frontiers | Research Topics

Novel modalities in cancer diagnostics and therapeutics

Edited by
Dong-Hua Yang and Haichang Li

Published in
Frontiers in Pharmacology
Frontiers in Oncology

FRONTIERS EBOOK COPYRIGHT STATEMENT

The copyright in the text of individual articles in this ebook is the property of their respective authors or their respective institutions or funders. The copyright in graphics and images within each article may be subject to copyright of other parties. In both cases this is subject to a license granted to Frontiers.

The compilation of articles constituting this ebook is the property of Frontiers.

Each article within this ebook, and the ebook itself, are published under the most recent version of the Creative Commons CC-BY licence. The version current at the date of publication of this ebook is CC-BY 4.0. If the CC-BY licence is updated, the licence granted by Frontiers is automatically updated to the new version.

When exercising any right under the CC-BY licence, Frontiers must be attributed as the original publisher of the article or ebook, as applicable.

Authors have the responsibility of ensuring that any graphics or other materials which are the property of others may be included in the CC-BY licence, but this should be checked before relying on the CC-BY licence to reproduce those materials. Any copyright notices relating to those materials must be complied with.

Copyright and source acknowledgement notices may not be removed and must be displayed in any copy, derivative work or partial copy which includes the elements in question.

All copyright, and all rights therein, are protected by national and international copyright laws. The above represents a summary only. For further information please read Frontiers' Conditions for Website Use and Copyright Statement, and the applicable CC-BY licence.

ISSN 1664-8714
ISBN 978-2-83251-045-2
DOI 10.3389/978-2-83251-045-2

About Frontiers

Frontiers is more than just an open access publisher of scholarly articles: it is a pioneering approach to the world of academia, radically improving the way scholarly research is managed. The grand vision of Frontiers is a world where all people have an equal opportunity to seek, share and generate knowledge. Frontiers provides immediate and permanent online open access to all its publications, but this alone is not enough to realize our grand goals.

Frontiers journal series

The Frontiers journal series is a multi-tier and interdisciplinary set of open-access, online journals, promising a paradigm shift from the current review, selection and dissemination processes in academic publishing. All Frontiers journals are driven by researchers for researchers; therefore, they constitute a service to the scholarly community. At the same time, the *Frontiers journal series* operates on a revolutionary invention, the tiered publishing system, initially addressing specific communities of scholars, and gradually climbing up to broader public understanding, thus serving the interests of the lay society, too.

Dedication to quality

Each Frontiers article is a landmark of the highest quality, thanks to genuinely collaborative interactions between authors and review editors, who include some of the world's best academicians. Research must be certified by peers before entering a stream of knowledge that may eventually reach the public - and shape society; therefore, Frontiers only applies the most rigorous and unbiased reviews. Frontiers revolutionizes research publishing by freely delivering the most outstanding research, evaluated with no bias from both the academic and social point of view. By applying the most advanced information technologies, Frontiers is catapulting scholarly publishing into a new generation.

What are Frontiers Research Topics?

Frontiers Research Topics are very popular trademarks of the *Frontiers journals series*: they are collections of at least ten articles, all centered on a particular subject. With their unique mix of varied contributions from Original Research to Review Articles, Frontiers Research Topics unify the most influential researchers, the latest key findings and historical advances in a hot research area.

Find out more on how to host your own Frontiers Research Topic or contribute to one as an author by contacting the Frontiers editorial office: frontiersin.org/about/contact

Novel modalities in cancer diagnostics and therapeutics

Topic editors
Dong-Hua Yang — New York College of Traditional Chinese Medicine, United States
Haichang Li — The Ohio State University, United States

Citation
Yang, D.-H., Li, H., eds. (2022). *Novel modalities in cancer diagnostics and therapeutics*. Lausanne: Frontiers Media SA. doi: 10.3389/978-2-83251-045-2

Table of contents

05 Editorial: Novel modalities in cancer diagnostics and therapeutics
Serena Li Zhao, Dong-Hua Yang and Haichang Li

08 Combination of Anlotinib and Celecoxib for the Treatment of Abdominal Desmoid Tumor: A Case Report and Literature Review
Jianzheng Wang, Hongle Li, Hui Wang, Qingli Li, Xuanye Bai, Huifang Lv, Caiyun Nie, Beibei Chen, Weifeng Xu, Shuiping Tu and Xiaobing Chen

14 A FAK Inhibitor Boosts Anti-PD1 Immunotherapy in a Hepatocellular Carcinoma Mouse Model
Yuhua Wei, Yufeng Wang, Nanbin Liu, Ran Qi, Yan Xu, Kun Li, Yu Feng and Baomin Shi

26 The Histone Acetyltransferase MOF Regulates SIRT1 Expression to Suppress Renal Cell Carcinoma Progression
Renbo Guo, Yiran Liang, Benkui Zou, Danyang Li, Zhen Wu, Fei Xie, Xu Zhang and Xiangzhi Li

38 Albuca Bracteata Polysaccharides Attenuate AOM/DSS Induced Colon Tumorigenesis via Regulating Oxidative Stress, Inflammation and Gut Microbiota in Mice
Ziyan Qin, Xinyu Yuan, Jian Liu, Zhuqing Shi, Leipeng Cao, Lexuan Yang, Kai Wu, Yongliang Lou, Haibin Tong, Lei Jiang and Jimei Du

53 IL7R Is Correlated With Immune Cell Infiltration in the Tumor Microenvironment of Lung Adenocarcinoma
Xin Wang, Shujian Chang, Teng Wang, Ruirong Wu, Zebo Huang, Junjie Sun, Jingjing Liu, Yan Yu and Yong Mao

65 ZWZ-3, a Fluorescent Probe Targeting Mitochondria for Melanoma Imaging and Therapy
Zengjin Liu, Hailan Wang, Changzhen Sun, Yuanmin He, Tong Xia, Jianv Wang, Xia Xiong, Qingbi Zhang, Sijin Yang and Li Liu

76 Vanillin Derivatives Reverse *Fusobacterium nucleatum*-Induced Proliferation and Migration of Colorectal Cancer Through E-Cadherin/β-Catenin Pathway
Zhongkun Zhou, Yiqing Wang, Rui Ji, Dekui Zhang, Chi Ma, Wantong Ma, Yunhao Ma, Xinrong Jiang, Kangjia Du, Rentao Zhang and Peng Chen

87 Engineered Exosomes-Mediated Transfer of hsa-miR-320a Overcomes Chemoresistance in Cervical Cancer Cells *via* Targeting MCL1
Jinling Zhou, Yuanhe Wang, Lizhu Zhang, Qin Chen, Xiaojun Zhu, Peiyue Jiang, Nan Jiang, Wei Zhao and Baohua Li

97 Roles and new Insights of Macrophages in the Tumor Microenvironment of Thyroid Cancer
Qi Liu, Wei Sun and Hao Zhang

111 The Histone Deacetylase Inhibitor I1 Induces Differentiation of Acute Leukemia Cells With MLL Gene Rearrangements *via* Epigenetic Modification
Jingfang Yao, Gentao Li, Zihui Cui, Peilei Chen, Jinhong Wang, Zhenbo Hu, Lei Zhang and Liuya Wei

124 CNST is Characteristic of Leukemia Stem Cells and is Associated With Poor Prognosis in AML
Haoyu Liu, Xu Zhang, Ziyan Zhao, Hongying Zhu, Danyang Li, Yang Yang, Wenbo Zhao, Fei Zhang, Yuefeng Wang, Lina Zhu, Zewen Ding and Xiangzhi Li

135 Individualized Treatment for Advanced Non-Small Cell Lung Cancer: A Case Report and Literature Review
Qianqian Sun, Weiqing Li, Taorui Liu and Huiqin Guo

142 Identification and Validation of an Apoptosis-Related Gene Prognostic Signature for Oral Squamous Cell Carcinoma
Shuqin Wang, Sien Zhang, Zhi Lin, Jingxin Ma, Lijun Zhu and Guiqing Liao

153 Sclerostin Suppression Facilitates Uveal Melanoma Progression Through Activating Wnt/β-Catenin Signaling *Via* Binding to Membrane Receptors LRP5/LRP6
Hanqing Wang, Sidi Zhao, Yang Liu, Fengyuan Sun, Xiaoming Huang and Tong Wu

167 Emerging Role of *Helicobacter pylori* in the Immune Evasion Mechanism of Gastric Cancer: An Insight Into Tumor Microenvironment-Pathogen Interaction
Zhifang Li, Wenqing Zhang, Jinyang Bai, Jing Li and Hong Li

174 Oxaliplatin Eluting CalliSpheres Microspheres for the Treatment of Unresectable or Recurrent Hepatocellular Carcinoma
Yonghua Bi, Kewei Ren, Jianzhuang Ren, Ji Ma and Xinwei Han

181 MOF negatively regulates estrogen receptor α signaling *via* CUL4B-mediated protein degradation in breast cancer
Xu Zhang, Yang Yang, Danyang Li, Zhen Wu, Haoyu Liu, Ziyan Zhao, Hongying Zhu, Fei Xie and Xiangzhi Li

frontiers | Frontiers in Pharmacology

TYPE Editorial
PUBLISHED 30 November 2022
DOI 10.3389/fphar.2022.1101506

Check for updates

OPEN ACCESS

EDITED AND REVIEWED BY
Heike Wulff,
University of California, Davis,
United States

*CORRESPONDENCE
Dong-Hua Yang,
yangd1@stjohns.edu
Haichang Li,
li.3714@osu.edu

†PRESENT ADDRESS
Dong-Hua Yang,
New York College of Traditional
Chinese Medicine, Mineola, NY,
United States

SPECIALTY SECTION
This article was submitted to
Experimental Pharmacology and Drug
Discovery, a section of the journal
Frontiers in Pharmacology

RECEIVED 17 November 2022
ACCEPTED 22 November 2022
PUBLISHED 30 November 2022

CITATION
Zhao SL, Yang D-H and Li H (2022),
Editorial: Novel modalities in cancer
diagnostics and therapeutics.
Front. Pharmacol. 13:1101506.
doi: 10.3389/fphar.2022.1101506

COPYRIGHT
© 2022 Zhao, Yang and Li. This is an open-access article distributed under the terms of the Creative Commons Attribution License (CC BY). The use, distribution or reproduction in other forums is permitted, provided the original author(s) and the copyright owner(s) are credited and that the original publication in this journal is cited, in accordance with accepted academic practice. No use, distribution or reproduction is permitted which does not comply with these terms.

Editorial: Novel modalities in cancer diagnostics and therapeutics

Serena Li Zhao[1], Dong-Hua Yang[2*†] and Haichang Li[3,4*]

[1]Department of Medicinal Chemistry and Pharmacognosy, The Ohio State University College of Pharmacy, Columbus, OH, United States, [2]Department of Pharmaceutical Sciences, College of Pharmacy and Health Sciences, St. John's University, New York, NY, United States, [3]Department of Surgery, The Ohio State University College of Medicine, Columbus, OH, United States, [4]Department of Veterinary Biosciences, The Ohio State University College of Veterinary Medicine, Columbus, OH, United States

KEYWORDS

cancer, technologies, diagnostics, therapeutics, novel modalities

Editorial on the Research Topic
Novel modalities in cancer diagnostics and therapeutics

This Research Topic "*Novel Modalities in Cancer Diagnostics and Therapeutics*" is the second issue following our previous topic "*New Technologies in Cancer Diagnostics and Therapeutics*" and continuously focuses on the newly emerging areas of cancer diagnostics, drug development, and molecular signaling pathways (Li et al., 2021). Our aim was to collect the latest findings in both basic research and clinic application to contribute to the future direction of drug development or novel therapy. To this end, we received 35 manuscripts and finally 17 articles were selected in this Research Topic.

This Research Topic comprises two review papers, two case reporters and thirteen research articles. Tumor microenvironment (TME) composed of tumor cells, immune cells such as macrophages, and plays an important function in the cancer development, progression, and prognosis. The review article by Liu et al. summarized the functions of tumor-associated macrophages (TAMs) in thyroid cancer and discussed the mechanisms by which TAMs maintain the stemness of thyroid cancer and potential strategies for targeting TAMs to treat thyroid cancer. Another review article by Li et al. highlighted the regulatory mechanisms underlying the crosstalk between *H. pylori* infection and immune cells in TME of gastric cancer. *H. pylori* is well known to induce immune response and inflammation in the stomach and involved in gastric cancer progression. The research demonstrated that the underlying molecular mechanism concerning the crosstalk between *H. pylori* and the TME of Gastric cancer may contribute to develop effective therapy against *H. pylori* -induced gastric cancer. The research article by Wang et al. provided evidence that Interleukin-7 receptor (IL7R) may function as a potential prognostic factor for lung adenocarcinoma and found that IL7R expression was positively correlated with the overall survival and progression-free survival of lung adenocarcinoma patients. Their findings suggest that IL7R inhibits tumor growth by regulating the proportion of immune infiltrating cells in TME. The case report article by Sun et al. presented a case study of a middle-aged male patient with advanced lung adenocarcinoma who underwent a descending surgery after nine cycles of individualized chemotherapy combined with targeted immunotherapy and continued adjuvant chemotherapy. Following a comprehensive analysis, they developed a precise individualized chemotherapy plan and the patient achieved complete response. Wang et al. reported a combined treatment study using anlotinib (a small molecule multi-target tyrosine kinase inhibitor) and celecoxib (COX-2 inhibitor) in a desmoid tumors (DTs) patient with aggressive fibromatosis in the abdominal cavity. They provided evidence that the patient achieved a partial response with mild toxicity and disappeared pain symptoms following a combined therapy.

Hepatocellular carcinoma (HCC) is one of the most common malignant tumors and the leading cause of cancer-related mortality worldwide. The immunotherapy which targets immune checkpoints, such as anti-programmed cell death 1(PD1) targeted immunotherapy, resulted in promising and encouraging effects in the treatment or various tumors. The studies from Wei et al. found that the combination of the FAK inhibitor (VS4718) and an anti-PD1 antibody could suppress tumor progression in murine model for hepatocellular carcinoma (HCC). The combination of the FAK inhibitor VS4718 and anti-PD1 could be a potential therapy for HCC by improving the immune environment, reducing liver fibrosis and simultaneously preventing PD1 from binding to the increased PD-L1 induced by FAK inhibitor. Drug-eluting beads-transarterial chemoembolization (DEB-TACE) has been widely used in unresectable and advanced hepatocellular carcinoma (HCC). Bi et al. assessed that the preliminary outcomes of DEB-TACE loaded with oxaliplatin for the treatment of patients with unresectable or recurrent HCC. The data suggested that DEB-TACE loaded with oxaliplatin-eluting CalliSpheres microspheres could be a safe, feasible, and efficacious palliative regimen in unresectable or recurrent HCC patients. Liu et al. investigated the expression of Consortin, a marker of poor differentiation of blood cells in the peripheral blood of acute myeloid leukemia (AML) patients by analyzing data from public databases and showed that CNST expression was inversely correlated with overall survival among AML patients and the genes negatively correlated with CNST are involved in various immune-related pathways. Mixed lineage leukemia gene rearrangements (MLLr) were found in about 10% of all the AML cases and in 22% of all the acute lymphoblastic leukemia (ALL) cases. Yao et al. investigated the Histone deacetylases inhibitor I1 (HDAC-I1), a chromatin-remodeling agent and found that a marked anti-proliferative effect on MLLr-AML and MLLr-ALL cells. HDAC-I1 inhibited HDAC and activated the hematopoietic cell lineage signaling, suggesting that HDAC-I1 could be a potential epigenetic agent for the treatment of Acute leukemia. Liu et al. developed the hemicyanine-based fluorescent probe ZWZ-3, which can be selectively enriched in the mitochondria of melanoma cells, thus promoting mitochondrial oxidative phosphorylation and inducing apoptosis and autophagy. Their data suggested that ZWZ-3 represents a potential therapeutic agent for detecting and treating melanoma. Qin et al. investigated the properties of polysaccharides of A. bracteate, named ABP and show that ABP increase anti-inflammatory cytokine IL-10, inhibited secretion of pro-inflammatory cytokines (IL-6, IFN-γ, and TNF-α), mitigated oxidative stress, and found that the CAC mice treated with ABP showed smaller tumor size and lower tumor incidence than untreated ones. Using database from TCGA and GEO, Wang et al. identified six risk biomarkers associated with prognosis of oral squamous cell carcinoma (OSCC). The expression of these risk genes in clinical specimens was higher in the non-survival patients than in the well-survival patients, suggesting that those gene signature and nomogram might provide a potential prognostic prediction and therapeutic for OSCC. Zhou et al. reported that miR-320a expression is lower in cisplatin (DDP) resistant cervical cancer (CC), and engineered miR-320a exosomes can attenuate DDP resistance *via* inhibiting Myeloid Cell Leukemia Sequence 1 (MCL1), a pro-survival and pro-proliferative factor which plays a critical role in tumorigenesis. The engineered miR-320a exosomes may represent a new therapy for chemoresistance cervical cancer treatment. Wang et al. studied the impact of sclerostin on malignant progression of Uveal melanoma (UM) and demonstrated that Sclerostin silencing through transfecting specific siRNA could heighten the proliferation, migration, and invasion as well as angiogenesis of human UM cells *via* activating Wnt/β-catenin signaling. Natural products with low toxicity are always important source for drug development. Zhou et al. investigated vanillin-derivate intervention by *in vitro* co-culturing with colorectal cancer cells and exploring the possible underlying mechanism. Their results showed that both vanillin derivatives were effective for *F. nucleatum*-infected Colorectal cancer (CRC) cells by inhibiting proliferation and migration through the E-cadherin/β-catenin pathway, suggesting potential natural product drug candidates for microbe-targeted strategies for the treatment of CRC.

Histone acetylation modification is one of the major significant epigenetic modifications, which are involved in various cellular biological processes including carcinogenesis (Langst and Manelyte, 2015). Dr. Xiangzhi Li's group has long been committed to studying the function of MOF (males absent on the first), a histone acetyltransferase in a variety of physiological and pathological processes including cancers (Li et al., 2009; Li et al., 2010; Li et al., 2012; Guo et al., 2020; Wang et al., 2021). In this Research Topic, Li's group further provides exciting evidence for the potential role of MOF in breast cancer (BC) (Zhang et al.) and renal cell carcinoma (RCC) (Guo et al.). Although the abnormal gene expression of MOF has been found in several types of cancers, more studies are still needed to comprehensively understand the function and complex regulatory mechanism of MOF in the initiation and progression of cancers and their relationship to cancer prognosis. Screening and discovering drugs or small molecules that can normalize the intracellular acetylation levels in cancer cells could be a prospective guide for further research and clinical applications.

In conclusion, this Research Topic "*Novel Modalities in Cancer Diagnostics and Therapeutics*" highlights multiple studies for developing potential targets or novel therapeutics for cancer diagnosis and treatment.

Author contributions

SZ and HL wrote the first draft. D-HY provided critical comments and revisions. All authors reviewed and approved the manuscript for submission.

Funding

This work was supported by the National Institutes of Health grants (RO1AG056919 and R21AR080628) to HL. We also appreciate the support from the OSU Comprehensive Cancer Center Startup Fund to HL.

Conflict of interest

The authors declare that the research was conducted in the absence of any commercial or financial relationships that could be construed as a potential conflict of interest.

Publisher's note

All claims expressed in this article are solely those of the authors and do not necessarily represent those of their affiliated organizations, or those of the publisher, the editors and the reviewers. Any product that may be evaluated in this article, or claim that may be made by its manufacturer, is not guaranteed or endorsed by the publisher.

References

Guo, X., Li, D., Song, J., Yang, Q., Wang, M., Yang, Y., et al. (2020). Mof regulates glucose level via altering different alpha-cell subset mass and intra-islet glucagon-like peptide-1, glucagon secretion. *Metabolism.* 109, 154290. doi:10.1016/j.metabol.2020.154290

Langst, G., and Manelyte, L. (2015). Chromatin remodelers: From function to dysfunction. *Genes* 6, 299–324. doi:10.3390/genes6020299

Li, X., Wu, L., Corsa, C. A., Kunkel, S., and Dou, Y. (2009). Two mammalian MOF complexes regulate transcription activation by distinct mechanisms. *Mol. Cell* 36, 290–301. doi:10.1016/j.molcel.2009.07.031

Li, X., Corsa, C. A., Pan, P. W., Wu, L., Ferguson, D., Yu, X., et al. (2010). MOF and H4 K16 acetylation play important roles in DNA damage repair by modulating recruitment of DNA damage repair protein Mdc1. *Mol. Cell. Biol.* 30, 5335–5347. doi:10.1128/MCB.00350-10

Li, X. Z., Li, L., Pandey, R., Byun, J. S., Gardner, K., Qin, Z. H., et al. (2012). The histone acetyltransferase MOF is a key regulator of the embryonic stem cell core transcriptional network. *Cell Stem Cell* 11, 163–178. doi:10.1016/j.stem.2012.04.023

Li, H., Zhao, S. L., Cohen, P., and Yang, D. H. (2021). Editorial: New technologies in cancer diagnostics and therapeutics. *Front. Pharmacol.* 12, 760833. doi:10.3389/fphar.2021.760833

Wang, M., Liu, H., Zhang, X., Zhao, W., Lin, X., Zhang, F., et al. (2021). Lack of MOF decreases susceptibility to hypoxia and promotes multidrug resistance in hepatocellular carcinoma via HIF-1α. *Front. Cell Dev. Biol.* 9, 718707. doi:10.3389/fcell.2021.718707

frontiers in Oncology

CASE REPORT
published: 13 January 2022
doi: 10.3389/fonc.2021.830672

Combination of Anlotinib and Celecoxib for the Treatment of Abdominal Desmoid Tumor: A Case Report and Literature Review

Jianzheng Wang[1†], *Hongle Li*[2†], *Hui Wang*[3], *Qingli Li*[4], *Xuanye Bai*[5], *Huifang Lv*[1], *Caiyun Nie*[1], *Beibei Chen*[1], *Weifeng Xu*[1], *Shuiping Tu*[4*] and *Xiaobing Chen*[1*]

[1] Department of Medical Oncology, Affiliated Cancer Hospital of Zhengzhou University, Henan Cancer Hospital, Zhengzhou, China, [2] Department of Molecular Pathology, Affiliated Cancer Hospital of Zhengzhou University, Henan Cancer Hospital, Zhengzhou, China, [3] Department of Endoscope Center, Affiliated Cancer Hospital of Zhengzhou University, Henan Cancer Hospital, Zhengzhou, China, [4] Department of Oncology, Renji Hospital, School of Medicine, Shanghai Jiaotong University, Shanghai, China, [5] Department of Pathology, Affiliated Cancer Hospital of Zhengzhou University, Henan Cancer Hospital, Zhengzhou, Henan, China

OPEN ACCESS

Edited by:
Dong-Hua Yang,
St. John's University, United States

Reviewed by:
Neeraj Kaushal,
St. John's University, United States
Shaoquan Zheng,
Sun Yat-sen University Cancer Center (SYSUCC), China

***Correspondence:**
Xiaobing Chen
zlyychenxb0807@zzu.edu.cn
Shuiping Tu
tushuiping@yahoo.com

†These authors have contributed equally to this work

Specialty section:
This article was submitted to Pharmacology of Anti-Cancer Drugs, a section of the journal Frontiers in Oncology

Received: 07 December 2021
Accepted: 20 December 2021
Published: 13 January 2022

Citation:
Wang J, Li H, Wang H, Li Q, Bai X, Lv H, Nie C, Chen B, Xu W, Tu S and Chen X (2022) Combination of Anlotinib and Celecoxib for the Treatment of Abdominal Desmoid Tumor: A Case Report and Literature Review. Front. Oncol. 11:830672. doi: 10.3389/fonc.2021.830672

Desmoid tumor is a rare disease, which is histologically characterized by local invasion, monoclonality, and fibroblast proliferation; and clinically characterized by a variable and often unpredictable course. The treatment of desmoid tumor is mainly surgical resection, but the recurrence rate is high. In recent years, a variety of treatment methods, including endocrine therapy, surgery, radiotherapy, chemotherapy, non-steroidal anti-inflammatory drugs, targeted drugs, interferon and more, have been used and achieved certain curative effects. In addition, in view of the inertia characteristics of desmoid tumor, observation is also a first-line scheme recommended by multiple guidelines. In the past, the research progress of targeted therapy for desmoid tumor is relatively slow and the curative effect is limited. Thus, targeted therapy is usually used as a remedial treatment after the failure of other conventional treatment methods. However, in recent years, with the rapid progress in the basic research of targeted therapy, some new targeted drugs are increasingly used for the clinical treatment of desmoid tumor and have achieved good results. Herein, we described a patient with aggressive fibromatosis in the abdominal cavity. Following a combined treatment using anlotinib and celecoxib, the patient achieved a partial response with mild toxicity. Simultaneously, the patient's pain symptoms completely disappeared. This case indicates that the combination of anlotinib and NSAIDs could be an effective treatment for desmoid tumor.

Keywords: desmoid tumors, anlotinib, celecoxib, targeted therapy, NSAIDs

BACKGROUND

Desmoid tumors (DTs), also known as aggressive fibromatosis, are local tumors of mesenchymal origin that can cause significant morbidity due to their infiltrating nature (1, 2). DTs are fibroblast clonal proliferative diseases originated from deep soft tissue. Most of them are found in connective tissues in muscles and fascia or aponeurosis. DT often infiltrates into adjacent muscle tissue or adipose tissue. It is usually easy to relapse after surgical resection, but in some cases, the disease can be stable and subside by itself (3). DTs include sporadic fibroma and familial adenomatous polyposis (FAP) associated fibroma. Most DTs are sporadic and are mainly caused by abnormalities in the Wnt/β-catenin signaling pathway, usually related to somatic β-catenin gene mutations (4, 5). At present, the treatment of DTs includes active monitoring, surgery, radiotherapy, chemotherapy, targeted therapy, endocrine and non-steroidal drug therapy (6). In the past, the research progress of targeted therapy for DTs is relatively slow and the curative effect is limited. Therefore, targeted therapy is often used as remedial treatment after the failure of other conventional treatment methods. However, in recent years, with the rapid progress of basic research on targeted therapy, some new targeted drugs, such as such as Imatinib (7–9), Pazopanib (10) and Sorafenib, are used in the clinical treatment of DTs and have achieved good curative effect (11).

Anlotinib is a small molecule multi-target tyrosine kinase inhibitor, which can effectively inhibit vascular endothelial growth factor receptor (VEGFR), platelet-derived growth factor receptor (PDGFR), fibroblast growth factor receptor (FGFR), stem cell growth factor receptor (c-Kit) and others, and has the effect of anti-tumor angiogenesis and inhibiting tumor growth (12). Anlotinib has shown encouraging anti-tumor effects and acceptable toxicity in advanced lung cancer and soft tissue sarcoma (13–15). However, the role of anlotinib in the treatment of DTs remains unknown. So far, there is no clinical study on using anlotinib for the treatment of DTs.

We have recently encountered a rare case of isolated aggressive fibromatosis located in the abdominal cavity. Our team innovatively used the combination of anlotinib and celecoxib for the treatment. The patient's tumor was significantly reduced and the progression-free survival (PFS) exceeded 18 months. This is the first case of successful treatment of DT using the combination of anlotinib and non-steroidal anti-inflammatory drugs (NSAIDs), which has not been previously reported.

CASE PRESENTATION

The patient is a 50 years old woman who had accidentally palpated a hard mass in the lower abdomen one and a half years ago. The mass had unclear boundaries and the patient had gradually worsening pain. The numerical rating scale (NRS) score was 7 points. A color Doppler ultrasound examination at the local hospital (2020-04-12) showed that there was an inhomogeneous echo mass about 9.5cm*7.7cm*6.8cm in the right front of the abdominal aorta in the upper mid-abdomen. She was admitted to Henan Cancer Hospital and an enhanced CT examination (2020-04-14) showed that there is a lump in the lower part of the abdomen and the upper part of the pelvis. The exploratory laparotomy was performed under general anesthesia on 2020-04-29. During the surgery, the size of the tumor was about 9cm*7cm*6cm, which invades the mesentery and causes mesangial contracture. The tumor envelops the main branches of the upper mesenteric blood vessels and is closely related to the blood vessels. Abdominal mass biopsy was performed after communicating with the patient's family. Postoperative pathology (2020-05-18) showed aggressive fibromatosis. Fluorescence *in situ* hybridization (FISH) detection:3p22/3 = 0.72,CTNNB1 gene deletion. Probe type: CSP3/GSP CTNNB1 (3p22) (**Figure 1**). Immunohistochemical staining was performed and showed CK(-), CD34(vascular+), SOX-10(-), Bcl-2 (-),β- catenin(+), SMA(-), Desmin(-), Ki-67 (about 1%), CD117 (-), Dog-1 (-), ER-, PR- (**Supplementary Figure 1**). After the surgery, the patient's NRS score was 6 points, and was given OxyContin 30 mg po q12h. We performed CT examination again before treatment as a baseline and the enhanced CT (2020-05-20) examination showed: 1. There is a soft tissue mass in the left lower abdominal cavity, with unclear borders, uneven enhancement, and unclear demarcation from the adjacent intestine. The larger section is about 84×65mm, and the surrounding fat gaps are blurred. We explain to the patient's family that there is currently no standard treatment plan for

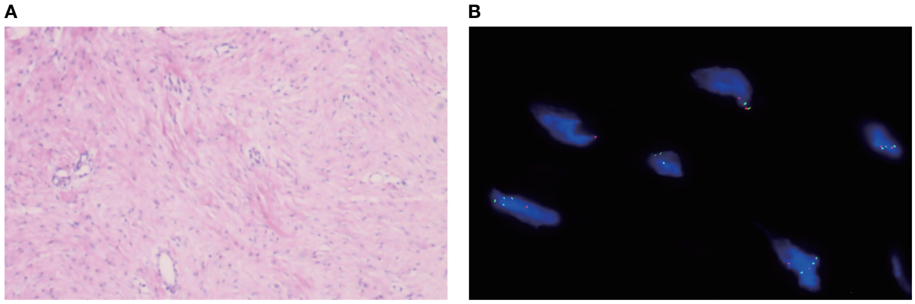

FIGURE 1 | **(A)** HE staining showing the fibromatosis. **(B)** Fluorescence *in situ* hybridization(FISH) detection:3p22/3 = 0.72,CTNNB1 gene deletion. Probe type: CSP3/GSP CTNNB1 (3p22).

aggressive fibromatosis, and anti-vascular targeted therapy combined with NSAIDs can be selected. The specific treatment regimen was: anlotinib: 10mg po bid d1-14, q21d and celecoxib: 0.1g po bid. From May 28, 2020 to December 02, 2021, anlotinib combined with celecoxib regimen was given for 22 cycles. The abdominal mass was significantly reduced after treatment (**Figure 2**). The treatment efficacy reached PR (partial response) (**Figure 3**), and the NRS score (2020-10-15) was 0 points (**Figure 4**). At present, the patient is generally in good condition, and the NRS score is 0 point. The patient is expected to obtain long-term survival with the continuation of treatment using anlotinib in combination with celecoxib.

DISCUSSION

DT is a rare soft tissue tumor with a low incidence, which can occur in all parts of the body (16). The World Health Organization (WHO) defines invasive fibromatosis as clonal fibroblastic proliferative tumor formed in deep soft tissue, which is characterized by invasive growth, local recurrence and no distant metastasis (17, 18). The proximal and abdominal parts of the upper and lower limbs are the most common sites. The diagnosis mainly depends on pathological examination. At present, comprehensive treatment including surgery is the main treatment mode for invasive fibroma. Imaging examination is of great significance for monitoring tumor growth.

The etiology of invasive fibromatosis is not clear, which may be due to the combined effect of genetic, endocrine and physical factors, leading to the defect of connective tissue growth regulation. Invasive fibromatosis patients with Gardner syndrome are familial, suggesting that the disease might has a genetic basis (19). It often occurs in pregnant or post-pregnant women, suggesting that endocrine factors may be involved in tumor growth. Thus, estrogen receptor blockers and aromatase inhibitors are often used for its clinical treatment (20, 21).

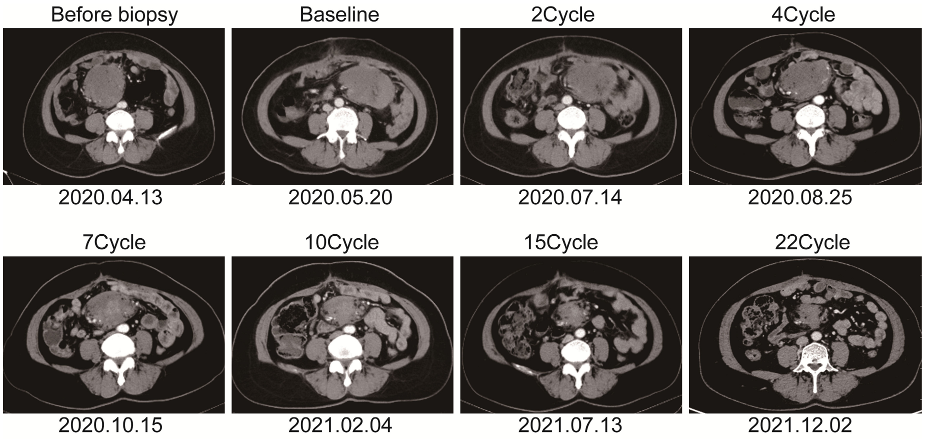

FIGURE 2 | The soft tissue mass in the left lower abdomen was scanned with enhanced computed tomography at different time points.

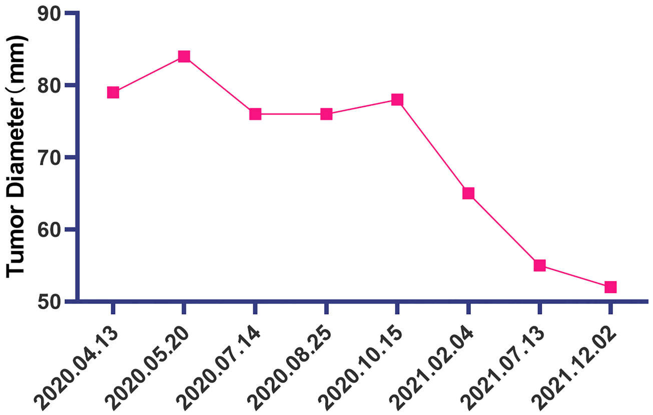

FIGURE 3 | The change of the diameter of the soft tissue mass in the left lower abdomen at different time points.

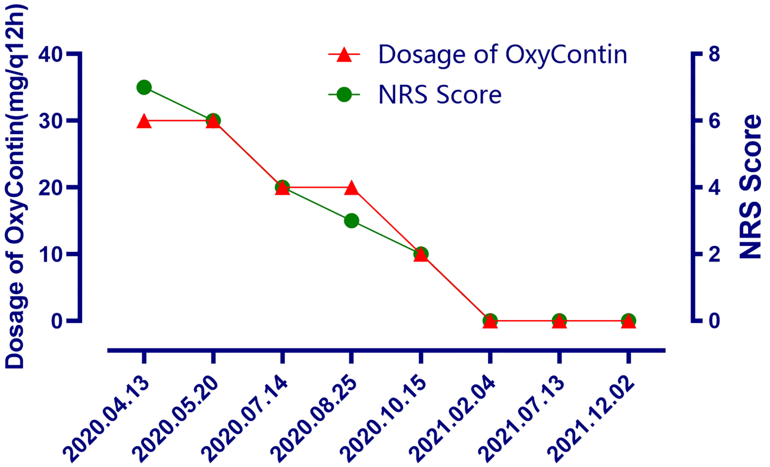

FIGURE 4 | The changes of the dosage of OxyContin and the changes of NRS scores after treatment at different time points.

At present, the treatment of DTs mainly includes active monitoring, surgery, radiotherapy, chemotherapy, targeted therapy and hormonal therapy. However, due to the lack of a comprehensive understanding of the pathogenesis of DTs and their natural evolution history, it is difficult to determine which types of DTs will not progress, and which DTs patients need active treatment. Studies have shown that the 5-year progression-free survival rate of asymptomatic DTs patients with active monitoring is 50% (22).

At present, drugs for targeted therapy of DTs mainly include tyrosine kinase inhibitors (TKIs), Wnt/β-catenin inhibitors and γ-secretase inhibitors. TKIs are one of the effective treatments for DTs. Clinically effective TKIs include imatinib, sorafenib, sunitinib, pazopani and anlotinib. But due to the low incidence of DTs, there is a lack of prospective studies with large number cases. Most of the current studies are retrospective. Imatinib is often used for remedial treatment of DTs after failure of other treatments. Kasper et al. (8) have shown that imatinib can inhibit tumor progression in DTs patients with Response Evaluation Criteria in Solid Tumours (RECIST) progress. For DTs patients with RECIST progress, the progression arrest rate (PAR) at 6 months after imatinib treatment is 65%.Penel et al. (7) showed that the PARs of patients with RECIST progression DTs and recurrent DTs at 6, 9 and 12 months after imatinib treatment were 80%, 69% and 67%, respectively. Sorafenib is one of the most studied TKIs drugs. It was found that in patients with progressive, refractory or symptomatic DTs, sorafenib could significantly prolong PFS and had long-term effects. The two-year PFS was 81% in the sorafenib-treatment group and 36% in the placebo group. The objective response rate (ORR) was 33% and 20%, respectively, in the two groups. In patients with effective treatment of DTs, the median time for sorafenib group to reach the RECIST efficacy evaluation standard was 9.6 months, and the placebo group was 13.3months (11). A phase II prospective study included 19 patients, including 9 sporadic fibromas and 10 FAP-related fibromas, to explore the efficacy of sunitinib on DTs. The results showed that partial response (PR) and stable disease (SD) were 26.3% and 42.1% respectively; the 2-year PFS was 74.7% and the overall survival (OS) was 94.4% (23). A phase II clinical trial found that pazopani showed efficacy for progressive DTs. Compared with methotrexate combined with vincristine, the PFS of pazopani for 6 months was 83.7% and 45.0%, and ORR was 55% and 37%, respectively. The short-term efficacy of pazopani was significantly better than that of the traditional second-line chemotherapy. A retrospective study explored the therapeutic effect of single-agent anlotinib on DTs. Anlotinib treated DTs patients in the extremities had the PFS of 95.2%, 90.5%, and 84.0% at 3, 6, and 12 months, respectively. The disease control rate (DCR) was 86.0% (18/21), and the ORR was 38.1% (8/21). The adverse reactions mainly included hand-foot syndrome, skin pigmentation, menstrual disorder, nausea and diarrhea, but they were all within the acceptable range (24). Although anlotinib has shown a certain effect on DTs, its final therapeutic effect still needs to be further confirmed by large-scale retrospective studies and prospective studies. So far, there is no report on the combination of anlotini and NSAIDs in the treatment of DTs. Our case shows for the first time that the combination of both has a good tumor inhibitory effect. At present, the patient is still in the treatment process, and it is expected to achieve a complete tumor regression effect.

Due to the critical role of Wnt/β-catenin signaling pathway in DTs formation, their inhibitors may be effective in this disease. Wnt/β-catenin inhibitor tegavivint is a new type of targeted drug and is being studied. It shows therapeutic effect on osteosarcoma both *in vitro* and *in vivo* (25). At present, there is no study on the therapeutic effect of tegavivint on DTs, and only one phase I clinical trial (NCT03459469) is recruiting DT patients.

γ-secretase inhibitor (GSI) is another new type of DTs targeted therapy drug. The γ-secretase inhibitor PF-03084014 acts on Notch pathway, interacts with Wnt/APC/β-catenin pathway, and indirectly regulates Wnt/APC/β-catenin pathway, reducing the proportion of cells in S phase and G2-M phase, thereby inhibiting the growth of DTs. However, PF-03084014 cannot cause cell apoptosis. That is, PF-03084014 cannot kill tumor cells. It can only control tumor progression by inhibiting tumor cell proliferation (26). Kummar et al. (27) suggested that PF-03084014 was effective in the treatment of refractory and progressive DTs. Among the 17 patients with DTs enrolled, 16 patients (94%) were evaluated as effective. Five cases (29%) were evaluated as PR, indicating the potential therapeutic effect of PF-03084014 on DTs. Another phase I clinical trial showed that the ORR of patients with DTs treated with PF-03084014 was high (5 out of 7 cases) (28). However, the existing research samples are small, and large sample studies are still needed to confirm the therapeutic effect of PF-03084014 on DTs.

Tyrosine kinase inhibitors are currently widely recognized drugs and are the main treatment when needed. Using targeted therapy, we need to consider the efficacy and also its toxicity. However, this would not be a problem if treatment with long-term toxicities is balanced against the potential benefit. Toxicity is usually assessed based on acute side effects. The emphasis on long-term toxicity is less, and such data of more recent drugs are not available. Tyrosine kinase inhibitor sorafenib is popular at present. However, they may lead to permanent hypertension and/or hypothyroidism (29). This is an issue that cannot be ignored because patients are generally young and have normal life expectancy. There is a characteristic peak age (approximately 30-40 years)for this disease, and we recognize a female predominance (30). Moreover, the long-term safety of these treatments has never been assessed, since these drugs were developed for patients with metastatic cancer and their life expectancy is very limited.

Research on the mechanism of DT indicated that it is characterized by WNT/oncogene pathway alterations triggering COX-2-mediated constitutive coactivation of PDGFR, and may therefore benefit from combined nonsteroidal anti-inflammatory drug and tyrosine kinase inhibitor treatment (31). We look forward to exploring more therapeutic regimens of PDGFR inhibitors combined with COX-2 inhibitors with less side effects. Anlotinib (PDGFR inhibitor) and celecoxib (COX-2 inhibitor) are very promising combinations. However, the optimal combination dose still needs to be explored. Therefore, it is still an open question to choose which treatment is good for drug therapy for DTs. We should clearly share all available and unknown information with patients in order to make the best decision on personalized treatment.

In general, DT is usually not a life-threatening disease. However, due to chronic pain, functional defects, and psychological problems, the quality of life of patients with DTs is generally decline. In particular, pain control should always be a priority whenever pain is present to allow active surveillance also for symptomatic patients as appropriate. There are few existing literature on the evaluation of health-related quality of life (HRQoL) in patients with DTs. We expect that the upcoming clinical trials should take HRQoL, including functional level and symptoms (most importantly, pain) as the endpoint of study. In this case, after the combined treatment of anlotinib and celecoxib, the pain was significantly reduced and the dose of OxyContin was decreased. Although the lesion was only stable in the first few cycles of CT efficacy evaluation, this suggests that the combination of anlotinib and NSAIDs drugs may be a very promising strategy in pain control. However, we cannot completely rule out that NSAIDs drugs play a certain role in enhancing the analgesic effect of opioids.

CONCLUSION

Although the management of DTs has undergone significant changes in recent years, there are many areas of controversy. For patients with active monitoring failure and/or postoperative recurrence of DTs, there is an urgent need for drug intervention. Exploring more efficient and low toxic drugs is the future direction, and the quality of life of patients should be the emphasized. As a physician, we should not only pay attention to the quality of life in the near future, but also to its long-term prediction. Our goal should always be to avoid or limit any possible harm. We expect that the combination of anlotinib and NSAIDs will be a potential treatment strategy for DTs in the future.

DATA AVAILABILITY STATEMENT

The original contributions presented in the study are included in the article/**Supplementary Material**. Further inquiries can be directed to the corresponding author.

AUTHOR CONTRIBUTIONS

JW and XC treated the patient. JW, HLL, HFL, CN, BC, and WX collected the data. JW wrote the original draft. HW, XB, QL, and ST analyzed the data and revised the draft. All authors contributed to the article and approved the submitted version.

FUNDING

This work was financially supported by the Science and Technique Foundation of Henan Province (No. 202102310121 for JW), the Medical Science and Technology Co-construction Project of Henan Province (No. LHGJ20200167), the 1000 Talents Program of Central plains (No. 204200510023 for XC), and the Sate Key Laboratory of Esophageal Cancer Prevention & Treatment (No. Z2020000X for XC).

SUPPLEMENTARY MATERIAL

The Supplementary Material for this article can be found online at: https://www.frontiersin.org/articles/10.3389/fonc.2021.830672/full#supplementary-material

REFERENCES

1. von Mehren M, Randall RL, Benjamin RS, Boles S, Bui MM, Ganjoo KN, et al. Soft Tissue Sarcoma, Version 2.2018, NCCN Clinical Practice Guidelines in Oncology. *J Natl Compr Canc Netw* (2018) 16(5):536–63. doi: 10.6004/jnccn.2018.0025
2. Devata S, Chugh R. Desmoid Tumors: A Comprehensive Review of the Evolving Biology, Unpredictable Behavior, and Myriad of Management Options. *Hematol Oncol Clin North Am* (2013) 27(5):989–1005. doi: 10.1016/j.hoc.2013.07.008
3. Lewis JJ, Boland PJ, Leung DH, Woodruff JM, Brennan MF. The Enigma of Desmoid Tumors. *Ann Surg* (1999) 229(6):866–72; discussion 872-3. doi: 10.1097/00000658-199906000-00014
4. Salas S, Chibon F, Noguchi T, Terrier P, Ranchere-Vince D, Lagarde P, et al. Molecular Characterization by Array Comparative Genomic Hybridization and DNA Sequencing of 194 Desmoid Tumors. *Genes Chromosomes Cancer* (2010) 49(6):560–8. doi: 10.1002/gcc.20766
5. Crago AM, Chmielecki J, Rosenberg M, O–Connor R, Byrne C, Wilder FG, et al. Near Universal Detection of Alterations in CTNNB1 and Wnt Pathway Regulators in Desmoid-Type Fibromatosis by Whole-Exome Sequencing and Genomic Analysis. *Genes Chromosomes Cancer* (2015) 54(10):606–15. doi: 10.1002/gcc.22272
6. Kasper B, Raut CP, Gronchi A. Desmoid Tumors: To Treat or Not to Treat, That Is the Question. *Cancer* (2020) 126(24):5213–21. doi: 10.1002/cncr.33233
7. Penel N, Le Cesne A, Bui BN, Perol D, Brain EG, Ray-Coquard I, et al. Imatinib for Progressive and Recurrent Aggressive Fibromatosis (Desmoid Tumors): An FNCLCC/French Sarcoma Group Phase II Trial With a Long-Term Follow-Up. *Ann Oncol* (2011) 22(2):452–7. doi: 10.1093/annonc/mdq341
8. Kasper B, Gruenwald V, Reichardt P, Bauer S, Rauch G, Limprecht R, et al. Imatinib Induces Sustained Progression Arrest in RECIST Progressive Desmoid Tumours: Final Results of a Phase II Study of the German Interdisciplinary Sarcoma Group (GISG). *Eur J Cancer* (2017) 76:60–7. doi: 10.1016/j.ejca.2017.02.001
9. Chugh R, Wathen JK, Patel SR, Maki RG, Meyers PA, Schuetze SM, et al. Efficacy of Imatinib in Aggressive Fibromatosis: Results of a Phase II Multicenter Sarcoma Alliance for Research Through Collaboration (SARC) Trial. *Clin Cancer Res* (2010) 16(19):4884–91. doi: 10.1158/1078-0432.CCR-10-1177
10. Toulmonde M, Pulido M, Ray-Coquard I, Andre T, Isambert N, Chevreau C, et al. Pazopanib or Methotrexate-Vinblastine Combination Chemotherapy in Adult Patients With Progressive Desmoid Tumours (DESMOPAZ): A non-Comparative, Randomised, Open-Label, Multicentre, Phase 2 Study. *Lancet Oncol* (2019) 20(9):1263–72. doi: 10.1016/S1470-2045(19)30276-1
11. Gounder MM, Mahoney MR, Van Tine BA, Ravi V, Attia S, Deshpande HA, et al. Sorafenib for Advanced and Refractory Desmoid Tumors. *N Engl J Med* (2018) 379(25):2417–28. doi: 10.1056/NEJMoa1805052
12. Sun Y, Niu W, Du F, Du C, Li S, Wang J, et al. Safety, Pharmacokinetics, and Antitumor Properties of Anlotinib, an Oral Multi-Target Tyrosine Kinase Inhibitor, in Patients With Advanced Refractory Solid Tumors. *J Hematol Oncol* (2016) 9(1):105. doi: 10.1186/s13045-016-0332-8
13. Chi Y, Fang Z, Hong X, Yao Y, Sun P, Wang G, et al. Safety and Efficacy of Anlotinib, a Multikinase Angiogenesis Inhibitor, in Patients With Refractory Metastatic Soft-Tissue Sarcoma. *Clin Cancer Res* (2018) 24(21):5233–8. doi: 10.1158/1078-0432.CCR-17-3766
14. Tang L, Yu W, Wang Y, Li H, Shen Z. Anlotinib Inhibits Synovial Sarcoma by Targeting GINS1: A Novel Downstream Target Oncogene in Progression of Synovial Sarcoma. *Clin Transl Oncol* (2019) 21(12):1624–33. doi: 10.1007/s12094-019-02090-2
15. Han B, Li K, Zhao Y, Li B, Cheng Y, Zhou J, et al. Anlotinib as a Third-Line Therapy in Patients With Refractory Advanced non-Small-Cell Lung Cancer: A Multicentre, Randomised Phase II Trial (Alter0302). *Br J Cancer* (2018) 118 (5):654–61. doi: 10.1038/bjc.2017.478
16. van Broekhoven DL, Grünhagen DJ, den Bakker MA, van Dalen T, Verhoef C. Time Trends in the Incidence and Treatment of Extra-Abdominal and Abdominal Aggressive Fibromatosis: A Population-Based Study. *Ann Surg Oncol* (2015) 22 (9):2817–23. doi: 10.1245/s10434-015-4632-y
17. Kruse AL, Luebbers HT, Grätz KW, Obwegeser JA. Aggressive Fibromatosis of the Head and Neck: A New Classification Based on a Literature Review Over 40 Years (1968-2008). *Oral Maxillofac Surg* (2010) 14(4):227–32. doi: 10.1007/s10006-010-0227-8
18. Eastley N, McCulloch T, Esler C, Hennig I, Fairbairn J, Gronchi A, et al. Extra-Abdominal Desmoid Fibromatosis: A Review of Management, Current Guidance and Unanswered Questions. *Eur J Surg Oncol* (2016) 42(7):1071–83. doi: 10.1016/j.ejso.2016.02.012
19. Xu B, Zhu LH, Wu JG, Wang XF, Matro E, Ni JJ. Pancreatic Solid Cystic Desmoid Tumor: Case Report and Literature Review. *World J Gastroenterol* (2013) 19 (46):8793–8. doi: 10.3748/wjg.v19.i46.8793
20. Shields CJ, Winter DC, Kirwan WO, Redmond HP. Desmoid Tumours. *Eur J Surg Oncol* (2001) 27(8):701–6. doi: 10.1053/ejso.2001.1169
21. Deyrup AT, Tretiakova M, Montag AG. Estrogen Receptor-Beta Expression in Extraabdominal Fibromatoses: An Analysis of 40 Cases. *Cancer* (2006) 106 (1):208–13. doi: 10.1002/cncr.21553
22. Bonvalot S, Eldweny H, Haddad V, Rimareix F, Missenard G, Oberlin O, et al. Extra-Abdominal Primary Fibromatosis: Aggressive Management Could be Avoided in a Subgroup of Patients. *Eur J Surg Oncol* (2008) 34(4):462–8. doi: 10.1016/j.ejso.2007.06.006
23. Jo JC, Hong YS, Kim KP, Lee JL, Lee J, Park YS, et al. A Prospective Multicenter Phase II Study of Sunitinib in Patients With Advanced Aggressive Fibromatosis. *Invest New Drugs* (2014) 32(2):369–76. doi: 10.1007/s10637-013-0059-0
24. Zheng C, Zhou Y, Wang Y, Luo Y, Tu C, Min L. The Activity and Safety of Anlotinib for Patients With Extremity Desmoid Fibromatosis: A Retrospective Study in a Single Institution. *Drug Des Devel Ther* (2020) 14:3941–50. doi: 10.2147/DDDT.S271008
25. Nomura M, Rainusso N, Lee YC, Dawson B, Coarfa C, Han R, et al. Tegavivint and the β-Catenin/ALDH Axis in Chemotherapy-Resistant and Metastatic Osteosarcoma. *J Natl Cancer Inst* (2019) 111(11):1216–27. doi: 10.1093/jnci/djz026
26. Shang H, Braggio D, Lee YJ, Al Sannaa GA, Creighton CJ, Bolshakov S, et al. Targeting the Notch Pathway: A Potential Therapeutic Approach for Desmoid Tumors. *Cancer* (2015) 121(22):4088–96. doi: 10.1002/cncr.29564
27. Kummar S, O'Sullivan Coyne G, Do KT, Turkbey B, Meltzer PS, Polley E, et al. Clinical Activity of the γ-Secretase Inhibitor PF-03084014 in Adults With Desmoid Tumors (Aggressive Fibromatosis). *J Clin Oncol* (2017) 35 (14):1561–9. doi: 10.1200/JCO.2016.71.1994
28. Messersmith WA, Shapiro GI, Cleary JM, Jimeno A, Dasari A, Huang B, et al. A Phase I, Dose-Finding Study in Patients With Advanced Solid Malignancies of the Oral γ-Secretase Inhibitor PF-03084014. *Clin Cancer Res* (2015) 21 (1):60–7. doi: 10.1158/1078-0432.CCR-14-0607
29. Walko CM, Aubert RE, La-Beck NM, Clore G, Herrera V, Kourlas H, et al. Pharmacoepidemiology of Clinically Relevant Hypothyroidism and Hypertension From Sunitinib and Sorafenib. *Oncologist* (2017) 22(2):208–12. doi: 10.1634/theoncologist.2016-0233
30. Kasper B, Ströbel P, Hohenberger P. Desmoid Tumors: Clinical Features and Treatment Options for Advanced Disease. *Oncologist* (2011) 16(5):682–93. doi: 10.1634/theoncologist.2010-0281
31. Signoroni S, Frattini M, Negri T, Pastore E, Tamborini E, Casieri P, et al. Cyclooxygenase-2 and Platelet-Derived Growth Factor Receptors as Potential Targets in Treating Aggressive Fibromatosis. *Clin Cancer Res an Off J Am Assoc Cancer Res* (2007) 13(17):5034–40. doi: 10.1158/1078-0432.CCR-07-0336

Conflict of Interest: The authors declare that the research was conducted in the absence of any commercial or financial relationships that could be construed as a potential conflict of interest.

Publisher's Note: All claims expressed in this article are solely those of the authors and do not necessarily represent those of their affiliated organizations, or those of the publisher, the editors and the reviewers. Any product that may be evaluated in this article, or claim that may be made by its manufacturer, is not guaranteed or endorsed by the publisher.

Copyright © 2022 Wang, Li, Wang, Li, Bai, Lv, Nie, Chen, Xu, Tu and Chen. This is an open-access article distributed under the terms of the Creative Commons Attribution License (CC BY). The use, distribution or reproduction in other forums is permitted, provided the original author(s) and the copyright owner(s) are credited and that the original publication in this journal is cited, in accordance with accepted academic practice. No use, distribution or reproduction is permitted which does not comply with these terms.

ORIGINAL RESEARCH
published: 18 January 2022
doi: 10.3389/fphar.2021.820446

A FAK Inhibitor Boosts Anti-PD1 Immunotherapy in a Hepatocellular Carcinoma Mouse Model

Yuhua Wei*[1†], *Yufeng Wang*[1†], *Nanbin Liu*[1], *Ran Qi*[1], *Yan Xu*[1], *Kun Li*[1], *Yu Feng*[2]* and *Baomin Shi*[1]

[1]Department of General Surgery, Tongji Hospital, Tongji University Medical School, Shanghai, China, [2]Shuguang Hospital, Shanghai University of Traditional Chinese Medicine, Shanghai, China

Anti-PD-1/PD-L1 immunotherapy has limited efficacy in hepatocellular carcinoma (HCC) and does not benefit all patients. A FAK inhibitor (VS-4718) has been reported to improve the microenvironment in some tumors. This study aimed to investigate the effect of the combination of the FAK inhibitor VS4718 and anti-PD1 for the treatment of HCC in a mouse model and its possible mechanism of action. The expression of FAK and infiltrated immune cells in human HCC from the data of TCGA were analyzed. A primary murine HCC model was established *via* protooncogene (c-Met/β-catenin) transfection. The pathological characteristics of tumors were examined after the mice were treated with VS4718 and/or anti-PD1 therapy. This study revealed that FAK is highly expressed in human HCC and is associated with poor prognosis of OS (overall survival) and PFS (progress free survival) in HCC patients. Immune cell infiltration ($CD8^+$ T, Tregs, M0, M2, CAFs and MDSCs) was correlated with FAK expression. In the experimental HCC model, the combination of a FAK inhibitor VS4718 and an anti-PD1 antibody had a better effect than monotherapy against HCC. VS4718 reduced the number of Tregs and macrophages but increased the number of $CD8^+$ T cells in HCC mice. Notably, FAK inhibitor promoted the expression of PD-L1 in HCC. This study suggested that combination of the FAK inhibitor VS4718 and anti-PD1 could be a potential therapy for HCC by improving the immune environment, reducing liver fibrosis and simultaneously preventing PD1 from binding to the increased PD-L1 induced by FAK inhibitor VS4718.

Keywords: hepatocellular carcinoma, FAK inhibitor (VS4718), PD1, PD-L1, combination

OPEN ACCESS

Edited by:
Dong-Hua Yang,
St. John's University, United States

Reviewed by:
Hadiar Rahman,
National Institutes of Health (NIH),
United States
Hao Zhang,
University of Pennsylvania,
United States

****Correspondence:***
Yu Feng
davisfy@126.com
Baomin Shi
tjshibaomin@tongji.edu.cn

†These authors share first authorship

Specialty section:
This article was submitted to
Pharmacology of Anti-Cancer Drugs,
a section of the journal
Frontiers in Pharmacology

Received: *23 November 2021*
Accepted: *17 December 2021*
Published: *18 January 2022*

Citation:
Wei Y, Wang Y, Liu N, Qi R, Xu Y, Li K, Feng Y and Shi B (2022) A FAK Inhibitor Boosts Anti-PD1 Immunotherapy in a Hepatocellular Carcinoma Mouse Model. Front. Pharmacol. 12:820446. doi: 10.3389/fphar.2021.820446

INTRODUCTION

Hepatocellular carcinoma (HCC) is one of the leading causes of cancer-related death (Yang et al., 2019). Due to the high rate of recurrence and metastasis of HCC and resistance to antitumor drugs, the 5-years survival rate of HCC patients is low (Greten et al., 2019; Xiang et al., 2019). Therefore, exploration of more effective treatments for HCC is an urgent need (Rimassa et al., 2019).

In recent years, attention has been given to the effectiveness of immunotherapy which targets immune checkpoints, such as anti-programmed cell death 1(PD1) targeted immunotherapy, which has resulted in encouraging effects in the treatment of some solid tumors (Motzer et al., 2020). PD1 belongs to the CD28 family and it regulates peripheral immune tolerance and autoimmunity in $CD8^+$ T cells, regulatory T cells (Tregs), and myeloid suppressor cells (MDSCs) (Yao et al., 2018; Pu et al., 2019). PD-L1 and PD-L2 are specific ligands of PD-1 and are mainly expressed in tumor cells and antigen-presenting cells. PD1 inhibits the function of effector T cells when it binds to PD-L1 or PD-L2 (Dong et al., 1999). The FDA has approved the anti-PD1 drugs nivolumab and pembrolizumab for the second-line treatment of HCC. However, not all patients are sensitive to these therapies, and the clinical efficacy of anti-PD1 is limited to a subset of patients, with a total effective rate of 20% or lower (Xu et al., 2018; Zhu et al., 2018). These results indicate that most patients are not suitable for anti-PD1 therapy. Therefore, it is of great significance to find ways to improve the sensitivity and effectiveness of anti-PD1 therapy.

Focal adhesion kinase (FAK) is encoded by the PTK2 gene. It is a nonreceptor tyrosine kinase in the integrin signal transduction cascade, which mediates the connection between cells and extracellular matrix (Evans and Müller, 2000). Highexpression of FAK is detected in a variety of human solid tumors (Song et al., 2021; Torres-Ayuso, et al., 2021). FAK can be phosphorylated and activated to target multiple downstream signaling pathways, promoting cell growth, development, invasion, and metastasis. FAK affects both cancer cells and tumor stromal cells (Shang et al., 2015; Shang et al., 2016; Lees et al., 2021). FAK can regulate the transcription of inflammatory genes and promote antitumor immune evasion (Jeong, et al., 2021). Previous studies have found that inhibition of FAK activity changed immune cell infiltration in tumor microenvironment (Jiang et al., 2016; Serrels et al., 2017; Canel et al., 2020). A FAK inhibitor VS4718, also named PND-1186, blocks FAK Tyr-397 phosphorylation and has become a potential anticancer drug (Wang et al., 2019; Dawson et al., 2021). The effect of VS4718 with PD1 blockade as a possible combination therapy has not been evaluated.

In this work, we used the c-Met/β-catenin plasmids to induce primary HCC model in C57BL/6 J mice. Using this mouse primary HCC model, we aimed to observe the efficacy of a FAK inhibitor (VS4718) in combination with an anti-PD1 antibody for the treatment of HCC and investigate the related mechanism.

MATERIALS AND METHODS

Data Source and Preprocessing

Gene expression data of LIHC projects (included 50 normal and 374 tumor tissues) with clinical information were obtained from TCGA (https://portal.gdc.cancer.gov/). Survival analyses, such as overall survival (OS), were measured from the date of study enrollment to death from any cause or last follow-up. Disease-free survival (DFS) is defined as the time between the treatment of intrahepatic lesions and the first discovery of recurrence or metastasis (Liu et al., 2018). The relationship between the expression of FAK and immune cells ($CD8^+$ T, Tregs, M0, M2, CAFs, and MDSCs) was analyzed by TIMER2.0 website (http://timer.cistrome.org/) (Li et al., 2016; Li et al., 2017; Li et al., 2020).

Plasmids

The plasmids pT3-EF1a-c-Met (Cat. #31784) and pT3-N90-β-catenin (Cat. #31785) were obtained from Addgene (United States). The plasmids pCMV/SB (Liang et al., 2018) was presented by Professor Dong (Naval Medical University, Shanghai, China). The plasmids were purified using EndoFree Maxi Plasmid Kit (Cat. #DP117) from Tiangen Biotech (China) for hydrodynamic tail vein injection.

Mice and Treatments

C57BL/6 J mice were purchased from Jiesijie (Shanghai, China). Mice were 6–8 weeks old and their body weight ranged from 18 to 22 g. The mice were placed in a micro-isolator cage in a room illuminated from 7:00 AM to 7:00 PM (12:12-HR light-dark cycle) and adequate food and water were provided. All animal experimental procedures were approved by the Institutional Animal Care and Use Committee of Tongji University.

To establish an HCC mouse model, we used the tail vein hydrodynamic high-pressure injection technique to inject 22.5 μg pT3-EF1α-c-MET; 22.5 μg pT3-EF1α-ΔN90-β-catenin; 5 μg pCMV/SB plasmid DNA dissolved in sterile saline (10% of the body weight of mice) into the mouse. After 4 weeks, the HCC mouse model was established which caused cancer only in liver (Shang et al., 2015).

The HCC mice were treated with drugs as following: 1) placebo group: A placebo is given orally (0.5% methylcellulose) or by injection (PBS) in equal doses and the same number of times. 2) anti-PD1 group: 200 μg PD1 antibody (anti-mPD1 clone RMP1-14, BioXcell, Cat. # BE0146) was injected by intraperitoneal injection, once every 3 days; 3) FAK inhibitor (VS4718) group: 50 mg/kg FAK inhibitor (VS4718) (Csnpharm, Cat. # CSN16593) dissolved in 0.5% methylcellulose (v/v, saline) was given to mice by gavage, twice a day. 4) The combination of anti-PD1 and FAK inhibitor group: 200 μg PD1 antibody was injected by intraperitoneal injection, once every 3 days and 50 mg/kg FAK inhibitor (VS4718) dissolved in 0.5% methylcellulose (v/v, saline) was given to mice by gavage, twice a day.

Protein Extraction and Western Blot

The mouse HCC tissues were added with RIPA (Thermo Scientific, 89,900) containing protease inhibitors (MCE, HY-K0010), placed on ice, and lysed for 30 min. After centrifugation at 12,000 rpm at 4°C for 10 min, the supernatant was transferred to a new EP tube. Then, the protein samples were quantified by the BCA method. The samples were placed in a metal bath and denatured at 100°C for 10 min. The protein samples were separated by electrophoresis on 10% SDS-PAGE gel and transferred to a 0.45 mm nitrocellulose membrane. Western blotting was performed with specific primary antibodies. Finally, imaging was performed using ECL (GE Health Care, United States). The detailed information about antibodies was listed in **Supplementary Table S1**.

ImmunoHistochemical Staining

The mouse HCC tissue was immobilized in 10% formalin and embedded in paraffin. Then, 5 μm thick slices were dewaxed in xylene and rehydrated in descending graded ethanol. A specific antigenic repair solution was used for antigenic repair. The slices were sealed in 10% BSA solution at room temperature for 1 h. The slides were then incubated overnight with specific antibodies at 4°C.The corresponding positive expression was detected by 3,3′ -diaminobenzidine (DAB) or indirect immunofluorescence. Positive staining was scored in at least three fields. At least three mice were included in each group.

RNA Extraction, cDNA Synthesis, and qPCR

The total RNAs were extracted from cells and tissues by the total RNA rapid extraction kit(Bioteke Corporation, RP4002). The cDNA was reverse-transcribed from 500 ng of total RNA using HiScript II Q RT SuperMix for qPCR kit (Vazyme, R222-01). The cDNA was diluted (1:20) for qPCR by ChamQ SYBR qPCR Master Mix (Vazyme, Q311-02) with gene-specific primers. β-actin was used as an endogenous control for normalization. The detailed information about the primer sequences was listed in **Supplementary Table S2**.

Statistical Analysis

GraphPad Prism 8.0.2 software was used for statistical analysis. Data were expressed as mean ± standard deviation (SD). Student’s *t*-test was used to compare two groups. Multiple groups were compared using one-way ANOVA. $p < 0.05$ was considered to be statistically significant. A Fishers’ exact test was used to analyze significance. The means ± SD are shown in the figures where applicable.

RESULTS

High Expression of FAK in Human HCC was Associated With Poor Prognosis and an Immunosuppressive TME

We analyzed the expression of FAK in human HCC and the correlation of FAK with patient outcome. It was found that FAK was highly expressed in HCC tissues ($p < 0.001$) (**Figure 1A**). In addition, we investigated FAK expression in the paired sample, and the expression of FAK was also higher in HCC tissues ($p < 0.001$) (**Figure 1B**). Cox regression analysis showed that high expression of FAK was associated with poor OS ($p = 0.049$) and PFS ($p = 0.027$), indicating that HCC patients with high FAK expression had a worse prognosis than those with low FAK expression (**Figures 1C,D**).

To evaluate whether FAK might impact the tumor microenvironment (TME), we analyzed the relationship between the expression of FAK and immune cells in HCC tumor tissues by TIMER2.0. The results showed that the expression of FAK was correlated with the number of CD8$^+$ T, Tregs, macrophages (M0, M2), CAFs and MDSCs (**Figure 1E**).

Combination of FAK Inhibition and Anti-PD1 Therapy Effectively Inhibited the Growth of HCC in Mice

To observe the efficacy of VS4718, anti-PD1 monotherapy or the combination of VS4718 and anti-PD1 in the treatment of HCC, we established a C57BL/6 J primary HCC model with complete immune function and then randomly grouped them for drug administration (**Figure 2A**). Compared with placebo, VS4718 or anti-PD1 monotherapy, the combination of VS4718 and anti-PD1 significantly inhibited HCC development in mice (**Figure 2B**). Compared with placebo and monotherapy, both liver weight and liver weight/mouse body weight were significantly lower in the combination treatment group (**Figures 2C,D**). It was found that the tumors were smaller and the liver tissue structure was relatively normal on H and E staining in the combination treatment group compared to the placebo and monotherapy groups (**Figure 2E**). These results suggest that a FAK inhibitor (VS4718) can promote the anti-PD1 immunotherapeutic efficacy in HCC in mice.

Combination of FAK Inhibition and Anti-PD1 Therapy Inhibited Proliferation and Promoted Apoptosis of HCC in Mice

To observe the effect of treatment on tumor status, including proliferation and apoptosis, PCNA immunohistochemical staining (**Figure 3A**) and TUNEL staining (**Figure 3B**) were performed. We analyzed the positive staining area in each group. We found that the combination treatment significantly inhibited tumor proliferation (**Figure 3C**) and promoted liver tumor cell apoptosis in mice compared with placebo and monotherapy (**Figure 3D**).

FAK Inhibition Reduced the Fibrosis of HCC in Mice

To determine the effect of drug treatments on fibrosis of HCC in mice, Sirius red staining (**Figure 4A**) and a-SMA immunohistochemical staining (**Figure 4B**) were performed. The anti-PD1 group showed a similar level of fibrosis compared with the placebo group. The FAK inhibitor group and combination group showed a significantly lower level of fibrosis (**Figures 4C,D**), implying that inhibition of FAK could reduce fibrosis in HCC mice.

FAK Inhibition Improved the Immune Microenvironment of HCC in Mice

To detect immune cell infiltration in HCC tissues of mice, CD8a, Foxp3, and F4/80 + immunohistochemical staining were used (**Figures 5A–C**). We found that the level of CD8a infiltration in HCC was higher in the FAK inhibitor monotherapy and combination groups than in the placebo or anti-PD1 groups (**Figure 5D**). Foxp3, a surface marker of Tregs, was significantly decreased (**Figure 5E**). F4/80 + expression decreased significantly (**Figure 5F**). These results suggest that a FAK inhibitor alone or in combination with an anti-PD1 antibody increases the number of CD8a T cells and decreases the number of Tregs and macrophages. We also detected the mRNA expression of some macrophage recruitment molecules (Ccl2, Flt3lg, Csf1, Csf2) and Tregs recruitment molecules (Ccl20, Cxcl13) in HCC tissues. The results showed that, compared with placebo and anti-PD1 monotherapy, a significantly lower expression of macrophage

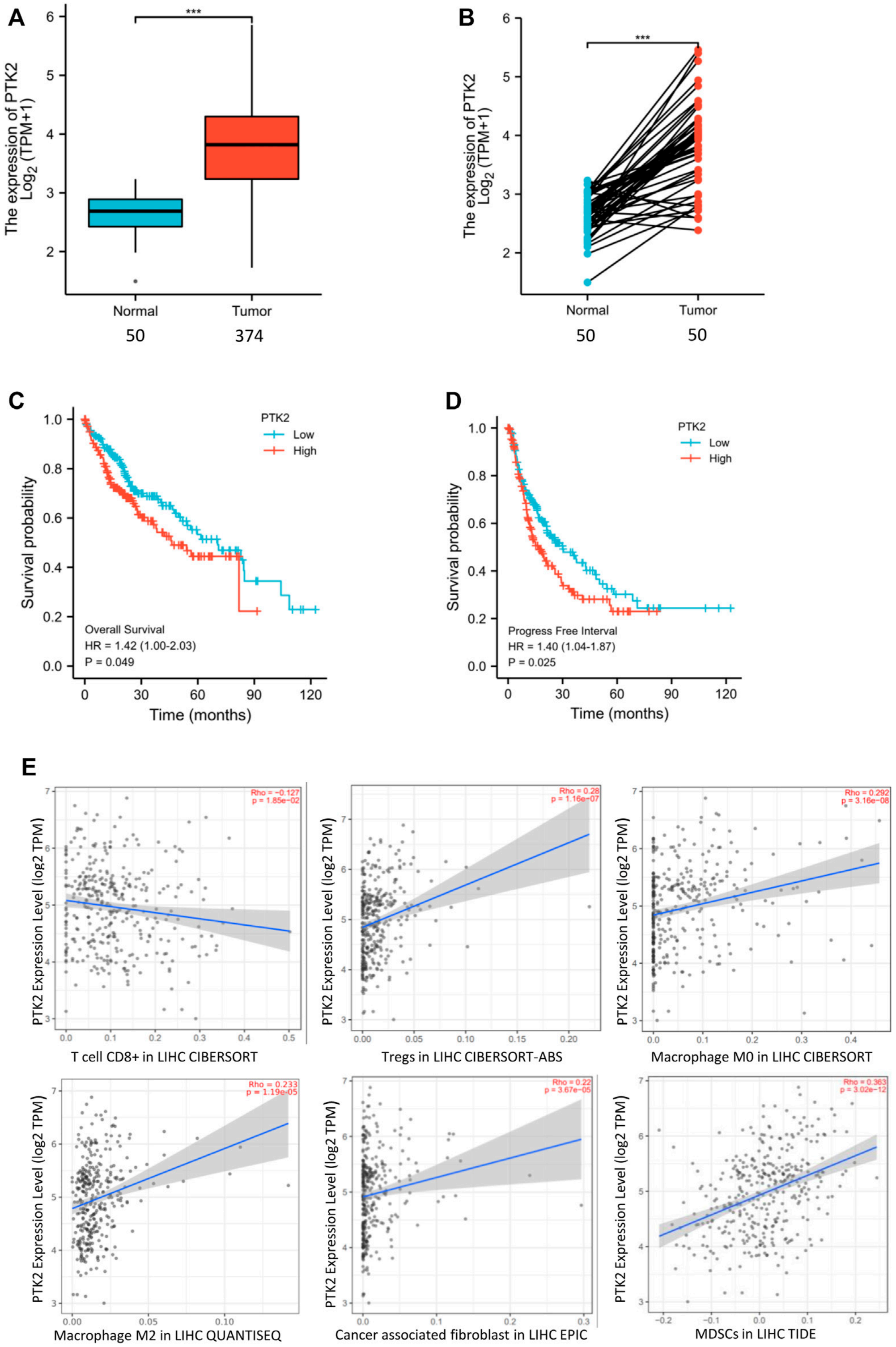

FIGURE 1 | High expression of FAK in human HCC is associated with poor prognosis and an immunosuppressive TME **(A)** FAK expression is higher in human HCC tissues than in paired normal tissues by Wilcoxon rank sum test ($p < 0.001$). **(B)** The expression of FAK significantly increased in HCC tissues compared with adjacent tissues in the paired samples with Wilcoxon signed-rank test. **(C–D)** Kaplan-Meier survival analysis showed that increased expression of FAK was significantly associated with poor Overall Survival ($p = 0.049$) and Progression-free survival ($p = 0.027$). **(E)** The relationship between FAK expression and CD8$^+$ T cells(Rho = -0.17 p = 1.85e-2), Tregs(Rho = 0.28 p = 1.16e-7),M0(Rho = 0.292; p = 3.16e-8),M2(Rho = 0.233; p = 1.19e-5),CAFs(Rho = 0.22; p = 3.67e-5) and MDSCs(Rho = 0.363; p = 3.02e-12).Significance identification: ns, $p \geq 0.05$; *, $p < 0.05$; **, $p < 0.01$; ***, $p < 0.001$.

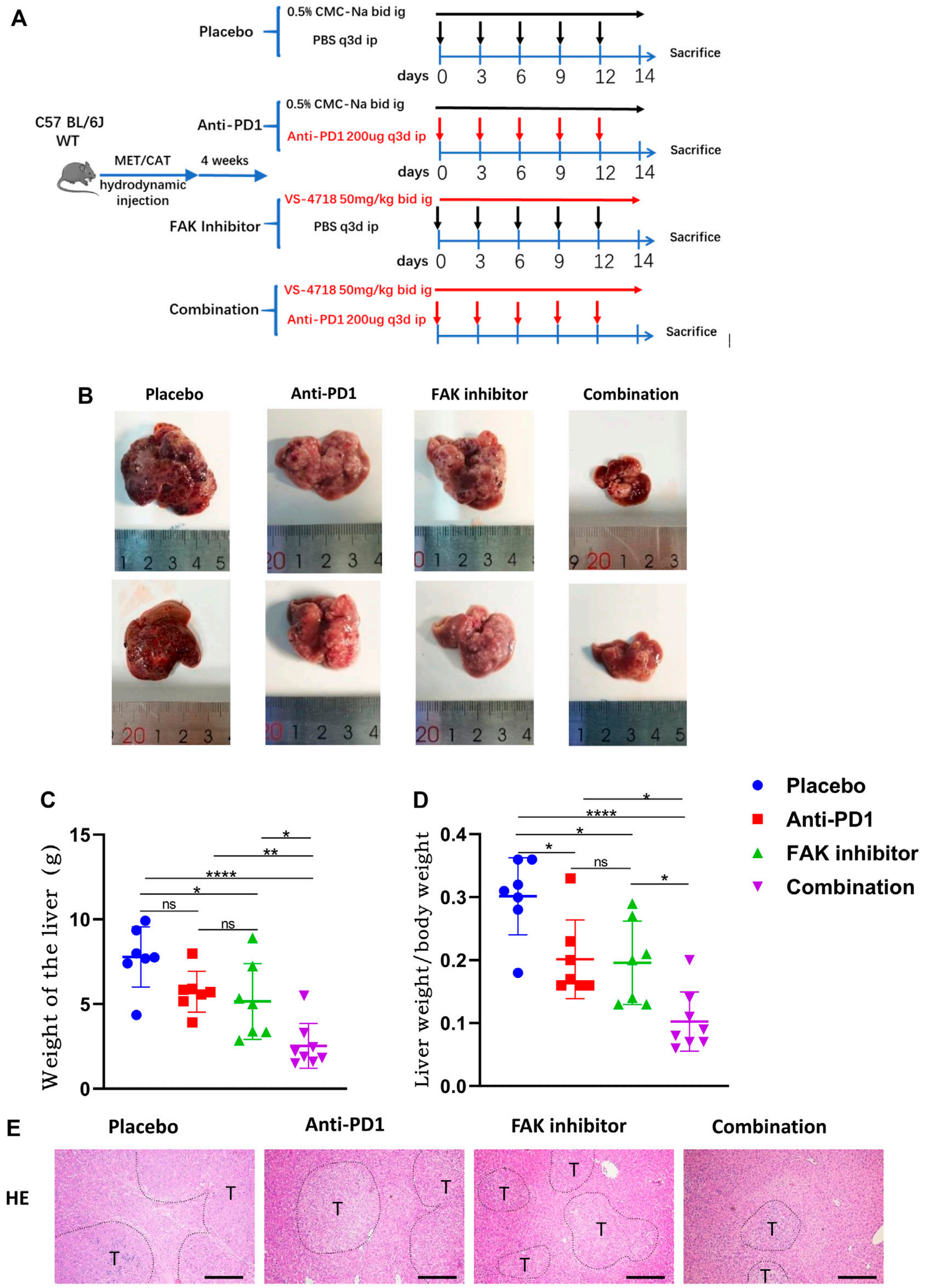

FIGURE 2 | Combination of FAK inhibition and anti-PD1 therapy effectively inhibited the growth of HCC in mice **(A)** After 4 weeks of plasmid injection in C57BL/6 J mice, a primary hepatocellular carcinoma model was established and the mice were randomly divided into four groups (Placebo group, *n* = 7; Anti-PD1 group, *n* = 7; FAK inhibitor group, *n* = 7; Combination group, *n* = 8), and specific information about the administration (time, dosage, and method). **(B)** The mouse liver after 2 weeks of medication. **(C–D)** The liver weight of mice and the liver weight/body weight of mice were compared in each group (Placebo group, *n* = 7; Anti-PD1 group, *n* = 7; FAK inhibitor group, *n* = 7; Combination group, *n* = 8). Significance identification: ns, $p \geq 0.05$; *, $p < 0.05$; **, $p < 0.01$; ***, $p < 0.001$. **(E)** HCC tissues of mice were histologically analyzed by H and E staining (scale bars, 400 μm).

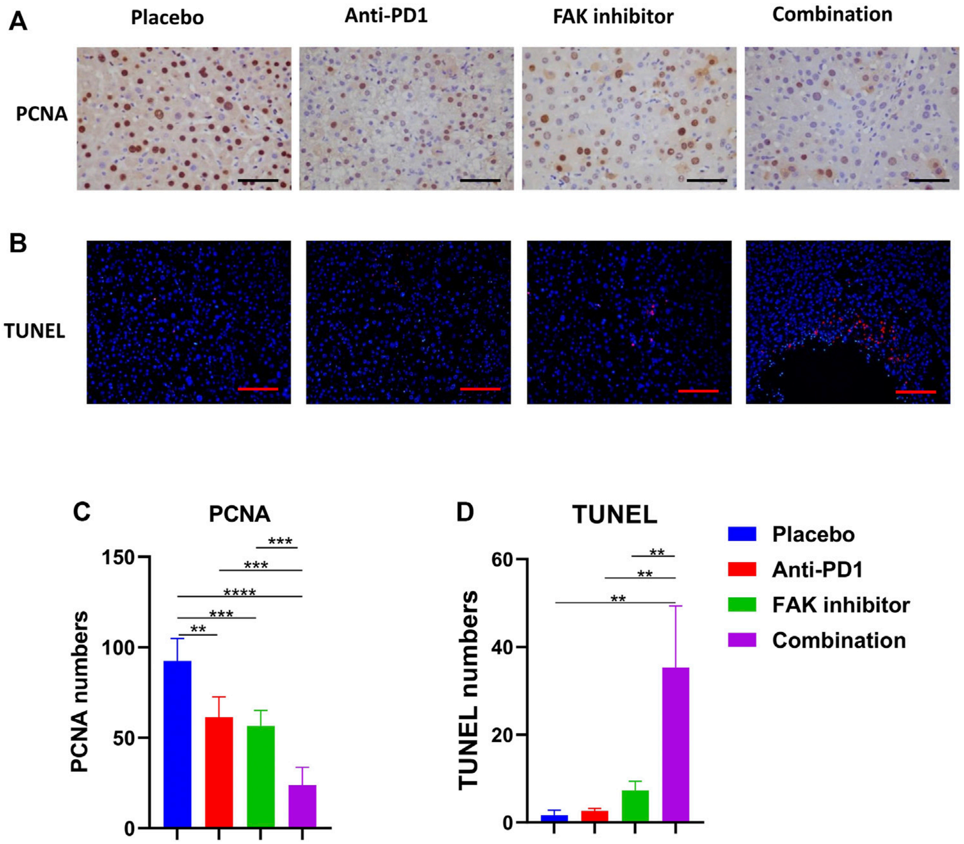

FIGURE 3 | Combination of FAK inhibition and anti-PD1 therapy inhibited proliferation and promoted apoptosis of HCC in mice **(A)** PCNA immunohistochemistry on HCC tissues of mice (scale bars, 100 μm). **(B)** HCC tissues of mice in each group were stained with TUNEL-staining (scale bars, 200 μm). **(C)** Quantification of PCNA staining ($n = 5$ mice/group). **(D)** Quantification of TUNEL staining ($n = 3$ mice/group). Significance identification: ns, $p \geq 0.05$; *, $p < 0.05$; **, $p < 0.01$; ***, $p < 0.001$.

recruitment molecules and Tregs recruitment molecules was observed in the FAK inhibitor monotherapy and combination groups (**Figure 5G**).

FAK Inhibition Increased the Expression of PD-L1 in HCC

To study whether the FAK inhibitor can affect PD-L1 expression in HCC in mice, we used qPCR to detect the mRNA expression of PD-L1. The results showed that the mRNA expression of PD-L1 in the FAK inhibitor monotherapy group and the combination group was higher than that in the placebo and anti-PD1 monotherapy groups (**Figure 6A**). Then, we extracted proteins from HCC in mice to perform Western blotting. We found that compared with the placebo group and anti-PD1 monotherapy group, *p*-FAK protein expression was decreased, but PD-L1 protein expression was significantly increased in the FAK inhibitor monotherapy group and the combination group (**Figure 6B**). To verify the expression of *p*-FAK and PD-L1, immunofluorescence staining was performed on the HCC tissues of mice. We also found that *p*-FAK expression was decreased in both the FAK inhibitor monotherapy group and the combination group, but PD-L1 protein expression was significantly increased (**Figure 6C**).

DISCUSSION

In this study, we observed the effect of a FAK inhibitor (VS4718) in combination with an anti-PD1 antibody for the treatment of HCC in a mouse model. The results suggested that VS4718 significantly enhanced the sensitivity of HCC to anti-PD1 and improved therapeutic effect in mice.

FAK, which is overexpressed and highly phosphorylated in a variety of cancer cells, can activate multiple signaling pathways (Zhang et al., 2020). FAK not only affects cancer cells but also the TME which is associated with tumor growth and apoptosis (Anderson et al., 2017; Hamidi and Ivaska, 2018). The high expression of FAK is related to inhibitory immune cell infiltration in some tumors (Li et al., 2016; Li et al., 2017; Li et al., 2020). At present, many small molecule FAK inhibitors have been evaluated or are undergoing clinical trials, and results show that FAK inhibitors have anticancer efficacy and tolerability (Brown et al., 2018; de Jonge et al., 2019; Mohanty et al., 2020). Previous research showed that FAK knockdown or pharmacological inhibition of FAK activity promoted apoptosis and induced tumor regression (Haun et al., 2018; Cooper and Giancotti, 2019). We found that FAK was highly expressed in human HCC tissues and associated with poor

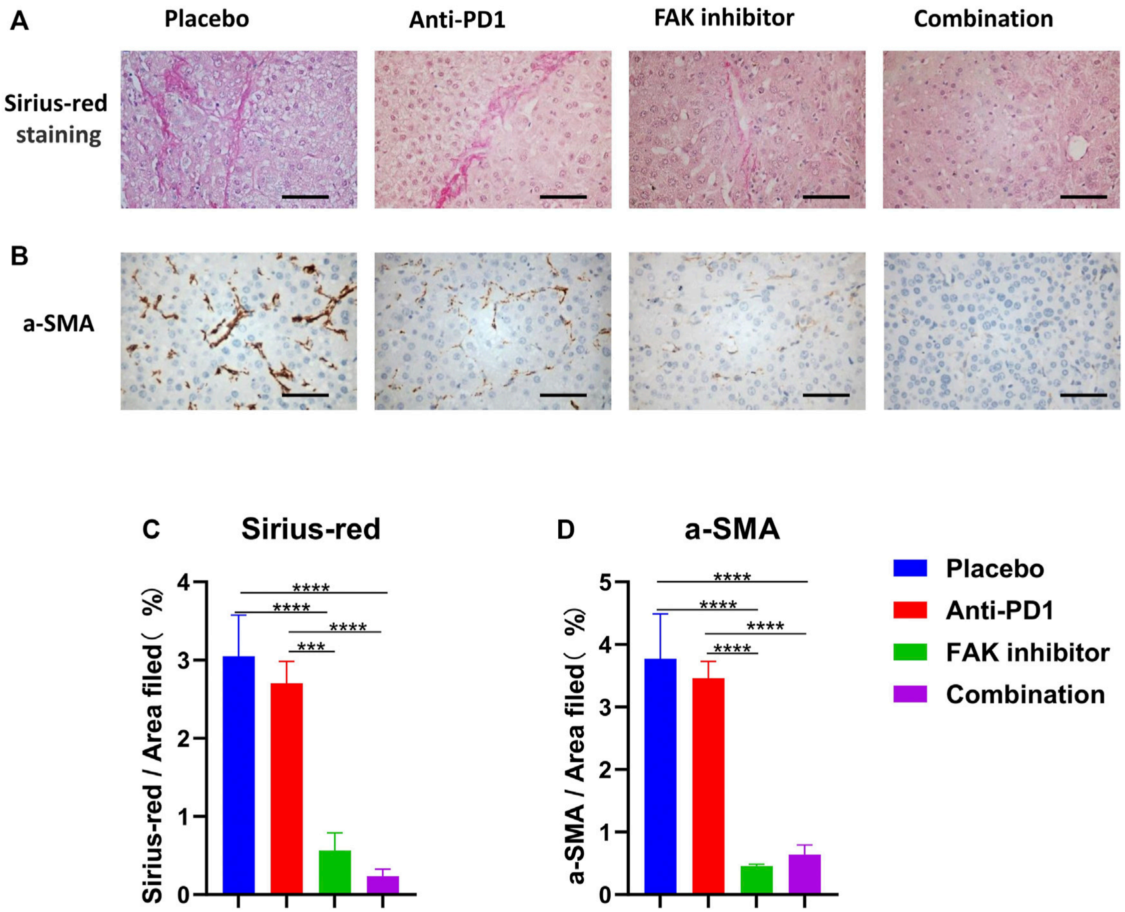

FIGURE 4 | FAK inhibition reduced the fibrosis of HCC in mice **(A)** Sirius-red staining was performed on HCC tissues of mice in each group (scale bars, 100 μm). **(B)** a-SMA immunohistochemistry was performed on HCC tissues of mice in each group (scale bars, 100 μm). **(C)** Quantification of Sirius-red staining (*n* = 3 mice/group). **(D)** Quantification of a-SMA staining (*n* = 3 mice/group). Significance identification: ns, $p \geq 0.05$; *, $p < 0.05$; **, $p < 0.01$; ***, $p < 0.001$.

prognosis of patients, which was consistent with the results of a clinical study (Fujii et al., 2004). Our experiment in mice showed that inhibition of the activity of FAK not only inhibited the growth of HCC but also reduced liver fibrosis and improved the immune microenvironment of HCC in mice.

Clinical trials showed that only 14.3% (22/154) of HCC patients responded to anti-PD1 therapy. (http://www.opdivohcp.com/advanced-hcc/efficacy/clinical-trial). Another challenge is that patients who respond initially may develop drug resistance later, leading to disease recurrence (Schoenfeld and Hellmann 2020). Therefore, some drugs combined with anti-PD1 are being explored to improve the sensitivity of HCC to treatment (Cheng et al., 2020). The immunosuppressive TME has been considered to be the reason for the failure of immunotherapy in HCC (Sangro et al., 2021). Extensive myeloid cell infiltration, such as macrophages and Tregs, may lead to dysfunction of infiltrating T cells (Mitchem et al., 2013), and cause tumor immunosuppression (Jiang, et al., 2016). These factors might contribute to the low sensitivity of tumors to anti-PD1 treatment. Similarly, in our experiments, anti-PD1 exhibited a weaker therapeutic effect on murine HCC, which is characterized by a higher degree of fibrosis and more immunosuppressive cell (macrophage and Treg) infiltration in the HCC tissues of mice. Some reports suggested that FAK inhibitors could act as immune modulators to improve the immune microenvironment of tumors (Jiang et al., 2016; Anderson et al., 2017; Osipov et al., 2019). Therefore, we evaluated the effect of FAK inhibitors on the liver tumor TME. A FAK inhibitor (VS4718) in combination with anti-PD1 therapy effectively inhibited the infiltration of macrophages and Tregs but increased $CD8^+$ T cell infiltration in tumors compared to anti-PD1 monotherapy. Mechanistically, the effect of the FAK inhibitor on HCC immune infiltration may be due to a decrease in some macrophage recruitment molecules (Ccl2, Flt3lg, Csf1, Csf2) (Soncin et al., 2018; Sterner et al., 2019) and Treg cell recruitment molecules (Ccl20, Cxcl13) (Chen et al., 2017; Ji et al., 2020) in HCC.

Another reason for the inhibitory TME could be the highly fibrotic stroma of tumor tissue (Robinson et al., 2016). A high density of stroma forms a barrier that makes it difficult for drugs to reach the tumor interior (Provenzano et al., 2012). Previous reports showed that inhibition of FAK reduced tumor fibrosis, thereby reducing the tumor barrier and improving the TME (Jiang et al.,

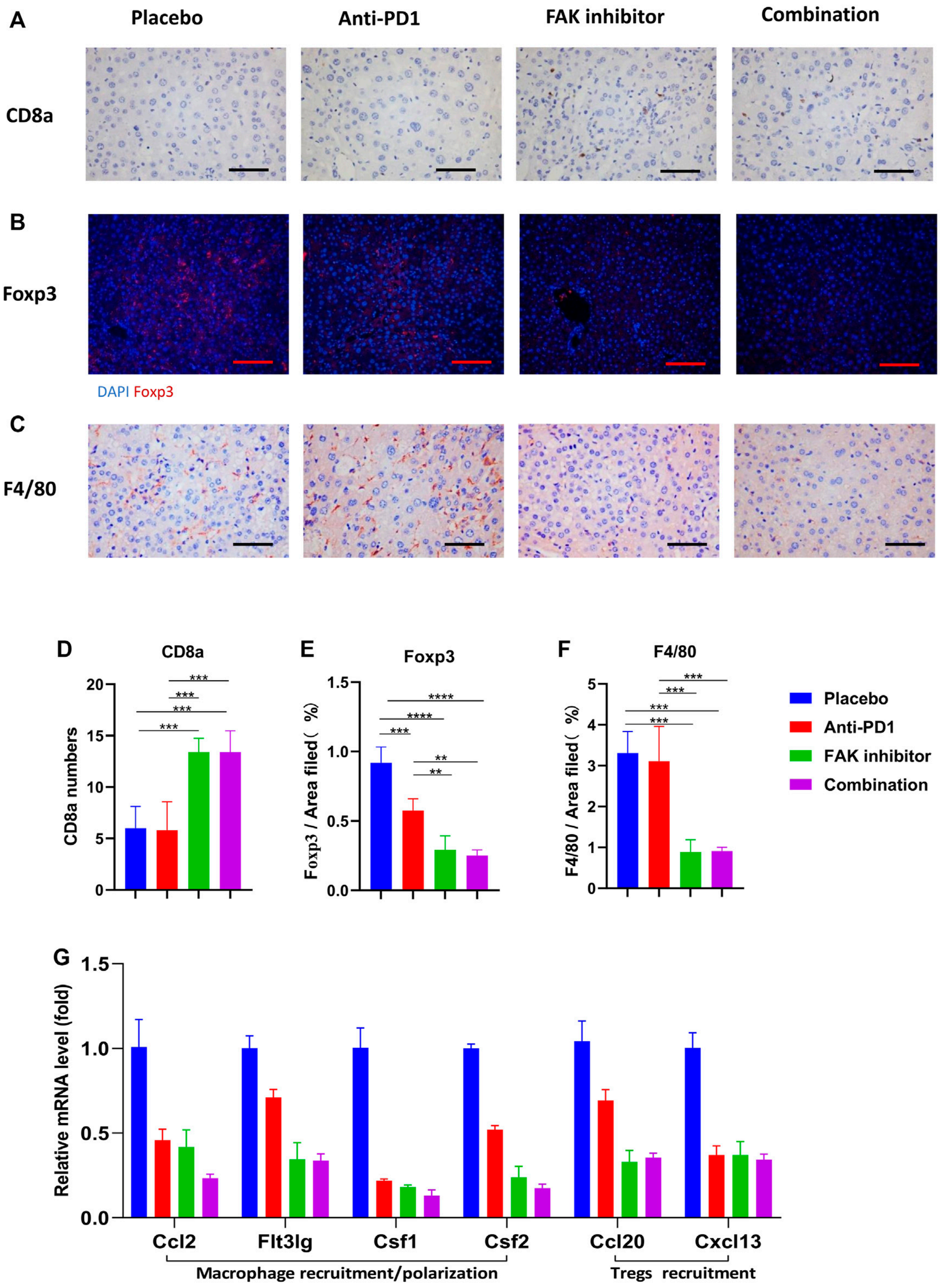

FIGURE 5 | FAK inhibition improved the immune microenvironment of HCC in mice **(A)** CD8a immunohistochemistry on HCC tissues of mice in each group (scale bars, 100 μm). **(B)** Foxp3 immunofluorescence on HCC tissues of mice in each group (scale bars, 200 μm). **(C)** F4/80 immunohistochemistry on HCC tissues of mice in each group (scale bars, 100 μm). **(D)** The number of CD8a positive cells in on HCC of mice (*n* = 5 mice/group). **(E)** Quantitative analysis of Foxp3 positive area per field by ImageJ (*n* = 4 mice/group). **(F)** Quantitative analysis of F4/80 positive area per field by ImageJ (*n* = 4 mice/group). Significance identification: ns, $p \geq 0.05$; *, $p < 0.05$; **, $p < 0.01$; ***, $p < 0.001$. **(G)** The mRNA expressions of macrophage recruitment/polarization factors (Ccl2, Flt3lg, Csf1, Csf2) and Tregs recruitment factors (Ccl20, Cxcl13) in HCC tissues of mice detected by q-PCR (*n* = 3 mice/group).

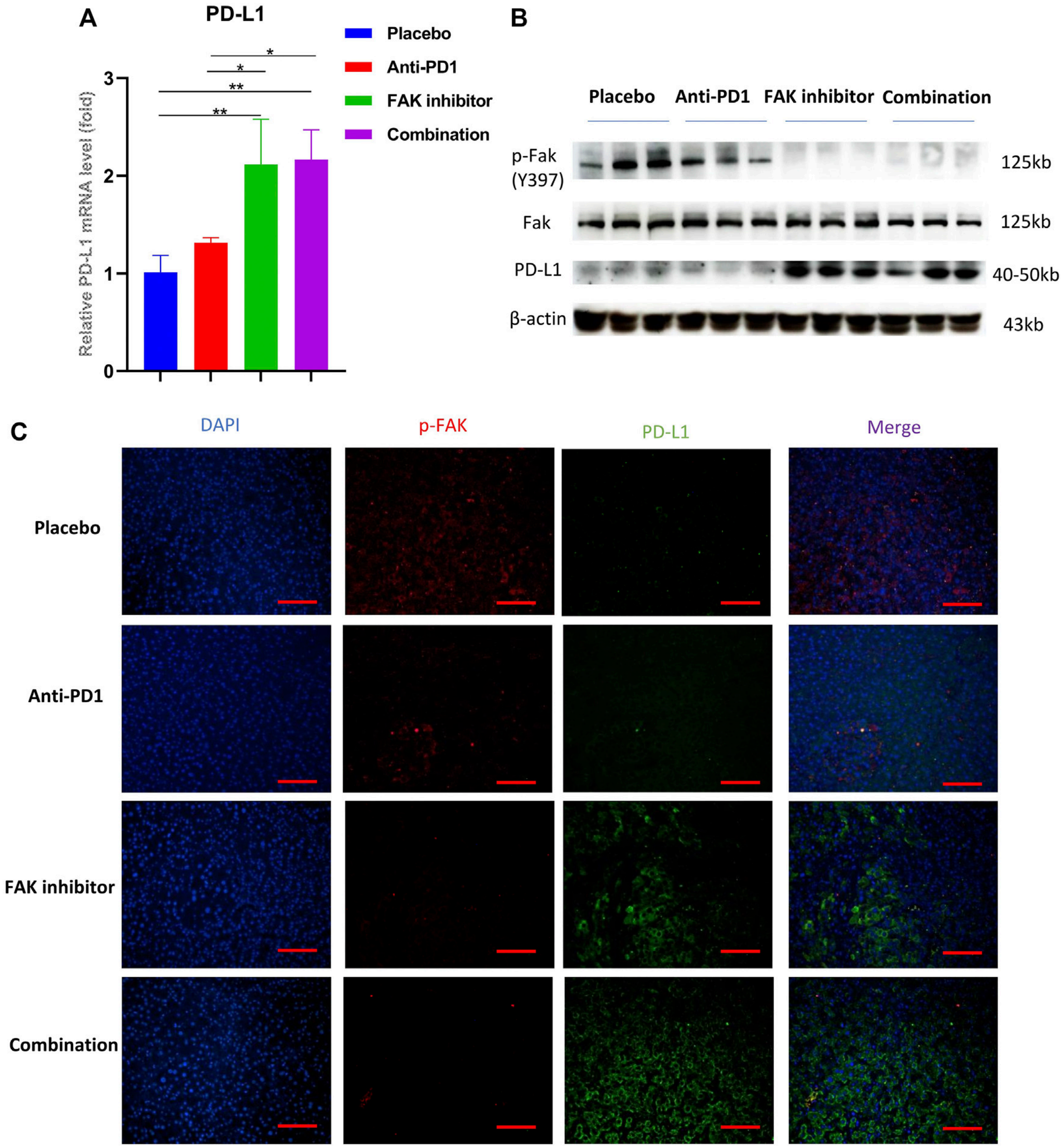

FIGURE 6 | FAK inhibition increased the expression of PD-L1 in HCC **(A)** The mRNA expressions of PD-L1 in HCC in mice detected by q-PCR ($n = 3$ mice/group). Significance identification: ns, $p \geq 0.05$; *, $p < 0.05$; **, $p < 0.01$; ***, $p < 0.001$. **(B)** The expression levels of *p*-Fak (Y397), Fak and PD-L1 in HCC in mice detected by Western Blotting ($n = 3$ mice/group). **(C)** Immunofluorescence staining of *p*-FAK and PD-L1 in HCC in mice (scale bar, 200 μm).

2016; Miller and Weissleder, 2017). Our results showed that a FAK inhibitor (VS4718) affects tumor fibrosis. We suggest that the antifibrotic effect of VS4718 plays a supporting role in the treatment of HCC. This effect might involve the inhibition of FAK on TGF-β/SMAD signaling pathway (Jiang et al., 2020).

Unexpectedly, we observed that treatment with VS4718 resulted in overexpression of PD-L1 in HCC. This finding differs from that of a previous study which showed that FAK inhibition induced the downregulation of PD-L1 in triple-negative breast cancer (Pan et al., 2019). High expression of PD-L1 may lead to the suppression of immune function (Topalian et al., 2016; Li et al., 2019). However, clinical studies have shown that patients with increased $CD8^+$ T cell infiltration and high PD-L1 positivity in HCC are more sensitive to anti-PD1 therapy and have a significantly improved disease control rate, which is significantly associated with prolonged PFS and OS (Aguiar et al., 2018; Han et al., 2019; Morita et al., 2021). The combination of VS4718 and an anti-PD1 antibody can not only increase the infiltration of $CD8^+$ T cells and reduce the infiltration of immunosuppressive Tregs and macrophages but also block the binding of PD1 on the surface of T cells to PD-L1 on the surface of tumor cells. This might be the main reason why the combination of a FAK inhibitor (VS4718) and an anti-PD1 antibody can better inhibit HCC in mice than FAK inhibitor (VS4718) monotherapy.

However, our murine model did not represent the heterogeneity of all HCC cases (Craig et al., 2020). The effect of a FAK inhibitor (VS4718) combined with an anti-PD1 antibody needs to be evaluated in different HCC models. The actual clinical therapeutic effect of FAK inhibitors combined with anti-PD1 antibodies on HCC patient needs further clinical research. In addition, the detailed mechanism of the combination of FAK inhibitor and anti-PD1 warrants further study.

In conclusion, our findings revealed that the combination of the FAK inhibitor VS4718 and an anti-PD1 antibody could suppress tumor progression in HCC mice and was better than monotherapy. The combined therapy improved the tumor immune microenvironment and reduced liver fibrosis. In addition, the combination therapy blocked the potential side effects of FAK inhibition-induced PD-L1 upregulation. Taken together, we demonstrate that the FAK inhibitor VS4718 enhances the efficacy of anti-PD1 immunotherapy in HCC. The combination of a FAK inhibitor and PD1 inhibitor could be a potential therapeutic strategy for the treatment of HCC.

DATA AVAILABILITY STATEMENT

The original contributions presented in the study are included in the article/**Supplementary Materials**, further inquiries can be directed to the corresponding author.

ETHICS STATEMENT

The animal study was reviewed and approved by the Animal Experiment Committee of Tongji Hospital, Tongji University Medical School.

AUTHOR CONTRIBUTIONS

BS conceived the research. BS and YF designed the methodology. YHW (1st author), YFW (2nd author), NL, RQ, YX, and KL performed the experiments. YHW wrote the original draft of the manuscript. BS and YF reviewed and edited the manuscript. YF supervised the study. All authors read and approved the final manuscript.

FUNDING

This work was supported by the National Natural Science Foundation of China (81874162).

ACKNOWLEDGMENTS

We would like to thank Xiaoni Kong, Hailong Wu, Fang Wang, Chang Yu, Jiacheng Lin, Liping You, Haochen Jiang, Junzhe Jiao, Lijie Ma, Xiaoqing Zhang, Miao Huang, Dongming Hua and others for their help. We also give our thanks to Dong for providing pCMV/SB plasmid and Professor Wei Qiu of Loyola University for his technical guidance. In addition, the results in part shown here are based on data generated by the TCGA network. We would like to thank the Cancer Genome Atlas Project, all tissue donors, and the researchers who contributed to obtaining and analyzing the samples used in this study.

SUPPLEMENTARY MATERIAL

The Supplementary Material for this article can be found online at: https://www.frontiersin.org/articles/10.3389/fphar.2021.820446/full#supplementary-material

REFERENCES

Aguiar, P. N., Perry, L. A., Penny-Dimri, J., Babiker, H., Tadokoro, H., de Mello, R. A., et al. (2018). The Effect of PD-L1 Testing on the Cost-Effectiveness and Economic Impact of Immune Checkpoint Inhibitors for the Second-Line Treatment of NSCLC. *Ann. Oncol.* 29 (4), 1078. doi:10.1093/annonc/mdx478

Anderson, K. G., Stromnes, I. M., and Greenberg, P. D. (2017). Obstacles Posed by the Tumor Microenvironment to T Cell Activity: A Case for Synergistic Therapies. *Cancer Cell* 31 (3), 311–325. doi:10.1016/j.ccell.2017.02.008

Brown, N. F., Williams, M., Arkenau, H. T., Fleming, R. A., Tolson, J., Yan, L., et al. (2018). A Study of the Focal Adhesion Kinase Inhibitor GSK2256098 in Patients with Recurrent Glioblastoma with Evaluation of Tumor Penetration of [11C] GSK2256098. *Neuro Oncol.* 20 (12), 1634–1642. doi:10.1093/neuonc/noy078

Canel, M., Taggart, D., Sims, A. H., Lonergan, D. W., Waizenegger, I. C., and Serrels, A. (2020). T-cell Co-stimulation in Combination with Targeting FAK Drives Enhanced Anti-tumor Immunity. *Elife* 9, e48092. doi:10.7554/eLife.48092

Chen, X., Takemoto, Y., Deng, H., Middelhoff, M., Friedman, R. A., Chu, T. H., et al. (2017). Histidine Decarboxylase (HDC)-expressing Granulocytic Myeloid Cells Induce and Recruit Foxp3+ Regulatory T Cells in Murine colon Cancer. *Oncoimmunology* 6 (3), e1290034. doi:10.1080/2162402X.2017.1290034

Cheng, A. L., Hsu, C., Chan, S. L., Choo, S. P., and Kudo, M. (2020). Challenges of Combination Therapy with Immune Checkpoint Inhibitors for Hepatocellular Carcinoma. *J. Hepatol.* 72 (2), 307–319. doi:10.1016/j.jhep.2019.09.025

Cooper, J., and Giancotti, F. G. (2019). Integrin Signaling in Cancer: Mechanotransduction, Stemness, Epithelial Plasticity, and Therapeutic Resistance. *Cancer Cell* 35 (3), 347–367. doi:10.1016/j.ccell.2019.01.007

Craig, A. J., von Felden, J., Garcia-Lezana, T., Sarcognato, S., and Villanueva, A. (2020). Tumour Evolution in Hepatocellular Carcinoma. *Gastroenterol. Hepatol.* 17 (3), 139–152. doi:10.1038/s41575-019-0229-4

Dawson, J. C., Serrels, A., Stupack, D. G., Schlaepfer, D. D., and Frame, M. C. (2021). Targeting FAK in Anticancer Combination Therapies. *Nat. Rev. Cancer* 21 (5), 313–324. doi:10.1038/s41568-021-00340-6

de Jonge, M. J. A., Steeghs, N., Lolkema, M. P., Hotte, S. J., Hirte, H. W., van der Biessen, D. A. J., et al. (2019). Phase I Study of BI 853520, an Inhibitor of Focal Adhesion Kinase, in Patients with Advanced or Metastatic Nonhematologic Malignancies. *Target. Oncol.* 14 (1), 43–55. doi:10.1007/s11523-018-00617-1

Dong, H., Zhu, G., Tamada, K., and Chen, L. (1999). B7-H1, a Third Member of the B7 Family, Co-stimulates T-Cell Proliferation and Interleukin-10 Secretion. *Nat. Med.* 5 (12), 1365–1369. doi:10.1038/70932

Evans, A. L., and Müller, U. (2000). Stereocilia Defects in the Sensory Hair Cells of the Inner Ear in Mice Deficient in Integrin Alpha8beta1. *Nat. Genet.* 24 (4), 424–428. doi:10.1038/74286

Fujii, T., Koshikawa, K., Nomoto, S., Okochi, O., Kaneko, T., Inoue, S., et al. (2004). Focal Adhesion Kinase Is Overexpressed in Hepatocellular Carcinoma and Can Be Served as an Independent Prognostic Factor. *J. Hepatol.* 41 (1), 104–111. doi:10.1016/j.jhep.2004.03.029

Greten, T. F., Lai, C. W., Li, G., and Staveley-O'Carroll, K. F. (2019). Targeted and Immune-Based Therapies for Hepatocellular Carcinoma. *Gastroenterology* 156 (2), 510–524. doi:10.1053/j.gastro.2018.09.051

Hamidi, H., and Ivaska, J. (2018). Every Step of the Way: Integrins in Cancer Progression and Metastasis. *Nat. Rev. Cancer* 18 (9), 533–548. doi:10.1038/s41568-018-0038-z

Han, H., Jain, A. D., Truica, M. I., Izquierdo-Ferrer, J., Anker, J. F., Lysy, B., et al. (2019). Small-Molecule MYC Inhibitors Suppress Tumor Growth and Enhance Immunotherapy. *Cancer cell* 36 (5), 483–497. doi:10.1016/j.ccell.2019.10.001

Haun, F. S., Neumann, L., Peintner, K., Wieland, J., Habicht, C., Schwan, K., et al. (2018). Identification of a Novel Anoikis Signalling Pathway Using the Fungal Virulence Factor Gliotoxin. *Nat. Commun.* 9 (1), 3524. doi:10.1038/s41467-018-05850-w

Jeong, K., Murphy, J. M., Erin Ahn, E. Y., and Steve Lim, S. T. (2021). FAK in the Nucleus Prevents VSMC Proliferation by Promoting P27 and P21 Expression *via* Skp2 Degradation. *Cardiovasc. Res.*, cvab132. doi:10.1093/cvr/cvab132

Ji, A. L., Rubin, A. J., Thrane, K., Jiang, S., Reynolds, D. L., Meyers, R. M., et al. (2020). Multimodal Analysis of Composition and Spatial Architecture in Human Squamous Cell Carcinoma. *Cell* 182 (2), 1661–1662. doi:10.1016/j.cell.2020.08.043

Jiang, H., Hegde, S., Knolhoff, B. L., Zhu, Y., Herndon, J. M., Meyer, M. A., et al. (2016). Targeting Focal Adhesion Kinase Renders Pancreatic Cancers Responsive to Checkpoint Immunotherapy. *Nat. Med.* 22 (8), 851–860. doi:10.1038/nm.4123

Jiang, H., Liu, X., Knolhoff, B. L., Hegde, S., Lee, K. B., Jiang, H., et al. (2020). Development of Resistance to FAK Inhibition in Pancreatic Cancer Is Linked to Stromal Depletion. *Gut* 69 (1), 122–132. doi:10.1136/gutjnl-2018-317424

Lees, D. M., Reynolds, L. E., Pedrosa, A. R., Roy-Luzarraga, M., and Hodivala-Dilke, K. M. (2021). Phosphorylation of Pericyte FAK-Y861 Affects Tumour Cell Apoptosis and Tumour Blood Vessel Regression. *Angiogenesis* 24 (3), 471–482. doi:10.1007/s10456-021-09776-8

Li, B., Severson, E., Pignon, J. C., Zhao, H., Li, T., Novak, J., et al. (2016). Comprehensive Analyses of Tumor Immunity: Implications for Cancer Immunotherapy. *Genome Biol.* 17 (1), 174. doi:10.1186/s13059-016-1028-7

Li, H., Li, C. W., Li, X., Ding, Q., Guo, L., Liu, S., et al. (2019). MET Inhibitors Promote Liver Tumor Evasion of the Immune Response by Stabilizing PDL1. *Gastroenterology* 156 (6), 1849–1861. doi:10.1053/j.gastro.2019.01.252

Li, T., Fan, J., Wang, B., Traugh, N., Chen, Q., Liu, J. S., et al. (2017). TIMER: A Web Server for Comprehensive Analysis of Tumor-Infiltrating Immune Cells. *Cancer Res.* 77 (21), e108–e110. doi:10.1158/0008-5472.CAN-17-0307

Li, T., Fu, J., Zeng, Z., Cohen, D., Li, J., Chen, Q., et al. (2020). TIMER2.0 for Analysis of Tumor-Infiltrating Immune Cells. *Nucleic Acids Res.* 48 (W1), W509–w514. doi:10.1093/nar/gkaa407

Liang, Y., Feng, Y., Zong, M., Wei, X. F., Lee, J., Feng, Y., et al. (2018). β-Catenin Deficiency in Hepatocytes Aggravates Hepatocarcinogenesis Driven by Oncogenic β-catenin and MET. *Hepatology* 67 (5), 1807–1822. doi:10.1002/hep.29661

Liu, J., Lichtenberg, T., Hoadley, K. A., Poisson, L. M., Lazar, A. J., Cherniack, A. D., et al. (2018). An Integrated TCGA Pan-Cancer Clinical Data Resource to Drive High-Quality Survival Outcome Analytics. *Cell* 173 (2), 400–416. doi:10.1016/j.cell.2018.02.052

Miller, M. A., and Weissleder, R. (2017). Imaging of Anticancer Drug Action in Single Cells. *Nat. Rev. Cancer* 17 (7), 399–414. doi:10.1038/nrc.2017.41

Mitchem, J. B., Brennan, D. J., Knolhoff, B. L., Belt, B. A., Zhu, Y., Sanford, D. E., et al. (2013). Targeting Tumor-Infiltrating Macrophages Decreases Tumor-Initiating Cells, Relieves Immunosuppression, and Improves Chemotherapeutic Responses. *Cancer Res.* 73 (3), 1128–1141. doi:10.1158/0008-5472.CAN-12-2731

Mohanty, A., Pharaon, R. R., Nam, A., Salgia, S., Kulkarni, P., and Massarelli, E. (2020). FAK-targeted and Combination Therapies for the Treatment of Cancer: an Overview of Phase I and II Clinical Trials. *Expert Opin. Investig. Drugs* 29 (4), 399–409. doi:10.1080/13543784.2020.1740680

Morita, M., Nishida, N., Sakai, K., Aoki, T., Chishina, H., Takita, M., et al. (2021). Immunological Microenvironment Predicts the Survival of the Patients with Hepatocellular Carcinoma Treated with Anti-PD-1 Antibody. *Liver cancer* 10 (4), 380–393. doi:10.1159/000516899

Motzer, R. J., Escudier, B., McDermott, D. F., Arén Frontera, O., Melichar, B., Powles, T., et al. (2020). Survival Outcomes and Independent Response Assessment with Nivolumab Plus Ipilimumab versus Sunitinib in Patients with Advanced Renal Cell Carcinoma: 42-month Follow-Up of a Randomized Phase 3 Clinical Trial. *J. Immunother. Cancer* 8 (2), e000891. doi:10.1136/jitc-2020-000891

Osipov, A., Saung, M. T., Zheng, L., and Murphy, A. G. (2019). Small Molecule Immunomodulation: the Tumor Microenvironment and Overcoming Immune Escape. *J. Immunother. Cancer* 7 (1), 224. doi:10.1186/s40425-019-0667-0

Pan, M. R., Wu, C. C., Kan, J. Y., Li, Q. L., Chang, S. J., Wu, C. C., et al. (2019). Impact of FAK Expression on the Cytotoxic Effects of CIK Therapy in Triple-Negative Breast Cancer. *Cancers (Basel)* 12 (1), 94. doi:10.3390/cancers12010094

Provenzano, P. P., Cuevas, C., Chang, A. E., Goel, V. K., Von Hoff, D. D., and Hingorani, S. R. (2012). Enzymatic Targeting of the Stroma Ablates Physical Barriers to Treatment of Pancreatic Ductal Adenocarcinoma. *Cancer Cell* 21 (3), 418–429. doi:10.1016/j.ccr.2012.01.007

Pu, N., Gao, S., Yin, H., Li, J. A., Wu, W., Fang, Y., et al. (2019). Cell-intrinsic PD-1 Promotes Proliferation in Pancreatic Cancer by Targeting CYR61/CTGF *via* the Hippo Pathway. *Cancer Lett.* 460, 42–53. doi:10.1016/j.canlet.2019.06.013

Rimassa, L., Danesi, R., Pressiani, T., and Merle, P. (2019). Management of Adverse Events Associated with Tyrosine Kinase Inhibitors: Improving Outcomes for Patients with Hepatocellular Carcinoma. *Cancer Treat. Rev.* 77, 20–28. doi:10.1016/j.ctrv.2019.05.004

Robinson, M. W., Harmon, C., and O'Farrelly, C. (2016). Liver Immunology and its Role in Inflammation and Homeostasis. *Cell Mol Immunol* 13 (3), 267–276. doi:10.1038/cmi.2016.3

Sangro, B., Sarobe, P., Hervás-Stubbs, S., and Melero, I. (2021). Advances in Immunotherapy for Hepatocellular Carcinoma. *Nat. Rev. Gastroenterol. Hepatol.* 18 (8), 525–543. doi:10.1038/s41575-021-00438-0

Schoenfeld, A. J., and Hellmann, M. D. (2020). Acquired Resistance to Immune Checkpoint Inhibitors. *Cancer Cell* 37 (4), 443–455. doi:10.1016/j.ccell.2020.03.017

Serrels, B., McGivern, N., Canel, M., Byron, A., Johnson, S. C., McSorley, H. J., et al. (2017). IL-33 and ST2 Mediate FAK-dependent Antitumor Immune Evasion through Transcriptional Networks. *Sci. Signal.* 10 (508), eaan8355. doi:10.1126/scisignal.aan8355

Shang, N., Arteaga, M., Zaidi, A., Cotler, S. J., Ding, P., Ding, X., et al. (2016). FAK Kinase Activity Is Required for the Progression of C-Met/β-Catenin-Driven Hepataocellular Carcinoma. *Gene Expr.* 17 (1), 79–88. doi:10.3727/105221616X691604

Shang, N., Arteaga, M., Zaidi, A., Stauffer, J., Cotler, S. J., Zeleznik-Le, N. J., et al. (2015). FAK Is Required for C-Met/β-Catenin-Driven Hepatocarcinogenesis. *Hepatology* 61 (1), 214–226. doi:10.1002/hep.27402

Soncin, I., Sheng, J., Chen, Q., Foo, S., Duan, K., Lum, J., et al. (2018). The Tumour Microenvironment Creates a Niche for the Self-Renewal of Tumour-Promoting Macrophages in colon Adenoma. *Nat. Commun.* 9 (1), 582. doi:10.1038/s41467-018-02834-8

Song, X., Xu, H., Wang, P., Wang, J., Affo, S., Wang, H., et al. (2021). Focal Adhesion Kinase (FAK) Promotes Cholangiocarcinoma Development and Progression *via* YAP Activation. *J. Hepatol.* 75, 888–899. doi:10.1016/j.jhep.2021.05.018

Sterner, R. M., Sakemura, R., Cox, M. J., Yang, N., Khadka, R. H., Forsman, C. L., et al. (2019). GM-CSF Inhibition Reduces Cytokine Release Syndrome and Neuroinflammation but Enhances CAR-T Cell Function in Xenografts. *Blood* 133 (7), 697–709. doi:10.1182/blood-2018-10-881722

Topalian, S. L., Taube, J. M., Anders, R. A., and Pardoll, D. M. (2016). Mechanism-driven Biomarkers to Guide Immune Checkpoint Blockade in Cancer Therapy. *Nat. Rev. Cancer* 16 (5), 275–287. doi:10.1038/nrc.2016.36

Torres-Ayuso, P., An, E., Nyswaner, K. M., Bensen, R. C., Ritt, D. A., Specht, S. I., et al. (2021). TNIK Is a Therapeutic Target in Lung Squamous Cell Carcinoma and Regulates FAK Activation through Merlin. *Cancer Discov.* 11 (6), 1411–1423. doi:10.1158/2159-8290.CD-20-0797

Wang, S., Hwang, E. E., Guha, R., O'Neill, A. F., Melong, N., Veinotte, C. J., et al. (2019). High-throughput Chemical Screening Identifies Focal Adhesion Kinase and Aurora Kinase B Inhibition as a Synergistic Treatment Combination in Ewing Sarcoma. *Clin. Cancer Res.* 25 (14), 4552–4566. doi:10.1158/1078-0432.CCR-17-0375

Xiang, D. M., Sun, W., Zhou, T., Zhang, C., Cheng, Z., Li, S. C., et al. (2019). Oncofetal HLF Transactivates C-Jun to Promote Hepatocellular Carcinoma Development and Sorafenib Resistance. *Gut* 68 (10), 1858–1871. doi:10.1136/gutjnl-2018-317440

Xu, F., Jin, T., Zhu, Y., and Dai, C. (2018). Immune Checkpoint Therapy in Liver Cancer. *J. Exp. Clin. Cancer Res.* 37 (1), 110. doi:10.1186/s13046-018-0777-4

Yang, J. D., Hainaut, P., Gores, G. J., Amadou, A., Plymoth, A., and Roberts, L. R. (2019). A Global View of Hepatocellular Carcinoma: Trends, Risk, Prevention and Management. *Nat. Rev. Gastroenterol. Hepatol.* 16 (10), 589–604. doi:10.1038/s41575-019-0186-y

Yao, H., Wang, H., Li, C., Fang, J. Y., and Xu, J. (2018). Cancer Cell-Intrinsic PD-1 and Implications in Combinatorial Immunotherapy. *Front. Immunol.* 9, 1774. doi:10.3389/fimmu.2018.01774

Zhang, J., Chen, Y., Lin, J., Jia, R., An, T., Dong, T., et al. (2020). Cyclovirobuxine D Exerts Anticancer Effects by Suppressing the EGFR-FAK-AKT/ERK1/2-Slug Signaling Pathway in Human Hepatocellular Carcinoma. *DNA Cell Biol* 39 (3), 355–367. doi:10.1089/dna.2019.4990

Zhu, A. X., Finn, R. S., Edeline, J., Cattan, S., Ogasawara, S., Palmer, D., et al. (2018). Pembrolizumab in Patients with Advanced Hepatocellular Carcinoma Previously Treated with Sorafenib (KEYNOTE-224): a Non-randomised, Open-Label Phase 2 Trial. *Lancet Oncol.* 19 (7), 940–952. doi:10.1016/S1470-2045(18)30351-6

Conflict of Interest: The authors declare that the research was conducted in the absence of any commercial or financial relationships that could be construed as a potential conflict of interest.

Publisher's Note: All claims expressed in this article are solely those of the authors and do not necessarily represent those of their affiliated organizations, or those of the publisher, the editors and the reviewers. Any product that may be evaluated in this article, or claim that may be made by its manufacturer, is not guaranteed or endorsed by the publisher.

Copyright © 2022 Wei, Wang, Liu, Qi, Xu, Li, Feng and Shi. This is an open-access article distributed under the terms of the Creative Commons Attribution License (CC BY). The use, distribution or reproduction in other forums is permitted, provided the original author(s) and the copyright owner(s) are credited and that the original publication in this journal is cited, in accordance with accepted academic practice. No use, distribution or reproduction is permitted which does not comply with these terms.

frontiers in Oncology

ORIGINAL RESEARCH
published: 16 February 2022
doi: 10.3389/fonc.2022.842967

The Histone Acetyltransferase MOF Regulates SIRT1 Expression to Suppress Renal Cell Carcinoma Progression

Renbo Guo[1,2], Yiran Liang[3], Benkui Zou[2], Danyang Li[1,4], Zhen Wu[1], Fei Xie[1], Xu Zhang[1] and Xiangzhi Li[1*]

[1] Shandong Provincial Key Laboratory of Animal Cell and Developmental Biology, School of Life Sciences, Shandong University, Qingdao, China, [2] Department of Urology, Shandong Cancer Hospital and Institute, Shandong First Medical University and Shandong Academy of Medical Sciences, Jinan, China, [3] Department of Breast Surgery, General Surgery, Qilu Hospital of Shandong University, Jinan, China, [4] Rehabilitation Center, Qilu Hospital, Cheelo College of Medicine, Shandong University, Jinan, China

OPEN ACCESS

Edited by:
Haichang Li,
The Ohio State University,
United States

Reviewed by:
Jiaxur Wu,
Fudan University, China
Lin-Yu Lu,
Zhejiang University, China

***Correspondence:**
Xiangzhi Li
xiangzhi@sdu.edu.cn

Specialty section:
This article was submitted to Pharmacology of Anti-Cancer Drugs, a section of the journal Frontiers in Oncology

Received: 24 December 2021
Accepted: 28 January 2022
Published: 16 February 2022

Citation:
Guo R, Liang Y, Zou B, Li D, Wu Z, Xie F, Zhang X and Li X (2022) The Histone Acetyltransferase MOF Regulates SIRT1 Expression to Suppress Renal Cell Carcinoma Progression. Front. Oncol. 12:842967. doi: 10.3389/fonc.2022.842967

Background: Renal cell carcinoma (RCC) is one of the most common and lethal human urological malignancies around the world. Although many advancements in diagnostic and therapeutic strategies have been acquired, the prognosis of patients with metastatic RCC was poor. Thus, there is an urgent need to understand the molecular mechanism of RCC.

Methods: The quantitative real-time PCR (qRT-PCR) was used to detect the RNA expression of MOF in human RCC tissues and cell lines. The protein expression of MOF was analyzed with immunohistochemistry (IHC) and Western blot. To understand the regulatory mechanism of MOF in liver cancer, ChIP-qPCR assay and dual-luciferase assay were performed. Moreover, a series of *in vivo* and *in vitro* experiments were conducted to evaluate the effect of MOF on renal cell carcinoma progression.

Results: In the present study, we found that Males absent on the first (MOF), a histone acetyltransferase involved in transcription activation, was significantly decreased in both RCC tissues and RCC cells compared to normal tissues and non-cancer cells. Moreover, MOF downregulation was associated with advanced histological grade, pathologic stage and distant metastasis of RCC patients. Ectopic expression of MOF could significantly attenuate cell proliferation and promote cell apoptosis. Besides, MOF overexpression also suppressed migration of RCC cells through inhibiting epithelial-mesenchymal transition (EMT). Importantly, the inhibition of tumor growth by MOF was further confirmed by *in vivo* studies. Mechanism dissection revealed that MOF could transcriptionally upregulate the expression of SIRT1, leading to attenuated STAT3 signaling, which was involved in cell proliferation and migration. Moreover, SIRT1 knockdown could restore the biological function induced by MOF overexpression.

Conclusions: Our findings indicated that MOF serves as a tumor suppressor *via* regulation of SIRT1 in the development and progression of RCC, and MOF might be a potent biomarker for diagnosis and prognosis prediction of RCC patients.

Keywords: renal cell carcinoma, MOF, SIRT1, progression, tumor suppressor

INTRODUCTION

Renal cell carcinoma (RCC) is a malignant tumor arising from urinary tubular epithelial cells (1), accounting for more than 90% of tumors in human kidney. It was reported that there were 403,262 new cases and 175,098 deaths in 2018 (2) and the incidence of RCC is gradually increasing every year. Radical nephrectomy is the major effective treatment for patients with RCC due to the poor effect to chemotherapy and radiotherapy (3). Moreover, although significant advances have been acquired in therapeutic strategies, including modified surgical techniques and improved systemic treatment with targeted agents, the prognosis of RCC is still far from satisfactory because of the tumor recurrence and metastasis (4). The median survival time of patients with metastatic RCC was only 13 months (5). Therefore, comprehension of the molecular mechanisms of RCC carcinogenesis and progression is essential for detecting diagnostic and therapeutic biomarkers.

Histone acetylation modification is one of the most significant epigenetic modifications involved in various cellular biological process (6), such as genetic transcription, chromosome constitution, cell cycle control, and DNA damage repair. The balance of global histone acetylation modification is regulated by histone acetyltransferases (HATs) and histone deacetylases (HDACs) (7), and its disturbance shows close association with the initiation and progression of various cancers. For example, the total acetylation levels of histone H3 were negatively correlated with Fuhrman grading, pT-stage, and distant metastasis of RCC (8), whereas the alteration of global H4K16ac was closely associated with the occurrence of tumors (9), indicating the diagnostic and prognostic value.

MOF, as a member of the MYST family of HATs in human cells, is responsible for H4K16ac (10). Depletion of MOF not only leads to global reduction of H4K16ac, but also influences various physiological and pathological processes (11–13), including cell proliferation, DNA damage repair, chromatic constitution, gene transcription, stem cell self-renewal, and embryonic development. Recently, mounting evidences revealed that abnormal expression of MOF was involved in various primary cancers, however, the expression patterns of MOF were varied among different cancers. The expression of MOF was upregulated in lung non-small cell lung cancer (NSCLC) tissues compared to normal tissues, and MOF overexpression led to enhanced cell proliferation, migration, adhesion, and drug resistance of NSCLC cells (14, 15). On the contrary, MOF was reported to be downregulated in multiple cancers, including breast cancer (16), medulloblastoma (17), gastric cancer (18), and ovarian cancer (19). Although the downregulation of MOF had been found in RCC (18, 20), it remains poorly understood about the functions and molecular mechanisms of MOF in RCC.

In this study, we assess the expression of MOF in RCC tissues and RCC cells, and further evaluate the association between MOF expression and corresponding clinicopathological features. In addition, the role of MOF in regulating RCC cell proliferation and mobility and the underlying mechanism was also investigated. Our results would help to comprehensively understand the function of MOF in RCC and provide a novel biomarker for diagnosis and treatment in RCC patients.

MATERIAL AND METHODS

Human Samples

A total of 52 RCC patients undergoing surgery in the department of urology at the Shandong Cancer Hospital and Institute were included in the present study. The RCC tissues and paired adjacent normal tissues were stored at − 80°C until use. None of the patients received chemotherapy or radiotherapy before surgery. Written informed consent was obtained from all participants, and all the experimental procedures were approved by the Ethics Committee of Shandong Cancer Hospital and Institute.

Gene Expression Profiles

The gene expression data matrix of normal tissue and RCC tissue was obtained from the GEO database (https://www.ncbi.nlm.nih.gov/geo/), which is accessible through the GEO platforms GPL570 (GSE53757).

Cell Culture

The human RCC cell lines, 786-O, Caki-1, 769-P, A498, ACHN and the immortalized proximal tubule epithelial cell line from normal adult human kidney (HK-2) were purchased from American Type Culture Collection (ATCC, Manassas, VA, USA). Mycoplasma detection was performed using a Mycoplasma Detection Set (Takara, Shiga, Japan) for all the cells. All the RCC cell lines were routinely cultured in Dulbecco's modified Eagle's medium (DMEM, Invitrogen, Carlsbad, CA, USA) supplemented with 10% fetal bovine serum (FBS), 100 U/ml Penicillin, and 100 μg/ml streptomycin in the humidified atmosphere with 5% CO2 at 37°C.

Cell Transfection

To overexpress MOF, pcDNA3.1-MOF vector containing the open reading frame (ORF) of MOF was used. Empty vector was used as a control. G418 (2mg/ml) was used for generating stably transfected cells. To knockdown MOF in RCC cells, duplexes of siRNA targeting MOF and negative control synthesized by GenePharma (Shanghai, China) were used. The cells were transfected using the Lipofectamine 2000 (Invitrogen) according to the manufacturer's instructions.

RNA Extraction and qRT-PCR

Total RNAs were isolated from tissues or cells using Trizol reagent (Invitrogen, Grand Island, USA) according to the manufacturer's instructions. One microgram of total RNA was subjected to reverse transcription using PrimeScript reverse transcriptase (RT) reagent kit (Takara, Shiga, Japan). Then, quantitative reverse transcriptase PCR (qRT-PCR) was conducted using SYBR green (Takara, Shiga, Japan) to determine the RNA expression level. Actin was used as the internal control, and expression of RNA was calculated by the relative quantification using $2^{-\Delta\Delta CT}$ method.

Western Blotting (WB)

Total proteins of tissues or cells were extracted by RIPA lysis buffer (Beyotime, China) containing protease inhibitor cocktail (MedChemExpress, China) according to the manufacturer's instructions. Then proteins were subjected to SDS-PAGE and then transferred to 0.22 μm PVDF membranes (Millipore, MA, USA). After being blocked with 5% skim milk powder and incubated with primary antibodies: anti-GAPDH (PTG, 60004-1-Ig), anti-MOF (Abcam, ab72056), anti-Fibronectin (PTG, 15613-1-AP), anti-N-cadherin (PTG, 22018-1-AP), anti-E-cadherin (PTG, 20874-1-AP), anti-Vimentin (PTG, 60330-1-Ig), anti-SIRT1 (Abcam, ab110304), anti-STAT3 (CST, 9139). Then, the membranes were incubated with HRP-conjugated anti-mouse (CST, 7076) or anti-rabbit (CST, 7074) secondary antibodies and detected through ECL detection system (Bio-Rad, USA). GAPDH was used as the internal control.

Cell Proliferation Assay

Transfected RCC cells were seeded in 96-well plates (1500 cells/well) and cultured for indicated time. 20 μl of 5 mg/ml MTT was added into each well and incubated for another 4 h in incubator at 37°C. After removal of the media, 100 μl DMSO was added. Then the absorbance was measured at 570 nm on a Microplate Reader (Bio-Rad) and the proliferation curves were calculated.

Colony Formation Assay

Transfected RCC cells were seeded in 6 cm plate (500 cells/plate) and cultured for 10-14 days. Then cell colonies were washed by PBS, fixed with ethanol and stained by crystal violet. The colonies were taken pictures and counted.

EdU Incorporation Assay

Transfected RCC cells were seeded in 96-well plates (1×10^4 cells/well) and incubated with 50 μM EdU for 2.5 h. The EdU Proliferation Kit (RiboBio Guangzhou, China) was used to evaluate cell proliferation viability following the standard protocol. Images were taken using an Olympus microscope (Olympus, Tokyo, Japan).

Cell Migration Assays

The invasive capability of RCC cells was determined by the transwell migration assays. 5 × 104 of infected RCC cells were harvested and seeded with serum-free DMEM into the upper chambers, and the bottom chambers were filled with medium containing 20% FBS. After incubation for 24 h at 37°C, the cells attached to the lower surface of the membrane were fixed by 4% methanol and stained with 0.1% crystal violet. Cells were counted and photographed using an Olympus light microscope.

Wound Healing Assay

Indicated cells were plated to confluence in 24-well plates. Then streaks across the plate were made in the monolayer with a pipette tip. Images were captured at 0 and 24 h after wounding using an Olympus light microscope.

Chromatin Immunoprecipitation (ChIP) Assay

ChIP assay was performed using the ChIP kit (CST, USA) according to the manufacturer's instruction. Briefly, transfected RCC cells were crosslinked with 4% formaldehyde for 10 min followed by sonication to yield genomic DNA fragments with an average length of 200-1000 bp. The lysates were then immunoprecipitated with anti-MOF antibodies (Abcam, Cambridge, UK) or normal rabbit IgG. The immunoprecipitated DNA was detected by qRT-PCR and the enrichment was expressed as fold enrichment compared to IgG.

Luciferase Assay

The SIRT1 gene promoter segment covering from -2000 bp to +1 bp was cloned into the pGL3-basic vector (Promega, Madison, WI, USA), which was termed as pGL3-SIRT1. The vector of pcDNA3.1-MOF was co-transfected with pGL3-SIRT1 and pRL-TK vector using Lipofectamine 2000 (Invitrogen). Luciferase activity was measured by dual-luciferase assay system (Promega) according to the manufacturer's manual.

Immunohistochemistry

Tissues were embedded in paraffin and cut into 4 μm sections. The sections were de-paraffinized in xylene and rehydrated in a series of alcohol. Then antigen retrieval was performed in 10 mM sodium citrate buffer (pH 6.0) using microwave heating. Endogenous peroxidase was blocked with 3% hydrogen peroxide and 5% BSA was used to block nonspecific binding. The sections were incubated with the primary antibody for MOF (1:200, Abcam, ab72056) and SIRT1 (1:200, Abcam, ab110304) overnight at 4°C. After incubation with corresponding secondary antibodies at 37°C for 1 h, the sections were stained with diaminobenzidine (DAB) and counterstained with hematoxylin. The representative images were taken using an Olympus light microscope.

Tumor Xenograft Formation and Lung Metastasis Model

Four-week-old nude mice were purchased from the Shanghai Experimental Animal Center and maintained in pathogen-free conditions. 769-P cells (1×10^7 cells) stably transfected with pcDNA3.1-MOF or control vectors were subcutaneously injected into one flank of each mice (n=5). Tumor sizes were measured using digital calipers every five days, and tumor volumes were calculated using the formula: $1/2 \times (\text{length} \times \text{width}^2)$. After 4 weeks, mice were killed, and tumors were excised and weighed. Hematoxylin and eosin (H&E) staining was performed for evaluation of tissue morphology and size of metastatic lesions. The animal experiments were conducted with approval from the Ethics Committee of Shandong Cancer Hospital and Institute.

Statistical Analysis

Statistical analysis was performed using SPSS 21.0 (Chicago, IL, USA) and GraphPad Prism 8.0 software. Data were expressed as mean ± S.D. from three independent experiments. Student's t-test was used for comparisons of two independent group and One-way ANOVA analysis was applied to compare statistical differences between groups. P-value < 0.05 was considered statistically significant.

RESULTS

MOF Is Downregulated in RCC Tissues and Cells

To investigate the role of MOF in RCC, the expression of MOF was analyzed in 52 paired RCC tissues and normal tissues. The qRT-PCR results revealed that the expression of MOF was significantly downregulated in RCC tissues compared to adjacent normal tissues (**Figure 1A**), which was consistent with the result (**Figure 1B**) obtained from GEO database (GSE53757). After analyzing the association between MOF expression and the clinicopathologic parameters, we found that low MOF expression level was significantly correlated with advanced histological grade, pathologic tumor stage and distant metastasis (**Figure 1C**). Moreover, the decreased expression of MOF in RCC tissues was further confirmed by western blot and immunohistochemistry (**Figures 1D, E**). Furthermore, we compared the levels of MOF in normal cells and RCC cells. Compared to normal renal tubular epithelial cells (HK2), the protein and mRNA levels of MOF in RCC cells (786-O, Caki-1, 769-P, A498, ACHN) were significantly decreased (**Figures 1F, G**). Taken together, MOF was significantly downregulated in RCC, and might serve as a tumor-suppressor in RCC.

MOF Overexpression Inhibited the Proliferation of RCC Cells

We further investigated the potential functional role of MOF in RCC cells. The knockdown or overexpression efficiency of MOF

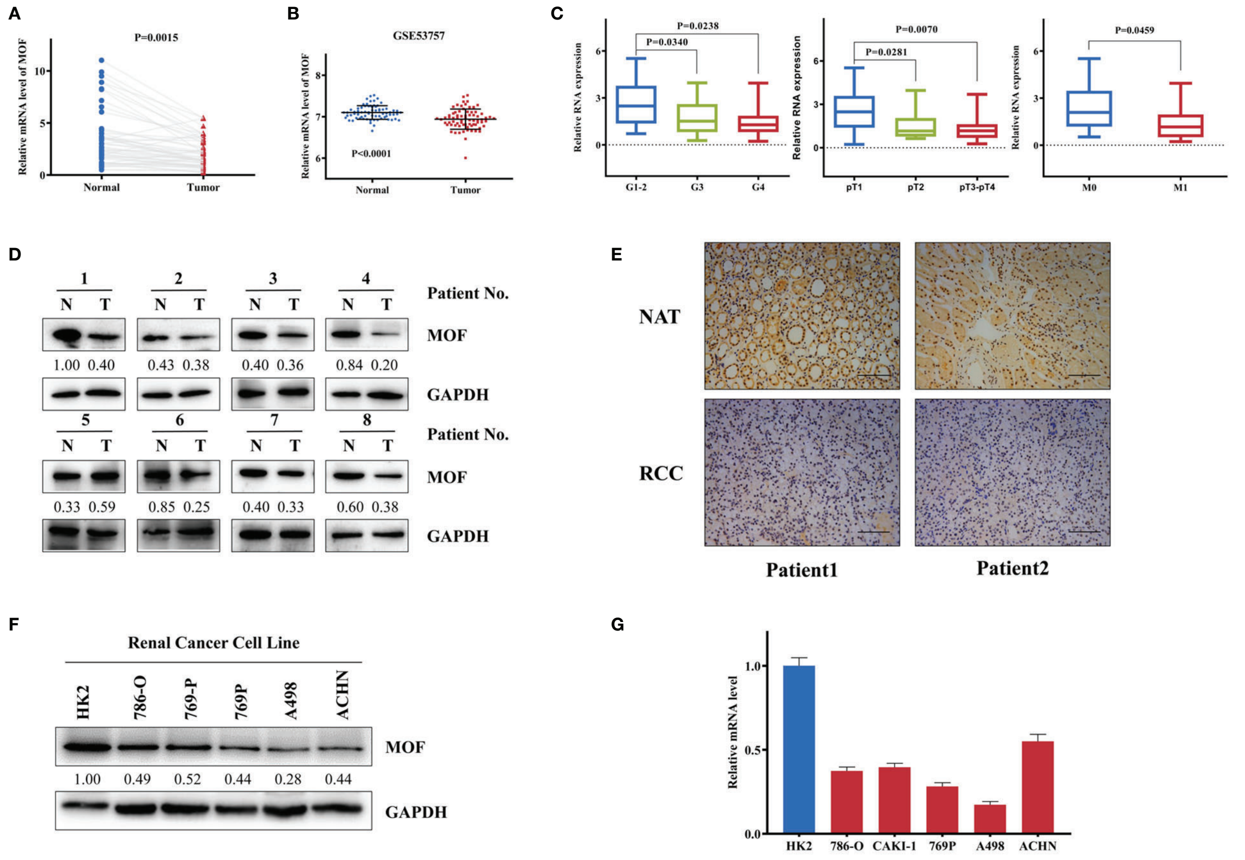

FIGURE 1 | MOF is downregulated in renal cell carcinoma tissues and cells. **(A)** MOF RNA level is decreased in renal cell carcinoma tissues (n=52) compared to normal tissues (n=52). **(B)** MOF expression level is down-regulated in renal cell carcinoma tissues (n=72) compared to normal tissues (n=72) according to GSE53757 database. **(C)** The expression of MOF was decreased in renal cell carcinoma tissues with advanced histological grade, pathologic tumor stage and distant metastasis. **(D)** MOF protein level is decreased in most renal cell carcinoma tissues. **(E)** The expression of MOF is reduced in renal cell carcinoma tissues. Scale bar, 100 µm. **(F, G)** MOF protein **(F)** and RNA **(G)** level is down-regulated in renal cell carcinoma cells.

in 786-O and 769-P cells were verified with western blot and qRT-PCR (**Figures 2A, B**). Both MTT assays and colony formation assays indicated that MOF knockdown led to increased proliferation of RCC cells, whereas MOF overexpression significantly inhibited the cell proliferation (**Figures 2C, D**). Moreover, EdU assays revealed that DNA synthesis activities of RCC cells were markedly increased after MOF knockdown and decreased after MOF overexpression (**Figure 2E**). Then flow cytometry analysis was performed to evaluate whether MOF could affect cell proliferation by modulating cell apoptosis. The results indicated that MOF knockdown led to a decreased apoptotic rate and ectopic expression of MOF promoted cell apoptosis (**Figure 2F**). These results suggested that MOF played an essential role in RCC cell proliferation.

MOF Overexpression Depressed the Migration and Invasion of RCC Cells

We then evaluated the effect of MOF on RCC cell motility. Knockdown of MOF observably increased the wound-healing ability of cells (**Figure 3A**). Consistently, the transwell migration and invasion assays revealed that MOF knockdown notably promoted the motility of RCC cells (**Figure 3B**). In accordance with the aforementioned results, MOF overexpression significantly attenuated cell migration and invasion (**Figures 3A, B**). Epithelial-mesenchymal transition (EMT) is one of the major mechanisms involved in cell malignant transformation, and our results indicated that MOF knockdown could decrease the expression of epithelial markers and increased the expression of mesenchymal markers, and MOF overexpression showed opposite effect on the expression of EMT-related proteins (**Figure 3C**). All these results indicated that MOF played an essential role in the migration and invasion of RCC cells.

MOF Regulated SIRT1 and Its Downstream Genes in RCC Cells

SIRT1 was reported to play a crucial role in the development and progression of various cancers (21). We wondered whether MOF could regulate the expression of SIRT1 in RCC. Using TCGA starbase, we found a closely positive association between MOF and SIRT1 (**Figure 4A**). Moreover, our results indicated that MOF knockdown significantly reduced the protein and mRNA levels of SIRT1, leading to the upregulated expression of its downstream target gene, STAT3 (**Figures 4B, C**). Consistently, overexpression of MOF led to the opposite results (**Figures 4B, C**). To explore the role of MOF in regulating SIRT1 expression, ChIP assay was performed. The results showed that MOF could bind to the promoter of SIRT1 (**Figure 4D**). In addition, the luciferase report assay demonstrated that knockdown of MOF could attenuate the promoter activity of SIRT1 (**Figure 4E**). These results indicated that MOF could transcriptionally regulate the expression of SIRT1 in RCC cells.

SIRT1 Contributed to the Biological Function of MOF in RCC Cells

To further prove SIRT1 upregulation as a mediator of MOF in RCC cells, we performed rescue experiment by co-transfecting MOF overexpression vectors and siRNAs against SIRT1 into 786-O and 769-P cells. The transfection efficiency was confirmed by qRT-PCR and western blot (**Figures 5A, B**). The functional results showed that SIRT1 knockdown could rescued the attenuated cell proliferation and motility caused by MOF overexpression (**Figures 5C, D**). These data demonstrated that SIRT1 is a direct functional target of MOF in RCC.

MOF Overexpression Attenuates RCC Growth and Progression *In Vivo*

Furthermore, *in vivo* experiments were performed to evaluate the functions of MOF. The 769-P cells stably transfected with MOF overexpression vectors or control vectors were subcutaneously injected into nude mice, and the results showed that the growth rates and tumor weights were significantly decreased in MOF-overexpressed group compared to the control group (**Figures 6A–C**). Consistently, IHC analysis revealed the increased MOF and SIRT1 expression in the MOF-overexpressed group (**Figure 6D**). Our findings indicate that MOF overexpression in RCC cells inhibited tumor growth *in vivo*.

DISCUSSION

Even though extensive advancement in diagnosis and treatment of renal cell carcinoma have been made over the decades, metastasis and recurrence is still the intractable problem for affecting the patient prognosis. However, the detailed mechanism of metastasis is still poorly understood. Recently, increasing evidence suggested that the histone modification status in cells is significantly associated with the gene expression pattern, and abnormal global histone modification would further lead to cell dysfunction, even cancer. Various chromatin modifying enzymes, such as histone acetyltransferases (HATs) and histone deacetylases (HDACs) have been shown to participate in the tumorigenesis and progression of several cancers.

MOF (also called MYST1), a member of the MYST family of histone acetyltransferases (HATs), is the human ortholog of Drosophila male absent on the first (MOF) protein (22). The aberrant expression of MOF has been found in various cancers, such as breast cancer (16), ovarian cancer (19), and gastric cancer (18), functioning as an oncogene or tumor suppressor. However, the exact expression and role of MOF in renal cell carcinoma and the underlying mechanism were still unknown. The expression patterns of MOF in different cancers were varied. In this study, using a large number of renal cell carcinoma tissues from our center, we demonstrated that the RNA expression level of MOF was downregulated in renal cell carcinoma tissues, which is consistent with the previous report (20). Moreover, the expression analysis using GSE53757 database also indicated the decreased expression of MOF in renal cell carcinoma tissues. We further analyze the association between MOF expression and the clinicopathologic parameters, and found that downregulated expression of MOF was associated with advanced renal cell carcinoma, indicating the potential role of MOF in metastasis

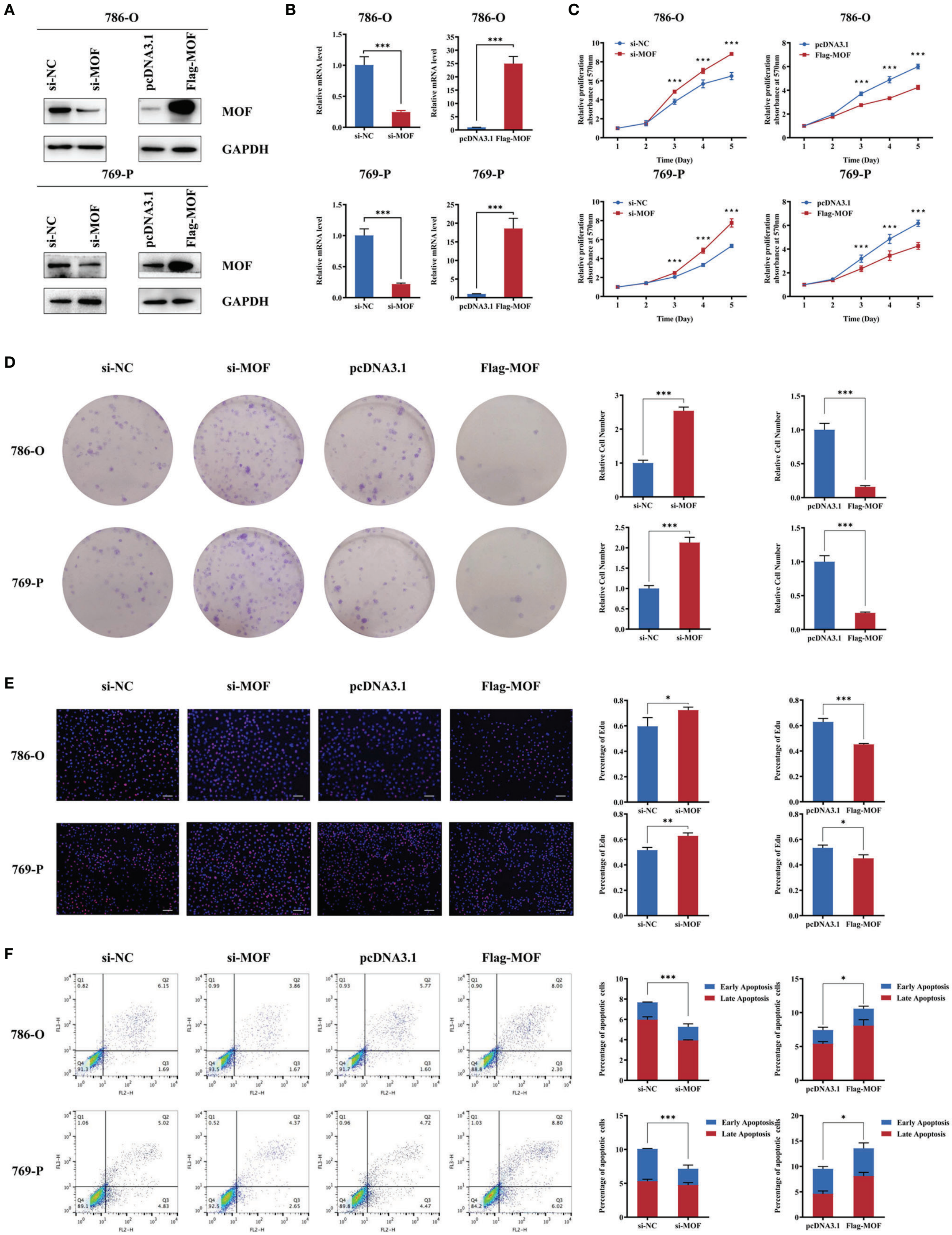

FIGURE 2 | MOF overexpression inhibits renal cell carcinoma cell proliferation. **(A, B)** The knockdown or overexpression efficiency of MOF in protein **(A)** or RNA **(B)** levels in 786-O and 769-P cells. **(C)** MOF knockdown promoted renal cell carcinoma cell proliferation, and MOF overexpression inhibited renal cell carcinoma cell proliferation. **(D)** MOF knockdown led to increased renal cell carcinoma cell colony formation ability, whereas MOF overexpression caused inhibited renal cell carcinoma cell colony formation ability. **(E)** MOF knockdown promotes DNA replication of renal cell carcinoma cells, and MOF overexpression inhibited DNA replication of renal cell carcinoma cells. Scale bar, 100 µm. **(F)** MOF knockdown inhibited renal cell carcinoma cell apoptosis, and MOF overexpression promoted renal cell carcinoma cell apoptosis. (*, $p < 0.05$, **, $p < 0.01$, ***, $p < 0.001$).

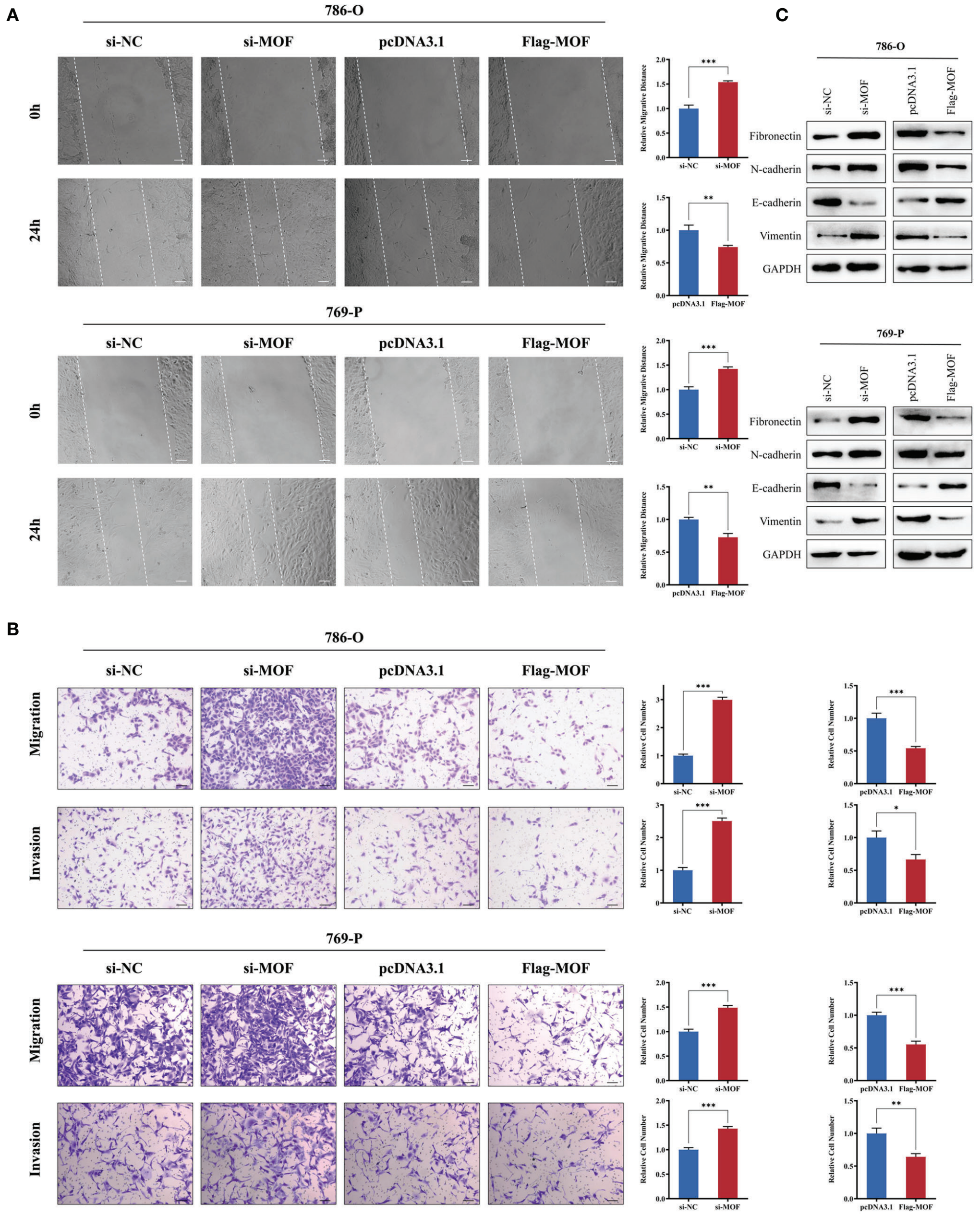

FIGURE 3 | MOF overexpression inhibits renal cell carcinoma cell migration and invasion. **(A, B)** The wound healing assay **(A)** and transwell assay **(B)** indicated that MOF knockdown led to inhibited renal cell carcinoma cell migration, whereas MOF overexpression caused the opposite results. Scale bar, 100 µm. **(C)** Western blot was used to detect the effect of MOF on the expression of EMT markers. (*, $p < 0.05$, **, $p < 0.01$, ***, $p < 0.001$).

prediction. Consistently, the abnormal protein expression of MOF was also validated in renal cell carcinoma cells. These results indicated that MOF might play a tumor-suppressive role in renal cell carcinoma.

Previous studies show that MOF could regulate several cellular processes through modulating the status of histone H4K16ac (11, 23, 24), such as DNA damage repair, genomic instability, and gene transcription. However, the role of MOF in different cancers remains controversial. The expression of MOF was found to be higher in non-small cell lung cancer (NSCLC) tissues compared to corresponding normal tissues, and MOF overexpression led to enhanced proliferation, metastasis, and radiation resistance of NSCLC cells (14, 25). Another study reported that MOF was significantly upregulated at the protein level in hepatocellular carcinoma with microvascular invasion, and MOF downregulation would reduce the intravasation and metastasis *in vitro* and *in vivo* (26). On the contrary, the mRNA and protein levels of MOF were abnormally down-regulated in

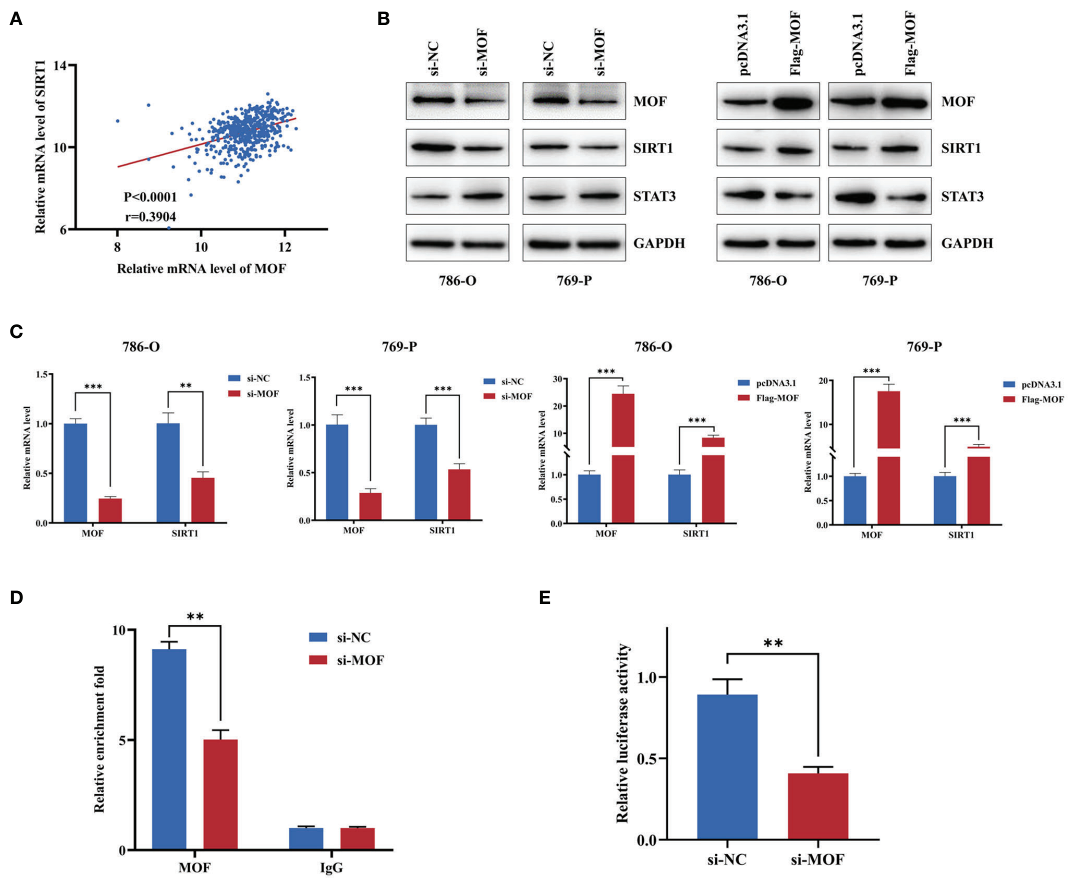

FIGURE 4 | MOF regulates SIRT1 in renal cell carcinoma cells. **(A)** The expression of MOF was positively associated with the expression of SIRT1 based on TCGA database. **(B, C)** The effect of MOF on the protein **(B)** and RNA **(C)** expression levels of SIRT1 and its target genes were detected. **(D)** ChIP assay indicated that MOF could bind with the promoter of SIRT1. **(E)** Luciferase assay showed that MOF knockdown decreased the SIRT1 promoter activity. (**, p < 0.01, ***, p < 0.001).

ovarian cancer tissues and cells, and the overexpression of MOF could inhibit the growth of ovarian cancer cells and promote cell apoptosis (27). Moreover, MOF-mediated H4K16Ac could promote the release of RNA polymerase II from pausing through recruiting BRD4 and pTEFb, and lead to reactivation of tumor suppressor TMS1 (16). These findings indicated that MOF had dual roles in cancers which largely depend upon the individual type of cancer itself with different cellular environment and various targets. In the study, we provided novel evidence for the tumor-suppressive role of MOF in renal cell carcinoma. The functional experiments demonstrated that MOF knockdown led to enhanced cell viability and motility, whereas overexpression of MOF inhibited cell proliferation and migration.

In order to discern the potential regulatory mechanism of MOF in renal cell carcinoma, we further explore its downstream pathway. Histone acetyltransferases (HATs) and histone deacetylases (HDACs) are major regulators for the overall level of acetylation in cells, which are in dynamic equilibrium and responsible for the function and expression of various genes (28). Aberrant expression of HATs and HDACs is associated with tumorigenesis and tumor development, and they are considered as novel anticancer targets for many cancers (29). Therefore, exploring the interaction between HATs and HDACs could help to find novel target for cancer treatment. The sirtuins (SIRT 1 to 7) belong to nicotinamide adenine dinucleotide (NAD+)-dependent class III HDACs with diverse roles in various biological activities (30, 31). Among them, SIRT1 is localized in cytoplasm and cell nucleus, and plays essential roles in the regulation of transcription factors and cellular metabolism through deacetylation of lysine residues (32, 33). Liu et al. revealed that MOF and SIRT1 were responsible for the acetylation level of WSTF, thus modulating the activities of WSTF and its effect on tumorigenesis (34). Moreover, SIRT1 could interact with MOF and deacetylate autoacetylated MOF, leading to increased recruitment of MOF to the chromatin and increased expression of its target gene HoxA9 (35). Another study reported that MOF could promote acetylation of DBC1 to inhibit DBC1-SIRT1 binding and increase the deacetylase activity of SIRT1, thus modulating cell response to DNA damage (36). These studies reveal that the interaction between MOF and SIRT1 serves as a significant mechanism in various

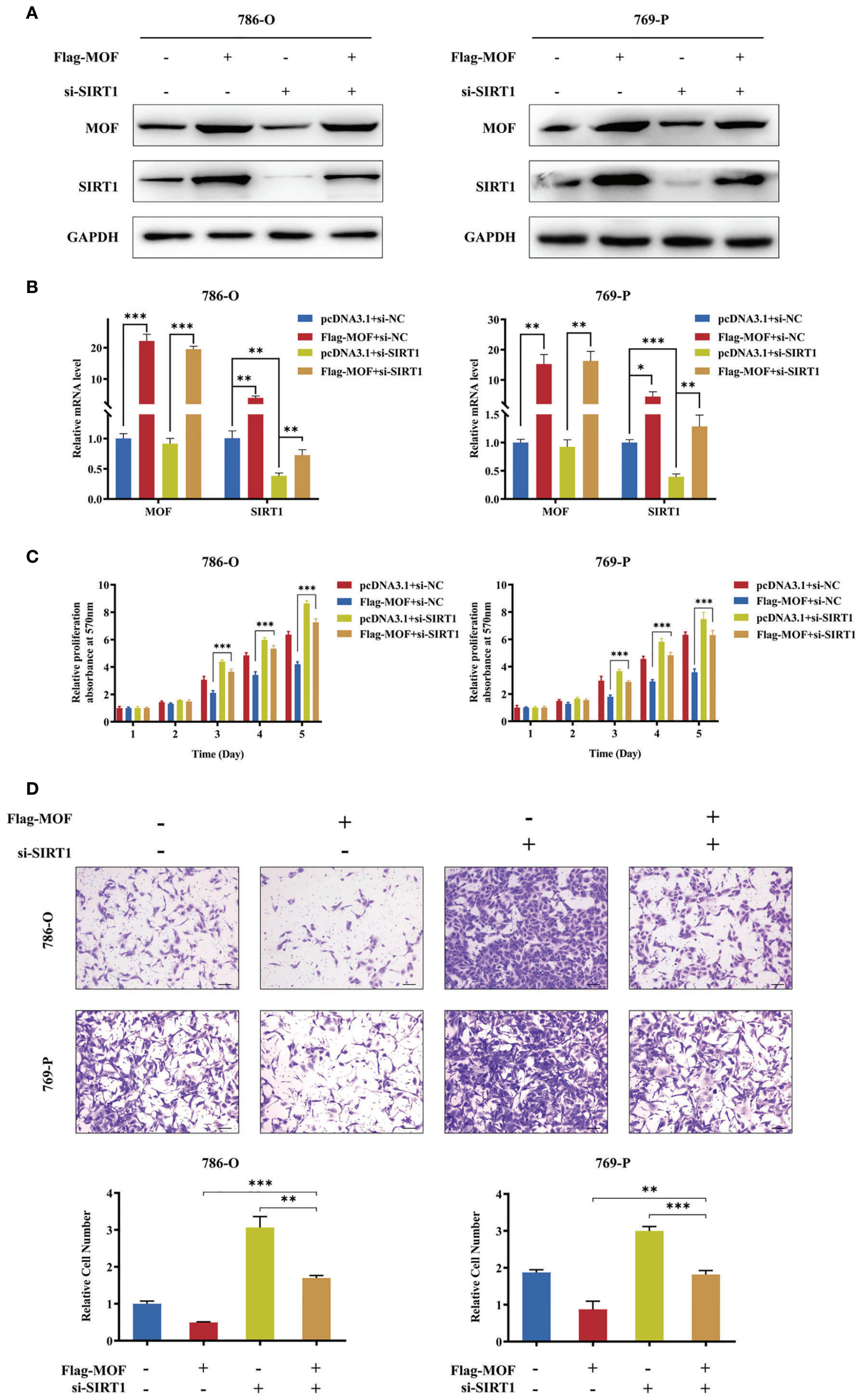

FIGURE 5 | SIRT1 knockdown restored MOF-induced inhibition of cell proliferation and migration. **(A, B)** Western blot **(A)** and qRT-PCR **(B)** assays demonstrated the efficiency of SIRT1 knockdown and MOF overexpression in 786-O and 769-P cells. **(C)** SIRT1 knockdown restored the inhibited cell proliferation induced by MOF overexpression. **(D)** SIRT1 knockdown restored the inhibited cell migration induced by MOF overexpression. Scale bar, 100 µm. (*, $p < 0.05$, **, $p < 0.01$, ***, $p < 0.001$).

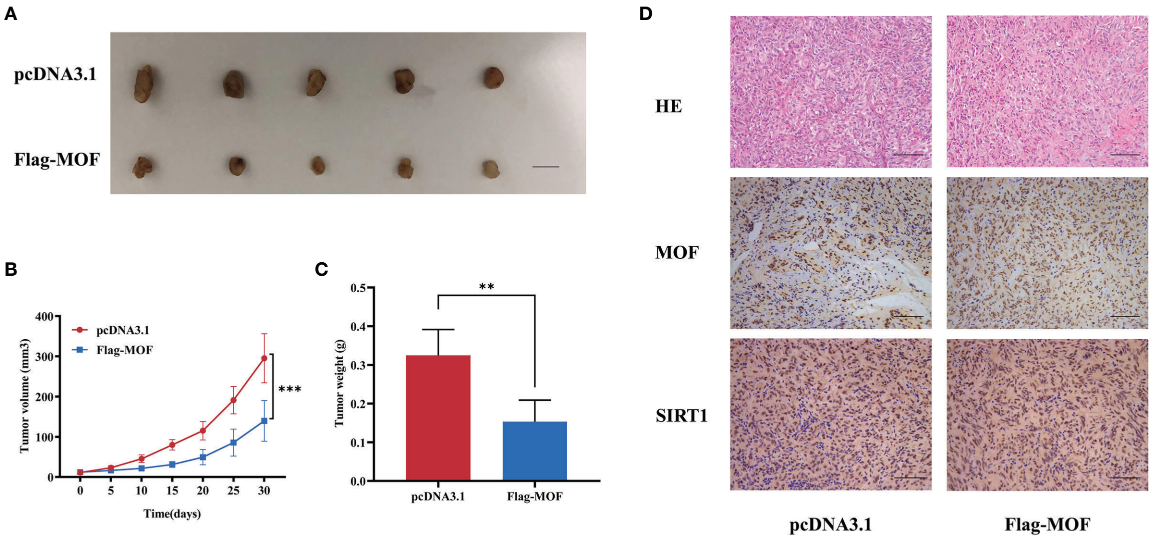

FIGURE 6 | The effect of MOF on renal cell carcinoma cell growth *in vivo*. **(A)** Tumor xenograft model in nude mice. MOF-overexpressed 769-P cells and control cells were inoculated to the flank of nude mice. Scale bar, 1 cm. **(B, C)** The tumor volume **(B)** and tumor weight **(C)** were analyzed. **(D)** H&E staining showed the tissue morphology. Representative images of MOF and SIRT1 staining in the indicated tumor tissues. Scale bar, 100 µm. (**, $p < 0.01$, ***, $p < 0.001$.).

biological processes and cancer development. However, the effect of MOF on SIRT1 expression and the functional role of SIRT1 in RCC remains unclear.

In this study, we found that the expression of MOF was positively associated with SIRT1 expression level. Knockdown of MOF led to decreased expression of SIRT1 in the protein and RNA levels, whereas MOF overexpression caused the opposite results. Further experiments indicated that, MOF could bind to the promoter of SIRT1, leading to the enhanced expression of SIRT1. Previous study reported that SIRT1 could deacetylate STAT3 and hence destabilize and negatively regulate STAT3 (21, 37). Consistently, our results also revealed that MOF overexpression led to decreased expression of the downstream target gene STAT3, whereas MOF knockdown upregulated the expression of STAT3. Multiple evidence found that the function of SIRT1 might be tissue or cell specific, and it could act as a tumor suppressor or oncogene in various cancers through regulating different biological pathways. Previous studies indicated that the expression of SIRT1 was upregulated in hepatocellular carcinoma tissues, and could directly deacetylate p62 to prevent its degradation (38). Moreover, SIRT1 expression was associated with tumor progression and poor prognosis in triple-negative breast cancer (39). In addition, SIRT1 overexpression led to enhanced expression of MMP2, promoting cell invasion in prostate cancer cells (40). On the contrary, the overexpression of SIRT1 in hormone receptor-positive patients and HER2+ patients were correlated with lower risks of lymph node metastasis (41). Moreover, the high expression level of SIRT1 was associated with a better survival rate in glioblastoma patients, and SIRT1 overexpression could enhance the inhibitory effect of Urolithin A on the tumor growth and metastasis of glioblastoma (42). Therefore, more efforts are needed to reveal the exact role of SIRT1 and its regulatory mechanism in RCC. In our study, the functional experiments indicated that knockdown of SIRT1 could promote the proliferation and migration of renal cancer cells, which further revealed that SIRT1 might act as an oncogene in renal cancer. Significantly, the inhibited effect of MOF overexpression on the proliferation and migration of renal cancer cells could be rescued by SIRT1 knockdown. These results further implicated that MOF might act as a tumor suppressor in renal cancer, partly through regulating the expression of SIRT1. Although our study and previous studies have revealed the significant role of MOF in tumor progression through modulating the expression of various genes (43, 44), such as SIRT6 and TNK2, more studies are needed to comprehensively understand the function and complex regulatory mechanism of MOF in the future.

In summary, our results indicated that MOF was downregulated in renal cell carcinoma tissues and cells, and the expression of MOF was negatively associated with the progression of renal cell carcinoma. We also identified the tumor-suppressive role of MOF *via* targeting SIRT1. These findings revealed that MOF might be a novel target for interventions in renal cell carcinoma.

CONCLUSION

In the present study, we discovered the suppressive role of MOF in tumor progression through regulating the expression of SIRT1, and provides a potential therapeutic target for renal cell carcinoma.

DATA AVAILABILITY STATEMENT

The original contributions presented in the study are included in the article/supplementary material. Further inquiries can be directed to the corresponding author.

ETHICS STATEMENT

The studies involving human participants were reviewed and approved by Ethics Committee of Shandong Cancer Hospital and Institute. The patients/participants provided their written informed consent to participate in this study. The animal study was reviewed and approved by Ethics Committee of Shandong Cancer Hospital and Institute.

AUTHOR CONTRIBUTIONS

RG and XL conceived and designed the experiments. RG, YL, DL, ZW, FX, and XZ performed the experiments. RG, YL, and BZ collected clinical samples. RG and YL analyzed the data. RG, YL, and XL wrote the manuscript. All authors read and approved the final manuscript.

FUNDING

This work was supported by the National Key Research and Development Program of China (No. 2016YFE0129200), National Natural Science Foundation of China (No. 31571321), Natural Science Foundation of Shandong Province (No. ZR2019PH077 and ZR2020LZL011), Research Funds of the Shandong Provincial Key Laboratory of Animal Cell and Developmental Biology (No. SDKLACDB-2019010), and Key Scientific and Medical Project of Shandong (No. 2011QZ016 and 2016GSF201042).

REFERENCES

1. Hsieh JJ, Purdue MP, Signoretti S, Swanton C, Albiges L, Schmidinger M, et al. Renal Cell Carcinoma. *Nat Rev Dis Primers* (2017) 3:17009. doi: 10.1038/nrdp.2017.9
2. Bray F, Ferlay J, Soerjomataram I, Siegel RL, Torre LA, Jemal A. Global Cancer Statistics 2018: GLOBOCAN Estimates of Incidence and Mortality Worldwide for 36 Cancers in 185 Countries. *CA Cancer J Clin* (2018) 68:394–424. doi: 10.3322/caac.21492
3. Najjar YG, Rini BI. Novel Agents in Renal Carcinoma: A Reality Check. *Ther Adv Med Oncol* (2012) 4:183–94. doi: 10.1177/1758834012443725
4. Kucharczyk J, Mandalapu K, Satti S, Matrana MR. Outcomes of Patients With Late-Relapse Metastatic Renal Cell Carcinoma Treated With Targeted Therapies: A Single Institution Experience. *Ochsner J* (2017) 17:331–4.
5. Cho IC, Chung J. Current Status of Targeted Therapy for Advanced Renal Cell Carcinoma. *Korean J Urol* (2012) 53:217–28. doi: 10.4111/kju.2012.53.4.217
6. Yamada T, Mizuno K, Hirota K, Kon N, Wahls WP, Hartsuiker E, et al. Roles of Histone Acetylation and Chromatin Remodeling Factor in a Meiotic Recombination Hotspot. *EMBO J* (2004) 23:1792–803. doi: 10.1038/sj.emboj.7600138
7. Bannister AJ, Kouzarides T. Regulation of Chromatin by Histone Modifications. *Cell Res* (2011) 21:381–95. doi: 10.1038/cr.2011.22
8. Mosashvilli D, Kahl P, Mertens C, Holzapfel S, Rogenhofer S, Hauser S, et al. Global Histone Acetylation Levels: Prognostic Relevance in Patients With Renal Cell Carcinoma. *Cancer Sci* (2010) 101:2664–9. doi: 10.1111/j.1349-7006.2010.01717.x
9. Zhu L, Yang J, Zhao L, Yu X, Wang L, Wang F, et al. Expression of hMOF, But Not HDAC4, Is Responsible for the Global Histone H4K16 Acetylation in Gastric Carcinoma. *Int J Oncol* (2015) 46:2535–45. doi: 10.3892/ijo.2015.2956
10. Taipale M, Rea S, Richter K, Vilar A, Lichter P, Imhof A, et al. hMOF Histone Acetyltransferase Is Required for Histone H4 Lysine 16 Acetylation in Mammalian Cells. *Mol Cell Biol* (2005) 25:6798–810. doi: 10.1128/MCB.25.15.6798-6810.2005
11. Sharma GG, So S, Gupta A, Kumar R, Cayrou C, Avvakumov N, et al. MOF and Histone H4 Acetylation at Lysine 16 Are Critical for DNA Damage Response and Double-Strand Break Repair. *Mol Cell Biol* (2010) 30:3582–95. doi: 10.1128/MCB.01476-09
12. Thomas T, Dixon MP, Kueh AJ, Voss AK. Mof (MYST1 or KAT8) Is Essential for Progression of Embryonic Development Past the Blastocyst Stage and Required for Normal Chromatin Architecture. *Mol Cell Biol* (2008) 28:5093–105. doi: 10.1128/MCB.02202-07
13. Li X, Li L, Pandey R, Byun JS, Gardner K, Qin Z, et al. The Histone Acetyltransferase MOF Is a Key Regulator of the Embryonic Stem Cell Core Transcriptional Network. *Cell Stem Cell* (2012) 11:163–78. doi: 10.1016/j.stem.2012.04.023
14. Zhao L, Wang DL, Liu Y, Chen S, Sun FL. Histone Acetyltransferase hMOF Promotes S Phase Entry and Tumorigenesis in Lung Cancer. *Cell Signal* (2013) 25:1689–98. doi: 10.1016/j.cellsig.2013.04.006
15. Chen Z, Ye X, Tang N, Shen S, Li Z, Niu X, et al. The Histone Acetylranseferase hMOF Acetylates Nrf2 and Regulates Anti-Drug Responses in Human non-Small Cell Lung Cancer. *Br J Pharmacol* (2014) 171:3196–211. doi: 10.1111/bph.12661
16. Kapoor-Vazirani P, Kagey JD, Vertino PM. SUV420H2-Mediated H4K20 Trimethylation Enforces RNA Polymerase II Promoter-Proximal Pausing by Blocking hMOF-Dependent H4K16 Acetylation. *Mol Cell Biol* (2011) 31:1594–609. doi: 10.1128/MCB.00524-10
17. Pfister S, Rea S, Taipale M, Mendrzyk F, Straub B, Ittrich C, et al. The Histone Acetyltransferase hMOF Is Frequently Downregulated in Primary Breast Carcinoma and Medulloblastoma and Constitutes a Biomarker for Clinical Outcome in Medulloblastoma. *Int J Cancer* (2008) 122:1207–13. doi: 10.1002/ijc.23283
18. Cao L, Zhu L, Yang J, Su J, Ni J, Du Y, et al. Correlation of Low Expression of hMOF With Clinicopathological Features of Colorectal Carcinoma, Gastric Cancer and Renal Cell Carcinoma. *Int J Oncol* (2014) 44:1207–14. doi: 10.3892/ijo.2014.2266
19. Liu N, Zhang R, Zhao X, Su J, Bian X, Ni J, et al. A Potential Diagnostic Marker for Ovarian Cancer: Involvement of the Histone Acetyltransferase, Human Males Absent on the First. *Oncol Lett* (2013) 6:393–400. doi: 10.3892/ol.2013.1380
20. Wang Y, Zhang R, Wu D, Lu Z, Sun W, Cai Y, et al. Epigenetic Change in Kidney Tumor: Downregulation of Histone Acetyltransferase MYST1 in Human Renal Cell Carcinoma. *J Exp Clin Cancer Res* (2013) 32:8. doi: 10.1186/1756-9966-32-8
21. Chen Y, Zhu Y, Sheng Y, Xiao J, Xiao Y, Cheng N, et al. SIRT1 Downregulated FGB Expression to Inhibit RCC Tumorigenesis by Destabilizing STAT3. *Exp Cell Res* (2019) 382:111466. doi: 10.1016/j.yexcr.2019.06.011
22. Neal KC, Pannuti A, Smith ER, Lucchesi JC. A New Human Member of the MYST Family of Histone Acetyl Transferases With High Sequence Similarity to Drosophila MOF. *Biochim Biophys Acta* (2000) 1490:170–4. doi: 10.1016/s0167-4781(99)00211-0
23. Zhao X, Su J, Wang F, Liu D, Ding J, Yang Y, et al. Crosstalk Between NSL Histone Acetyltransferase and MLL/SET Complexes: NSL Complex Functions in Promoting Histone H3K4 Di-Methylation Activity by MLL/SET Complexes. *PloS Genet* (2013) 9:e1003940. doi: 10.1371/journal.pgen.1003940
24. Gupta A, Guerin-Peyrou TG, Sharma GG, Park C, Agarwal M, Ganju RK, et al. The Mammalian Ortholog of Drosophila MOF That Acetylates Histone H4 Lysine 16 Is Essential for Embryogenesis and Oncogenesis. *Mol Cell Biol* (2008) 28:397–409. doi: 10.1128/MCB.01045-07
25. Li N, Tian GW, Tang LR, Li G. hMOF Reduction Enhances Radiosensitivity Through the Homologous Recombination Pathway in non-Small-Cell Lung Cancer. *Onco Targets Ther* (2019) 12:3065–75. doi: 10.2147/OTT.S192568

26. Pote N, Cros J, Laouirem S, Raffenne J, Negrao M, Albuquerque M, et al. The Histone Acetyltransferase hMOF Promotes Vascular Invasion in Hepatocellular Carcinoma. *Liver Int* (2020) 40:956–67. doi: 10.1111/liv.14381
27. Cai M, Hu Z, Han L, Guo R. MicroRNA-572/hMOF/Sirt6 Regulates the Progression of Ovarian Cancer. *Cell Cycle* (2020) 19:2509–18. doi: 10.1080/15384101.2020.1809258
28. Shahbazian MD, Grunstein M. Functions of Site-Specific Histone Acetylation and Deacetylation. *Annu Rev Biochem* (2007) 76:75–100. doi: 10.1146/annurev.biochem.76.052705.162114
29. Noureen N, Rashid H, Kalsoom S. Identification of Type-Specific Anticancer Histone Deacetylase Inhibitors: Road to Success. *Cancer Chemother Pharmacol* (2010) 66:625–33. doi: 10.1007/s00280-010-1324-y
30. Michishita E, Park JY, Burneskis JM, Barrett JC, Horikawa I. Evolutionarily Conserved and Nonconserved Cellular Localizations and Functions of Human SIRT Proteins. *Mol Biol Cell* (2005) 16:4623–35. doi: 10.1091/mbc.e05-01-0033
31. Roth M, Chen WY. Sorting Out Functions of Sirtuins in Cancer. *Oncogene* (2014) 33:1609–20. doi: 10.1038/onc.2013.120
32. Davenport AM, Huber FM, Hoelz A. Structural and Functional Analysis of Human SIRT1. *J Mol Biol* (2014) 426:526–41. doi: 10.1016/j.jmb.2013.10.009
33. Chen C, Zhou M, Ge Y, Wang X. SIRT1 and Aging Related Signaling Pathways. *Mech Ageing Dev* (2020) 187:111215. doi: 10.1016/j.mad.2020.111215
34. Liu Y, Zhang YY, Wang SQ, Li M, Long YH, Li YF, et al. WSTF Acetylation by MOF Promotes WSTF Activities and Oncogenic Functions. *Oncogene* (2020) 39:5056–67. doi: 10.1038/s41388-020-1350-0
35. Lu L, Li L, Lv X, Wu XS, Liu DP, Liang CC. Modulations of hMOF Autoacetylation by SIRT1 Regulate hMOF Recruitment and Activities on the Chromatin. *Cell Res* (2011) 21:1182–95. doi: 10.1038/cr.2011.71
36. Zheng H, Yang L, Peng L, Izumi V, Koomen J, Seto E, et al. hMOF Acetylation of DBC1/CCAR2 Prevents Binding and Inhibition of Sirt1. *Mol Cell Biol* (2013) 33:4960–70. doi: 10.1128/MCB.00874-13
37. Ao N, Liu Y, Feng H, Bian X, Li Z, Gu B, et al. Ubiquitin-Specific Peptidase USP22 Negatively Regulates the STAT Signaling Pathway by Deubiquitinating SIRT1. *Cell Physiol Biochem* (2014) 33:1863–75. doi: 10.1159/000362964
38. Feng L, Chen M, Li Y, Li M, Hu S, Zhou B, et al. Sirt1 Deacetylates and Stabilizes P62 to Promote Hepato-Carcinogenesis. *Cell Death Dis* (2021) 12:405. doi: 10.1038/s41419-021-03666-z
39. Chung SY, Jung YY, Park IA, Kim H, Chung YR, Kim JY, et al. Oncogenic Role of SIRT1 Associated With Tumor Invasion, Lymph Node Metastasis, and Poor Disease-Free Survival in Triple Negative Breast Cancer. *Clin Exp Metastasis* (2016) 33:179–85. doi: 10.1007/s10585-015-9767-5
40. Lovaas JD, Zhu L, Chiao CY, Byles V, Faller DV, Dai Y. SIRT1 Enhances Matrix Metalloproteinase-2 Expression and Tumor Cell Invasion in Prostate Cancer Cells. *Prostate* (2013) 73:522–30. doi: 10.1002/pros.22592
41. Chung YR, Kim H, Park SY, Park IA, Jang JJ, Choe JY, et al. Distinctive Role of SIRT1 Expression on Tumor Invasion and Metastasis in Breast Cancer by Molecular Subtype. *Hum Pathol* (2015) 46:1027–35. doi: 10.1016/j.humpath.2015.03.015
42. Liu CL, Zhao D, Li JJ, Liu S, An JJ, Wang D, et al. Inhibition of Glioblastoma Progression by Urolithin A *In Vitro* and *In Vivo* by Regulating Sirt1-FOXO1 Axis *via* ERK/AKT Signaling Pathways. *Neoplasma* (2021). doi: 10.4149/neo_2021_210623N834
43. Li D, Yang Y, Chen B, Guo X, Gao S, Wang M, et al. MOF Regulates TNK2 Transcription Expression to Promote Cell Proliferation in Thyroid Cancer. *Front Pharmacol* (2020) 11:607605. doi: 10.3389/fphar.2020.607605
44. Zhang J, Liu H, Pan H, Yang Y, Huang G, Yang Y, et al. The Histone Acetyltransferase hMOF Suppresses Hepatocellular Carcinoma Growth. *Biochem Biophys Res Commun* (2014) 452:575–80. doi: 10.1016/j.bbrc.2014.08.122

Conflict of Interest: The authors declare that the research was conducted in the absence of any commercial or financial relationships that could be construed as a potential conflict of interest.

Publisher's Note: All claims expressed in this article are solely those of the authors and do not necessarily represent those of their affiliated organizations, or those of the publisher, the editors and the reviewers. Any product that may be evaluated in this article, or claim that may be made by its manufacturer, is not guaranteed or endorsed by the publisher.

Copyright © 2022 Guo, Liang, Zou, Li, Wu, Xie, Zhang and Li. This is an open-access article distributed under the terms of the Creative Commons Attribution License (CC BY). The use, distribution or reproduction in other forums is permitted, provided the original author(s) and the copyright owner(s) are credited and that the original publication in this journal is cited, in accordance with accepted academic practice. No use, distribution or reproduction is permitted which does not comply with these terms.

frontiers
in Pharmacology

ORIGINAL RESEARCH
published: 21 February 2022
doi: 10.3389/fphar.2022.833077

Albuca Bracteata Polysaccharides Attenuate AOM/DSS Induced Colon Tumorigenesis via Regulating Oxidative Stress, Inflammation and Gut Microbiota in Mice

Ziyan Qin[1†], Xinyu Yuan[1†], Jian Liu[2], Zhuqing Shi[1], Leipeng Cao[1], Lexuan Yang[3], Kai Wu[4], Yongliang Lou[1], Haibin Tong[2]*, Lei Jiang[3]* and Jimei Du[1]*

[1]Department of Microbiology and Immunology, School of Laboratory Medicine, Wenzhou Medical University, Wenzhou Key Laboratory of Sanitary Microbiology, Wenzhou, China, [2]College of Life and Environmental Science, Wenzhou University, Wenzhou, China, [3]Central Laboratory, School of the First Clinical Medicine and the First Affiliated Hospital of Wenzhou Medical University, Wenzhou, China, [4]Laboratory Animal Center, Wenzhou Medical University, Wenzhou, China

OPEN ACCESS

Edited by:
Dong-Hua Yang,
St. John's University, United States

Reviewed by:
Lingzhi Li,
University of Texas MD Anderson Cancer Center, United States
Peng Song,
Lanzhou University, China
Hossein Fahimi,
Islamic Azad University of Medical Sciences, Iran

****Correspondence:***
Haibin Tong
tonghaibin@gmail.com
Lei Jiang
jiangleistone79@163.com
Jimei Du
djm@wmu.edu.cn

†These authors share first authorship

Specialty section:
This article was submitted to Experimental Pharmacology and Drug Discovery, a section of the journal Frontiers in Pharmacology

Received: *10 December 2021*
Accepted: *11 January 2022*
Published: *21 February 2022*

Citation:
Qin Z, Yuan X, Liu J, Shi Z, Cao L, Yang L, Wu K, Lou Y, Tong H, Jiang L and Du J (2022) Albuca Bracteata Polysaccharides Attenuate AOM/DSS Induced Colon Tumorigenesis via Regulating Oxidative Stress, Inflammation and Gut Microbiota in Mice.
Front. Pharmacol. 13:833077.
doi: 10.3389/fphar.2022.833077

Inflammation is an important risk factor in the development of inflammatory bowel disease (IBD) and colitis-associated colorectal cancer (CAC). Accumulating evidence indicates that some phytochemicals have anti-cancer properties. Polysaccharides extracted from Albuca bracteata (AB) have been reported to possess anti-neoplastic activities on colorectal cancer (CRC) models. However, it is still unclear whether they exert therapeutic effects on colorectal cancer. In this study, we investigate the properties of polysaccharides of A. bracteate, named ABP. The average molecular weight of ABP was 18.3 kDa and ABP consisted of glucose, mannose, galactose, xylose, galacturonic acid, glucuronic acid at a molar ratio of 37.8:8:2.5:1.7:1:1. An Azoxymethane/Dextran sodium sulfate (AOM/DSS) induced CAC mouse model was established. The CAC mice treated with ABP showed smaller tumor size and lower tumor incidence than untreated ones. ABP increased anti-inflammatory cytokine IL-10, inhibited secretion of pro-inflammatory cytokines (IL-6, IFN-γ, and TNF-α), mitigated oxidative stress by increasing GSH and decreasing MDA levels, suppressed the activation of STAT3 and expressions of its related genes c-Myc and cyclin D1. Moreover, ABP treatment increased the relative abundance of beneficial bacteria (*f*_Ruminococcaceae, *g_Roseburia, g_Odoribacter, g_Oscillospira,* and *g_Akkermansia*) and the levels of fecal short-chain fatty acid (SCFA) in CAC model mice. In summary, our data suggest that ABP could be a potential therapeutic agent for treating CAC.

Keywords: colitis-associated colorectal cancer, CAC, polysaccharides, anti-inflammation, anti-oxidant, anti-tumor, gut microbiota, short-chain fatty acid

INTRODUCTION

Colorectal cancer (CRC) is the third most common cause of tumor-related death worldwide (Siegel et al., 2021). Accumulating evidence reveals that inflammation is a vital factor that contributes to CRC development and growth, and inflammatory bowel disease (IBD) is a known risk factor for colitis-associated colorectal cancer (CAC) (Ullman and Itzkowitz, 2011; Robles et al., 2016). The Azoxymethane/Dextran sodium sulfate (AOM/DSS) mouse model is commonly used for studying colitis-related carcinogenesis and cancer-preventive intervention. Application of the AOM/DSS model has been used to unravel the pathogenesis of CAC from the perspectives of signaling pathways (Fukata et al., 2007; Grivennikov et al., 2009), anti-oxidant machinery (Barrett et al., 2013) and the influence of gut microbiota (Uronis et al., 2009).

CAC development is closely associated with gut flora (Kang and Martin, 2017), and the gut microbiota of CAC is altered with decreased probiotic bacteria (Li et al., 2019) concurrently with enriched pathogenic and opportunistic bacteria (Chattopadhyay et al., 2021). Dysbiosis of gut microbiota increases intestinal permeability, allowing microbial products and microbes to translocate from intestinal lumen to mucosa. After recognizing microbes *via* the Toll-like receptor, intestinal immune cells and epithelial cells activate downstream molecules of inflammatory signaling pathways, including STAT3 (Waldner and Neurath, 2015). The transcriptional activity of STAT3 involves multiple cellular processes, such as cell survival, proliferation, angiogenesis, and immune evasion (Yu et al., 2009; Yu et al., 2014). Accumulation of pathogenic bacteria ultimately provides a proinflammatory environment that favors tumor promotion (Papapietro et al., 2013). While probiotics like *Lactobacillus* or *Bifidobacterium* exerts anti-cancer roles by inhibiting inflammation and angiogenesis, and modulating the intestinal barrier function by generating short-chain fatty acids (SCFAs) (Zhong et al., 2014). Numerous studies have indicated that gut microbiota plays a critical role in host metabolism and immune system development. Thus, regulating the balance of gut microbiota may be therapeutically viable and promising for IBD and CAC treatment (Song et al., 2018).

Polysaccharides have attracted increasing attention for their therapeutic activity in cancer treatment with few side effects. Several polysaccharides have been used to prevent and treat CAC (Sanders et al., 2016; Ji et al., 2018). Studies have shown that polysaccharides attenuate intestinal mucositis with immunomodulatory, various pharmacological effects and anti-neoplastic effects (Liu et al., 2018b; Ren et al., 2018). Zou et al. reported that *Ficus carica* polysaccharides elevated the expression of tight junction protein Claudin-1 and inhibited the formation of cytokines (TNF-α and IL-1β) to prevent DSS-induced colitis in C57BL/6J mice (Zou et al., 2020). Liu et al. reported that tea polysaccharides inhibited colon tumorigenesis in mice by regulating signaling pathways (Liu et al., 2018c).

Albuca bracteata (Thunb.) J.C.Manning and *Goldblatt* (AB) has long been cultivated in China and used as an herbal remedy for diabetes, hepatitis, cancers, and other diseases (Zhang et al., 2017). In many parts of China, particularly in the southeast region, bulbs of AB are commonly used as a dietary therapy for improving anti-tumor immunity and relieving tumor-induced pain or side effects of chemotherapy. In a previous study (Yuan et al., 2021), ABP showed anti-tumor effects on a homograft CRC mouse model, indicating that ABP may be a potential anti-tumor therapeutic agent for treating CRC. However, it is still unclear whether ABP exert therapeutic effects on CAC.

In this study, the molecular composition of ABP was analyzed, and treatment effects and potential mechanisms of ABP against tumor were explored in an AOM/DSS-induced CAC mice model. The results showed that ABP exhibited various bio-activities, including anti-inflammation, anti-oxidant, regulating gut microbiota, and anti-tumor effects. ABP could be a valuable therapeutic agent for CAC and a good candidate for agents in medicine and functional foods.

MATERIALS AND METHODS

Extraction of ABP

ABP was extracted and purified as previously described by Chen et al. (Chen et al., 2012) with minor modifications. Briefly, bulbs of AB were washed and sliced into small pieces, dried at 60°C for 48 h and then ground in a high-speed disintegrator. The dried AB powder (particle size: 0.6 mm) was soaked overnight in 95% ethanol at a ratio of 1:10 (weight/volume) to remove oligosaccharides, small molecule chemicals and colored materials. Then the pretreated powder was oven-dried at 60°C overnight. The powder was extracted with distilled water for 3 h using the Soxhlet apparatus at 95°C, and the extracts were collected, filtrated, and concentrated using a rotary evaporator. ABP was precipitated by adding ethanol to the final concentration of 75% by volume, and the ABP was collected after centrifugation and dried under nitrogen gas flow.

Analysis of Chemical Compositions

The total carbohydrate content of ABP was determined by the phenol sulfuric acid method (Liu et al., 2020). The uronic acid content was quantified *via* the *m*-hydroxydiphenyl method as previously described by Liu et al. (2021b) using D-glucuronic acid as the standard. The protein content was measured using Bradford's method (Wu et al., 2019). The characteristics of chemical groups and bonds in ABP were determined using the Fourier transform-infrared (FT-IR) spectroscopy (BRUKER Tensor 27, Ettlingen, Germany) and KB-disk method and recorded in the frequency range of 4,000–500 cm^{-1}.

Molecular Weight of ABP

The average molecular weight (Mw) of ABP was measured via high-performance gel-permeation chromatography (HPGPC) using an Agilent 1,260 Infinity II HPLC system, equipped with a TSK-GEL G4000 PW_{XL} column (Φ7.8 mm × 300 mm, TOSOH, Japan) and the Agilent 1260-RID detector, eluted with Na_2SO_4 solution (0.1 M). A standard curve of molecular weight was established using Dextran standards (180 Da, 4.6 kDa, 7.1 kDa, 21.4 kDa, 41.1 kDa, 150 kDa, and 2000 kDa).

Monosaccharide Composition

The monosaccharide composition of ABP was analyzed based on a previously described method (Wu et al., 2019) with some modifications. Briefly, the sample ABP was hydrolyzed in trifluoroacetic acid (2 M) at 120°C for 3 h. The filtered hydrolysate was analyzed by an Agilent 1,260 Infinity II HPLC system equipped with a Hypersil ODS-2 column (5 μm, 4.6 mm ×

250 mm) and Agilent 1260-DAD detector. The optimal analysis conditions were set as follows. The eluent was 0.05 M phosphate buffer solution (pH 6.8) and acetonitrile (83:17, v/v), the flow rate was 0.8 ml/min, injection volume was 10 μl, monitored absorbance was 254 nm.

Animal Studies

Animal experiments were performed according to protocols approved by the Institutional Animal Care and Use Committee of Wenzhou Medical University (wydw 2021–0224). Female BALB/c mice (4–5 weeks old) purchased from Laboratory Animal Center of Wenzhou Medical University were randomly divided into four groups: the normal group, A/D group (AOM/DSS), ABP-L group (AOM/DSS +0.5 mg/ml ABP), and ABP-H group (AOM/DSS +1 mg/ml ABP). On the first day of the experiment, mice in the A/D, ABP-L, and ABP-H groups received an intraperitoneal injection of AOM (10 mg/kg), while those in the normal group received physiological saline. After the administration of sterile water for 1 week, 2% DSS was added into the drinking water of the A/D, ABP-L, and ABP-H groups for another week, followed by sterile drinking water for 2 weeks. This DSS water cycle was repeated thrice. Mice in the normal group received sterile water throughout the study. Once the DSS cycles finished, mice in the ABP-L and ABP-H groups received ABP (0.2 ml/per mice) *via* oral gavage for 11 weeks, while those in the A/D group received an equivalent volume of sterile drinking water. During the experiment, body weight of all mice was recorded. Mice were sacrificed using anesthesia, and colorectal tissue, mucosa, fecal and serum of individual mouse were collected after three or 11 weeks of treatment. Serum was used for ELISA experiments, fecal was used for the analysis of SCFAs, colon mucosa was used for 16S rRNA gene sequencing. A portion of colon tissue fixed in 4% paraformaldehyde was prepared for hematoxylin-eosin (HE) staining, and the other portion was stored at -80°C for subsequent GSH, MDA and Western blot assays.

Western Blot

Western blots were performed as described before (Luo et al., 2021). The primary antibodies used were as follows: anti-Cyclin D1 (#ab40754, Abcam, Cambridge, MA, United States), anti-c-Myc (#ab32072, Abcam, Cambridge, MA, United States), anti-P-STAT3 (#9145, Cell Signaling Technology, Danvers, MA,United States), anti-STAT3 (#12640, Cell Signaling Technology, Danvers, MA,United States), anti-COX-2 (#AF7003, Affinity Biosciences, Cincinnati, OH, United States), and anti-GAPDH (#5174, Cell Signaling Technology, Danvers, MA,United States).

16S rRNA Gene Sequencing and Microbiome Analysis

Samples were collected, and total genomic DNA was extracted as described previously (Zhang et al., 2020; Lou et al., 2021). Bacterial sequencing of 16S rRNA genes was performed with the Illumina HiSeq6000 platform (Hangzhou Guhe Information and Technology Co., Ltd., Zhejiang, China). Mcirobiome analysis was done using Quantitative Insights Into Microbial Ecology (QIIME2, V.2020.6) pipeline, PICRUSt and the Statistical Analysis of Metagenomic Profiles (STAMP) software package V.2.1.3 as described previously (Lou et al., 2021).

Analysis of Short-Chain Fatty Acid in Feces

The quantitative analysis of fecal SCFAs was determined by a trace ultra gas chromatograph coupled with an ISQ mass spectrometer (TRACE 1310-ISQ, Thermo, MA, United States). Briefly, fecal samples were homogenized with 50 μl of 15% phosphoric acid, 100 mg of glass beads, and 100 μl of isocaproic acid as the internal standard for 10 min using a vortex mixer. After acidification, 400 μl of diethyl ether was added to each sample for SCFAs extraction, and then centrifuged the mix for 10 min at 12,000 rpm (4°C). The levels of SCFAs were quantitatively determined by the GC-MS (gas chromatography–mass spectrometry). The GC-MS analysis was performed by a trace ultra GC equipped with an HP-Innowax MS capillary column (30 m × 0.25 mm × 0.5 μm film thickness, Agilent Technologies). Temperature of injector, ion source quadrupole, the GC-MS interface was 250°C, 230°C, 150°C, and 250°C, respectively. The flow rate of helium carrier gas was kept at 1.0 ml/min. Samples were injected (1 μl) with a split injection (split ratio: 10:1). The initial column temperature was 90°C, increased to 120°C at the rate of 10°C/min, then elevated at a rate of 5°C/min to 150°C, and finally increased to 250°C at a rate of 25°C/min and held for 2 min. The mass spectrometer was used in electron impact (EI) ionization mode (70 eV).

Determination of Reduced Glutathione (GSH) and Malondialdehyde (MDA)

Reduced glutathione (GSH) and malondialdehyde (MDA) were performed to evaluate oxidative stress. GSH was measured by using the GSH assay kit (A006, Nanjing Jiancheng Bioengineering Institute, Nanjing, China) and MDA by MDA assay kit (A003, Nanjing Jiancheng Bioengineering Institute, Nanjing, China). Assays were carried out according to the manufacturer's instructions.

Hematoxylin-Eosin Staining and Histological Analysis

Hematoxylin and eosin (HE) staining was performed for histological observation. Colon tissues were paraffin-embedded, dewaxed, rehydrated, and stained with HE. The staining was performed as described previously (Zhu et al., 2021). The histological score of each mouse was record and values ranged from 0 to 10 according to the extent of colon injury. The scoring criteria were presented in **Supplementary Table S2**.

Measurement of Cytokine Levels

Serum cytokines were measured and quantified with the Mouse IL-6 ELISA Kit (Catalogue Number: SU-B20012, Konodee Biotechnology Co., Fujian., China), Mouse IL-10 ELISA Kit (Catalogue Number: SU-B20005, Konodee Biotechnology Co.,

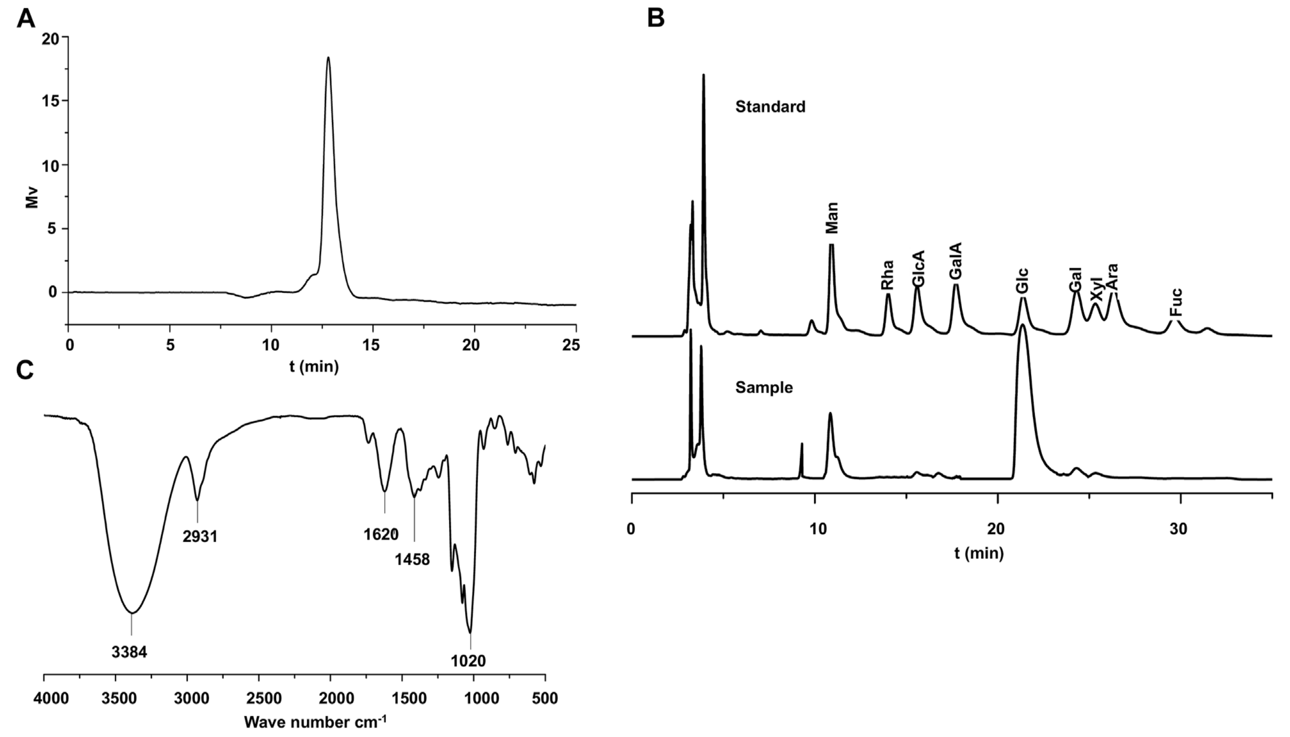

FIGURE 1 | Chemical Composition of ABP. **(A)** HP-GPC profiling of ABP.**(B)** Liquid chromatogram of standard monosaccharide derivatives and liquid chromatogram of hydrolyzed monosaccharide derivatives of ABP. **(C)** FT-IR spectrum of ABP.

Fujian., China), Mouse TNF-α ELISA Kit (Catalogue Number: SU-B20220, Konodee Biotechnology Co., Fujian., China) and Mouse IFN-γ ELISA Kit (Catalogue Number: SU-B20652, Konodee Biotechnology Co., Fujian., China), according to the manufactures instructions.

Statistical Analysis

Data were presented as means ± standard deviation (SD) or median. Normally distributed data were analyzed by student's *t*-test, non-normal distributed data were analyzed using the Kruskal–Wallis test (SPSS 23.0, SPSS Company, Inc., United States). The threshold for significance was $p < 0.05$.

RESULTS

Chemical Composition of ABP

The total carbohydrate, uronic acid, and protein contents of ABP were 92.58%, 1.63%, and 1.70%, respectively (**Tabel S1**). Dextran standards with the molecular weight from 180 Da to 2,000 kDa were applied onto an HPLC system to calibrate the column. According to the standard curve Log(Mw) = 2.35–0.421 t_R (Mw is the average molecular weight, t_R is the retention time, correlation coefficient $R^2 = 0.997$), the Mw of ABP was 18.3 kDa, and the HPGPC profile of ABP (**Figure 1A**) showed a single and symmetrically sharp peak, indicating that ABP was a homogeneous polysaccharide. The composition of component monosaccharides is an important parameter for assessing polysaccharide characteristics. According to the HPLC analysis with a PMP (1-phenyl-3-methyl-5-pyrazolone) pre-column derivatization method, the monosaccharide compositions of ABP were shown in **Figure 1B** and **Supplementary Table S1**. Overall, the data indicated that ABP was a hetero-polysaccharide composed of glucose, mannose, galactose, xylose, galacturonic acid, glucuronic acid in a ratio of 37.8: 8: 2.5: 1.7: 1: 1. Glucose is the major monosaccharide. The FT-IR spectrum of ABP (**Figure 1C**) showed intense absorption peaks at 3,384 cm^{-1} for O-H stretching vibration (Li et al., 2017; Su and Li, 2020) and 2,931 cm^{-1} for C-H stretching vibration (Wang et al., 2012; Hashemifesharaki et al., 2020; Ma et al., 2020). The absorption peak at 1,620 cm^{-1} and 1,458 cm^{-1} were the characteristic absorption peaks of C=O (Cao et al., 2018; Zeng et al., 2020) and C-H groups (Sun et al., 2013; Meng et al., 2017). Furthermore, the peak at 1,020 cm^{-1} corresponded to the stretching vibration of C-O groups (Biao et al., 2020; Hu et al., 2020).

ABP Treatment Ameliorated AOM/DSS Induced Weight Loss and Colonic Damage

An AOM/DSS-induced CAC model was established to determine the anti-tumor effect of ABP on CAC mice (**Figure 2A**). At the end of ABP treatment, compared with the A/D group (18.0 ± 5.788), the ABP-L group (11 ± 3.536, $p < 0.05$) and ABP-H group (6.6 ± 4.099, $p < 0.01$) demonstrated a significant reduction in the number of tumors (**Figures 2B,C**). Treatment with ABP also alleviated the shortening of the colon (**Figure 2D**, ABP-L, $p < 0.01$, ABP-H, $p < 0.001$) and weight loss (**Figure 2E**). Colon tissue

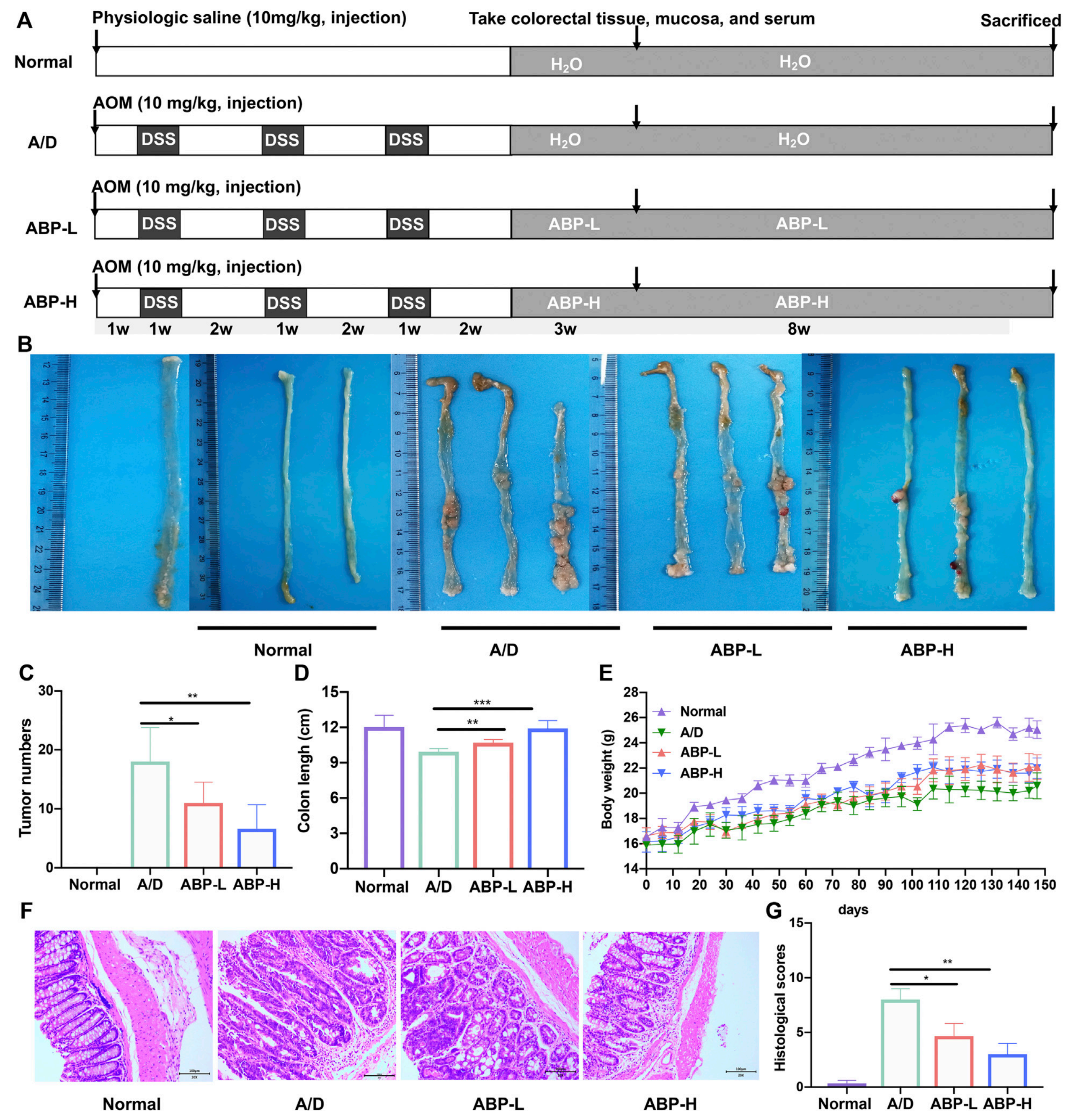

FIGURE 2 | ABP treatment ameliorated weight loss and AOM/DSS-induced pathological damage of colon. **(A)** The overview of the animal experiment design. **(B-C)** Colon tumor burden in each group. **(D)** Colon lengths of mice in each group. **(E)** Body weights of mice in each group. **(F)** Micrographs of HE-stained colon tissues in11 weeks treatment group. **(G)** Histological scores of each group. Compared with the A/D group, **p* < 0.05, ***p* < 0.01.

sections in the A/D group showed noticeable pathological changes, including colonic epithelial cell destruction, loss of goblet cells, and varying degrees of inflammatory cell infiltration, whereas those of ABP treatment groups displayed a remarkable reduction in symptoms (**Figures 2F,G, Supplementary Table S2**). These results indicated that intervention with ABP ameliorated weight loss, clinical signs of inflammation and tumor development in AOM/DSS-induced CAC mice.

To evaluate the effect of long-term oral consumption of ABP on the general health of mice, we introduced a group of ABP alone. Results indicated that long-term consumption of ABP did not lead to shortening of the colon (**Supplementary Figure S1A, B**), loss of body weight (**Supplementary Figure S1C**), and

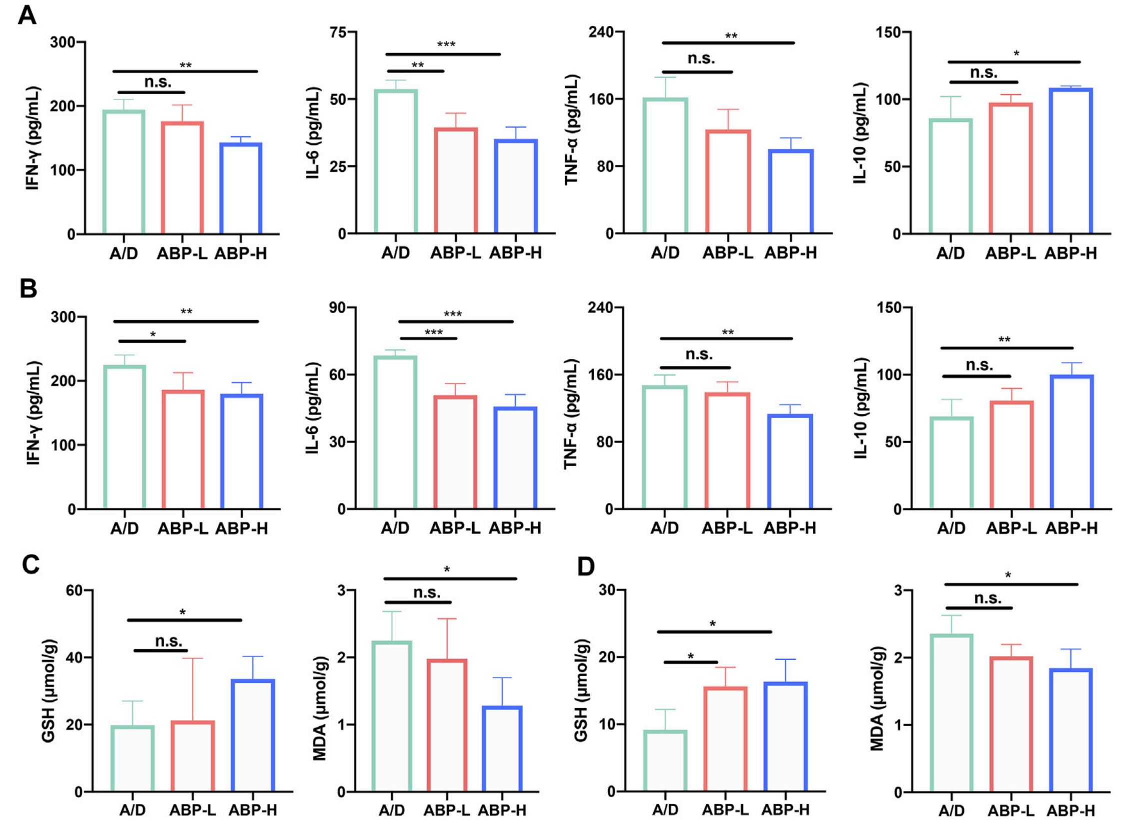

FIGURE 3 | ABP treatment attenuated the production of oxide- and inflammatory-cytokines of AOM/DSS-induced CAC mice. **(A-B)** Leves of IL-6, TNF-α, IFN-γ, IL-10 in serum of mice treated with ABP for 3 weeks **(A)** and 11 weeks **(B)**. **(C-D)** Levels of MDA and GSH in colon tissue treated with ABP for 3 weeks **(C)** and 11 weeks **(D)**. Compared with the A/D group, $^{*}p < 0.05$, $^{**}p < 0.01$.

pathological changes in the colon (**Supplementary Figure S1D**). Besides, no side effects were observed in the long-term use of ABP.

ABP Treatment Attenuated the Production of Oxide- and Inflammatory- Cytokines in AOM/DSS-Induced CAC Mice

Because inflammation and oxidative stress might lead to cancer progression, serum levels of inflammatory cytokines and oxidative stress indicators of the colon in CAC mice treated with ABP for three or 11 weeks were detected by ELISA assays and commercial kits. At 3 weeks, the level of pro-inflammatory cytokines TNF-α, IFN-γ, and IL-6 decreased while the anti-inflammatory cytokine IL-10 increased in ABP treatment groups (**Figure 3A**). A similar phenomenon was also observed at 11 weeks (**Figure 3B**). An increased level of GSH and decreased level of MDA in the colon were observed in the mice of ABP treatment groups both in 3 weeks (**Figure 3C**) and 11 weeks of treatment (**Figure 3D**). These data implied that ABP might in favor of reducing the occurrence and development of CAC by suppressing pro-inflammatory-related cytokines, upregulating anti-inflammatory cytokines, and reducing oxidative damages.

ABP Treatment Suppressed the Activation of STAT3 in the Colonic Tissue of AOM/DSS-Induced CAC Mice

To gain more insights into the regulatory role of ABP in anti-inflammation, we examined proteins related to the IL-6/STAT3 signaling pathway (**Figures 4A,B**) by Western Blot. It was found that, both in 3 and 11 consecutive weeks of treatment (**Figures 4C,D**), expressions of P-STAT3, Cyclin D1 and c-Myc were inhibited in ABP treated groups and COX-2 in ABP-H groups. The expression of COX-2 decreased in the 11 consecutive weeks of ABP-L treatment, while no similar trend was found in the 3-weeks group. These results indicated that ABP treatment might regulate expressions of P-STAT3, c-Myc, and Cyclin D1 in CAC mice, suppress the activation of the IL-6/STAT3 signaling pathway and reduce the inflammatory response.

ABP Treatment Regulated the Intestinal Microflora of AOM/DSS Induced CAC Mice

To reveal ABP treatment effects on gut microbiota composition of AOM/DSS induced CAC mice, 16S rRNA gene sequencing was performed on colon mucosal samples. The gut microbiota

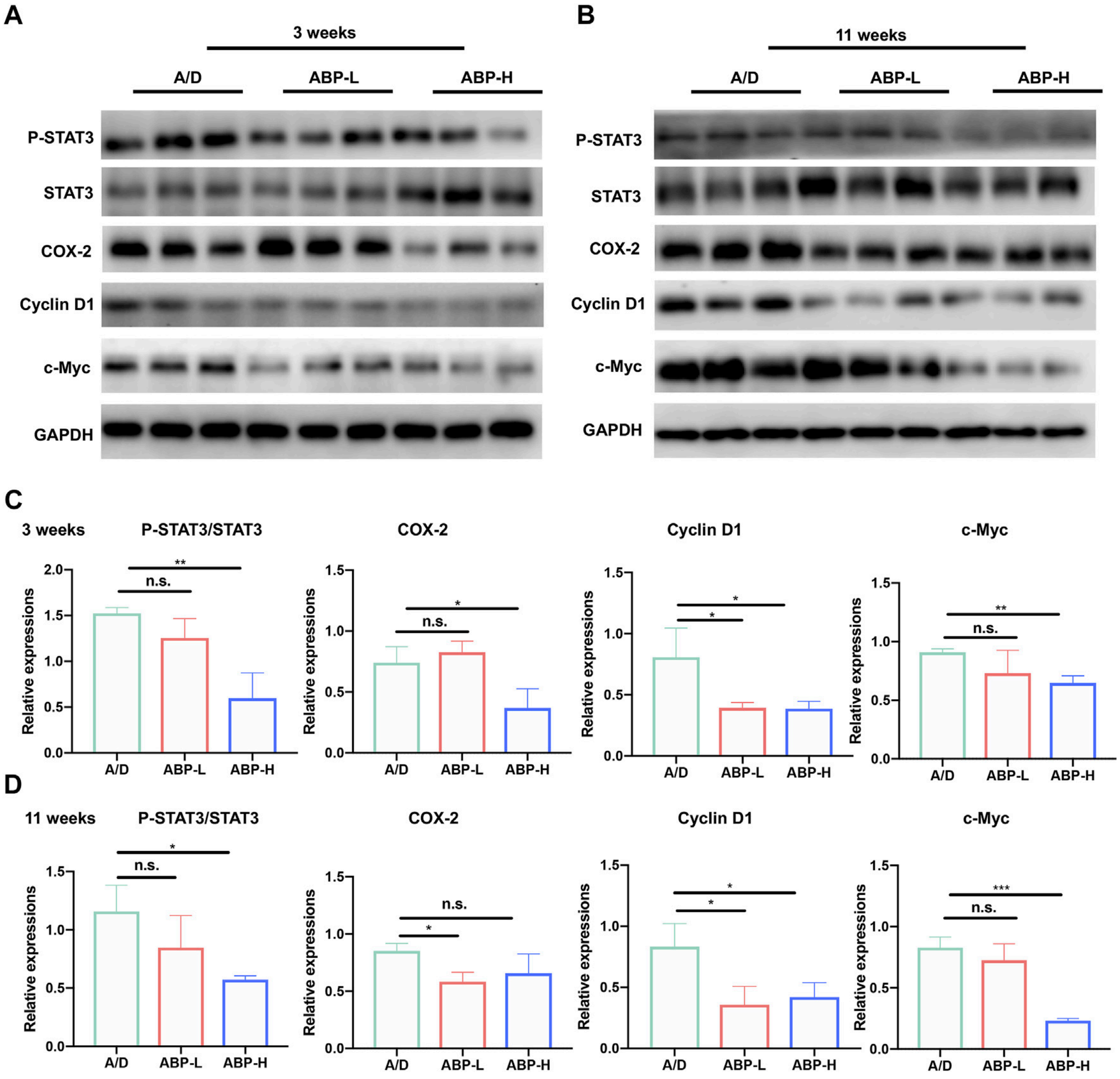

FIGURE 4 | ABP treatment suppressed the activation of STAT3 in the colonic tissue in AOM/DSS-induced CAC mice. **(A-B)** Western blotting of STAT3, P-STAT3, COX-2, Cyclin D1, c-Myc and GAPDH in colon tissue treated with ABP for 3 weeks **(A)** and 11 weeks **(B)**. **(C-D)** P-STAT3 protein expression relative to STAT3. COX-2, c-Myc and Cyclin D1 protein expressions relative to GAPDH in colon tissues treated with ABP for 3 weeks **(C)** and 11 weeks **(D)**. Compared with the A/D group, $^*p < 0.05$, $^{**}p < 0.01$.

diversity and richness were evaluated by Chao1, Shannon, and Simpson indexes.

No significant change was found among all groups' alpha diversity, no matter treated for 3 weeks or 11 weeks (**Figures 5A–C**, **Supplementary Figures S2A, B**). The principal coordinates analysis (PCoA) showed an obscure difference between the A/D and ABP groups treated for 3 weeks (**Supplementary Figures S2C, D**). Compared to the A/D group, the PCoA results showed an apparent difference in the normal group (**Figure 5D**, $p = 0.043$) and the ABP-H group (**Figure 5E**, $p = 0.024$) treated for 11 weeks, showed no difference between the ABP-L group and the A/D group (**Figure 5F**). These results indicated that ABP might influence the intestinal flora composition, and adequate treatment of ABP was required to improve microbiota in CAC mice.

To clarify the effects of ABP on the microflora of CAC model mice, the community composition of each group was analyzed at the phylum, family, and genus levels. The heatmap showed that (**Supplementary Figures S3A–C**) *g_Lysinibacillus, g_Streptococcus, g_Acinetobacter, g_Gordonia, g_Ochrobactrum, g_Halomonas, and g_Ralstonia* were enriched in the A/D group, while *f_*Rikenellaceae and *g_Turicibacter* were enriched in the ABP-L group treated for 3weeks, *g_Ruminococcus_, g_Enterococcus, g_Odoribacter* and *g_Dehalobacterium* were enriched in the ABP-H group. In the 11-week treatment groups, the heatmap showed that (**Figures 6A–C**) some potential pathogenic bacteria (*g_Ralstonia*, *g_Proteus*, *g_Adlercreutzia*, and *g_Streptococcus*) enriched in the A/D group, while some beneficial bacteria enriched in the ABP-L group (*p_Verrucomicrobia*, *g_Ruminococcus_*, *g_Roseburia*) and the ABP-H group (*f_*Ruminococcaceae, *g_Oscillospira*, *g_Odoribacter*, *g_Coprococcus*).

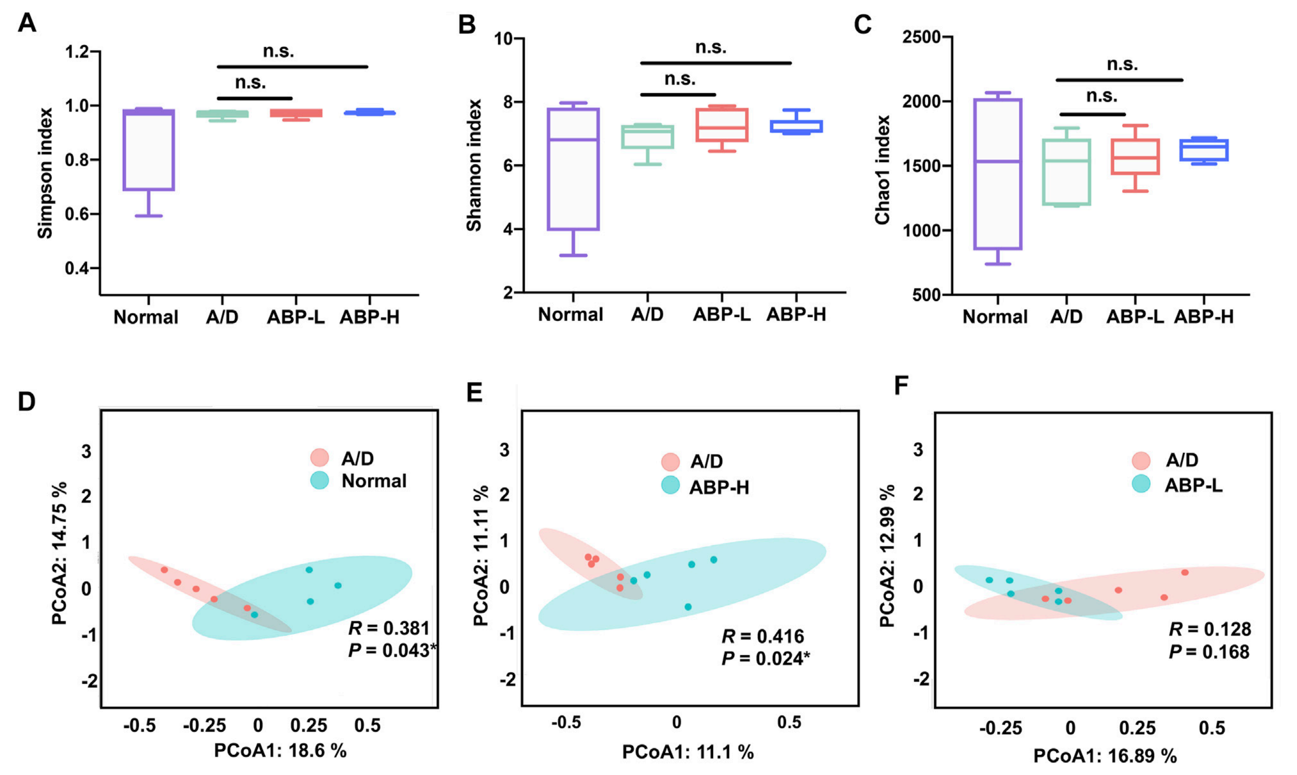

FIGURE 5 | ABP treatment altered the abundance and diversity of gut microbes in AOM/DSS-induced CAC mice (treatment with ABP for 11 weeks). **(A-C)** Analysis of alpha diversity; **(A)** Simpson index. **(B)** Shannon index. **(C)** Chao1 index. **(D-F)** Analysis of beta diversity. principal coordinates analysis (PCoA).

Differences among groups at family and genus level were also analyzed by liner discriminate analysis (LDA), effect size measurements (LEfSe) and the Kruskal Wallis test (**Figures 7A,B**, **Supplementary Figures S4A, B**). The ABP-L group treated for 3 weeks (**Supplementary Figure S4C**) had higher relative abundance of some bacteria (*g_Turicibacter*, $p < 0.01$; *g_AF12*, $p < 0.01$) and lower opportunistic pathogens (*g_Streptococcus*, $p < 0.001$; *g_Ralstonia*, $p < 0.01$; *g_Corynebacterium*, $p < 0.05$). The ABP-H group had a higher relative abundance of *g_Odoribacter* ($p < 0.01$) *and g_AF12* ($p < 0.05$), and a less relative abundance of *g_Streptococcus* ($p < 0.05$). The ABP-L group (**Figure 7C**) treated for 11 weeks had enriched probiotics (*g_Roseburia*, $p < 0.05$, *g_Akkermansia*, $p < 0.01$), decreased potential pathogenic and inflammation-promoting bacteria (*g_Corynebacterium*, $p < 0.01$; *g_Anaeroplasma*, $p < 0.01$). The ABP-H group had much higher relative abundance of *f*_Ruminococcaceae ($p < 0.01$) and *g_Oscillospira* ($p < 0.05$), but less abundance of CAC related bacteria that were enriched in the A/D group (*f_S24-7*, $p < 0.05$; *f*_Coriobacteriaceae, $p < 0.01$; *f*_Prevotellaceae, $p < 0.05$; *g_Bacteroides*, $p < 0.01$; *g_Adlercreutzia*, $p < 0.01$; *g_Proteus*, $p < 0.05$ and *g_Anaeroplasma*, $p < 0.05$).

We also focused on changes of certain bacteria over time. As shown in **Supplementary Figure S5**, along with the extension of time, the relative abundance of *f_S24-7*, *g_Streptococcus*, *g_Acinetobacter*, *g_Anaeroplasma* increased in the A/D group. ABP treatment decreased the relative abundance of the four bacteria, increased the relative abundance of *g_Odoribacter*, *f*_Ruminococcaceae, *g_Oscillospira*, *g_Coprococcus* gradually. These data proved that ABP might ameliorate gut microbiota dysbiosis, elevate beneficial bacteria levels, and downregulate certain pathogenic bacteria levels in AOM/DSS-induced CAC mice.

ABP Treatment Improved Fecal SCFA Levels of AOM/DSS Induced CAC Mice

The effect of ABP treatment on the metabolism of the intestinal tract was assessed by fecal SCFAs measurement and analysis. PLS-DA and PCoA analysis showed a clear difference between the ABP-H and A/D groups (**Figures 8A,B**). As shown in **Figure 8C**, mice in the ABP-H group had a higher concentration of total SCFAs ($p < 0.01$) and individual acetic acid ($p < 0.001$), propionic acid ($p < 0.01$), and valeric acid ($p < 0.05$) than those of the A/D group. These data indicated that ABP could significantly increase the production of SCFAs in mice. The changes in fecal SCFA levels of mice treated with ABP were consistent with the altered composition of the intestinal microbiome.

DISCUSSION

In mice, colitis induced by DSS is characterized by colon mucosal inflammation accompanied by shortening of the

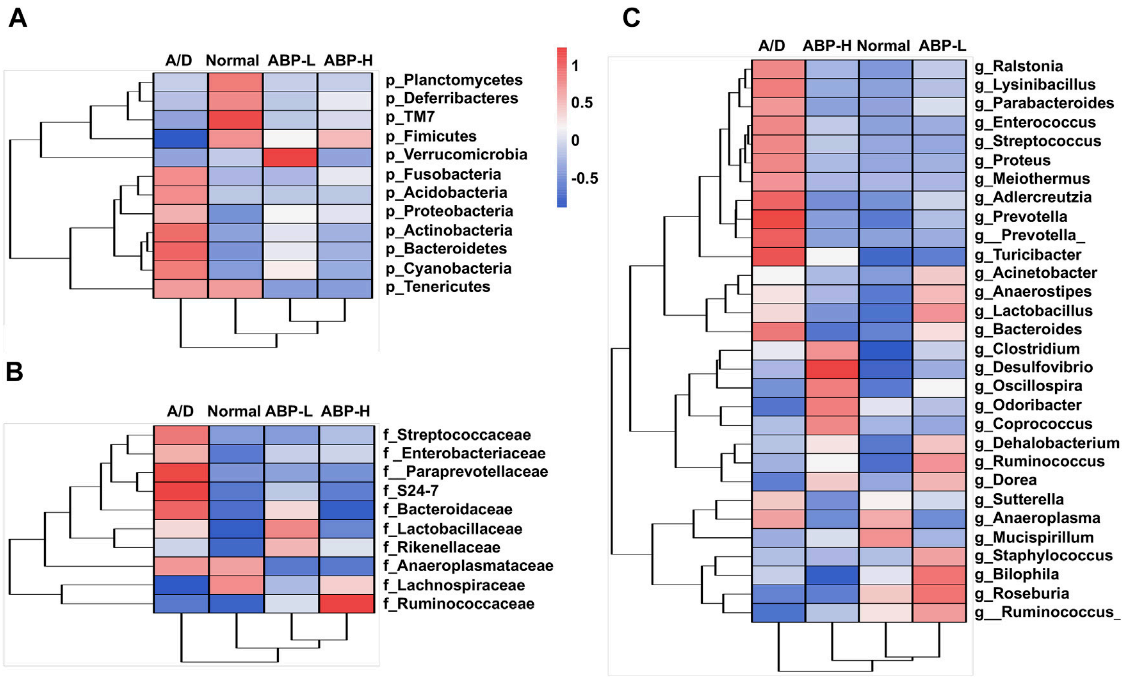

FIGURE 6 | ABP treatment improved the composition of the intestinal microflora in AOM/DSS-induced CAC mice (treatment with ABP for 11 weeks). **(A-C)** Heatmap of bacterial taxa based at the phylum, family and genus levels.

colorectum and body weight loss (Matsunaga et al., 2021). Current research has focused on using natural substances with low toxicity and few side effects on normal cells or organs to offer alternative anti-inflammation and anti-tumor therapies (Giner et al., 2016). Some polysaccharides, such as *Hericium Erinaceus* polysaccharide and *Astragalus* polysaccharide, have been reported to alleviate ulcerative colitis development by suppressing inflammatory cytokines and regulating gut microbiota in animals (Zhao et al., 2016; Ren et al., 2018).

Phytochemical analysis revealed that AB had various components with bio-active properties, such as saponins, flavonoids, polysaccharides, etc. that exhibit anti-oxidant, anti-inflammatory, anti-diabetic, and anti-neoplastic effects (Zhou et al., 2005; Iguchi et al., 2017). In this study, AB was farmed by ourselves and ABP was extracted from bulbs of AB. At first, we determined the Mw, monosaccharide composition and FT-IR spectrum of ABP and the results showed that ABP was a homogeneous polysaccharide with an Mw of 18.3 kDa and mainly composed of glucose, mannose, galactose, and xylose. Next, we confirmed that ABP had antioxidant and anti-inflammatory properties *in vivo*, and ABP treatment could effectively inhibit tumorigenesis and progression by attenuating colon shortening, body weight loss, and histological damages in AOM/DSS induced CAC mice.

Furthermore, we explored the probable mechanisms of ABP against CAC. TNF-α and IL-6 are pro-inflammatory cytokines that play important roles in the process of inflammation (Francescone et al., 2015). The production of these cytokines is regulated by signaling pathways such as the STAT3 pathway. The STAT3 transcription factor induces the expression of cell proliferation related genes (cyclin D1, PCNA) and suppresses apoptotic genes (Bcl-2, Bcl-XL) (Becker et al., 2005; Klampfer, 2008). It is well accepted that STAT3 signaling drives pathological processes, including cell proliferation, recruitment of inflammatory mediators, and angiogenesis (Francescone et al., 2015). Indeed, many inflammatory mediators are positively associated with the prevalence of colorectal adenomas (Kim et al., 2008; Basavaraju et al., 2015; Song et al., 2016). For example, serum levels of IL-6 are higher in CRC patients than in healthy controls (Knupfer and Preiss, 2010). Grivennikov et al. reported that IL-6 promoted colon tumor growth in an AOM/DSS-induced CAC mouse model (Grivennikov et al., 2009). IL-10 is an anti-inflammatory cytokine critical for maintaining intestinal immune homeostasis. IL-10-deficient mice develop intestinal inflammation in the presence of normal gut microflora (Burrello et al., 2018). In this experiment, ABP treatment inhibited the phosphorylation of STAT3, reduced the expression of IL-6 and increased the expression of IL-10, indicating that the anti-inflammatory effect of ABP may be one of its anti-tumor effects.

Oxidative stress has been proposed as a mechanism of IBD. With the production of MDA, excessive NO produces oxygen free radicals that cause tissue damage and the formation of colitis (Zhu and Li, 2012; Li et al., 2016). We found that in CAC mice treated with ABP, MDA contents were significantly decreased and the level of GSH was increased, suggesting that ABP had anti-oxidative capacity and can scavenge free radicals.

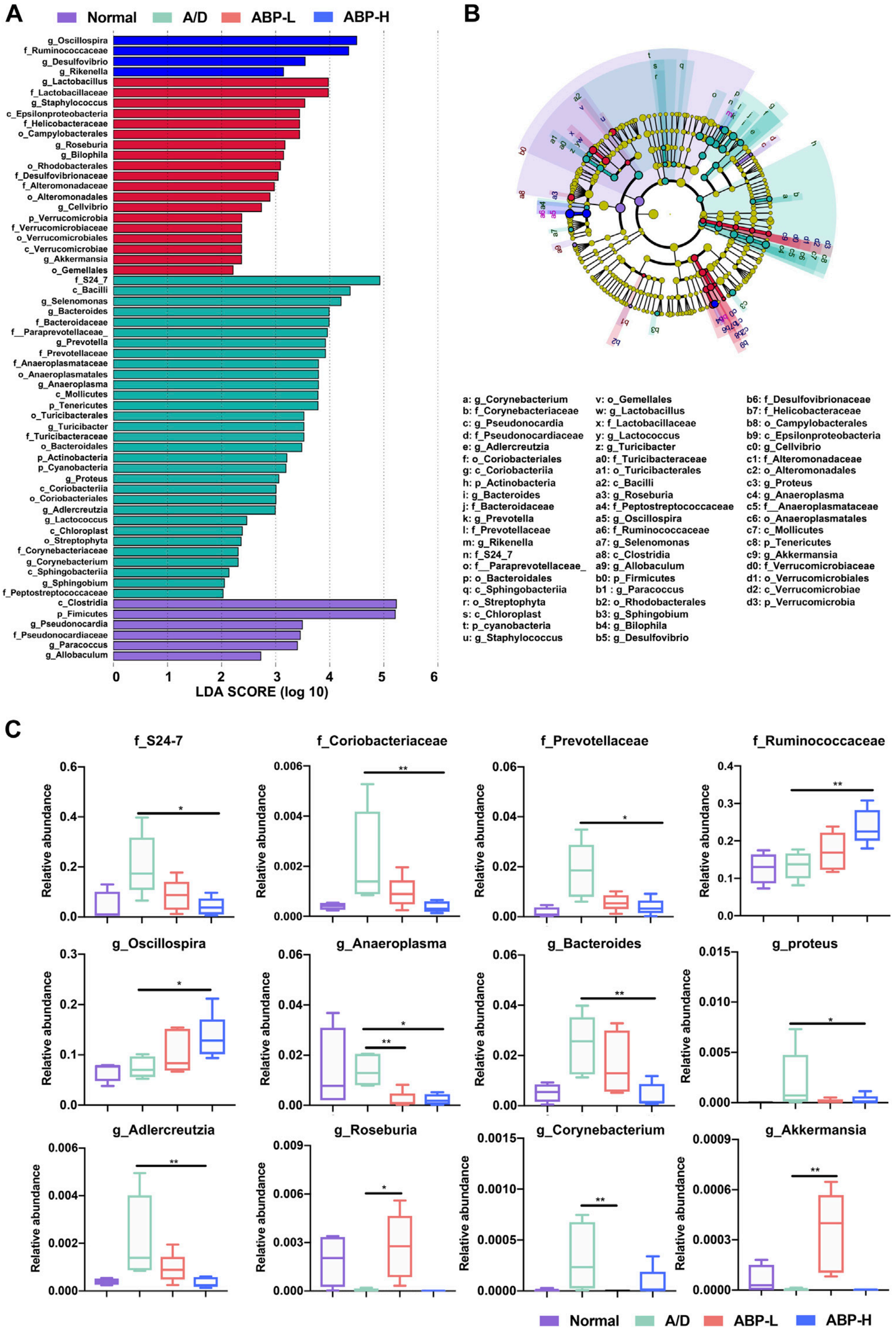

FIGURE 7 | Distribution of colon microbiota in each group (treatment with ABP for 11 weeks). **(A-B)** LEfSe analysis of bacterial taxa differences in each group. **(C)** Box plots demonstrating the characteristic bacteria at the family and genus levels. Compared with the A/D group, *$p < 0.05$, **$p < 0.01$.

The intestinal microbiota plays a pivotal role in physiological homeostasis and pathophysiology of diseases, destruction of intestinal barrier and signals of epithelial cells are closely related to microbiota dysbiosis (Arthur and Jobin, 2013; Jackson and Theiss, 2020). The impaired gut microbiota may result in the damage of enteric mucosa and various inflammation. Therefore, invasive bacteria might cross the barrier and trigger a pro-inflammatory response (Abreu, 2010). As the most

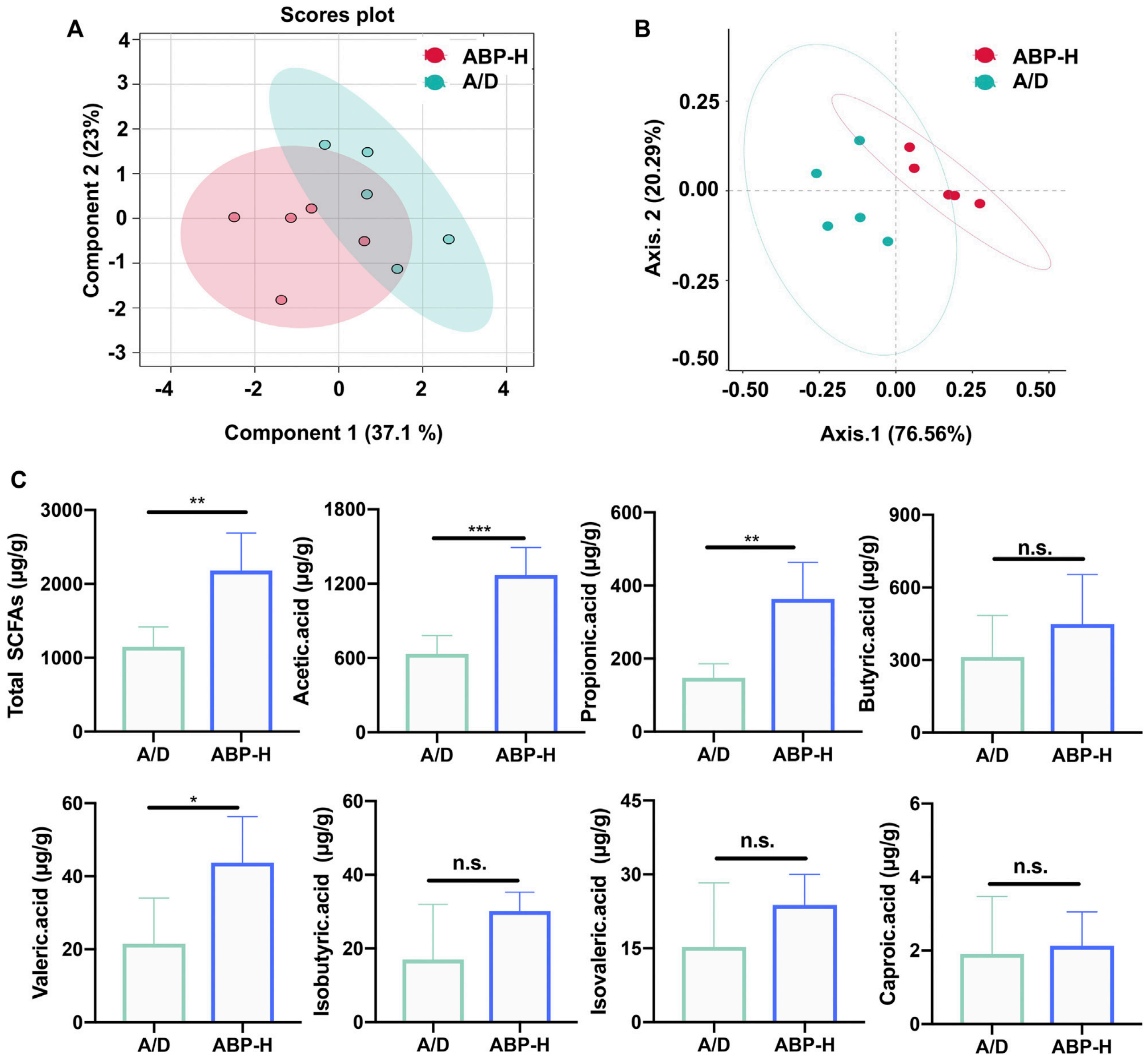

FIGURE 8 | ABP treatment increased the fecal SCFA levels in AOM/DSS-induced CRC mice (treatment with ABP for 11 weeks). **(A-B)** PCoA and PLS-DA analysis. **(C)** Bar plots for fecal SCFA content. Compared with the A/D group, **p* < 0.05, ***p* < 0.01.

commonly used specimen for gut microbiota sequencing, feces may not reflect the real flora of the intestinal surface. There are two main reasons: food consumption and certain bacteria that have penetrated the intestinal barrier cannot be detected precisely, such as *Akkermansia*. *Akkermansia* plays a critical role in maintaining human immunity and metabolism, can strengthen the intestinal barrier by promoting mucus secretion (van der Lugt et al., 2019), thus it has been deemed a promising therapeutic probiotic (Zou and Chen, 2020; Yu et al., 2021). Hence, we selected mucosal specimens instead of feces in this study.

SCFAs are the main metabolites produced by anaerobic bacteria, which confer healthy outcomes to the host (den Besten et al., 2013; Tan et al., 2014). The beneficial roles of SCFAs for the host include their capacity to strengthen intestinal barrier function, reduce oxidative stress, and anti-inflammatory, anti-carcinogenic effects (Sun and O'Riordan, 2013; van der Beek et al., 2017). Liu et al. reported that pumpkin polysaccharides increased the relative abundance of *g_Oscillospira* altered and increased SCFAs production in diabetic rats (Liu G. et al., 2018). Liu et al. found dietary supplementation of berry anthocyanin extracts enriched levels of SCFA producing bacteria and elevated production of fecal SCFAs in high-fat-fed C57BL/6J mice (Liu et al., 2021a). Xia et al. found that Adaptogenic flower buds increased the relative abundance of SCFA producing bacteria and strengthened the epithelial tight junction complex and immune responses (Xia W. et al., 2020). In this study,

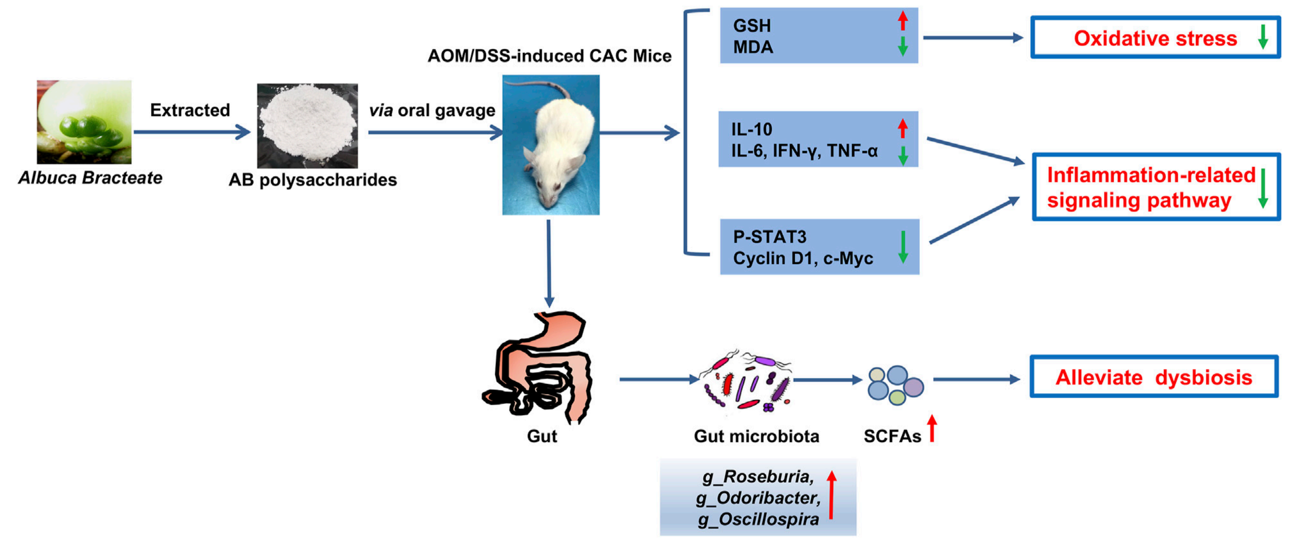

FIGURE 9 | Schematic diagram depicting the mechanism of action underlying the effect of ABP as a regulator of CRC progression.

we found that ABP treatment enriched the relative abundance of SCFA producing bacteria and elevated fecal SCFA levels in AOM-DSS induced CAC mice.

The heat map and LEfSe analysis showed that ABP decreased the relative abundance of some potentially pathogenic bacteria (*g_Streptococcus, g_Proteus, g_Corynebacterium, g_Anaeroplasma, g_Acinetobacter,* and *g_Ralstonia*) (Wu et al., 2018; Liu et al., 2019; Xia X. et al., 2020; Zorron Cheng Tao Pu et al., 2020; Marongiu et al., 2021; Zhang et al., 2021). GC-MS results revealed that ABP increased the levels of SCFAs in AOM/DSS induced CAC mice. In this study, changes in SCFA levels in ABP treated mice coincided with intestinal microbiome changes.

As expected, the A/D group showed a gradual increase of some bacteria along with time extension, implying these bacteria may be positively related to progression of AOM/DSS induced CAC. In ABP treatment groups, both decreasing trends of relative abundance of CAC related bacteria and increasing trends of SCFA producing bacteria were more apparent in mice treated for 11 weeks than those in 3 weeks, implying that regulation of ABP on the intestinal flora is a continuous and accumulating process. Combined with the long-term use of ABP having no side effect on the ABP alone group, we supposed that ABP could be used for long-term treatment against CAC.

Taken together, ABP treatment inhibited tumor progression in the AOM/DSS induced CAC mice by improving microbiota, increasing the abundance of beneficial bacteria and fecal SCFAs, reducing oxidative damage in the colon, suppressing inflammatory signaling pathways (**Figure 9**). ABP may be a potential therapeutic agent for treating CAC.

DATA AVAILABILITY STATEMENT

The datasets presented in this study can be found in online repositories. The names of the repository/repositories and accession number(s) can be found below: https://www.ncbi.nlm.nih.gov/sra; PRJNA785339.

ETHICS STATEMENT

The animal study was reviewed and approved by Institutional Animal Care and Use Committee of Wenzhou Medical University (wydw 2021-0224).

AUTHOR CONTRIBUTIONS

HT, LJ, and JD conceived and supervised the project and designed the experiments. JD and LJ contributed to the design of the experiments, ZQ and XY performed most of the experiments, JL, ZS, LC, LY, and KW performed part of the experiments. XY and ZQ analyzed the results and wrote the manuscript. ZQ and XY analyzed the data and created the figures. XY, ZQ, YL, and ZS performed the literature review. HT, LJ and JD revised the manuscript. ZQ and XY are co-first authors, they contributed equally to this work. HT, LJ, and JD are the corresponding authors. All authors provided their final approval for the publication of this manuscript.

FUNDING

This research was supported by the Fundamental Public Welfare Research Program of Zhejiang Province (No. LGF18H180012).

ACKNOWLEDGMENTS

The authors thank Guohua Deng for his kind help with cultivating the AB on his farm. We also express our gratefulness to Professor Pan Li of Zhejiang University. We also extend our appreciation to Hangzhou Guhe Information and Technology Co., Ltd., Zhejiang, China. for their sequencing and metabolomic profiling services.

SUPPLEMENTARY MATERIAL

The Supplementary Material for this article can be found online at: https://www.frontiersin.org/articles/10.3389/fphar.2022.833077/full#supplementary-material

REFERENCES

Abreu, M. T. (2010). Toll-like Receptor Signalling in the Intestinal Epithelium: How Bacterial Recognition Shapes Intestinal Function. *Nat. Rev. Immunol.* 10 (2), 131–144. doi:10.1038/nri2707

Arthur, J. C., and Jobin, C. (2013). The Complex Interplay between Inflammation, the Microbiota and Colorectal Cancer. *Gut Microbes* 4 (3), 253–258. doi:10.4161/gmic.24220

Barrett, C. W., Ning, W., Chen, X., Smith, J. J., Washington, M. K., Hill, K. E., et al. (2013). Tumor Suppressor Function of the Plasma Glutathione Peroxidase Gpx3 in Colitis-Associated Carcinoma. *Cancer Res.* 73 (3), 1245–1255. doi:10.1158/0008-5472.CAN-12-3150

Basavaraju, U., Shebl, F. M., Palmer, A. J., Berry, S., Hold, G. L., El-Omar, E. M., et al. (2015). Cytokine Gene Polymorphisms, Cytokine Levels and the Risk of Colorectal Neoplasia in a Screened Population of Northeast Scotland. *Eur. J. Cancer Prev.* 24 (4), 296–304. doi:10.1097/CEJ.0000000000000087

Becker, C., Fantini, M. C., Wirtz, S., Nikolaev, A., Lehr, H. A., Galle, P. R., et al. (2005). IL-6 Signaling Promotes Tumor Growth in Colorectal Cancer. *Cell Cycle* 4 (2), 217–220. doi:10.4161/cc.4.2.1413

Biao, Y., Jiannan, H., Yaolan, C., Shujie, C., Dechun, H., Julian Mcclements, D., et al. (2020). Identification and Characterization of Antioxidant and Immune-Stimulatory Polysaccharides in Flaxseed hull. *Food Chem.* 315, 126266. doi:10.1016/j.foodchem.2020.126266

Burrello, C., Garavaglia, F., Cribiù, F. M., Ercoli, G., Lopez, G., Troisi, J., et al. (2018). Therapeutic Faecal Microbiota Transplantation Controls Intestinal Inflammation through IL10 Secretion by Immune Cells. *Nat. Commun.* 9 (1), 5184. doi:10.1038/s41467-018-07359-8

Cao, J., Tang, D., Wang, Y., Li, X., Hong, L., and Sun, C. (2018). Characteristics and Immune-Enhancing Activity of Pectic Polysaccharides from Sweet Cherry (Prunus Avium). *Food Chem.* 254, 47–54. doi:10.1016/j.foodchem.2018.01.145

Chattopadhyay, I., Dhar, R., Pethusamy, K., Seethy, A., Srivastava, T., Sah, R., et al. (2021). Exploring the Role of Gut Microbiome in Colon Cancer. *Appl. Biochem. Biotechnol.* 193 (6), 1780–1799. doi:10.1007/s12010-021-03498-9

Chen, R., Li, Y., Dong, H., Liu, Z., Li, S., Yang, S., et al. (2012). Optimization of Ultrasonic Extraction Process of Polysaccharides from Ornithogalum Caudatum Ait and Evaluation of its Biological Activities. *Ultrason. Sonochem.* 19 (6), 1160–1168. doi:10.1016/j.ultsonch.2012.03.008

den Besten, G., van Eunen, K., Groen, A. K., Venema, K., Reijngoud, D. J., and Bakker, B. M. (2013). The Role of Short-Chain Fatty Acids in the Interplay between Diet, Gut Microbiota, and Host Energy Metabolism. *J. Lipid Res.* 54 (9), 2325–2340. doi:10.1194/jlr.R036012

Francescone, R., Hou, V., and Grivennikov, S. I. (2015). Cytokines, IBD, and Colitis-Associated Cancer. *Inflamm. Bowel Dis.* 21 (2), 409–418. doi:10.1097/MIB.0000000000000236

Fukata, M., Chen, A., Vamadevan, A. S., Cohen, J., Breglio, K., Krishnareddy, S., et al. (2007). Toll-like Receptor-4 Promotes the Development of Colitis-Associated Colorectal Tumors. *Gastroenterology* 133 (6), 1869–1881. doi:10.1053/j.gastro.2007.09.008

Giner, E., Recio, M. C., Ríos, J. L., Cerdá-Nicolás, J. M., and Giner, R. M. (2016). Chemopreventive Effect of Oleuropein in Colitis-Associated Colorectal Cancer in C57bl/6 Mice. *Mol. Nutr. Food Res.* 60 (2), 242–255. doi:10.1002/mnfr.201500605

Grivennikov, S., Karin, E., Terzic, J., Mucida, D., Yu, G. Y., Vallabhapurapu, S., et al. (2009). IL-6 and Stat3 Are Required for Survival of Intestinal Epithelial Cells and Development of Colitis-Associated Cancer. *Cancer Cell* 15 (2), 103–113. doi:10.1016/j.ccr.2009.01.001

Hashemifesharaki, R., Xanthakis, E., Altintas, Z., Guo, Y., and Gharibzahedi, S. M. T. (2020). Microwave-assisted Extraction of Polysaccharides from the Marshmallow Roots: Optimization, Purification, Structure, and Bioactivity. *Carbohydr. Polym.* 240, 116301. doi:10.1016/j.carbpol.2020.116301

Hu, D., Bao, T., Lu, Y., Su, H., Ke, H., and Chen, W. (2020). Polysaccharide from Mulberry Fruit (Morus alba L.) Protects against Palmitic-Acid-Induced Hepatocyte Lipotoxicity by Activating the Nrf2/ARE Signaling Pathway. *J. Agric. Food Chem.* 68 (46), 13016–13024. doi:10.1021/acs.jafc.9b03335

Iguchi, T., Kuroda, M., Naito, R., Watanabe, T., Matsuo, Y., Yokosuka, A., et al. (2017). Structural Characterization of Cholestane Rhamnosides from Ornithogalum Saundersiae Bulbs and Their Cytotoxic Activity against Cultured Tumor Cells. *Molecules* 22 (8), 1243. doi:10.3390/molecules22081243

Jackson, D. N., and Theiss, A. L. (2020). Gut Bacteria Signaling to Mitochondria in Intestinal Inflammation and Cancer. *Gut Microbes* 11 (3), 285–304. doi:10.1080/19490976.2019.1592421

Ji, X., Peng, Q., and Wang, M. (2018). Anti-colon-cancer Effects of Polysaccharides: A Mini-Review of the Mechanisms. *Int. J. Biol. Macromol* 114, 1127–1133. doi:10.1016/j.ijbiomac.2018.03.186

Kang, M., and Martin, A. (2017). Microbiome and Colorectal Cancer: Unraveling Host-Microbiota Interactions in Colitis-Associated Colorectal Cancer Development. *Semin. Immunol.* 32, 3–13. doi:10.1016/j.smim.2017.04.003

Kim, S., Keku, T. O., Martin, C., Galanko, J., Woosley, J. T., Schroeder, J. C., et al. (2008). Circulating Levels of Inflammatory Cytokines and Risk of Colorectal Adenomas. *Cancer Res.* 68 (1), 323–328. doi:10.1158/0008-5472.CAN-07-2924

Klampfer, L. (2008). The Role of Signal Transducers and Activators of Transcription in colon Cancer. *Front. Biosci.* 13, 2888–2899. doi:10.2741/2893

Knüpfer, H., and Preiss, R. (2010). Serum Interleukin-6 Levels in Colorectal Cancer Patients-Aa Summary of Published Results. *Int. J. Colorectal Dis.* 25 (2), 135–140. doi:10.1007/s00384-009-0818-8

Li, M. Y., Luo, H. J., Wu, X., Liu, Y. H., Gan, Y. X., Xu, N., et al. (2019). Anti-Inflammatory Effects of Huangqin Decoction on Dextran Sulfate Sodium-Induced Ulcerative Colitis in Mice through Regulation of the Gut Microbiota and Suppression of the Ras-PI3K-Akt-HIF-1α and NF-κB Pathways. *Front. Pharmacol.* 10, 1552. doi:10.3389/fphar.2019.01552

Li, Q., Wang, W., Zhu, Y., Chen, Y., Zhang, W., Yu, P., et al. (2017). Structural Elucidation and Antioxidant Activity a Novel Se-Polysaccharide from Se-Enriched Grifola Frondosa. *Carbohydr. Polym.* 161, 42–52. doi:10.1016/j.carbpol.2016.12.041

Li, R., Chen, Y., Shi, M., Xu, X., Zhao, Y., Wu, X., et al. (2016). Gegen Qinlian Decoction Alleviates Experimental Colitis via Suppressing TLR4/NF-κB Signaling and Enhancing Antioxidant Effect. *Phytomedicine* 23 (10), 1012–1020. doi:10.1016/j.phymed.2016.06.010

Liu, F., Liu, A., Lu, X., Zhang, Z., Xue, Y., Xu, J., et al. (2019). Dysbiosis Signatures of the Microbial Profile in Tissue from Bladder Cancer. *Cancer Med.* 8 (16), 6904–6914. doi:10.1002/cam4.2419

Liu, G., Liang, L., Yu, G., and Li, Q. (2018a). Pumpkin Polysaccharide Modifies the Gut Microbiota during Alleviation of Type 2 Diabetes in Rats. *Int. J. Biol. Macromol* 115, 711–717. doi:10.1016/j.ijbiomac.2018.04.127

Liu, J., Hao, W., He, Z., Kwek, E., Zhu, H., Ma, N., et al. (2021a). Blueberry and cranberry Anthocyanin Extracts Reduce Bodyweight and Modulate Gut Microbiota in C57BL/6 J Mice Fed with a High-Fat Diet. *Eur. J. Nutr.* 60 (5), 2735–2746. doi:10.1007/s00394-020-02446-3

Liu, J., Wu, S., Chen, Y., Li, Q., Su, L., Yang, Y., et al. (2021b). Sargassum fusiforme Alginate Relieves Hyperglycemia and Modulates Intestinal Microbiota and Metabolites in Type 2 Diabetic Mice. *Nutrients* 13 (8). doi:10.3390/nu13082887

Liu, J., Wu, S. Y., Chen, L., Li, Q. J., Shen, Z. Y., Jin, L., et al. (2020). Different Extraction Methods Bring About Distinct Physicochemical Properties And Antioxidant Activities Of Sargassum Fusiforme Fucoidans. *Int. J. Biol. Macromol* 155, 1385–1392. doi:10.1016/j.ijbiomac.2019.11.113

Liu, L. Q., Li, H. S., Nie, S. P., Shen, M. Y., Hu, J. L., and Xie, M. Y. (2018b). Tea Polysaccharide Prevents Colitis-Associated Carcinogenesis in Mice by

Inhibiting the Proliferation and Invasion of Tumor Cells. *Int. J. Mol. Sci.* 19 (2), 506. doi:10.3390/ijms19020506

Liu, L. Q., Nie, S. P., Shen, M. Y., Hu, J. L., Yu, Q., Gong, D., et al. (2018c). Tea Polysaccharides Inhibit Colitis-Associated Colorectal Cancer via Interleukin-6/STAT3 Pathway. *J. Agric. Food Chem.* 66 (17), 4384–4393. doi:10.1021/acs.jafc.8b00710

Lou, M., Cao, A., Jin, C., Mi, K., Xiong, X., Zeng, Z., et al. (2021). Deviated And Early Unsustainable Stunted Development Of Gut Microbiota In Children With Autism Spectrum Disorder. *Gut.* doi:10.1136/gutjnl-2021-325115

Luo, L., Sun, W., Zhu, W., Li, S., Zhang, W., Xu, X., et al. (2021). BCAT1 Decreases the Sensitivity of Cancer Cells to Cisplatin by Regulating mTOR-Mediated Autophagy via Branched-Chain Amino Acid Metabolism. *Cell Death Dis* 12 (2), 169. doi:10.1038/s41419-021-03456-7

Ma, F., Wang, R., Li, X., Kang, W., Bell, A. E., Zhao, D., et al. (2020). Physical Properties of Mucilage Polysaccharides from Dioscorea Opposita Thunb. *Food Chem.* 311, 126039. doi:10.1016/j.foodchem.2019.126039

Marongiu, L., Landry, J. J. M., Rausch, T., Abba, M. L., Delecluse, S., Delecluse, H. J., et al. (2021). Metagenomic Analysis of Primary Colorectal Carcinomas and Their Metastases Identifies Potential Microbial Risk Factors. *Mol. Oncol.* 15, 3363–3384. doi:10.1002/1878-0261.13070

Matsunaga, Y., Hasei, S., Yamamotoya, T., Honda, H., Kushiyama, A., Sakoda, H., et al. (2021). Pathological Role of Pin1 in the Development of DSS-Induced Colitis. *Cells* 10 (5), 1230. doi:10.3390/cells10051230

Meng, Q., Li, Y., Xiao, T., Zhang, L., and Xu, D. (2017). Antioxidant and Antibacterial Activities of Polysaccharides Isolated and Purified from Diaphragma Juglandis Fructus. *Int. J. Biol. Macromol* 105 (Pt 1), 431–437. doi:10.1016/j.ijbiomac.2017.07.062

Papapietro, O., Teatero, S., Thanabalasuriar, A., Yuki, K. E., Diez, E., Zhu, L., et al. (2013). R-spondin 2 Signalling Mediates Susceptibility to Fatal Infectious Diarrhoea. *Nat. Commun.* 4, 1898. doi:10.1038/ncomms2816

Ren, Y., Geng, Y., Du, Y., Li, W., Lu, Z. M., Xu, H. Y., et al. (2018). Polysaccharide of Hericium erinaceus Attenuates Colitis in C57BL/6 Mice via Regulation of Oxidative Stress, Inflammation-Related Signaling Pathways and Modulating the Composition of the Gut Microbiota. *J. Nutr. Biochem.* 57, 67–76. doi:10.1016/j.jnutbio.2018.03.005

Robles, A. I., Traverso, G., Zhang, M., Roberts, N. J., Khan, M. A., Joseph, C., et al. (2016). Whole-Exome Sequencing Analyses of Inflammatory Bowel Disease-Associated Colorectal Cancers. *Gastroenterology* 150 (4), 931–943. doi:10.1053/j.gastro.2015.12.036

Sanders, K., Moran, Z., Shi, Z., Paul, R., and Greenlee, H. (2016). Natural Products for Cancer Prevention: Clinical Update 2016. *Semin. Oncol. Nurs.* 32 (3), 215–240. doi:10.1016/j.soncn.2016.06.001

Siegel, R. L., Miller, K. D., Fuchs, H. E., and Jemal, A. (2021). Cancer Statistics, 2021. *CA A. Cancer J. Clin.* 71 (1), 7–33. doi:10.3322/caac.21654

Song, H., Wang, W., Shen, B., Jia, H., Hou, Z., Chen, P., et al. (2018). Pretreatment with Probiotic Bifico Ameliorates Colitis-Associated Cancer in Mice: Transcriptome and Gut flora Profiling. *Cancer Sci.* 109 (3), 666–677. doi:10.1111/cas.13497

Song, M., Mehta, R. S., Wu, K., Fuchs, C. S., Ogino, S., Giovannucci, E. L., et al. (2016). Plasma Inflammatory Markers and Risk of Advanced Colorectal Adenoma in Women. *Cancer Prev. Res. (Phila)* 9 (1), 27–34. doi:10.1158/1940-6207.CAPR-15-0307

Su, Y., and Li, L. (2020). Structural Characterization and Antioxidant Activity of Polysaccharide from Four Auriculariales. *Carbohydr. Polym.* 229, 115407. doi:10.1016/j.carbpol.2019.115407

Sun, Y., and O'Riordan, M. X. (2013). Regulation of Bacterial Pathogenesis by Intestinal Short-Chain Fatty Acids. *Adv. Appl. Microbiol.* 85, 93–118. doi:10.1016/B978-0-12-407672-3.00003-4

Sun, Y. D., Wang, Z. H., and Ye, Q. S. (2013). Composition Analysis and Anti-proliferation Activity of Polysaccharides from Dendrobium Chrysotoxum. *Int. J. Biol. Macromol* 62, 291–295. doi:10.1016/j.ijbiomac.2013.08.046

Tan, J., McKenzie, C., Potamitis, M., Thorburn, A. N., Mackay, C. R., and Macia, L. (2014). The Role of Short-Chain Fatty Acids in Health and Disease. *Adv. Immunol.* 121, 91–119. doi:10.1016/B978-0-12-800100-4.00003-9

Ullman, T. A., and Itzkowitz, S. H. (2011). Intestinal Inflammation and Cancer. *Gastroenterology* 140 (6), 1807–1816. doi:10.1053/j.gastro.2011.01.057

Uronis, J. M., Mühlbauer, M., Herfarth, H. H., Rubinas, T. C., Jones, G. S., and Jobin, C. (2009). Modulation of the Intestinal Microbiota Alters Colitis-Associated Colorectal Cancer Susceptibility. *PLoS One* 4 (6), e6026. doi:10.1371/journal.pone.0006026

van der Beek, C. M., Dejong, C. H. C., Troost, F. J., Masclee, A. A. M., and Lenaerts, K. (2017). Role of Short-Chain Fatty Acids in Colonic Inflammation, Carcinogenesis, and Mucosal protection and Healing. *Nutr. Rev.* 75 (4), 286–305. doi:10.1093/nutrit/nuw067

van der Lugt, B., van Beek, A. A., Aalvink, S., Meijer, B., Sovran, B., Vermeij, W. P., et al. (2019). Akkermansia Muciniphila Ameliorates the Age-Related Decline in Colonic Mucus Thickness and Attenuates Immune Activation in Accelerated Aging Ercc1 -/Δ7 Mice. *Immun. Ageing* 16, 6. doi:10.1186/s12979-019-0145-z

Waldner, M. J., and Neurath, M. F. (2015). Mechanisms of Immune Signaling in Colitis-Associated Cancer. *Cell Mol Gastroenterol Hepatol* 1 (1), 6–16. doi:10.1016/j.jcmgh.2014.11.006

Wang, R., Chen, P., Jia, F., Tang, J., and Ma, F. (2012). Optimization of Polysaccharides from Panax Japonicus C.A. Meyer by RSM and its Anti-oxidant Activity. *Int. J. Biol. Macromol* 50 (2), 331–336. doi:10.1016/j.ijbiomac.2011.12.023

Wu, P., Zhang, G., Zhao, J., Chen, J., Chen, Y., Huang, W., et al. (2018). Profiling the Urinary Microbiota in Male Patients with Bladder Cancer in China. *Front Cel Infect Microbiol* 8, 167. doi:10.3389/fcimb.2018.00167

Wu, S., Zhang, X., Liu, J., Song, J., Yu, P., Chen, P., et al. (2019). Physicochemical Characterization of Sargassum Fusiforme Fucoidan Fractions and Their Antagonistic Effect against P-Selectin-Mediated Cell Adhesion. *Int. J. Biol. Macromol* 133, 656–662. doi:10.1016/j.ijbiomac.2019.03.218

Xia, W., Khan, I., Li, X. A., Huang, G., Yu, Z., Leong, W. K., et al. (2020a). Adaptogenic Flower Buds Exert Cancer Preventive Effects by Enhancing the SCFA-Producers, Strengthening the Epithelial Tight junction Complex and Immune Responses. *Pharmacol. Res.* 159, 104809. doi:10.1016/j.phrs.2020.104809

Xia, X., Wu, W. K. K., Wong, S. H., Liu, D., Kwong, T. N. Y., Nakatsu, G., et al. (2020b). Bacteria Pathogens Drive Host Colonic Epithelial Cell Promoter Hypermethylation of Tumor Suppressor Genes in Colorectal Cancer. *Microbiome* 8 (1), 108. doi:10.1186/s40168-020-00847-4

Yu, H., Lee, H., Herrmann, A., Buettner, R., and Jove, R. (2014). Revisiting STAT3 Signalling in Cancer: New and Unexpected Biological Functions. *Nat. Rev. Cancer* 14 (11), 736–746. doi:10.1038/nrc3818

Yu, H., Pardoll, D., and Jove, R. (2009). STATs in Cancer Inflammation and Immunity: a Leading Role for STAT3. *Nat. Rev. Cancer* 9 (11), 798–809. doi:10.1038/nrc2734

Yu, Y., Lu, J., Sun, L., Lyu, X., Chang, X. Y., Mi, X., et al. (2021). Akkermansia Muciniphila: A Potential Novel Mechanism of Nuciferine to Improve Hyperlipidemia. *Biomed. Pharmacother.* 133, 111014. doi:10.1016/j.biopha.2020.111014

Yuan, X., Xue, J., Tan, Y., Yang, Q., Qin, Z., Bao, X., et al. (2021). Albuca Bracteate Polysaccharides Synergistically Enhance the Anti-tumor Efficacy of 5-Fluorouracil against Colorectal Cancer by Modulating β-Catenin Signaling and Intestinal Flora. *Front. Pharmacol.* 12, 736627. doi:10.3389/fphar.2021.736627

Zeng, F., Chen, W., He, P., Zhan, Q., Wang, Q., Wu, H., et al. (2020). Structural Characterization of Polysaccharides with Potential Antioxidant and Immunomodulatory Activities from Chinese Water Chestnut Peels. *Carbohydr. Polym.* 246, 116551. doi:10.1016/j.carbpol.2020.116551

Zhang, J., Zhou, H. C., He, S. B., Zhang, X. F., Ling, Y. H., Li, X. Y., et al. (2021). The Immunoenhancement Effects of Sea Buckthorn Pulp Oil in Cyclophosphamide-Induced Immunosuppressed Mice. *Food Funct.* 12 (17), 7954–7963. doi:10.1039/d1fo01257f

Zhang, Y., Fang, F., Fan, K., Zhang, Y., Zhang, J., Guo, H., et al. (2017). Effective Cytotoxic Activity of OSW-1 on colon Cancer by Inducing Apoptosis *In Vitro* and *In Vivo*. *Oncol. Rep.* 37 (6), 3509–3519. doi:10.3892/or.2017.5582

Zhang, Y., Liu, Q., Yu, Y., Wang, M., Wen, C., and He, Z. (2020). Early and Short-Term Interventions in the Gut Microbiota Affects Lupus Severity, Progression, and Treatment in MRL/lpr Mice. *Front. Microbiol.* 11, 628. doi:10.3389/fmicb.2020.00628

Zhao, H. M., Wang, Y., Huang, X. Y., Huang, M. F., Xu, R., Yue, H. Y., et al. (2016). Astragalus Polysaccharide Attenuates Rat Experimental Colitis by Inducing Regulatory T Cells in Intestinal Peyer's Patches. *World J. Gastroenterol.* 22 (11), 3175–3185. doi:10.3748/wjg.v22.i11.3175

Zhong, L., Zhang, X., and Covasa, M. (2014). Emerging Roles of Lactic Acid Bacteria in protection against Colorectal Cancer. *World J. Gastroenterol.* 20 (24), 7878–7886. doi:10.3748/wjg.v20.i24.7878

Zhou, Y., Garcia-Prieto, C., Carney, D. A., Xu, R. H., Pelicano, H., Kang, Y., et al. (2005). OSW-1: a Natural Compound with Potent Anticancer Activity and a Novel Mechanism of Action. *J. Natl. Cancer Inst.* 97 (23), 1781–1785. doi:10.1093/jnci/dji404

Zhu, H., and Li, Y. R. (2012). Oxidative Stress and Redox Signaling Mechanisms of Inflammatory Bowel Disease: Updated Experimental and Clinical Evidence. *Exp. Biol. Med. (Maywood)* 237 (5), 474–480. doi:10.1258/ebm.2011.011358

Zhu, H. C., Jia, X. K., Fan, Y., Xu, S. H., Li, X. Y., Huang, M. Q., et al. (2021). Alisol B 23-Acetate Ameliorates Azoxymethane/Dextran Sodium Sulfate-Induced Male Murine Colitis-Associated Colorectal Cancer via Modulating the Composition of Gut Microbiota and Improving Intestinal Barrier. *Front. Cel Infect Microbiol* 11, 640225. doi:10.3389/fcimb.2021.640225

Zorron Cheng Tao Pu, L., Yamamoto, K., Honda, T., Nakamura, M., Yamamura, T., Hattori, S., et al. (2020). Microbiota Profile Is Different for Early and Invasive Colorectal Cancer and Is Consistent throughout the colon. *J. Gastroenterol. Hepatol.* 35 (3), 433–437. doi:10.1111/jgh.14868

Zou, Q., Zhang, X., Liu, X., Li, Y., Tan, Q., Dan, Q., et al. (2020). Ficus Carica Polysaccharide Attenuates DSS-Induced Ulcerative Colitis in C57BL/6 Mice. *Food Funct.* 11 (7), 6666–6679. doi:10.1039/d0fo01162b

Zou, Y., and Chen, T. (2020). Engineered Akkermansia Muciniphila: A Promising Agent against Diseases (Review). *Exp. Ther. Med.* 20 (6), 285. doi:10.3892/etm.2020.9415

Conflict of Interest: The authors declare that the research was conducted in the absence of any commercial or financial relationships that could be construed as a potential conflict of interest.

Publisher's Note: All claims expressed in this article are solely those of the authors and do not necessarily represent those of their affiliated organizations, or those of the publisher, the editors and the reviewers. Any product that may be evaluated in this article, or claim that may be made by its manufacturer, is not guaranteed or endorsed by the publisher.

Copyright © 2022 Qin, Yuan, Liu, Shi, Cao, Yang, Wu, Lou, Tong, Jiang and Du. This is an open-access article distributed under the terms of the Creative Commons Attribution License (CC BY). The use, distribution or reproduction in other forums is permitted, provided the original author(s) and the copyright owner(s) are credited and that the original publication in this journal is cited, in accordance with accepted academic practice. No use, distribution or reproduction is permitted which does not comply with these terms.

ORIGINAL RESEARCH
published: 21 February 2022
doi: 10.3389/fphar.2022.857289

IL7R Is Correlated With Immune Cell Infiltration in the Tumor Microenvironment of Lung Adenocarcinoma

Xin Wang[1], Shujian Chang[1], Teng Wang[1], Ruirong Wu[1], Zebo Huang[1], Junjie Sun[1], Jingjing Liu[1], Yan Yu[2]* and Yong Mao[1]*

[1]*Department of Medical Oncology, Affiliated Hospital of Jiangnan University, Wuxi, China,* [2]*Department of Medical Oncology, Harbin Medical University Cancer Hospital, Harbin, China*

OPEN ACCESS

Edited by:
Dong-Hua Yang,
St. John's University, United States

Reviewed by:
Zhihui Song,
Fox Chase Cancer Center,
United States
Yibing Ji,
University at Buffalo, United States

***Correspondence:**
Yan Yu
Yuyan@hrbmu.edu.cn
Yong Mao
mydoctorwx@aliyun.com

Specialty section:
This article was submitted to
Pharmacology of Anti-Cancer Drugs,
a section of the journal
Frontiers in Pharmacology

Received: *18 January 2022*
Accepted: *04 February 2022*
Published: *21 February 2022*

Citation:
Wang X, Chang S, Wang T, Wu R, Huang Z, Sun J, Liu J, Yu Y and Mao Y (2022) IL7R Is Correlated With Immune Cell Infiltration in the Tumor Microenvironment of Lung Adenocarcinoma.
Front. Pharmacol. 13:857289.
doi: 10.3389/fphar.2022.857289

Tumor microenvironment plays an important role in the development, progression, and prognosis of lung adenocarcinoma. Exploring new biomarkers based on the immune microenvironment of lung adenocarcinoma can effectively predict the prognosis and provide effective clinical treatment. In this study, we used the ESTIMATE algorithm to score the immune and stromal components in lung adenocarcinoma data downloaded from the TCGA database. The result showed that the immune/stromal score was associated with clinical features and prognosis of lung adenocarcinoma patients. Interleukin-7 receptor (IL7R) is an important prognostic biomarker identified by intersection analysis of protein-protein interaction networks and Cox regression survival analysis. According to TCGA and Oncomine database analysis, IL7R expression in adenocarcinoma tissues was significantly lower than that in normal lung tissues and was further verified in clinical tissue samples. Survival analysis showed IL7R was an independent prognostic factor of lung adenocarcinoma. IL7R expression was positively correlated with the overall survival and progression-free survival of lung adenocarcinoma patients and negatively correlated with tumor size. Our results suggest that IL7R inhibits tumor growth by regulating the proportion of immune infiltrating cells in the tumor immune microenvironment. IL7R could be a beneficial prognostic marker in patients with lung adenocarcinoma and has great potential in immune therapy.

Keywords: IL7R, tumor immunological microenvironment, tumor infiltrating lymphocytes, lung adenocarcinoma, prognosis

INTRODUCTION

Lung cancer is the leading cause of cancer-related death with increasing morbidity and mortality over the years. Non-small cell lung cancer (NSCLC) accounts for about 85% of lung cancers, and lung adenocarcinoma (LUAD) is a common pathological type of NSCLC with a 5 year survival rate of less than 20% (Chen et al., 2015; DeSantis et al., 2016; Bray et al., 2018; Siegel et al., 2021). Tumor immunotherapy, such as immune checkpoint blockade (ICB), has dramatically changed the landscape of cancer treatment and improved the survival of various cancer patients (Lambrechts et al., 2018; Zappasodi et al., 2018). Since not all tumor patients respond to immunotherapy, searching for effective therapeutic targets and prognostic biomarkers for individualized treatment has become an urgent need.

Previous studies have suggested that the positive response of immunotherapy usually depends on the dynamic interaction between tumor cells and immune modulators in the tumor microenvironment (TME) (Dougan and Dranoff, 2009a). The inhibitory effects and heterogeneity of TME have a great influence on the occurrence and development of tumors and the efficacy of immunotherapy (Dougan and Dranoff, 2009b). The TME is composed of vascular, extracellular matrix (ECM), cancer-associated fibroblasts (CAFs) and tumor-infiltrating lymphocytes (TILs). The tumor immune microenvironment plays an important role in the development and progression of primary lung cancer (Lavin et al., 2017). In this study, the immune and stromal components in the TME of lung adenocarcinoma were scored by the ESTIMATE algorithm. We found that the immune and stromal scores were related to the pathological molecular subtypes, clinical stages, and survival prognosis of LUAD patients. Based on different immune/stromal scores, we screened out differential expression genes related to the immune microenvironment and identified prognostic genes associated with survival. IL7R was confirmed to be associated with prognosis and immune cell infiltration in LUAD patients. IL7R may be a prognostic factor and a potential therapeutic target for immunotherapy for patients with LUAD.

MATERIALS AND METHODS

Ethics Statement

The pathological tissue sections used in this study were approved by the Ethics Committee of Jiangnan university affiliated hospital. Each patient signed a consent form for participating in the study.

Data Acquisition and Analysis

The mRNA expression data and clinical information of lung adenocarcinoma were obtained from the TCGA and GEO database (GSE68465). There are three molecular subtypes of lung adenocarcinoma: bronchoid, magnoid, and squamoid (Hayes et al., 2006). The stromal and immune scores were calculated by the ESTIMATE algorithm using the TCGA data (Yoshihara et al., 2013). The survminer package was used to analyze the relationship between stromal score or immune score and overall survival of LUAD patients. The optimal cut-off points were calculated by smoothHR (Smooth Hazard Ratio Curves Taking a Reference Value) algorithm. The expression of IL7R in lung adenocarcinoma tissues and normal tissues was analyzed by TCGA and Oncomine database. CIBERSORT computational method was applied for estimating the TIL abundance profile in all tumor samples (Chen et al., 2018). The relationship between IL7R and TIL was evaluated by the Timer website (Li et al., 2017).

Differential Expression Genes and Functional Enrichment

Differential expression genes (DEGs) were screened out using the limma package of R language, Fold change (FC) >1 and $p < 0.05$ (Li et al., 2017). Heatmap was generated using ClustVis (Ritchie et al., 2015). Functional enrichment analysis on DEGs was conducted by the web tool DAVID. False discovery rate (FDR) < 0.05 (Metsalu and Vilo, 2015). The KEGG pathway function of IL7R was enriched and analyzed by GSEA (Huang et al., 2009).

Protein-Protein Interaction Network Construction and Cox Survival Analysis

The Protein-Protein Interaction (PPI) network was constructed by the STRING database (Subramanian et al., 2005) and visualized with the Cytoscape software (Szklarczyk et al., 2015). Nodes were selected with an interaction relationship greater than 0.5 ((Shannon et al., 2003)). The Cox survival analysis was analyzed using the software package survival to screen prognostic genes ($p < 0.05$).

Patients and Tissue Samples

In this study,40 cases of LUAD and 35 cases of adjacent normal tissues were collected from LUAD patients who underwent surgery and then received care and follow-up in our hospital between the period of July 2014 and August 2016.

Cell Culture

A panel of LUAD cell lines H1975, H1650, H1299, A549, PC9, H661, and the normal lung epithelial cell line HBE were used for *in vitro* validation. All cells were purchased from the ATCC. The PC9 cell line was maintained in DMEM medium (Gibco, NY, United States), and the other cells were maintained in 1,640 medium (Gibco, NY, United States), both mediums containing 10% FBS. All cells were incubated in 5% CO_2 air at 37°C.

Immunohistochemical Analysis

The paraffin sections were dewaxed with xylene, immersed in the EDTA antigen extraction buffer for antigen repair, blocked with 3% hydrogen peroxide, incubated with rabbit anti-IL7R polyclonal antibody (1:200; ABclonal; A13503) overnight. Tissue sections were incubated with the secondary antibody (Zhongshan Golden Bridge, PV-6001), then stained with DAB.

Immunohistochemical (IHC) staining results were evaluated by two experienced pathologists who were blinded to all original data. IL7R staining is mainly located in the cytoplasm of bronchial epithelium or alveolar epithelium of lung tissue, and also in the cytoplasm of tumor cells. In the IL7R staining evaluation, a semiquantitative scoring method was used to assess the IHC staining result, which included the staining intensity score and score of staining density. We calculated the intensity of staining (0, no staining; 1, low-intensity staining; 2, moderate-intensity staining; 3, strong intensity staining) and the staining density (1, 0–10%; 2, 11–50%; 3, 51–100%). The total IHC score (staining intensity score × staining density score) ranged from 0 to 9. The IHC score <4 was defined as IL7R low expression and the IHC score ≥4 was defined as IL7R high expression.

RT-qPCR

Total RNA was extracted and reverse transcription was performed based on the manufacturer's protocol. A NanoDrop 2000 (Thermo, MA, United States) was used to measure the RNA concentration. RT-qPCR was performed with an ABI Illumina instrument

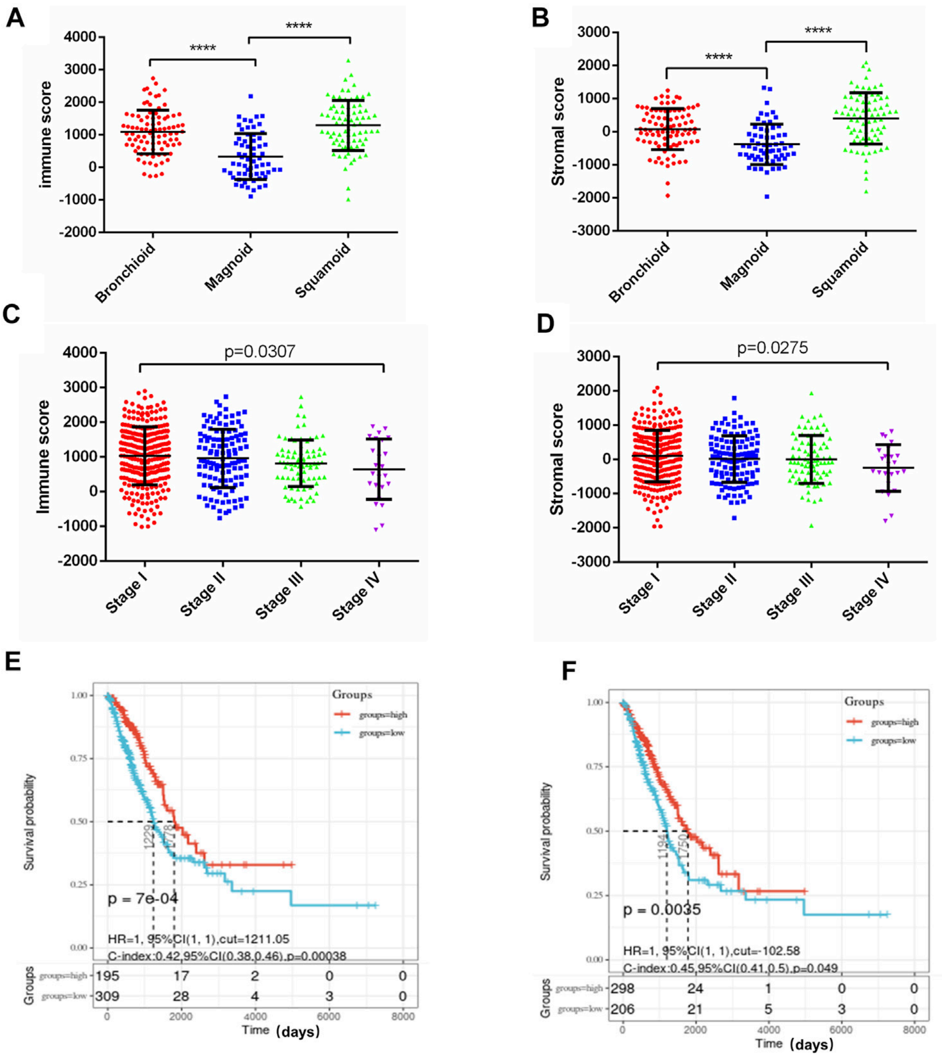

FIGURE 1 | Immune scores and stromal scores are associated with LUAD subtypes, clinical stage, and survival. **(A)** Distribution of immune scores in LUAD molecular subtypes. Box-plot shows a significant association between molecular subtypes and the level of immune scores ($n = 516$, $p < 0.001$). **(B)** Distribution of stromal scores of LUAD molecular subtypes. Box-plot shows a significant association between LUAD molecular subtypes and the level of stromal scores ($n = 516$, $p < 0.001$). **(C)** Distribution of immune scores for LUAD clinical stage. Box-plot shows a significant association between the clinical stage and the level of immune scores ($n = 516$, $p = 0.0307$). **(D)** Distribution of stromal scores for LUAD clinical stage. Box-plot shows a significant association between the clinical stage and the level of immune scores ($n = 516$, $p = 0.0275$). **(E)** The Kaplan-Meier survival curve showed the overall survival of the high score group is longer than the low score group, $p = 7e\text{-}04$. **(F)** LUAD cases were divided into two groups based on their stromal scores, the overall survival of the high score group is longer than the low score group, $p = 0.035$. **** $p < 0.0001$.

(Steponeplus, United States) using SYBRGreen (Roche, Swiss). Semi-quantitative analysis of the mRNA expression level was quantified by the $2^{-\Delta\Delta Ct}$ method.

Western Blot

Cells were harvested and lysed with RIPA lysis solution (Solarbio, China) supplemented with protease and phosphorylase inhibitors. The concentration of cell protein was determined by the BCA assay kit (Beyotime, China) and equal amounts of proteins were resolved by SDS-PAGE gel and transferred to the PVDF membrane. Afterward, the primary and secondary antibodies were added for incubation. Finally, the membranes were washed with PBST and visualized with ECL detection reagent (Beyotime, China). The primary antibodies were as follows: IL7R (1:1,000; ABclonal; A13503) and β-actin (1:1,000; Zhongshan Golden Bridge; TA-09).

Statistical Analysis

Discrete and continuous data are presented as a count with proportion and mean (± standard deviation) or median (interquartile range [IQR]), respectively, with standard methods for group comparison. Comparison between two groups was performed by Students t-test. One way-ANOVA was used for comparison in multiple groups. The association between IL7R expression and clinicopathological parameters was performed by the chi-squared test. Survival curves were drawn

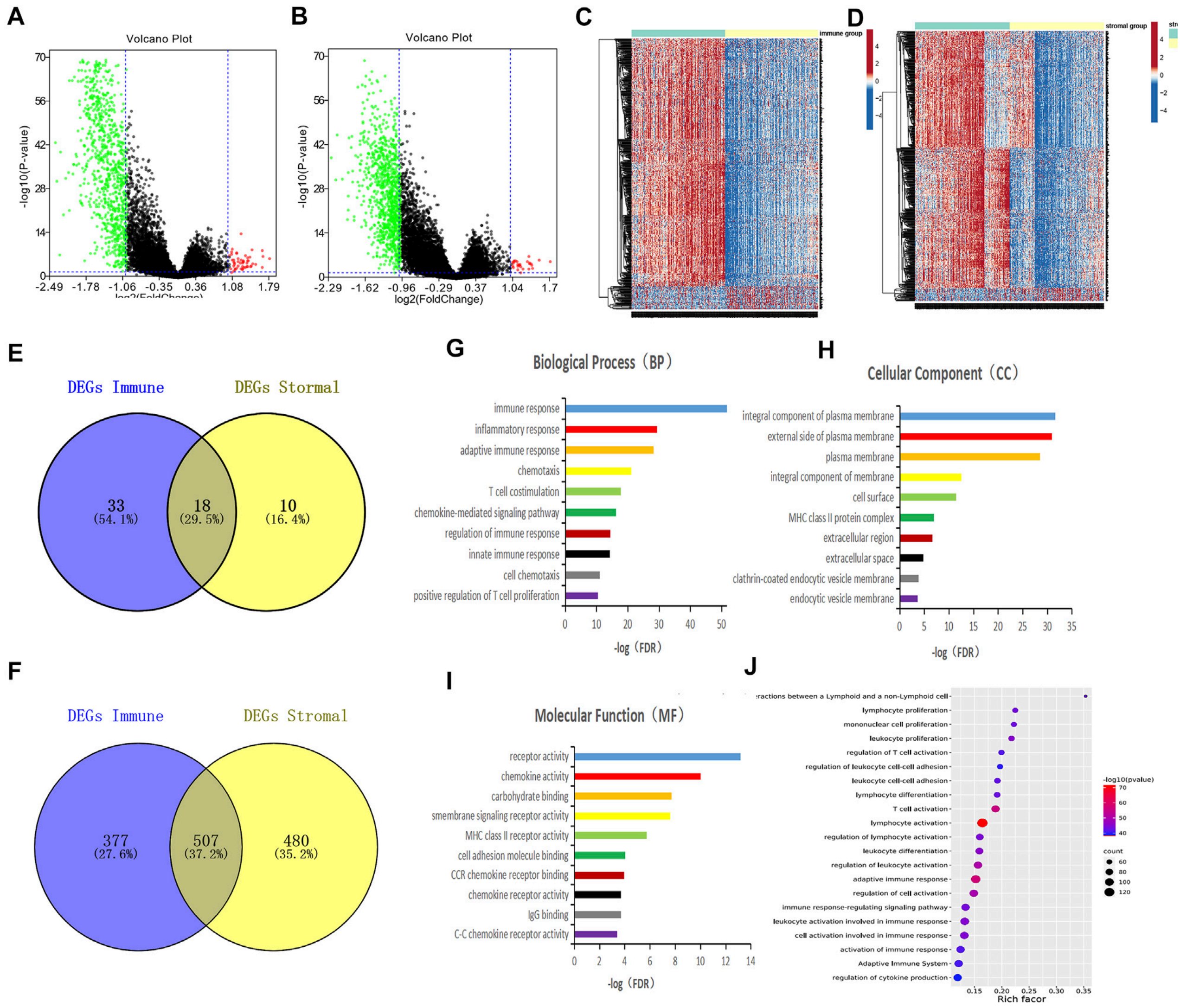

FIGURE 2 | Screening differential genes related to tumor immune microenvironment in lung adenocarcinoma. **(A,B)** Patients with LUAD were grouped according to immune/stromal scores, volcano plots were drawn using Limma package of R language, $|\log2FC|>1$, $p < 0.05$. Genes with high expression are shown in red, low expression is shown in green, genes with the same expression level are in black. **(C,D)** Heatmap of the DEGs of immune/stromal scores of top half (high score) vs bottom half (low score). $p < 0.05$, FC > 1) **(E,F)** Venn diagrams showing the number of commonly upregulated **(E)** or downregulated **(F)** DEGs in stromal and immune score groups. **(G–I)** Top 10 GO terms. False discovery rate (FDR) of GO analysis was acquired from DAVID functional annotation tool, $p < 0.05$. **(J)** Bubble plots showed the annotation of the DEGs KEGG pathway, $p < 0.05$.

based on the Kaplan-Meier method. $p < 0.05$ was considered significantly different. All statistical analyses were performed by using the R language (version 3.5.3).

RESULTS

Immune Scores and Stromal Scores Are Significantly Associated With LUAD Molecular Subtypes, Clinical Stage, and Survival

We downloaded the data of lung adenocarcinoma mRNA expression and clinical profiles from the TCGA database. In this study, we obtained information about 516 LUAD patients from the TCGA database and calculated the immune score and stromal score of each sample by ESTIMATE algorithm. The range of immune score was from −13,355.85 to 3,286.67, and the range of stromal score was from −1959.31 to 2098.77. We found that the immune score and stromal score were significantly associated with LUAD molecular subtypes, clinical stage, and survival. The squamoid subtype had the highest average immune score, followed by the bronchoid subtype. Patients with the magnoid subtype had the lowest immune scores, $p < 0.0001$ (**Figure 1A**). The trend of the stromal score was consistent with the immune score, with squamoid subtype having the highest score, magnoid having the lowest score, and bronchoid subtype having the score

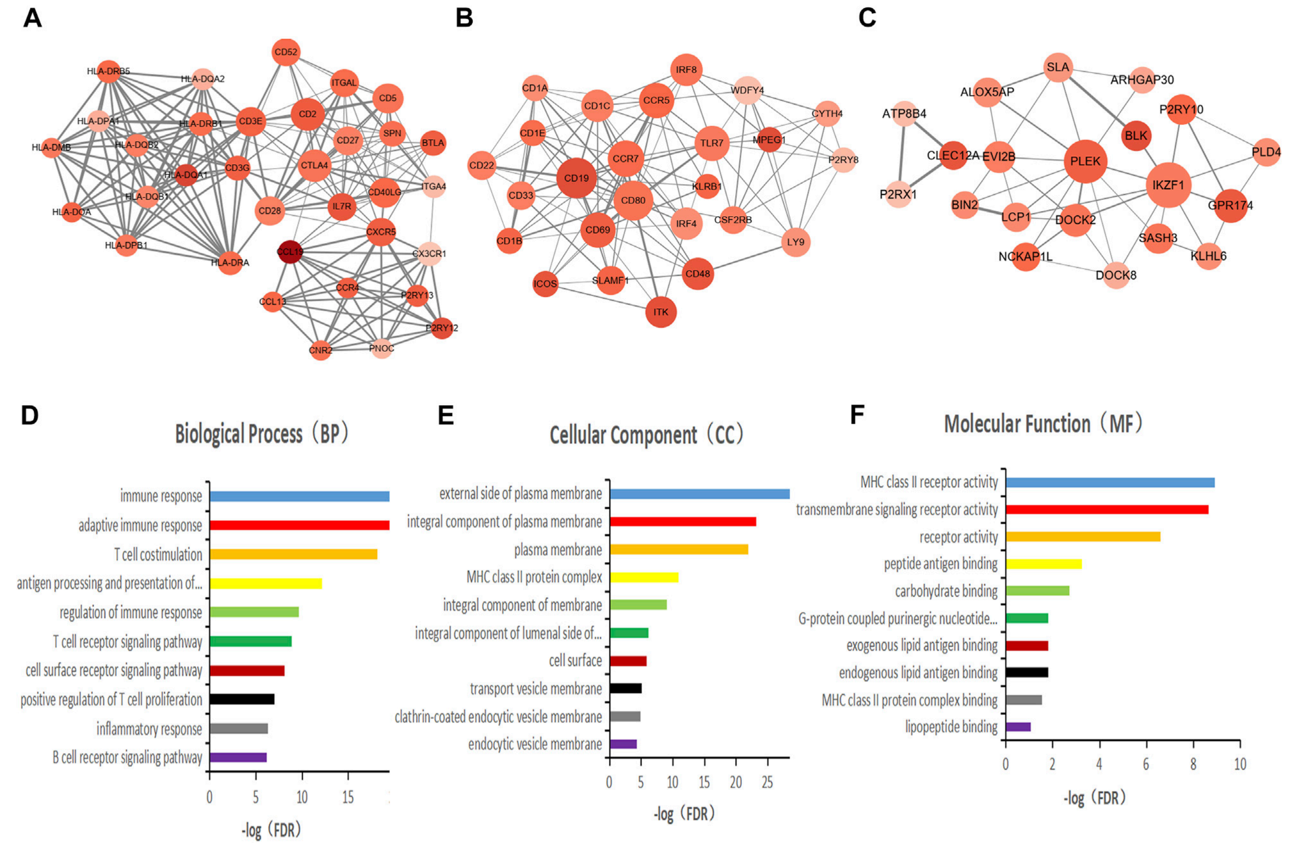

FIGURE 3 | PPI network was constructed to screen the key genes of immune function. **(A–C)** Interaction network constructed with the nodes with interaction confidence value > 0.5. The color of the nodes in the PPI network reflects the log(FC) value of the Z value of gene expression, and the size of the nodes represents the number of proteins interacting with the specified protein. **(D–F)** Top 10 GO terms of the mode gene in figure A. False discovery rate (FDR) of GO analysis was acquired from DAVID functional annotation tool, $p < 0.05$.

in the middle, $p < 0.0001$ (**Figure 1B**). In addition, the immune score and stromal score were decreased with the elevated clinical stage of lung adenocarcinoma. The immune/stromal score of stage I patients was significantly higher than that of stage IV patients (**Figures 1C,D**). Patients with LUAD were grouped into low-and high-immune/stromal score groups based on the cut-off value for immune scores (1,211.05) or stromal scores (102.58). Survival analysis showed that LUAD patients with higher immune or stromal scores had significantly better overall survival than those with lower scores (**Figures 1E,F**).

Screening Differential Genes Related to Tumor Immune Microenvironment in Lung Adenocarcinoma

To identify genes that play important roles in the TME of LUAD, we evaluated the mRNA sequencing data of 516 LUAD patients in the TCGA database which were divided into high and low score groups according to immune/stromal scores. The differential expression genes (DEGs) were screened out by the Limma package of R language, the results were shown in the Volcano plots (**Figures 2A,B**). There were 51 up-regulated genes and 884 down-regulated genes in the high immune score group compared with the low score group. Based on stromal scores, 28 genes were up-regulated and 987 genes were down-regulated in the high stromal score group ($|\log2FC|>1, p < 0.05$). The heatmap showed distinct expression profiles of the DEGs in LUAD patients according to the immune/stromal scores (**Figures 2C,D**). A total of 18 up-regulated genes and 507 down-regulated genes were screened as DEGs by drawing a Venn diagram for intersection (**Figures 2E,F**). Then, we performed GO functional enrichment analysis on 507 down-regulated genes. The result showed the top 10 GO terms of the biological process included immune response, inflammatory response, adaptive immune response, chemotaxis, T cell costimulation, Chemokine-mediated signaling pathway, regulation of immune response, innate immune response, cell chemotaxis, and positive regulation of T cell proliferation (**Figure 2G**); MHC class II protein complex was shown in the top Go terms of CC(**Figure 2H**); and receptor activity, chemokine activity, MHC class II receptor activity, IgG binding were indicated in the top GO terms of MF (**Figure 2I**). The GO enrichment function of the KEGG pathway showed the DEGs were significantly related to the immune response pathway (**Figure 2J**).

PPI Network Was Constructed to Screen the Key Genes of Immune Function

To better understand the interactions of the DEGs, we constructed protein-protein interaction (PPI) networks using the STRING online tool. The network consisted of eight modules, 221 nodes, and 1,604 edges. We used Cytoscape software to analyze the PPI network and screened out the most important three modules for further analysis (**Figures 3A–C**). GO functional enrichment analysis was conducted on the genes in the three modules, and we found that only the first module of the gene set was functionally enriched in the immune function, including immune response, adaptive immune response, T cell costimulation, antigen processing and presentation, regulation of immune response, T cell receptor signaling pathway, cell surface receptor signaling pathway, positive regulation of T cell proliferation, inflammatory response, and B cell receptor signaling pathway (**Figures 3D–F**).

Screening Prognostic Genes for Lung Adenocarcinoma

To explore the potential role of DEGs in the overall survival of LUAD, we performed Cox survival analysis on 507 DEGs. The results showed 294 genes were associated with the OS in patients with LUAD by log-rank test, $p < 0.05$. We also downloaded the GSE68465 data set from the GEO database and screened 59 genes related to the prognosis of LUAD by Cox survival analysis. A total of 43 DEGs were determined to be related to LUAD prognosis after the intersection analysis of the above two datasets by the Venn diagram (**Figure4A**). GO functional enrichment analysis of these 43 genes showed a significant correlation with immune response, including immune cell activation, signal transduction, and antigen-antibody response (**Figures 4B–E**). By comparing 43 prognostic genes with 35 immune-related genes, we identified six immune microenvironment-related genes that could predict prognosis, including CD27, IL7R, CD40LG, CD28, CD2, and HLA-DQB1. We then downloaded a list of the immune genes from the Import website, which contains 2,483 immune genes symbols. Four prognostic immune genes were identified by comparing the list. According to the Cox survival analysis of the four genes, the univariate survival analysis result showed that tumor stage ($p < 0.001$), tumor size ($p < 0.001$), lymph node metastasis ($p < 0.001$), distant metastasis ($p = 0.002$), as well as the expression of IL7R ($p = 0.002$), CD40LG ($p = 0.001$), CD28($p = 0.024$), and HLA-DQB1($p = 0.014$) all affected the prognosis of LUAD patients (**Figure 4F**). Multivariate Cox analysis showed that **Figure 4F** only IL7R expression was an independent prognostic factor affecting the prognosis of lung adenocarcinoma, $p = 0.007$ (**Figure 4G**).

Relationship Between IL7R Expression and Clinical Features and Survival in Patients With Lung Adenocarcinoma

To clarify the relationship between IL7R and the clinical characteristics of LUAD patients, we analyzed the TCGA data and found that the expression level of IL7R in LUAD tissues was significantly lower than that in normal lung tissues, $p < 0.001$ (**Figure 5A**). The Oncomine datasets showed the expression of IL7R in lung cancer tissues was decreased in all 13 datasets (**Figure 5B**). The detailed analysis data were shown in **Table 1**. Then, we analyzed the relationship between IL7R and clinical features, and the survival of patients with lung adenocarcinoma was analyzed using datasets from TCGA. The expression of IL7R was correlated with the tumor size, the IL7R expression in the T1 stage was significantly higher than in other T stages (**Figure 5C**). We also found that the LUAD patients with high IL7R expression had significantly better overall survival (OS) and progression-free survival (PFS) than those with low IL7R expression (**Figures 5D,E**). Further verification was conducted in 40 tissue samples from LUAD patients and 35 cases of adjacent normal tissues, and it was found that the expression of IL7R was negative in lung adenocarcinoma tissues and positive in adjacent normal lung tissues. In lung adenocarcinoma tissue samples, the expression of IL7R is mainly located in the cytoplasm of tumor cells, and most of them are negative or weakly positive (**Figure 5F**). In addition, we analyzed the expression of IL7R in lung adenocarcinoma tissue samples with different growth patterns. The tissues of 40 LUAD patients included 20 cases of acinar adenocarcinoma (ACI). 15 cases of solid adenocarcinoma with mucin production (SPA), 3 cases were micropapillary predominant adenocarcinoma (MPA) and 2 cases were lepidic predominant adenocarcinoma (LPA). The result showed there was no correlation between the expression of IL7R and the growth pattern of lung adenocarcinoma ($p = 0.075$). We also found that the expression of IL7R in normal lung epithelial cell line was higher than that in lung adenocarcinoma cell lines (**Figures 5G,H**).

IL7R is Associated With Tumor Microenvironmental Status of Lung Adenocarcinoma

Due to the significant difference in the expression of IL7R in lung adenocarcinoma and normal tissues, we conducted a GSEA functional enrichment analysis of the KEGG pathway for IL7R, and the results confirmed that when IL7R expression was elevated, the KEGG pathway was mainly enriched in immune-related activities, including chemokine signaling pathway, natural killer cell-mediated cytotoxicity, B cell receptor signaling pathway, cytokine-cytokine receptor interaction, leukocyte transendothelial migration, and T cell receptor signaling pathway (**Figure 6A**). The decrease of IL7R expression was mainly concentrated in cell metabolic activities, such as glycan biosynthesis, peroxisome, clycosylphosphatidylinositol anchor (**Figure 6B**). These results suggested IL7R could be a potential indicator of TME status.

IL7R Is Associated With Immune Cell Infiltration in Lung Adenocarcinoma

To explore the mechanism of IL7R affecting the TME of lung adenocarcinoma, we analyzed the relationship between IL7R expression and the components of tumor-infiltrating lymphocytes in the TME of lung adenocarcinoma. The

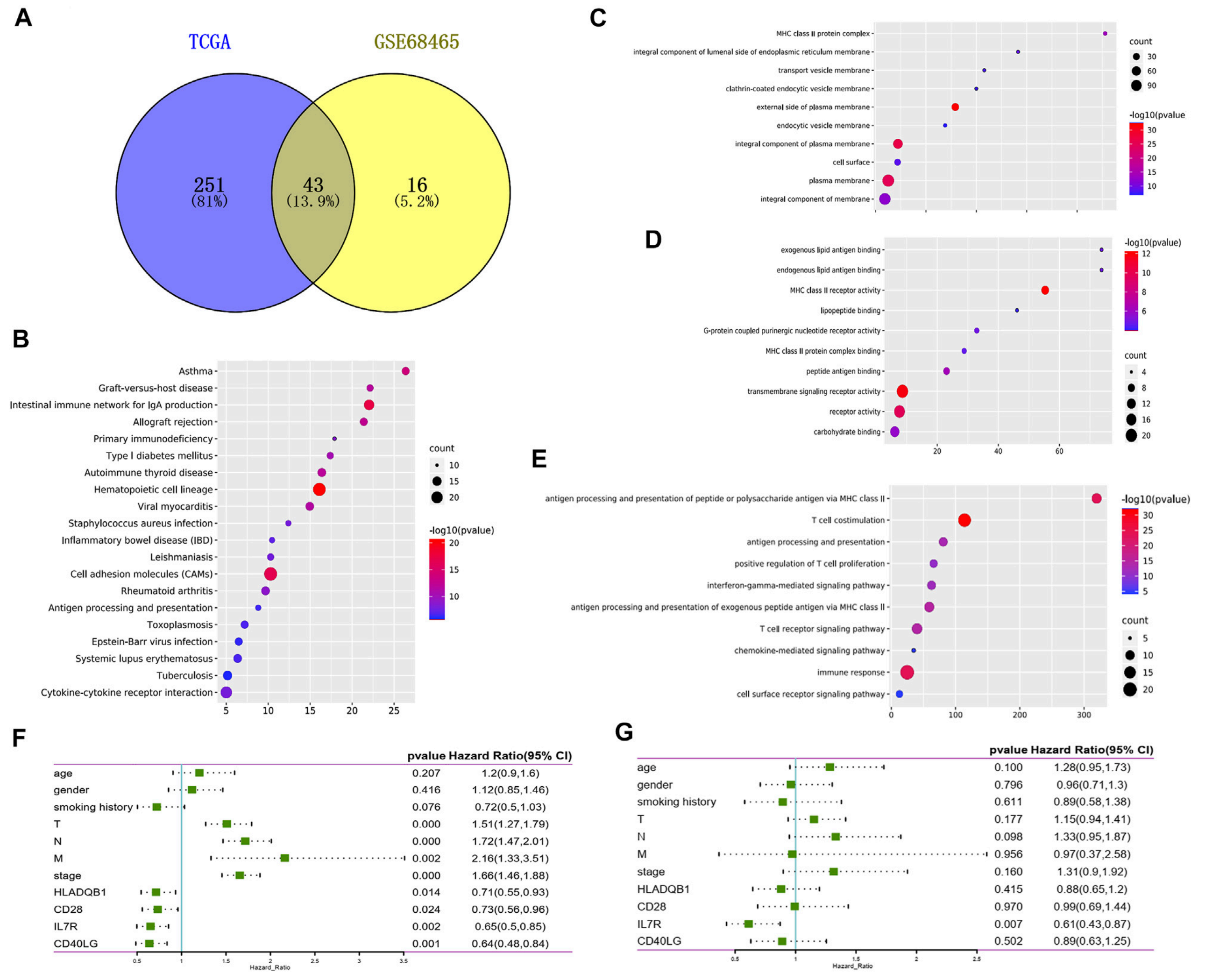

FIGURE 4 | Screening prognostic genes for lung adenocarcinoma. **(A)** Venn plot showed the prognostic gene shared by the TCGA and GSE68465 dataset in univariate COX analysis. **(B)** Bubble plots showed the annotation of the prognostic gene in KEGG pathway. **(C–E)** Top 10 GO terms of the prognostic gene. False discovery rate (FDR) of GO analysis was acquired from the DAVID functional annotation tool, $p < 0.05$. **(F)** Univariate Cox survival analysis of immune microenvironment related prognostic genes based on TCGA lung adenocarcinoma data. **(G)** Variate Cox survival analysis of immune microenvironment related prognostic genes based on TCGA lung adenocarcinoma data.

proportion of lung adenocarcinoma TIL was estimated using CIBERSORT analysis. The proportions and correlation of various TIL in TCGA lung adenocarcinoma samples were shown in **Figure 7A**. Grouped according to the median expression of IL7R, the infiltrating levels of 13 groups of TIL cells were found to be altered (**Figure 7B**). Next, the TIL ratio of TCGA lung adenocarcinoma samples was estimated by Timer algorithm, and the relationship between the changes of TIL components and the expression of IL7R was analyzed. We found the IL7R gene copy number variation significantly affected the infiltration levels of B cells, CD4 + T cells, and DC cells (**Figure 7C**).IL7R was negatively correlated with the tumor purity of lung adenocarcinoma and positively correlated with the expression of B cells, CD8+T cells, CD4+T cells, macrophages, monocytes, and DC cells (**Figure 7D**). Survival analysis showed the overall survival of patients with lung adenocarcinoma was positively correlated with the expression of B cells, DC cells, and IL7R (**Figure 7E**).

DISCUSSION

TME is composed of various types of immune cells, their secreted products (cytokines, chemokines), and extracellular matrix (Killock, 2018). Previous studies have suggested that the immune microenvironment plays an important role in the occurrence and development of primary lung cancer, and affects the treatment and prognosis of lung cancer (Almatroodi et al., 2016; Condamine et al., 2016; Bauer et al., 2017; Carrega and Ferlazzo, 2017; Janakiram et al., 2017). Studying the relationship

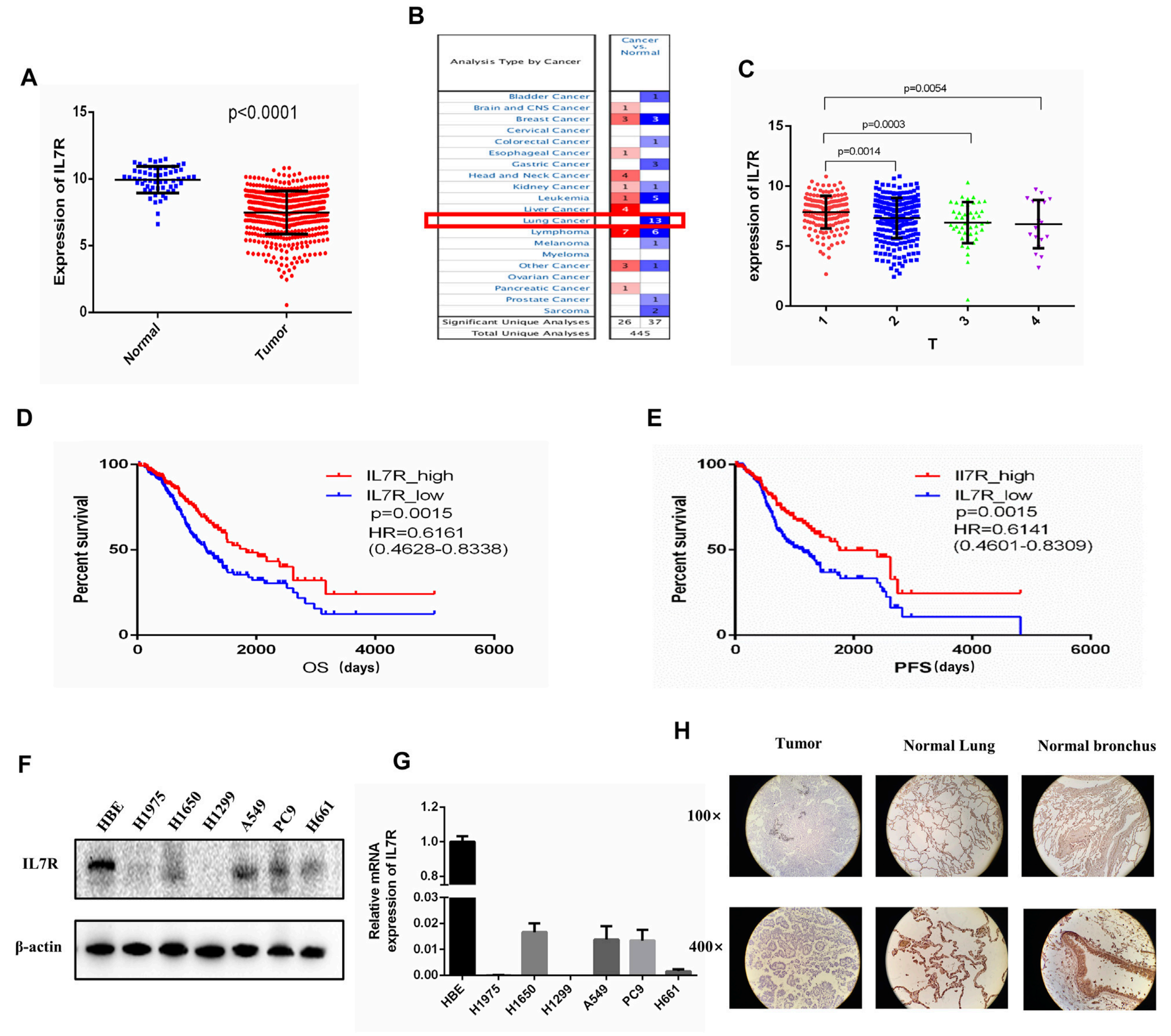

FIGURE 5 | The expression of IL7R in lung adenocarcinoma tissues was lower than that in normal tissues and correlated with tumor size and patient survival. **(A)** IL7R expression in lung adenocarcinoma tissue was significantly lower than that in normal lung tissue based on TCGA data, *p* < 0.001. **(B)** The Oncomine database showed that the expression level of IL7R in lung cancer tissues in 13 data sets was lower than that in normal tissues. **(C)** The expression level of IL7R was negatively correlated with tumor size. **(D)** Kaplan-Meier survival curves showed the LUAD patients with high IL7R expression had better overall survival than those with low IL7R expression, *p* = 0.0015. **(E)** Patients with high IL7R expression also had better progression-free survival than those with low IL7R expression, *p* = 0.0015. **(F)**The expression of IL7R in normal lung epithelial cell line HBE was higher than that in lung adenocarcinoma cell lines assayed by Western blot and **(G)** qRT-PCR. **(H)** Immunohistochemical staining showed IL7R was expressed at low level in LUAD tumors (left) compared with para-carcinoma tissue (lung tissue, middle; bronchus, right), (×100 and×400, respectively).

between DEGs and the immune microenvironment, exploring the underlying mechanism may provide a new landscape for immunotherapy. In this study, we mined the expression profile data of a large number of lung adenocarcinoma samples from TCGA, evaluated the immune and stromal components of the samples, and calculated the immune/stromal scores. The immune/stromal score was determined to be significantly correlated with the molecular subtypes, clinical stage, and overall survival of lung adenocarcinoma, demonstrating that the immune microenvironment of lung adenocarcinoma is highly correlated with the clinicopathological features of lung adenocarcinoma.

Lung adenocarcinoma can be divided into three molecular subtypes, named bronchioid, squamoid, and magnoid according to its genetic pattern (Almatroodi et al., 2016; Condamine et al., 2016; Bauer et al., 2017; Carrega and Ferlazzo, 2017; Janakiram et al., 2017). These subtypes are associated with prognosis, patients with bronchioid subtype may have a superior survival and the survival was worse in magnoid tumors compared with both

TABLE 1 | Transcription expression of IL7R between LUAD and normal lung tissues (Oncomine).

Types of LUAD vs. Lung	Fold change	*p*-value	*t*-test	Ref
Lung adenocarcinoma	−6.208	1.5E-6	−6.419	Bhattacharjee Lung
Lung adenocarcinoma	−2.816	1.9E-7	−6.159	Stearman Lung
Lung adenocarcinoma	−2.278	7.41E-4	−4.914	Garber Lung
Lung adenocarcinoma	−2.420	5.7E-8	−6.126	Su Lung
Lung adenocarcinoma	−2.646	1.17E-15	−9.377	Landi Lung
Lung adenocarcinoma	−2.406	1.40E-11	−7.896	Hou Lung
Lung adenocarcinoma	−2.252	1.38E-10	−6.925	Selamat Lung
Lung adenocarcinoma	−1.976	1.77E-4	−4.686	Beer Lung
Lung adenocarcinoma	−1.833	1.25E-5	−5.188	Okayama Lung

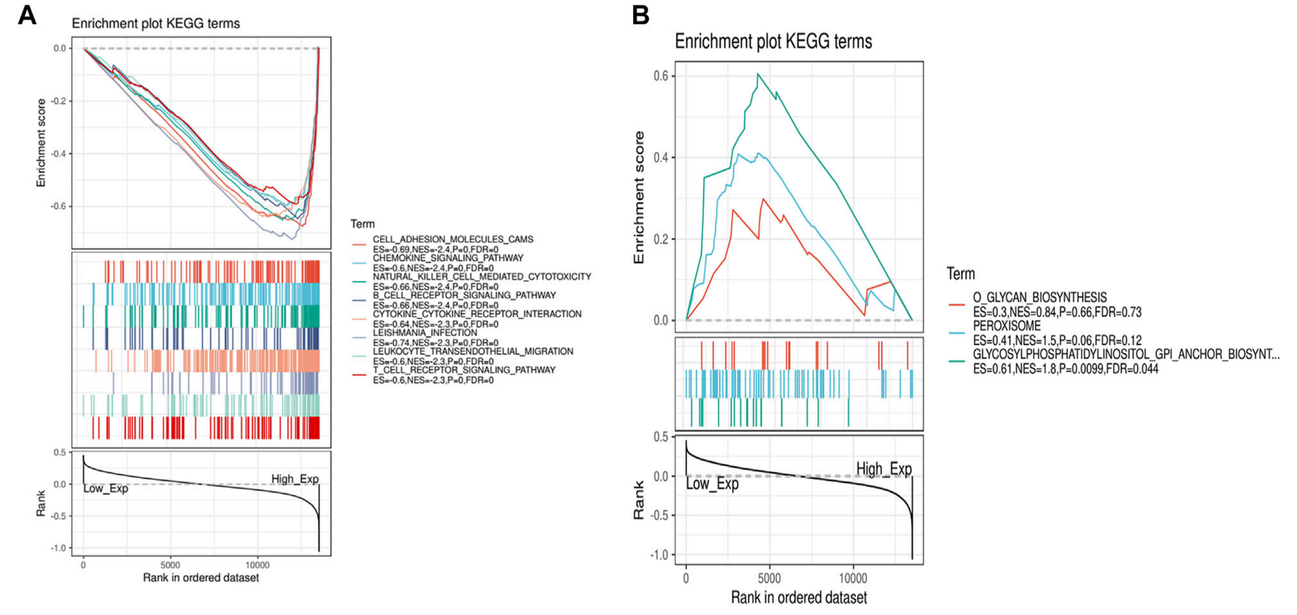

FIGURE 6 | GSEA for samples with high IL7R expression and low expression. **(A)** The enriched gene sets in HALLMARK collection by the high IL7R expression sample. Each line representing one particular gene set with unique color, $p < 0.05$ were considered significant. **(B)** The enriched gene sets in HALLMARK by samples with low IL7R expression, $p < 0.05$.

bronchioid and squamoid tumors (Wilkerson et al., 2012). Our result showed that both the squamoid and bronchioid subtypes had higher immune and stromal scores than the magnoid subtype. These results further suggested that high immune/stromal scores may be associated with better outcomes in patients with bronchioid subtypes. With the increase of tumor diameter, the immune/stromal scores decreased, suggesting that the immune microenvironment components of LUAD may have inhibitory effects on the formation and proliferation of tumors. Survival analysis showed that patients with high immune/stromal scores had better OS and PFS than those with low scores, indicating that the immune/stromal score of lung adenocarcinoma is a good prognostic marker for lung adenocarcinoma. Therefore, we believed the TME of lung adenocarcinoma played an important role in the development of tumors and the prognosis of patients.

To identify immune-related genes that play crucial roles in the TME of lung adenocarcinoma, we screened DEGs according to the immune/stromal scores. A total of 525 DEGs were screened by intersection analysis, among which 18 genes were up-regulated and 507 genes were down-regulated. GO enrichment functional analysis was performed on all down-regulated genes, and we found that the functions of DEGs were mainly focused on the immune response. Then, we identified 35 genes with important functions among the DEGs by constructing PPI networks. These hub genes showed significant roles related to immune response, indicating that these 35 genes play an important role in the TME of LUAD.

To search for prognostic genes for LUAD, we performed Cox survival analysis on lung adenocarcinoma data of TCGA and GSE68465 datasets. There were 294 prognostic genes in the TCGA dataset and 59 prognostic genes in the GSE68465 dataset. By intersection analysis of the prognostic genes from the above two datasets, 43 prognostic genes were screened out. These prognostic genes were found to be associated with T cell

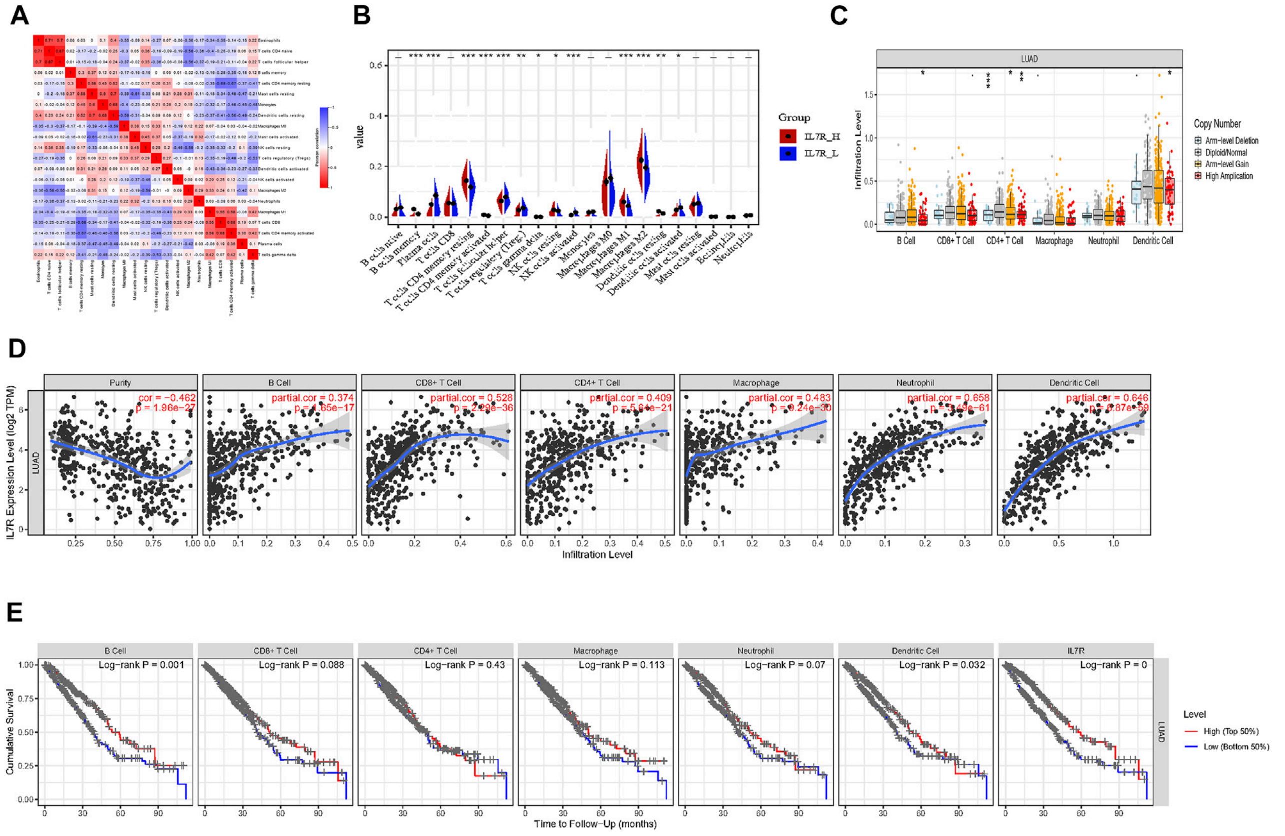

FIGURE 7 | IL7R is associated with immune cell infiltration in lung adenocarcinoma. **(A)** Heatmap showing the correlation between 21 kinds of TIL and the shade of each tiny color box represented corresponding correlation value between two types of cells. **(B)** Violin plot showed the ratio differentiation of 21 kinds of immune cells between LUAD tumor samples with low or high IL7R expression, and Wilcoxon rank-sum was used for the significance test. **(C)** IL7R gene copy number variation significantly affected the infiltration levels of B cells, CD4 + T cells, and DC cells. **(D)** IL7R was negatively correlated with the tumor purity of lung adenocarcinoma and positively correlated with the expression of B cells, CD8+T cells, CD4+T cells, macrophages, monocytes, and DC cells. **(E)** Survival analysis showed the overall survival of patients with lung adenocarcinoma was positively correlated with the expression of B cells, DC cells, and IL7R.

synthesis, MHCII receptor function, antigen presentation, and other immune responses. We compared the previous 35 immune microenvironment-related genes with 43 prognostic genes and finally obtained six overlapping genes. We downloaded the list of immune gene symbols for lung adenocarcinoma from the Immport website for comparison, and four of them were determined to be immunity-related genes. Therefore, we suggest that these four genes are key genes that play important roles in the TME of LUAD and influence the prognosis of patients. Cox survival analysis of these four genes revealed that only IL7R was an independent prognostic factor for OS in LUAD patients.

TCGA and Oncomine database analysis showed that the expression of IL7R was significantly higher in normal lung tissues than in LUAD tissues, this result was further verified by tissue samples and cell lines. The IL7R expression was negatively correlated with tumor size and positively correlated with overall survival and progression-free survival in LUAD patients. In order to clarify the functional mechanism of IL7R in LUAD, we performed GSEA functional enrichment analysis on IL7R. The results showed that the function of IL7R was related to the B cell receptor, T cell receptor, NK cell regulation of cytotoxicity, leukocyte chemotaxis, and other immune functions. Therefore, we speculate that IL7R may be involved in the regulation of lymphocyte infiltration in the TME, thus influencing the progression of lung adenocarcinoma.

TIL is an important component of TME, mainly consisting of T lymphocytes, B lymphocytes, natural killer (NK) cells, and other immune cells. These immune lymphocyte phenotypes can promote or inhibit the development of tumors (Rosenberg et al., 1986). TIL distribution characteristics can be used to predict the prognosis of cancer patients and the efficacy of immunotherapy (Keren et al., 2018). By the CIBOSORT analysis, we found that there were significant differences in the proportion of TIL among LUAD patients with different IL7R expression levels, which proved that IL7R could regulate TIL infiltration status. Based on the infiltration levels of TIL in groups with different IL7R expression levels, we found 12 groups of TILs had significant changes in the infiltration levels. Next, we evaluated the correlation between the IL7R expression and the infiltration level of TIL using the Timer algorithm. The result indicated that the expression of IL7R was positively correlated with all six types of TILs, and the gene copy number variation of IL7R has significantly affected the infiltration level of B cells, CD4 + T cells, and DC cells. Survival analysis showed only B cells, DC cells, and IL7R were significantly associated with the OS of LUAD patients. Above all, we believe IL7R inhibits the progression of lung adenocarcinoma by modulating the infiltration levels of B cells, DC cells, and CD4 + T cells, thus affecting the survival of patients.

IL7R is a protein-coding gene, which encodes the receptor of interleukin 7 (IL7) (Mazzucchelli and Durum, 2007). It is critical for the development of T cells and B cells, the survival of juvenile T cells, and the maintenance of memory T cells (Clark et al., 2014; Leung et al., 2019). It is necessary for the development and maintenance of innate lymphoid cells, also for the generation and development of the lymphoid structural barriers (Seddon et al., 2002). IL7R deficiency is associated with severe combined immunodeficiency (SCID) (Puel et al., 1998; Roifman et al., 2000). In our study, we found that IL7R was significantly associated with infiltration of B cell, $CD4^+$ T cell, DC cell, and it also affected the prognosis of patients with LUAD. The infiltrating B lymphocyte is an important part of tertiary lymphoid structures (TLSs), which is an ectopic lymphoid organ that forms in non-lymphoid tissues during chronic inflammation and tumor progression (Sautès-Fridman et al., 2019). B cell infiltration and the formation of TLSs were found to be positively correlated with the immunotherapy response in patients with different tumor types. It is suggested that infiltrating B lymphocytes play an important role in the treatment of ICB and predict the prognosis (Cabrita et al., 2020; Helmink et al., 2020; Petitprez et al., 2020).CD4+ T cells are mainly expressed as helper T cells, and assist in the activation of other cells. Cytokines secreted by Th1 cells in the subsets of $CD4^+$ helper T cells, especially interleukin-2 (IL-2) and IFN-γ, can activate and promote the function of CD8+T cells and NK cells (Knutson and Disis, 2005). Dendritic Cells (DC) are professional Antigen-presenting Cells (APC), which have attracted much attention in recent years. DC cells can absorb, process, and present antigens to initiate T cell-mediated immune response (Laoui et al., 2016). Above all, our results suggest that IL7R can influence the distribution of TIL, and inhibit tumor occurrence and progression by increasing the infiltration proportion of the above three TILs.

In conclusion, IL7R is a biomarker for predicting a good prognosis of lung adenocarcinoma. IL7R could also be a potential therapeutic target for the treatment of lung adenocarcinoma.

DATA AVAILABILITY STATEMENT

The datasets presented in this study can be found in online repositories. The names of the repository/repositories and accession number(s) can be found in the article/ **Supplementary Material**.

ETHICS STATEMENT

The studies involving human participants were reviewed and approved by the Ethics Committee of Jiangnan University affiliated hospital. The patients/participants provided their written informed consent to participate in this study.

AUTHOR CONTRIBUTIONS

XW, YM, YY designed research; XW performed the experiments and drafted the manuscript; SJC and JJL contributed to the qRT-PCR assay; TW and ZBH were involved in the western blot assay; XW collected the human LUAD tissues; XW, JJS and RRW analyzed data; YM reviewed the manuscript. All authors read and approved the final manuscript.

FUNDING

The work was funded by the National Cancer Center of China Climbing Fund (NCC201808B017).

SUPPLEMENTARY MATERIAL

The Supplementary Material for this article can be found online at: https://www.frontiersin.org/articles/10.3389/fphar.2022.857289/full#supplementary-material

REFERENCES

Almatroodi, S. A., McDonald, C. F., Darby, I. A., and Pouniotis, D. S. (2016). Characterization of M1/M2 Tumour-Associated Macrophages (TAMs) and Th1/Th2 Cytokine Profiles in Patients with NSCLC. *Cancer Microenviron* 9 (1), 1–11. doi:10.1007/s12307-015-0174-x

Bauer, A. K., Velmurugan, K., Xiong, K. N., Alexander, C. M., Xiong, J., and Brooks, R. (2017). Epiregulin Is Required for Lung Tumor Promotion in a Murine Two-Stage Carcinogenesis Model. *Mol. Carcinog* 56 (1), 94–105. doi:10.1002/mc.22475

Bray, F., Ferlay, J., Soerjomataram, I., Siegel, R. L., Torre, L. A., and Jemal, A. (2018). Global Cancer Statistics 2018: GLOBOCAN Estimates of Incidence and Mortality Worldwide for 36 Cancers in 185 Countries. *CA Cancer J. Clin.* 68 (6), 394–424. doi:10.3322/caac.21492

Cabrita, R., Lauss, M., Sanna, A., Donia, M., Skaarup Larsen, M., Mitra, S., et al. (2020). Tertiary Lymphoid Structures Improve Immunotherapy and Survival in Melanoma. *Nature* 577 (7791), 561–565. doi:10.1038/s41586-019-1914-8

Carrega, P., and Ferlazzo, G. (2017). Natural Killers Are Made Not Born: How to Exploit NK Cells in Lung Malignancies. *Front. Immunol.* 8, 277. doi:10.3389/fimmu.2017.00277

Chen, B., Khodadoust, M. S., Liu, C. L., Newman, A. M., and Alizadeh, A. A. (2018). Profiling Tumor Infiltrating Immune Cells with CIBERSORT. *Methods Mol. Biol.* 1711, 243–259. doi:10.1007/978-1-4939-7493-1_12

Chen, W., Zheng, R., Baade, P. D., Zhang, S., Zeng, H., Bray, F., et al. (2015). Cancer Statistics in China, 2015. *CA Cancer J. Clin.* 66 (2), 115–132. doi:10.3322/caac.21338

Clark, M. R., Mandal, M., Ochiai, K., and Singh, H. (2014). Orchestrating B Cell Lymphopoiesis through Interplay of IL-7 Receptor and Pre-B Cell Receptor Signalling. *Nat. Rev. Immunol.* 14 (2), 69–80. doi:10.1038/nri3570

Condamine, T., Dominguez, G. A., Youn, J. I., Kossenkov, A. V., Mony, S., Alicea-Torres, K., et al. (2016). Lectin-type Oxidized LDL Receptor-1 Distinguishes Population of Human Polymorphonuclear Myeloid-Derived Suppressor Cells in Cancer Patients. *Sci. Immunol.* 1, 1aaf8943–aaf8943. doi:10.1126/sciimmunol.aaf8943

DeSantis, C. E., Siegel, R. L., Sauer, A. G., Miller, K. D., Fedewa, S. A., Alcaraz, K. I., et al. (2016). Cancer Statistics for African Americans, 2016: Progress and Opportunities in Reducing Racial disparitiesProgress and Opportunities in Reducing Racial Disparities. CA Cancer J Clin. *CA Cancer J. Clin.* 66 (4), 290–308. doi:10.3322/caac.21340

Dougan, M., and Dranoff, G. (2009). Immune Therapy for Cancer. *Annu. Rev. Immunol.* 27 (1), 83–117. doi:10.1146/annurev.immunol.021908.132544

Dougan, M., and Dranoff, G. (2009). The Immune Response to Tumors. *Curr. Protoc. Immunol.* 20, 11. doi:10.1002/0471142735.im2011s85

Hayes, D. N., Monti, S., Parmigiani, G., Gilks, C. B., Naoki, K., Bhattacharjee, A., et al. (2006). Gene Expression Profiling Reveals Reproducible Human Lung Adenocarcinoma Subtypes in Multiple Independent Patient Cohorts. *J. Clin. Oncol.* 24 (31), 5079–5090. doi:10.1200/JCO.2005.05.1748

Helmink, B. A., Reddy, S. M., Gao, J., Zhang, S., Basar, R., Thakur, R., et al. (2020). B Cells and Tertiary Lymphoid Structures Promote Immunotherapy Response. *Nature* 577 (7791), 549–555. doi:10.1038/s41586-019-1922-8

Huang, da. W., Sherman, B. T., and Lempicki, R. A. (2009). Systematic and Integrative Analysis of Large Gene Lists Using DAVID Bioinformatics Resources. *Nat. Protoc.* 4 (1), 44–57. doi:10.1038/nprot.2008.211

Janakiram, M., Shah, U. A., Liu, W., Zhao, A., Schoenberg, M. P., and Zang, X. (2017). The Third Group of the B7-CD28 Immune Checkpoint Family: HHLA2, TMIGD2, B7x, and B7-H3. *Immunol. Rev.* 276 (1), 26–39. doi:10.1111/imr.12521

Keren, L., Bosse, M., Marquez, D., Angoshtari, R., Jain, S., Varma, S., et al. (2018). A Structured Tumor-Immune Microenvironment in Triple Negative Breast Cancer Revealed by Multiplexed Ion Beam Imaging. *Cell.* 174 (6), 1373–e19. doi:10.1016/j.cell.2018.08.039

Killock, D. (2018). Sequencing Cells of the Immune TME. *Nat. Rev. Clin. Oncol.* 15 (9), 531. doi:10.1038/s41571-018-0069-0

Knutson, K. L., and Disis, M. L. (2005). Tumor Antigen-specific T Helper Cells in Cancer Immunity and Immunotherapy. *Cancer Immunol. Immunother.* 54 (8), 721–728. doi:10.1007/s00262-004-0653-2

Lambrechts, D., Wauters, E., Boeckx, B., Aibar, S., Nittner, D., Burton, O., et al. (2018). Phenotype Molding of Stromal Cells in the Lung Tumor Microenvironment. *Nat. Med.* 24 (8), 1277–1289. doi:10.1038/s41591-018-0096-5

Laoui, D., Keirsse, J., Morias, Y., Van Overmeire, E., Geeraerts, X., Elkrim, Y., et al. (2016). The Tumour Microenvironment Harbours Ontogenically Distinct Dendritic Cell Populations with Opposing Effects on Tumour Immunity. *Nat. Commun.* 7 (1), 13720. doi:10.1038/ncomms13720

Lavin, Y., Kobayashi, S., Leader, A., Amir, E. D., Elefant, N., Bigenwald, C., et al. (2017). Innate Immune Landscape in Early Lung Adenocarcinoma by Paired Single-Cell Analyses. *Cell.* 169 (4), 750–e17. doi:10.1016/j.cell.2017.04.014

Leung, G. A., Cool, T., Valencia, C. H., Worthington, A., Beaudin, A. E., and Forsberg, E. C. (2019). The Lymphoid-Associated Interleukin 7 Receptor (IL7R) Regulates Tissue-Resident Macrophage Development. *Development* 146 (14), 146dev176180. doi:10.1242/dev.176180

Li, T., Fan, J., Wang, B., Traugh, N., Chen, Q., Liu, J. S., et al. (2017). TIMER: A Web Server for Comprehensive Analysis of Tumor-Infiltrating Immune Cells. *Cancer Res.* 77 (21), e108–10. doi:10.1158/0008-5472.CAN-17-0307

Mazzucchelli, R., and Durum, S. K. (2007). Interleukin-7 Receptor Expression: Intelligent Design. *Nat. Rev. Immunol.* 7 (2), 144–154. doi:10.1038/nri2023

Metsalu, T., and Vilo, J. (2015). ClustVis: a Web Tool for Visualizing Clustering of Multivariate Data Using Principal Component Analysis and Heatmap. *Nucleic Acids Res.* 43 (W1), W566–W570. doi:10.1093/nar/gkv468

Petitprez, F., de Reyniès, A., Keung, E. Z., Chen, T. W., Sun, C. M., Calderaro, J., et al. (2020). B Cells Are Associated with Survival and Immunotherapy Response in Sarcoma. *Nature* 577 (7791), 556–560. doi:10.1038/s41586-019-1906-8

Puel, A., Ziegler, S. F., Buckley, R. H., and Leonard, W. J. (1998). Defective IL7R Expression in T(-)B(+)NK(+) Severe Combined Immunodeficiency. *Nat. Genet.* 20 (4), 394–397. doi:10.1038/3877

Ritchie, M. E., Phipson, B., Wu, D., Hu, Y., Law, C. W., Shi, W., et al. (2015). Limma powers Differential Expression Analyses for RNA-Sequencing and Microarray Studies. *Nucleic Acids Res.* 43 (7), e47. doi:10.1093/nar/gkv007

Roifman, C. M., Zhang, J., Chitayat, D., and Sharfe, N. (2000). A Partial Deficiency of interleukin-7R Alpha Is Sufficient to Abrogate T-Cell Development and Cause Severe Combined Immunodeficiency. *Blood* 96 (8), 2803–2807. doi:10.1182/blood.v96.8.2803

Rosenberg, S. A., Spiess, P., and Lafreniere, R. (1986). A New Approach to the Adoptive Immunotherapy of Cancer with Tumor-Infiltrating Lymphocytes. *Science* 233 (4770), 1318–1321. doi:10.1126/science.3489291

Sautès-Fridman, C., Petitprez, F., Calderaro, J., and Fridman, W. H. (2019). Tertiary Lymphoid Structures in the Era of Cancer Immunotherapy. *Nat. Rev. Cancer* 19 (6), 307–325. doi:10.1038/s41568-019-0144-6

Seddon, B., Zamoyska, R., and Il-7 Receptor Signals (2002). TCR and IL-7 Receptor Signals Can Operate Independently or Synergize to Promote Lymphopenia-Induced Expansion of Naive T Cells. *J. Immunol.* 169 (7), 3752–3759. doi:10.4049/jimmunol.169.7.3752

Shannon, P., Markiel, A., Ozier, O., Baliga, N. S., Wang, J. T., Ramage, D., et al. (2003). Cytoscape: A Software Environment for Integrated Models of Biomolecular Interaction Networks. *Genome Res.* 13 (11), 2498–2504. doi:10.1101/gr.1239303

Siegel, R. L., Miller, K. D., Fuchs, H. E., and JemalCancer Statistics, A. (2021). Cancer Statistics, 2021. *CA A. Cancer J. Clin.* 71 (1), 7–33. doi:10.3322/caac.21654

Subramanian, A., Tamayo, P., Mootha, V. K., Mukherjee, S., Ebert, B. L., Gillette, M. A., et al. (2005). Gene Set Enrichment Analysis: a Knowledge-Based Approach for Interpreting Genome-wide Expression Profiles. *Proc. Natl. Acad. Sci. U S A.* 102 (43), 15545–15550. doi:10.1073/pnas.0506580102

Szklarczyk, D., Franceschini, A., Wyder, S., Forslund, K., Heller, D., Huerta-Cepas, J., et al. (2015). STRING V10: Protein-Protein Interaction Networks, Integrated over the Tree of Life. *Nucleic Acids Res.* 43 (D1), D447–D452. doi:10.1093/nar/gku1003

Wilkerson, M. D., Yin, X., Walter, V., Zhao, N., Cabanski, C. R., Hayward, M. C., et al. (2012). Differential Pathogenesis of Lung Adenocarcinoma Subtypes Involving Sequence Mutations, Copy Number, Chromosomal Instability, and Methylation. *PLoS ONE* 7 (5), e36530. doi:10.1371/journal.pone.0036530

Yoshihara, K., Shahmoradgoli, M., Martínez, E., Vegesna, R., Kim, H., Torres-Garcia, W., et al. (2013). Inferring Tumour Purity and Stromal and Immune Cell Admixture from Expression Data. *Nat. Commun.* 4 (1), 2612. doi:10.1038/ncomms3612

Zappasodi, R., Merghoub, T., and Wolchok, J. D. (2018). Emerging Concepts for Immune Checkpoint Blockade-Based Combination Therapies. *Cancer Cell.* 33 (4), 581–598. doi:10.1016/j.ccell.2018.03.005

Conflict of Interest: The authors declare that the research was conducted in the absence of any commercial or financial relationships that could be construed as a potential conflict of interest.

Publisher's Note: All claims expressed in this article are solely those of the authors and do not necessarily represent those of their affiliated organizations, or those of the publisher, the editors, and the reviewers. Any product that may be evaluated in this article, or claim that may be made by its manufacturer, is not guaranteed or endorsed by the publisher.

Copyright © 2022 Wang, Chang, Wang, Wu, Huang, Sun, Liu, Yu and Mao. This is an open-access article distributed under the terms of the Creative Commons Attribution License (CC BY). The use, distribution or reproduction in other forums is permitted, provided the original author(s) and the copyright owner(s) are credited and that the original publication in this journal is cited, in accordance with accepted academic practice. No use, distribution or reproduction is permitted which does not comply with these terms.

frontiers
in Pharmacology

ORIGINAL RESEARCH
published: 23 February 2022
doi: 10.3389/fphar.2022.829684

ZWZ-3, a Fluorescent Probe Targeting Mitochondria for Melanoma Imaging and Therapy

Zengjin Liu[1]†, Hailan Wang[2,3]†, Changzhen Sun[1], Yuanmin He[2], Tong Xia[2], Jianv Wang[2], Xia Xiong[2], Qingbi Zhang[3], Sijin Yang[1]* and Li Liu[2]*

[1] National Traditional Chinese Medicine Clinical Research Base and Drug Research Center of the Affiliated Traditional Chinese Medicine Hospital of Southwest Medical University, Luzhou, China, [2] Department of Dermatology, The Affiliated Hospital of Southwest Medical University, Luzhou, China, [3] School of Public Health, Southwest Medical University, Luzhou, China

OPEN ACCESS

Edited by:
Dong-Hua Yang,
St. John's University, United States

Reviewed by:
Xuan Zhao,
Shandong University of Traditional Chinese Medicine, China
Francoise Degoul,
Institut National de la Santé et de la Recherche Médicale (INSERM), France

***Correspondence:**
Li Liu
liuli@swmu.edu.cn
Sijin Yang
ysjimn@swmu.edu.cn

†These authors have contributed equally to this work

Specialty section:
This article was submitted to Experimental Pharmacology and Drug Discovery,
a section of the journal Frontiers in Pharmacology

Received: 06 December 2021
Accepted: 24 January 2022
Published: 23 February 2022

Citation:
Liu Z, Wang H, Sun C, He Y, Xia T, Wang J, Xiong X, Zhang Q, Yang S and Liu L (2022) ZWZ-3, a Fluorescent Probe Targeting Mitochondria for Melanoma Imaging and Therapy. Front. Pharmacol. 13:829684. doi: 10.3389/fphar.2022.829684

The increased drug resistance and metastasis of melanoma resulted in poor prognosis of patients. Here, we designed and synthesized a novel hemicyanine-based fluorescent probe ZWZ-3, and investigated its application for melanoma imaging and treatment both *in vitro* and *in vivo*. ZWZ-3 preferentially accumulated in melanoma cells *via* a process that depended on the organic anion-transporting polypeptide (OATP), which targeted mitochondria on the hemicyanine cationic nitrogen. In addition, we investigated the effect and molecular mechanism of ZWZ-3 in melanoma. *In vitro* studies showed that ZWZ-3 promoted the generation of reactive oxygen species and induced mitochondrial-mediated cell apoptosis by upregulating Bax and activating caspase-3, caspase-9, and PARP. Importantly, ZWZ-3 also induced autophagy by upregulating LC-3II and Atg5 and downregulating P62. It significantly suppressed tumor growth of A375 xenograft tumor in mice without notable side effects. Histological and immunohistochemical analyses revealed that ZWZ-3 induced apoptosis and inhibited tumor cell proliferation. Thus, ZWZ-3 represents a novel theranostic agent that can be used to effectively targeting, detecting, and treating melanoma. It could also help monitoring disease progression and response to treatment.

Keywords: hemicyanine-based fluorescent probe, anti-cancer, mitochondrial-targeted, autophagy, apoptosis

INTRODUCTION

Melanoma is one of the most malignant tumors with high metastatic potential. Although it represents only 4% of dermal tumor cases, melanoma is the most dangerous and deadly form of dermal tumor, accounting for 75% of skin cancer-related deaths (Apalla et al., 2017; Hessler et al., 2020). Early-stage melanoma can be treated with surgical intervention, with relatively high 5-year survival rate, yet metastatic melanoma significantly shorten survival rate (Smart et al., 2021). Due to its aggressiveness, melanoma patients are often diagnosed at advanced stages with local infiltration or distant metastasis, which cannot be treated with surgery alone (Tse et al., 2017; Zhu et al., 2017). In addition, melanoma is one of the most potent drug-resistant cancers (Wang et al., 2015). Thus, multifunctional theranostic agents with the potential of simultaneous imaging-guided, tumor targeting and treatment are urgently needed to improve the timely diagnosis and treatment of the disease.

Cancer cell death involves various pathways including apoptosis, necrosis and autophagy. Apoptosis is a type of programmed cell death in which reactive oxygen species (ROS) are abnormally generated in response to diverse external stimuli, which enhanced oxidative stress in mitochondria and dysregulated the mitochondrial membrane and proteins (Cotter, 2009; D'Arcy, 2019). The released mitochondrial protein cytochrome C causes activation of caspase-like proteases, and leading to apoptotic cell death (Bajpai et al., 2020). Autophagy plays an important role of "garbage collector", which removed damaged cellular components or abnormal metabolites. During the process of autophagy, autophagosomes engulf cytoplasmic components, during which the cytosolic form of LC3, called LC3-I, converts into the autophagosome-associated LC3-II form (Huang et al., 2013; Zada et al., 2021). This conversion can therefore be used for tracking autophagy, as can the interaction between LC3 and the adapter protein p62 during autophagosome formation (Islam et al., 2018). The adapter protein P62 also interacts with polyubiquitinated proteins through the ubiquitin-associated domain to promote the autophagic degradation of ubiquitinated substrates (Zhang et al., 2013). Furthermore, p62 complexes with SQSTM1 could act as a selective autophagy receptor that degrades the autolysosome when autophagic flux increases (Xiang et al., 2021).

Mitochondria, the energy center of cells, are involved in different physiological processes and play essential roles in cancer development and progression. The dysfunction of mitochondria causes various disorders and affects the process of cancer cell survival and death. Accumulating evidence indicates that abnormal mitochondria accelerate tumor development and progression, including proliferation, migration, invasion, oxidative phosphorylation and apoptosis (Fu et al., 2019; Chiu et al., 2020). Although targeting mitochondria is widely recognized as important for effective anticancer therapy, most anti-cancer drugs are difficult to target this organelle (Wu et al., 2018). Based on the differences of mitochondria between normal cells and cancer cells, many mitochondrial-targeted agents have been developed for monitoring drug distribution and achieving specific therapies (Zhang et al., 2011; Zhang et al., 2021).

In particular, researchers have been developing "theranostic" compounds that could not only treat cancers but also detect or monitor their response to therapy. Current theranostics are based mainly on nanotechnology (Vinod and Jena, 2021; Wu et al., 2021) or conjugation with tumor-specific ligands (Zhao et al., 2019), contrast agents (Shu et al., 2021), and anticancer drugs (Kong et al., 2016; Jeyamogan et al., 2021). To some extent, these methods have been proofed to be promising, but there are some debates about the selectivity and specificity of these theranostics (Zhang et al., 2011). Therefore, it is crucial to develop alternative or innovative strategies for solving the above problems. Recently, small molecule-based fluorophores with unique inherent-targeting have attracted interests of researchers, because theranostic agents with this structure not only solves the problem of targeting but also benefits for large-scale application in the future (Wang et al., 2018). For instance, multifunctional heptamethine dyes that can be selectively enriched in the mitochondria of various human tumor xenografts have been developed for tumor imaging and therapy (von Kiedrowski et al., 2020; Zhang et al., 2021). However, they also exert some undesired side effects due to their poor water solubility and non-ideal antitumor activity.

Hemicyanines, as a principal member of the cyanine family, are commonly used in fluorescent sensors owing to their good optical properties, specifically, long absorption and emission wavelength, high fluorescence quantum yield and large Stokes shift (Kong et al., 2016; Zeng et al., 2021). Recently, several studies have reported the use of hemicyanine dyes as fluorescent probes for disease diagnosis in response to various biomarkers, including ROS

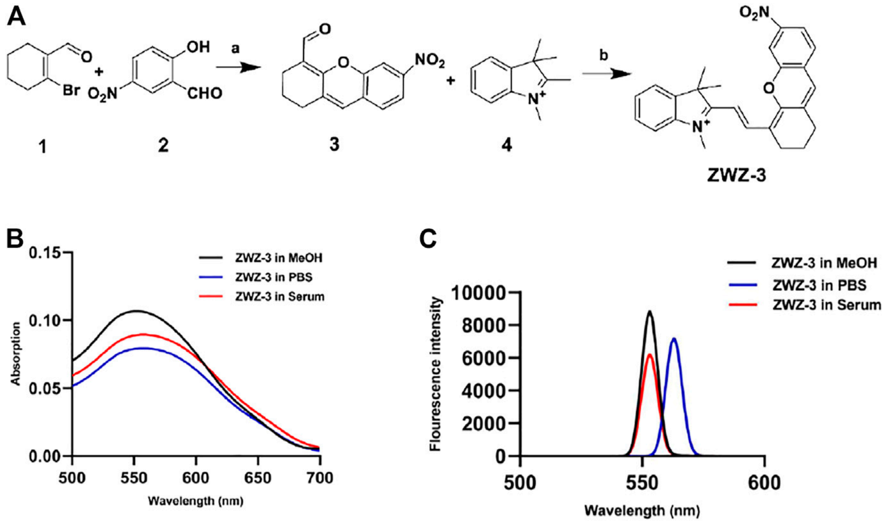

FIGURE 1 | Chemical synthesis and optical properties of ZWZ-3. **(A)** Synthetic route and chemical structure of ZWZ-3. a: Cs_2CO_3, DMF, 25°C, 12 h, yield: 50%; b: K_2CO_3, Ac_2O, 80°C, 12 h, yield: 73%. **(B)** The absorption spectra of 5 μM ZWZ-3 in methanol, PBS and 10% foetal bovine serum (FBS), respectively. **(C)** The fluorescence intensity of 5 μM ZWZ-3 in methanol, PBS and 10% FBS, respectively. All experiments were performed in triplicate.

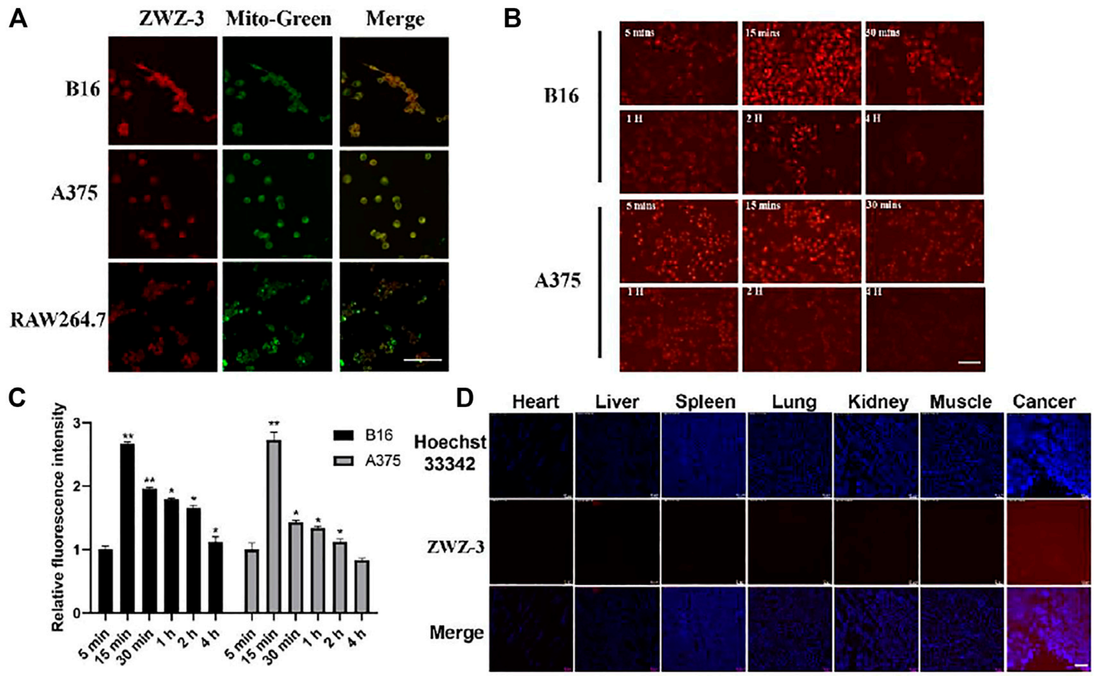
A
ZWZ-3
Mito-Green
Merge
B16
A375
RAW264.7
B
B16
5 mins
15 mins
30 mins
1 H
2 H
4 H
A375
5 mins
15 mins
30 mins
1 H
2 H
4 H
C
Relative fluorescence intensity
0
1
2
3
B16
A375
5 min
15 min
30 min
1 h
2 h
4 h
**
**
*
*
*
**
*
*
*
D
Heart
Liver
Spleen
Lung
Kidney
Muscle
Cancer
Hoechst 33342
ZWZ-3
Merge

FIGURE 2 | ZWZ-3 specifically locates to the mitochondria of cancer cells and targets tumor tissue. **(A)** Colocalization of ZWZ-3 with a mitochondria-specific tracker (Mito Tracker Green) in B16, A375 and RAW264.7 cells, imaged using a confocal microscope. **(B) (C)** fluorescence intensity in B16 and A375 cells was evaluated after incubation with the same concentration of ZWZ-3 (5 μM) for various times (*n* = 3). **(D)** C57BL/6J mice with B16 subcutaneous tumor xenografts were subjected to histopathologic analysis after a single-dose intravenous administration of ZWZ-3 at 2 mg/kg for 24 h. Organs and xenografts were imaged by fluorescence microscope. All experiments were conducted in three time and each point represents the mean ± SD (**p* < .05; ***p* < .01). Scale bar = 100 μm.

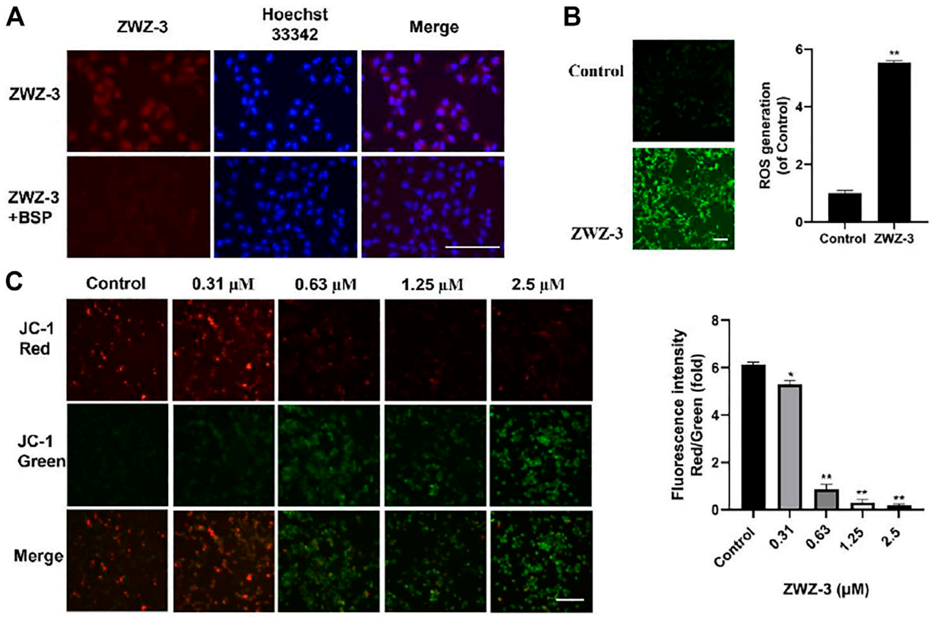
A
ZWZ-3
Hoechst 33342
Merge
ZWZ-3
ZWZ-3 +BSP
B
Control
ZWZ-3
ROS generation (of Control)
0
2
4
6
**
Control
ZWZ-3
C
Control
0.31 μM
0.63 μM
1.25 μM
2.5 μM
JC-1 Red
JC-1 Green
Merge
Fluorescence Intensity Red/Green (fold)
0
2
4
6
8
*
**
**
**
Control
0.31
0.63
1.25
2.5
ZWZ-3 (μM)

FIGURE 3 | ZWZ-3 enters the mitochondria of tumor cells through OATP to induce the production of ROS and mitochondrial membrane depolarization. **(A)** B16 cells were pretreated with vehicle control, sulfobromophthalein (BSP) (250 μM) for 20 min, then treated with 5 μM ZWZ-3 for 1 h prior to fluorescence microscope observations. **(B)** Intracellular ROS productions were detected using DCFH-DA. **(C)** B16 cells were pretreated with ZWZ-3 for 24 h, then treated with JC-1 for 20 min prior to fluorescence microscope observations. All experiments were carried out in triplicate and each point represents the mean ± SD (**p* < .05; ***p* < .01). Scale bar = 100 μm.

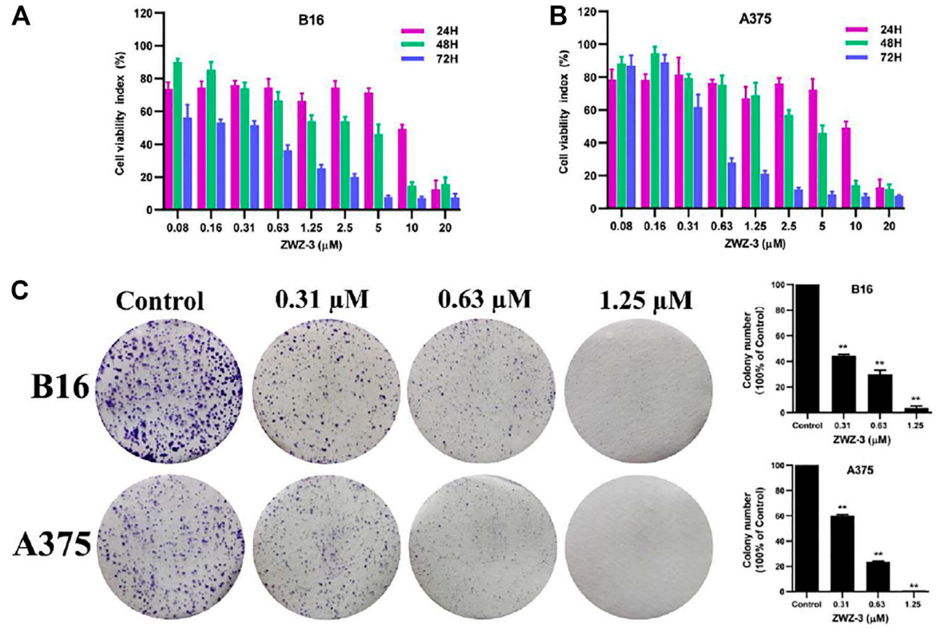

FIGURE 4 | *In vitro* anticancer activity of ZWZ-3 against melanoma cells. **(A,B)** melanoma cell lines (B16 and A375) were treated with various concentrations of ZWZ-3 for 24, 48 and 72 h respectively, and IC_{50} values were calculated. **(C)** B16 and A375 cells were treated with control or gradient concentrations of ZWZ-3 for 7 days. Then, the colony formation in each group was counted. Quantification is displayed on the right of each cell line. Dates are expressed as mean ± SD for 3 independent experiments (**$p < .01$).

and nitrogen species (Xie et al., 2016), biothiols (Chen et al., 2015), enzymes (Liu et al., 2019), and pH (Li et al., 2015). Furthermore, hemicyanine dyes have been widely applied for cancer imaging and imaging-guided surgical resection (Luo et al., 2018), but they have rarely been directly used in anti-cancer therapy.

In the present study, we developed the hemicyanine-based fluorescent probe ZWZ-3, which can be selectively enriched in the mitochondria of melanoma cells, thus promoting mitochondrial oxidative phosphorylation and inducing apoptosis and autophagy. In this way, ZWZ-3 shows promise as a novel theranostic agent for characterization and treatment of melanoma.

MATERIALS AND METHODS

Materials

All reactions were performed under magnetic stirring and in dried glassware. Unless otherwise stated, all chemicals and solvents were obtained from commercial sources and used without further purification. Analytical thin-layer chromatography was conducted on 0.20 mm silica gel plates (Haiyang, Qingdao, Shandong, China) under the indicator of QF-254 UV. Column chromatography was performed on Haiyang silica gel 60 (200–300 mesh). Mass spectra was obtained from the Agilent (United States). ^1H NMR and ^{13}C NMR spectra were analyzed on a Bruker DMX600 NMR spectrometer under tetramethyllsilane (TMS) as an internal standard. Peak multiplicity of NMR signals was as stated below: s, singlet; d, doublet; t, triplet; q, quartet; m, multiplet. Chemical shift (δ): ppm relative to Me4Si (internal standard). Coupling constant: J (Hz).

MTT (3-[4,5-dimethyl-2-thiazolyl]-2,5-diphenyl-2-H-tetrazolium bromide, thiazolyl blue tetrazolium bromide), H33342 were purchased from YuanYe Bio-Technology, China. AnnexinV-FITC/PI was purchased from Biosharp, China. DCFH-DA, JC-1, MitoTracker Green were purchased from Beyotime, China. Lipfiter transfection reagent was purchased from Hanbio, China. Sulfobromophthalein (BSP, a competitive inhibitor of OATP transporters) was purchased from BT Reagent, NAC (a pharmacological inhibitor of ROS) was purchased from Bestbio. Antibodies against Atg5 (#12994), P62 (#39749), PARP (#9532T), BAX (#2772S), LC3A/B (#12741S), Ki-67 (#12202S) were purchased from SCT. Cleaved Caspase 9 (#ab202068) was purchased from Abcam. Cleaved Caspase 3 (#341034), β-actin (#T200068-8F10), Anti-mouse HRP (#511203), Anti-rabbit HRP (#511103) were purchased from Zen Bioscience.

Synthesis and Structural Characterization

A mixture of 2-bromocyclohex-1-ene-1-carbaldehyde **1** (370 mg, 2 mM), 2-hydroxy-5-nitrobenzaldehyde **2** (167 mg, 1 mM) and Cs_2CO_3 (1.95 g, 6.0 mM) in DMF (2 ml) was stirred for 12 h at 25°C. The solvent was removed under reduced pressure by evaporation, and the residue was purified by silica gel chromatography to afford 6-nitro-2,3-dihydro-1H-xanthene-4-carbaldehyde **3** as a yellow solid (128 mg, 50% yield). A mixture of 3 (25.7 mg, 0.1 mM), 1,2,3,3-tetramethyl-3H-indol-1-ium **4** (17.4 mg, 0.1 mM) and K_2CO_3 (65 mg, 0.2 mM) in Ac_2O (2.0 ml) was stirred at 80°C for 12 h. The

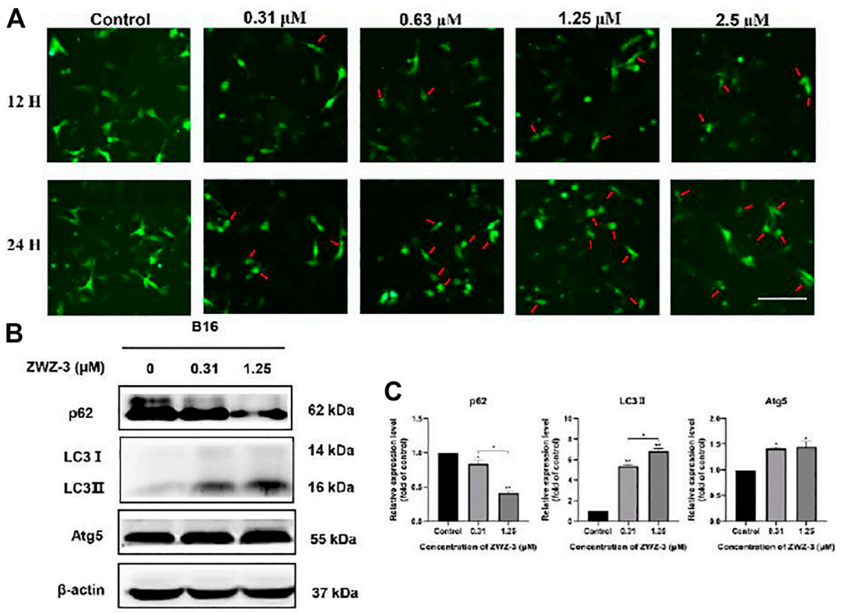

FIGURE 5 | ZWZ-3 promotes autophagy in melanoma cells. **(A)** B16 cells expressing GFP-LC3 were treated with complete medium or ZWZ-3. The distribution of GFP-LC3 was examined using fluorescence microscope. **(B,C)** The levels of P62, LC3-II and Atg5 were determined via western blotting. Protein expressions were qualified by the densitometry analysis using ImageJ. Dates are expressed as mean ± SD for 3 independent experiments (*$p < .05$, **$p < .01$).

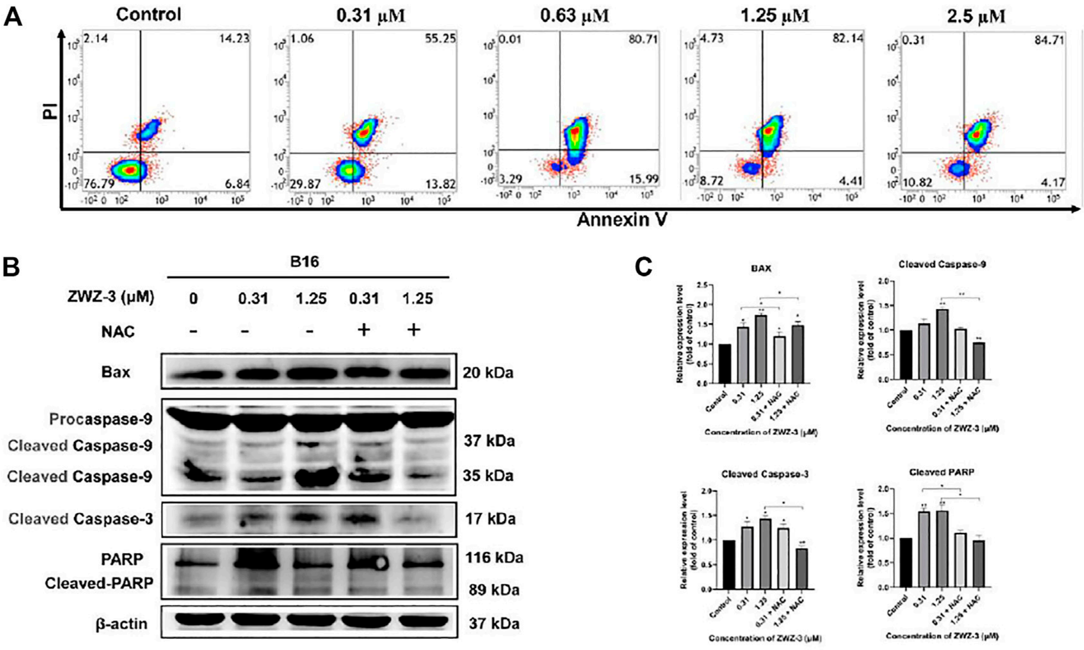

FIGURE 6 | ZWZ-3 induces apoptosis in melanoma cells. **(A)** FCM analysis of B16 cells stained with Annexin V-FITC/PI after treatment with ZWZ-3 for 24 h **(B,C)** Cells were pretreated with ROS inhibitors (NAC, 10 mM) for 30 min followed by treatment with ZWZ-3 for 24 h. The expression of Bax, cleaved caspase 9, cleaved caspase 3 and cleaved PARP were measured by western blotting. Protein expressions were qualified by the densitometry analysis using ImageJ. Dates are expressed as mean ± SD for 3 independent experiments (*$p < .05$, **$p < .01$).

solvent was removed by evaporation under reduced pressure, and the residue was subjected to silica gel chromatography to afford ZWZ-3 as a purple solid (30 mg, 73% yield). ^{1}H NMR (400 MHz, $CDCl_3$) δ 8.59 (d, 1H, J = 15.32 Hz), 8.01 (d, 1H, J = 15.32 Hz), 7.95 (s, 1H), 7.49–7.53(m, 5H), 7.09(s, 1H), 6.96 (d, 1H, J = 15.32 Hz), 4.25 (s, 3H), 2.85–2.96 (m, 2H), 1.88–1.95

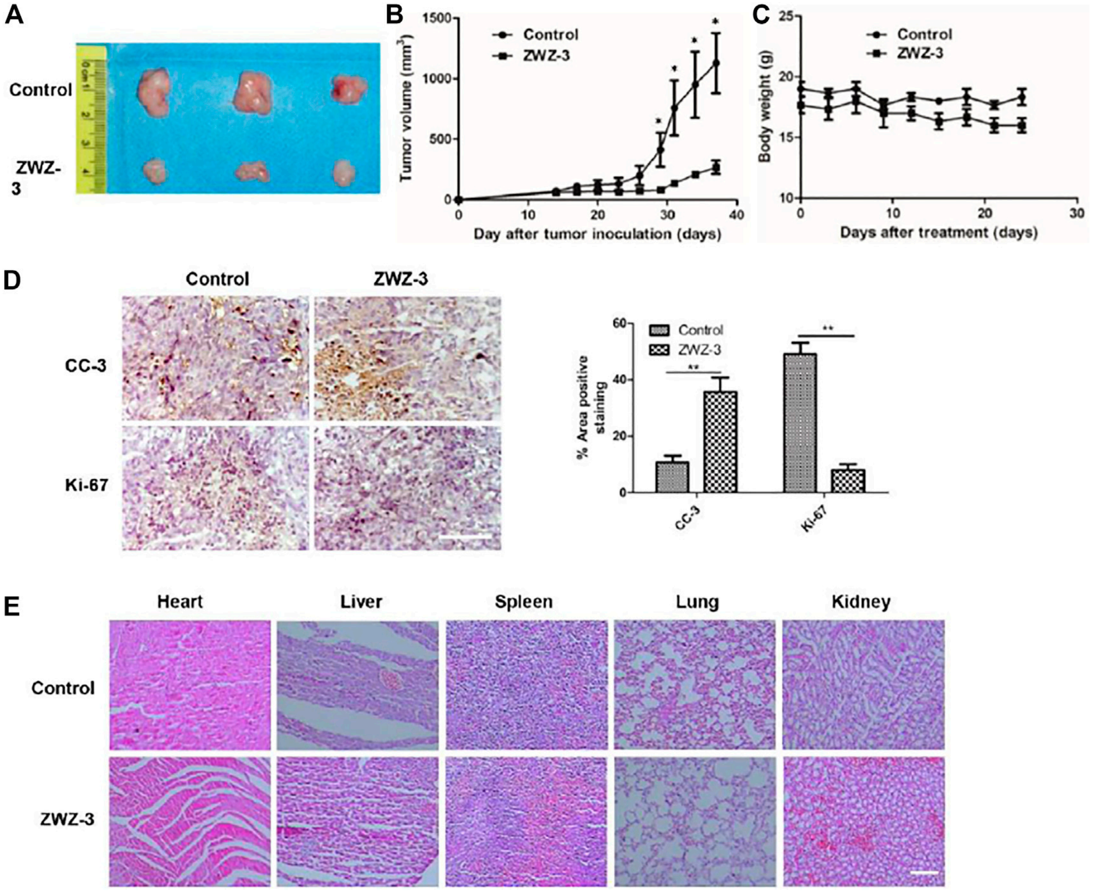

FIGURE 7 | ZWZ-3 reduces tumor cell proliferation and induces tumor apoptosis *in vivo*. **(A)** Tumor pictures from mice treated with indicated ZWZ-3 on the final day. In A375 xenograft model, the mice were treated with ZWZ-3 (5 mg/kg) or vehicle. Tumor volumes **(B)** and body weight **(C)** were measured every 3 days. **(D)** Tumor tissues from A375 xenograft treated with control or ZWZ-3 were immunohistochemically analyzed with anti-Ki67 and cleaved caspase 3 (CC-3) antibodies. The statistical data of CC-3 and Ki-67 positive cell number were displayed on the right. **(E)** H&E stain vital organ sections of mice treated with vehicle or ZWZ-3. Dates are expressed as mean ± SD for 3 independent experiments (*$p < .05$; **$p < .01$). Scale bar = 100 μm.

(m, 2H), 1.84 (s, 6H), MS: m/z calculated for $C_{26}H_{25}N_2O_3^+$, 413.1860, found 413.1860.

Determination of Optical Properties

To study the optical properties of ZWZ-3 in methanol, serum and phosphate buffered saline (PBS), ZWZ-3 was incubated with methanol or 10% fetal bovine serum (FBS, Gibco) or PBS at 37°C. The absorbance of ZWZ-3 was measured on a UV–Vis scanning spectrophotometer Puxi TU-1900. Fluorescence intensities were detected using an Agilent F-7000 fluorescence spectrophotometer (United States) (550 nm excitation, continuous wavelength from 500 to 600 nm emission).

Cell Lines and Cell Culture

Murine melanoma cell line (B16), human melanoma cell line (A375) and murine macrophage cell line (RAW264.7) were obtained from ATCC (Manassas, VA, United States) and cultured in ATCC suggested media with 10% FBS. Cells were supplied with 1% antibiotic-antimycotic solution and incubated at 37°C humidfied atmosphere with 5% CO_2.

MTT and Colony Formation Assays

The effect of ZWZ-3 on cells viabilities was performed by standard MTT method and colony formation assay. In the MTT assay, the cells were seeded in 96-well plates at $1–5\times10^3$ cells/well and incubation for 24 h. 100 μl medium with various concentrations of ZWZ-3 were added to each well and incubated for 24, 48 and 72 h, respectively. Then, 20 μl MTT solution were added to each well to a final concentration of 0.5 mg/ml, followed by incubation for 2–4 h at 37°C. Finally, the medium of each well was replaced by 150 μl DMSO and incubated for 15–20 min. The absorbance of each well was detected at 570 nm wavelength using Spectra MAXM5 microplate spectrophotometer (Molecular Devices), then the growth inhibiting rates was calculated. Data were derived from at least three separate experiments.

In the colony formation assay, the cells were seeded in six-well plates at 200–500 cells/well and incubated for 24 h. Then the cells were incubated with 2 ml medium containing indicated concentrations of ZWZ-3 for 7 days. After washing with PBS, fixed with 4% paraformldehyde and stained with crystal violet solution (0.5% in methanol), the cells were observed and counted by the microscope. Each assay was replicated three times.

Detection of ΔΨm and ROS Levels in Cells

DCFH-DA (6.7 μM) and JC-1 (10 μg/ml) were used to measure mitochondrial membrane potential (ΔΨm) and reactive oxygen species (ROS) levels. After treated with ZWZ-3 for 2 h or 24 h, the melanoma cells were treated with DCFH-DA or JC-1 at 37°C in the dark for 40 or 20 min. The cells were washed with PBS, and the fluorescence of cells was observed using fluorescence microscope. Image J software was employed to measure the fluorescence intensity. Each assay was replicated three times.

Fluorescent Imaging For Biodistribution and Tumor-Targeted

Confocal laser technique was conducted to assess for subcellular colocalization of ZWZ-3 *in vitro*. In brief, A375, B16 and RAW264.7 cells in the logarithmic growth phase were seeded in 35 mm glass-bottomed culture dishes at 37°C and 5% CO_2 for 24 h. After co-incubating with ZWZ-3 (5 μM) for 1 h, the fresh medium was replaced. Then, apply MitoTracker Green (Beyotime, China) to make the final concentration of 200 nM, incubated for 45 min. After washed with PBS for three times, the cells were observed by laser scanning confocal microscope (Leica TSC SP8) (ZWZ-3: 638 nm excitation, continuous wavelength from 450 to 700 nm emission; MitoTracker Green: 490 nm excitation, continuous wavelength from 450 to 700 nm emission).

To assess the localization of ZWZ-3 *in vivo*, the organs of subcutaneous tumor model mice were made into frozen sections for observation. Briefly, after the tissues of heart, liver, spleen, lung, kidney, paracancerous and tumor were cut into frozen sections on a cryostat microtome (Leica CM1950), they were fixed with ice acetone for 15 min, drained and washed with PBS for 5 min. Then, the frozen sections were stained by Hoechst33342 (2 μg/ml) (YuanYe Bio-Technology, Shanghai, China) at 37°C for 10 min and washed with PBS for two to three times, 5 min each time. A fluorescence microscope (Leica DMi8) was performed for observing.

To investigate the mechanism affecting the selective entry of ZWZ-3 into tumor cells, B16 cells were added in six-well plates and cultured overnight. B16 cells were incubated with 250 μM BSP for 20 min and then incubated with 5 μM ZWZ-3 for 1 h. After being washed with PBS solution, cells were incubated with 1 μg/ml Hoechst33342 for 10 min. Finally, the cells were cleaned by PBS solution and observed by fluorescence microscope.

Detection of Cells Apoptosis

The detection of cells apoptosis was conducted according to Annexin V-FITC/PI detection kit (Biosharp, China). The A375 and B16 cells (2×10^5 cells/well) in the logarithmic growth phase were seeded in six-well plates and incubated overnight. After treatment with various concentration of ZWZ-3 (0 ~ 2.5 μM) for 24 h, the cells were collected, cleaned with cold PBS and stained with 5 μl Annexin V-FITC at room temperature in the dark for 20 min. Subsequently, 10 μl of PI was added for 5 min. FCM was used to measure the apoptosis induced by ZWZ-3. The data was carried out using FlowJo software.

Western Blotting Analysis

The B16 cells were collected, lysed and quantified (BCA; Beyotime, China). Western blot analyses were conducted using the indicated antibodies. Protein densitometric analysis of all bands were performed using the Image J software. Data were depicted as fold difference over untreated control. GAPDH was conducted as an internal control.

Measurement of GFP-LC3 Aggregates

For visualization of the autophagosomes, cells were transfected with GFP-LC3 plasmid, which was presented to me by Dr. F. Jianguo (Southwest Medical University, Luzhou, China). Briefly, B16 cells were seeded into a 24-well plate and cultured overnight. Next, cells were transfected with GFP-LC3 plasmid for 12 h. The cells were exposed to different concentration of ZWZ-3 for 12 or 24 h. Lastly, fluorescence microscope was conducted to observe the GFP-LC3 aggregates.

Tumor Xenograft Models

Mice used in this study were purchased from the Chengdu Dossy Laboratory Animals Company (Chengdu, China) and were housed in a specific-pathogen-free (SPF) condition facility with an air-conditioned room at 25 ± 2°C with 40%–70% relative humidity, and a 12-h light/dark cycle. For subcutaneous tumor model, mice engrafted subcutaneously with 1×10^7 A375 cells were randomized to groups when tumor volume was around 100 mm^3 and were given by intraperitoneal injection of ZWZ-3 5 mg/kg or vehicle once 3 days. Tumor size and body weight were measured every 3 days. The mice were sacrificed when reached the endpoint defined by the tumor size (~1,000 mm^3). Tumor volume is calculated as follows: Volume = $0.5 \times a \times b^2$, where a (mm) represents the length and b (mm) represents the width of the tumor. All animal experiments have been approved by the Laboratory Animal Management Committee of the Affiliated 190 Hospital of Southwest Medical University in China (Permit Number: 20200201) and were conducted in accordance with the approved guidelines.

Hematoxylin and Eosin (H&E) Staining

The tissues of mice were fixed with 10% formaldehyde solution for 24 h and embedded in paraffin, then cut into 4 mm-thick sections. Finally, the sections were stained by hematoxylin and eosin (H&E) and observed using microscope (Nikon, NiE, Japan).

Immunohistochemistry

Immunohistochemical staining for Ki-67 and CC-3 was performed on xenograft tumor tissues using antibodies against Ki-67 and CC-3 respectively.

Statistical Analysis

The data were expressed as the mean ± standard deviation and analyzed using SPSS 17.0 software. The differences of two groups were analyzed by t-test of two independent samples. $p < 0.05$ were considered statistically significant.

RESULTS

Chemical Synthesis and Optical Properties of ZWZ-3

The general synthetic route of compound ZWZ-3 is illustrated in **Figure 1A**. The structural characterization of ZWZ-3 was determined by ^{1}H-NMR (**Supplementary Figure S1**), 13C-NMR (**Supplementary Figure S2**) and high resolution mass spectrometry (HRMS) (**Supplementary Figure S3**). The absorption and fluorescence spectra of ZWZ-3 were investigated in methanol (MeOH), PBS and 10% fetal bovine serum. It was found that the absorption and emission peak of ZWZ-3 was in the 550–560 nm (**Figure 1B**). ZWZ-3 presented a good stability in 10% FBS and methanol (**Figure 1C**), indicating that it has potential as a novel fluorescence probe for biomedical imaging.

ZWZ-3 Specifically Localizes to the Mitochondria of Cancer Cells and Targets Tumor Tissues

Hemicyanines are known to target mitochondria due to the presence of cationic nitrogen (Li et al., 2016). A subcellular localization assay, using colocalization with a mitochondrial tracker (MitoTracker Green) in B16, A375 and RAW264.7 cells, showed that ZWZ-3 preferentially accumulated in the mitochondria of tumor cells in a time-dependent manner (**Figures 2A–C**). Fluorescence began to appear at 5 min, and it was at the strongest at 15 min. After 15 min, the fluorescence intensity gradually weakened and there was almost no fluorescence at 4 h. C57BL/6J mice with B16 subcutaneous tumor xenografts were subjected to histopathologic analysis after a single-dose intravenous administration of ZWZ-3 at 2 mg/kg. Histopathologic analysis of organs and tumor frozen sections (**Figure 2D**) indicated that ZWZ-3 preferentially accumulates in tumor tissues. Thus, ZWZ-3 could be a promising fluorescence probe for targeting mitochondria and biomedical imaging in melanoma based on our results.

ZWZ-3 Selectively Accumulates in the Mitochondria of Tumor Cells *via* a Mechanism Dependent on organic anion-transporting polypeptide

OATPs are multispecific transport proteins, which can transport cations, anions and neutral compounds in cells, and plays an important role in drug absorption, distribution and excretion *in vivo* (Obaidat et al., 2012; Liu et al., 2018). Shi found that OATP mediates the selective accumulation of the heptamethine dye IR-780 in tumor cells (Zhang et al., 2010). To verify whether ZWZ-3 enters tumor cell through the same pathway, B16 cells were pretreated with sulfobromophthalein (BSP, a competitive inhibitor of OATP transporters) for 20 min. BSP significantly inhibited the tumor accumulation of ZWZ-3 (**Figure 3A**), suggesting that ZWZ-3 enters the cytosol in an OATP-dependent manner. In addition, similar results were observed in A375 cells (**Supplementary Figure S4**).

Mitochondrial membrane potential ($\Delta\Psi$m) plays a key role in cell health and function. Mitochondria-mediated intrinsic apoptotic pathway is always accompanied by the disruption of $\Delta\Psi$m. Here, we treated B16 cells and A375 cells with ZWZ-3 for 24 h, then used the cationic dye (JC-1) to assess $\Delta\Psi$m. As shown in **Figure 3B** and **Supplementary Figure S5**, ZWZ-3 induced mitochondrial membrane depolarization in a dose-dependent manner.

High levels of ROS were shown to promote mitochondria-mediated intrinsic apoptotic pathway (Idelchik et al., 2017). To determine whether ZWZ-3 affects ROS production, ROS products were measured after stimulating the cell with 5 μM ZWZ-3 for 2 h. As shown in **Figure 3C**, we found that ZWZ-3 increased the intracellular ROS levels in melanoma cells in a dose-dependent manner. These results suggest that the fluorescent probe ZWZ-3 can selectively accumulate in the mitochondria of tumor cells in an OATP-dependent manner, inducing mitochondrial membrane depolarization and ROS production.

ZWZ-3 Suppresses the Growth of Melanoma Cells *in vitro*

Given the tumor targeting and imaging property of ZWZ-3, further investigation of anti-tumor effects of ZWZ-3 was conducted. The effect of ZWZ-3 on cancer cells proliferation was evaluated by MTT assay (**Supplementary Figure S6**). In A549 and MDA-MB-231 cell lines, the IC_{50} of ZWZ-3 were calculated as 0.48 and 0.93 μM, respectively. ZWZ-3 displayed relatively strong activity against B16 and A375 cell lines (IC_{50} 0.2 and 0.43 μM, respectively) at 72 h. These results indicated that among the tested tumor cell lines, melanoma cells were the most sensitive to ZWZ-3. Additionally, ZWZ-3 suppressed melanoma cells viability in a concentration and time—dependent manner (**Figures 4A,B**). Similarly, in a colony formation assay, ZWZ-3 suppressed proliferation of both cell lines and reduced colony numbers in a dose-dependent manner (**Figure 4C**).

ZWZ-3 Induces Autophagy by Regulating Autophagy-Related Proteins in Melanoma Cells

The role of autophagy in cell survival and death has been reported in several studies. Accumulating evidence has revealed that LC3 (microtubule-associated protein 1A/1B-light chain 3) is a vital autophagosome marker and that p62/SQSTM1 is a selective autophagy receptor that is degraded within the autolysosome after an increase in autophagic flux (Xiang et al., 2021). Therefore, to detect the effect of ZWZ-3 on autophagy, we evaluated the level of crucial autophagic marker LC3-II *via* B16 cells that expressed GFP-LC3. We found that ZWZ-3 could efficiently induce GFP-LC3 puncta in a dose- and time-dependent manner (**Figure 5A**). Additionally, as shown in **Figures 5B,C**, p62 protein levels were notably decreased after ZWZ-3 treatment. LC3-II and Atg5 protein levels were increased following ZWZ-3 treatment for 24 h in B16 cells. The above-mentioned results indicated that ZWZ-3 induced autophagy in a concentration- and time-dependent manner in melanoma cells.

ZWZ-3 Induces Mitochondria-Mediated Apoptosis in Melanoma Cells

To explore whether ZWZ-3 induce apoptosis in melanoma cells, we treated B16 cells or A375 cells (**Supplementary Figure S7**) with different ZWZ-3 concentrations, then analyzed them by flow cytometry. Treatment with 0.31 μM ZWZ-3 for 24 h led to an apoptosis rate of 55.25% (**Figure 6A**), and this effect was dose-dependent, since 0.63 μM led to a rate of 80.71%; 1.25 μM, 82.14%; and 2.5 μM, 84.71%. These data indicated that ZWZ-3 induced melanoma cell apoptosis in a dose-dependent manner. Western blot analysis displayed that ZWZ-3 increased the levels of Bax, cleaved caspase 9, cleaved caspase 3 and cleaved PARP (**Figures 6B,C**). These effects of ZWZ-3 were reversed by NAC (a pharmacological inhibitor of ROS), suggesting that the fluorescent probe ZWZ-3 induces mitochondria-mediated apoptosis through the ROS pathway.

ZWZ-3 Inhibits Melanoma Growth *in vivo*

To evaluate the potential therapeutic effect of ZWZ-3 *in vivo*, A375 cells were injected into the right flank of BALB/c nude mice. ZWZ-3-treated mice show significantly reduced tumor volume compared to the control group, without significant body weight loss (**Figures 7A–C**). The growth inhibition rates at day 38 post-inoculation were 76.3%.

Tumor tissues form untreated and ZWZ-3-treated mice were immunohistochemically analyzed to investigate the potential mechanisms through which ZWZ-3 inhibited A375 melanoma growth. Compared with the control group, ZWZ-3 significantly reduced the number of Ki67-positive cells and increased the number of cleaved caspase-3-positive cells (**Figure 7D**). These results suggest that ZWZ-3 can inhibit proliferation and promote apoptosis in melanoma tumors, consistent with our *in vitro* experiments. Moreover, H&E staining of vital organs (Heart, liver, spleen, lung, kidney) showed that long-term administration of ZWZ-3 did not affect tissue architecture or cell morphology (**Figure 7E**). These data indicated that ZWZ-3 significantly inhibited melanoma growth without causing obvious toxicities *in vivo*.

DISCUSSION

Melanoma is a highly aggressive cancer that accounts for most deaths related to skin cancer, yet it is usually diagnosed at late stage and its prognosis is poor. In the present study, we synthesized and identified a new tumor-targeted fluorophore dye ZWZ-3 with great optical properties and stability in 10% FBS and methanol, and tselectively accumulates in the mitochondria of melanoma cells. In a mouse model, ZWZ-3 preferably accumulated in tumor tissues within 24 h after intravenous injection, and it suppressed tumor growth without obvious side effects. These results justify for further investigation of ZWZ-3 as a safe and effective theranostic agent for imaging and treatment of melanoma.

As a cationic lipophile, the heptamethine core can specifically accumulates in the mitochondria of cancer cells through an OATP-mediated pathway (Wang et al., 2018). Consistently, our hemicyanine-based fluorescent probe ZWZ-3 selectively accumulated in the mitochondria of melanoma cells in an (OATP)-dependent manner, inducing mitochondrial ROS production and promoting cell apoptosis in a time- and dose-dependent manner. In addition, ZWZ-3 significantly reduced ΔΨm, while upregulating Bax and activating caspase-3, caspase-9, and PARP. These effects of ZWZ-3 were reversed by adding NAC to inhibit ROS production, suggesting that ZWZ-3 induces apoptosis by increasing ROS levels (Yang et al., 1998).

Autophagy helps normal cells resist nutrient deprivation or metabolic stress (Chen et al., 2021), and it can be exploited for anticancer therapy. Radiation and chemotherapy work, in part, by inducing autophagy in cancer cells (Amaravadi et al., 2019; Li et al., 2020). Two hallmarks of autophagy are the conversion of the soluble form of LC3-I to the autophagosome-associated form LC3-II, as well as the degradation of p62 (Zheng et al., 2018). ATG5 helps catalyze the LC3 lipidation, which is essential for autophagosome formation and expansion (Yang et al., 2021). In our study, ZWZ-3 significantly increased the levels of ATG5 and LC3-II in a dose-dependent manner while promoting degradation of p62, indicating that ZWZ-3 can effectively induce autophagy by regulating the expression of autophagy-related proteins.

Our *in vivo* studies in mice bearing A375 xenografts showed that ZWZ-3 effectively suppressed tumor growth at an inhibitory rate of 76.3%. Consistent with *in vitro* results, tumor sections of ZWZ-3-treated mice showed significantly upregulated cleaved caspase-3 (indicating apoptosis), and downregulated Ki-67 (indicating reduced proliferation). At the same time, ZWZ-3 showed no obvious toxicity *in vivo*, suggesting its potential as a safe, effective theranostic agent.

In summary, we designed and synthesized a novel theranostic agent that can selectively accumulate in the mitochondria of melanoma cells in an OATP-dependent manner. ZWZ-3 can inhibit proliferation and induce apoptosis of melanoma cells by altering levels of various apoptosis- and autophagy-related proteins. Our work may promote the development of this and other dual-functional hemicyanine-based dyes as novel tumor-targeting therapeutic agent.

DATA AVAILABILITY STATEMENT

The original contributions presented in the study are included in the article/**Supplementary Material**, further inquiries can be directed to the corresponding authors.

ETHICS STATEMENT

The animal study was reviewed and approved by the Laboratory Animal Management Committee of the Affiliated 190 Hospital of Southwest Medical University in China.

AUTHOR CONTRIBUTIONS

LL, ZL, and HW participated in most of the experiments. ZL, CS performed the compound synthesis and structural analysis, optical properties. LL and HW cell phenotypes, animal studies and fluorescence imaging. JW performed the histopathology. SY, XX, and QZ conceived and supervised the project. LL, SY, HW, and ZL wrote the manuscript.

FUNDING

The authors are grateful to financial support from National Natural Science Foundation of China (82003716, 82074378), Sichuan Science and Technology Department Project (2020YJ0191) and Luzhou Municipal People's Government-Southwest Medical University Science and Technology Strategic Cooperation Project (2018LZXNYD-ZK20).

SUPPLEMENTARY MATERIAL

The Supplementary Material for this article can be found online at: https://www.frontiersin.org/articles/10.3389/fphar.2022.829684/full#supplementary-material

REFERENCES

Amaravadi, R. K., Kimmelman, A. C., and Debnath, J. (2019). Targeting Autophagy in Cancer: Recent Advances and Future Directions. *Cancer Discov.* 9 (9), 1167–1181. doi:10.1158/2159-8290.Cd-19-0292

Apalla, Z., Lallas, A., Sotiriou, E., Lazaridou, E., and Ioannides, D. (2017). Epidemiological Trends in Skin Cancer. *Dermatol. Pract. Concept* 7 (2), 1–6. doi:10.5826/dpc.0702a01

Bajpai, V. K., Khan, I., Shukla, S., Kang, S. M., Aziz, F., Tripathi, K. M., et al. (2020). Multifunctional N-P-Doped Carbon Dots for Regulation of Apoptosis and Autophagy in B16F10 Melanoma Cancer Cells and *In Vitro* Imaging Applications. *Theranostics* 10 (17), 7841–7856. doi:10.7150/thno.42291

Chen, C., Ding, W., Li, J., Geng, X., Zhang, H., and Sun, Y. (2021). The Anticancer Activity of Root Extract from Quercus Acutissima Carruth. Via Regulating Apoptosis and Autophagy in Breast Cancer Cells. *J. Ethnopharmacol*, 114730. doi:10.1016/j.jep.2021.114730

Chen, H., Dong, B., Tang, Y., and Lin, W. (2015). Construction of a Near-Infrared Fluorescent Turn-On Probe for Selenol and its Bioimaging Application in Living Animals. *Chemistry* 21 (33), 11696–11700. doi:10.1002/chem.201502226

Chiu, H. Y., Tay, E. X. Y., Ong, D. S. T., and Taneja, R. (2020). Mitochondrial Dysfunction at the Center of Cancer Therapy. *Antioxid. Redox Signal.* 32 (5), 309–330. doi:10.1089/ars.2019.7898

Cotter, T. G. (2009). Apoptosis and Cancer: the Genesis of a Research Field. *Nat. Rev. Cancer* 9 (7), 501–507. doi:10.1038/nrc2663

D'Arcy, M. S. (2019). Cell Death: a Review of the Major Forms of Apoptosis, Necrosis and Autophagy. *Cell Biol Int* 43 (6), 582–592. doi:10.1002/cbin.11137

Fu, A., Hou, Y., Yu, Z., Zhao, Z., and Liu, Z. (2019). Healthy Mitochondria Inhibit the Metastatic Melanoma in Lungs. *Int. J. Biol. Sci.* 15 (12), 2707–2718. doi:10.7150/ijbs.38104

Hessler, M., Jalilian, E., Xu, Q., Reddy, S., Horton, L., Elkin, K., et al. (2020). Melanoma Biomarkers and Their Potential Application for *In Vivo* Diagnostic Imaging Modalities. *Int. J. Mol. Sci.* 21 (24). doi:10.3390/ijms21249583

Huang, A. C., Lien, J. C., Lin, M. W., Yang, J. S., Wu, P. P., Chang, S. J., et al. (2013). Tetrandrine Induces Cell Death in SAS Human Oral Cancer Cells through Caspase Activation-dependent Apoptosis and LC3-I and LC3-II Activation-dependent Autophagy. *Int. J. Oncol.* 43 (2), 485–494. doi:10.3892/ijo.2013.1952

Idelchik, M. D. P. S., Begley, U., Begley, T. J., and Melendez, J. A. (2017). Mitochondrial ROS Control of Cancer. *Semin. Cancer Biol.* 47, 57–66. doi:10.1016/j.semcancer.2017.04.005

Islam, M. A., Sooro, M. A., and Zhang, P. (2018). Autophagic Regulation of P62 Is Critical for Cancer Therapy. *Int. J. Mol. Sci.* 19 (5). doi:10.3390/ijms19051405

Jeyamogan, S., Khan, N. A., and Siddiqui, R. (2021). Application and Importance of Theranostics in the Diagnosis and Treatment of Cancer. *Arch. Med. Res.* 52 (2), 131–142. doi:10.1016/j.arcmed.2020.10.016

Kong, F., Liang, Z., Luan, D., Liu, X., Xu, K., and Tang, B. (2016). A Glutathione (GSH)-Responsive Near-Infrared (NIR) Theranostic Prodrug for Cancer Therapy and Imaging. *Anal. Chem.* 88 (12), 6450–6456. doi:10.1021/acs.analchem.6b01135

Li, D. P., Wang, Z. Y., Cao, X. J., Cui, J., Wang, X., Cui, H. Z., et al. (2016). A Mitochondria-Targeted Fluorescent Probe for Ratiometric Detection of Endogenous Sulfur Dioxide Derivatives in Cancer Cells. *Chem. Commun. (Camb)* 52 (13), 2760–2763. doi:10.1039/c5cc09092j

Li, L., Liu, W. L., Su, L., Lu, Z. C., and He, X. S. (2020). The Role of Autophagy in Cancer Radiotherapy. *Curr. Mol. Pharmacol.* 13 (1), 31–40. doi:10.2174/1874467212666190809154518

Li, Y., Wang, Y., Yang, S., Zhao, Y., Yuan, L., Zheng, J., et al. (2015). Hemicyanine-based High Resolution Ratiometric Near-Infrared Fluorescent Probe for Monitoring pH Changes *In Vivo*. *Anal. Chem.* 87 (4), 2495–2503. doi:10.1021/ac5045498

Liu, S. Y., Xiong, H., Li, R. R., Yang, W. C., and Yang, G. F. (2019). Activity-Based Near-Infrared Fluorogenic Probe for Enabling *In Vitro* and *In Vivo* Profiling of Neutrophil Elastase. *Anal. Chem.* 91 (6), 3877–3884. doi:10.1021/acs.analchem.8b04455

Liu, X., Chen, L., Liu, M., Zhang, H., Huang, S., Xiong, Y., et al. (2018). Ginsenoside Rb1 and Rd Remarkably Inhibited the Hepatic Uptake of Ophiopogonin D in Shenmai Injection Mediated by OATPs/oatps. *Front. Pharmacol.* 9, 957. doi:10.3389/fphar.2018.00957

Luo, Z., Huang, Z., Li, K., Sun, Y., Lin, J., Ye, D., et al. (2018). Targeted Delivery of a γ-Glutamyl Transpeptidase Activatable Near-Infrared-Fluorescent Probe for Selective Cancer Imaging. *Anal. Chem.* 90 (4), 2875–2883. doi:10.1021/acs.analchem.7b05022

Obaidat, A., Roth, M., and Hagenbuch, B. (2012). The Expression and Function of Organic Anion Transporting Polypeptides in normal Tissues and in Cancer. *Annu. Rev. Pharmacol. Toxicol.* 52, 135–151. doi:10.1146/annurev-pharmtox-010510-100556

Shu, G., Chen, M., Song, J., Xu, X., Lu, C., Du, Y., et al. (2021). Sialic Acid-Engineered Mesoporous Polydopamine Nanoparticles Loaded with SPIO and Fe3+ as a Novel Theranostic Agent for T1/T2 Dual-Mode MRI-Guided Combined Chemo-Photothermal Treatment of Hepatic Cancer. *Bioact Mater.* 6 (5), 1423–1435. doi:10.1016/j.bioactmat.2020.10.020

Smart, J. A., Oleksak, J. E., and Hartsough, E. J. (2021). Cell Adhesion Molecules in Plasticity and Metastasis. *Mol. Cancer Res.* 19 (1), 25–37. doi:10.1158/1541-7786.Mcr-20-0595

Tse, A. K., Chen, Y. J., Fu, X. Q., Su, T., Li, T., Guo, H., et al. (2017). Sensitization of Melanoma Cells to Alkylating Agent-Induced DNA Damage and Cell Death via Orchestrating Oxidative Stress and IKKβ Inhibition. *Redox Biol.* 11, 562–576. doi:10.1016/j.redox.2017.01.010

Vinod, C., and Jena, S. (2021). Nano-Neurotheranostics: Impact of Nanoparticles on Neural Dysfunctions and Strategies to Reduce Toxicity for Improved Efficacy. *Front. Pharmacol.* 12, 612692. doi:10.3389/fphar.2021.612692

von Kiedrowski, V., Hübner, R., Kail, D., Cheng, X., Schirrmacher, R., Wängler, C., et al. (2020). Synthesis, Characterization and Optimization of *In Vitro* Properties of NIR-Fluorescent Cyclic α-MSH Peptides for Melanoma Imaging. *J. Mater. Chem. B* 8 (46), 10602–10608. doi:10.1039/d0tb01798a

Wang, H. X., Sharma, C., Knoblich, K., Granter, S. R., and Hemler, M. E. (2015). EWI-2 Negatively Regulates TGF-β Signaling Leading to Altered Melanoma Growth and Metastasis. *Cell Res* 25 (3), 370–385. doi:10.1038/cr.2015.17

Wang, Y., Luo, S., Zhang, C., Liao, X., Liu, T., Jiang, Z., et al. (2018). An NIR-Fluorophore-Based Therapeutic Endoplasmic Reticulum Stress Inducer. *Adv. Mater.* 30, 1800475. doi:10.1002/adma.201800475

Wu, J., Li, J., Wang, H., and Liu, C. B. (2018). Mitochondrial-targeted Penetrating Peptide Delivery for Cancer Therapy. *Expert Opin. Drug Deliv.* 15 (10), 951–964. doi:10.1080/17425247.2018.1517750

Wu, Y. X., Zhang, D., Hu, X., Peng, R., Li, J., Zhang, X., et al. (2021). Multicolor Two-Photon Nanosystem for Multiplexed Intracellular Imaging and Targeted Cancer Therapy. *Angew. Chem. Int. Ed.* 60 (22), 12569–12576. doi:10.1002/anie.202103027

Xiang, X., Tian, Y., Hu, J., Xiong, R., Bautista, M., Deng, L., et al. (2021). Fangchinoline Exerts Anticancer Effects on Colorectal Cancer by Inducing Autophagy via Regulation AMPK/mTOR/ULK1 Pathway. *Biochem. Pharmacol.* 186, 114475. doi:10.1016/j.bcp.2021.114475

Xie, X., Yang, X., Wu, T., Li, Y., Li, M., Tan, Q., et al. (2016). Rational Design of an α-Ketoamide-Based Near-Infrared Fluorescent Probe Specific for Hydrogen Peroxide in Living Systems. *Anal. Chem.* 88 (16), 8019–8025. doi:10.1021/acs.analchem.6b01256

Yang, H. W., Hwang, K. J., Kwon, H. C., Kim, H. S., Choi, K. W., and Oh, K. S. (1998). Detection of Reactive Oxygen Species (ROS) and Apoptosis in Human Fragmented Embryos. *Hum. Reprod.* 13 (4), 998–1002. doi:10.1093/humrep/13.4.998

Yang, J., Rao, S., Cao, R., Xiao, S., Cui, X., and Ye, L. (2021). miR-30a-5p Suppresses Lung Squamous Cell Carcinoma via ATG5 - Mediated Autophagy. *Aging (Albany NY)* 13 (13), 17462–17472. doi:10.18632/aging.203235

Zada, S., Hwang, J. S., Ahmed, M., Lai, T. H., Pham, T. M., Elashkar, O., et al. (2021). Cross Talk between Autophagy and Oncogenic Signaling Pathways and Implications for Cancer Therapy. *Biochim. Biophys. Acta Rev. Cancer* 1876 (1), 188565. doi:10.1016/j.bbcan.2021.188565

Zeng, Z., Liew, S. S., Wei, X., and Pu, K. (2021). Hemicyanine-Based Near-Infrared Activatable Probes for Imaging and Diagnosis of Diseases. *Angew. Chem. Int. Ed.* 60, 26454–26475. doi:10.1002/anie.202107877

Zhang, C., Liu, T., Su, Y., Luo, S., Zhu, Y., Tan, X., et al. (2010). A Near-Infrared Fluorescent Heptamethine Indocyanine Dye with Preferential Tumor Accumulation for *In Vivo* Imaging. *Biomaterials* 31 (25), 6612–6617. doi:10.1016/j.biomaterials.2010.05.007

Zhang, C., Liu, T., Luo, P., Gao, L., Liao, X., Ma, L., et al. (2021). Near-infrared Oxidative Phosphorylation Inhibitor Integrates Acute Myeloid Leukemia-Targeted Imaging and Therapy. *Sci. Adv.* 7 (1). doi:10.1126/sciadv.abb6104

Zhang, E., Zhang, C., Su, Y., Cheng, T., and Shi, C. (2011). Newly Developed Strategies for Multifunctional Mitochondria-Targeted Agents in Cancer Therapy. *Drug Discov. Today* 16, 140–146. doi:10.1016/j.drudis.2010.12.006

Zhang, Y. B., Gong, J. L., Xing, T. Y., Zheng, S. P., and Ding, W. (2013). Autophagy Protein p62/SQSTM1 Is Involved in HAMLET-induced Cell Death by Modulating Apotosis in U87MG Cells. *Cell Death Dis* 4, e550. doi:10.1038/cddis.2013.77

Zhao, J., Li, S., Jin, Y., Wang, J. Y., Li, W., Wu, W., et al. (2019). Multimerization Increases Tumor Enrichment of Peptide‑Photosensitizer Conjugates. *Molecules* 24 (4). doi:10.3390/molecules24040817

Zheng, Y., Wang, K., Wu, Y., Chen, Y., Chen, X., Hu, C. W., et al. (2018). Pinocembrin Induces ER Stress Mediated Apoptosis and Suppresses Autophagy in Melanoma Cells. *Cancer Lett.* 431, 31–42. doi:10.1016/j.canlet.2018.05.026

Zhu, L., Kalimuthu, S., Gangadaran, P., Oh, J. M., Lee, H. W., Baek, S. H., et al. (2017). Exosomes Derived from Natural Killer Cells Exert Therapeutic Effect in Melanoma. *Theranostics* 7 (10), 2732–2745. doi:10.7150/thno.18752

Conflict of Interest: The authors declare that the research was conducted in the absence of any commercial or financial relationships that could be construed as a potential conflict of interest.

Publisher's Note: All claims expressed in this article are solely those of the authors and do not necessarily represent those of their affiliated organizations, or those of the publisher, the editors and the reviewers. Any product that may be evaluated in this article, or claim that may be made by its manufacturer, is not guaranteed or endorsed by the publisher.

Copyright © 2022 Liu, Wang, Sun, He, Xia, Wang, Xiong, Zhang, Yang and Liu. This is an open-access article distributed under the terms of the Creative Commons Attribution License (CC BY). The use, distribution or reproduction in other forums is permitted, provided the original author(s) and the copyright owner(s) are credited and that the original publication in this journal is cited, in accordance with accepted academic practice. No use, distribution or reproduction is permitted which does not comply with these terms.

frontiers in Pharmacology

ORIGINAL RESEARCH
published: 04 March 2022
doi: 10.3389/fphar.2022.841918

Vanillin Derivatives Reverse *Fusobacterium nucleatum*-Induced Proliferation and Migration of Colorectal Cancer Through E-Cadherin/β-Catenin Pathway

Zhongkun Zhou[1], Yiqing Wang[2], Rui Ji[2], Dekui Zhang[3], Chi Ma[3], Wantong Ma[1], Yunhao Ma[1], Xinrong Jiang[1], Kangjia Du[1], Rentao Zhang[1] and Peng Chen[1]*

[1]School of Pharmacy, Lanzhou University, Lanzhou, China, [2]The First Hospital of Lanzhou University, Lanzhou, China, [3]The Second Hospital of Lanzhou University, Lanzhou, China

Colorectal cancer (CRC) is a common clinical malignant tumor and closely related to intestinal microbiome disorders. Especially, *Fusobacterium nucleatum* (*F. nucleatum*) is one of the most prevalent pathogens in CRC. However, its change in CRC patients of Northwest China, an area with a high incidence of gastrointestinal tumors, is unclear, and therapeutic strategies targeting *F. nucleatum* remain unresolved. Here, fecal samples of healthy people and CRC patients were studied using 16S rRNA sequencing to explore microbial community alterations. Additionally, vanillin derivate (IPM711 and IPM712) intervention by coculture with CRC cells and potential mechanism were investigated. Results showed that intestinal microbial homeostasis was gradually dysregulated, and the abundance of *Fusobacterium* was higher in CRC patients. Moreover, IPM711 and IPM712 showed better anti-*F. nucleatum* activity than vanillin by increasing cell membrane permeability and destroying bacterial integrity. In addition, IPM711 and IPM712 could downregulate the expression of E-cadherin and β-catenin, thus, suppressing the migration of HCT116. Collectively, IPM711 and IPM712 have both anticolorectal cancer and anti-*F. nucleatum* activities, providing potential natural product drug candidates for microbe-targeted strategies for the treatment of CRC.

Keywords: colorectal cancer, microbiome, vanillin derivatives, *Fusobacterium nucleatum*, 16S rRNA sequencing

OPEN ACCESS

Edited by:
Haichang Li,
The Ohio State University,
United States

Reviewed by:
Rebekka Einenkel,
University of Bonn, Germany
Priyia Pusparajah,
Monash University Malaysia, Malaysia

***Correspondence:**
Peng Chen
chenpeng@lzu.edu.cn

Specialty section:
This article was submitted to Experimental Pharmacology and Drug Discovery, a section of the journal Frontiers in Pharmacology

Received: *23 December 2021*
Accepted: *21 January 2022*
Published: *04 March 2022*

Citation:
Zhou Z, Wang Y, Ji R, Zhang D, Ma C, Ma W, Ma Y, Jiang X, Du K, Zhang R and Chen P (2022) Vanillin Derivatives Reverse Fusobacterium nucleatum-Induced Proliferation and Migration of Colorectal Cancer Through E-Cadherin/β-Catenin Pathway. Front. Pharmacol. 13:841918. doi: 10.3389/fphar.2022.841918

INTRODUCTION

Colorectal cancer (CRC) is the third most prevalent cancer in both sexes combined, with an incidence of 6.1% and mortality of 9.2% (Bray et al., 2018). Development of CRC is a multifactorial process, among which gut microbes widely participated in the initiation, progression, metastasis, and chemoresistance (Wong and Yu, 2019). Although precise regulation of intestinal microbes for CRC treatment is not available clinically, microbiome intervention therapy, such as fecal microbiota transplantation and target-specific drugs, has caused wide attention. Specially, compared with chemotherapy drugs, natural products are potential lead compounds for new drug development with low toxicity and high efficiency.

Hundreds of microbes are related to CRC, yet only several of them have been studied in detail, including *Fusobacterium nucleatum* (*F. nucleatum*), *Bacteroides fragilis*, and certain strains of

Escherichia coli (Zhou et al., 2020). *F. nucleatum* is an oral anaerobic bacteria and can cause opportunistic infections; however, Castellarin et al. reported that it was prevalent in human colorectal carcinoma for the first time (Castellarin et al., 2012). As a mutualist, infectious agent, and oncogenic microorganism, *F. nucleatum* was reported to be more enriched in CRC tissues of patients with recurrence and strongly associated with shorter recurrence-free survival (RFS) (Yu et al., 2017). It can promote colorectal carcinogenesis, exhibiting increased virulence in CRC when compared with the normal tissues (Rubinstein et al., 2013). Furthermore, *Fusobacterium* is associated with liver metastases from primary human colorectal cancers and positive lymph node metastasis (Bullman et al., 2017; Chen et al., 2020). Also, *F. nucleatum* helps tumors to construct an immune microenvironment, such as expansion of myeloid-derived immune cells and low tumor stromal CD3 lymphocytes, and is significantly associated with MSI-high (mismatch repair deficiency) independent of CIMP (CpG island methylator phenotype) and BRAF mutation status (Kostic et al., 2013; Mima et al., 2016; Borowsky et al., 2021). Recently, evidence revealed that high amounts of *F. nucleatum* were responsible for drug-resistance in CRC, including 5-fluorouracil and cisplatin (Zhang et al., 2019). Over the last decades, the carcinogenic mechanism of this pathogen is gradually elucidated. *F. nucleatum* adheres to and invades CRC cells via its unique FadA adhesin, binding to E-cadherin and forming FadA–E-cadherin–Annexin A1-β-catenin complex in cancerous cells. It can also induce oncogenic and inflammatory responses (Rubinstein et al., 2013). Fusobacterial Fap2 can recognize Gal–Gal–NAc to localize to CRC through a hematogenous route and increase proliferation of cancer cells (Yang et al., 2017). Moreover, *F. nucleatum* can promote distant metastases and chemoresistance *via* TLR4 and MYD88 innate immune signaling and autophagy pathway, providing target for clinical management as well as new drug development (Bullman et al., 2017; Yu et al., 2017). Recently, Yeoh and his colleagues found that southern Chinese populations harbor non-nucleatum Fusobacteria, being absent in western and rural populations (Yeoh et al., 2020). However, changes in gut microbiome, especially *F. nucleatum* in CRC patients in Northwest China, are rarely studied, which is an area with higher incidence of gastrointestinal tumors.

Apart from microbiota disorders, targeting and regulating pathogenic bacteria remain another issue. Treatment by traditional broad-spectrum antibiotics may point to both pathogen and other microbiota. Chemotherapy drugs will cause serious side effects and lead to chemotherapy resistance induced by some bacteria. For example, although metronidazole can decrease *Fusobacterium* load, it targets a range of anaerobic bacteria (Bullman et al., 2017). Recently, researchers reported that metformin relieved the symptoms induced by *F. nucleatum* administration in $APC^{\mathrm{Min}/+}$ mice, rescuing *F. nucleatum*-induced tumorigenicity. It also corroborates that *Fusobacterium*-abundant CRC will benefit from non-antibiotic antifusobacterial therapy (Yu et al., 2017; Huang et al., 2020). Furthermore, it was reported that tungstate treatment selectively inhibited molybdenum-cofactor-dependent microbial respiratory pathways to ameliorate colitis (Zhu et al., 2018). Therefore, regulation of intestinal microbes is promising and will facilitate personalized cancer treatment.

Vanillin (4-hydroxy-3-methoxybenzaldehyde) is derived from the orchid *Vanilla planifolia* and used as one kind of flavor in various industries, such as ice creams and pharmaceuticals. Vanillin and its derivatives have different bioactive properties and are changing from a popular flavor to therapeutic molecules (Arya et al., 2021). It was found that vanillin could inhibit respiration of *E. coli* and *L. innocua*, increase the permeability of cell membranes, and cause more severe membrane damage after hydroxyl modification (Fitzgerald et al., 2004). Additionally, when combined with conventional antibiotics, vanillin could modulate the action of antibiotics against resistant bacteria, including *E. coli*, *Staphylococcus aureus*, and *Pseudomonas aeruginosa* (Bezerra et al., 2017). Furthermore, our previous studies showed that vanillin derivatives 4-[1H-imidazo(4,5-f)(1,10)phenanthrolin-2-yl]-2-methoxyphenol and 2-[1H-imidazo(4,5-f) (1,10)phenanthrolin-2-yl]-6-methoxyphenol (IPM711 and IPM712) could inhibit the growth, invasion, and migration of HT29 and HCT116 cells through the Wnt/β-catenin signaling pathway. After hydroxyl modification, derivative IPM712 showed better anticancer activity than 5-Fu and low toxicity at therapeutic concentrations. Further mechanism research demonstrated that it could affect the function of the PI3K/AKT signal pathway (Ma et al., 2020). However, whether vanillin derivatives can rescue opportunistic pathogen-induced (especially *F. nucleatum*) colorectal tumorigenesis deserves further study.

With this background, fecal samples of CRC patients and healthy people were used to explore the changes in intestinal microbial community and diversity. In addition, we tested the antibacterial activity of vanillin derivatives against *F. nucleatum* as well as its potential mechanism. Results indicated that IPM711 and IPM712 are potential novel agents for colorectal cancer treatment.

MATERIALS AND METHODS

Sample Collection

Fecal samples were collected from the First Hospital of Lanzhou University and the Second Hospital of Lanzhou University. Those patients above 18 years old who went through colonoscopy examination were selected by reading medical records, including CRC, polypus, and healthy cases. The exclusion criteria were as follows: 1) had antibiotics for treatment in the last 3 months; 2) on a vegetarian diet; 3) experiencing surgeries in the last 3 months; 4) inflammatory bowel disease (IBD), Crohn's disease, and diarrhea; 5) had any other cancer history; and 6) had received radiotherapy or chemotherapy. Samples were collected either prior to colonoscopy or 1–2 weeks after colonoscopy, placed on ice, transported to the laboratory, and stored at −80°C immediately. The study protocol was approved by the Ethical Review Board of the hospital (LDYYLL 2020-241 and 2021A-152). Informed consent was obtained from all study patients.

TABLE 1 | Primers used for qPCR in this study.

Name	Sequences
GAPDH-F	5′-GGAGCGAGATCCCTCCAAAAT-3′
GAPDH-R	5′-GGCTGTTGTCATACTTCTCTCATGG-3′
RASA-F	5′-GTGGCCGGTGCTGCTGTTGC-3′
RASA-R	5′-TGGCCACCTGTTCCTCCTCGTATT-3′
MYD88-F	5′-GCCGCCGGATGGTGGTGGTTGT-3′
MYD88-R	5′-TTGGTGCAGGGGTTGGTGTAGTCG-3′
E-cadherin-F	5′-ATTTTTCCCTCGACACCCGAT-3′
E-cadherin-R	5′-TCCCAGGCGTAGACCAAGA-3′
PI3KCA-F	5′-TGAAGCACCTGAATAGGCAAGTCG-3′
PI3KCA-R	5′-TCTGGTCGCCTCATTTGCTCAAC-3′
β-catenin-F	5′-CAACTAAACAGGAAGGGATGGA-3′
β-catenin-R	5′-CTATACCACCCACTTGGCAGAC-3′
AKT-F	5′-AGCGACGTGGCTATTGTGAAG-3′
AKT-R	5′-GCCATCATTCTTGAGGAGGAAGT-3′
GSK-3β-F	5′-GACTAAGGTCTTCCGACCCC-3′
GSK-3β-R	5′-AAGAGTGCAGGTGTGTCTCG-3′

16S rRNA Sequencing and Bioinformatics Analysis

Genomic DNA was extracted using the TIANamp Stool DNA Kit (TIANGEN BIOTECH) following the manufacturer’s instructions. Quality and quantity of DNA were verified with NanoDrop 2000 and 1% agarose gel. Bacterial V3–V4 regions of the 16S rRNA gene were amplified with universal primers 343F and 798R. PCR products were purified with AMPure XP beads (Agencourt) and quantified using Qubit dsDNA assay kit.

Paired-end reads were then preprocessed using Trimmomatic software and assembled using FLASH software (Reyon et al., 2012; Bolger et al., 2014). Sequences were performed further denoising as follows: reads with ambiguous, homologous sequences or below 200 bp were abandoned. Reads with 75% of bases above Q20 were retained. Then reads with chimera were detected and removed using the QIIME software (version 1.8.0) (Caporaso et al., 2010). Clean reads were subjected to clustering to generate operational taxonomic units (OTUs) using the Vsearch software with 97% similarity cutoff (Edgar et al., 2011). Species richness was represented by observed species, while community diversity was expressed using phylogenetic diversity (Faith, 1992).

Bacteria and Cell Culture

F. nucleatum was purchased from the China General Microbiological Culture Collection Center (CGMCC) and cultured with EG medium (Euglena gracilis medium) in an anaerobic box at 37°C, and the number of *F. nucleatum* was determined by the standard curve. HCT116 cell line was cultured in RPMI-1640 medium supplemented with 10% FBS and 1% antibiotics at 37°C and 5% CO_2. *F. nucleatum* and cancer cells (multiplicity of infection, MOI = 100) were cocultured for 2 h at 37°C and treated with compounds at the half maximal inhibitory concentration (IC_{50}) for 48 h. Experiments were performed with cells of passage numbers 4 to 20. Experiments were repeated three times.

Minimum Inhibitory Concentrations and Minimum Bactericidal Concentrations Test

F. nucleatum was harvested at logarithmic growth period (24–48 h), and the concentration of the bacterial solution was adjusted to 10^6 CFU/ml. IPM711 and IPM712 were diluted to 40, 80, 120, 160, and 200 μM with EG medium. Then 50 μl of compound solution and 50 μl of bacterial solution were added to 96-well plates and mixed for 10 min. After 48 h of anaerobic culture at 37°C, concentrations of clarified wells were determined as the minimum inhibitory concentrations. Finally, 50 μl of culture solution was collected from each clarified well and spotted onto the EG plates, and concentrations of plate without colonies were determined as the minimum bactericidal concentrations (MBC). Experiments were repeated three times.

MTT Assay for Inhibition

MTT was used to determine the inhibition, and L-cysteine was removed from the medium formula. *F. nucleatum* was harvested and diluted to an optical density at 600 nm (OD_{600nm}) of 0.2. Next, 50 μl of bacterial solution and the same volume of compound solution were added to the 96-well plate with the final concentration at 20, 40, 60, 80, and 100 μM, which were cultivated for 24 h under anaerobic conditions at 37°C. Finally, absorbance (Abs) values were detected at 490 nm, and the cell viability was calculated according to the formula = 100% × (sample Abs)/(control Abs). Penicillin–streptomycin and EG medium were set as positive and negative controls, respectively.

Effects on Bacterial Membrane Permeability

Propidium iodide (PI) was used to study the effect on bacterial membrane permeability, which could only bind to the nucleus through broken cell membranes. First, the density of *F. nucleatum* was diluted to 0.4 at OD_{600nm}. Then 1 ml of bacterial solution and compound solution were mixed and incubated for 24 h under anaerobic conditions at 37°C. Next, the solution was centrifuged for 2 min at 10,000 rpm and washed twice with 1× phosphate-buffered solution (PBS). Finally, *F. nucleatum* was stained with 50 mg/ml of PI solution for 20 min. To determine the total bacteria, it was fixed using 4% paraformaldehyde. Measurements were made using fluorescence microscope (BX53, Olympus). Experiments were repeated three times.

Effects on Bacterial Integrity

The density of *F. nucleatum* was diluted to 0.4 at OD_{600nm} and incubated with compounds (MIC). Three hours later, the bacterial suspension was centrifuged for 5 min at 10,000 rpm and fixed with 2.5% glutaraldehyde for 4 h at 4°C. Then it was centrifuged to remove the supernatant and dehydrated with 20%, 50%, 80%, and 100% (twice) ethanol for 15 min each time. Next, the bacterial solution was adjusted to a suitable concentration and frozen dried for 4 h. Finally, a layer of gold was sprayed onto the surface, and *F. nucleatum* was observed using a scanning electron microscope (SEM, JSM-6701F, JEOL).

Real-Time Quantitative PCR

After coculture with *F. nucleatum*, HCT 116 cells (1 × 10^6 cells) were treated with IPM711 and IPM712 at the concentration of

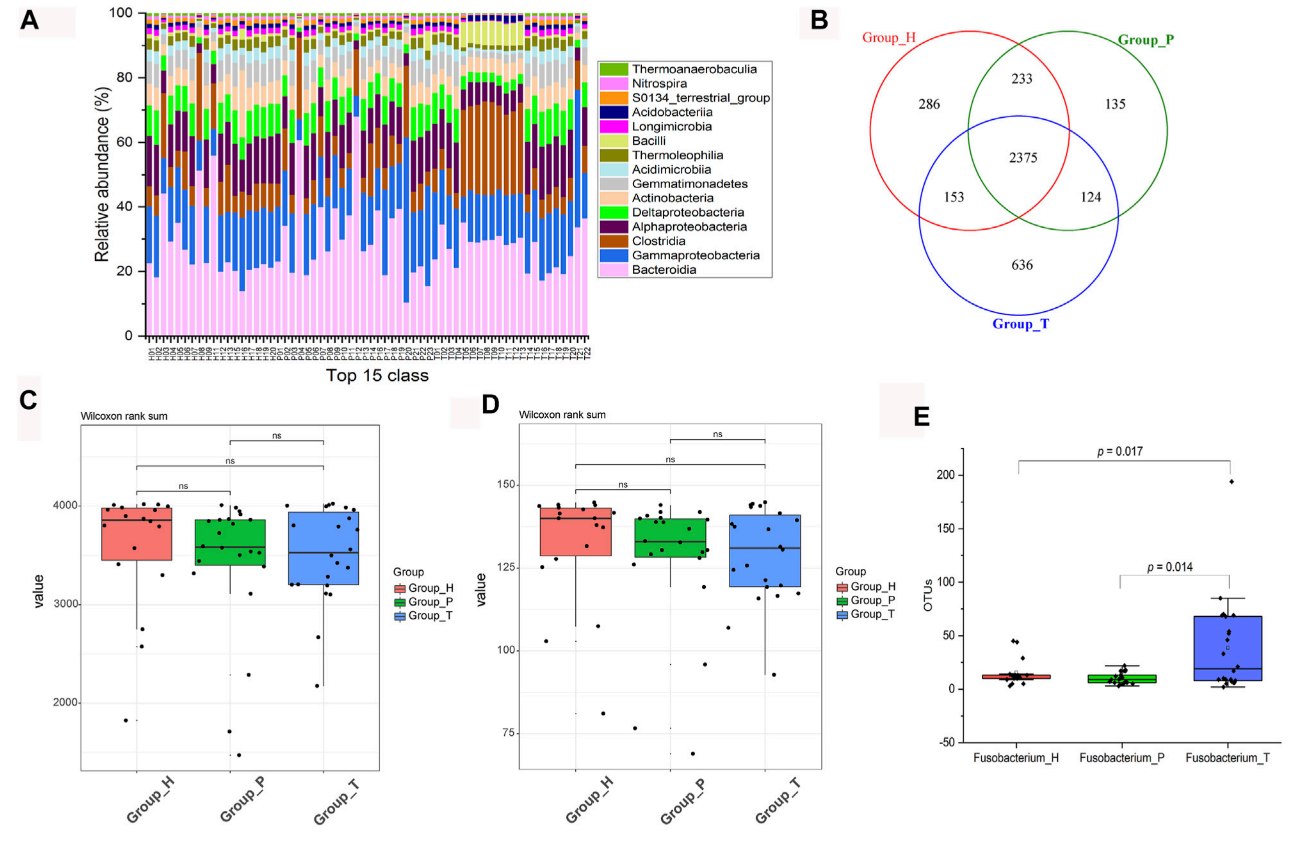

FIGURE 1 | Changes in microbial community and diversity. Relative abundance of the top 15 classes (H, healthy people; P, polyp patients; T, CRC patients) **(A)**. Venn diagram of different groups **(B)**. Comparation among observed species **(C)**. Comparation among phylogenetic diversity **(D)**. Absolute abundance (OTU numbers) of *Fusobacterium* in different groups **(E)**.

IC_{50} (6.69 and 1.40 μM, respectively) for 48 h. Total RNA was extracted using RNAsimple Total RNA Kit and subjected to reverse transcription with FastKing gDNA Dispelling RT SuperMix (TIANGEN BIOTECH) following the manufacturer's instructions. Quantitative PCR (qPCR) assay was used to measure the relative abundance of the gene. Each 10 μl of reaction volume contained 1× SuperReal PreMix Plus (SYBR Green, TIANGEN BIOTECH), 0.3 μM of each primer, 1× ROX reference dye. Primers used here are listed in **Table 1** and the conditions were as follows: 15 min at 95°C, 40 cycles of 15 s at 95°C, and 32 s at 60°C. A melting curve step was run after the qPCR reaction to verify the specificity of each primer. All qPCR amplifications were run on the Applied Biosystems QuantStudio 5 Real-Time PCR Systems (Applied Biosystems, USA). The relative abundance was calculated using $2^{-\Delta\Delta Ct}$ method. All experiments were performed in triplicate.

Western Blot

For Western blot experiments, 1×10^6 cells were seeded into six-well plates. The coculture and treatment were the same as described above. Then the total proteins were extracted with RIPA buffer containing 1% PMSF and detected with Brasford assay. Proteins of different sizes were separated using 10% sodium dodecyl sulfate-polyacrylamide gel electrophoresis (SDS-PAGE). Afterward, proteins were transferred onto a 0.22-μm PVDF membrane and incubated with Tris buffer containing 5% nonfat milk, which was further incubated with primary antibodies, including E-cadherin (#bs-1519R, 1:1,000, Bioss) and β-catenin (#bs-1165R, 1:1,000, Bioss), and secondary antibody (#bs-40295G-HRP, 1:5,000, Bioss) for 12 and 1 h, respectively. Subsequently, the expression of proteins was analyzed using the chemiluminescence analysis system and ImageJ 1.43 software. GAPDH (#bs-10900R, 1:5,000, Bioss) was used as a control for whole-cell lysates. All experiments were performed in triplicate.

Migration Assay

HCT116 cells (1×10^6 cells) were seeded into six-well plates and cocultured with *F. nucleatum* for 2 h under anaerobic conditions. Then cells were washed with PBS three times and seeded at a density of 1×10^5 cells/0.1 ml in RPMI-1640 (1% FBS) into the upper chambers (8-μm pore size, Corning). The lower chamber was filled with 500 μl of media with 20% FBS. After incubation for 48 h, cells were fixed with 4% paraformaldehyde for 20 min at room temperature, and then stained with 0.1% crystal violet for 20 min. Migrating

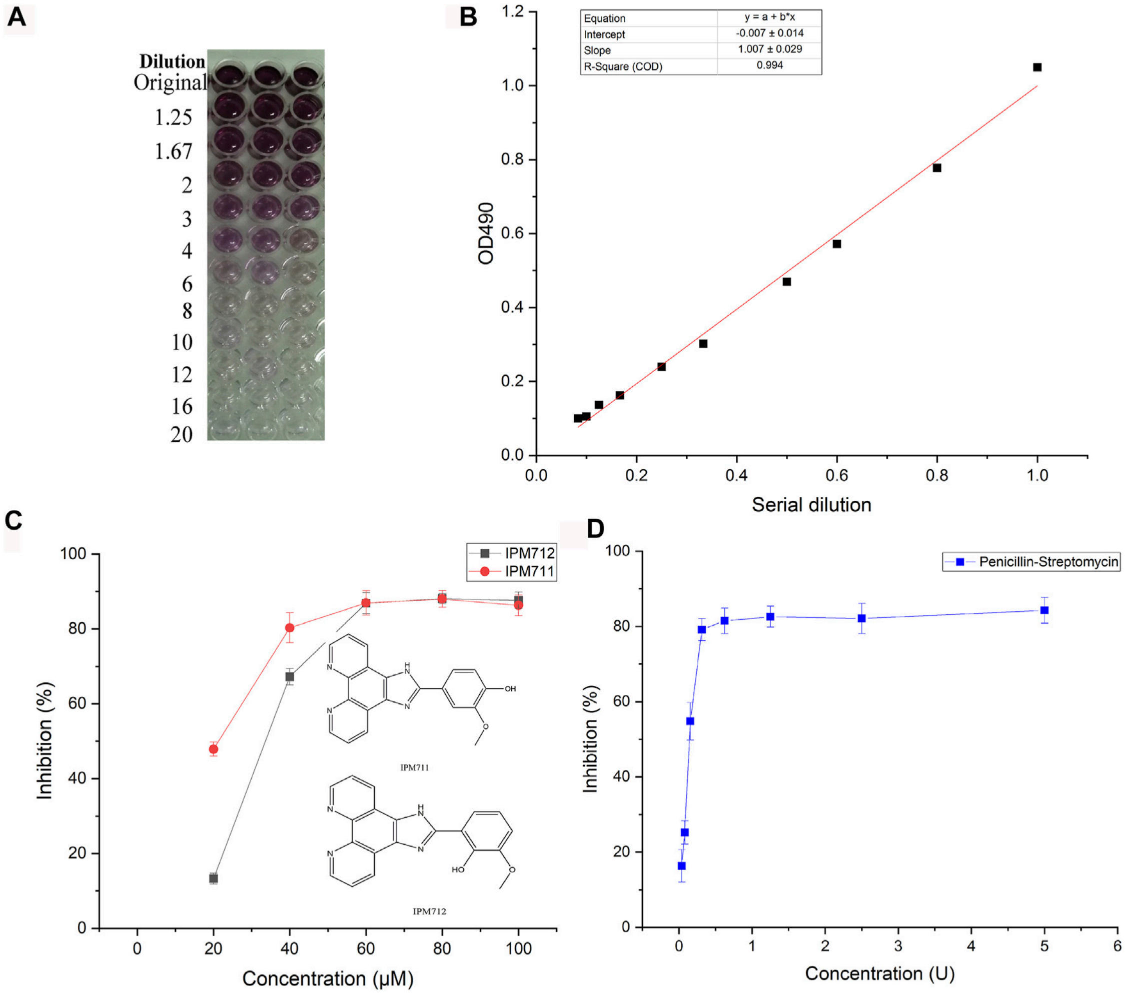

FIGURE 2 | Anti-*F. nucleatum* activities of IPM711 and IPM712. Gradient changes in color in a 96-well plate at different *F. nucleatum* concentrations using the MTT method and corresponding standard curve at 490 nm **(A,B)**. Inhibition rates of IPM711 (red point), IPM712 (black point), and penicillin–streptomycin (blue point) against *F. nucleatum* **(C,D)**.

cells were visualized by microscopy at ×40 magnification and counted with the ImageJ 1.43 software. All experiments were performed in triplicate.

Statistical Analysis

Transcriptome data from colorectal cancer and the adjacent normal tissues infected with *F. nucleatum* in the public GEO datasets were used as external validation. Additionally, gene expression abundance, and overall survival of healthy people and CRC patients were analyzed using GEPIA (http://gepia.cancer-pku.cn/) (Tang et al., 2017).

All statistical analysis were performed with the OriginPro software (OriginLab Corporation, United States) and R Project for Statistical Computing environment. qPCR data were analyzed using QuantStudio™ Design and Analysis Software (Thermo Fisher Technology). Statistical differences between groups were analyzed using t-test. All results were expressed as the mean ± standard deviation of independent experiments. A value of $p <$ 0.05 was considered statistically significant.

RESULTS

Changes of Microbial Community and Diversity

The overall study population consists of 22 CRC patients, 22 cases with different degrees of polypus, and 18 controls who went through colonoscopy but with no disease symptoms. The mean age of the cohort is 59.5 years old, and female subjects account for 40.0%. The number of valid tags of each sample was distributed between 26,376 and 37,118, with the average length distributed between 414.35 and 420.06 bp.

To investigate the signature of the three groups, microbial community structure and alpha diversity were used for

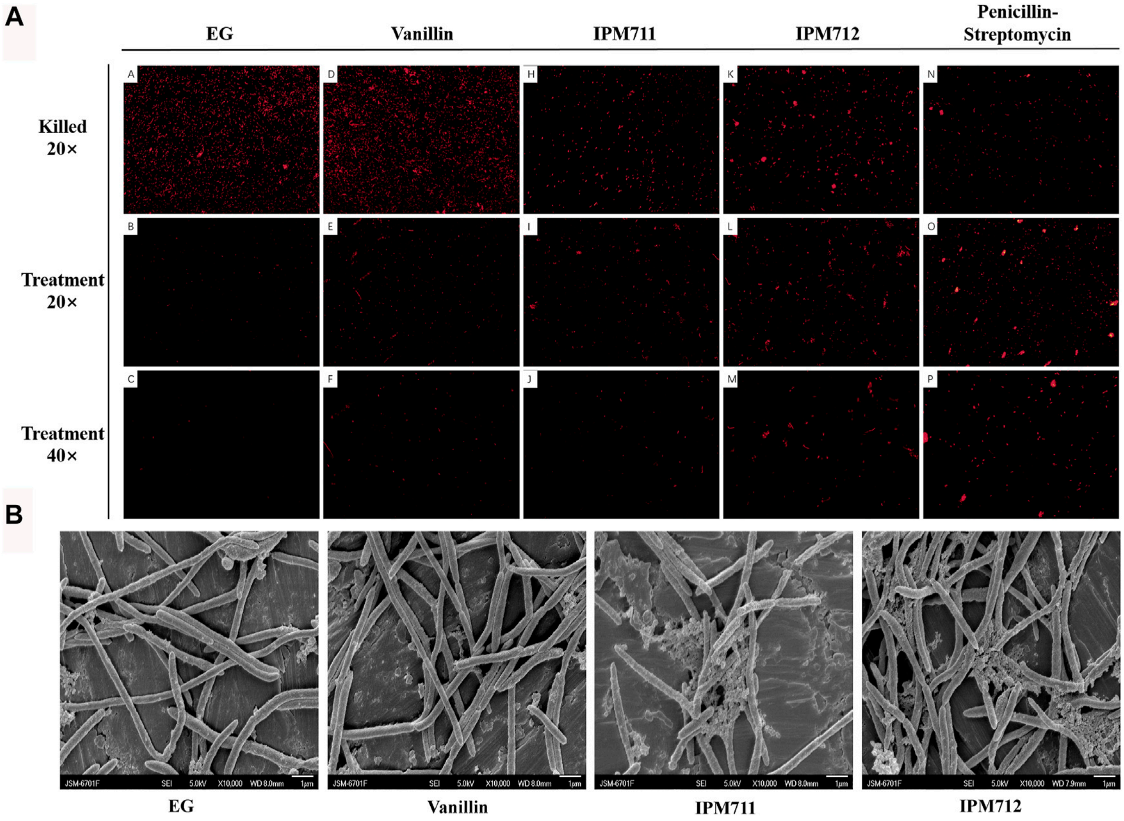

FIGURE 3 | Fluorescence microscope observation after propidium iodide (PI) staining and bacterial morphology after exposure to vanillin and its derivatives. Observation (20×) after 4% paraformaldehyde fixation and stain (marked as "killed" on the first row). Observation (20×) after *Euglena gracilis* (EG) medium, vanillin, IPM711, IPM712, and penicillin–streptomycin treatments (the second row). Observation (40×) after treatment (the third row) **(A)**. Scanning electron microscope (SEM) observation after EG medium, vanillin, IPM711, and IPM 712 treatments **(B)**.

comparison. In CRC patients, the abundance of Clostridia and Bacilli was higher, while the healthy group contained more Gammaproteobacteria and Deltaproteobacteria (**Figure 1A**). Compared with the polyp group, the difference in composition of species between healthy and cancer groups was bigger (**Figure 1B**). In addition, both species richness and community diversity showed a stepwise decreased frequency from controls, to dysplasia and to cancers, indicating that the development of CRC was accompanied with depletion of gut microbes (**Figures 1C, D**). We further studied the change in *Fusobacterium* and found that its abundance gradually increased along the deterioration of the disease (the sample H06 was excluded according to the F-test) (**Figure 1E**).

Antimicrobial Effect of IPM711 and IPM712

As one of the most prevailing pathogenic bacteria, *F. nucleatum* was used for antibacterial test of IPM711 and IPM712. Results showed that their MIC values were 80 and 60 μM, respectively. Both MBC values were 80 μM. Furthermore, MTT assay was applied for the detection of inhibition rate, and the standard curve showed that there was a good linear relationship between the number of viable bacteria and the absorbance ($R^2 > 0.99$, **Figures 2A, B**). The inhibition rates of IPM711, IPM712, and antibiotics were 88.09%, 88.00%, and 87.25% at 100 μM/5 U (**Figures 2C,D**). Overall, IPM712 has a higher antibacterial activity, demonstrating that the change in the hydroxyl position reduces the steric hindrance and increases the activity, which is consistent with their antitumor effects.

Morphology Changes of Bacterial Cells

Based on the antibacterial activity results, PI staining and SEM were carried out to observe the bacterial morphology change after exposure to compounds. Paraformaldehyde-treated bacteria were used to display all the *F. nucleatum* in the different groups, and results showed a decreased number of *F. nucleatum* after treatment of compounds (**Figure 3A**). Additionally, compared with EG medium and vanillin groups, IPM711 and IPM712 groups had stronger fluorescence, indicating that they could strongly increase the permeability of cell membranes, which was similar to the penicillin–streptomycin group. SEM observation showed that the outer surface of *F. nucleatum* was complete and smooth after treatment with EG medium and vanillin, yet the bacteria became rough and some broke after treatment with IPM711 and IPM712 (**Figure 3B**). Results

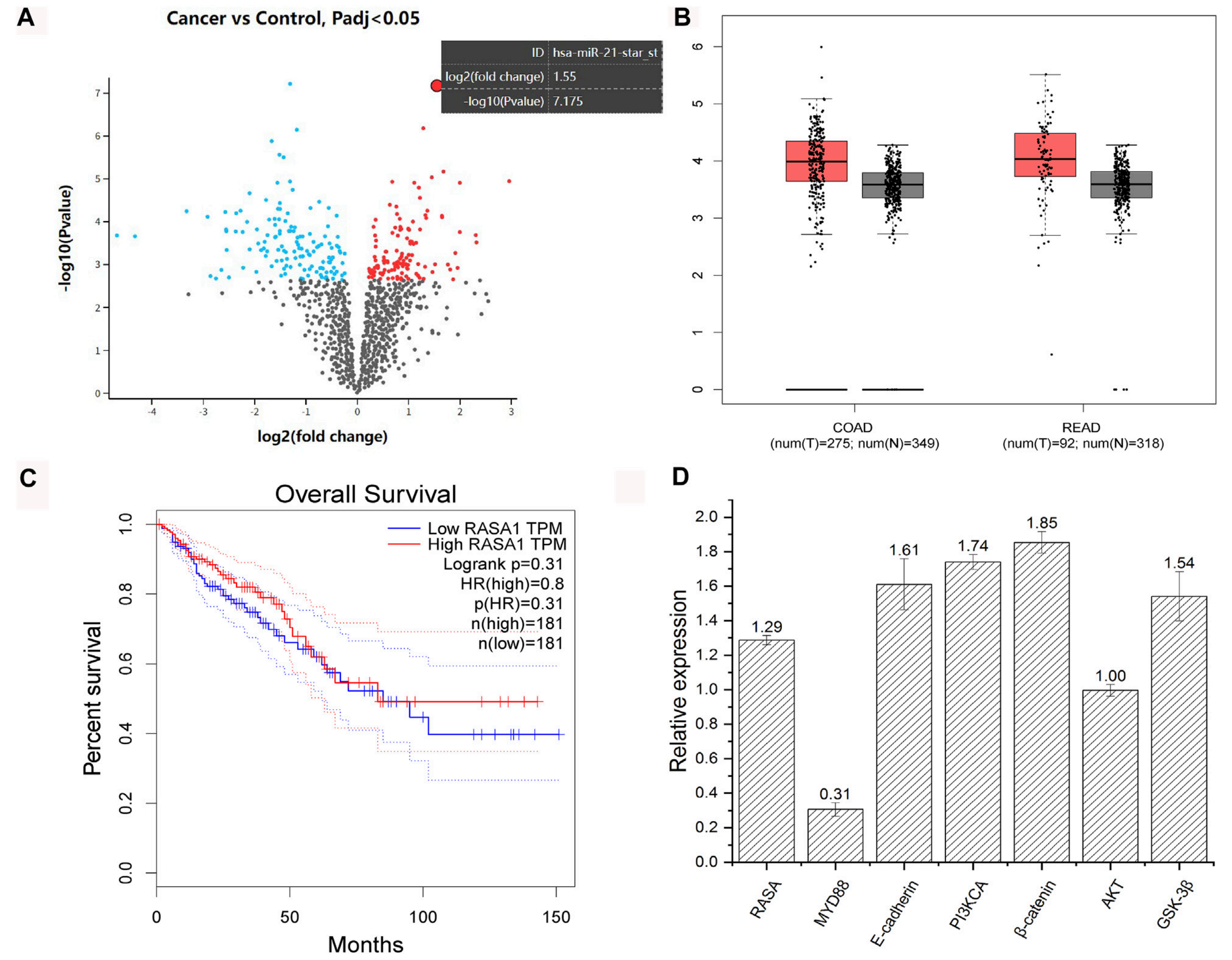

FIGURE 4 | Analysis of GSE122182 dataset and validation with qPCR. Volcano map of gene expression of colorectal cancer and the adjacent normal tissues infected with *F. nucleatum* (red points represent upregulated genes and blue points represent downregulated genes) **(A)**. Expression difference of *RASA* gene between healthy people and CRC patients (COAD, colon cancer; RECD, rectal cancer; T, tumor patients; N, normal people) **(B)**. Survival curve of patients with high and low expression of *RASA* gene (obtained from GEPIA, http://gepia.cancer-pku.cn/) **(C)**. Changes in gene expressions of HCT116 after coculture with *F. nucleatum* (numbers represent the fold change in gene expression) **(D)**.

suggested that IPM711 and IPM712 could cause the breakage of bacterial cells and destroy the integrity, thus, exerting better antibacterial activity than vanillin.

F. nucleatum Induce Colorectal Tumourigenesis

F. nucleatum was reported to be more abundant in CRC tissues, and expression data (GSE122182) of miRNA profile from colorectal cancer and the adjacent normal tissues infected with *F. nucleatum* showed that miRNA 21 was the most upregulated, whose corresponding gene is *RASA* (**Figure 4A**). Further analysis showed that the expression level of *RASA* was higher in CRC patients. Those patients with high *RASA* expressions displayed shorter survival period (GEPIA, http://gepia.cancer-pku.cn/, **Figures 4B, C**). In addition, after coculture of *F. nucleatum* and HCT116 cells, qPCR experiments showed that *F. nucleatum* induced upregulated expression of *RASA*, *PI3KCA*, *β-catenin*, *E-cadherin*, and *GSK-3β*, yet without any influence on the *AKT* gene. Meanwhile, expression of *MYD88* was downregulated (**Figure 4D**). Those genes were previously reported to be associated with apoptosis, invasion, and chemotherapy resistance of colorectal cancer.

IPM711 and IPM712 Reverse *Fusobacterium nucleatum*-Induced Colorectal Tumorigenesis

To verify whether IPM711 and IPM712 are able to treat CRC after *F. nucleatum* infection, compound treatments were performed after coculture of *F. nucleatum* and HCT116 cells. qPCR results showed that IPM711 and IPM712 could downregulate the

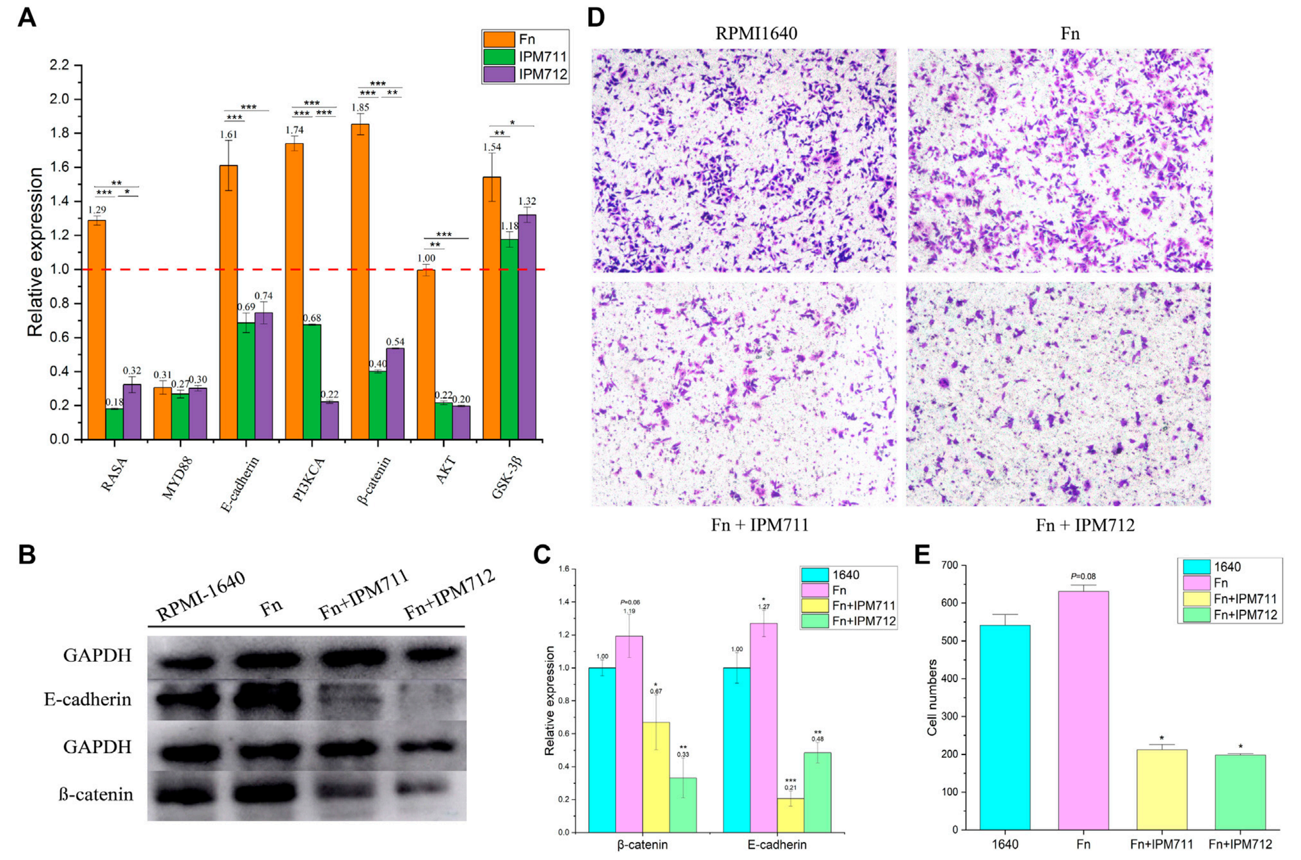

FIGURE 5 | Changes in gene and protein expression. Changes in related genes of HCT116 after cocultivation with *F. nucleatum* (Fn, MOI = 100, 2 h) and treatments with IPM711 and IPM712 at the concentration of IC_{50} **(A)**. Changes in E-cadherin and β-catenin proteins of HCT116 after cocultivation with *F. nucleatum* (MOI = 100, 2 h) and treatments with IPM711 and IPM712 (IC_{50}) **(B)**. Statistical analysis, $^{*}p < 0.05$, $^{**}p < 0.01$, $^{***}p < 0.001$ compared with control group **(C)**. Characterization of migratory capacity of HCT116 cells after treatment with RPMI-1640, *F. nucleatum*, *F. nucleatum* and IPM711, and *F. nucleatum* and IPM712 **(D)**. Statistical analysis, $^{*}p < 0.05$ compared with control group **(E)**.

overexpressed *RASA* gene significantly, but without any effect on *MYD88* gene, suggesting that IPM711 and IPM712 might rescue *F. nucleatum*-induced chemoresistance somehow instead of the TRL4/MYD88 pathway. Moreover, the expression of *E-cadherin*, *PI3KCA*, *β-catenin*, *AKT*, and *GSK-3β* were downregulated, indicating that IPM711 and IPM712 could reduce the proliferation and migration of cancer cells as well as the adhesion of *F. nucleatum* (**Figure 5A**). Western blot results also showed that E-cadherin and β-catenin proteins were downregulated after IPM711 and IPM712 treatments, corroborating the gene expression changes (**Figures 5B, C**). Finally, migration assay proved that IPM711 and IPM712 still exerted anticancer effect in the case of *F. nucleatum* infection (**Figure 5D**).

DISCUSSION

Gut microbiome dysbiosis and increase in *Fusobacterium* are common in CRC patients and verified in our sample set in Northwest China for the first time. In addition, vanillin derivatives, IPM711 and IPM712, showed better anti-*F. nucleatum* activity after structural modification. Furthermore, intervention experiments *in vitro* indicated that they were effective for *F. nucleatum*-infected CRC cells by inhibiting proliferation and migration through the E-cadherin/β-catenin pathway (**Figure 6**).

Disorders of the gut microbiome have been acknowledged as one important factor of CRC development, and panels of different microbes can be used as biomarkers for early diagnosis. People from different countries or areas carry different microbiome characteristics, which may result from their unique regional environmental factors. Fusobacteria is not relatively abundant in healthy people but common in CRC patients. However, *Fusobacterium* are prevalent in most CRC populations in China, though several *Fusobacterium* taxa are comparatively more abundant in southern Chinese populations (Yang et al., 2020; Yeoh et al., 2020). Northwest China, especially Gansu and Ningxia, are areas with a high incidence of gastrointestinal tumors (Zhang et al., 2021), yet the gut microbiome changes in CRC patients in these areas are unclear. Our results showed that patients' intestinal microbiome gradually changed with the development of the disease, manifested as an increase in harmful bacteria, a

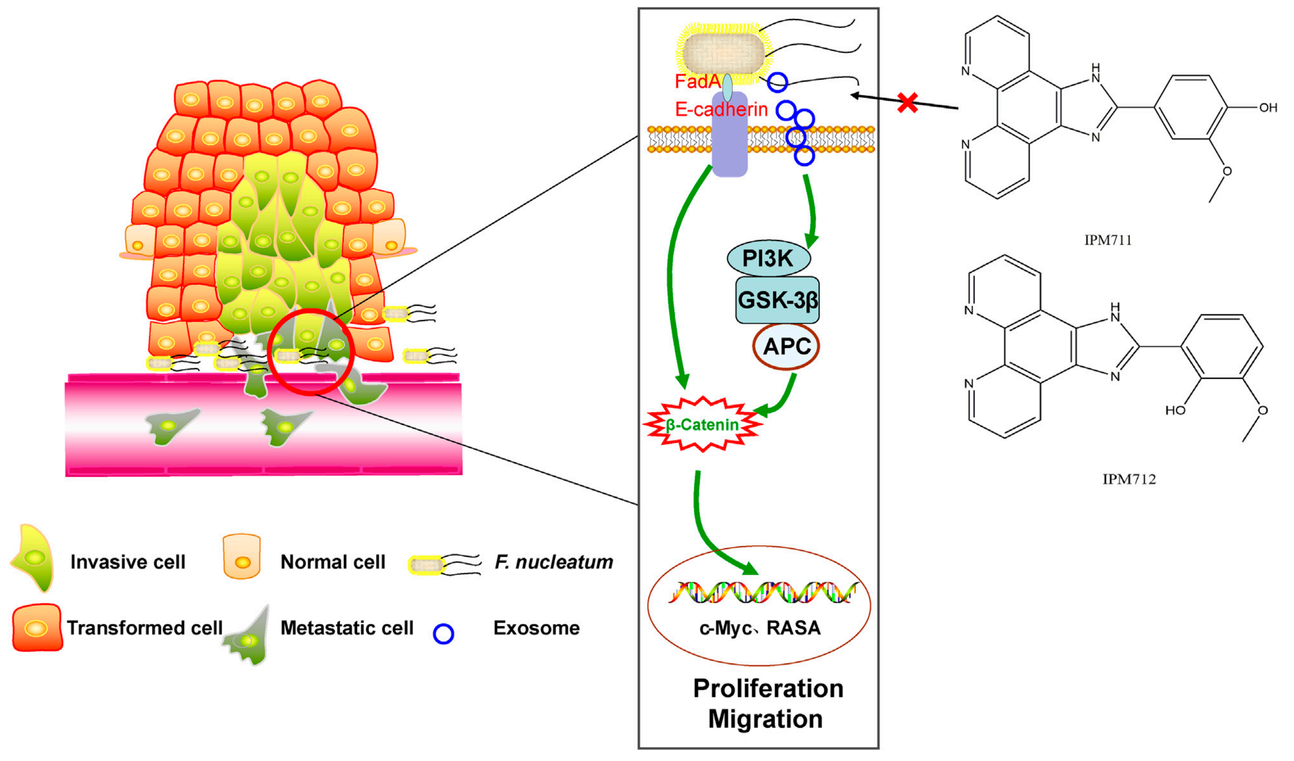

FIGURE 6 | Vanillin derivatives reverse *F. nucleatum*-induced proliferation and migration of CRC through the E-cadherin/β-catenin pathway.

decrease in beneficial bacteria, and a gradual decline in overall diversity. Moreover, predictions in the Kyoto Encyclopedia of Genes and Genomes (KEGG) displayed that pathways of CRC patients were mainly related with the calcium signaling pathway, various types of N-glycan biosynthesis, the GnRH signaling pathway, endocytosis, and Fc gamma R-mediated phagocytosis, while the main functions in healthy people included glycolysis/gluconeogenesis, cysteine and methionine metabolism, primary immunodeficiency, and peptidoglycan biosynthesis (**Supplementary Figure S1**), suggesting that the dysregulation in the gut microbiome might be accompanied by changes in metabolic function. Most importantly, *Fusobacterium* is more abundant in CRC patients in Northwest China, whereas the specific taxa and associated functions need further exploration using powerful tools, such as metagenomic and metatranscriptome sequencing. Another limitation is that changes in the microbial community or *Fusobacterium* are based on the microorganisms shed into the feces. Although fecal samples are more convenient for collection and noninvasive for early diagnosis (Wong et al., 2017), they may contain the bacteria throughout the digestive tract. Therefore, tissue samples are needed to further verify those changes.

F. nucleatum can produce volatile sulfur compounds, such as H_2S and CH_3SH, being considered to be related to oral halitosis initially. Subsequently it was found to be prevalent in human colorectal carcinoma. To reduce these kinds of bacteria, many natural products and active molecules had been tested to inhibit *F. nucleatum*, including Labrador tea, peppermint, winter savory essential oils, tea polyphenols, wild blueberry polyphenols, *Litsea japonica* leaf extract, curcumin, dietary (poly) phenols, graphene oxide, and macrolides (Nagaoka et al., 2013; Ben Lagha et al., 2015; He et al., 2015; Shahzad et al., 2015; Izui et al., 2016; Ben Lagha et al., 2017; Yun et al., 2018; Ben Lagha et al., 2020), indicating that phenolic compounds possess superior activity against *F. nucleatum*. A study evaluated the resistance of natural and synthetic phenolic compounds to oral bacteria, finding that lipophilicity and steric effect were two key factors. They acted as non-ionic surfactants and destroyed the lipoprotein interface (Greenberg et al., 2008). Similarly, after structural modification, ortho-hydroxyl groups enhanced the antibacterial activity of vanillin derivatives, which was consistent with the anticancer effect (Ma et al., 2020). Currently, narrow-spectrum antibiotics targeting *F. nucleatum* are not available, thus, combining conventional chemotherapy (5-fluorouracil, cisplatin, etc.) with well-tolerated natural compounds may help to better respond to treatment and improve patients' quality of life. Recently, a systematic review summarized natural compounds possessing anti-CRC activities and proposed advantages of combination therapy, including reduction of resistance to cancer drugs, alleviation of the toxic burden on the patient's body, and increased sensitivity to chemotherapeutic drug by targeting multiple metabolic pathways (Rejhová et al., 2018). Therefore, natural products, such as vanillin derivatives, are potential candidates for the treatment of *F. nucleatum*-infected CRC, which will lead to chemotherapy resistance to 5-fluorouracil and cisplatin (Yu et al., 2017; Zhang et al., 2019).

Results of qPCR and Western blot suggested that IPM711 and IPM712 inhibited the expression of E-cadherin (the occurrence of double bonds might result from the slightly poor specificity of polyclonal antibody) and β-catenin, which were indispensable for the adherence of *F. nucleatum* to HCT116 cells. E-cadherin mediates bacterial adhesion to mammalian cells, and β-catenin (also called CTNNB) is necessary for the creation and maintenance of epithelial cell layers by regulating cell growth and adhesion between cells, both of which are overexpressed in tumor tissues (**Supplementary Figure S2**). Previous studies demonstrated that *F. nucleatum* could stimulate growth of CRC cells through its FadA adhesion, which binds to E-cadherin and activated β-catenin signaling (Rubinstein et al., 2013). Another research found that FadA, E-cadherin, Annexin A1, and β-catenin could form a complex in cancerous cells, and FadA adhesin from *F. nucleatum* upregulated Annexin A1 expression through E-cadherin (Rubinstein et al., 2019). The protein encoded by the *RASA* gene is part of the GAP1 family of GTPase-activating proteins, thereby, allowing control of cellular proliferation and differentiation. Upregulation of miR-223 was associated with the downregulation of *RASA* in CRC tissues, and C/EBP-β-activated miR-223 improved colorectal cancer cell growth and stimulated tumorigenesis by targeting *RASA* in CRC (Sun et al., 2013; Sun et al., 2015). Furthermore, overexpression of *RASA* could abolish the promotive effects of exosome-transmitted miR-335-5p on CRC cell migration, invasion, and epithelial–mesenchymal transition (Sun et al., 2021). Recently, it was reported that *F. nucleatum* could activate TLR4 signaling to MYD88 and reduce levels of *RASA*, thus, leading to chemoresistance (Yang et al., 2017). IPM711 and IPM712 could significantly downregulate the expression *RASA* gene and might relieve chemoresistance. Furthermore, IPM711 and IPM712 also changed the upregulation of *GSK-3β* induced by *F. nucleatum*, which was recently proved to be associated with exosomes derived from *F. nucleatum* (Guo et al., 2021), suggesting that they might inhibit the proliferation and migration of CRC cells by influencing the exosomes. With the discovery of the carcinogenic mechanisms of *F. nucleatum*, treatment of CRC by targeting the bacteria has become a feasible strategy. Natural products are important source of drug development with low toxicity and high efficiency. It is of great significance to develop natural medicines that can resist both colorectal cancer and pathogenic bacteria.

DATA AVAILABILITY STATEMENT

The datasets presented in this study can be found in online repositories. The names of the repository/repositories and accession number(s) can be found below. The datasets (16S rRNA sequencing) for this study can be found in the NCBI Short Read Archive (PRJNA763872).

ETHICS STATEMENT

The studies involving human participants were reviewed and approved by the First Hospital of Lanzhou University and the Second Hospital of Lanzhou University. The patients/participants provided their written informed consent to participate in this study.

AUTHOR CONTRIBUTIONS

PC and ZZ conceived the project and contributed to the experimental designs. ZZ, YW, RJ, DZ, CM, YM, XJ, RZ, and KD performed the experiments, generated the figures, and wrote the manuscript. PC, ZZ, YW, RJ, DZ, CM, and WM interpreted the results. PC supervised the project. All authors discussed the results and approved the manuscript.

FUNDING

This work was supported by the Key Research and Development Program of Gansu Province (Grant No. 21YF5FA112), the Technological Innovation Guidance Program of Gansu Province (Grant No. 21CX6QA127), and the College Students' Innovation and Entrepreneurship Training Program of Lanzhou University (Grant Nos. 20210260002, 20210260009).

SUPPLEMENTARY MATERIAL

The Supplementary Material for this article can be found online at: https://www.frontiersin.org/articles/10.3389/fphar.2022.841918/full#supplementary-material

REFERENCES

Arya, S. S., Rookes, J. E., Cahill, D. M., and Lenka, S. K. (2021). Vanillin: a Review on the Therapeutic Prospects of a Popular Flavouring Molecule. *Adv. Tradit Med. (Adtm)* 21, 1–17. doi:10.1007/s13596-020-00531-w

Ben Lagha, A., Dudonné, S., Desjardins, Y., and Grenier, D. (2015). Wild Blueberry (Vaccinium Angustifolium Ait.) Polyphenols Target Fusobacterium Nucleatum and the Host Inflammatory Response: Potential Innovative Molecules for Treating Periodontal Diseases. *J. Agric. Food Chem.* 63 (31), 6999–7008. doi:10.1021/acs.jafc.5b01525

Ben Lagha, A., Haas, B., and Grenier, D. (2017). Tea Polyphenols Inhibit the Growth and Virulence Properties of Fusobacterium Nucleatum. *Sci. Rep.* 7 (1), 44815. doi:10.1038/srep44815

Ben Lagha, A., Vaillancourt, K., Maquera Huacho, P., and Grenier, D. (2020). Effects of Labrador tea, Peppermint, and winter Savory Essential Oils on Fusobacterium Nucleatum. *Antibiotics (Basel)* 9 (11), 794. doi:10.3390/antibiotics9110794

Bezerra, C. F., Camilo, C. J., do Nascimento Silva, M. K., de Freitas, T. S., Ribeiro-Filho, J., and Coutinho, H. D. M. (2017). Vanillin Selectively Modulates the Action of Antibiotics against Resistant Bacteria. *Microb. Pathog.* 113, 265–268. doi:10.1016/j.micpath.2017.10.052

Bolger, A. M., Lohse, M., and Usadel, B. (2014). Trimmomatic: a Flexible Trimmer for Illumina Sequence Data. *Bioinformatics* 30 (15), 2114–2120. doi:10.1093/bioinformatics/btu170

Borowsky, J., Haruki, K., Lau, M. C., Dias Costa, A., Väyrynen, J. P., Ugai, T., et al. (2021). Association of Fusobacterium Nucleatum with Specific T-Cell Subsets in the Colorectal Carcinoma Microenvironment. *Clin. Cancer Res.* 27 (10), 2816–2826. doi:10.1158/1078-0432.Ccr-20-4009

Bray, F., Ferlay, J., Soerjomataram, I., Siegel, R. L., Torre, L. A., and Jemal, A. (2018). Global Cancer Statistics 2018: GLOBOCAN Estimates of Incidence and Mortality Worldwide for 36 Cancers in 185 Countries. *CA Cancer J. Clin.* 68 (6), 394–424. doi:10.3322/caac.21492

Bullman, S., Pedamallu, C. S., Sicinska, E., Clancy, T. E., Zhang, X., Cai, D., et al. (2017). Analysis of Fusobacterium Persistence and Antibiotic Response in Colorectal Cancer. *Science* 358 (6369), 1443–1448. doi:10.1126/science.aal5240

Caporaso, J. G., Kuczynski, J., Stombaugh, J., Bittinger, K., Bushman, F. D., Costello, E. K., et al. (2010). QIIME Allows Analysis of High-Throughput Community Sequencing Data. *Nat. Methods* 7 (5), 335–336. doi:10.1038/nmeth.f.303

Castellarin, M., Warren, R. L., Freeman, J. D., Dreolini, L., Krzywinski, M., Strauss, J., et al. (2012). Fusobacterium Nucleatum Infection Is Prevalent in Human Colorectal Carcinoma. *Genome Res.* 22 (2), 299–306. doi:10.1101/gr.126516.111

Chen, S., Su, T., Zhang, Y., Lee, A., He, J., Ge, Q., et al. (2020). Fusobacterium Nucleatum Promotes Colorectal Cancer Metastasis by Modulating KRT7-AS/KRT7. *Gut Microbes* 11 (3), 511–525. doi:10.1080/19490976.2019.1695494

Edgar, R. C., Haas, B. J., Clemente, J. C., Quince, C., and Knight, R. (2011). UCHIME Improves Sensitivity and Speed of Chimera Detection. *Bioinformatics* 27 (16), 2194–2200. doi:10.1093/bioinformatics/btr381

Faith, D. P. (1992). Systematics and Conservation: on Predicting the Feature Diversity of Subsets of Taxa. *Cladistics* 8 (4), 361–373. doi:10.1111/j.1096-0031.1992.tb00078.x

Fitzgerald, D. J., Stratford, M., Gasson, M. J., Ueckert, J., Bos, A., and Narbad, A. (2004). Mode of Antimicrobial Action of Vanillin against *Escherichia coli*, Lactobacillus Plantarum and Listeria Innocua. *J. Appl. Microbiol.* 97 (1), 104–113. doi:10.1111/j.1365-2672.2004.02275.x

Greenberg, M., Dodds, M., and Tian, M. (2008). Naturally Occurring Phenolic Antibacterial Compounds Show Effectiveness against Oral Bacteria by a Quantitative Structure-Activity Relationship Study. *J. Agric. Food Chem.* 56 (23), 11151–11156. doi:10.1021/jf8020859

Guo, S., Chen, J., Chen, F., Zeng, Q., Liu, W.-L., and Zhang, G. (2021). Exosomes Derived from Fusobacterium Nucleatum-Infected Colorectal Cancer Cells Facilitate Tumour Metastasis by Selectively Carrying miR-1246/92b-3p/27a-3p and CXCL16. *Gut* 70 (8), 1507–1519. doi:10.1136/gutjnl-2020-321187

He, J., Zhu, X., Qi, Z., Wang, C., Mao, X., Zhu, C., et al. (2015). Killing Dental Pathogens Using Antibacterial Graphene Oxide. *ACS Appl. Mater. Inter.* 7 (9), 5605–5611. doi:10.1021/acsami.5b01069

Huang, X., Hong, X., Wang, J., Sun, T., Yu, T., Yu, Y., et al. (2020). Metformin Elicits Antitumour Effect by Modulation of the Gut Microbiota and Rescues Fusobacterium Nucleatum-Induced Colorectal Tumourigenesis. *EBioMedicine* 61, 103037. doi:10.1016/j.ebiom.2020.103037

Izui, S., Sekine, S., Maeda, K., Kuboniwa, M., Takada, A., Amano, A., et al. (2016). Antibacterial Activity of Curcumin against Periodontopathic Bacteria. *J. Periodontol.* 87 (1), 83–90. doi:10.1902/jop.2015.150260

Kostic, A. D., Chun, E., Robertson, L., Glickman, J. N., Gallini, C. A., Michaud, M., et al. (2013). Fusobacterium Nucleatum Potentiates Intestinal Tumorigenesis and Modulates the Tumor-Immune Microenvironment. *Cell Host Microbe* 14 (2), 207–215. doi:10.1016/j.chom.2013.07.007

Ma, W., Zhang, Q., Li, X., Ma, Y., Liu, Y., Hu, S., et al. (2020). IPM712, a Vanillin Derivative as Potential Antitumor Agents, Displays Better Antitumor Activity in Colorectal Cancers Cell Lines. *Eur. J. Pharm. Sci.* 152, 105464. doi:10.1016/j.ejps.2020.105464

Mima, K., Nishihara, R., Qian, Z. R., Cao, Y., Sukawa, Y., Nowak, J. A., et al. (2016). Fusobacterium Nucleatum in Colorectal Carcinoma Tissue and Patient Prognosis. *Gut* 65 (12), 1973–1980. doi:10.1136/gutjnl-2015-310101

Nagaoka, K., Yanagihara, K., Harada, Y., Yamada, K., Migiyama, Y., Morinaga, Y., et al. (2013). Macrolides Inhibit Fusobacterium Nucleatum-Induced MUC5AC Production in Human Airway Epithelial Cells. *Antimicrob. Agents Chemother.* 57 (4), 1844–1849. doi:10.1128/AAC.02466-12

Rejhová, A., Opattová, A., Čumová, A., Slíva, D., and Vodička, P. (2018). Natural Compounds and Combination Therapy in Colorectal Cancer Treatment. *Eur. J. Med. Chem.* 144, 582–594. doi:10.1016/j.ejmech.2017.12.039

Reyon, D., Tsai, S. Q., Khayter, C., Foden, J. A., Sander, J. D., and Joung, J. K. (2012). FLASH Assembly of TALENs for High-Throughput Genome Editing. *Nat. Biotechnol.* 30 (5), 460–465. doi:10.1093/bioinformatics/btr50710.1038/nbt.2170

Rubinstein, M. R., Wang, X., Liu, W., Hao, Y., Cai, G., and Han, Y. W. (2013). Fusobacterium Nucleatum Promotes Colorectal Carcinogenesis by Modulating E-Cadherin/β-Catenin Signaling via its FadA Adhesin. *Cell Host Microbe* 14 (2), 195–206. doi:10.1016/j.chom.2013.07.012

Rubinstein, M. R., Baik, J. E., Lagana, S. M., Han, R. P., Raab, W. J., Sahoo, D., et al. (2019). Fusobacterium Nucleatum Promotes Colorectal Cancer by Inducing Wnt/β-Catenin Modulator Annexin A1. *EMBO Rep.* 20 (4), e47638. doi:10.15252/embr.201847638

Shahzad, M., Millhouse, E., Culshaw, S., Edwards, C. A., Ramage, G., and Combet, E. (2015). Selected Dietary (Poly)phenols Inhibit Periodontal Pathogen Growth and Biofilm Formation. *Food Funct.* 6 (3), 719–729. doi:10.1039/C4FO01087F

Sun, D., Yu, F., Ma, Y., Zhao, R., Chen, X., Zhu, J., et al. (2013). MicroRNA-31 Activates the RAS Pathway and Functions as an Oncogenic MicroRNA in Human Colorectal Cancer by Repressing RAS P21 GTPase Activating Protein 1 (RASA1). *J. Biol. Chem.* 288 (13), 9508–9518. doi:10.1074/jbc.M112.367763

Sun, D., Wang, C., Long, S., Ma, Y., Guo, Y., Huang, Z., et al. (2015). C/EBP-β-activated microRNA-223 Promotes Tumour Growth through Targeting RASA1 in Human Colorectal Cancer. *Br. J. Cancer* 112 (9), 1491–1500. doi:10.1038/bjc.2015.107

Sun, X., Lin, F., Sun, W., Zhu, W., Fang, D., Luo, L., et al. (2021). Exosome-transmitted miRNA-335-5p Promotes Colorectal Cancer Invasion and Metastasis by Facilitating EMT via Targeting RASA1. *Mol. Ther. Nucleic Acids* 24, 164–174. doi:10.1016/j.omtn.2021.02.022

Tang, Z., Li, C., Kang, B., Gao, G., Li, C., and Zhang, Z. (2017). GEPIA: a Web Server for Cancer and normal Gene Expression Profiling and Interactive Analyses. *Nucleic Acids Res.* 45 (W1), W98–w102. doi:10.1093/nar/gkx247

Wong, S. H., and Yu, J. (2019). Gut Microbiota in Colorectal Cancer: Mechanisms of Action and Clinical Applications. *Nat. Rev. Gastroenterol. Hepatol.* 16 (11), 690–704. doi:10.1038/s41575-019-0209-8

Wong, S. H., Kwong, T. N. Y., Chow, T. C., Luk, A. K. C., Dai, R. Z. W., Nakatsu, G., et al. (2017). Quantitation of Faecal Fusobacterium Improves Faecal Immunochemical Test in Detecting Advanced Colorectal Neoplasia. *Gut* 66 (8), 1441–1448. doi:10.1136/gutjnl-2019-31853210.1136/gutjnl-2016-312766

Yang, Y., Weng, W., Peng, J., Hong, L., Yang, L., Toiyama, Y., et al. (2017). Fusobacterium Nucleatum Increases Proliferation of Colorectal Cancer Cells and Tumor Development in Mice by Activating Toll-like Receptor 4 Signaling to Nuclear Factor-Kb, and Up-Regulating Expression of MicroRNA-21. *Gastroenterology* 152 (4), 851–e24. doi:10.1053/j.gastro.2016.11.018

Yang, J., Li, D., Yang, Z., Dai, W., Feng, X., Liu, Y., et al. (2020). Establishing High-Accuracy Biomarkers for Colorectal Cancer by Comparing Fecal Microbiomes in Patients with Healthy Families. *Gut Microbes* 11 (4), 918–929. doi:10.1080/19490976.2020.1712986

Yeoh, Y. K., Chen, Z., Wong, M. C. S., Hui, M., Yu, J., Ng, S. C., et al. (2020). Southern Chinese Populations Harbour Non-nucleatum Fusobacteria Possessing Homologues of the Colorectal Cancer-Associated FadA Virulence Factor. *Gut* 69 (11), 1998–2007. doi:10.1136/gutjnl-2019-319635

Yu, T., Guo, F., Yu, Y., Sun, T., Ma, D., Han, J., et al. (2017). Fusobacterium Nucleatum Promotes Chemoresistance to Colorectal Cancer by Modulating Autophagy. *Cell* 170 (3), 548–e16. doi:10.1016/j.cell.2017.07.008

Yun, I. G., Ahn, S. H., Yoon, W. J., Kim, C. S., Lim, Y. K., Kook, J. K., et al. (2018). Litsea Japonica Leaf Extract Suppresses Proinflammatory Cytokine Production in Periodontal Ligament Fibroblasts Stimulated with Oral Pathogenic Bacteria or Interleukin-1β. *Int. J. Mol. Sci.* 19 (9), 2494. doi:10.3390/ijms19092494

Zhang, S., Yang, Y., Weng, W., Guo, B., Cai, G., Ma, Y., et al. (2019). Fusobacterium Nucleatum Promotes Chemoresistance to 5-fluorouracil by Upregulation of BIRC3 Expression in Colorectal Cancer. *J. Exp. Clin. Cancer Res.* 38 (1), 14. doi:10.1186/s13046-018-0985-y

Zhang, S., Sun, K., Zheng, R., Zeng, H., Wang, S., Chen, R., et al. (2021). Cancer Incidence and Mortality in China, 2015. *J. Natl. Cancer Cent.* 1 (1), 2–11. doi:10.1016/j.jncc.2020.12.001

Zhou, Z., Ge, S., Li, Y., Ma, W., Liu, Y., Hu, S., et al. (2020). Human Gut Microbiome-Based Knowledgebase as a Biomarker Screening Tool to Improve the Predicted Probability for Colorectal Cancer. *Front. Microbiol.* 11, 596027. doi:10.3389/fmicb.2020.596027

Zhu, W., Winter, M. G., Byndloss, M. X., Spiga, L., Duerkop, B. A., Hughes, E. R., et al. (2018). Precision Editing of the Gut Microbiota Ameliorates Colitis. *Nature* 553 (7687), 208–211. doi:10.1038/nature25172

Conflict of Interest: The authors declare that the research was conducted in the absence of any commercial or financial relationships that could be construed as a potential conflict of interest.

Publisher's Note: All claims expressed in this article are solely those of the authors and do not necessarily represent those of their affiliated organizations, or those of the publisher, the editors, and the reviewers. Any product that may be evaluated in this article, or claim that may be made by its manufacturer, is not guaranteed or endorsed by the publisher.

Copyright © 2022 Zhou, Wang, Ji, Zhang, Ma, Ma, Ma, Jiang, Du, Zhang and Chen. This is an open-access article distributed under the terms of the Creative Commons Attribution License (CC BY). The use, distribution or reproduction in other forums is permitted, provided the original author(s) and the copyright owner(s) are credited and that the original publication in this journal is cited, in accordance with accepted academic practice. No use, distribution or reproduction is permitted which does not comply with these terms.

frontiers | Frontiers in Pharmacology

ORIGINAL RESEARCH
published: 04 April 2022
doi: 10.3389/fphar.2022.883445

Engineered Exosomes-Mediated Transfer of hsa-miR-320a Overcomes Chemoresistance in Cervical Cancer Cells *via* Targeting MCL1

Jinling Zhou[1], Yuanhe Wang[1], Lizhu Zhang[2], Qin Chen[3], Xiaojun Zhu[1], Peiyue Jiang[1], Nan Jiang[4], Wei Zhao[5] and Baohua Li[1]**

[1]Department of Obstetrics and Gynecology, Women's Hospital, Zhejiang University School of Medicine, Hangzhou, China, [2]Institute of Nanjing Nanxin Pharmaceutical Technology Research, Nanjing, China, [3]Department of Pathology, Women's Hospital, Zhejiang University School of Medicine, Hangzhou, China, [4]Department of Clinical Laboratory, Women's Hospital, Zhejiang University School of Medicine, Hangzhou, China, [5]Department of Biomedical Sciences and Tung Biomedical Sciences Centre, City University of Hong Kong, Hong Kong, Hong Kong SAR, China

In cervical cancer (CC), cisplatin resistance greatly restricts the application in clinical. Here, we report that engineered exosomes-mediated transfer of hsa-miR-320a overcomes chemoresistance in cervical cancer cells via targeting Myeloid Cell Leukemia Sequence 1 (MCL1). In DDP resistant CC tissues, as well as cell lines, it was found that miR-320a expression is lower, engineered miR-320a exosomes were used to attenuate DDP resistance in Hela/DDP and Caski/DDP cells. Mechanistically, we find that MCL1, which is a target of miR-320a, overcomes DDP resistance in Hela/DDP cells and in mice. In conclusion, we report that the engineered miR-320a exosomes is proved to be effective and safe.

Keywords: engineered exosomes, cervical cancer, has-miR-320a, Mcl1, chemoresistance

OPEN ACCESS

Edited by:
Dong-Hua Yang,
St. John's University, United States

Reviewed by:
Wenjun Wu,
Fox Chase Cancer Center, United States
Yibing Ji,
University at Buffalo, United States

****Correspondence:***
Wei Zhao
zw198626520@126.com
Baohua Li
lbh19787@zju.edu.cn

Specialty section:
This article was submitted to Pharmacology of Anti-Cancer Drugs, a section of the journal Frontiers in Pharmacology

Received: *25 February 2022*
Accepted: *21 March 2022*
Published: *04 April 2022*

Citation:
Zhou J, Wang Y, Zhang L, Chen Q, Zhu X, Jiang P, Jiang N, Zhao W and Li B (2022) Engineered Exosomes-Mediated Transfer of hsa-miR-320a Overcomes Chemoresistance in Cervical Cancer Cells via Targeting MCL1. Front. Pharmacol. 13:883445. doi: 10.3389/fphar.2022.883445

INTRODUCTION

In women, CC is the fourth malignant cancer (Arbyn et al., 2020). The causes that associated with the development of CC include human papillomavirus (HPV) infection, reproductive factors, long-term oral contraceptives, smoking, obesity, genetic changes, epigenetic aberrations, and so on (Arora et al., 2019).

The CC patient survival rate is low because of its metastasis and recurrence, even there are progress in surgical and r chemoradiotherapy (Pfaendler et al., 2018). Nowadays, cisplatin (DDP)-based chemoradiotherapy is the main treatment. However, cisplatin resistance is a big challenge for the clinical application (Zhu et al., 2016). Overcoming cisplatin resistance could improve the efficacy of cisplatin-based therapy.

MiR-320a is related to chemoresistance and cisplatin resistance in lung adenocarcinoma (Lu et al., 2020) and laryngeal carcinoma (Yuan et al., 2018), doxorubicin resistance in osteosarcoma (Zhou et al., 2018), imatinib resistance in gastrointestinal stromal tumors (Gao et al., 2014), 5-FU resistance in human pancreatic cancer (Wang et al., 2016), and tamoxifen resistance in other type such as breast cancer (Lu et al., 2015). Whether miR-320a is involved in cisplatin resistance in cervical cancer is unknown.

Exosomes are nano-sized vesicles with a 30–150 nm diameter, and are enclosed by a lipid bilayer, nucleic acids or miRNAs (Dong et al., 2021). Exosomes can be transferred to influence the phenotype

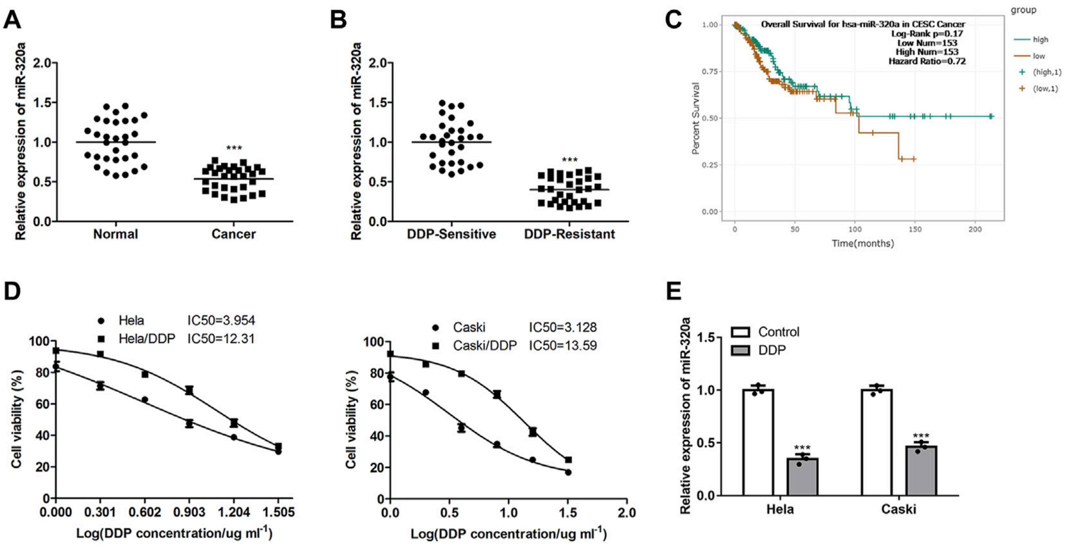

FIGURE 1 | The miR-320a expression levels are inhibited in DDP resistant CC cells. **(A)** The miR-320a expressions in para-cancer and CC tissues were determined by qRT-PCR analysis. **(B)** The miR-320a expressions in DDP sensitive clinical CC tissues and DDP resistant clinical CC tissues were determined by qRT-PCR analysis. **(C)** The overall survival of miR-320a high- and low expression patients analyzed by the Kaplan-Meier method. **(D)** IC50 values of DDP resistant CC cell line Hela/DDP and Caski/DDP were verified by MTT assay. **(E)** The miR-320a expressions of DDP sensitive or resistant CC cell lines Hela and Caski were measured by qRT-PCR. ***, $p < 0.001$ vs. Control group.

of recipient cells regulating and serving as a potential tool for therapy. Compared with liposome and nanoparticle, the exosomes are with high efficiency and biocompatibility.

It was reported that MCL1 is a key molecule in cisplatin resistance, such as. MCL1 in non-small cell lung cancer (NSCLC) (Ma et al., 2016; Lu et al., 2021) and hypopharyngeal squamous cell carcinoma (Liu X. et al., 2021). The miR-320a/MCL1 axis mediates the doxorubicin resistance of osteosarcoma (Zhou et al., 2018). Thus, we hypothesis that miR-320a/MCL1 may mediate DDP resistance in cervical cancer.

Here, we report that miR-320a expression is lower in DDP resistant CC, and engineered miR-320a exosomes can attenuate DDP resistance. The miR-320a molecule directly combines with and negatively regulates MCL1, resulting in alleviation of DDP resistance. The effectiveness and safety of engineered miR-320a exosomes in DDP resistant cervical cancer provides a new therapy strategy.

MATERIALS AND METHODS

Cells and Animals

Hela and Caski cell lines were from Shanghai Culture Collection of Chinese Academy of Sciences. Hela and Caski cells were cultured in RPMI-1640 (Gibco, United States) medium. The medium contains 10% fetal bovine serum (FBS, Gibco, United States) with 100 U/ml penicillin/streptomycin (Gibco, United States) at 37°Cand 5% CO_2 in a humidified incubator.

C57BL/6J female mice of 8–10 weeks were from Shanghai SLAC Laboratory Animal Co., Ltd. (Shanghai, China). Mice were maintained at 25 ± 1°C under light and dark cycles. Three mice were randomly selected for each experiment. All animal experiments were approved by the Animal Care Committee of Zhejiang University School of Medicine.

qRT-PCR

The total RNA was isolated from cells using Trizol (Invitrogen) and quantified with Nanodrop 2000 (Thermo Fisher Scientific). qPCR was performed on ABI 7300 Thermocycler (Thermo Fisher Scientific) with SYBR Premix Ex Taq kit (Thermo Fisher Scientific). We use GAPDH and U6 as internal control. The relative expressions were calculated by the $2^{-\Delta\Delta Ct}$ method. The sequences employed are as follows: GAPDH forward (F): 5′-AAC GGATTTGGTCGTATTGG-3′ and Reverse (R): 5′-TTGATTTTG GAGGGATCTCG-3′; MCL1 F: 5′-CCAGAGGTGAACCACAGC G-3′, and R: 5′-AGCCCCTGTCAATCCTCCT-3′; U6 F: 5′-CTC GCTTCGGCAGCACA-3′, and R: 5′-AACGCTTCACGAATTTGC GT-3′; miR-320a, 5′-AAAAGCUGGGUUGAGAGGGCGA-3′.

MTT Assay

The cells were plated in 96-well plates at a density of 5,000 cells/well, incubated overnight, and then treated. Cells were incubated with 20 μl MTT for 4 h at 37°C. The formazan crystals were dissolved in 150 μl DMSO, and the OD490 values were measured with a BioTek instrument (Winooski, Vermont, United States).

Engineered miR-320a Exosome Preparation and Identification

A miR-320a lentiviral vector was from GenePharma, Shanghai. HEK293 cells were incubated with retroviral supernatant and selected by puromycin dihydrochloride (Thermo Fisher). The

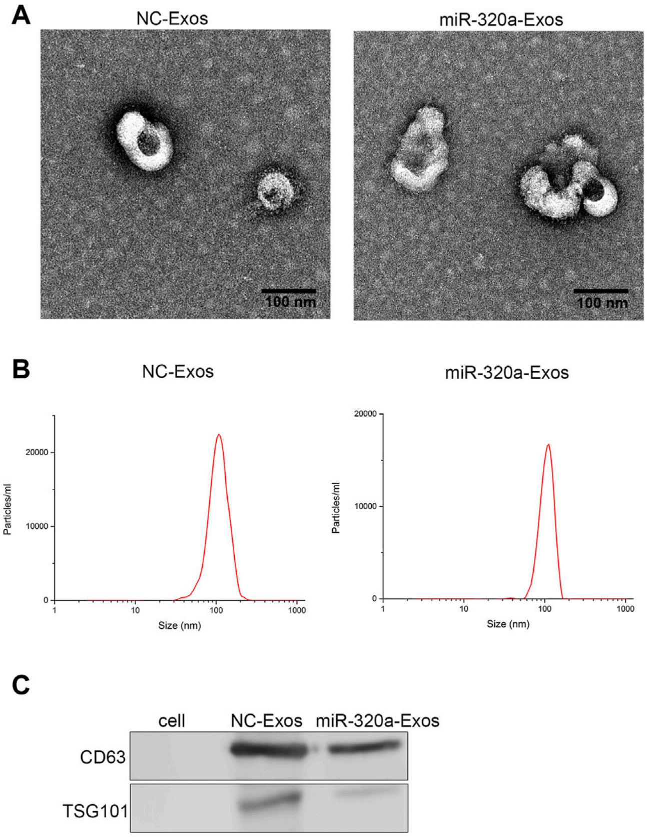

FIGURE 2 | The characterization of engineered miR-320a exosomes. The morphology and diameter distribution of non-engineered HEK293 exosomes and engineered miR-320a exosomes were detected by TEM **(A)** and DLS **(B)**. **(C)** The exosomal specific markers CD63 and TSG101 were detected by Western blotting.

conditioned medium (CM) was harvested to isolate exosomes. Briefly, the CM was centrifuged at 300×g (15 min) and 2000×g (15 min) and filtered by a 0.22-μm filter (Merck Millipore, United States). Then, the solution was ultracentrifuged at 100,000×g (90 min) in an ultracentrifuge (Beckman, United States). The pellets were resuspended in PBS and ultracentrifuged at 100,000×g (90 min). In order to quantify the exosomes, Nanoparticle Tracking Analysis was used. Transmission electron microscopy (TEM) was used for the morphology of exosomes.

Western Blotting

For protein extraction, cells were washed and suspended with RIPA buffer. The protein was obtained by centrifugation with 12,000 rpm for 30 min at 4°C. Protein was separated by 10% SDS-PAGE. The bands were transferred onto nitrocellulose membrane (PALL, United States), then blocked with 5% skim milk and incubated with primary conjugated antibodies (CD63: Proteintech, Cat No. 25682-1-AP; TSG101: Proteintech, Cat No. 67381-1-Ig; Bax: Proteintech, Cat No. 50599-2-Ig; Bcl-2: Proteintech, Cat No. 12789-1-AP; Cleaved Caspase3: CST, Cat No. 9661; Cleaved Caspase9: CST, Cat No. 7237; MCL1: Proteintech, Cat No. 16225-1-AP; β-actin: Proteintech, Cat no. 66009-1-Ig). Then the nitrocellulose membrane was incubated with the secondary conjugated antibody (HRP-conjugated Affinipure Goat Anti-Rabbit: Proteintech, Cat no. SA00001-2; HRP-conjugated Affinipure Goat Anti-Mouse IgG: Proteintech, Cat no. SA00001-1) for 4 h at room temperature and washed with TBST. The target protein bands were imaged by ECL (Advansta, United States), analyzed, and quantified by Bio-Rad ChemiDoc™ MP system (Bio-Rad, United States).

CCK-8 Assay

For the proliferation assay, a CCK-8 kit (Beyotime Biotechnology Inc., China) was used. Cells were seeded into 96-well plates at a density of 2×10^3 cells/well and incubated for 24, 48, 72 or 96 h at 37°C. Then, 20 μl of 10% CCK-8 reagent was added per well and incubated at 37°C for 2 h. The optical density was measured at 450 nm using an Enzyme Immunoassay Analyzer (Bio-Rad Laboratories, Inc.).

Apoptosis Analysis

The flow cytometry was used for the apoptosis. The cell pellets from each group were harvested, collected, and dissolved in 500 μl binding buffer, incubated with 5 μl AnnexinV-FITC and 5 μl PI in darkness for 30 min at RT and immediately subjected to flow cytometry analysis.

Luciferase Reporter Assays

The 3′UTR of MCL1 containing miR-320a binding sites were synthesized by Genepharma (Shanghai, China). These fragments were linked to the luciferase reporter gene vector (Promega, Madison, WI, United States). The luciferase activity was measured using the Dual-Luciferase Reporter Assay System (Promega, United States).

RIP Assay

The EZ-Magna RIP Kit (Sigma, St. Louis, MO, United States) was used for the RIP assay. In brief, the lysate of 1×10^7 cells in RIP lysis buffer was incubated with Anti-IgG or Anti-Ago2-coated magnetic beads for 6 h. RNAs of MCL1 and miR-320a enriched on the beads was extracted and quantified by reverse-transcription quantitative polymerase chain reaction (qRT-PCR).

TUNEL Assay

Fixed cells were used for TUNEL assay (Beyotime, Shanghai, China). Briefly, the cells were incubated with 50 μl of TUNEL reaction buffer for 50 min and diaminobenzidine (DAB) for 3 min, the results were photographed using an epifluorescence microscope at ×400 magnification (Nikon Eclipse 80i).

Immunofluorescence Staining

For immunofluorescence Staining, the mainly procedure was described in previously report (Zhang et al., 2022). Briefly, the

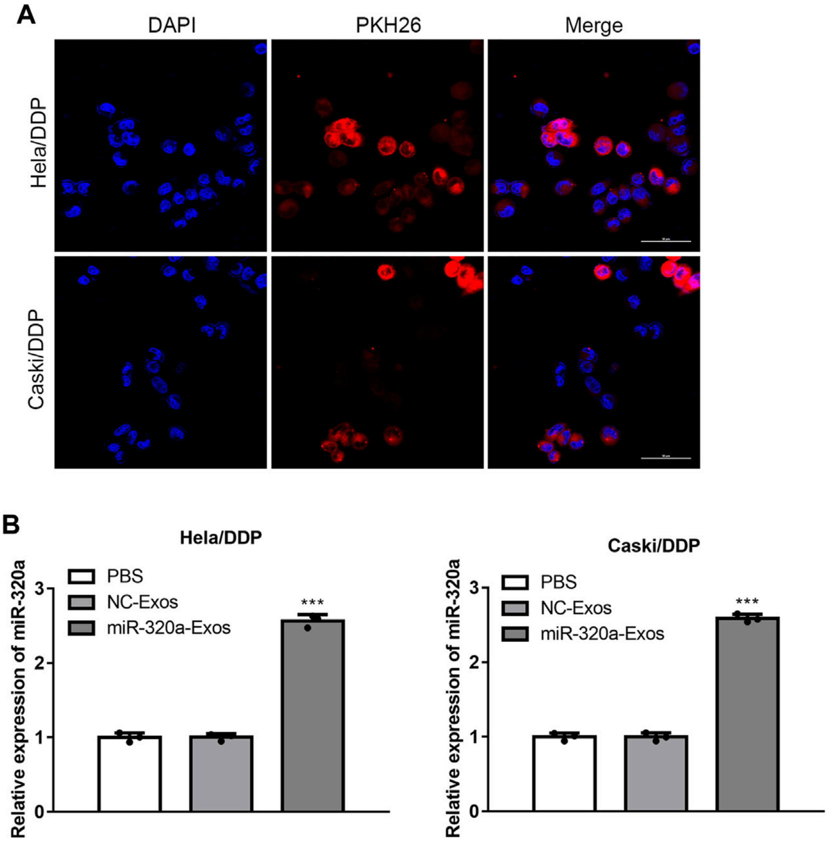

FIGURE 3 | Engineered miR-320a exosomes can be effectively up-taken by Hela/DDP and Caski/DDP cells. **(A)** The uptake of engineered miR-320a exosomes by Hela/DDP and Caski/DDP was confirmed by laser confocal microscopy. **(B)** The miR-320a expression in Hela/DDP and Caski/DDP cells after internalizing the engineered miR-320a exosomes was determined by qRT-PCR. ***, $p < 0.001$ vs. PBS group.

treated Hela/DDP and Caski/DDP cells were washed by PBS and fixed by ice chilled methanol. The exosome was labeled by PKH26 (Puzar Dominkus et al., 2018) using PKH26 Red Fluorescent Cell Linker Kits for General Cell Membrane Labeling (Sigma-Aldrich). DAPI (Sigma-Aldrich) stained cellular nucleus with following the instruction, slides were imaged by confocal laser scanning microscopy (Olympus).

Hematoxylin-Eosin (HE) Staining and Immunohistochemistry (IHC) Assays

Dissected solid tumors were fixed with 10% formalin and imaged by a microscope at 400×. For IHC assays, the paraffin slices were dewaxed by xylene, rehydrated by gradient ethanol, immerged in 3% H_2O_2 for 30 min, then the primary antibody (PCNA: Proteintech, Cat No. 24036-1-AP) was incubated at 4°C overnight. Then, the slides were incubated with peroxidase-conjugated streptavidin at 37°C for 25 min. The slides were counterstained with hematoxylin, dehydrated by gradient ethanol and clarified by xylene, imaged by a microscope (Olympus, Japan) with 200×. The brown staining indicates the positive reactions.

Statistical Analysis

Overall survival analysis was performed using the Kaplan-Meier method. All data are presented as mean ± SD. Data were analyzed by ANOVA, followed by Turkey post hoc test. A p value below 0.05 was considered that there were statistically significant differences. *, $p < 0.05$; **, $p < 0.01$; ***, $p < 0.001$.

RESULTS

MiR-320a Expression is Lower in DDP Resistant CC Cells

Firstly, we found that the miR-320a expression were decreased in CC tissues (**Figure 1A**), and further decreased in DDP resistant CC tissues (**Figure 1B**). However, there were no significant differences in overall survival of patients between miR-320a high- and low-expression (**Figure 1C**). Next, after the DDP resistances of CC cell line Hela/DDP and Caski/DDP being verified (**Figure 1D**), miR-320a expression was also inhibited in these DDP resistant CC cell lines (**Figure 1E**). These data indicate MiR-320a expression is downregulated in DDP resistant CC cells.

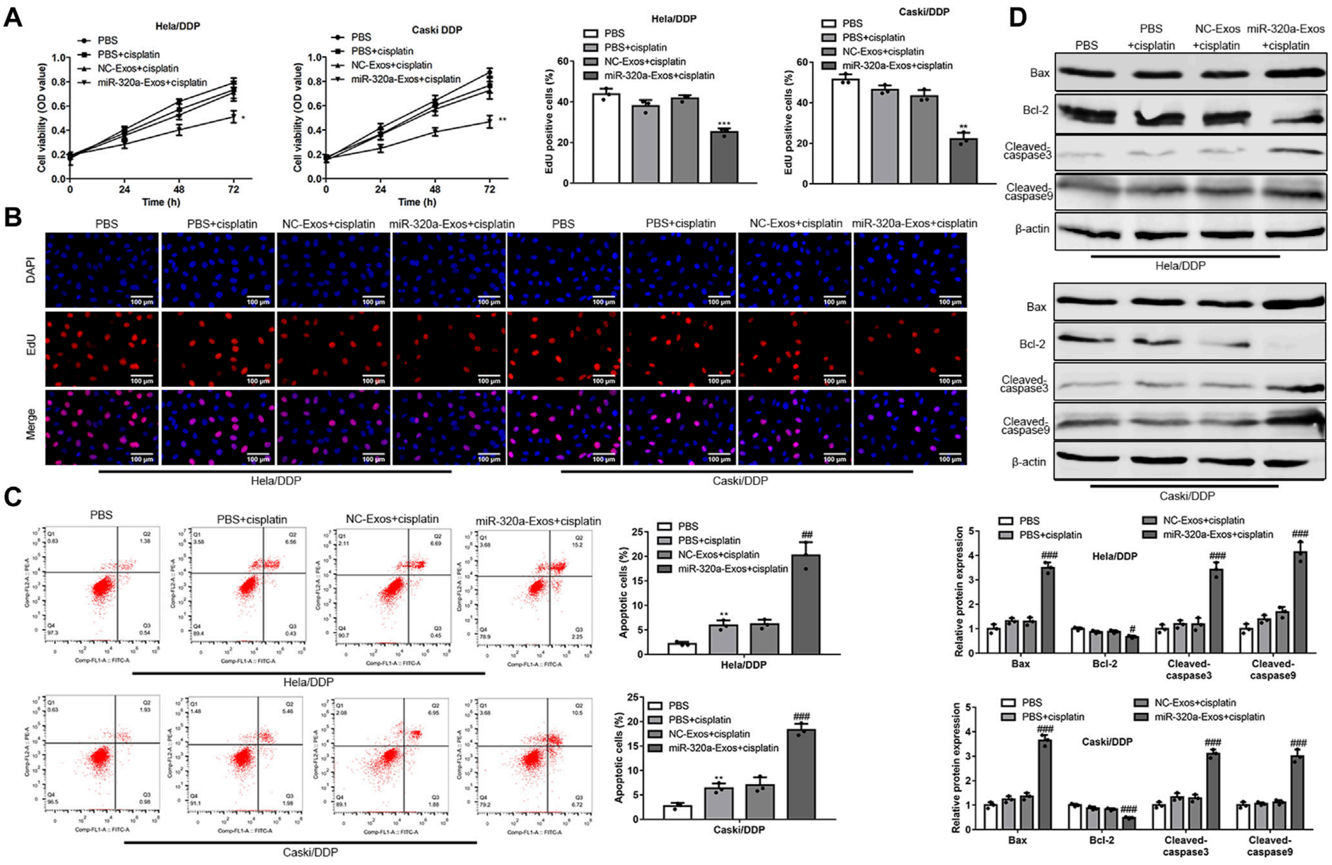

FIGURE 4 | Engineered miR-320a exosomes attenuates DDP resistance in Hela/DDP and Caski/DDP cells. **(A)** The cell viability, proliferation, apoptosis rate, and apoptosis associated proteins of DDP induced Hela/DDP and Caski/DDP cells affected by engineered miR-320a exosomes were measured by CCK-8 assay **(A)**, 5-Ethynyl-2′-deoxyuridine (EdU) assay **(B)**, annexin V-FITC/PI apoptotic kit **(C)**, and Western blot **(D)**, respectively. *, $p < 0.05$; **, $p < 0.01$; ***, $p < 0.001$ vs. PBS group; #, $p < 0.05$; ##, $p < 0.01$; ###, $p < 0.001$ vs. PBS + cisplatin group.

Engineered miR-320a Exosomes can be Effectively Up-Taken by Hela/DDP and Caski/DDP Cells

MiR-320a overexpressing cells were constructed, And the exosomes were obtained. According to transmission electron microscopy (TEM) (**Figure 2A**) and dynamic light scattering (DLS) (**Figure 2B**), it was found that the engineered miR-320a exosomes were spherical microvesicles ranged from 40 to 130 nm. Western blotting for exosomal characteristic markers (CD63 and TSG101) further confirmed the specific molecule of the exosomes (**Figure 2C**). Moreover, these data indicate that there are no differences in morphology and specific markers between the non-engineered HEK293 exosomes and engineered miR-320a exosomes. Next, we observed that the engineered miR-320a exosomes could be phagocytized into both Hela/DDP and Caski/DDP cells via laser confocal microscopy (**Figure 3A**). The qRT-PCR analysis for miR-320a showed that miR-320a in Hela/DDP and Caski/DDP cells were promoted by engineered cell exosomes (**Figure 3B**). These results show that the engineered miR-320a exosomes are effectively up-taken by Hela/DDP and Caski/DD cells.

Engineered miR-320a Exosomes Attenuate DDP Resistance in Hela/DDP and Caski/DDP Cells

To investigate whether the engineered miR-320a exosomes, which were up-taken by Hela/DDP and Caski/DDP cells, affected the cell sensitivity to DDP, the Hela/DDP and Caski/DDP cells were treated with exosomes from non-engineered HEK293 and engineered miR-320a exosomes, and stimulated with DDP (1ug/ml) at 24, 48, 72 h. The results suggested that, compared with non-engineered HEK293 exosomes, engineered miR-320a exosomes increased the inhibitory function of DDP on Hela/DDP and Caski/DDP cell viability (**Figure 4A**) and proliferation (**Figure 4B**). Additionally, engineered miR-320a exosomes enhanced the DDP induced apoptosis rates of Hela/DDP and Caski/DDP cells (**Figure 4C**). Consistent with the apoptosis rates, the levels of pro-apoptotic protein markers, Bax/Bcl-2 ratio, cleaved-caspase3, and cleaved-caspase9, were increased in the DDP stimulated Hela/DDP and Caski/DDP cells by engineered miR-320a exosomes (**Figure 4D**). These data

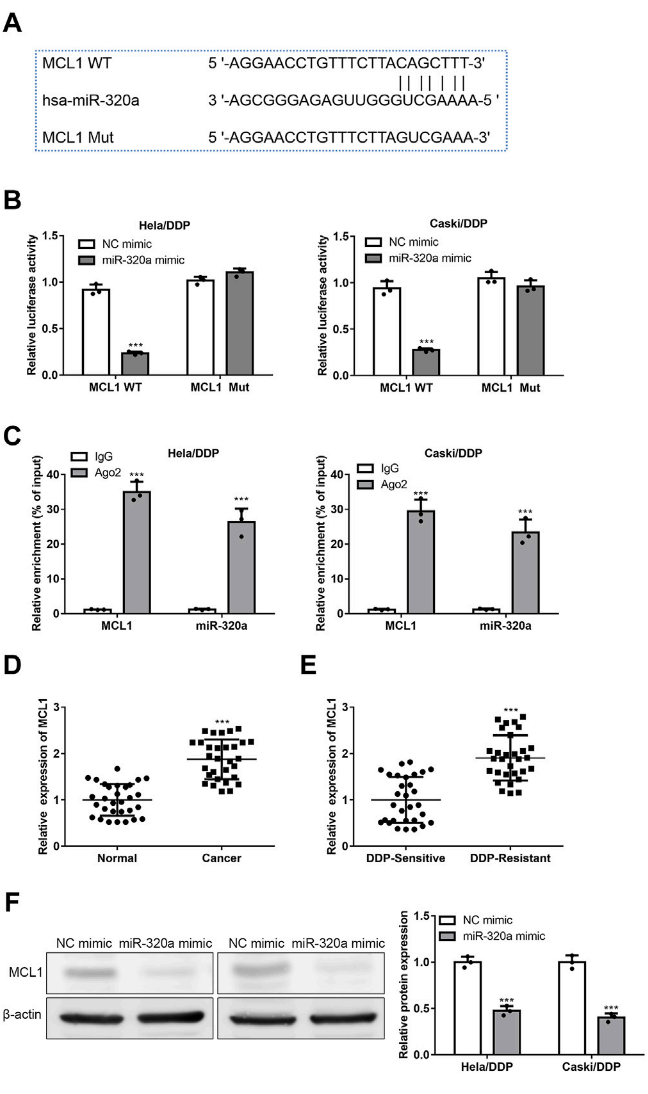

FIGURE 5 | MCL1 is a target of miR-320a. **(A)** The complementary sequences of 3′-UTR of MCL1 mRNA and miR-320a were analyzed by StarBase website. **(B)** The level of MCL1 expression regulated by miR-320a is verified by the luciferase reporter assay. **(C)** The combination of MCL1 mRNA and miR-320a is confirmed by RIP assay. **(D)** The mRNA levels of MCL1 in CC tissues were detected by qRT-PCR. **(E)** The mRNA levels of MCL1 in DDP resistant CC tissues were detected by qRT-PCR. **(F)** The MCL1 proteins regulated by miR-320a were confirmed by Western blot. ***, $p <$ 0.001 vs. Control group.

indicate that engineered miR-320a exosomes overcome DDP resistant CC cell line Hela/DDP and Caski/DDP cells.

MCL1 is a Target of miR-320a

Among the potential targets of miR-320a, MCL1 has been reported as a target of miR-320a (PMID: 30119255). MCL1, as an anti-apoptotic protein, is a therapeutic target of CC (PMID: 32715755). Thus, our study focused on whether MCL1 is regulated by miR-320a in Hela/DDP and Caski/DDP cells. The bioinformatics results showed that the 3′-UTR of MCL1 mRNA displayed complementary sequences for miR-320a (**Figure 5A**). Then, dual-luciferase reporter assay was carried out, the results indicated the decreased of MCL1-WT luciferase activity in Hela/DDP and Caski/DDP cells in the addition of miR-320a, relative to MCL1-MUT (**Figure 5B**). And the results of RIP assay suggested that MCL1 mRNA was directly combined with miR-320a (**Figure 5C**). Next, we validated that the levels of MCL1 mRNA were increased in CC (**Figure 5D**) and DDP resistant CC (**Figure 5E**) in clinical samples. And MCL1 protein expression was proved to be downregulated by miR-320a in Hela/DDP and Caski/DDP cells (**Figure 5F**). These data indicate that MCL1 directly combines and negatively regulated by miR-320a.

MiR-320a Overcomes DDP Resistance in Hela/DDP Cells by Regulating MCL1

To further evaluate whether miR-320a regulate DDP resistance in Hela/DDP cells *via* MCL1, MCL1 was overexpressed in Hela/DDP cells. The data showed that, MCL1 overexpression abolished the suppression of cell viability (**Figure 6A**) and proliferation (**Figure 6B**) by engineered miR-320a exosomes in Hela/DDP cells. Additionally, MCL1 overexpression canceled the enhanced apoptotic rates (**Figure 6C**) and upregulated pro-apoptotic protein markers (Bax/Bcl-2 ratio, cleaved-caspase3, and cleaved-caspase9) (**Figure 6D**) induced by engineered miR-320a exosomes in Hela/DDP cells. It is evidenced by our data that miR-320a overcomes DDP resistance in Hela/DDP cells by regulating MCL1.

Engineered miR-320a Exosomes Ameliorate DDP Resistance *In Vivo*

To evaluate the function of engineered miR-320a exosomes on DDP resistance *in vivo*, engineered miR-320a exosomes were isolated and injected into the tail vein of the mice with subcutaneous Hela/DDP cells tumor. Th volumes and weights of tumor were inhibited by engineered miR-320a exosomes injection (**Figures 7A,B**). The Tunel assay showed that engineered miR-320a exosomes enhanced the apoptosis of tumor cells in the mice with subcutaneous tumor formation of Hela/DDP cells (**Figure 7C**), which is consistent with the inhibited proliferation *in vitro* (**Figure 7C**). Then, the expression of MCL1 mRNA was suppressed by the injection of engineered miR-320a exosomes (**Figure 7D**). These data are in consistent with *in vitro*, suggesting that engineered miR-320a exosomes overcome DDP resistance in CC.

The Safety of Engineered miR-320a Exosomes Injection *In Vivo*

We evaluated the safety of engineered miR-320a exosomes which were injected into the tail vein. No significant difference was found in the body weights between the non-

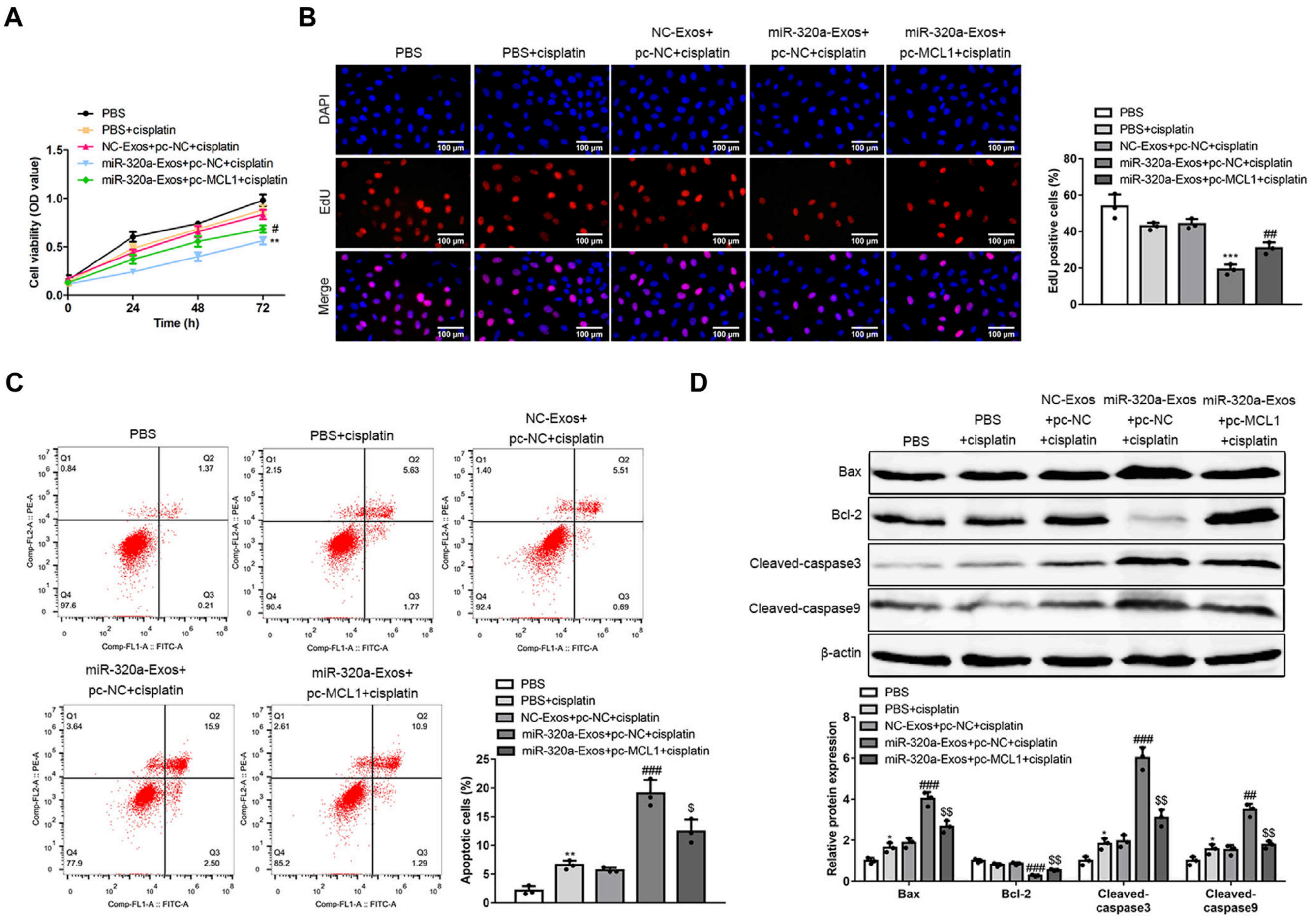

FIGURE 6 | MiR-320a overcomes DDP resistance in Hela/DDP cells by regulating MCL1. **(A)** The cell viability, proliferation, apoptosis rate, and apoptosis associated proteins of DDP induced Hela/DDP and Caski/DDP cells affected by engineered miR-320a exosomes and MCL1 overexpression were measured by CCK-8 assay **(A)**, 5-Ethynyl-2′-deoxyuridine (EdU) assay **(B)**, annexin V-FITC/PI apoptotic assay **(C)**, and Western blot **(D)**, respectively. *, $p < 0.05$; **, $p < 0.01$; ***, $p < 0.001$ vs. PBS group; #, $p < 0.05$; ##, $p < 0.01$; ###, $p < 0.001$ vs. NC-Exo + pc-NC + cisplatin group; $, $p < 0.05$; $$, $p < 0.01$ vs. miR-320a-Exo + pc-NC + cisplatin group.

engineered HEK293 exosomes injected mice and the engineered miR-320a exosomes injected mice (**Figure 8A**). Furthermore, ALT, AST, ALP, WBC, RBC, and PLT in the serum were not different in the engineered miR-320a exosomes injected mice compared with the non-engineered HEK293 exosomes injected mice (**Figure 8B**). And the histopathological staining of heart, liver, spleen, lung, and kidney did not show observable change in the engineered miR-320a exosomes injected mice compared with the non-engineered HEK293 exosomes injected mice (**Figure 8C**). These data indicate that tail vein injection of engineered miR-320a exosomes is safe.

DISCUSSION

Although major progress has been made in improving the effectiveness of DDP for CC chemotherapy, DDP resistance remains a serious problem, which is urgent to be solved. Here, we confirm the effectiveness and safety of engineered miR-320a exosomes in DDP resistant cervical cancer. And the bioinformatics analysis and the dual-luciferase reporter assay confirms that miR-320a directly binds to the 3′-UTR of MCL1 mRNA and negatively regulates its function, improving the DDP chemoresistance.

MiR-320a has been considered as an inhibitor of carcinoma. A recent study showed that low level of miR-320a promoted glioma proliferation through FOXM1 expression (Qi et al., 2021). Additionally, it was reported that miR-320a, the expression of which is modulated by demethylation, ameliorated DDP resistance in lung adenocarcinoma (Lu et al., 2020). Moreover, as a downstream target of long non-coding RNA AFAP1-AS1, the low expression of miR-320a promoted the stemness and DDP chemoresistance of laryngeal carcinoma cells by negative regulation of RBPJ mRNA and protein (Yuan et al., 2018). Consistent with these results, here, we verified the effectiveness of miR-320a in DDP resistant cervical cancer.

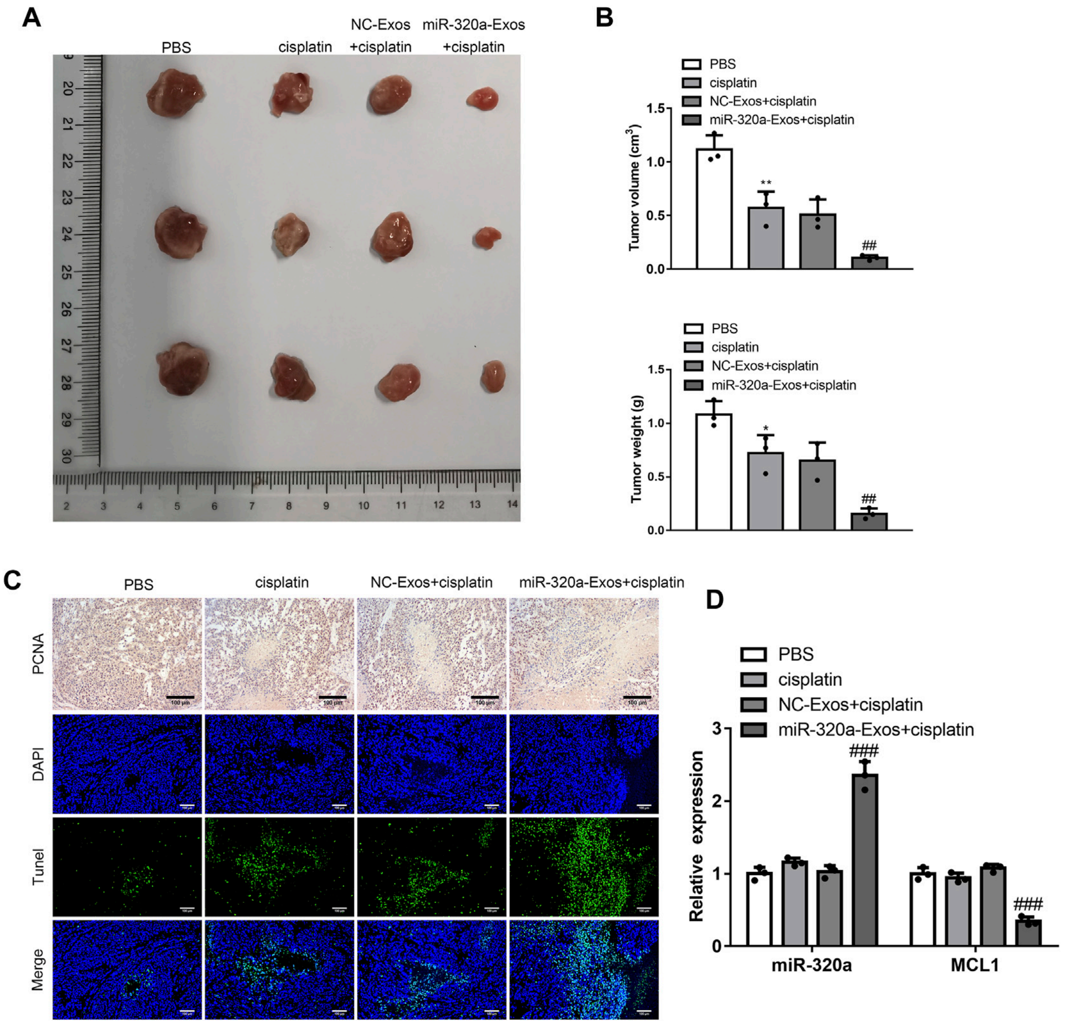

FIGURE 7 | Engineered miR-320a exosomes ameliorate DDP resistance *in vivo*. **(A)** The tumor images, and. **(B)** The tumor volumes and weights of the mice with subcutaneous tumor formation of Hela/DDP cells affected by tail vein injection of engineered miR-320a exosomes. **(C)** The apoptosis and proliferation of tumor tissues detected by Tunel assay and immunohistochemistry. **(D)** MCL1 mRNA expression regulated by engineered miR-320a exosomes injection is evaluated by qRT-PCR. *, $p < 0.05$; **, $p < 0.01$ vs. PBS group; ##, $p < 0.01$; ###, $p < 0.001$ vs. NC-Exos + cisplatin group.

Exosomes are nano-sized vesicles with the diameter of 30–150 nm, they contain various biomolecules, and can be secreted by almost all mammalian cell types. Based on the structure, engineered exosomes have become a possibility in the treatment of numerous diseases. A recent study indicated that miR-317b-5b-loaded engineered exosomes can transfer itself both *in vitro* and *in vivo* for the anti-tumor functions (Xue et al., 2021). In addition, engineered miR-181b exosomes regulate macrophage polarization, thus to improve osteointegration (Liu W. et al., 2021). In this study, engineered miR-320a exosomes were used to alleviate DDP resistance in CC.

MCL1, a pro-survival and pro-proliferative factor, plays a critical role in many tumor types. The deubiquitination and stabilisation of MCL1 was considered to be required for the proliferation of CC cells (Morgan et al., 2021). What's more, MCL1 siRNA-silencing demonstrated high efficacy on CC cell lines (Lechanteur et al., 2017). All these data support that MCL1 is a therapeutic target for CC. In contrast, we confirmed that MCL1 functioned as the target of miR-320a for ameliorating DDP resistance in CC, which was consistent with the previous study that miR-320a/MCL1 axis mediated the doxorubicin resistance of osteosarcoma (Zhou et al., 2018).

Besides the effect we mentioned above, miR-320a has a great number of functions in numerous aspects. For example, by inhibiting MafF, the pancreatic beta cells loss its function in diabetes (Du et al., 2021); it also regulates endoplasmic reticulum stress as well as autophagy in diffuse large B-cell lymphoma (Cui et al., 2021); and human glucagon expression (Jo et al., 2021). Although the safety of engineered miR-320a exosomes was assessed by measuring body weights, ALT, AST, ALP, WBC, RBC, and PLT in the serum, and the histopathological staining, more

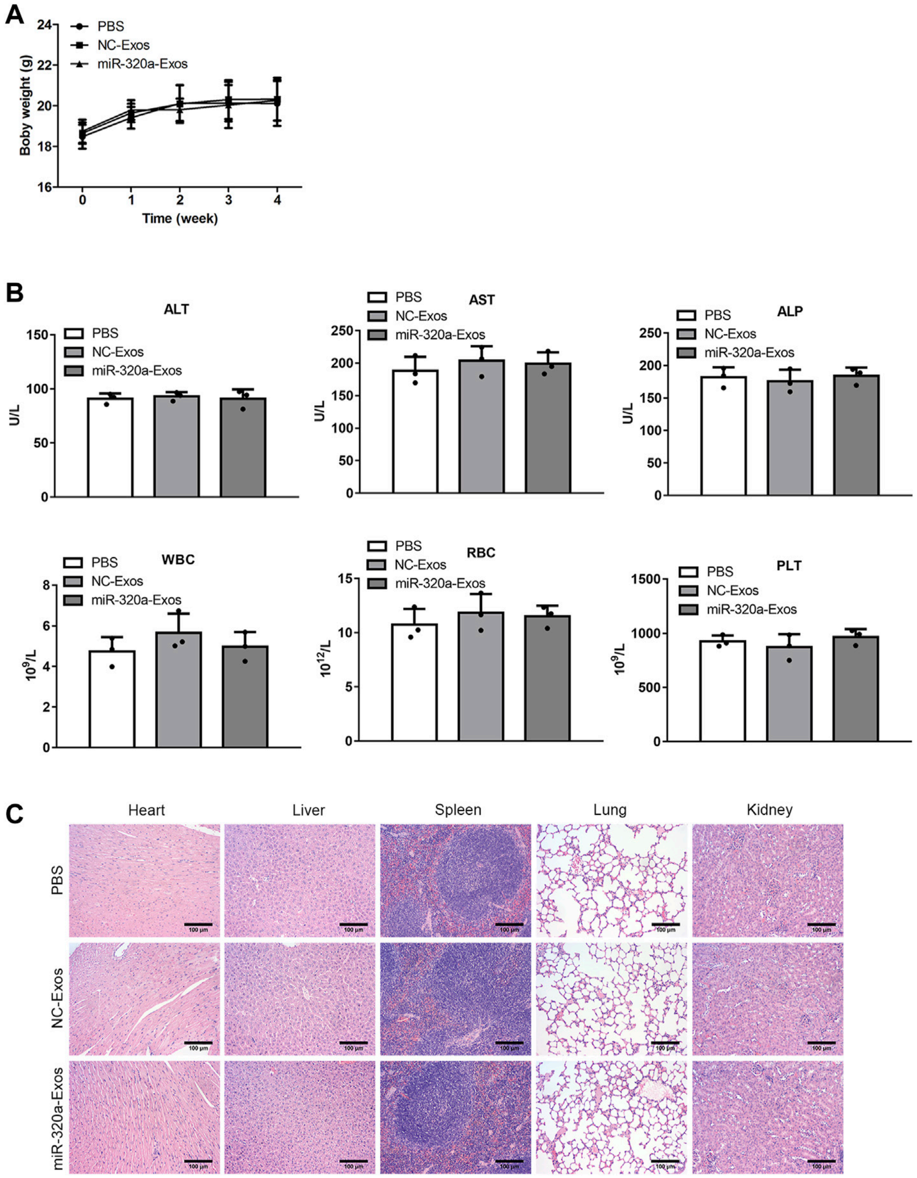

FIGURE 8 | The safety of engineered miR-320a exosomes injection *in vivo*. **(A)** The body weights between the non-engineered HEK293 exosomes injected mice and the engineered miR-320a exosomes injected mice. **(B)** The differences of ALT, AST, ALP, WBC, RBC, and PLT in the serum of the engineered miR-320a exosomes injected mice compared with the non-engineered HEK293 exosomes injected mice. **(C)** The histopathological staining of heart, liver, spleen, lung, and kidney of the engineered miR-320a exosomes injected mice compared with the non-engineered HEK293 exosomes injected mice.

comprehensive evaluation is required to investigate the impact of miR-320a.

In conclusion, we confirmed that miR-320a is downregulated in DDP resistant CC and engineered miR-320a exosomes can attenuate DDP resistance by inhibiting MCL1.

DATA AVAILABILITY STATEMENT

The original contributions presented in the study are included in the article/Supplementary Material, further inquiries can be directed to the corresponding authors.

ETHICS STATEMENT

The animal study was reviewed and approved by the Animal Care Committee of Zhejiang University School of Medicine.

AUTHOR CONTRIBUTIONS

WZ and BL conceived and designed the work. JZ, YW, LZ, QC, XZ, PJ and NJ performed experiments. JZ, YW and LZ collected and analyzed the data. WZ and BL checked the raw data and results. PJ obtained funding. WZ and BL drafted the manuscript. All authors revised and approved the final manuscript.

FUNDING

This work was supported by National Natural Science Foundation of China (81902625) and Zhejiang Provincial Natural Science Foundation of China under Grant (LQ19H160028).

REFERENCES

Arbyn, M., Weiderpass, E., Bruni, L., de Sanjosé, S., Saraiya, M., Ferlay, J., et al. (2020). Estimates of Incidence and Mortality of Cervical Cancer in 2018: a Worldwide Analysis. *Lancet Glob. Health* 8 (2), e191–e203. doi:10.1016/S2214-109X(19)30482-6

Arora, I., Sharma, M., and Tollefsbol, T. O. (2019). Combinatorial Epigenetics Impact of Polyphenols and Phytochemicals in Cancer Prevention and Therapy. *Int. J. Mol. Sci.* 20 (18). doi:10.3390/ijms20184567

Cui, Y., Xu, H., Yang, Y., Zhao, D., Wen, Y., Lv, C., et al. (2021). The Regulation of miR-320a/XBP1 axis through LINC00963 for Endoplasmic Reticulum Stress and Autophagy in Diffuse Large B-Cell Lymphoma. *Cancer Cel Int* 21 (1), 305. doi:10.1186/s12935-021-01992-y

Dong, Z., Gu, H., Guo, Q., Liang, S., Xue, J., Yao, F., et al. (2021). Profiling of Serum Exosome MiRNA Reveals the Potential of a MiRNA Panel as Diagnostic Biomarker for Alzheimer's Disease. *Mol. Neurobiol.* 58 (7), 3084–3094. doi:10.1007/s12035-021-02323-y

Du, H., Yin, Z., Zhao, Y., Li, H., Dai, B., Fan, J., et al. (2021). miR-320a Induces Pancreatic β Cells Dysfunction in Diabetes by Inhibiting MafF. *Mol. Ther. Nucleic Acids* 26, 444–457. doi:10.1016/j.omtn.2021.08.027

Gao, X., Shen, K., Wang, C., Ling, J., Wang, H., Fang, Y., et al. (2014). MiR-320a Downregulation Is Associated with Imatinib Resistance in Gastrointestinal Stromal Tumors. *Acta Biochim. Biophys. Sin (Shanghai)* 46 (1), 72–75. doi:10.1093/abbs/gmt118

Jo, S., Xu, G., Jing, G., Chen, J., and Shalev, A. (2021). Human Glucagon Expression Is under the Control of miR-320a. *Endocrinology* 162 (3). doi:10.1210/endocr/bqaa238

Lechanteur, A., Furst, T., Evrard, B., Delvenne, P., Piel, G., and Hubert, P. (2017). Promoting Vaginal Distribution of E7 and MCL-1 siRNA-Silencing Nanoparticles for Cervical Cancer Treatment. *Mol. Pharm.* 14 (5), 1706–1717. doi:10.1021/acs.molpharmaceut.6b01154

Liu, W., Yu, M., Chen, F., Wang, L., Ye, C., Chen, Q., et al. (2021a). A Novel Delivery Nanobiotechnology: Engineered miR-181b Exosomes Improved Osteointegration by Regulating Macrophage Polarization. *J. Nanobiotechnol* 19 (1), 269. doi:10.1186/s12951-021-01015-y

Liu, X., Zhang, Z., Kan, S., Lv, Z., Zhou, S., Liu, X., et al. (2021b). PHF20 Inhibition Promotes Apoptosis and Cisplatin Chemosensitivity via the OCT4-p-STAT3-MCL1 S-ignaling P-athway in H-ypopharyngeal S-quamous C-ell C-arcinoma. *Int. J. Oncol.* 59 (1). doi:10.3892/ijo.2021.5218

Lü, M., Ding, K., Zhang, G., Yin, M., Yao, G., Tian, H., et al. (2015). MicroRNA-320a Sensitizes Tamoxifen-Resistant Breast Cancer Cells to Tamoxifen by Targeting ARPP-19 and ERRγ. *Sci. Rep.* 5, 8735. doi:10.1038/srep08735

Lu, M., Hu, C., Wu, F., Shu, L., Pan, Y., Liu, X., et al. (2020). MiR-320a Is Associated with Cisplatin Resistance in Lung Adenocarcinoma and its Clinical Value in Non-small Cell Lung Cancer: A Comprehensive Analysis Based on Microarray Data. *Lung Cancer* 147, 193–197. doi:10.1016/j.lungcan.2020.06.020

Lu, T., Lu, W., Jia, C., Lou, S., and Zhang, Y. (2021). Knockdown of miR-15b Partially Reverses the Cisplatin Resistance of NSCLC through the GSK-3β/MCL-1 Pathway. *Adv. Clin. Exp. Med.* 30 (8), 849–857. doi:10.17219/acem/135701

Ma, J., Zhao, Z., Wu, K., Xu, Z., and Liu, K. (2016). MCL-1 Is the Key Target of Adjuvant Chemotherapy to Reverse the Cisplatin-Resistance in NSCLC. *Gene* 587 (2), 147–154. doi:10.1016/j.gene.2016.04.054

Morgan, E. L., Patterson, M. R., Barba-Moreno, D., Scarth, J. A., Wilson, A., and Macdonald, A. (2021). The Deubiquitinase (DUB) USP13 Promotes Mcl-1 Stabilisation in Cervical Cancer. *Oncogene* 40 (11), 2112–2129. doi:10.1038/s41388-021-01679-8

Pfaendler, K. S., Liu, M. C., and Tewari, K. S. (2018). Bevacizumab in Cervical Cancer: 5 Years after. *Cancer J.* 24 (4), 187–192. doi:10.1097/PPO.0000000000000324

Pužar Dominkuš, P., Stenovec, M., Sitar, S., Lasič, E., Zorec, R., Plemenitaš, A., et al. (2018). PKH26 Labeling of Extracellular Vesicles: Characterization and Cellular Internalization of Contaminating PKH26 Nanoparticles. *Biochim. Biophys. Acta (Bba) - Biomembranes* 1860 (6), 1350–1361. doi:10.1016/j.bbamem.2018.03.013

Qi, L., Wang, W., Zhao, G., Jiang, H., Zhang, Y., Zhao, D., et al. (2021). Circular RNA circCCDC66 Promotes Glioma Proliferation by Acting as a ceRNA for miR-320a to Regulate FOXM1 Expression. *Aging (Albany NY)* 13 (13), 17673–17689. doi:10.18632/aging.203258

Wang, W., Zhao, L., Wei, X., Wang, L., Liu, S., Yang, Y., et al. (2016). MicroRNA-320a Promotes 5-FU Resistance in Human Pancreatic Cancer Cells. *Sci. Rep.* 6, 27641. doi:10.1038/srep27641

Xue, Q., Yang, Y., Yang, L., Yan, X., Shen, Z., Liu, J., et al. (2021). miR-371b-5p-Engineered Exosomes Enhances Tumor Inhibitory Effect. *Front Cel Dev Biol* 9, 750171. doi:10.3389/fcell.2021.750171

Yuan, Z., Xiu, C., Song, K., Pei, R., Miao, S., Mao, X., et al. (2018). Long Non-coding RNA AFAP1-AS1/miR-320a/RBPJ axis Regulates Laryngeal Carcinoma Cell Stemness and Chemoresistance. *J. Cel Mol Med* 22 (9), 4253–4262. doi:10.1111/jcmm.13707

Zhang, L., Zhao, W., Huang, J., Li, F., Sheng, J., Song, H., et al. (2022). Development of a Dendritic Cell/Tumor Cell Fusion Cell Membrane Nano-Vaccine for the Treatment of Ovarian Cancer. *Front. Immunol.* 13, 828263. doi:10.3389/fimmu.2022.828263

Zhou, B., Li, L., Li, Y., Sun, H., and Zeng, C. (2018). Long Noncoding RNA SNHG12 Mediates Doxorubicin Resistance of Osteosarcoma via miR-320a/MCL1 axis. *Biomed. Pharmacother.* 106, 850–857. doi:10.1016/j.biopha.2018.07.003

Zhu, H., Luo, H., Zhang, W., Shen, Z., Hu, X., and Zhu, X. (2016). Molecular Mechanisms of Cisplatin Resistance in Cervical Cancer. *Drug Des. Devel Ther.* 10, 1885–1895. doi:10.2147/DDDT.S106412

Conflict of Interest: The authors declare that the research was conducted in the absence of any commercial or financial relationships that could be construed as a potential conflict of interest.

Publisher's Note: All claims expressed in this article are solely those of the authors and do not necessarily represent those of their affiliated organizations or those of the publisher, the editors, and the reviewers. Any product that may be evaluated in this article, or claim that may be made by its manufacturer, is not guaranteed or endorsed by the publisher.

Copyright © 2022 Zhou, Wang, Zhang, Chen, Zhu, Jiang, Jiang, Zhao and Li. This is an open-access article distributed under the terms of the Creative Commons Attribution License (CC BY). The use, distribution or reproduction in other forums is permitted, provided the original author(s) and the copyright owner(s) are credited and that the original publication in this journal is cited, in accordance with accepted academic practice. No use, distribution or reproduction is permitted which does not comply with these terms.

frontiers | Frontiers in Pharmacology

REVIEW
published: 11 April 2022
doi: 10.3389/fphar.2022.875384

Roles and new Insights of Macrophages in the Tumor Microenvironment of Thyroid Cancer

*Qi Liu, Wei Sun and Hao Zhang**

Department of Thyroid Surgery, The First Hospital of China Medical University, Shenyang, China

Although most thyroid cancers have a good and predictable prognosis, the anaplastic, medullary, and refractory thyroid cancers still prone to recurrence and metastasis, resulting in poor prognosis. Although a number of newly developed targeted therapies have begun to be indicated for the above types of thyroid cancer in recent years, their ability to improve overall survival remain hindered by low efficacy. As the largest component of immune cells in tumor microenvironment, tumor-associated macrophages play a key role in the invasion and metastasis of thyroid cancer. There is much evidence that the immune system, tumor microenvironment and cancer stem cell interactions may revolutionize traditional therapeutic directions. Tumor-associated macrophages have been extensively studied in a variety of tumors, however, research on the relationship between thyroid cancer and macrophages is still insufficient. In this review, we summarize the functions of tumor-associated macrophages in different types of thyroid cancer, their cytokines or chemokines effect on thyroid cancer and the mechanisms that promote tumor proliferation and migration. In addition, we discuss the mechanisms by which tumor-associated macrophages maintain the stemness of thyroid cancer and potential strategies for targeting tumor-associated macrophages to treat thyroid cancer.

Keywords: thyroid cancer, cancer stem cell, tumor microenvironment, tumor associated macrophages, cytokines

OPEN ACCESS

Edited by:
Dong-Hua Yang,
St. John's University, United States

Reviewed by:
Zhenhai Li,
Shenzhen University, China
Nella Prevete,
University of Naples Federico II, Italy
Zhengyu Jiang,
Janssen Research and Development,
United States

****Correspondence:***
Hao Zhang
haozhang@cmu.edu.cn

Specialty section:
This article was submitted to
Pharmacology of Anti-Cancer Drugs,
a section of the journal
Frontiers in Pharmacology

Received: *14 February 2022*
Accepted: *21 March 2022*
Published: *11 April 2022*

Citation:
Liu Q, Sun W and Zhang H (2022)
Roles and new Insights of
Macrophages in the Tumor
Microenvironment of Thyroid Cancer.
Front. Pharmacol. 13:875384.
doi: 10.3389/fphar.2022.875384

INTRODUCTION

In recent years, thyroid cancer (TC) has attracted more and more attention due to its rapid increase in incidence. TC ranks the fifth in the incidence of all malignant tumors and has become the most common endocrine tumor (Cabanillas et al., 2016). It is important to note that the incidence of TC is also increased in children and adolescents (Person et al., 2021). The incidence of TC continues to increase not only because of environmental pollution, radiation exposure and other external factors, but also because of the improvement of imaging or ultrasound diagnostic technology and biopsy diagnosis (La Vecchia et al., 2015). Papillary thyroid carcinoma (PTC) and follicular thyroid carcinoma (FTC) account for 80%–85% and 10%–15% of TCs respectively (LiVolsi, 2011; Sowder et al., 2018). Patients with these differentiated TCs can benefit from surgery, radioiodine therapy, and thyroid stimulating hormone (TSH) inhibition therapy, and thus have a better prognosis. In contrast, medullary thyroid carcinoma (MTC) is one of the relatively rare thyroid malignant tumors, accounting for 1%–2% of all TCs, but it has a worse prognosis with a 10-year overall survival (OS) of only 81.2% (Cabanillas et al., 2016; Kotwal et al., 2021). Notably, there are approximately 2% of anaplastic thyroid cancer (ATC) (Smallridge et al., 2012), though rare, is often associated with resistance to radioiodine treatment and is characterized by an aggressive phenotype and poor prognosis, with an average survival time of few months (Cabanillas et al., 2016; Veschi et al., 2020). Currently, the clinical treatment for ATC is a great challenge.

Macrophages are highly plastic cells with multiple functions and these cells originate in the bone marrow from myeloid derived progenitor cells (Varol et al., 2015). Tumor-associated macrophages (TAMs) are derived from tumor-infiltrating monocytes in peripheral blood. Current studies indicate that TAM population is in a constant transition between M1 and M2 type (Pan et al., 2020). M1-macrophages have antitumor effects, through the identification of tumor cells and finally kill tumor cells, the study revealed M1-macrophages by two different mechanism of killing tumor cells, one is mediated cytotoxicity to kill tumor cells directly, and the other is antibody dependent cell-mediated cytotoxicity to kill tumor cells. M2-macrophages are divided into multiple subtypes, M2a is involved in tissue fiber formation, M2b contributes to tumor progression, M2c is responsible for tissue remodeling, and M2d promotes angiogenesis (Wang et al., 2019a). TAMs can promote tumor progression by secreting cytokines, such as vascular endothelial growth factor (VEGF) or fibroblast growth factor (FGF) (Mantovani et al., 2002). Therefore TAMs promote angiogenesis and are often associated with high density of blood vessels (Coffelt et al., 2010). In TCs, TAMs mainly exhibit the M2 phenotype (Solinas et al., 2010). Therefore, how to control the phenotypic transformation of TAMs may be the focus of future research. These cytokines or chemokines originate from cancer cells and macrophages, but the mechanisms by which these cytokines or chemokines act on tumors have not been fully elucidated. TAMs maintains the survival, proliferation and invasion of cancer cells and may be a potential therapeutic target (Bolli et al., 2017; Mantovani et al., 2017; Cassetta and Pollard, 2018).

Tumor microenvironment (TME) is mainly composed of tumor cells, innate and adaptive immune cells, fibroblasts, vascular, cytokines and chemokines, et al. TME can not only provide a suitable environment for tumor to promote tumor growth and metastasis, but also inhibit the occurrence and development of tumor through changes in metabolism, secretion, immunity and other conditions (Ben-Baruch, 2006; de Visser et al., 2006). TME is a complex and interactive network regulated by immune cells, cytokines and other elements. Tumor cells are regulated by their own genes and external factors, which jointly promote tumor development and phenotypic changes, such as EMT of tumor cells (Pradella et al., 2017; Weng et al., 2019). TC cells can maintain growth by secreting a variety of cytokines and also by secreting chemokines to recruit different immune cells (Lumachi et al., 2010; Fozzatti and Cheng, 2020). These cytokines or chemokines affect the progression of TC and changes in the immune microenvironment (Menicali et al., 2020). Innate immune cells, especially natural-killer cells (NK cells) and macrophages play a key role in the regulation of tumor progression and inhibition (Goldberg and Sondel, 2015). Similarly, these immune cells can also secrete some cytokines and angiogenic factors to remodeling the TME of TC (Poschke et al., 2011). In addition, tumor progression can also destroy the balance of the original microenvironment, making it conducive to tumor proliferation and migration. Immune surveillance is the function of the immune system to identify, kill and remove mutated cells from the body to prevent tumor development. Tumor immune escape is a phenomenon in which tumor cells evade recognition and attack by the immune system through various mechanisms, thus allowing them to survive and proliferate *in vivo* (Prendergast et al., 2010). Although immune cells tend to kill tumor cells in the early stage of tumor genesis, they seem to evade immune surveillance eventually, and even inhibit the cytotoxic effect of immune cells on tumor through various mechanisms (Lei et al., 2020).

At present, it is believed that TC is closely associated with the occurrence and development of inflammation, and about 20% of PTC is caused by chronic thyroiditis (Fugazzola et al., 2011). Chronic inflammatory is an important factor mediating tumorigenesis (Noy and Pollard, 2014). The original concept of "inflammation causes tumors" is gradually changed to "inflammation causes tumors, and tumors cause inflammation (Allavena et al., 2011)." In this review, we discuss the types of TAMs and their effects on TCs, the interaction between cytokines and chemokines in TME, cancer stem cell (CSC), and new strategies for immunotherapy of TCs.

TUMOR-ASSOCIATED MACROPHAGES IN THE THYROID TUMOR MICROENVIRONMENT

Similar to other malignant tumors, the thyroid-TME is composed of immune cells (macrophages, mast cells, neutrophils, and lymphocytes) and soluble mediators (chemokines, cytokines, and growth factors) that are active in and around cancer cells (Yapa et al., 2017). Currently, TAMs infiltration in TME is believed to be through recruitment of circulating monocytes. Cytokines and chemokines in TME promote polarization of macrophages and affect the functions of TAMs, such as promoting tumor proliferation, stemness, gene instability, blood vessel and lymphatic proliferation, immunosuppression, et al. (Mantovani and Allavena, 2015). A schematic diagram of the interaction between TC and TAM is shown in **Figure 1**.

TC is commonly associated with a complex genetic background and gene mutations, that could be involved in mutations in BRAF, RAS and PI3K signaling pathways. Losing or inhibiting the functions of PTEN, p53 and Β-catenin is commonly seen in poorly differentiated TCs (Hou et al., 2007). $\mathrm{BRAF}^{\mathrm{V600E}}$ mutation is most frequent in PTCs or ATCs (Cancer Genome Atlas Research, 2014). While RAS mutation mostly exist in FTCs and other variant of PTCs (Cabanillas et al., 2016). RET proto-oncogene mutation is thought to be the cause of most MTC, while a low proportion of TCs is caused by sporadic RAS mutation (Ciampi et al., 2013; Wells et al., 2015). In an *in vivo* study of nude mice, high CXCL16 expression is associated with M2-macrophage infiltration in $\mathrm{BRAF}^{\mathrm{V600E}}$ mutated PTC, promoting tumor angiogenesis and resulting in poor prognosis (Kim et al., 2019). In another study, In $\mathrm{BRAF}^{\mathrm{V600E}}$ and $\mathrm{BRAF}^{\mathrm{WT}}$, the average ratio of immune cell populations CD68 +/CD163 + cells tends to decrease, resulting

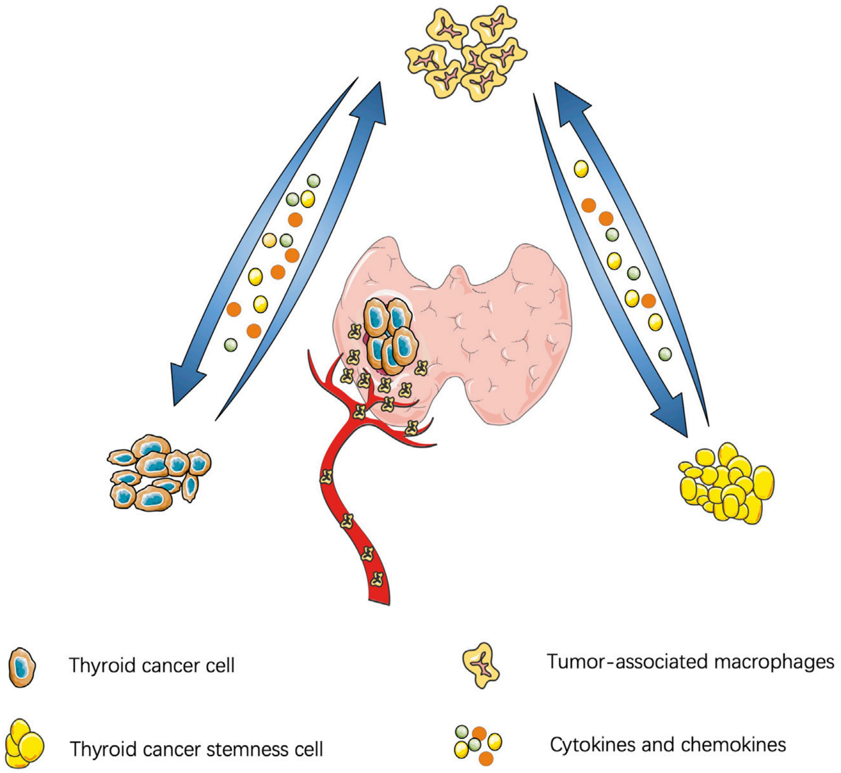

FIGURE 1 | Interaction between thyroid cancer and tumor-associatated macrophages: Thyroid cancer cells secrete cytokines to manitain the stemness of cancer cells and cancer stem cells feedback to promote tumor proliferation and migration. Thyroid cancer can also secrete chemokines to recruit macrophages and polarize into M2 subtype. Similarly, cytokines derived from tumor-association macrophages promote tumor migration.

in extensive immunosuppression of TC in BRAF^{V600E} (Angell et al., 2014).

Polarization of Tumor-Associated Macrophages in Tumor Microenvironment

Macrophages recruited from circulating monocytes into tumor tissues and endowed with tumor-promoting or suppressive effects are called TAMs (Pathria et al., 2019; Cassetta and Pollard, 2020). Once TAMs from peripheral blood monocytes are recruited to TME by tumor secreted chemokines and polarized into M1/M2 macrophages under various stimuli. TAMs can also show significant plasticity within the TME, transforming from one phenotype to another in response to certain stimuli (Sica and Mantovani, 2012).

M1-TAMs are involved in the activation of Th1 type immune response and they have a high capacity of antigen presentation, secreting some cytokines and chemokines such as IL-1β, IL-6, IL-12, IL-23, CXCL9, CXCL10, TNF-α, etc., (Porta et al., 2015; Wu et al., 2020). In addition, Some surface proteins of M1-TAMs, CD68, CD80 and CD86, are also upregulated (de Sousa et al., 2016). In contrast, M2-TAMs primarily upregulated the expression of anti-inflammatory cytokines and chemokines, including IL-10, TGF-β, CCL17, CCL18, CCL22, and CCL24. Similarly, some surface proteins of M2-TAMs are upregulated including CD163, CD204 and CD206 (Biswas et al., 2013; Jayasingam et al., 2019).

Although many markers related to TAMs polarization have been discovered, some markers of M1 or M2 phenotype can be co-expressed on an individual cell (Chong et al., 2015). Therefore, the anti-tumor or pro-tumor effects of M1 or M2 macrophages are still controversial. Their effects can be determined not only by the high and low expression of markers, but also by the complex activation mechanism of the mutual transformation between the two phenotypes (**Figure 2**).

Roles of Tumor Associated Macrophages in Tumor Microenvironment

Hypoxia is an effective means to induce TME to recruit TAMs, and imbalance of TME oxygen supply may inhibit TAMs migration. Hypoxia inducible factor-1α (HIF-1α) is a key transcription factor regulating hypoxia-induced gene expression, and its high expression can induce TAMs to enter hypoxia region continuously. HIF-1α upregulates CXCR4 and its ligand CXCL12 in monocytes/macrophages and induces these chemotactic responses (Kumar and Gabrilovich, 2014).

After recruitment and polarization, M2-TAMs can secrete a series of cytokines to stimulate tumor cell proliferation and survival including epithelial growth factor (EGF), epithelial

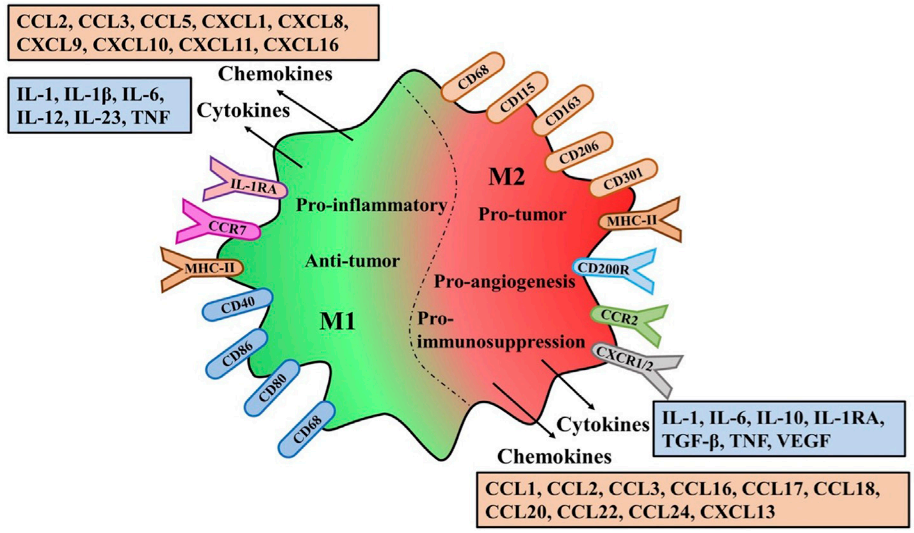
CCL2, CCL3, CCL5, CXCL1, CXCL8, CXCL9, CXCL10, CXCL11, CXCL16
Chemokines
IL-1, IL-1β, IL-6, IL-12, IL-23, TNF
Cytokines
CD68
CD115
CD163
CD206
CD301
MHC-II
CD200R
CCR2
CXCR1/2
IL-1RA
CCR7
MHC-II
CD40
CD86
CD80
CD68
Pro-inflammatory
Anti-tumor
M1
M2
Pro-tumor
Pro-angiogenesis
Pro-immunosuppression
Cytokines
IL-1, IL-6, IL-10, IL-1RA, TGF-β, TNF, VEGF
Chemokines
CCL1, CCL2, CCL3, CCL16, CCL17, CCL18, CCL20, CCL22, CCL24, CXCL13

FIGURE 2 | Polarization characteristics surface markers receptors and secretions of TAMs.The variation of M1/M2-TAMS in the Tumor microenviroment the same or different markers and receptors on the membrane surface are explained. Different types of Polarization secreted different cytokines and chemokines and different effects on tumors

growth ligands of the factor receptor (EGFR) and basic fibroblast growth factor (bFGF) (Yin et al., 2016). Polarization of TAMs has been confirmed to be associated with proliferation and metastasis of various malignant tumors. In ovarian cancer, TAMs can promote tumor proliferation and migration by upregulating insulin like growth factor (IGF1) signaling pathway (Liu et al., 2018a). Gastric cancer derived mesenchymal cells secrete IL-6 and IL-8 (CXCL8) through JAK2/STAT3 signaling pathway and induce polarization of gastric cancer M2-macrophages. M2-macrophages significantly promote gastric cancer metastasis through promoting epithelial-mesenchymal transition (EMT) mechanism (Li et al., 2019). In a study on exosomes and TME, Mir-183-5p level of M2-TAMs exosomes was significantly increased, which targeted THEM4-mediated Akt/NF-κB and inhibited the mRNA and protein expression, promoted the proliferation and invasion of colon cancer cells, and inhibited apoptosis. Downregulation of Mir-183-5p reversed the M2-TAMs mediated tumor promotion (Zhang et al., 2021a). In some clinical studies of non-small cell lung cancer, M2-TAMs infiltrate induce tumor cell invasion and progression, resulting in poor prognosis (Sumitomo et al., 2019; Sedighzadeh et al., 2021). Pulmonary macrophage accumulation is one of the important factors leading to lung metastasis of ATC (Li et al., 2016). Recent studies have found that some gene mutations can cause imbalance of M1/M2-TAMs. For example, a recent animal study revealed that Mettl3-deficient mice showed increased infiltration of M1/M2-TAMs. Deletion of METTL3 disrupts YTHDF1-mediated translation of SPRED2, thereby enhancing NF-kB and STAT3 activation through the ERK pathway, leading to increased tumor growth and metastasis (Yin et al., 2021). When the mTOR pathway is activated, the monocyte macrophage phenotype is converted to M2-TAMs, enhancing pro-angiogenic capacity. On the contrary, when the mTOR pathway is inhibited, the cell phenotype is transformed into M1-TAMs, and its decreased angiogenesis ability can inhibit tumor growth (Li et al., 2020). Therefore, under the structure of TME, M2-TAMs can not only secrete cytokines or chemokines to induce tumor development, but also promote tumor proliferation and migration through cross talk with tumor cells.

There is substantial evidence that inflammatory responses at tumor sites can promote tumor growth and progression. Inflammation and immune evasion are considered to be hallmarks of cancer.

Interaction of Tumor-Associated Macrophages With Thyroid Cancer Stem Cells

CSC is a subpopulation of cancer cells with the ability to self-renew and proliferate heterogeneous cancer cells. CSCs have an important role in tumor survival, proliferation, metastasis, drug resistance and recurrence (Ayob and Ramasamy, 2018). CSCs are primarily found inside tumors, named stem cell niches, under specific microenvironmental conditions, that consist of multiple types of stromal cells, including the vascular system, mesenchymal cells, immune cells, extracellular matrix, and cytokines (Borovski et al., 2011). In 2005, Takano and his colleagues proposed that TC cells were derived from stem cells or precursor cells of fetal origin in normal thyroid gland rather than from differentiated thyroid follicular cells.

Based on this hypothesis, many scholars believe that TC is a CSC-driven disease that may originate from the transformation of stem cells or from the dedifferentiation process of cancer cells (Zhang et al., 2006; Zito et al., 2008). CSCs are predominantly found in different specific TME, where the dynamic balance between intracellular and extracellular cytokines produced by the TME allows the maintenance of a stem cell phenotype characterized by a lack of tissue-specific differentiation, slow cell cycle rate, quiescence and a theoretically unlimited capacity for self-renewal (Pietras et al., 2014; Chan et al., 2019; Grassi et al., 2021). A growing number of studies have shown that CSCs are closely associated with radiotherapy tolerance, tumor metastasis and recurrence (Magee et al., 2012; Mertins, 2014). The transition of stem cells to differentiated cancer cells is stimulated by growth factors and cytokines that are present in the TME in which the stem cells are located (Gianì et al., 2020). TAMs secretes multiple cytokines or chemokines to support self-renewal and maintenance of stemness. Similarly, CSCs secrete pro-tumor signals to activate TAMs, which further promotes tumor development (Sainz et al., 2016). The expression of EMT biomarkers was strongly correlated with the presence of CSCs in TC and the role of TAMs (Lan et al., 2013; Hardin et al., 2018). CSCs are currently thought to drive TC heterogeneity, contributing to their metastatic potential and therapeutic resistance (Grassi et al., 2021). CSCs can also secrete exosomes to regulate the polarization of TAMs toward the M2 phenotype, inhibit NK-cell activity, and promote suppression of the immune microenvironment in CSC niches (Caruso Bavisotto et al., 2019; Baig et al., 2020). The current view is that eradication of CSCs may inhibit tumor recurrence, while failure to completely remove CSCs eventually leads to tumor recurrence (Nguyen et al., 2012). Although current research is limited, there is evidence that TAMs can enhance the stemness of CSC (Chanmee et al., 2014). In a study of head and neck cancer, TAMs can affect CD44 signal through PI3K-4EBP1-SOX2 pathway to mediate stemness enhancement, and *In vivo* experiments, Targeting CD44 reduced PI3K-4EBP1-SOX2 signal, inhibited tumor growth, and attenuated stemness (Gomez et al., 2020). Periostin secreted by glioma stem cells recruited peripheral blood mononuclear cells into glioblastoma tissue. Moreover, TAMs and glioma stem cells co-distribute in perivascular niches to maintain the characteristics of M2 macrophages and secrete tumour-supportive factors to promote glioblastoma growth and progression (Zhou et al., 2015).

Although the current research results on thyroid CSCs and TAMs are still insufficient. However, existing studies can show that there is a mutual promotion between thyroid CSCs, TAMs and TME, that is, TAMs can maintain the stemness of thyroid CSCs, and CSCs can also promote polarization of TAMs to M2 macrophages. Finally, CSCs and TAMSs establish a positive loop by a cross talk mechanism.

FUNCTIONS AND MECHANISMS OF MACROPHAGES IN THYROID CANCER

TAMs accounts for a large proportion of tumor-infiltrating immune cells in TME and are highly plastic (Chen et al., 2019). TAMs are infiltrating immune cells that can occupy up to 50% of the total volume of thyroid tumors (Ryder et al., 2008). TAMs respond to cytokines or chemokines secreted by tumor cells and polarize into M1 or M2-TAMs. but in TME, M2-TAMs are usually predominant. M1-TAMs play a key role in killing tumor cells by producing reactive oxygen/nitrogen species (ROS/RNS) and pro-inflammatory cytokines such as IL-1β, IL-6, and TNF-α, and thus M1-TAMs are macrophages with anti-tumor effects (Jeannin et al., 2018; Chen et al., 2019). Typically, most TAMs are M2-TAMs with a Th2 immune response, which can enhance tumor cell immune escape (Galdiero et al., 2013; Ferrari et al., 2019).

TC cells and M2-macrophages can promote each other. M2-TAMs promotes TC dedifferentiation, proliferation and metastasis by secreting Wnt1 and Wnt3 ligands, that activate the Wnt signaling pathway and promote β-catenin activation (Lv et al., 2021a). Inhibition of the Akt-mTOR signaling pathway inhibits TC-induced cytokines production by macrophages (Sloot et al., 2019a). Mazzoni et al. found that TC cells activate PGE2 secretion to promote M2 polarization, enhancing tumor invasiveness (Mazzoni et al., 2019). On the contrary, TCs can induce macrophages polarization, which in turn acts on tumor cells to lead to tumor progression and metastasis. For example, senescent thyroid tumor cells can induce M2-macrophages polarization with increased expression of CCL17,CCL18,IL-18,TGFβ1, that ultimately promotes tumor migration by activating NF-κB signaling pathway (Zhang et al., 2021b). In addition, gene mutations also have an impact on TAM polarization, such as BRAF^{V600E} mutation, which can lead to an increase in the proportion of M2-TAMs and promote tumor growth (Ryder et al., 2013). Some drugs or compounds can alter polarization of M2. For example, a recent study by Juan LV et al. found that Zoledronic acid inhibits M2-induced TC proliferation, stemness and metastasis by inhibiting M2 polarization and suppressing the Wnt/β-catenin signaling pathway (Lv et al., 2020). TNF-α derived from TAMs can induce IL-32β expression in TC cells. Although IL-32β does not directly affect TC cells migration, alternative splicing of IL-32 towards the IL-32β isoform may be beneficial for TC cell survival through induction of the pro-survival chemokine IL-8 (CXCL8) (Sloot et al., 2019b).

M1-Macrophage Transformation in Thyroid Cancer

M1-macrophages can inhibit tumor proliferation and migration in a variety of malignant tumors. However, due to the limitations of various factors and conditions, studies on TC are still insufficient. Reversing the polarization of M2-macrophages has also emerged as one of the potential new strategies for TC treatment. Metabolic reprogramming of M1-macrophages has been found in autoimmune diseases to enhance glycolysis and inhibit oxidative phosphorylation, which may be one of the clues of autoimmune thyroiditis (Murray et al., 2014).

In PTC, the normal thyroid tissue had higher density of M1-macrophages than the cancer tissue. And the proportion of M1-macrophages in stage I and II is higher than that in other stages (Xie et al., 2020). More importantly, CIBERSORT results showed that some anti-tumor immune cells such as M1-macrophages, plasma cells and CD8^{+} T cells were positively correlated. Similarly, A the cancer genome atlas (TCGA) prognostic model of TC revealed that a higher proportion of

M1-macrophages and dendritic resting cells in the low-risk group (Zhang et al., 2021c). In addition, the endocrine system is also involved in regulating the polarization of macrophages. *In vitro* results showed that triiodothyronine (T3) had a negative effect on triggering the differentiation of bone marrow derived monocytes into nonpolarized macrophages. M1-macrophages polarization of macrophages induced by T3 (Perrotta et al., 2014). *In vitro* experiments, the co-culture system of TPC-1 cells and bleomycin revealed that low-dose bleomycin could transform M2-TAMs into M1-TAMs, and the proliferation, migration and invasion abilities of TPC-1 cells were significantly reduced (Liu et al., 2018b). Another *in vitro* study found that in Graves disease (GD), activated NK-cells drive macrophages to differentiate to M1 phenotype, which in turn is cytotoxic to cancer cells and downregulates the M2 phenotype (Imam et al., 2019). This will open up new prospects for immunotherapy of TC. Macrophage/innate immunity can modulate from M2 phenotype to M1 phenotype to help treat TC as naturally done by GD.

Functions of M2-Macrophages in Papillary Thyroid Cancer

The most common route of metastasis for PTC is lymphatic metastasis. Current studies have found that PTC can achieve the purpose of macrophage recruitment in TME by upregulation of some chemokine transcription programs (Guarino et al., 2010; Muzza et al., 2010). Previous studies have demonstrated that high density of M2-TAMs leads to lymph node metastasis in PTC (Gulubova and Ivanova, 2019). It was reported that M2 macrophages accumulated around the lymphatic vessels at the PTC tumor margins implicated lymphatic invasion of cancer cells (Kabasawa et al., 2021). M2-TAMs around lymphatic vessels enhance lymphatic invasion by upregulating MMP2. Yang et al. found that Mir-324-5p/PTPRD/CEBPD axis induces Human Umbilical Vein Endothelial Cells (HUVEC) invasion/migration and M2-macrophages polarization through VEGF and IL4/IL13, respectively, and participates in the progression of PTC (Yang et al., 2020a). TAMs conditioned medium co-cultured with PTC cell enhanced the invasion of PTC. More importantly, this study found that CXCL8 promotes PTC metastasis *in vivo*, confirming that TAMs may promote PTC metastasis through the interaction between CXCL8 and its receptor, CXCr1/2 (Fang et al., 2014). In addition, other cytokines secreted by TAMs also promote the invasion and metastasis of PTC. For example, The combination of CXCL16 derived from M2-TAMs with angiogenic genes leads to high aggressiveness of PCT, and knockout of endogenous CXCL16 delayed tumor growth in athymic mice (Cho et al., 2016). M2-macrophages also have immunosuppressive function, which can mediate immune escape and promote the proliferation and metastasis of TC. M2-TAMs promote the proliferation and metastasis of TC through a variety of paracrine methods. In addition, the upregulated level of VEGF and EGF secreted by M2-macrophages can promote tumor microangiogenesis by recruiting endothelial cells (Chandler et al., 2019). Hypoxia is also a major driver of tumor angiogenesis, and a large number of TAMs have been found in hypoxia areas of tumors, especially necrotic tissues (Yang et al., 2020b).

Functions of M2-Macrophages in Anaplastic Thyroid Cancer

The density of M2-macrophages varied among thyroid tumors, with higher density in PTC and highest in ATC. The density of M2-macrophages is closely associated with tumor prognosis (Jung et al., 2015; Ferrari et al., 2019). The presence of a high density of macrophages in ATC, which are dominated by polarized M2-TAMs, is associated with tumor aggressiveness, and therefore M2-TAMs can be used as a biomarker to predict prognosis (Sica et al., 2006; Caillou et al., 2011). However, the high density of TAMs aggregation is not sufficient to evaluate the prognosis. It is critical to evaluate their function and signaling pathways (MacDonald et al., 2020). The infiltrating cells of ATCs include lymphocyte infiltrate (mainly CD8$^+$ cytotoxic T cells) and TAMs (Cameselle-García et al., 2021; Prete et al., 2021). M2-TAMs can secrete insulin-like growth factors (IGF) to activate IR-A/IGF1R and mediate PI3K/AKT/mTOR signaling pathway to accelerate ATC cells metastasis and enhance stem cell viability and stemness (Lv et al., 2021b). A recent study revealed that blocking CD47 inhibits the growth of ATCs and reduces TAMs density, thereby suppressing tumor growth (Schürch et al., 2019). Caluo and his colleagues identified a specific type of TAM in ATC, called "ramified TAM" (RTAM), which is not present in other types of TCs, and forms a high dense network interlinked with tumor cells in ATC, providing signals and nutrients for tumor growth (Caillou et al., 2011).

Functions of M2-Macrophages in Medullary Thyroid Cancer and Follicular Thyroid Cancer

A recent *in vitro* study showed that CCL15 derived from FTC cells can effectively recruit TAMs to TME, thus providing a favorable microenvironment for tumor growth (Huang et al., 2016). MALAT1-mediated TAMs secretes FGF2 (bFGF) to inhibit the release of inflammatory cytokines, promote the proliferation, migration and invasion of FTC133 cells, and induce angiogenesis (Huang et al., 2017). In transgenic mouse models of FTC, a mechanism was found that advanced cancer in emasculated men was due to increased expression of tumor suppressor genes:GLIPR1 and SFRP1, resulting in increased tumor invasion of M1-macrophages and CD8 cells. In addition, GLIPR1 slows down the growth of cancer cells and increases the secretion of CCL5, which leads to the activation of immune cells (Zhang et al., 2015). However, studies on TAMs in FTC is still lacking due to tumor samples limitations, and large samples of clinical and basic studies are needed to confirm this function. Interestingly, there is still no study or report on MTC and TAMs, and the relationship between the two is still unclear.

MACROPHAGE-DERIVED CYTOKINES AND CHEMOKINES INTERACT IN THYROID CANCER

Macrophage-Derived Cytokines in Thyroid Cancer

TAMs not only provide structural support for tumor growth, but also participate in tumor development by secreting signaling molecules (Kogure et al., 2019). Although TAMs have insufficient secretory function, they can secrete cytokines or directly stimulate TC cells. Though some of the macrophage phenotypes will have anti-tumor immune function, but in recent years, there are evidence that TAMs can reconstruct TME, promote tumor cell proliferation and survival, promote angiogenesis and lymphatic vessel formation, and suppress T cell response to tumors (Mantovani and Allavena, 2015).

TAMs can also increase angiogenic factors to promote tumor angiogenesis. A recent study confirmed that TAMs promote tumor angiogenesis by upregulating VEGF (Hughes et al., 2015; Osterberg et al., 2016). In addition, VEGF secreted by TAMs increased the growth and activity of tumor microvasculature, providing suitable microenvironment for TC infiltration and metastasis. Examples include VEGF, platform-derived growth factor (PDGF), bFGF (Melaccio et al., 2021). In addition, it can also produce the matrix metalloproteases (MMPS) (Ojalvo et al., 2010; Cheng et al., 2021). Angiogenesis is related to tumor growth and metastasis and plays an important role in tumor development. Therefore, TAMs are one of the important factors in tumor angiogenesis (Chen et al., 2019).

In a BRAF^{V600E} mutation-induced mouse tumor model, TC cells and TAMs secrete TGF-β, which leads to tumorigenic EMT and increases the invasiveness of TC cells (Knauf et al., 2011). TAMs not only secretes some cytokines to promote the EMT of TC, but also maintains the stemness of TC. In TC, IL-6 is dependent on the activation of the IL6/JAK1/STAT3 signaling pathway to promote thyroid CSC proliferation and colony formation and to enhance the properties of thyroid CSCs and EMT (Zheng et al., 2019). IL-10 is secreted by both TAMs and malignant tumor cells. IL-10 has various effects in the immune system, most notably in the form of immunosuppression. IL-10 is found to be overexpressed in TCs and its expression was shown to be correlated with tumor size and tumor extension, suggesting that IL-10 might enhance the function of tumor progression (Mocellin et al., 2005; Cunha et al., 2017).

In summary, after monocytes are recruited near the tumor and differentiate into TAMs, TAMs secrete a variety of molecules, including growth factors, cytokines, and proteases, that promote tumor angiogenesis, immunosuppression, and tumor metastasis.

Macrophage-Derived Chemokines in Thyroid Cancer

Chemokines are classified into four subtypes: C, CC, CXC, and CX3C, and CC in the predominant one of these subtypes (Yapa et al., 2017). The role of cytokines is to create a concentration gradient to induce motility or chemotaxis for specific receptor cells, inducing the migration of immune cells such as NK-cells, dendritic cells, and others (Mukaida et al., 2014). Previous studies have identified a variety of chemokine-mediated immune cells that promote progression of TCs (Yapa et al., 2017). However, the signaling pathways by which these chemokines mediate immune cells are diverse. TC cells or normal thyroid cells secrete a variety of chemokines in the basal state or under stimulation (Mironska et al., 2019).

In the studies on chemokine-mediated macrophages, cellular CXCL8 was the first chemokines found to be associated with TC, and cell lines from PTC and ATC were found to contain high levels of CXCL8 and TAMs, leading to tumor proliferation and metastasis (Kobawala et al., 2011). When CXCL8 is blocked, the metastatic potential of PTC is significantly reduced, and conversely, increasing exogenous CXCL8 promotes the metastatic potential of PTC (Fang et al., 2014). In addition, Visciano and his colleagues used *in vitro* cell culture to demonstrate that (IL-8) CXCL8 induces EMT in TC and enhances the stemness of thyroid CSCs through the Akt-Slug signaling pathway (Visciano et al., 2015). These chemokines also have the function of promoting EMT in TC (Pradella et al., 2017).

In a study of another chemokine receptor, CXCR4, whose ligand is CXCL12, activates G protein-mediated signaling pathways, including AKT, JAK/STAT, and MAPK (Pawig et al., 2015), and promotes migration and invasion of a variety of malignancies, including TCs. High expression of CXCR4 promotes cell proliferation and lymph node metastasis in PTCs and ATCs (Hwang et al., 2003; Wagner et al., 2008). In addition, there are many chemokines that can enhance the proliferation and invasion of TC. For example, CCL2/MCP-1 (monocyte chemotactic protein-1) promotes lymph node metastasis in PTC by recruiting TAMs expressing CCR2, and patients with high CCL2 expression are more likely to recurrence (Tanaka et al., 2009). The chemokine CCL21 and its receptor CCR7 were found to play crucial roles in the proliferation and migration of PTC and MTC by Sancho et al. (2006). In PTC, patients with elevated CCL2 are more likely to develop lymph metastases and have a high recurrence risk (Tanaka et al., 2009). In another experiment found that PTC overexpression of CXCL16 is correlated with M2 polarization and promote tumor angiogenesis (Kim et al., 2019). A recent study confirmed that high CXCR6 expression was positively associated with PTC lymph metastasis and that CXCL16 mediated macrophages invasion of PTC and altered the macrophages phenotype to M2-TAMs in the TME (Cho et al., 2016).

TARGETING TUMOR-ASSOCIATED MACROPHAGES IS A POTENTIAL TREATMENT FOR THYROID CANCER

For all types of TC, surgical treatment is still the best means of treatment, and TSH inhibition therapy could be performed according to the postoperative pathological results such as lymph node metastasis of patients and the risk of recurrence (Haugen et al., 2015). If necessary, ^{131}I therapy, external radiation or targeted therapy should be performed (Wang et al., 2019b). Tumor immunotherapy is an effective anti-tumor therapy

TABLE.1 | Tyrosine kinase inhibitors and new immunotherapeutics in development for thyroid cancer.

Drug	Therapeutic target	Indication	Dose	Results	Research progress	Reference
Dabrafenib plus Trametinib	BRAF and MEK	ATC	150 twice daily and 2 mg once daily	63% PR	In clinical trial	Subbiah et al. (2018)
Selpercatinib	RET	MTC	160 twice daily	61% PR	Approved for clinical use	Wirth et al. (2020)
Anlotinib	VEGF, VEGFR, PDGFR, c-Kit, RET	MTC	12mg once daily	56.9% PR	Approved for clinical use	Sun et al. (2018)
Pralsetinib	RET	MTC	400 mg once daily	91%	Approved for clinical use	Markham (2020)
Vandetanib	RET, VEGF, VEGFR	MTC	300 mg once daily	45% PR	Approved for clinical use	Koehler et al. (2021)
Cabozantinib	RET, VEGFR, c-MET	MTC	140 mg once daily	28% PR	Approved for clinical use	Koehler et al. (2021)
Axitinib	VEGF, VEGFR	ATC	5 mg twice daily	30% PR	In clinical trial	Cohen et al. (2014)
Lenvatinib	VEGF, VEGFR, FGFR, RET, c-kit	ATC/MTC	24 mg daily	24%/ 36% PR	Approved for clinical use	Tahara et al. (2017)
Pazopanib	VEGFR, PDGFR, FGFR, c- kit	MTC	800 mg daily	14% PR	In clinical trial	Bible et al. (2014)
Sorafenib	VEGFR, PDGFR, RET, c-kit, BRAF	MTC	400 mg twice daily	24% PR	Approved for clinical use	Lam et al. (2010)
Sunitinib	VEGFR, GIST, PDGFR, RET, c-kit, CSF-1R, Flt-3	MTC	37.5 mg daily	24% PR	In clinical trial	Carr et al. (2010)

Immunotherapy strategies and therapeutic targets for thyroid cancer under development.

Drug	Therapeutic target	Research progress	Indication	Drug	Therapeutic target	Research progress	Indication
LY3022855	CSF-1R, TAM	In clinical trial	TC	Cemiplimab	PD-1, PD-L1	In clinical trial	ATC
PLX3397 plus Paclitaxel	CSF-1R, TAM	In clinical trial	TC	MLN0128(mTORi)	mTOR1/2	In clinical trial	ATC
LY3022855 plus Tremelimumab or Durvalumab	CSF-1R, TAM, PD-1	In clinical trial	TC	Pembrolizumab	PD-1, PD-L1	Approved for clinical use	ATC
PLX3397 plus Pembrolizumab	CSF-1R, TAM, PD-1	In clinical trial	TC	Trametinib plus Paclitaxel	MEK	In clinical trial	ATC

strategy developed in recent years. There is considerable evidence that macrophages are polarized into the M2 phenotype in the development of many solid tumors (Komohara et al., 2016; Movahedi and Van Ginderachter, 2016). Therefore, targeting TAMs is a potential therapeutic strategy for solid tumors. The transformation of M2 to M1-macrophages is a potential new antitumor immunotherapy, and its mechanism is related to the upregulation of macrophage phagocytosis. Current strategies for macrophage therapy are mainly through two approaches: inhibition of recruitment and/or clearance, and reversal of differentiation. Blocking macrophages recruitment has been extensively studied in preclinical models, and is being evaluated for feasibility of clinical application. Several monoclonal antibodies that have been approved for clinical use in the treatment of tumors have been shown to work therapeutically, primarily by increasing the phagocytic activity of macrophages. Targeted regulation of TAMs plays a key role in the activity of antitumor drugs (Germano et al., 2013).

Transform or Inhibit the Polarization of M2-Macrophages

Inhibition of cytokines or chemokines, such as CCL2 and colony stimulating factor (CSF-1), that promote the polarization of macrophages into M2 phenotype, is a promising immunotherapy (Kim et al., 2013; Richards et al., 2013). Tyrosinase inhibitors for TC and immunotherapy drugs under development are listed in **Table 1**. A recent study showed that PLX4720 (The main active molecule is 7-azaindole, which is a potent and selective inhibitor of B-Raf V600E) combined with anti-PD-L1/PD-1 antibody significantly reduced ATC tumor volume, increased the density and cytotoxicity of CD8$^+$ T cells and NK cells, increased M1-TAMs, prolonged survival, improved TME, and enhanced anti-tumor immune effect (Gunda et al., 2018). In addition, Rituximab is a chimeric monoclonal antibody that specifically binds to the transmembrane antigen CD20 and inhibit the growth of non-Hodgkin's lymphoma cells by promoting macrophage phagocytosis (Chao et al., 2010). Trastuzumab blocks the attachment of human EGF to Her2 by attaching itself to Her2 and mediate macrophage killing of Her-2 overexpressing in breast cancer cells (Shi et al., 2015). Similarly, bleomycin mainly interferes with DNA synthesis, but low dose bleomycin can reverse the M2 to M1-macrophages, and the proliferation, migration and invasion of TPC-1 cells are significantly reduced, suggesting that bleomycin can inhibit the progression of PTC by modulating macrophages polarization (Liu et al., 2018b). Similarly, selective elimination of M2-TAMs inhibits PTC growth, and CSF-1 signaling may serve as a potential therapeutic target for inhibiting BRAF^{V600E} mutation-induced PTC (Ryder et al., 2013). More interestingly, A bisphosphonate (zoledronic acid) binds to microcalcification in tumor tissue and is subsequently phagocytized by TAM to induce apoptosis, and also promotes polarization of M2 towards M1-macrophages (Hattori et al., 2015). A mouse model of combined anti-macrophage zoledronic acid and tumor cytotoxic docetaxel showed that the combined strategy significantly inhibited tumor growth and pulmonary metastasis (Sun et al., 2015). Blocking and targeting the CCL-2/CCR2 and CSF-1/CSF-1R pathways is a promising approach in ATC. This approach can not only inhibit the recruitment of tumor M2-macrophages, but also re-polarize them into the M1 phenotype (Naoum et al., 2018).

Blocking the Secretion of Cytokines/Chemokines or Their Receptors in the TME

Blocking common TAM-related chemokines such as CCL2 and CXCL8 and their associated receptors may also be a potential therapeutic strategy. Since ELR- can counteract the effect of ELR+, targeting ELR + CXC chemokines can also inhibit tumorigenesis (Mukaida et al., 2014). Stassi et al. found that IL-4 and IL-10 promoted the progression of TC cells and resistance to chemotherapy through upregulation of anti-apoptotic proteins. Therefore, IL-4 and IL-10 may be new therapeutic targets for TC (Stassi et al., 2003). In addition, TC cells have some functional receptors that receive signals of chemokines for proliferation, immunosuppression, angiogenesis and other activities to maintain the growth and metastatic potential of tumor cells (Mantovani et al., 2010; Allavena et al., 2011). In a BRAF^{V600E} mutant PTC mouse model, IL-12 treatment significantly reduced tumor size and weight and improved OS (Parhar et al., 2016). Another study identified IL-12 as a pro-inflammatory cytokine with anti-tumor activity, demonstrating inhibition of ATC growth (Lu, 2017). Possible molecular mechanisms are associated with NF-κB activation and NF-κ B-dependent MMP-3 upregulation. Therefore, molecular therapies targeting CCL20 and CCR6 may provide promising intervention strategies for TC (Cunha et al., 2012; Zeng et al., 2014). In a animal model experiment, the change of secretory CXCL8 in the treatment of MTC can be used as a biomarker for the clinical efficacy of sunitinib (Broutin et al., 2011). In addition to MTC and ATC, the prognosis of PTC is also closely related to TME. Researchers are looking for an immunotherapy to modify TME to enhance the outcome of surgery and RAI (Na and Choi, 2018). Balkwill et al. demonstrated that CXCR7, when downregulated in PTC, inhibits cell growth and invasion, leads to S-phase arrest, and promotes apoptosis, suggesting that CXCR7 may be a promising target for therapeutic intervention of PTC (Balkwill, 2012).

The plasticity of macrophages highlights the potential of macrophage reprogramming as a therapeutic strategy to inhibit tumor progression, enabling these cells to adapt their functions to meet the needs of tumor resistance. In order to better understand the activation status of TAMs in TME, further studies on specific markers are needed to distinguish the different functions of antitumor or pro-tumor TAMs.

CONCLUSION AND PERSPECTIVES

In recent decades, there has been no significant improvement in the survival of patients with progressive or recurrent TCs, despite systematic and multidisciplinary treatments. Therefore, for the postoperative management of TC patients, in addition to histological classification, other pathological parameters such as mutational status, activation of molecular signaling pathways, tumor cell differentiation, and associated immunophenotype need to be considered. TME plays an important role in TC development, metastasis, stemness, and TAMs account for the largest proportion of cells in TME. Although it is currently believed that high infiltration of M2-TAMs supports the TME and promotes the growth of TC, it has also been suggested that mixed immune cell infiltration may be associated with a good prognosis in differentiated TC. The study of TAMs in TC is a novel field and more research is needed to unravel the complex and dynamic crosstalk between TC cells and their microenvironment. Although current research has evidence to support that targeting TAMs can significantly improve the efficacy of conventional therapies and immunotherapy, there is still a long way to go to understand the role and mechanisms of TAMs in TC progression and the use of TAM-based immunotherapy.

AUTHOR CONTRIBUTIONS

QL: Conceptualization, Writing—Original draft preparation. WS: Writing—Reviewing and Editing, Validation. HZ: Supervision.

FUNDING

This works was funded by National Natural Science Foundation of China (81902726), Science and Technology Project of Shenyang City (21-173-9-31).

REFERENCES

Allavena, P., Germano, G., Marchesi, F., and Mantovani, A. (2011). Chemokines in Cancer Related Inflammation. *Exp. Cel Res* 317 (5), 664–673. doi:10.1016/j.yexcr.2010.11.013

Angell, T. E., Lechner, M. G., Jang, J. K., Correa, A. J., LoPresti, J. S., and Epstein, A. L. (2014). BRAF V600E in Papillary Thyroid Carcinoma Is Associated with Increased Programmed Death Ligand 1 Expression and Suppressive Immune Cell Infiltration. *Thyroid* 24 (9), 1385–1393. doi:10.1089/thy.2014.0134

Ayob, A. Z., and Ramasamy, T. S. (2018). Cancer Stem Cells as Key Drivers of Tumour Progression. *J. Biomed. Sci.* 25 (1), 20. doi:10.1186/s12929-018-0426-4

Baig, M. S., Roy, A., Rajpoot, S., Liu, D., Savai, R., Banerjee, S., et al. (2020). Tumor-derived Exosomes in the Regulation of Macrophage Polarization. *Inflamm. Res.* 69 (5), 435–451. doi:10.1007/s00011-020-01318-0

Balkwill, F. R. (2012). The Chemokine System and Cancer. *J. Pathol.* 226 (2), 148–157. doi:10.1002/path.3029

Ben-Baruch, A. (2006). Inflammation-associated Immune Suppression in Cancer: the Roles Played by Cytokines, Chemokines and Additional Mediators. *Semin. Cancer Biol.* 16 (1), 38–52. doi:10.1016/j.semcancer.2005.07.006

Bible, K. C., Suman, V. J., Molina, J. R., Smallridge, R. C., Maples, W. J., Menefee, M. E., et al. (2014). A Multicenter Phase 2 Trial of Pazopanib in Metastatic and Progressive Medullary Thyroid Carcinoma: MC057H. *J. Clin. Endocrinol. Metab.* 99 (5), 1687–1693. doi:10.1210/jc.2013-3713

Biswas, S. K., Allavena, P., and Mantovani, A. (2013). Tumor-associated Macrophages: Functional Diversity, Clinical Significance, and Open Questions. *Semin. Immunopathol* 35 (5), 585–600. doi:10.1007/s00281-013-0367-7

Bolli, E., Movahedi, K., Laoui, D., and Van Ginderachter, J. A. (2017). Novel Insights in the Regulation and Function of Macrophages in the Tumor Microenvironment. *Curr. Opin. Oncol.* 29 (1), 55–61. doi:10.1097/CCO.0000000000000344

Borovski, T., De Sousa E Melo, F., Vermeulen, L., and Medema, J. P. (2011). Cancer Stem Cell Niche: the Place to Be. *Cancer Res.* 71 (3), 634–639. doi:10.1158/0008-5472.CAN-10-3220

Broutin, S., Ameur, N., Lacroix, L., Robert, T., Petit, B., Oumata, N., et al. (2011). Identification of Soluble Candidate Biomarkers of Therapeutic Response to Sunitinib in Medullary Thyroid Carcinoma in Preclinical Models. *Clin. Cancer Res.* 17 (7), 2044–2054. doi:10.1158/1078-0432.CCR-10-2041

Cabanillas, M. E., McFadden, D. G., and Durante, C. (2016). Thyroid Cancer. *Lancet* 388 (10061), 2783–2795. doi:10.1016/S0140-6736(16)30172-6

Caillou, B., Talbot, M., Weyemi, U., Pioche-Durieu, C., Al Ghuzlan, A., Bidart, J. M., et al. (2011). Tumor-associated Macrophages (TAMs) Form an Interconnected Cellular Supportive Network in Anaplastic Thyroid Carcinoma. *PLoS One* 6 (7), e22567. doi:10.1371/journal.pone.0022567

Cameselle-García, S., Abdulkader-Sande, S., Sánchez-Ares, M., Rodríguez-Carnero, G., Garcia-Gómez, J., Gude-Sampedro, F., et al. (2021). PD-L1 Expression and Immune Cells in Anaplastic Carcinoma and Poorly Differentiated Carcinoma of the Human Thyroid Gland: A Retrospective Study. *Oncol. Lett.* 22 (1), 553. doi:10.3892/ol.2021.12814

Cancer Genome Atlas Research, N. (2014). Integrated Genomic Characterization of Papillary Thyroid Carcinoma. *Cell* 159 (3), 676–690. doi:10.1016/j.cell.2014.09.050

Carr, L. L., Mankoff, D. A., Goulart, B. H., Eaton, K. D., Capell, P. T., Kell, E. M., et al. (2010). Phase II Study of Daily Sunitinib in FDG-PET-Positive, Iodine-Refractory Differentiated Thyroid Cancer and Metastatic Medullary Carcinoma of the Thyroid with Functional Imaging Correlation. *Clin. Cancer Res.* 16 (21), 5260–5268. doi:10.1158/1078-0432.CCR-10-0994

Caruso Bavisotto, C., Cipolla, C., Graceffa, G., Barone, R., Bucchieri, F., Bulone, D., et al. (2019). Immunomorphological Pattern of Molecular Chaperones in Normal and Pathological Thyroid Tissues and Circulating Exosomes: Potential Use in Clinics. *Int. J. Mol. Sci.* 20 (18). doi:10.3390/ijms20184496

Cassetta, L., and Pollard, J. W. (2018). Targeting Macrophages: Therapeutic Approaches in Cancer. *Nat. Rev. Drug Discov.* 17 (12), 887–904. doi:10.1038/nrd.2018.169

Cassetta, L., and Pollard, J. W. (2020). Tumor-associated Macrophages. *Curr. Biol.* 30 (6), R246–R248. doi:10.1016/j.cub.2020.01.031

Chan, T. S., Shaked, Y., and Tsai, K. K. (2019). Targeting the Interplay between Cancer Fibroblasts, Mesenchymal Stem Cells, and Cancer Stem Cells in Desmoplastic Cancers. *Front. Oncol.* 9, 688. doi:10.3389/fonc.2019.00688

Chandler, K. B., Costello, C. E., and Rahimi, N. (2019). Glycosylation in the Tumor Microenvironment: Implications for Tumor Angiogenesis and Metastasis. *Cells* 8 (6). doi:10.3390/cells8060544

Chanmee, T., Ontong, P., Konno, K., and Itano, N. (2014). Tumor-associated Macrophages as Major Players in the Tumor Microenvironment. *Cancers (Basel)* 6 (3), 1670–1690. doi:10.3390/cancers6031670

Chao, M. P., Alizadeh, A. A., Tang, C., Myklebust, J. H., Varghese, B., Gill, S., et al. (2010). Anti-CD47 Antibody Synergizes with Rituximab to Promote Phagocytosis and Eradicate Non-hodgkin Lymphoma. *Cell* 142 (5), 699–713. doi:10.1016/j.cell.2010.07.044

Chen, Y., Song, Y., Du, W., Gong, L., Chang, H., and Zou, Z. (2019). Tumor-associated Macrophages: an Accomplice in Solid Tumor Progression. *J. Biomed. Sci.* 26 (1), 78. doi:10.1186/s12929-019-0568-z

Cheng, N., Bai, X., Shu, Y., Ahmad, O., and Shen, P. (2021). Targeting Tumor-Associated Macrophages as an Antitumor Strategy. *Biochem. Pharmacol.* 183, 114354. doi:10.1016/j.bcp.2020.114354

Cho, S. W., Kim, Y. A., Sun, H. J., Kim, Y. A., Oh, B. C., Yi, K. H., et al. (2016). CXCL16 Signaling Mediated Macrophage Effects on Tumor Invasion of Papillary Thyroid Carcinoma. *Endocr. Relat. Cancer* 23 (2), 113–124. doi:10.1530/ERC-15-0196

Chong, B. F., Tseng, L. C., Hosler, G. A., Teske, N. M., Zhang, S., Karp, D. R., et al. (2015). A Subset of CD163+ Macrophages Displays Mixed Polarizations in Discoid Lupus Skin. *Arthritis Res. Ther.* 17, 324. doi:10.1186/s13075-015-0839-3

Ciampi, R., Mian, C., Fugazzola, L., Cosci, B., Romei, C., Barollo, S., et al. (2013). Evidence of a Low Prevalence of RAS Mutations in a Large Medullary Thyroid Cancer Series. *Thyroid* 23 (1), 50–57. doi:10.1089/thy.2012.0207

Coffelt, S. B., Lewis, C. E., Naldini, L., Brown, J. M., Ferrara, N., and De Palma, M. (2010). Elusive Identities and Overlapping Phenotypes of Proangiogenic Myeloid Cells in Tumors. *Am. J. Pathol.* 176 (4), 1564–1576. doi:10.2353/ajpath.2010.090786

Cohen, E. E., Tortorici, M., Kim, S., Ingrosso, A., Pithavala, Y. K., and Bycott, P. (2014). A Phase II Trial of Axitinib in Patients with Various Histologic Subtypes of Advanced Thyroid Cancer: Long-Term Outcomes and Pharmacokinetic/pharmacodynamic Analyses. *Cancer Chemother. Pharmacol.* 74 (6), 1261–1270. doi:10.1007/s00280-014-2604-8

Cunha, L. L., Morari, E. C., Guihen, A. C., Razolli, D., Gerhard, R., Nonogaki, S., et al. (2012). Infiltration of a Mixture of Immune Cells May Be Related to Good Prognosis in Patients with Differentiated Thyroid Carcinoma. *Clin. Endocrinol. (Oxf)* 77 (6), 918–925. doi:10.1111/j.1365-2265.2012.04482.x

Cunha, L. L., Morari, E. C., Nonogaki, S., Marcello, M. A., Soares, F. A., Vassallo, J., et al. (2017). Interleukin 10 Expression Is Related to Aggressiveness and Poor Prognosis of Patients with Thyroid Cancer. *Cancer Immunol. Immunother.* 66 (2), 141–148. doi:10.1007/s00262-016-1924-4

de Sousa, J. R., de Sousa, R. P., Aarão, T. L., Dias, L. B., Jr., Carneiro, F. R., Fuzii, H. T., et al. (2016). *In Situ* expression of M2 Macrophage Subpopulation in Leprosy Skin Lesions. *Acta Trop.* 157, 108–114. doi:10.1016/j.actatropica.2016.01.008

de Visser, K. E., Eichten, A., and Coussens, L. M. (2006). Paradoxical Roles of the Immune System during Cancer Development. *Nat. Rev. Cancer* 6 (1), 24–37. doi:10.1038/nrc1782

Fang, W., Ye, L., Shen, L., Cai, J., Huang, F., Wei, Q., et al. (2014). Tumor-associated Macrophages Promote the Metastatic Potential of Thyroid Papillary Cancer by Releasing CXCL8. *Carcinogenesis* 35 (8), 1780–1787. doi:10.1093/carcin/bgu060

Ferrari, S. M., Fallahi, P., Galdiero, M. R., Ruffilli, I., Elia, G., Ragusa, F., et al. (2019). Immune and Inflammatory Cells in Thyroid Cancer Microenvironment. *Int. J. Mol. Sci.* 20 (18). doi:10.3390/ijms20184413

Fozzatti, L., and Cheng, S. Y. (2020). Tumor Cells and Cancer-Associated Fibroblasts: A Synergistic Crosstalk to Promote Thyroid Cancer. *Endocrinol. Metab. (Seoul)* 35 (4), 673–680. doi:10.3803/EnM.2020.401

Fugazzola, L., Colombo, C., Perrino, M., and Muzza, M. (2011). Papillary Thyroid Carcinoma and Inflammation. *Front. Endocrinol. (Lausanne)* 2, 88. doi:10.3389/fendo.2011.00088

Galdiero, M. R., Garlanda, C., Jaillon, S., Marone, G., and Mantovani, A. (2013). Tumor Associated Macrophages and Neutrophils in Tumor Progression. *J. Cel Physiol* 228 (7), 1404–1412. doi:10.1002/jcp.24260

Germano, G., Frapolli, R., Belgiovine, C., Anselmo, A., Pesce, S., Liguori, M., et al. (2013). Role of Macrophage Targeting in the Antitumor Activity of Trabectedin. *Cancer Cell* 23 (2), 249–262. doi:10.1016/j.ccr.2013.01.008

Gianì, F., Vella, V., Tumino, D., Malandrino, P., and Frasca, F. (2020). The Possible Role of Cancer Stem Cells in the Resistance to Kinase Inhibitors of Advanced Thyroid Cancer. *Cancers (Basel)* 12 (8). doi:10.3390/cancers12082249

Goldberg, J. L., and Sondel, P. M. (2015). Enhancing Cancer Immunotherapy via Activation of Innate Immunity. *Semin. Oncol.* 42 (4), 562–572. doi:10.1053/j.seminoncol.2015.05.012

Gomez, K. E., Wu, F., Keysar, S. B., Morton, J. J., Miller, B., Chimed, T. S., et al. (2020). Cancer Cell CD44 Mediates Macrophage/Monocyte-Driven Regulation of Head and Neck Cancer Stem Cells. *Cancer Res.* 80 (19), 4185–4198. doi:10.1158/0008-5472.CAN-20-1079

Grassi, E. S., Ghiandai, V., and Persani, L. (2021). Thyroid Cancer Stem-like Cells: From Microenvironmental Niches to Therapeutic Strategies. *J. Clin. Med.* 10 (7). doi:10.3390/jcm10071455

Guarino, V., Castellone, M. D., Avilla, E., and Melillo, R. M. (2010). Thyroid Cancer and Inflammation. *Mol. Cel Endocrinol* 321 (1), 94–102. doi:10.1016/j.mce.2009.10.003

Gulubova, M. V., and Ivanova, K. V. (2019). The Expression of Tumor-Associated Macrophages and Multinucleated Giant Cells in Papillary Thyroid Carcinoma. *Open Access Maced J. Med. Sci.* 7 (23), 3944–3949. doi:10.3889/oamjms.2019.715

Gunda, V., Gigliotti, B., Ndishabandi, D., Ashry, T., McCarthy, M., Zhou, Z., et al. (2018). Combinations of BRAF Inhibitor and Anti-PD-1/pd-L1 Antibody Improve Survival and Tumour Immunity in an Immunocompetent Model of Orthotopic Murine Anaplastic Thyroid Cancer. *Br. J. Cancer* 119 (10), 1223–1232. doi:10.1038/s41416-018-0296-2

Hardin, H., Helein, H., Meyer, K., Robertson, S., Zhang, R., Zhong, W., et al. (2018). Thyroid Cancer Stem-like Cell Exosomes: Regulation of EMT via Transfer of lncRNAs. *Lab. Invest.* 98 (9), 1133–1142. doi:10.1038/s41374-018-0065-0

Hattori, Y., Shibuya, K., Kojima, K., Miatmoko, A., Kawano, K., Ozaki, K., et al. (2015). Zoledronic Acid Enhances Antitumor Efficacy of Liposomal Doxorubicin. *Int. J. Oncol.* 47 (1), 211–219. doi:10.3892/ijo.2015.2991

Haugen, B. R., Alexander, E. K., Bible, K. C., Doherty, G. M., Mandel, S. J., Nikiforov, Y. E., et al. (2015). 2015 American Thyroid Association Management Guidelines for Adult Patients with Thyroid Nodules and Differentiated Thyroid Cancer: The American Thyroid Association Guidelines Task Force on Thyroid Nodules and Differentiated Thyroid Cancer. *Thyroid* 26 (1), 1–133. doi:10.1089/thy.2015.0020

Hou, P., Liu, D., Shan, Y., Hu, S., Studeman, K., Condouris, S., et al. (2007). Genetic Alterations and Their Relationship in the Phosphatidylinositol 3-kinase/Akt Pathway in Thyroid Cancer. *Clin. Cancer Res.* 13 (4), 1161–1170. doi:10.1158/1078-0432.CCR-06-1125

Huang, F. J., Zhou, X. Y., Ye, L., Fei, X. C., Wang, S., Wang, W., et al. (2016). Follicular Thyroid Carcinoma but Not Adenoma Recruits Tumor-Associated Macrophages by Releasing CCL15. *BMC Cancer* 16, 98. doi:10.1186/s12885-016-2114-7

Huang, J. K., Ma, L., Song, W. H., Lu, B. Y., Huang, Y. B., Dong, H. M., et al. (2017). LncRNA-MALAT1 Promotes Angiogenesis of Thyroid Cancer by Modulating Tumor-Associated Macrophage FGF2 Protein Secretion. *J. Cel Biochem* 118 (12), 4821–4830. doi:10.1002/jcb.26153

Hughes, R., Qian, B. Z., Rowan, C., Muthana, M., Keklikoglou, I., Olson, O. C., et al. (2015). Perivascular M2 Macrophages Stimulate Tumor Relapse after Chemotherapy. *Cancer Res.* 75 (17), 3479–3491. doi:10.1158/0008-5472.CAN-14-3587

Hwang, J. H., Hwang, J. H., Chung, H. K., Kim, D. W., Hwang, E. S., Suh, J. M., et al. (2003). CXC Chemokine Receptor 4 Expression and Function in Human Anaplastic Thyroid Cancer Cells. *J. Clin. Endocrinol. Metab.* 88 (1), 408–416. doi:10.1210/jc.2002-021381

Imam, S., Dar, P., Paparodis, R., Almotah, K., Al-Khudhair, A., Hasan, S. A., et al. (2019). Nature of Coexisting Thyroid Autoimmune Disease Determines success or Failure of Tumor Immunity in Thyroid Cancer. *J. Immunother. Cancer* 7 (1), 3. doi:10.1186/s40425-018-0483-y

Jayasingam, S. D., Citartan, M., Thang, T. H., Mat Zin, A. A., Ang, K. C., and Ch'ng, E. S. (2019). Evaluating the Polarization of Tumor-Associated Macrophages into M1 and M2 Phenotypes in Human Cancer Tissue: Technicalities and Challenges in Routine Clinical Practice. *Front. Oncol.* 9, 1512. doi:10.3389/fonc.2019.01512

Jeannin, P., Paolini, L., Adam, C., and Delneste, Y. (2018). The Roles of CSFs on the Functional Polarization of Tumor-Associated Macrophages. *FEBS J.* 285 (4), 680–699. doi:10.1111/febs.14343

Jung, K. Y., Cho, S. W., Kim, Y. A., Kim, D., Oh, B. C., Park, D. J., et al. (2015). Cancers with Higher Density of Tumor-Associated Macrophages Were Associated with Poor Survival Rates. *J. Pathol. Transl Med.* 49 (4), 318–324. doi:10.4132/jptm.2015.06.01

Kabasawa, T., Ohe, R., Aung, N. Y., Urano, Y., Kitaoka, T., Tamazawa, N., et al. (2021). Potential Role of M2 TAMs Around Lymphatic Vessels during Lymphatic Invasion in Papillary Thyroid Carcinoma. *Sci. Rep.* 11 (1), 1150. doi:10.1038/s41598-020-80694-3

Kim, M. J., Sun, H. J., Song, Y. S., Yoo, S. K., Kim, Y. A., Seo, J. S., et al. (2019). CXCL16 Positively Correlated with M2-Macrophage Infiltration, Enhanced Angiogenesis, and Poor Prognosis in Thyroid Cancer. *Sci. Rep.* 9 (1), 13288. doi:10.1038/s41598-019-49613-z

Kim, S., Cho, S. W., Min, H. S., Kim, K. M., Yeom, G. J., Kim, E. Y., et al. (2013). The Expression of Tumor-Associated Macrophages in Papillary Thyroid Carcinoma. *Endocrinol. Metab. (Seoul)* 28 (3), 192–198. doi:10.3803/EnM.2013.28.3.192

Knauf, J. A., Sartor, M. A., Medvedovic, M., Lundsmith, E., Ryder, M., Salzano, M., et al. (2011). Progression of BRAF-Induced Thyroid Cancer Is Associated with Epithelial-Mesenchymal Transition Requiring Concomitant MAP Kinase and TGFβ Signaling. *Oncogene* 30 (28), 3153–3162. doi:10.1038/onc.2011.44

Kobawala, T. P., Patel, G. H., Gajjar, D. R., Patel, K. N., Thakor, P. B., Parekh, U. B., et al. (2011). Clinical Utility of Serum Interleukin-8 and Interferon-Alpha in Thyroid Diseases. *J. Thyroid Res.* 2011, 270149. doi:10.4061/2011/270149

Koehler, V. F., Adam, P., Frank-Raue, K., Raue, F., Berg, E., Hoster, E., et al. (2021). Real-World Efficacy and Safety of Cabozantinib and Vandetanib in Advanced Medullary Thyroid Cancer. *Thyroid* 31 (3), 459–469. doi:10.1089/thy.2020.0206

Kogure, A., Kosaka, N., and Ochiya, T. (2019). Cross-talk between Cancer Cells and Their Neighbors via miRNA in Extracellular Vesicles: an Emerging Player in Cancer Metastasis. *J. Biomed. Sci.* 26 (1), 7. doi:10.1186/s12929-019-0500-6

Komohara, Y., Fujiwara, Y., Ohnishi, K., and Takeya, M. (2016). Tumor-associated Macrophages: Potential Therapeutic Targets for Anti-cancer Therapy. *Adv. Drug Deliv. Rev.* 99 (Pt B), 180–185. doi:10.1016/j.addr.2015.11.009

Kotwal, A., Erickson, D., Geske, J. R., Hay, I. D., and Castro, M. R. (2021). Predicting Outcomes in Sporadic and Hereditary Medullary Thyroid Carcinoma over Two Decades. *Thyroid* 31 (4), 616–626. doi:10.1089/thy.2020.0167

Kumar, V., and Gabrilovich, D. I. (2014). Hypoxia-inducible Factors in Regulation of Immune Responses in Tumour Microenvironment. *Immunology* 143 (4), 512–519. doi:10.1111/imm.12380

La Vecchia, C., Malvezzi, M., Bosetti, C., Garavello, W., Bertuccio, P., Levi, F., et al. (2015). Thyroid Cancer Mortality and Incidence: a Global Overview. *Int. J. Cancer* 136 (9), 2187–2195. doi:10.1002/ijc.29251

Lam, E. T., Ringel, M. D., Kloos, R. T., Prior, T. W., Knopp, M. V., Liang, J., et al. (2010). Phase II Clinical Trial of Sorafenib in Metastatic Medullary Thyroid Cancer. *J. Clin. Oncol.* 28 (14), 2323–2330. doi:10.1200/JCO.2009.25.0068

Lan, L., Luo, Y., Cui, D., Shi, B. Y., Deng, W., Huo, L. L., et al. (2013). Epithelial-mesenchymal Transition Triggers Cancer Stem Cell Generation in Human Thyroid Cancer Cells. *Int. J. Oncol.* 43 (1), 113–120. doi:10.3892/ijo.2013.1913

Lei, X., Lei, Y., Li, J. K., Du, W. X., Li, R. G., Yang, J., et al. (2020). Immune Cells within the Tumor Microenvironment: Biological Functions and Roles in Cancer Immunotherapy. *Cancer Lett.* 470, 126–133. doi:10.1016/j.canlet.2019.11.009

Li, W., Zhang, X., Wu, F., Zhou, Y., Bao, Z., Li, H., et al. (2019). Gastric Cancer-Derived Mesenchymal Stromal Cells Trigger M2 Macrophage Polarization that Promotes Metastasis and EMT in Gastric Cancer. *Cell Death Dis* 10 (12), 918. doi:10.1038/s41419-019-2131-y

Li, X., Shan, C., Wu, Z., Yu, H., Yang, A., and Tan, B. (2020). Emodin Alleviated Pulmonary Inflammation in Rats with LPS-Induced Acute Lung Injury through Inhibiting the mTOR/HIF-1α/VEGF Signaling Pathway. *Inflamm. Res.* 69 (4), 365–373. doi:10.1007/s00011-020-01331-3

Li, X. J., Gangadaran, P., Kalimuthu, S., Oh, J. M., Zhu, L., Jeong, S. Y., et al. (2016). Role of Pulmonary Macrophages in Initiation of Lung Metastasis in Anaplastic Thyroid Cancer. *Int. J. Cancer* 139 (11), 2583–2592. doi:10.1002/ijc.30387

Liu, H., Dong, H., Jiang, L., Li, Z., and Ma, X. (2018). Bleomycin Inhibits Proliferation and Induces Apoptosis in TPC-1 Cells through Reversing M2-Macrophages Polarization. *Oncol. Lett.* 16 (3), 3858–3866. doi:10.3892/ol.2018.9103

Liu, L., Wang, X., Li, X., Wu, X., Tang, M., and Wang, X. (2018). Upregulation of IGF1 by Tumor-Associated Macrophages Promotes the Proliferation and Migration of Epithelial Ovarian Cancer Cells. *Oncol. Rep.* 39 (2), 818–826. doi:10.3892/or.2017.6148

LiVolsi, V. A. (2011). Papillary Thyroid Carcinoma: an Update. *Mod. Pathol.* 24 (Suppl. 2), S1–S9. doi:10.1038/modpathol.2010.129

Lu, X. (2017). Impact of IL-12 in Cancer. *Curr. Cancer Drug Targets* 17 (8), 682–697. doi:10.2174/1568009617666170427102729

Lumachi, F., Basso, S. M., and Orlando, R. (2010). Cytokines, Thyroid Diseases and Thyroid Cancer. *Cytokine* 50 (3), 229–233. doi:10.1016/j.cyto.2010.03.005

Lv, J., Chen, F. K., Liu, C., Liu, P. J., Feng, Z. P., Jia, L., et al. (2020). Zoledronic Acid Inhibits Thyroid Cancer Stemness and Metastasis by Repressing M2-like Tumor-Associated Macrophages Induced Wnt/β-Catenin Pathway. *Life Sci.* 256, 117925. doi:10.1016/j.lfs.2020.117925

Lv, J., Feng, Z. P., Chen, F. K., Liu, C., Jia, L., Liu, P. J., et al. (2021). M2-like Tumor-Associated Macrophages-Secreted Wnt1 and Wnt3a Promotes Dedifferentiation and Metastasis via Activating β-catenin Pathway in Thyroid Cancer. *Mol. Carcinog* 60 (1), 25–37. doi:10.1002/mc.23268

Lv, J., Liu, C., Chen, F. K., Feng, Z. P., Jia, L., Liu, P. J., et al. (2021). M2-like T-umour-associated M-acrophage-secreted IGF P-romotes T-hyroid C-ancer S-temness and M-etastasis by A-ctivating the PI3K/AKT/mTOR P-athway. *Mol. Med. Rep.* 24 (2). doi:10.3892/mmr.2021.12249

MacDonald, L., Jenkins, J., Purvis, G., Lee, J., and Franco, A. T. (2020). The Thyroid Tumor Microenvironment: Potential Targets for Therapeutic Intervention and Prognostication. *Horm. Cancer* 11 (5-6), 205–217. doi:10.1007/s12672-020-00390-6

Magee, J. A., Piskounova, E., and Morrison, S. J. (2012). Cancer Stem Cells: Impact, Heterogeneity, and Uncertainty. *Cancer Cell* 21 (3), 283–296. doi:10.1016/j.ccr.2012.03.003

Mantovani, A., and Allavena, P. (2015). The Interaction of Anticancer Therapies with Tumor-Associated Macrophages. *J. Exp. Med.* 212 (4), 435–445. doi:10.1084/jem.20150295

Mantovani, A., Marchesi, F., Malesci, A., Laghi, L., and Allavena, P. (2017). Tumour-associated Macrophages as Treatment Targets in Oncology. *Nat. Rev. Clin. Oncol.* 14 (7), 399–416. doi:10.1038/nrclinonc.2016.217

Mantovani, A., Savino, B., Locati, M., Zammataro, L., Allavena, P., and Bonecchi, R. (2010). The Chemokine System in Cancer Biology and Therapy. *Cytokine Growth Factor. Rev.* 21 (1), 27–39. doi:10.1016/j.cytogfr.2009.11.007

Mantovani, A., Sozzani, S., Locati, M., Allavena, P., and Sica, A. (2002). Macrophage Polarization: Tumor-Associated Macrophages as a Paradigm for Polarized M2 Mononuclear Phagocytes. *Trends Immunol.* 23 (11), 549–555. doi:10.1016/s1471-4906(02)02302-5

Markham, A. (2020). Pralsetinib: First Approval. *Drugs* 80 (17), 1865–1870. doi:10.1007/s40265-020-01427-4

Mazzoni, M., Mauro, G., Erreni, M., Romeo, P., Minna, E., Vizioli, M. G., et al. (2019). Senescent Thyrocytes and Thyroid Tumor Cells Induce M2-like Macrophage Polarization of Human Monocytes via a PGE2-dependent Mechanism. *J. Exp. Clin. Cancer Res.* 38 (1), 208. doi:10.1186/s13046-019-1198-8

Melaccio, A., Sgaramella, L. I., Pasculli, A., Di Meo, G., Gurrado, A., Prete, F. P., et al. (2021). Prognostic and Therapeutic Role of Angiogenic Microenvironment in Thyroid Cancer. *Cancers (Basel)* 13 (11). doi:10.3390/cancers13112775

Menicali, E., Guzzetti, M., Morelli, S., Moretti, S., and Puxeddu, E. (2020). Immune Landscape of Thyroid Cancers: New Insights. *Front. Endocrinol. (Lausanne)* 11, 637826. doi:10.3389/fendo.2020.637826

Mertins, S. D. (2014). Cancer Stem Cells: a Systems Biology View of Their Role in Prognosis and Therapy. *Anticancer Drugs* 25 (4), 353–367. doi:10.1097/CAD.0000000000000075

Mironska, A., Łukaszewicz-Zajac, M., and Mroczko, B. (2019). Clinical Significance of Selected Chemokines in Thyroid Cancer. *Anticancer Res.* 39 (6), 2715–2720. doi:10.21873/anticanres.13397

Mocellin, S., Marincola, F. M., and Young, H. A. (2005). Interleukin-10 and the Immune Response against Cancer: a Counterpoint. *J. Leukoc. Biol.* 78 (5), 1043–1051. doi:10.1189/jlb.0705358

Movahedi, K., and Van Ginderachter, J. A. (2016). The Ontogeny and Microenvironmental Regulation of Tumor-Associated Macrophages. *Antioxid. Redox Signal.* 25 (14), 775–791. doi:10.1089/ars.2016.6704

Mukaida, N., Sasaki, S., and Baba, T. (2014). Chemokines in Cancer Development and Progression and Their Potential as Targeting Molecules for Cancer Treatment. *Mediators Inflamm.* 2014, 170381. doi:10.1155/2014/170381

Murray, P. J., Allen, J. E., Biswas, S. K., Fisher, E. A., Gilroy, D. W., Goerdt, S., et al. (2014). Macrophage Activation and Polarization: Nomenclature and Experimental Guidelines. *Immunity* 41 (1), 14–20. doi:10.1016/j.immuni.2014.06.008

Muzza, M., Degl'Innocenti, D., Colombo, C., Perrino, M., Ravasi, E., Rossi, S., et al. (2010). The Tight Relationship between Papillary Thyroid Cancer, Autoimmunity and Inflammation: Clinical and Molecular Studies. *Clin. Endocrinol. (Oxf)* 72 (5), 702–708. doi:10.1111/j.1365-2265.2009.03699.x

Na, K. J., and Choi, H. (2018). Immune Landscape of Papillary Thyroid Cancer and Immunotherapeutic Implications. *Endocr. Relat. Cancer* 25 (5), 523–531. doi:10.1530/ERC-17-0532

Naoum, G. E., Morkos, M., Kim, B., and Arafat, W. (2018). Novel Targeted Therapies and Immunotherapy for Advanced Thyroid Cancers. *Mol. Cancer* 17 (1), 51. doi:10.1186/s12943-018-0786-0

Nguyen, L. V., Vanner, R., Dirks, P., and Eaves, C. J. (2012). Cancer Stem Cells: an Evolving Concept. *Nat. Rev. Cancer* 12 (2), 133–143. doi:10.1038/nrc3184

Noy, R., and Pollard, J. W. (2014). Tumor-associated Macrophages: from Mechanisms to Therapy. *Immunity* 41 (1), 49–61. doi:10.1016/j.immuni.2014.06.010

Ojalvo, L. S., Whittaker, C. A., Condeelis, J. S., and Pollard, J. W. (2010). Gene Expression Analysis of Macrophages that Facilitate Tumor Invasion Supports a Role for Wnt-Signaling in Mediating Their Activity in Primary Mammary Tumors. *J. Immunol.* 184 (2), 702–712. doi:10.4049/jimmunol.0902360

Osterberg, N., Ferrara, N., Vacher, J., Gaedicke, S., Niedermann, G., Weyerbrock, A., et al. (2016). Decrease of VEGF-A in Myeloid Cells Attenuates Glioma Progression and Prolongs Survival in an Experimental Glioma Model. *Neuro Oncol.* 18 (7), 939–949. doi:10.1093/neuonc/now005

Pan, Y., Yu, Y., Wang, X., and Zhang, T. (2020). Tumor-Associated Macrophages in Tumor Immunity. *Front. Immunol.* 11, 583084. doi:10.3389/fimmu.2020.583084

Parhar, R. S., Zou, M., Al-Mohanna, F. A., Baitei, E. Y., Assiri, A. M., Meyer, B. F., et al. (2016). IL-12 Immunotherapy of Braf(V600E)-Induced Papillary Thyroid Cancer in a Mouse Model. *Lab. Invest.* 96 (1), 89–97. doi:10.1038/labinvest.2015.126

Pathria, P., Louis, T. L., and Varner, J. A. (2019). Targeting Tumor-Associated Macrophages in Cancer. *Trends Immunol.* 40 (4), 310–327. doi:10.1016/j.it.2019.02.003

Pawig, L., Klasen, C., Weber, C., Bernhagen, J., and Noels, H. (2015). Diversity and Inter-connections in the CXCR4 Chemokine Receptor/Ligand Family: Molecular Perspectives. *Front. Immunol.* 6, 429. doi:10.3389/fimmu.2015.00429

Perrotta, C., Buldorini, M., Assi, E., Cazzato, D., De Palma, C., Clementi, E., et al. (2014). The Thyroid Hormone Triiodothyronine Controls Macrophage Maturation and Functions: Protective Role during Inflammation. *Am. J. Pathol.* 184 (1), 230–247. doi:10.1016/j.ajpath.2013.10.006

Person, L., Lacour, B., Faure, L., Guissou, S., Poulalhon, C., Orbach, D., et al. (2021). Childhood Head and Neck Cancer in France: Incidence, Survival and Trends from 2000 to 2015. *Int. J. Pediatr. Otorhinolaryngol.* 150, 110858. doi:10.1016/j.ijporl.2021.110858

Pietras, A., Katz, A. M., Ekström, E. J., Wee, B., Halliday, J. J., Pitter, K. L., et al. (2014). Osteopontin-CD44 Signaling in the Glioma Perivascular Niche Enhances Cancer Stem Cell Phenotypes and Promotes Aggressive Tumor Growth. *Cell Stem Cell* 14 (3), 357–369. doi:10.1016/j.stem.2014.01.005

Porta, C., Riboldi, E., Ippolito, A., and Sica, A. (2015). Molecular and Epigenetic Basis of Macrophage Polarized Activation. *Semin. Immunol.* 27 (4), 237–248. doi:10.1016/j.smim.2015.10.003

Poschke, I., Mougiakakos, D., and Kiessling, R. (2011). Camouflage and Sabotage: Tumor Escape from the Immune System. *Cancer Immunol. Immunother.* 60 (8), 1161–1171. doi:10.1007/s00262-011-1012-8

Pradella, D., Naro, C., Sette, C., and Ghigna, C. (2017). EMT and Stemness: Flexible Processes Tuned by Alternative Splicing in Development and Cancer Progression. *Mol. Cancer* 16 (1), 8. doi:10.1186/s12943-016-0579-2

Prendergast, G. C., Metz, R., and Muller, A. J. (2010). Towards a Genetic Definition of Cancer-Associated Inflammation: Role of the Ido Pathway. *Am. J. Pathol.* 176 (5), 2082–2087. doi:10.2353/ajpath.2010.091173

Prete, A., Matrone, A., Gambale, C., Torregrossa, L., Minaldi, E., Romei, C., et al. (2021). Poorly Differentiated and Anaplastic Thyroid Cancer: Insights into Genomics, Microenvironment and New Drugs. *Cancers (Basel)* 13 (13). doi:10.3390/cancers13133200

Richards, D. M., Hettinger, J., and Feuerer, M. (2013). Monocytes and Macrophages in Cancer: Development and Functions. *Cancer Microenviron* 6 (2), 179–191. doi:10.1007/s12307-012-0123-x

Ryder, M., Ghossein, R. A., Ricarte-Filho, J. C., Knauf, J. A., and Fagin, J. A. (2008). Increased Density of Tumor-Associated Macrophages Is Associated with Decreased Survival in Advanced Thyroid Cancer. *Endocr. Relat. Cancer* 15 (4), 1069–1074. doi:10.1677/ERC-08-0036

Ryder, M., Gild, M., Hohl, T. M., Pamer, E., Knauf, J., Ghossein, R., et al. (2013). Genetic and Pharmacological Targeting of CSF-1/CSF-1R Inhibits Tumor-Associated Macrophages and Impairs BRAF-Induced Thyroid Cancer Progression. *PLoS One* 8 (1), e54302. doi:10.1371/journal.pone.0054302

Sainz, B., Jr., Carron, E., Vallespinós, M., and Machado, H. L. (2016). Cancer Stem Cells and Macrophages: Implications in Tumor Biology and Therapeutic Strategies. *Mediators Inflamm.* 2016, 9012369. doi:10.1155/2016/9012369

Sancho, M., Vieira, J. M., Casalou, C., Mesquita, M., Pereira, T., Cavaco, B. M., et al. (2006). Expression and Function of the Chemokine Receptor CCR7 in Thyroid Carcinomas. *J. Endocrinol.* 191 (1), 229–238. doi:10.1677/joe.1.06688

Schürch, C. M., Roelli, M. A., Forster, S., Wasmer, M. H., Brühl, F., Maire, R. S., et al. (2019). Targeting CD47 in Anaplastic Thyroid Carcinoma Enhances Tumor Phagocytosis by Macrophages and Is a Promising Therapeutic Strategy. *Thyroid* 29 (7), 979–992. doi:10.1089/thy.2018.0555

Sedighzadeh, S. S., Khoshbin, A. P., Razi, S., Keshavarz-Fathi, M., and Rezaei, N. (2021). A Narrative Review of Tumor-Associated Macrophages in Lung Cancer: Regulation of Macrophage Polarization and Therapeutic Implications. *Transl Lung Cancer Res.* 10 (4), 1889–1916. doi:10.21037/tlcr-20-1241

Shi, Y., Fan, X., Deng, H., Brezski, R. J., Rycyzyn, M., Jordan, R. E., et al. (2015). Trastuzumab Triggers Phagocytic Killing of High HER2 Cancer Cells *In Vitro* and *In Vivo* by Interaction with Fcγ Receptors on Macrophages. *J. Immunol.* 194 (9), 4379–4386. doi:10.4049/jimmunol.1402891

Sica, A., and Mantovani, A. (2012). Macrophage Plasticity and Polarization: *In Vivo* Veritas. *J. Clin. Invest.* 122 (3), 787–795. doi:10.1172/JCI59643

Sica, A., Schioppa, T., Mantovani, A., and Allavena, P. (2006). Tumour-associated Macrophages Are a Distinct M2 Polarised Population Promoting Tumour Progression: Potential Targets of Anti-cancer Therapy. *Eur. J. Cancer* 42 (6), 717–727. doi:10.1016/j.ejca.2006.01.003

Sloot, Y. J. E., Rabold, K., Netea, M. G., Smit, J. W. A., Hoogerbrugge, N., and Netea-Maier, R. T. (2019). Effect of PTEN Inactivating Germline Mutations on Innate Immune Cell Function and Thyroid Cancer-Induced Macrophages in Patients with PTEN Hamartoma Tumor Syndrome. *Oncogene* 38 (19), 3743–3755. doi:10.1038/s41388-019-0685-x

Sloot, Y. J. E., Rabold, K., Ulas, T., De Graaf, D. M., Heinhuis, B., Händler, K., et al. (2019). Interplay between Thyroid Cancer Cells and Macrophages: Effects on IL-32 Mediated Cell Death and Thyroid Cancer Cell Migration. *Cel Oncol (Dordr)* 42 (5), 691–703. doi:10.1007/s13402-019-00457-9

Smallridge, R. C., Ain, K. B., Asa, S. L., Bible, K. C., Brierley, J. D., Burman, K. D., et al. (2012). American Thyroid Association Guidelines for Management of Patients with Anaplastic Thyroid Cancer. *Thyroid* 22 (11), 1104–1139. doi:10.1089/thy.2012.0302

Solinas, G., Schiarea, S., Liguori, M., Fabbri, M., Pesce, S., Zammataro, L., et al. (2010). Tumor-conditioned Macrophages Secrete Migration-Stimulating Factor: a New Marker for M2-Polarization, Influencing Tumor Cell Motility. *J. Immunol.* 185 (1), 642–652. doi:10.4049/jimmunol.1000413

Sowder, A. M., Witt, B. L., and Hunt, J. P. (2018). An Update on the Risk of Lymph Node Metastasis for the Follicular Variant of Papillary Thyroid Carcinoma with the New Diagnostic Paradigm. *Head Neck Pathol.* 12 (1), 105–109. doi:10.1007/s12105-017-0835-9

Stassi, G., Todaro, M., Zerilli, M., Ricci-Vitiani, L., Di Liberto, D., Patti, M., et al. (2003). Thyroid Cancer Resistance to Chemotherapeutic Drugs via Autocrine Production of Interleukin-4 and Interleukin-10. *Cancer Res.* 63 (20), 6784–6790.

Subbiah, V., Kreitman, R. J., Wainberg, Z. A., Cho, J. Y., Schellens, J. H. M., Soria, J. C., et al. (2018). Dabrafenib and Trametinib Treatment in Patients with Locally Advanced or Metastatic BRAF V600-Mutant Anaplastic Thyroid Cancer. *J. Clin. Oncol.* 36 (1), 7–13. doi:10.1200/JCO.2017.73.6785

Sumitomo, R., Hirai, T., Fujita, M., Murakami, H., Otake, Y., and Huang, C. L. (2019). M2 Tumor-Associated Macrophages Promote Tumor Progression in Non-small-cell Lung Cancer. *Exp. Ther. Med.* 18 (6), 4490–4498. doi:10.3892/etm.2019.8068

Sun, X., Gao, D., Gao, L., Zhang, C., Yu, X., Jia, B., et al. (2015). Molecular Imaging of Tumor-Infiltrating Macrophages in a Preclinical Mouse Model of Breast Cancer. *Theranostics* 5 (6), 597–608. doi:10.7150/thno.11546

Sun, Y., Du, F., Gao, M., Ji, Q., Li, Z., Zhang, Y., et al. (2018). Anlotinib for the Treatment of Patients with Locally Advanced or Metastatic Medullary Thyroid Cancer. *Thyroid* 28 (11), 1455–1461. doi:10.1089/thy.2018.0022

Tahara, M., Kiyota, N., Yamazaki, T., Chayahara, N., Nakano, K., Inagaki, L., et al. (2017). Lenvatinib for Anaplastic Thyroid Cancer. *Front. Oncol.* 7, 25. doi:10.3389/fonc.2017.00025

Tanaka, K., Kurebayashi, J., Sohda, M., Nomura, T., Prabhakar, U., Yan, L., et al. (2009). The Expression of Monocyte Chemotactic Protein-1 in Papillary Thyroid Carcinoma Is Correlated with Lymph Node Metastasis and Tumor Recurrence. *Thyroid* 19 (1), 21–25. doi:10.1089/thy.2008.0237

Varol, C., Mildner, A., and Jung, S. (2015). Macrophages: Development and Tissue Specialization. *Annu. Rev. Immunol.* 33, 643–675. doi:10.1146/annurev-immunol-032414-112220

Veschi, V., Verona, F., Lo Iacono, M., D'Accardo, C., Porcelli, G., Turdo, A., et al. (2020). Cancer Stem Cells in Thyroid Tumors: From the Origin to Metastasis. *Front. Endocrinol. (Lausanne)* 11, 566. doi:10.3389/fendo.2020.00566

Visciano, C., Liotti, F., Prevete, N., Cali', G., Franco, R., Collina, F., et al. (2015). Mast Cells Induce Epithelial-To-Mesenchymal Transition and Stem Cell Features in Human Thyroid Cancer Cells through an IL-8-Akt-Slug Pathway. *Oncogene* 34 (40), 5175–5186. doi:10.1038/onc.2014.441

Wagner, P. L., Moo, T. A., Arora, N., Liu, Y. F., Zarnegar, R., Scognamiglio, T., et al. (2008). The Chemokine Receptors CXCR4 and CCR7 Are Associated with Tumor Size and Pathologic Indicators of Tumor Aggressiveness in Papillary Thyroid Carcinoma. *Ann. Surg. Oncol.* 15 (10), 2833–2841. doi:10.1245/s10434-008-0064-2

Wang, J. R., Zafereo, M. E., Dadu, R., Ferrarotto, R., Busaidy, N. L., Lu, C., et al. (2019). Complete Surgical Resection Following Neoadjuvant Dabrafenib Plus Trametinib in BRAFV600E-Mutated Anaplastic Thyroid Carcinoma. *Thyroid* 29 (8), 1036–1043. doi:10.1089/thy.2019.0133

Wang, L. X., Zhang, S. X., Wu, H. J., Rong, X. L., and Guo, J. (2019). M2b Macrophage Polarization and its Roles in Diseases. *J. Leukoc. Biol.* 106 (2), 345–358. doi:10.1002/JLB.3RU1018-378RR

Wells, S. A., Jr., Asa, S. L., Dralle, H., Elisei, R., Evans, D. B., Gagel, R. F., et al. (2015). Revised American Thyroid Association Guidelines for the Management of Medullary Thyroid Carcinoma. *Thyroid* 25 (6), 567–610. doi:10.1089/thy.2014.0335

Weng, Y. S., Tseng, H. Y., Chen, Y. A., Shen, P. C., Al Haq, A. T., Chen, L. M., et al. (2019). MCT-1/miR-34a/IL-6/IL-6R Signaling axis Promotes EMT Progression, Cancer Stemness and M2 Macrophage Polarization in Triple-Negative Breast Cancer. *Mol. Cancer* 18 (1), 42. doi:10.1186/s12943-019-0988-0

Wirth, L. J., Sherman, E., Robinson, B., Solomon, B., Kang, H., Lorch, J., et al. (2020). Efficacy of Selpercatinib in RET-Altered Thyroid Cancers. *N. Engl. J. Med.* 383 (9), 825–835. doi:10.1056/NEJMoa2005651

Wu, K., Lin, K., Li, X., Yuan, X., Xu, P., Ni, P., et al. (2020). Redefining Tumor-Associated Macrophage Subpopulations and Functions in the Tumor Microenvironment. *Front. Immunol.* 11, 1731. doi:10.3389/fimmu.2020.01731

Xie, Z., Li, X., He, Y., Wu, S., Wang, S., Sun, J., et al. (2020). Immune Cell Confrontation in the Papillary Thyroid Carcinoma Microenvironment. *Front. Endocrinol. (Lausanne)* 11, 570604. doi:10.3389/fendo.2020.570604

Yang, L., Shi, P., Zhao, G., Xu, J., Peng, W., Zhang, J., et al. (2020). Targeting Cancer Stem Cell Pathways for Cancer Therapy. *Signal. Transduct Target. Ther.* 5 (1), 8. doi:10.1038/s41392-020-0110-5

Yang, Y., Xia, S., Zhang, L., Wang, W., Chen, L., and Zhan, W. (2020). MiR-324-5p/PTPRD/CEBPD axis Promotes Papillary Thyroid Carcinoma Progression via Microenvironment Alteration. *Cancer Biol. Ther.* 21 (6), 522–532. doi:10.1080/15384047.2020.1736465

Yapa, S., Mulla, O., Green, V., England, J., and Greenman, J. (2017). The Role of Chemokines in Thyroid Carcinoma. *Thyroid* 27 (11), 1347–1359. doi:10.1089/thy.2016.0660

Yin, H., Zhang, X., Yang, P., Zhang, X., Peng, Y., Li, D., et al. (2021). RNA m6A Methylation Orchestrates Cancer Growth and Metastasis via Macrophage Reprogramming. *Nat. Commun.* 12 (1), 1394. doi:10.1038/s41467-021-21514-8

Yin, M., Li, X., Tan, S., Zhou, H. J., Ji, W., Bellone, S., et al. (2016). Tumor-associated Macrophages Drive Spheroid Formation during Early Transcoelomic Metastasis of Ovarian Cancer. *J. Clin. Invest.* 126 (11), 4157–4173. doi:10.1172/JCI87252

Zeng, W., Chang, H., Ma, M., and Li, Y. (2014). CCL20/CCR6 Promotes the Invasion and Migration of Thyroid Cancer Cells via NF-Kappa B Signaling-

Induced MMP-3 Production. *Exp. Mol. Pathol.* 97 (1), 184–190. doi:10.1016/j.yexmp.2014.06.012

Zhang, C., Gu, X., Pan, M., Yuan, Q., and Cheng, H. (2021). Senescent Thyroid Tumor Cells Promote Their Migration by Inducing the Polarization of M2-like Macrophages. *Clin. Transl Oncol.* 23 (6), 1253–1261. doi:10.1007/s12094-020-02516-2

Zhang, L. J., Xiong, Y., Nilubol, N., He, M., Bommareddi, S., Zhu, X., et al. (2015). Testosterone Regulates Thyroid Cancer Progression by Modifying Tumor Suppressor Genes and Tumor Immunity. *Carcinogenesis* 36 (4), 420–428. doi:10.1093/carcin/bgv001

Zhang, P., Zuo, H., Ozaki, T., Nakagomi, N., and Kakudo, K. (2006). Cancer Stem Cell Hypothesis in Thyroid Cancer. *Pathol. Int.* 56 (9), 485–489. doi:10.1111/j.1440-1827.2006.01995.x

Zhang, S., Chen, S., Wang, Y., Zhan, Y., Li, J., Nong, X., et al. (2021). Association of a Novel Prognosis Model with Tumor Mutation Burden and Tumor-Infiltrating Immune Cells in Thyroid Carcinoma. *Front. Genet.* 12, 744304. doi:10.3389/fgene.2021.744304

Zhang, S., Li, D., Zhao, M., Yang, F., Sang, C., Yan, C., et al. (2021). Exosomal miR-183-5p Shuttled by M2 Polarized Tumor-Associated Macrophage Promotes the Development of Colon Cancer via Targeting THEM4 Mediated PI3K/AKT and NF-Kb Pathways. *Front. Oncol.* 11, 672684. doi:10.3389/fonc.2021.672684

Zheng, R., Chen, G., Li, X., Wei, X., Liu, C., and Derwahl, M. (2019). Effect of IL-6 on Proliferation of Human Thyroid Anaplastic Cancer Stem Cells. *Int. J. Clin. Exp. Pathol.* 12 (11), 3992–4001.

Zhou, W., Ke, S. Q., Huang, Z., Flavahan, W., Fang, X., Paul, J., et al. (2015). Periostin Secreted by Glioblastoma Stem Cells Recruits M2 Tumour-Associated Macrophages and Promotes Malignant Growth. *Nat. Cel Biol* 17 (2), 170–182. doi:10.1038/ncb3090

Zito, G., Richiusa, P., Bommarito, A., Carissimi, E., Russo, L., Coppola, A., et al. (2008). *In Vitro* identification and Characterization of CD133(pos) Cancer Stem-like Cells in Anaplastic Thyroid Carcinoma Cell Lines. *PLoS One* 3 (10), e3544. doi:10.1371/journal.pone.0003544

Conflict of Interest: The authors declare that the research was conducted in the absence of any commercial or financial relationships that could be construed as a potential conflict of interest.

Publisher's Note: All claims expressed in this article are solely those of the authors and do not necessarily represent those of their affiliated organizations, or those of the publisher, the editors and the reviewers. Any product that may be evaluated in this article, or claim that may be made by its manufacturer, is not guaranteed or endorsed by the publisher.

Copyright © 2022 Liu, Sun and Zhang. This is an open-access article distributed under the terms of the Creative Commons Attribution License (CC BY). The use, distribution or reproduction in other forums is permitted, provided the original author(s) and the copyright owner(s) are credited and that the original publication in this journal is cited, in accordance with accepted academic practice. No use, distribution or reproduction is permitted which does not comply with these terms.

Frontiers in Pharmacology
ORIGINAL RESEARCH
published: 27 April 2022
doi: 10.3389/fphar.2022.876076

The Histone Deacetylase Inhibitor I1 Induces Differentiation of Acute Leukemia Cells With MLL Gene Rearrangements *via* Epigenetic Modification

Jingfang Yao[1,2†], *Gentao Li*[2†], *Zihui Cui*[2†], *Peilei Chen*[2], *Jinhong Wang*[2], *Zhenbo Hu*[1]*, *Lei Zhang*[2]* and *Liuya Wei*[2]*

[1]Laboratory for Stem Cell and Regenerative Medicine, Affiliated Hospital of Weifang Medical University, Weifang, China, [2]School of Pharmacy, Weifang Medical University, Weifang, China

Acute leukemia (AL) is characterized by excessive proliferation and impaired differentiation of leukemic cells. AL includes acute myeloid leukemia (AML) and acute lymphoblastic leukemia (ALL). Previous studies have demonstrated that about 10% of AML and 22% of ALL are mixed lineage leukemia gene rearrangements (MLLr) leukemia. The prognosis of MLLr leukemia is poor and new therapeutics are urgently needed. Differentiation therapy with all-trans-retinoic acid (ATRA) has prolonged the 5-years disease-free survival rate in acute promyelocytic leukemia (APL), a subtype of AML. However, the differentiation therapy has not been effective in other acute leukemia. Here, we aim to explore the cell differentiation effect of the potent HDACs inhibitor, I1, and the possible mechanism on the MLLr-AML and MLLr-ALL cells (MOLM-13, THP-1, MV4-11 and SEM). It is shown that I1 can significantly inhibit the proliferation and the colony-forming ability of MOLM-13, THP-1, MV4-11 and SEM cells by promoting cell differentiation coupled with cell cycle block at G0/G1 phase. We show that the anti-proliferative effect of I1 attributed to cell differentiation is most likely associated with the HDAC inhibition activity, as assessed by the acetylation of histone H3 and H4, which may dictates the activation of hematopoietic cell lineage pathway in both MOLM-13 and THP-1 cell lines. Moreover, the activity of HDAC inhibition of I1 is stronger than that of SAHA in MOLM-13 and THP-1 cells. Our findings suggest that I1, as a chromatin-remodeling agent, could be a potent epigenetic drug to overcome differentiation block in MLLr-AL patients and would be promising for the treatment of AL.

Keywords: acute leukemia, mixed lineage leukemia rearranged, differentiation therapy, HDAC inhibitor, epigenetic modification

OPEN ACCESS

Edited by:
Dong-Hua Yang,
St. John's University, United States

Reviewed by:
Hua Zhu,
The Ohio State University,
United States
Zhi Shi,
Jinan University, China
Dora Visnjic,
University of Zagreb, Croatia

***Correspondence:**
Liuya Wei
xiaoyawfmc@163.com
Lei Zhang
leizhangchemical@gmail.com
Zhenbo Hu
huzhenbo@wfmc.edu.cn

†These authors have contributed equally to this work

Specialty section:
This article was submitted to Experimental Pharmacology and Drug Discovery,
a section of the journal Frontiers in Pharmacology

Received: *15 February 2022*
Accepted: *02 March 2022*
Published: *27 April 2022*

Citation:
Yao J, Li G, Cui Z, Chen P, Wang J, Hu Z, Zhang L and Wei L (2022) The Histone Deacetylase Inhibitor I1 Induces Differentiation of Acute Leukemia Cells With MLL Gene Rearrangements via Epigenetic Modification.
Front. Pharmacol. 13:876076.
doi: 10.3389/fphar.2022.876076

INTRODUCTION

Acute leukemia (AL) includes acute myeloid leukemia (AML) and acute lymphoblastic leukemia (ALL). AML is a hematological malignancy characterized by increased self-renewal of leukemia stem/progenitor cells that are blocked in myeloid differentiation (Yu et al., 2016). ALL represents 25% of all the cancers diagnosed among children younger than 15 years and 0.1% of all the adult cancers (Allen and Ahmed, 2016). Most cases of ALL arise from the immature hematopoietic stem/progenitor cells with self-renewal and differentiation capacity (George et al., 2001). Hence, the blockade of cellular differentiation represents a hallmark of both AML and ALL.

Mixed lineage leukemia (MLL) gene rearrangements (MLLr) were found in about 10% of all the AML cases (Schoch et al., 2003) and in 22% of all the ALL cases (Gole and Wiesmüller, 2015). Despite great improvements in the treatment for ALL, MLLr-ALL have a particularly poor outcome with low survival rate compared with those of other forms of ALL (Wuchter et al., 2000). Similarly, very few MLLr- AML have either a good or an intermediate outcome (Szczepański et al., 2010). Therefore, there is an urgent need for development of new therapeutics for the MLLr-AL. Acute promyelocytic leukemia (APL) is the M3 subtype of AML, which is one of the most aggressive types and accounts for 10–15% of AML (Prange et al., 2017). Fortunately, the differentiation inducer ATRA is effective in the treatment of APL (Wang and Chen, 2008). However, the differentiation therapy with ATRA has not been effective in the treatment of the other subtypes of AML and ALL.

Histone deacetylases (HDACs) are enzymes that remove acetyl groups from histones and other proteins and thus regulate chromatin accessibility and expression of target genes (Manzotti et al., 2019). It is well documented that inhibition of HDACs promotes growth arrest and cell differentiation or apoptosis through altering the acetylation status of histone and non-histone proteins (Rosato et al., 2003; Manal et al., 2016). So far, there are four FDA-approved anticancer drugs targeting HDAC, i.e., SAHA (Suberoylanilide hydroxamic acid), FK-228, PXD-101 and LBH-589 (O'Connor et al., 2006; West and Johnstone, 2014). SAHA is a well-studied and most famous HDAC inhibitor (HDACi), which is used for the treatment of cutaneous T cell lymphoma.

In our previous study, I1 (4-(4-(1H-indol-3-yl)butanamido)-N-hydroxybenzamide, $C_{19}H_{20}N_3O_3$) is a HDACs inhibitor, which has considerable HDAC inhibitory potency with the percentage inhibitory rate of 53.81% compared with SAHA (59.91%) at the concentration of 1 μM (Chen et al., 2021). In the present study, we evaluate whether I1 has inhibitory activity by inducing cell differentiation on MLLr-AML and MLLr-ALL cell lines (MOLM-13, THP-1, MV4-11 and SEM). The possible mechanism of action of I1 is also explored.

MATERIALS AND METHODS

Chemicals

I1 was prepared by our lab. **Figure 1A** shows the chemical structure of I1 with a molecular weight of 338 and SAHA. I1 or SAHA was dissolved in dimethyl sulfoxide (DMSO) to prepare a 10 mM stock solution and stored at −20°C. The stock solutions were diluted to the desired concentrations with RPMI-1640 medium. The same concentration of DMSO as that of the I1 solution was used as control. The final

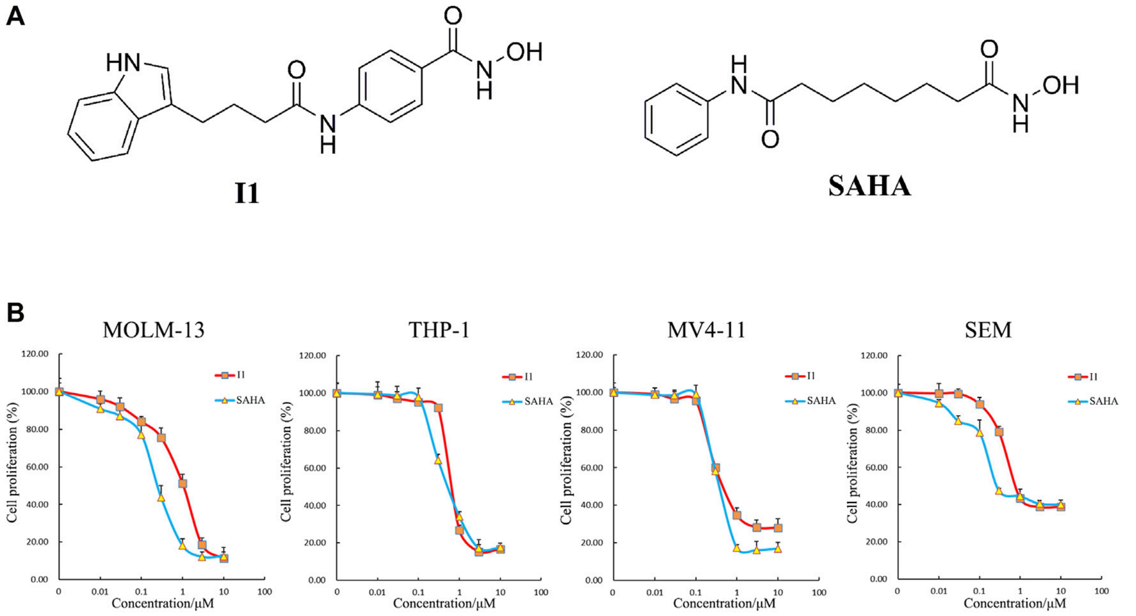

FIGURE 1 | I1 inhibited the proliferation of MOLM-13, THP-1, MV4-11 and SEM cells. **(A)** The chemical structure of I1 and SAHA. **(B)** CCK-8 assay on cells treated with different concentrations of I1 or SAHA (0–10 μM) for 72 h. Data presented as mean ± SD. The CCK-8 assay was carried out for three times in triplicate.

concentration of DMSO (not exceed 0.1%) in the cell culture had few toxic effect on the cells. Fluorescein Isothiocyanate (FITC)/Annexin V Apoptosis Detection Kit and Propidium iodide (PI)/RNase staining solution were obtained from BD Biosciences (San Jose, CA, United States). Cell Counting Kit-8 (CCK-8) was purchased from Solarbio (Beijing, China). FITC anti- CD11b (cat #301403, RRID:AB_314167), PE anti- CD13 (cat #301704, RRID:AB_314180), FITC anti- CD14 (cat #301804, RRID: AB_314186) and PE anti- CD15 (cat #301906, RRID: AB_314198) were obtained from Biolegend Inc. (San Diego, CA, United States). PE anti-human HLA-DR (FAB4869P) were obtained from R&D systems (Minneapolis, MN, United States). Anti -human HLA-DP (sc-33719) was obtained from Santa Cruz Biotechnology, Inc. (Dallas, TX, United States). MethoCult H4100 (cat #04100) and H4435 (cat #04435) were obtained from STEMCELL Technologies (Vancouver, BC, Canada). Antibodies against GAPDH (Cat #5174), Histone H3 (Cat #4499), Histone H4 (Cat #2935), Acetyl-Histone H3 (Ac-H3, Cat #8173), Acetyl-Histone H4 (Ac-H4, Cat #2594), HLA-DRA (Cat #97971T), CD13 (Cat #32720S) and CIITA (Cat #3793S) were obtained from Cell Signaling Technology (Beverly, MA, United States). Antibody against CD59 (BF0017) was purchased from Affinity Biosciences (Affinity Biosciences, OH, United States). The 2×SYBR Green qPCR Mix (cat #AH0104-B), SPARKscript II RT Plus kit (cat #AG0304-B), Spark ECL Plus A (cat #ED0015-C), Spark ECL Plus B (cat #ED0016-C) and RIPA buffer (SparkJade EA0002) were purchased from SPARKJADE (Shandong, China).

Cell Lines and Cell Culture

MOLM-13 (M5 subtype of AML expressing MLL-AF9 fusion gene, DSMZ No.: ACC 554), THP-1 (M5 subtype of AML expressing MLL-AF9 fusion gene, DSMZ No.: ACC 16), MV4-11 (AML expressing MLL-AF4 fusion gene, DSMZ No.: ACC 102), and SEM (ALL carrying MLL-AF4 fusion gene, DSMZ No.: ACC 546) cell lines were used. These cell lines were grown in RPMI-1640 medium at 37°C with 5% CO_2, and the medium contained fetal bovine serum (10%) and streptomycin/penicillin (1%).

Cell Proliferation Assay

The CCK-8 assay was used to detect the proliferation of MOLM-13, THP-1, MV4-11 and SEM cells. Briefly, cells were cultured in 96-well plates at approximately 5,000 cells/well for 24 h and were treated with I1 or SAHA (0–10 μM). After 72 h, 5 μM CCK-8 was added to each well and placed in a 37°C incubator for 4 h. An Opsys microplate reader (Dynex Technologies, Chantilly, Virginia, United States) was used to measure the light absorbance at 450 nm. The results are expressed as percentage of cell proliferation normalized to DMSO-treated control cells.

Colony Formation Assay

MOLM-13, THP-1, MV4-11 and SEM cells were incubated with I1 (0–2 μM) in a sterile 24-well flat-bottomed culture plate containing 2.6% methylcellulose medium and 10% FBS for 15 days. A CX43 microscope (Olympus, Shinjuku, Tokyo, Japan) and an Olympus EP50 camera (Olympus, Shinjuku, Tokyo, Japan) were used to count the number of colonies. A colony consisting of approximately 50 cells was counted.

Cell Cycle Analysis

MOLM-13, MV4-11, THP-1 and SEM cells were incubated with indicated concentration of I1 for 24, 48 or 72 h. After collecting the cells, they were fixed with 70% pre-chilled ethanol and stored at −20°C for at least 24 h. Then cells were washed with PBS, then stained with 50 mg/ml PI and 100 mg/ml RNase A in the dark at room temperature for 30 min. Finally, the Beckman-Coulter DXFLEX flow cytometer (Miami, Florida, United States) was used to detect the percentage of cells in G0/G1, S, and G2/M phases, and the data was analyzed and fitted using ModFit software.

Cell Apoptosis Analysis

MOLM-13, THP-1, MV4-11 and SEM cells were treated with I1 (0–2 μM) or indicated concentration of SAHA for 72 h. Cells were collected and resuspended in 1× binding buffer then incubated with FITC/Annexin V and PI double labeling in the dark at room temperature for 30 min. Finally, the apoptotic rate was detected by a Beckman-Coulter DXFLEX flow cytometer.

Analysis of Cell Morphology

MOLM-13, THP-1, MV4-11 and SEM cells were cultured with indicated concentration of I1 for 72 h, and then the cells were collected. Slides were made by cytospin and then air-dried. The cells were stained with Wright-Giemsa, and their morphological characteristics were observed with an optical microscope.

Cell Surface Antigens Measurement

The MOLM-13, THP-1, MV4-11 and SEM cells were treated with indicated concentration of I1 for 72 h, and the cells were collected and incubated with different antibodies and placed in the dark at room temperature for 30 min, then the expression of differentiation markers was determined by a Beckman-Coulter DXFLEX flow cytometer. Finally, the mean fluorescence intensity (MFI) of antigens of each experiment groups were compared with that of control using the SPSS software.

mRNA-Sequencing Analysis

mRNA-Sequencing (mRNA-seq) was performed for THP-1 and MOLM-13 cell lines. After 48 h of incubation with indicated concentration of I1, the cells were collected for RNA extraction. Sequencing libraries were prepared and then sequenced. The mRNAs expression levels were determined using FPKM (fragments per kilobase of exon per million fragments mapped). Differential expression analysis was performed using DESeq R packages. The threshold for differential expressions of genes (DEGs) is set as a corrected p value of 0.05 and absolute value of $\log_2$ FC (fold change) ≥ 0.58. The method of geometric test was used to enrich the DEGs from the Gene Ontology and Kyoto Encyclopedia of Genes and Genomes (KEGG) databases

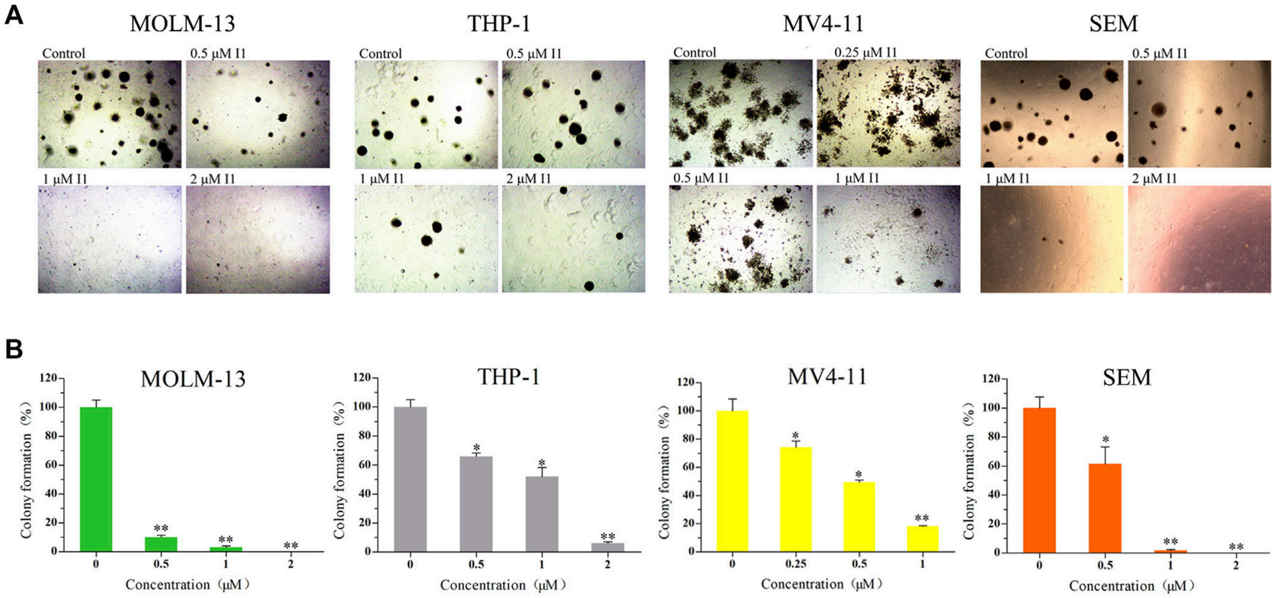

FIGURE 2 | I1 suppressed the colony formation of MOLM-13, THP-1, MV4-11 and SEM cells. **(A)** Cells were treated with I1 at the concentrations of 0.25–2 μM for 15 days then the cell morphology was observed under light microscopy. **(B)** Graph bars exhibited the statistical analysis of the number of colonies (*p < 0.05, **p < 0.01). The colony formation assay was performed three times.

for both cell lines. The clusterProfiler package of R software was used to the enrichment analysis of DEGs. The pathways with a FDR value of <0.05 were considered significantly enriched.

Verification of Expression of Differential Genes by Real-Time PCR

Trizol reagent was used to extract total RNA from MOLM-13 and THP-1 cells treated with indicated concentration of I1 for 24, 48, or 72 h. Reverse transcription of the first cDNA strand was performed using the Primerscript RT kit. The following primers are used to amplify cDNA: forward GAPDH 5′-TGGGTGTGAACCATGAGAAGT-3′, reverse GAPDH 5′-TGAGTCCTTCCACGATACCAA-3′; forward CD59 5′-CAGTGCTACAACTGTCCTAACC-3′, reverse CD59 5′-TGAGACACGCATCAAAATCAGAT-3′; forward CD13 5′-GAAGGACAGCCAGTATGAGATG-3′, reverse CD13 5′-GGATAAGCGTGATGTTGAACTC-3′; forward HLA-DRA 5′-AGTCCCTGTGCTAGGATTTTTCA-3′, reverse HLA-DRA 5′-ACATAAACTCGCCTGATTGGTC-3′; forward CIITA 5′-CCTGGAGCTTCTTAACAGCGA-3′, reverse CIITA 5′-TGTGTCGGGTTCTGAGTAGAG-3′.

Western Blotting Analysis

After treatment of MOLM-13 and THP-1 cells with indicated concentration of I1 for 72 h, the cells were collected and lysed with RIPA buffer containing protease inhibitors. The protein lysate was separated by sodium dodecyl sulfate-polyacrylamide gel (SDS-PAGE) and then transferred to PVDF membrane. After blocking the PVDF membrane with 10% skimmed milk, the membrane was incubated with specific primary antibodies at 4°C overnight, and incubated with goat anti-rabbit or goat anti-mouse immunoglobulin G (lgG) antibody for 1 h at room temperature. Finally, the enhanced chemiluminescence (ECL) reagent detection system was used to visualize the protein expression.

Statistical Analysis

All experiments were repeated for three times. All data were expressed as mean ± standard deviation (SD). One-way ANOVA was used for the comparison of experiment groups with the control using the SPSS software. $p < 0.05$ was considered statistically significant.

RESULTS

I1 Possesses Significant Anti-proliferation Activity Against AML and ALL Cells With MLL Gene Rearrangements

The effect of I1 on cell proliferation compared with SAHA was determined by CCK-8 assay. As shown in **Figure 1B**, I1 significantly reduced the proliferation of MOLM-13, THP-1, MV4-11 and SEM cells with the IC_{50} value of 1.04, 0.75, 0.58, and 0.87 μM, respectively, that was comparable with that of SAHA 0.26, 0.63, 0.44, and 0.28 μM, respectively. These results indicate that I1 can effectively inhibit the proliferation of AML and ALL cells with MLL gene rearrangements. Moreover, I1 has a similar potency of anti-proliferation as SAHA on these cells.

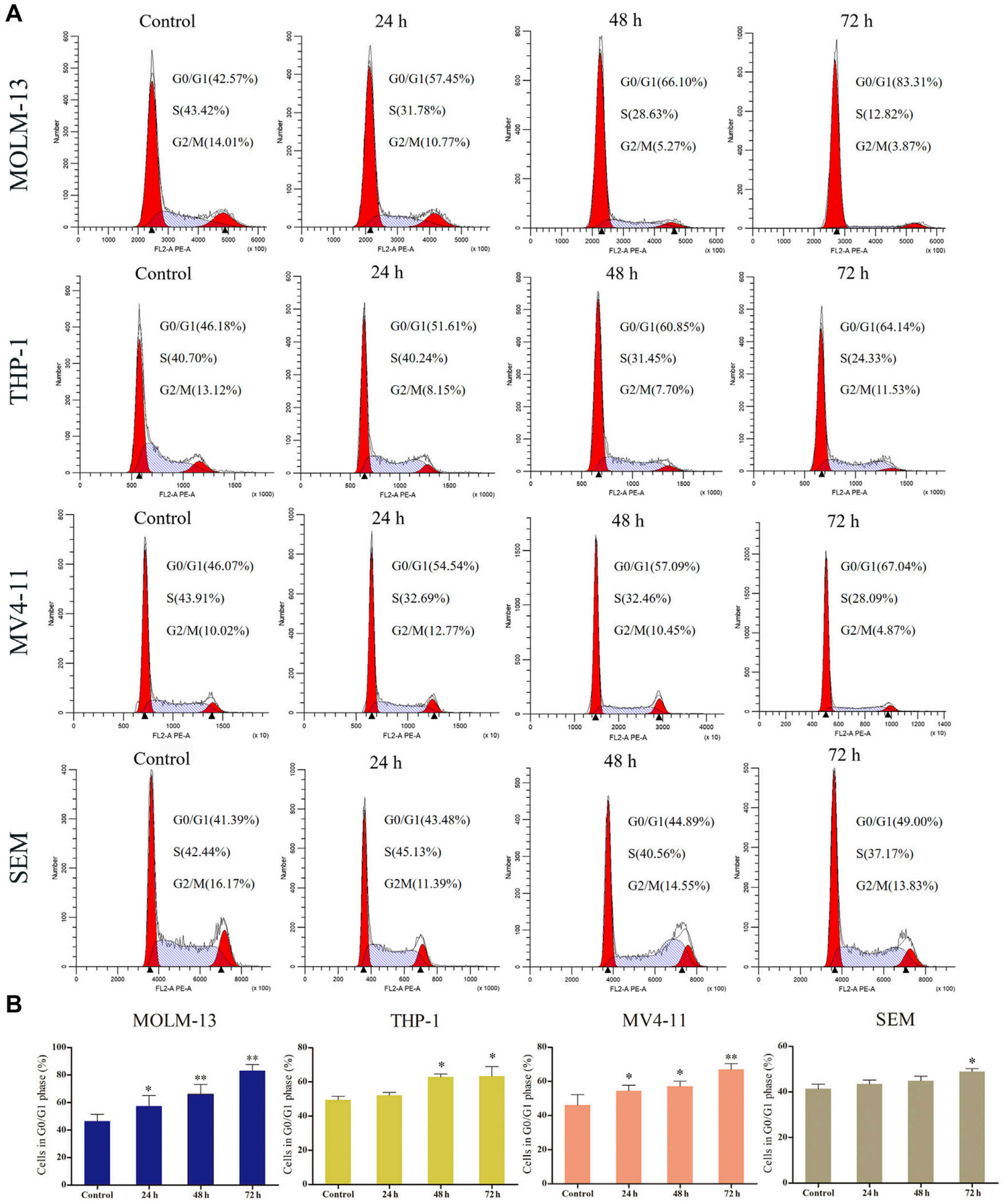

FIGURE 3 | I1 induces cell-cycle exit of MOLM-13, THP-1, MV4-11 and SEM cells. **(A)** MOLM-13, THP-1, MV4-11 and SEM cells were treated with I1 at the concentrations of 1, 0.7, 0.5 or 0.7 μM, respectively for 24, 48 or 72 h, then stained with PI, and detected using flow cytometry. **(B)** Graph bars show the percentage of cells at G0/G1 phase. (*$p < 0.05$, **$p < 0.01$). The cell cycle analysis was performed three times.

I1 Markedly Inhibits Colony Formation of AML and ALL Cells With MLL Gene Rearrangements

The effect of I1 on the colony forming ability of MOLM-13, THP-1, MV4-11 and SEM cells was explored. As shown in **Figures 2A,B**, I1 at 0.25–2 μM remarkably inhibited colony formation capacity of MOLM-13, THP-1, MV4-11 and SEM cells in a concentration-dependent manner. In addition, it was found that these cells rarely formed colonies when they were treated with I1 at a concentration of 2 μM. This result indicates that I1 could significantly inhibit the colony-formation capacity of AML and ALL cells with MLL gene rearrangements at a low concentration.

I1 Induces Cell Cycle Arrest at G0/G1 in AML and ALL Cells With MLL Gene Rearrangements

The effect of I1 on the cell cycle progression of MOLM-13, THP-1, MV4-11 and SEM cells was evaluated. As shown in **Figures 3A,B**, the percentage of cells in G0/G1 phase increased in these cells with increasing treatment time. This result suggests that I1 inhibits cell proliferation through inducing a G0/G1 cell cycle exit in MLLr -AL cells.

I1 Induces Minimal Signs of Apoptosis in AML and ALL Cells With MLL Gene Rearrangements

In order to determine whether the anti-proliferative effect of I1 on MOLM-13, THP-1, MV4-11 and SEM cells is related to the induction of apoptosis, these cells were treated with indicated concentrations of I1 or SAHA for 72 h. As shown in **Figures 4A,B**, no significant apoptosis was observed when MOLM-13, THP-1, MV4-11, and SEM cells were incubated with I1 at a concentration of no higher than 2, 1.4, 1 or 1.4 μM, respectively. In contrast, SAHA induced obvious apoptosis in all cell lines at a specific concentration, which may suggest that the mechanism for the anti-proliferation activity of I1 and SAHA is different, particularly in THP-1 and MV4-11 cells. This is consistent with the finding that SAHA induced apoptosis of acute myeloid leukemia cell line HL-60 coupled with at G0/G cell cycle arrest (Wang et al., 2007). This data indicates that the cell cycle arrest was not associated with cell apoptosis in MOLM-13, THP-1, MV4-11 and SEM cells treated with I1 at 1, 0.7, 0.5, 0.7 μM, respectively. These concentrations of I1 is used in the following experiment to explore its effect on cell differentiation. Since SAHA inhibited the proliferation of AML cell line by inducing apoptosis but not cell differentiation, we did not use it as positive control in the following experiments including morphology, the expression of differentiation markers and mRNA-seq.

I1 Promotes Cell Differentiation in AML and ALL Cells With MLL Gene Rearrangements

Since I1 did not induce apoptosis of MOLM-13, THP-1, MV4-11 and SEM cells at indicated concentrations, the morphological change and cell surface antigen were analyzed to evaluate the differentiation of these cells treated with I1. The cell phenotype was analyzed by evaluating a set of six differentiation biomarkers (CD11b (a monocyte/granulocyte marker), CD13 (a macrophage/monocyte marker), CD14 (a monocyte/macrophage monocyte/macrophage), CD15 (a monocyte/macrophage marker), CD59 (an erythrocyte marker), HLA-DP and HLA-DR (major histocompatibility complex (MHC) class II genes, immune regulation antigens)). It was found that all the cells showed increased cell size and decreased nuclear/cytoplasmic ratio, indicating that I1 induced cell differentiation with morphological changes (**Figure 5A**). Moreover, I1 increased the expression of CD59 while decreased the expression of CD13 in MOLM-13 cells. Similarly, I1 increased the expression of CD11b, CD13, CD15, and HLA-DR in THP-1 cells. In addition, the expression of CD11b and CD13 was up-regulated in the MV4-11 cells incubated with I1. Similarly, the expression of CD14 and HLA-DP increased in the SEM cells incubated with I1 (**Figures 5B,C**). These results indicate that I1 induces differentiation of AML and ALL cells with MLL gene rearrangements.

I1 Induces Cell Differentiation Through Activating Hematopoietic Cell Lineage Signaling Pathway in MOLM-13 and THP-1 Cells

We performed global gene expression analyses using mRNA-seq to explore the molecular mechanism of I1-mediated cell differentiation in MOLM-13 and THP-1 cells. It was found that 352 genes were up-regulated and 329 genes were down-regulated in MOLM-13 cells. Similarly, the expression of 175 genes increased and the expression of 212 genes decreased in THP-1 cells, indicating that I1 has different effects on the expression of genes. The volcano maps of these genes in MOLM-13 and THP-1 are shown in **Figure 6A**. This result suggested that the effect of I1 on the mRNA expression of all genes is not universal in these cells. As shown in **Figure 6B**, CD59, HLA-DQB1, HLA-DMA, CR1 and IL7R were significantly up-regulated, while ANPEP (CD13), CD9, FCER2 (CD23) and TNF were markedly down-regulated in MOLM-13 cells incubated with I1. Similarly, HLA-DRA, HLA-DQB1, HLA-DRB5, and CIITA were significantly up-regulated whereas CD36, KITLG and TNF were markedly down-regulated in THP-1 cells treated with I1. Furthermore, the KEGG analysis showed that these differentially expressed genes (CD59, HLA-DQB1, HLA-DMA, CR1, IL7R, CD13, CD9, CD23 and TNF) were enriched in hematopoietic cell lineage signaling pathway in MOLM-13 cells, and HLA-DRA, HLA-DQB1, HLA-DRB5, CD36, KITLG and TNF genes were also enriched in hematopoietic cell lineage signaling pathway in THP-1 cells (**Figure 6C**).

In addition, some representative differentially expressed genes screened by mRNA-seq were confirmed by RT-PCR and Western blotting in MOLM-13 and THP-1 cells. As shown in **Figures 7A–C**, I1 treatment significantly changed the expression of CD59 and CD13 mRNA and protein in MOLM-13 cells. In THP-1 cells, the transcription and protein levels of HLA-DRA and CIITA were significantly up-regulated. These results are consistent with the expression identified by mRNA-seq.

Since I1 is a HDAC inhibitor, we explored the effect of I1 on the activity of HDAC inhibition by determining the level of acetylated histone protein H3 and H4 *via* Western blotting analysis. As shown in **Figures 7B,C**, the acetylated histone H3 and H4 increased in a concentration-dependent manner in MOLM-13 and THP-1 cells treated with I1. Moreover, at the concentration of 1 and 0.7 μM, at which I1 did not induce cell apoptosis but promoted cell differentiation of MOLM-13 and THP-1 cells, respectively, the level of acetylated H3 and H4 is higher in THP-1 cells than that in MOLM-13 cells. In contrast,

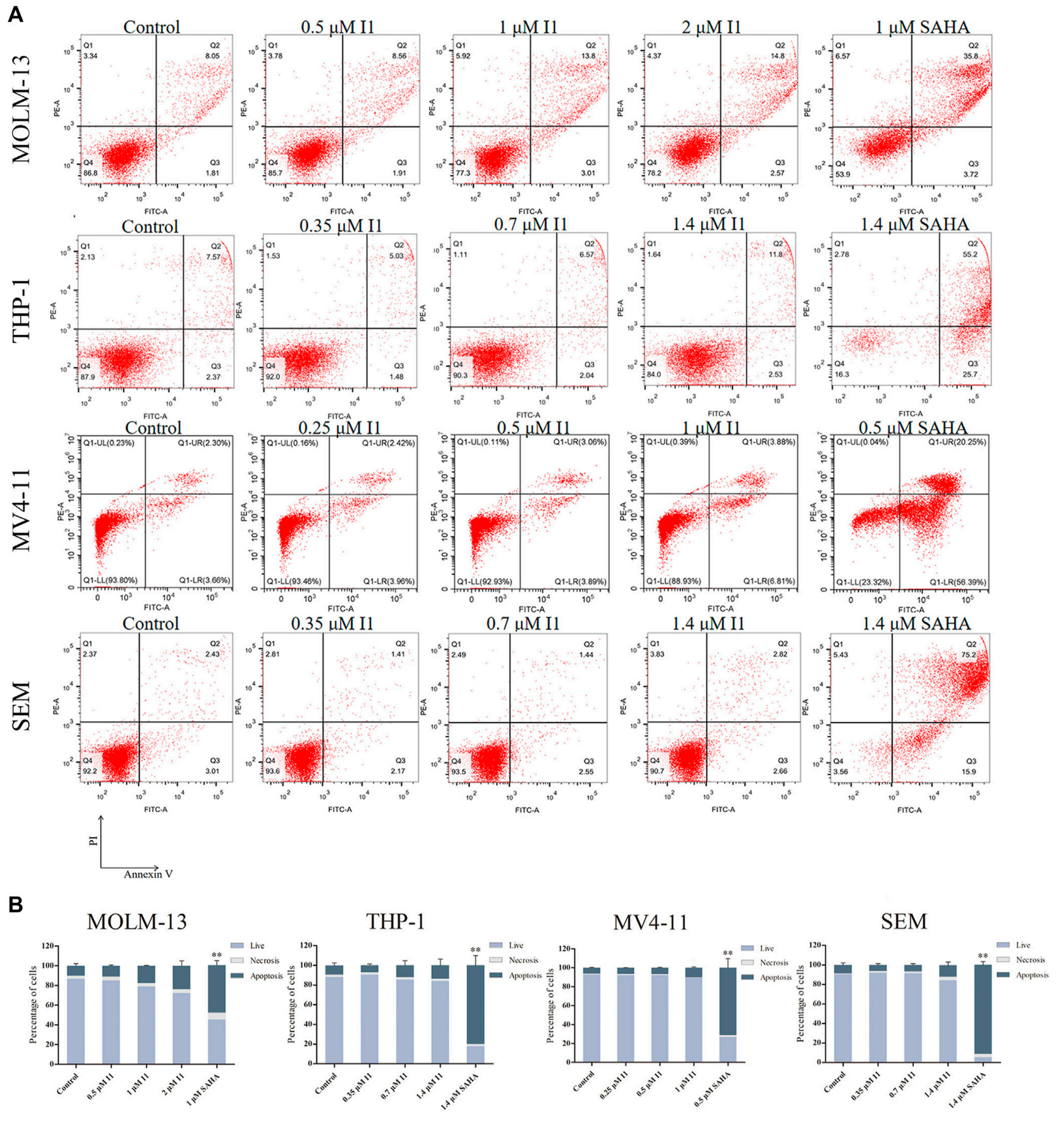

FIGURE 4 | I1 does not induce apoptosis in MOLM-13, THP-1, MV4-11 and SEM cells. **(A)** Cells were treated with I1 or SAHA for 72 h and cell apoptotic rate was determined quantitatively using a flow cytometric apoptosis assay. **(B)** Graph bars show the statistical analysis of apoptosis ratio. MOLM-13 cell was treated with 0.5, 1, 2 μM I1 or 1 μM SAHA. MV4-11 cell was treated with 0.25, 0.5, 1 μM I1 or 0.5 μM SAHA. THP-1 and SEM cells were treated with 0.35, 0.7, 1.4 μM I1 or 1.4 μM SAHA for 72 h (**$p < 0.01$). The analysis of cell apoptotic rate was performed three times.

the same concentration of SAHA did not increase in the acetylated histone H4 in MOLM-13 cells and did not alter the level of acetylated histone protein H3 and H4 in THP-1 cells. This data suggested that the activity of HDAC inhibition of I1 is stronger than that of SAHA in MOLM-13 and THP-1 cells at comparative treatment concentration.

DISCUSSION

It is well documented that about 10%–20% of patients with acute leukemia carry chromosomal rearrangements involving the MLL gene (Pui et al., 2002; Xu et al., 2020). MLLr-AML mainly occurs in young-to-middle-aged adults whereas MLLr-ALL manifests

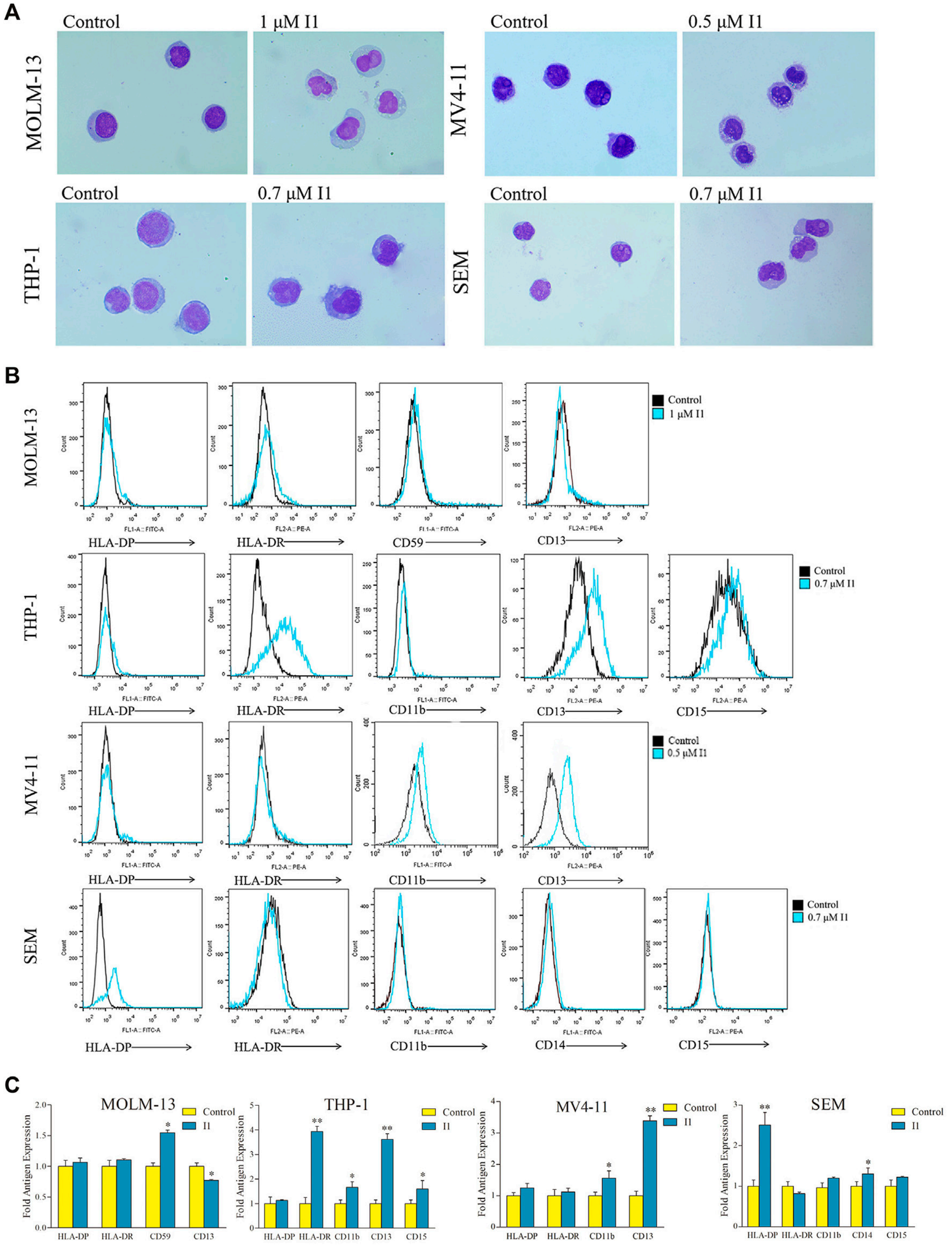

FIGURE 5 | I1 induces differentiation of MOLM-13, THP-1, MV4-11 and SEM cells. **(A)** The morphology of Wright-Giemsa stained cells examined by oil immersion lens (×1,000). **(B)** The expression of different antigens of cells measured by flow cytometry. **(C)** Graph bars show the mean fluorescence intensity (MFI) of antigens. MOLM-13, THP-1, MV4-11 and SEM cells were incubated with 1, 0.7, 0.5 or 0.7 μM I1, repectively for 72 h (**p* < 0.05, ***p* < 0.01). The figures are representative of three independent experiments.

predominantly in infants younger than 1- year-old. Despite great improvements in the treatment of AML and ALL, literature data suggest that most patients with MLLr-AL have poor clinical outcome (Balgobind et al., 2009; Szczepański et al., 2010). Therefore, there is a pressing need for the development of alternative or complementary therapies against MLLr-AML

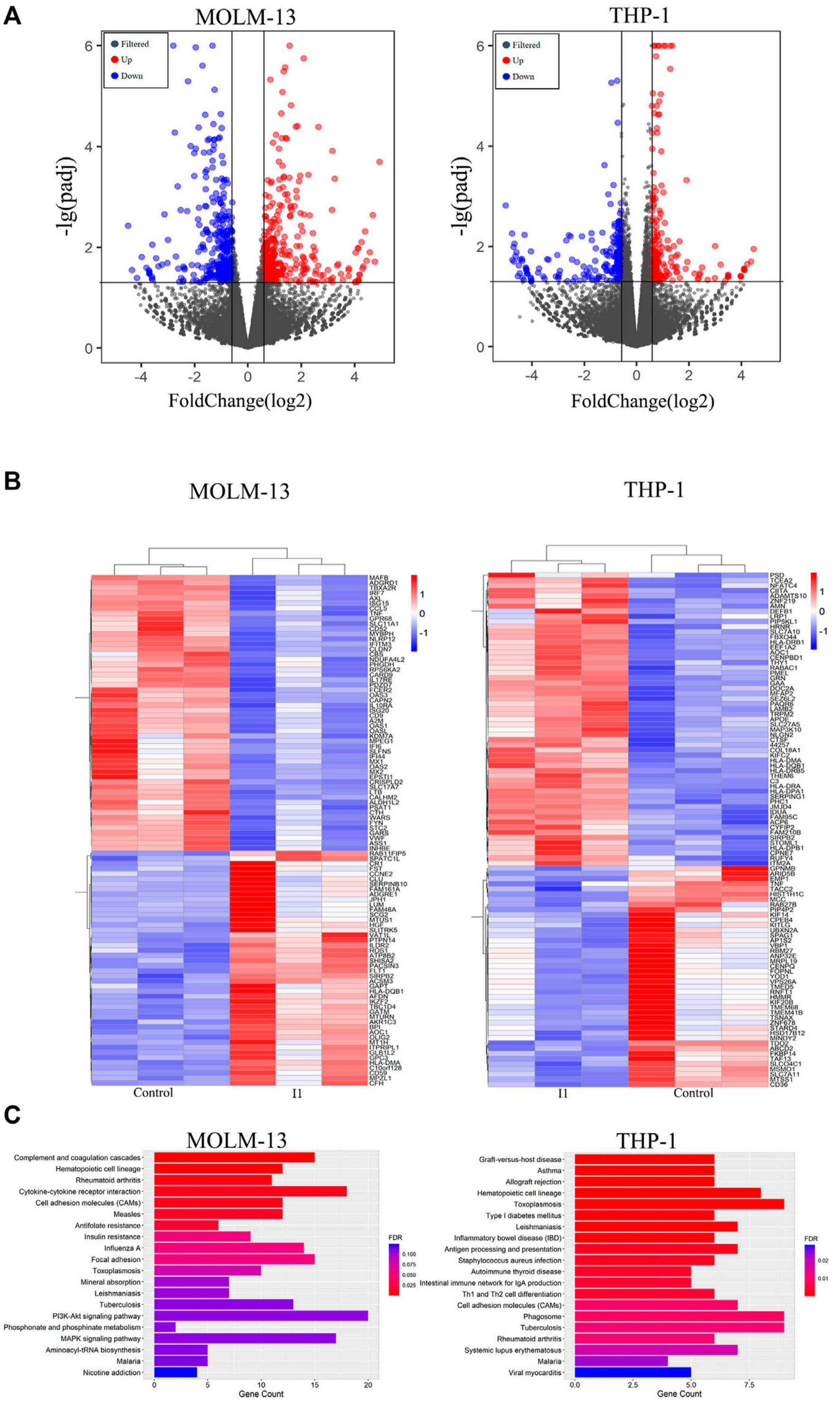

FIGURE 6 | I1 promotes cell differentiation *via* activating hematopoietic cell lineage pathway in MOLM-13 and THP-1 Cells. **(A)** Volcano plots of MOLM-13 and THP-1 cells. **(B)** The heatmap of differentially expressed genes (DEGs). The bars from blue to red denotes the expression levels of DEGs from low to high. (100 genes with $p < 0.05$ and $|\log 2 \text{ FC}| > 0.58$ based on their p value in both cell lines). **(C)** KEGG pathway analyses on all DEGs. MOLM-13 and THP-1 cells were incubated with 1, or 0.7 μM I1, respectively for 48 h. The figures are representative of three independent experiments.

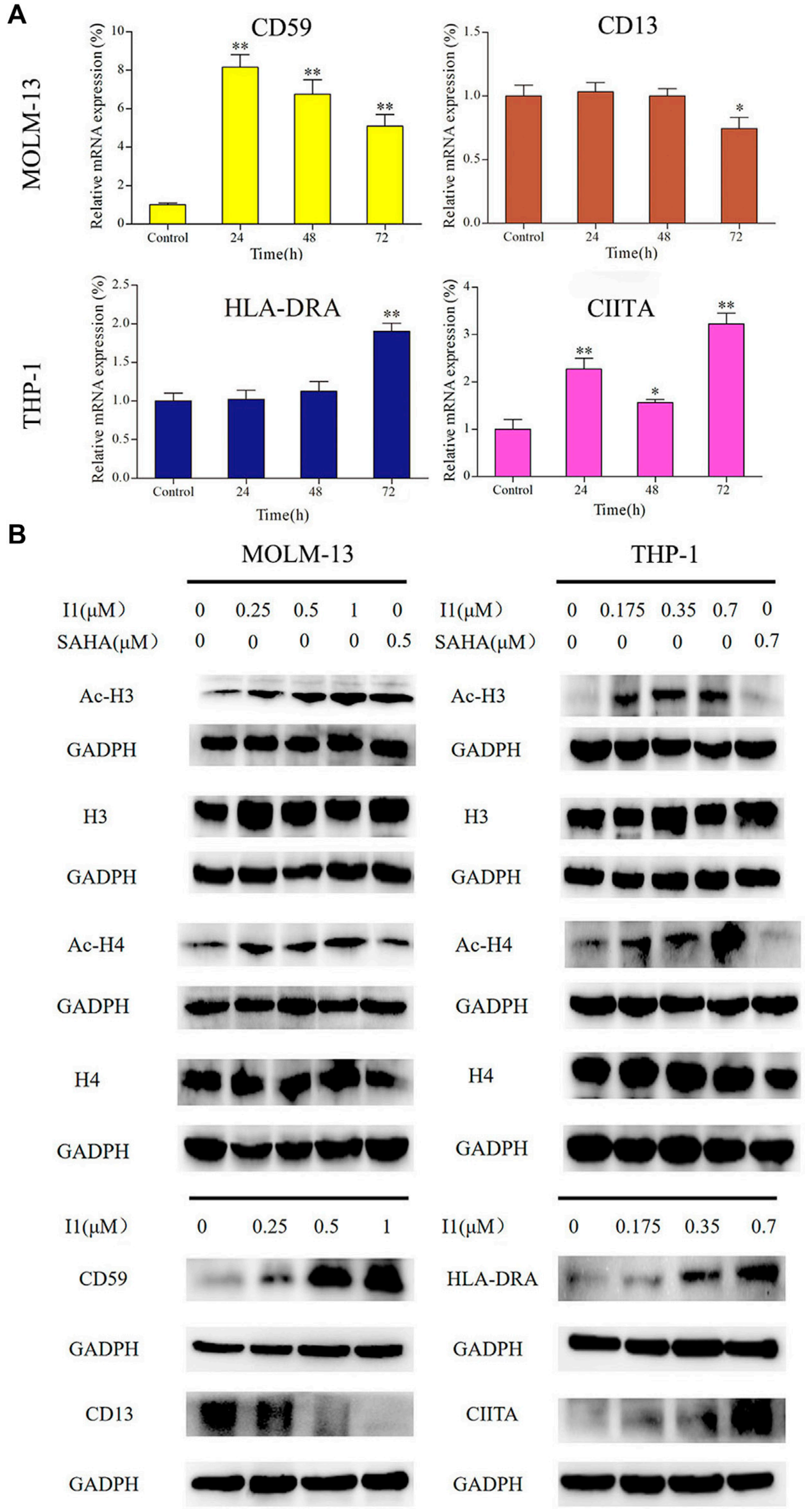

FIGURE 7 | The RT-PCR and Western blotting analysis of cell differentiation related genes in MOLM-13 and THP-1 cell lines. **(A)** The effects of I1 on the mRNA expression of CD59, CD13, HLA-DRA and CIITA evaluated by RT-PCR. MOLM-13 and THP-1 cells were incubated with 1, or 0.7 μM I1 repectively, for 24, 48, or 72 h **(B)** H3, Ac-H3, H4, Ac-H4, CD59, CD13, HLA-DRA and CIITA protein levels measured by Western blotting analysis. **(C)** Graph bars show the protein expression visualized and quantified by AI600 imager. MOLM-13 were incubated with 0.25, 0.5, 1 μM I1, or 0.5 μM SAHA for 72 h. THP-1 cells were incubated with 0.175, 0.35, 0.7 μM I1, or 0.7 μM SAHA for 72 h(*$p < 0.05$, **$p < 0.01$).

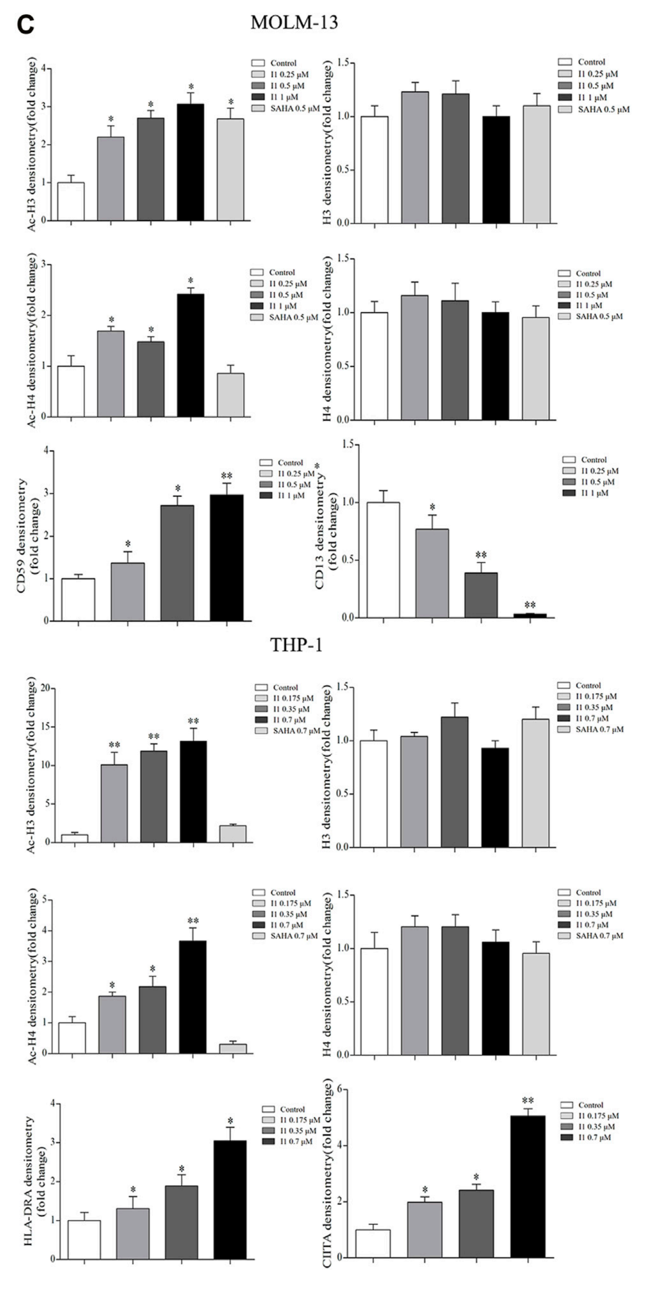

FIGURE 7 | Continued.

and MLLr-ALL. Many efforts have been made to develop inhibitors for MLL-MEN1 and MLL-LEDGF interactions, the SET domain of MLL and AF4-MLL, DOT1L and BET proteins (BRD4) (Marschalek, 2015). However, further clinical evaluation is required for these new drugs. Moreover, the impact of these new drugs on both MLL and DOT1L must be very carefully assessed in order to avoid side-effects.

Epigenetic modification regulates gene expression in the absence of alterations in DNA sequences but through nucleosome structural modification (Vidal et al., 2014). Histone modification, a key mechanism of epigenetic regulation, control gene expression by changing the configuration of chromatin and modifying the access of transcription factors to gene promoters (Li et al., 2021). The histone modifications include methylation, acetylation, phosphorylation, ubiquitination, ADP-ribosylation, and sumoylation. Among these, histone acetylation and methylation are most commonly assessed (Manal et al., 2016). Histone deacetylases (HDACs) are chromatin-remodeling enzymes whose enzymatic activity controls the acetylation of histone or non-histone proteins through its influence on chromatin conformation (Johnstone, 2002). Furthermore, histone acetylation affects the transcription and gene replication to activate gene expression. Thus, HDACs play a key epigenetic function as they remove acetyl group from histone or non-histone proteins to regulate gene expression. Therefore, HDACi have been shown to own the activity to induce differentiation or apoptosis and to inhibit cell proliferation in solid or hematopoietic cancers *via* the acetylation of histone or non-histone proteins both *in vitro* and *in vivo* (Göttlicher et al., 2001; Nebbioso et al., 2005). HDACis are generally divided into five groups based on the chemical structure, including hydroxamic acids, cyclic peptides, aminobenzamides, carboxylic acids, and hybrid molecules.

Compared with SAHA (Suberoylanilide hydroxamic acid), I1 is an indole-3-butyric acid bearing HDAC inhibitor with phenyl group in the linker. Similarly, hydroxamic acid group was utilized as the zinc binding group of I1 (**Figure 1A**). Our previous study demonstrated that I1 exhibited considerable HDAC inhibitory activity compared with SAHA in a study which investigated the enzyme inhibitory potency using HeLa nuclear extract containing a mixture of HDAC isoforms (Chen et al., 2021). This study at the first study showed that I1 had the differentiation-inducing activity in MLLr-AML and MLLr-AL cells. We showed that I1 significantly inhibited the cell proliferation and colony forming ability of MOLM-13, THP-1, MV4-11 and SEM cells by inducing cell differentiation, which is confirmed by the morphological changes and alteration on the expression of the cell surface antigens CD11b, CD13, CD14, CD15, CD59, HLA-DP or HLA-DR. Furthermore, cell differentiation was accompanied by G0/G1 cell cycle exit. Mechanistically, it was revealed that the hematopoietic cell lineage signaling pathway was engaged in the MOLM-13 and THP-1 cells treated with I1. Moreover, it is revealed that I1 showed marked HDAC inhibitory activity through the acetylation of histone H3 and H4 in MOLM-13 and THP-1 cells. In addition, the effect of I1 on the HDAC inhibition activity in THP-1 cells is higher than that in MOLM-13 cells, which is consistent with the IC_{50} values of I1 towards MOLM-13 and THP-1 cells. Taken together, we found that I1 induces cell differentiation and inhibits cell proliferation in MLLr-AML and MLLr-ALL cells.

Genes including CD59, CD13, HLA-DQB1, HLA-DMA, CR1, IL7R, CD9, CD23 and TNF were significantly enriched in hematopoietic cell lineage signaling pathway in MOLM-13 cells. HLA-DRA, HLA-DQB1, HLA-DRB5, CD36, KITLG and TNF were enriched in the signaling pathway in THP-1 cells. It is known that hematopoietic cell lineage signaling pathway, a differentiation-related pathway, denotes the development and differentiation of the hematopoietic cells into various cell types of hematopoietic lineages such as erythrocytes, neutrophils, basophils, eosinophils, macrophages, and myeloid derived dendritic cells (Tenen, 2003; Zhang et al., 2017). Our present study showed that I1 treatment induced cell differentiation with morphological changes, increasing the expression of CD59 and HLA-DR and decreasing the expression of CD13 in MOLM-13 cells. Similarly, I1 up-regulated the expressions of HLA-DR, CD11b, CD13, CD15 in THP-1 cells. I1 treatment also significantly increased the mRNA and protein level of CIITA (a HLA trans-activator) and HLA-DRA in THP-1 cells. This data was in consistent with the finding that up-regulation of CIITA expression enhances the expression of HLA class II antigens (Lazzaro et al., 2001). Therefore, I1-mediated differentiation of MOLM-13 and THP-1 cells might be associated with the hematopoietic cell lineage pathway.

As mentioned above, I1 exhibited significant HDAC inhibitory activity assessed by the acetylation of histone H3 and H4 in MOLM-13 and THP-1 cells. Moreover, growing evidence suggests that HDACi such as valproic acid (VPA) and trichostatin A (TSA), and chromatin-remodeling agents, induced myeloid precursors committed to cell differentiation (Milhem et al., 2004; Bug et al., 2005; De Felice et al., 2005). It reveals that cell fate involved in lineage commitment might be dictated by targeting enzymes with chromatin-remodeling activity such as HDACs (Zardo et al., 2008). Therefore, I1 treatment induces cell differentiation likely originate from the HDAC inhibition activity, as assessed by the acetylation of histone H3 and H4, which may trigger the hematopoietic cell lineage pathway.

In conclusion, our findings show that the HDAC inhibitor I1, as a chromatin-remodeling agent, has a marked anti-proliferative effect on MLLr-AML and MLLr-ALL cells by inducing cell differentiation. Importantly, I1 presented the properties of HDAC inhibition and activated the hematopoietic cell lineage signaling pathway. Moreover, the HDAC inhibition effect of I1 is higher than that of SAHA. I1 could overcome the cell differentiation block of MLLr-AL cells, indicating that I1 could be a potential epigenetic drug worth of further investigation including *in vivo* studies and anti-proliferation activity on primary myeloid leukemia cells and development to surmount differentiation block and be effective in MLLr-AL. Moreover, the induction of cell differentiation would be promising for the treatment of AL.

DATA AVAILABILITY STATEMENT

The datasets presented in this study can be found in online repositories. The names of the repository/repositories and accession number(s) can be found below: https://www.ncbi.nlm.nih.gov; GSE193965.

AUTHOR CONTRIBUTIONS

JY: conceptualization, methodology, and writing-original draft. GL, ZC, PC, JW: methodology. ZH: supervision. LZ: conceptualization and supervision. LW: editing and supervision. All authors contributed to the article and approved the submitted version.

FUNDING

The research was supported by the grant of Shandong Provincial Natural Science Foundation of China (ZR2020KC016 to ZH), the Weifang Science and Technology Bureau (2020YQFK013 to ZH). Natural Science Foundation of Shandong Province (ZR2016HM47 to LW). Science and technology support plan for youth innovation in universities of Shandong Province (2019KJM001 to LZ), Natural Foundation of Shandong Province (Youth Found, ZR2019QH005 to LZ) and the innovation training program for college students of Shandong Province (Grant X2021376 to ZC).

REFERENCES

Allen, T., and Ahmed, A. (2016). Immunotherapy and Acute Lymphoblastic Leukemia. *EC Cancer* 2, 141–147.

Balgobind, B. V., Raimondi, S. C., Harbott, J., Zimmermann, M., Alonzo, T. A., Auvrignon, A., et al. (2009). Novel Prognostic Subgroups in Childhood 11q23/MLL-Rearranged Acute Myeloid Leukemia: Results of an International Retrospective Study. *Blood* 114 (12), 2489–2496. doi:10.1182/blood-2009-04-215152

Bug, G., Gül, H., Schwarz, K., Pfeifer, H., Kampfmann, M., Zheng, X., et al. (2005). Valproic Acid Stimulates Proliferation and Self-Renewal of Hematopoietic Stem Cells. *Cancer Res.* 65 (7), 2537–2541. doi:10.1158/0008-5472.CAN-04-3011

Chen, Y., Zhang, L., Zhang, L., Jiang, Q., and Zhang, L. (2021). Discovery of Indole-3-Butyric Acid Derivatives as Potent Histone Deacetylase Inhibitors. *J. Enzyme Inhib. Med. Chem.* 36 (1), 425–436. doi:10.1080/14756366.2020.1870457

De Felice, L., Tatarelli, C., Mascolo, M. G., Gregorj, C., Agostini, F., Fiorini, R., et al. (2005). Histone Deacetylase Inhibitor Valproic Acid Enhances the Cytokine-Induced Expansion of Human Hematopoietic Stem Cells. *Cancer Res.* 65 (4), 1505–1513. doi:10.1158/0008-5472.CAN-04-3063

George, A. A., Franklin, J., Kerkof, K., Shah, A. J., Price, M., Tsark, E., et al. (2001). Detection of Leukemic Cells in the Cd34(+)cd38(-) Bone Marrow Progenitor Population in Children with Acute Lymphoblastic Leukemia. *Blood* 97 (12), 3925–3930. doi:10.1182/blood.V97.12.3925

Gole, B., and Wiesmüller, L. (2015). Leukemogenic Rearrangements at the Mixed Lineage Leukemia Gene (MLL)-multiple rather Than a Single Mechanism. *Front. Cel Dev. Biol.* 3, 41. doi:10.3389/fcell.2015.00041

Göttlicher, M., Minucci, S., Zhu, P., Krämer, O. H., Schimpf, A., Giavara, S., et al. (2001). Valproic Acid Defines a Novel Class of HDAC Inhibitors Inducing Differentiation of Transformed Cells. *EMBO J.* 20 (24), 6969–6978. doi:10.1093/emboj/20.24.6969

Johnstone, R. W. (2002). Histone-deacetylase Inhibitors: Novel Drugs for the Treatment of Cancer. *Nat. Rev. Drug Discov.* 1, 287–299. doi:10.1038/nrd772

Lazzaro, B., Anderson, A. E., Kajdacsy-Balla, A., and Hessner, M. J. (2001). Antigenic Characterization of Medullary Carcinoma of the Breast: HLA-DR Expression in Lymph Node Positive Cases. *Appl. Immunohistochem. Mol. Morphol.* 9 (3), 234–241. doi:10.1097/00129039-200109000-00007

Li, K., Han, J., and Wang, Z. (2021). Histone Modifications Centric-Regulation in Osteogenic Differentiation. *Cell Death Discov.* 7 (1), 91. doi:10.1038/s41420-021-00472-6

Manal, M., Chandrasekar, M. J. N., Gomathi Priya, J., and Nanjan, M. J. (2016). Inhibitors of Histone Deacetylase as Antitumor Agents: A Critical Review. *Bioorg. Chem.* 67, 18–42. doi:10.1016/j.bioorg.2016.05.005

Manzotti, G., Ciarrocchi, A., and Sancisi, V. (2019). Inhibition of BET Proteins and Histone Deacetylase (HDACs): Crossing Roads in Cancer Therapy. *Cancers (Basel)* 11 (3), 304–331. doi:10.3390/cancers11030304

Marschalek, R. (2015). MLL Leukemia and Future Treatment Strategies. *Arch. Pharm. (Weinheim)* 348 (4), 221–228. doi:10.1002/ardp.201400449

Milhem, M., Mahmud, N., Lavelle, D., Araki, H., DeSimone, J., Saunthararajah, Y., et al. (2004). Modification of Hematopoietic Stem Cell Fate by 5aza 2'deoxycytidine and Trichostatin A. *Blood* 103 (11), 4102–4110. doi:10.1182/blood-2003-07-2431

Nebbioso, A., Clarke, N., Voltz, E., Germain, E., Ambrosino, C., Bontempo, P., et al. (2005). Tumor-selective Action of HDAC Inhibitors Involves TRAIL Induction in Acute Myeloid Leukemia Cells. *Nat. Med.* 11 (1), 77–84. doi:10.1038/nm1161

O'Connor, O. A., Heaney, M. L., Schwartz, L., Richardson, S., Willim, R., MacGregor-Cortelli, B., et al. (2006). Clinical Experience with Intravenous and Oral Formulations of the Novel Histone Deacetylase Inhibitor Suberoylanilide Hydroxamic Acid in Patients with Advanced Hematologic Malignancies. *J. Clin. Oncol.* 24 (1), 166–173. doi:10.1200/JCO.2005.01.9679

Prange, K. H. M., Mandoli, A., Kuznetsova, T., Wang, S. Y., Sotoca, A. M., Marneth, A. E., et al. (2017). MLL-AF9 and MLL-AF4 Oncofusion Proteins Bind a Distinct Enhancer Repertoire and Target the RUNX1 Program in 11q23 Acute Myeloid Leukemia. *Oncogene* 36, 3346–3356. doi:10.1038/onc.2016.488

Pui, C. H., Gaynon, P. S., Boyett, J. M., Chessells, J. M., Baruchel, A., Kamps, W., et al. (2002). Outcome of Treatment in Childhood Acute Lymphoblastic Leukaemia with Rearrangements of the 11q23 Chromosomal Region. *Lancet* 359 (9321), 1909–1915. doi:10.1016/S0140-6736(02)08782-2

Rosato, R. R., Almenara, J. A., and Grant, S. (2003). The Histone Deacetylase Inhibitor MS-275 Promotes Differentiation or Apoptosis in Human Leukemia Cells through a Process Regulated by Generation of Reactive Oxygen Species and Induction of p21CIP1/WAF1 1. *Cancer Res.* 63 (13), 3637–3645. doi:10.1109/APS.1989.134877

Schoch, C., Schnittger, S., Klaus, M., Kern, W., Hiddemann, W., and Haferlach, T. (2003). AML with 11q23/MLL Abnormalities as Defined by the WHO Classification: Incidence, Partner Chromosomes, FAB Subtype, Age Distribution, and Prognostic Impact in an Unselected Series of 1897 Cytogenetically Analyzed AML Cases. *Blood* 102 (7), 2395–2402. doi:10.1182/blood-2003-02-0434

Szczepański, T., Harrison, C. J., and van Dongen, J. J. (2010). Genetic Aberrations in Paediatric Acute Leukaemias and Implications for Management of Patients. *Lancet Oncol.* 11, 880–889. doi:10.1016/S1470-2045(09)70369-9

Tenen, D. G. (2003). Disruption of Differentiation in Human Cancer: AML Shows the Way. *Nat. Rev. Cancer* 3 (2), 89–101. doi:10.1038/nrc989

Vidal, S. J., Rodriguez-Bravo, V., Galsky, M., Cordon-Cardo, C., and Domingo-Domenech, J. (2014). Targeting Cancer Stem Cells to Suppress Acquired Chemotherapy Resistance. *Oncogene* 33, 4451–4463. doi:10.1038/onc.2013.411

Wang, Z. Y., and Chen, Z. (2008). Acute Promyelocytic Leukemia: from Highly Fatal to Highly Curable. *Blood* 111 (5), 2505–2515. doi:10.1182/blood-2007-07-102798

Wang, Y., Wang, S. Y., Hou, C. M., Xu, Y. J., Du, Z. Y., and Yu, X. D. (2007). Histone Deacetylase Inhibitor SAHA Induces Inactivation of MAPK Signaling and Apoptosis in HL-60 Cells. *Zhongguo Shi Yan Xue Ye Xue Za Zhi* 15 (2), 267–271.

West, A. C., and Johnstone, R. W. (2014). New and Emerging HDAC Inhibitors for Cancer Treatment. *J. Clin. Invest.* 124 (1), 30–39. doi:10.1172/JCI69738

Wuchter, C., Harbott, J., Schoch, C., Schnittger, S., Borkhardt, A., Karawajew, L., et al. (2000). Detection of Acute Leukemia Cells with Mixed Lineage Leukemia (MLL) Gene Rearrangements by Flow Cytometry Using Monoclonal Antibody 7.1. *Leukemia* 14 (7), 1232–1238. doi:10.1038/sj.leu.2401840

Xu, X., Wang, L., Hu, L., Dirks, W. G., Zhao, Y., Wei, Z., et al. (2020). Small Molecular Modulators of Jmjd1c Preferentially Inhibit Growth of Leukemia Cells. *Int. J. Cancer* 146 (2), 400–412. doi:10.1002/ijc.32552

Yu, Z. Y., Xiao, H., Wang, L. M., Shen, X., Jing, Y., Wang, L., et al. (2016). Natural Product Vibsanin a Induces Differentiation of Myeloid Leukemia Cells through Pkc Activation. *Cancer Res.* 76, 2698–2709. doi:10.1158/0008-5472.CAN-15-1616

Zardo, G., Cimino, G., and Nervi, C. (2008). Epigenetic Plasticity of Chromatin in Embryonic and Hematopoietic Stem/progenitor Cells: Therapeutic Potential of Cell Reprogramming. *Leukemia* 22 (8), 1503–1518. doi:10.1038/leu.2008.141

Zhang, Q., Chen, L., Cui, S., Li, Y., Zhao, Q., Cao, W., et al. (2017). Expression and Regulation of Long Noncoding RNAs during the Osteogenic Differentiation of Periodontal Ligament Stem Cells in the Inflammatory Microenvironment. *Sci. Rep.* 7 (1), 13991. doi:10.1038/s41598-017-14451-4

Conflict of Interest: The authors declare that the research was conducted in the absence of any commercial or financial relationships that could be construed as a potential conflict of interest.

Publisher's Note: All claims expressed in this article are solely those of the authors and do not necessarily represent those of their affiliated organizations, or those of the publisher, the editors, and the reviewers. Any product that may be evaluated in this article, or claim that may be made by its manufacturer, is not guaranteed or endorsed by the publisher.

Copyright © 2022 Yao, Li, Cui, Chen, Wang, Hu, Zhang and Wei. This is an open-access article distributed under the terms of the Creative Commons Attribution License (CC BY). The use, distribution or reproduction in other forums is permitted, provided the original author(s) and the copyright owner(s) are credited and that the original publication in this journal is cited, in accordance with accepted academic practice. No use, distribution or reproduction is permitted which does not comply with these terms.

frontiers | Frontiers in Pharmacology

ORIGINAL RESEARCH
published: 18 May 2022
doi: 10.3389/fphar.2022.888243

CNST is Characteristic of Leukemia Stem Cells and is Associated With Poor Prognosis in AML

Haoyu Liu[1†], Xu Zhang[1†], Ziyan Zhao[1], Hongying Zhu[1], Danyang Li[1,2], Yang Yang[1,3], Wenbo Zhao[4], Fei Zhang[1], Yuefeng Wang[1], Lina Zhu[1], Zewen Ding[5] and Xiangzhi Li[1]*

[1]Shandong Provincial Key Laboratory of Animal Cell and Developmental Biology, School of Life Sciences, Advanced Medical Research Institute, Shandong University, Qingdao, China, [2]Rehabilitation Center, Qilu Hospital, Cheelo College of Medicine, Shandong University, Jinan, China, [3]School of Pharmacy, Binzhou Medical University, Yantai, China, [4]Department of Hematology, Shandong Provincial Hospital Affiliated to Shandong First Medical University, Jinan, China, [5]Centre for Discovery Brain Sciences, University of Edinburgh, Edinburgh, United Kingdom

OPEN ACCESS

Edited by:
Haichang Li,
The Ohio State University,
United States

Reviewed by:
Hui Zhang,
Chinese Academy of Medical Sciences, China
Wen-Jie Song,
Kumamoto University Hospital, Japan

***Correspondence:**
Xiangzhi Li
xiangzhi@sdu.edu.cn

[†]These authors have contributed equally to this work

Specialty section:
This article was submitted to Experimental Pharmacology and Drug Discovery,
a section of the journal Frontiers in Pharmacology

Received: 02 March 2022
Accepted: 28 March 2022
Published: 18 May 2022

Citation:
Liu H, Zhang X, Zhao Z, Zhu H, Li D, Yang Y, Zhao W, Zhang F, Wang Y, Zhu L, Ding Z and Li X (2022) CNST is Characteristic of Leukemia Stem Cells and is Associated With Poor Prognosis in AML.
Front. Pharmacol. 13:888243.
doi: 10.3389/fphar.2022.888243

Consortin (CNST) is a protein located on the trans-Golgi network that can target transmembrane proteins to the plasma membrane. Although CNST was discovered more than 10 years ago, there are still not enough studies on its function. During our search for possible new acute myeloid leukemia (AML) markers, we found that CNST was overexpressed in almost all patients with AML. By analyzing profiling data from public databases, we found that CNST expression inversely correlated with overall survival among AML patients. There was a great variation in CNST expression among different subtypes of AML, and the expression was the highest in the t(8,21) subtype, which was probably due to the direct regulation of CNST transcription by RUNX1-RUNX1T1. In addition, we analyzed the expression of CNST in different cells of the hematopoietic system. We found that CNST was associated with the low differentiation degrees of hematopoietic cells and had the highest expression level in leukemia stem cells (LSCs). Finally, we analyzed the CNST-related gene network and found that the genes negatively correlated with CNST are involved in various immune-related pathways, which indicates that CNST is likely related to immune evasion, LSC niche retention, and assembly of stress granules. In conclusion, our study suggests that CNST has the potential to be a diagnostic and prognostic biomarker for AML.

Keywords: acute myeloid leukemia, consortin, leukemia stem cell, prognosis, biomarker

INTRODUCTION

Acute myeloid leukemia (AML) is a malignant disease that occurs in the hematopoietic system. It is characterized by abnormal proliferation and differentiation of hematopoietic stem cells (HSCs) (Khwaja et al., 2016). The proliferation of immature myeloid cells leads to the accumulation of immature progenitor cells, which impairs normal hematopoiesis and causes severe infection, anemia, and hemorrhage (Newell and Cook, 2021). Standard intensive chemotherapy with combination of anthracyclines and cytarabine for AML has been used for more than 40 years (Dombret and Gardin, 2016). Recent progresses in molecular biology, have gradually offered a deeper understanding of the pathophysiology of AML. Consequently, many different treatment options have been derived, which enables us to provide more individualized treatment plans for different patients (Carter et al., 2020).

However, AML is still considered a disease that is complicated and difficult to treat, suggesting that more effective and targeted treatments are still needed.

Consortin (CNST) is a receptor located on the trans-Golgi network (TGN) and cytoplasmic transport vesicles (del Castillo et al., 2010), which is a binding partner of connexins for the plasma membrane targeting and recycling of connexins. CNST directly interacts with the TGN clathrin linkers GGA1 and GGA2, and knockdown of CNST results in a decrease in the number of connexin plaques at the plasma membrane (del Castillo et al., 2010).

CNST is thought to be involved in pathways related to inherited non-syndromic hearing impairment (DFNB1) (del Castillo et al., 2010); in mice, CNST may affect bone volume and microarchitecture (Mohan et al., 2013); the expression level of CNST increased during the depolarization of rat myocardial fibroblasts after the addition of TGF-β1 (Salvarani et al., 2017). Currently, there is limited research on CNST and the diseases it may affect.

In this study, we investigated the expression of CNST in the blood system and AML, and its impact on the prognosis of AML by analyzing data from public databases. Moreover, the possible function of CNST in AML was analyzed.

MATERIALS AND METHODS

Public Database

CNST expression data for 33 tumors were obtained from Gene Expression Profiling Interactive Analysis (GEPIA) (Tang et al., 2017). Gene expression data were obtained from the Beat AML (Tyner et al., 2018) http://www.vizome.org/additional_figures_BeatAML.html, and the Gene Expression Omnibus (GEO) repository [https://www.ncbi.nlm.nih.gov/gds.GSE13159 (Haferlach et al., 2010), GSE114868 (Huang et al. , 2019), GSE15061 (Mills et al., 2009), GSE63270 (Jung et al., 2015), GSE75384 (Corces et al., 2016), GSE42519 (Rapin et al., 2014), GSE24006 (Gentles et al., 2010), GSE116256 (van Galen et al., 2019), GSE10358 (Tomasson et al., 2008), GSE14468 (Wouters et al., 2009), GSE30285 (Li et al., 2012), GSE11504 (Jensen et al., 2010), GSE69408 (Nilsson et al., 2016),GSE61804 (Metzelder et al., 2015), GSE75461 (Tregnago et al., 2016), GSE65427 (Li Y. et al., 2016), GSE14924 (Le Dieu et al., 2009),GSE127200 (Paczulla et al., 2019), GSE83533 (Li S. et al., 2016), GSE66525 (Hackl et al., 2015), GSE117090 (Radpour et al., 2019), GSE153264 (Stengel et al., 2021), GSE146173 (Bamopoulos et al., 2020)]. The Cancer Genome Atlas (TCGA) project on AML (Cancer Genome Atlas Research et al., 2013) transcriptomic cohorts were obtained from [https://portal.gdc.cancer.gov] (https://portal.gdc.cancer.gov/).

Transcriptomic Data Analysis

We used directly the already normalized transcriptome data. For unprocessed count data, we used the CPM method in edgeR to replace the count value with the CPM value. Differentially expressed genes between different groups were found using the limma (version 3.48.3) (Ritchie et al., 2015) package, and pathway enrichment analysis was performed through enrichGO in the clusterProfiler (Yu et al., 2012). Gene Set Enrichment Analysis (GSEA) (Mootha et al., 2003; Subramanian et al., 2005) was performed with GSEA software (Broad Institute).

Analysis of Single-Cell RNA-Seq

For the downstream analysis of single-cell RNA-seq, we selected cells with at least 1000 UMIS (gene count, indicating the number of captured transcripts) mapped to at least 200 unique genes. We also excluded cells with more than 20% of gene counts reflecting mitochondrial genes or ribosomal RNA. We normalized gene counts to a total of 10,000 for each cell. The type definitions for different cells used in the cell annotations were provided in the data.

Single-cell transcriptome sequencing data were visualized using a combination of principal component analysis (PCA) and t-distributed stochastic neighbor embedding (t-SNE), The top 50 principal components were selected for downstream analysis. Specifically, PCA was performed using prcomp, which was followed by t-SNE visualization using the Rtsne package. The maximum number of iterations was 2000, and the random seed was the seed (1,000).

High variable genes for clustering: HSC/hematopoietic progenitor cells (HPC): SPINK2, ZFAS1, NRIP1, GAS5, JUN, MEIS1, HLF, EGR1, CRHBP, NPR3; LSC: NPTX2, H1F0, EMP1, MEIS1, CALCRL, TPSD1, TPT1, CRHBP, CLNK, TSC22D1; leukemic progenitor cell (LPC): CDK6, HSP90AB1, SPINK2, EEF1B2, PCNP, TAPT1-AS1, HINT1, LRRC75A-AS1, DSE, PEBP1.

Data Visualizations

Gene expression data plots in different tumors were built with the Gene Expression Profiling Interactive Analysis (GEPIA) web tool. The chromatin immunoprecipitation followed by sequencing (ChIP-seq) data were visualized using the WashU Epigenome Browser (Li et al., 2019), and the rest of the data were visualized using ggplot2 (version 3.3.5) (Ginestet, 2011) in the R statistical language.

Cell Culture

KG-1a, THP-1, HL-60, HEL, and KO-52 cells were cultured in RPMI-1640 (M&C Gene Technology) containing 10% FBS (LONSA SCIENCE SRL), maintained at 37°C with 5% CO2. Kasumi-1 cells were cultured in RPMI-1640 containing 20% FBS.

Cell Preparation

$CD34^+$ cells were enriched using the CD34 Positive Isolation Kit (Thermo). CD34-enriched AML cells were then incubated with CD34-FITC (FITC-65111; Proteintech) and CD38-PE (PE-65183; Proteintech) monoclonal antibodies and sorted on a flow cytometer (BD FACSAria Fusion).

RNA extraction, reverse transcription, and quantitative real time polymerase chain reaction (qRT-PCR).

Total RNA was extracted with RNAiso Plus (Takara). Reverse transcription was performed using the M5 Sprint qPCR RT kit (Mei5 Biotechnology). Afterward, RT-PCR was performed using THUNDERBIRD SYBR qPCR Mix (TOYOBO) on a LineGene

4840 Real-time PCR system (Bioer). Glyceraldehyde 3-phosphate dehydrogenase (GAPDH) was used as an endogenous control. GAPDH gene Forward primer: TGGCACCGTCAAGGCTGA GAA; Reverse primer: TGGTGAAGACGCCAGTGGACTC. CNST gene Forward primer: GCCACTTCGGGATGCTTC TGAG; Reverse primer: GCCACTTCGGGATGCTTCTGAG.

Western Blot

Cells were lysed in sodium dodecyl sulfate (SDS) lysis buffer (1% SDS, 5% glycerol, 1 mM EDTA, 25 mM Tris, and 150 mM NaCl) supplemented with protease inhibitors and sonicated to shear DNA. Protein samples were separated by SDS-PAGE, transferred to the PVDF membrane (Millipore). Antibodies:

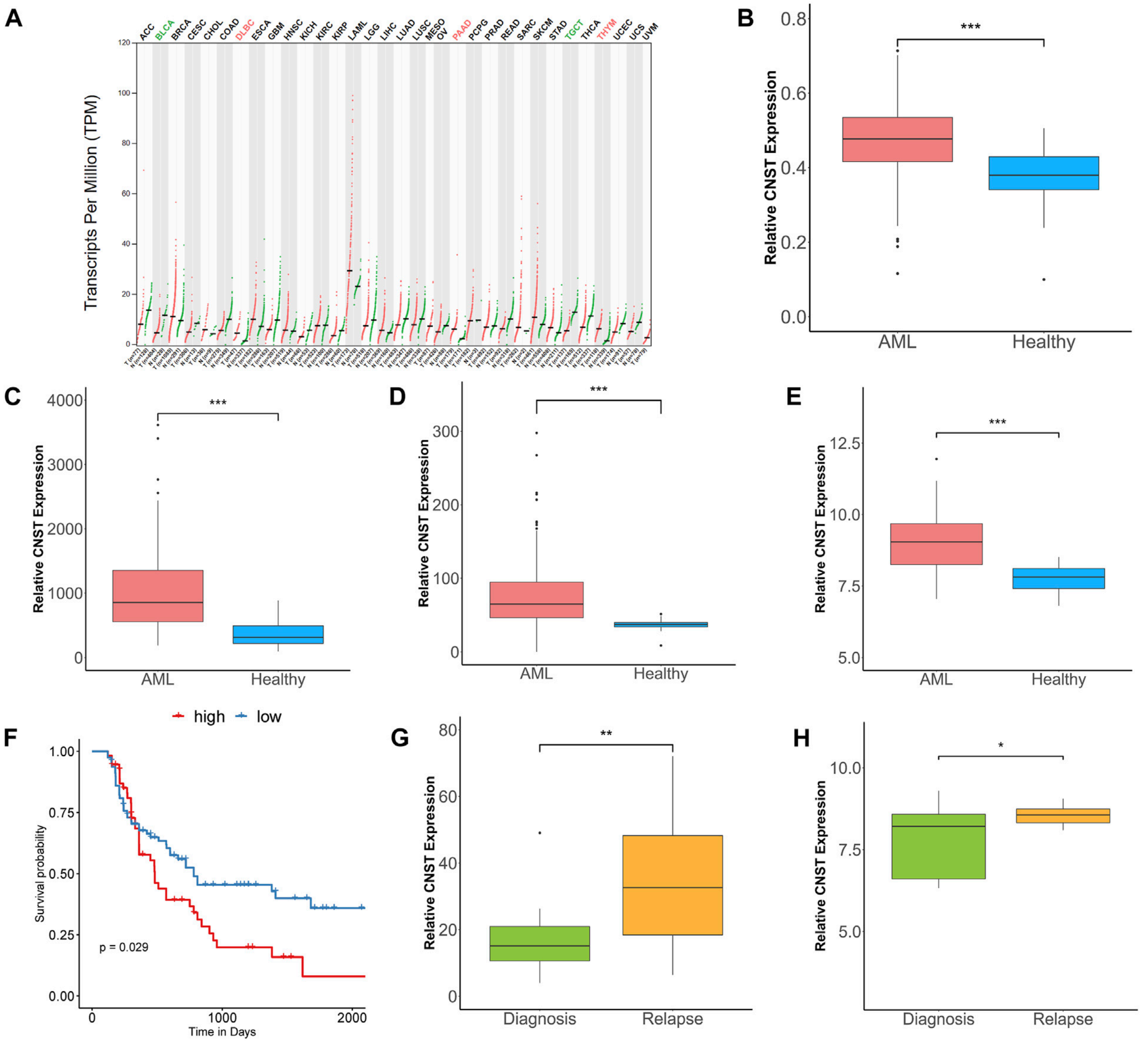

FIGURE 1 | CNST expression is elevated in acute myeloid leukemia (AML) and correlates with poor prognosis. **(A)** The expression of CNST in 33 types of tumors compared with normal subjects in Gene Expression Profiling Interactive Analysis (GEPIA) database. Comparison of CNST expression in AML and normal bone marrow in Beat AML **(B)**, GSE13159 **(C)**, GSE114868 **(D)**, and GSE15061 **(E)**. **(F)** Kaplan–Meier analysis of overall survival (OS) in AML using TCGA database [CNST^{high} (*n* = 67) vs. CNST^{low} (*n* = 67)] (cut-off point: median CNST expression level). Comparison of CNST expression levels at relapse and initial diagnosis in GSE83533 **(G)** and GSE66525 **(H)**. $^{*}p < 0.05$, $^{**}p < 0.01$, $^{***}p < 0.001$. Abbreviations: ACC, Adrenocortical carcinoma; BLCA, Bladder Urothelial Carcinoma; BRCA, Breast invasive carcinoma; CESC, Cervical squamous cell carcinoma and endocervical adenocarcinoma; CHOL, Cholangio carcinoma; COAD, Colon adenocarcinoma; DLBC, Lymphoid Neoplasm Diffuse Large B-cell Lymphoma; ESCA, Esophageal carcinoma; GBM, Glioblastoma multiforme; HNSC, Head and Neck squamous cell carcinoma; KICH, Kidney Chromophobe; KIRC, Kidney renal clear cell carcinoma; KIRP, Kidney renal papillary cell carcinoma; LAML, Acute Myeloid Leukemia; LGG, Brain Lower Grade Glioma; LIHC, Liver hepatocellular carcinoma; LUAD, Lung adenocarcinoma; LUSC, Lung squamous cell carcinoma; MESO, Mesothelioma; OV, Ovarian serous cystadenocarcinoma; PAAD, Pancreatic adenocarcinoma; PCPG, Pheochromocytoma and Paraganglioma; PRAD, Prostate adenocarcinoma; READ, Rectum adenocarcinoma; SARC, Sarcoma; SKCM, Skin Cutaneous Melanoma; STAD, Stomach adenocarcinoma; TGCT, Testicular Germ Cell Tumors; THCA, Thyroid carcinoma; THYM, Thymoma; UCEC, Uterine Corpus Endometrial Carcinoma; UCS, Uterine Carcinosarcoma; UVM, Uveal Melanoma.

CNST (26322-1-AP; Proteintech), GAPDH (60004-1-Ig; Proteintech).

Statistical Analysis

All statistical analyses were performed using R4.1.1 and third-party R packages based on R. The Shapiro–Wilk test was used to determine whether the variables were normally distributed. Student's *t*-test or Mann–Whitney *U* test was used to examine whether there was a difference between the two groups of data, and analysis of variance (ANOVA) or Kruskal–Wallis test was used to evaluate the relationship between a categorical variable and a continuous variable, as appropriate. For ANOVA test, multiple comparisons were performed using Tukey test. For Kruskal–Wallis test, multiple comparisons were performed using Kruskal–Wallis H test. The correlation between genes was estimated using the Pearson correlation coefficient. The prognostic effect of CNST expression was analyzed through Kaplan–Meier analysis using the log-rank test. The p value < 0.05 (two-tailed) was defined as statistically significant in all statistical analyses.

RESULTS

CNST is Overexpressed in AML and Correlates With Poor Prognosis

We analyzed CNST expression in 33 types of tumors by using the GEPIA tool. We found that CNST expression was abnormally higher in AML compared with paired normal tissues (**Figure 1A**). We then compared CNST expression data from AML patients and healthy human bone marrow cells in four large-scale datasets and found that CNST showed significantly higher expression in AML patients (Mann–Whitney test, Beat AML, $p < 0.001$; GSE13159, $p < 0.001$; GSE114868, $p < 0.001$; GSE15061, $p < 0.001$; **Figures 1B–E**). To investigate whether the higher expression of CNST in AML affects the prognosis of AML patients, we used the TCGA database to analyze the relationship between CNST expression and the survival time of AML patients. The expression of CNST was found to have an adverse effect on the survival time of AML patients ($p = 0.029$; **Figure 1F**). Furthermore, the GSE83533 and GSE66525 datasets showed that CNST expression was significantly higher in relapsed AML patients (Mann–Whitney test, GSE83533, $p = 0.002$; GSE66525, $p = 0.033$) (**Figures 1G,H**).

CNST Expression Correlates With Specific Subtypes of AML

To verify the ability of CNST as a diagnostic marker, we further examined whether CNST expression is associated with the demographic, molecular and biological characteristics of AML, including those based on age, morphology, cytogenetics, and genomic lesions. We analyzed five independent large clinical datasets and focused on bone marrow samples. In GSE10358 and GSE14468 datasets, the expression of CNST in young patients (aged < 60 years) was higher than that in the elderly group, but this trend was not found in GSE30285, TCGA, and Beat AML. To further explore whether CNST expression is related to age, we used the data of GSE11504 and GSE69408 to analyze the expression of CNST in bone marrow cells and HSCs from different ages of people. We found that there was little change in CNST expression in bone marrow cells and HSCs of different ages. CNST expression showed a significant variation according to the French–American–British classification, which subclassified AML into different categories based on the cytology as well as enzymatic profile (Hasserjian, 2021), in all of the analyzed datasets. M0, M1, M4, and M7 subtypes showed higher CNST expression. Moreover, all cohorts showed a significant variation in CNST expression between AML forms with different karyotypes. The expression levels of CNST in AML patients with the t (8; 21) karyotype were significantly higher than those in AML patients with other karyotypes (Kruskal–Wallis test, $p < 0.001$; **Figure 2A**). In addition, we also analyzed the effect of NPM1 and FLT3 mutations on CNST expression and found that NPM1 and FLT3 mutations did not show any effect on CNST expression.

CNST May Be a Direct Downstream Transcript of RUNX1–RUNX1T1

Patients with t (8; 21) karyotype have been shown to have mutations in the RUNX1–RUNX1T1 fusion protein (Erickson et al., 1992). Therefore, we analyzed the CNST expression levels of AML with different fusion proteins in GSE61804 and GSE75461 cohorts. The results showed that AML with the RUNX1–RUNX1T1 fusion protein had a higher expression of CNST than other cases. However, this difference was not shown for those AMLs with RUNX1 mutations in GSE146173. We also analyzed data at the single-cell level with GSE116256 and revealed that patients with RUNX1–RUNX1T1 had the highest CNST expression levels (**Figures 2B,C**). We identified differentially expressed genes between AML patients with RUNX1–RUNX1T1 and other AML patients in TCGA data, and found that CNST was highly expressed in AML patients with RUNX1–RUNX1T1 (**Figure 2D**). We compared the expression levels of CNST in the leukemia cell lines Kasumi-1 and KO-52, where the Kasumi-1 cell line expresses RUNX1–RUNX1T1 and the KO-52 does not, and the results showed that the expression of CNST was higher in Kasumi-1 (Student's *t*-test, $p < 0.001$; **Figures 2E,F**). The data from GSE153281 showed that CNST expression decreased only 2 h after adding dTAG-47 to degrade RUNX1–RUNX1T1 (Kruskal–Wallis test, $p < 0.001$; **Figure 2G**). According to ChIP-seq data for RUNX1, RUNX1–RUNX1T1 binds more strongly to the transcriptional start site of CNST than does normal RUNX1 (**Figure 2H**), suggesting that RUNX1–RUNX1T1 is likely to directly regulate CNST expression.

CNST is Associated With a Low Degree of Differentiation of Myeloid Cells and is Highly Expressed in LSCs

CNST was also highly expressed in the M0–M2 subtypes of AML and decreased with the degree of differentiation, which may suggest that CNST expression may be related to the degree of differentiation of AML (Kruskal–Wallis test, $p < 0.001$; **Figure 3A**). For this reason, we first examined the expression of CNST in AML cell lines from different patients. The results showed that the expression of CNST was the highest in the least differentiated KG-1a cell line (ANOVA test, $p < 0.001$; **Figures 3B,C**). We then analyzed the expression of CNST in different cells of the hematopoietic system of AML patients and healthy individuals from the GSE75384 cohort (Kruskal–Wallis test, $p < 0.001$; **Figure 3D**). In the hematopoietic system, the expression of CNST decreased with the differentiation of myeloid cells. CNST expression was extremely low in monocytes and nucleated red blood cells and was higher in less differentiated HSCs and multipotent progenitors (MPPs). Exceptionally, CNST expression was also high in megakaryocytes, which was consistent with the higher expression of CNST in the M7 subtype of AML. However, in lymphocyte lineages, the expression of CNST did not significantly decrease in differentiated B cells, T cells, and NK cells. To verify this expression trend of CNST, we analyzed the GSE42519 and GSE63270 cohorts, and the conclusion was equivalent to that of the GSE75384 cohort. Specifically, CNST was most highly expressed in HSCs, while it showed lower expression in differentiated myeloid cells such as granulocytes and monocytes. In all AML cells, especially in LSCs, CNST expression levels were higher than those in normal myeloid cells (Kruskal–Wallis test, $p < 0.001$; **Figure 3D**). CNST was overexpressed in LSCs compared with HSCs. Elevated CNST levels were also detected in leukemic cells compared with hematopoietic progenitor cells (Mann–Whitney test; **Figures 3E,F**). Similarly, the expression of CNST in leukemic progenitor cells (LPCs) was also higher than that in HPCs. We then used the GSE116256 dataset to analyze the expression of CNST at the single-cell level, and the results showed that the expression of CNST was higher in LSCs and adjacent cells (**Figure 3G**). We also analyzed the correlation between the expression of CNST and that of 17 genes used to evaluate LSC (17-gene LSC score, LSC17) (Ng et al., 2016) in the TCGA dataset. CD33, a common AML marker gene, and ACTB were used together as control genes for the analysis of CNST. It was demonstrated that the expression of CNST was positively correlated with that of the 17 genes of LSC, such as CD34, but CD33 and ACTB as control genes did not show this correlation. (**Figures 3H–J**). We compared CNST expression in sorted $CD34^{+}CD38^{-}$, $CD34^{+}CD38^{+}$, and $CD34^{-}$ KG-1a cells and found that CNST expression was significantly higher in HSC-like ($CD34^{+}CD38^{-}$) KG-1a cells (ANOVA test, $p < 0.001$; **Figures 3K, L**). Taken together, these data indicate that in the hematopoietic system, CNST is a marker of immature hematopoietic cells. Compared with healthy blood cells of similar degree of differentiation, the expression of CNST is elevated in AML cells.

CNST-Related Gene Networks in AML

To investigate the biological function of CNST in AML, we separately analyzed RNA-sequencing data from AML patients' bone marrow and the sorted LSCs. We first analyzed five different AML datasets (TCGA, Beat AML, GSE6891, GSE13159, GSE114868). Differentially expressed genes (DEGs) between $CNST^{high}$ and $CNST^{low}$ groups were found in these datasets. Gene Ontology (GO) enrichment analyses were performed on these DEGs, and pathways enriched in at least three datasets were selected. These included 325 pathways that positively correlated with CNST expression and 619 pathways that negatively correlated with CNST expression (**Figures 4A,B**). The DEGs that are positively related to CNST are involved in the establishment of protein localization to membrane, protein transport along the microtubule, and protein import. This is in agreement with the previously reported CNST function, and stem cell population maintenance is consistent with our conclusions in the previous section of the article. Interestingly, as shown in our study, CNST is also involved in pathways such as stress granule (SG) assembly, P-body, and macroautophagy. DEGs negatively related to CNST are involved in myeloid cell differentiation, aging, and a large number of immune-related pathways, including neutrophil activation, antigen processing and presentation, response to interferon-gamma, T cell activation, toll-like receptor signaling pathway, and the production of various interleukins. To confirm the role of CNST in immunity, we analyzed the GSE127200 dataset, which groups AML cells based on the presence or absence of NKG2D ligands (NKG2DLs) on the surface. NKG2DL-negative AML cells often exhibit the ability to escape immune response. Our results showed that CNST expression was significantly elevated in the NKG2DL-negative group (Mann–Whitney test, $p < 0.001$, **Figure 4D**). The TCGA data also showed that PD-L1 expression was higher in $CNST^{high}$ AML (Mann–Whitney test, $p = 0.002$, **Figure 4E**). Since CNST is mainly expressed in LSCs, we used GSE117090 to perform GO analysis on LSCs with different CNST expression levels. Our results revealed that a variety of adhesion-related pathways were enriched in LSCs with high CNST expression. These pathways included regulation of cell–substrate adhesion, regulation of cell–matrix adhesion, integrin-mediated signaling pathway, and focal adhesion assembly (**Figure 4F**). The adhesion of LSCs to the microenvironment is thought to be involved in LSC niche retention, which is considered an important mechanism of AML drug resistance. We found that multiple integrins, such as ITGA6, ITGA9, and ITGB1, were highly expressed in LSCs of the $CNST^{high}$ group (Mann–Whitney test, ITGA6, $p < 0.001$; ITGA9, $p < 0.001$; ITGB1, $p < 0.001$; **Figure 4G**).

DISCUSSION

CNST is a protein located on the TGN that mediates the targeting of transmembrane proteins to the plasma membrane. At present, there is limited information about CNST, and the function of CNST is still poorly understood. Here, we investigated the expression patterns of CNST in AML and normal hematopoietic system and analyzed the possible role of CNST in AML.

CNST was significantly elevated in AML compared with normal bone marrow and was associated with a poorer prognosis. In multiple different independent patient cohorts, CNST expression of AML patients with various subtypes showed higher expression

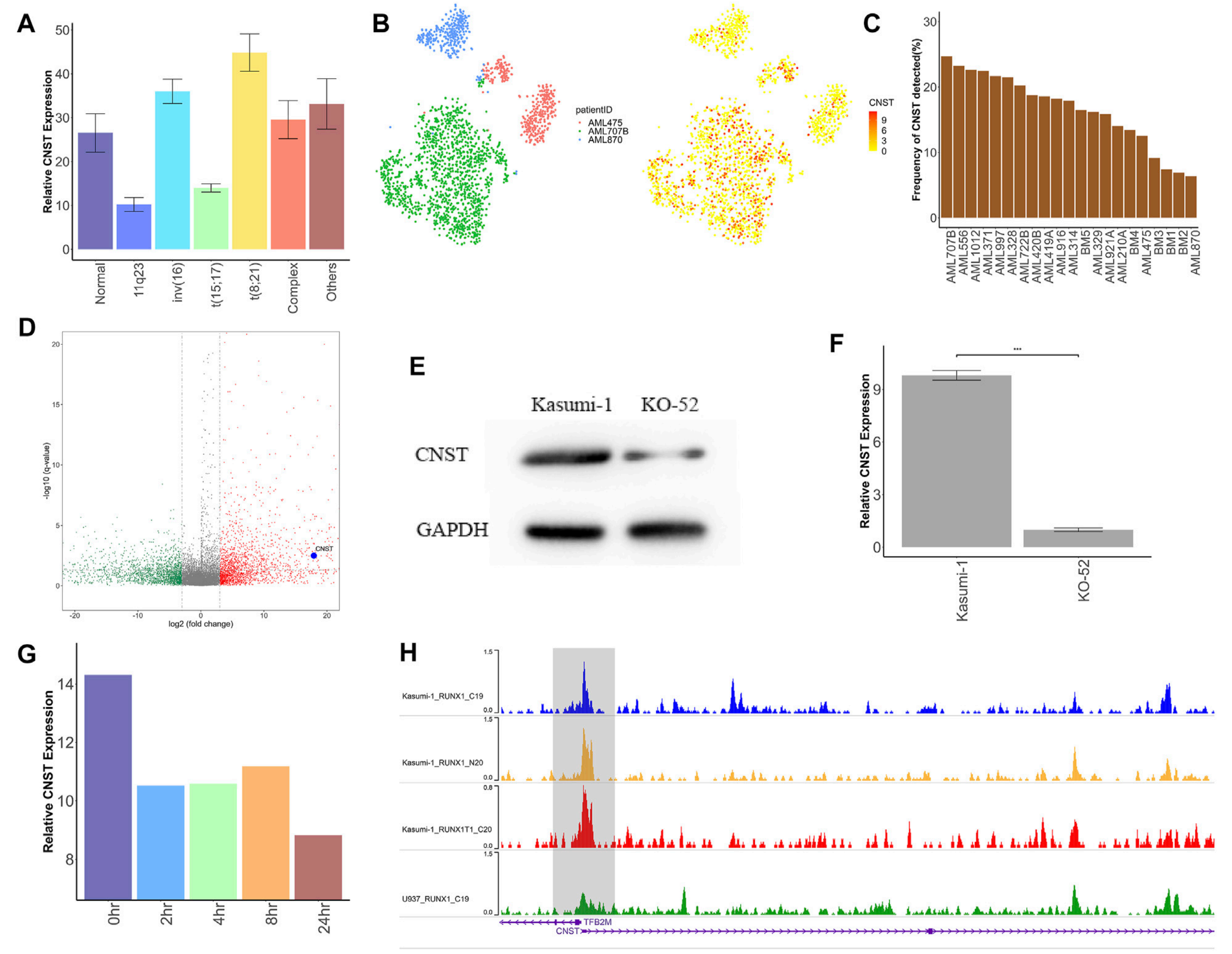

FIGURE 2 | CNST may be directly transcribed by RUNX1–RUNX1T1. **(A)** Expression analysis of CNST in AML with different abnormal karyotypes in TCGA. **(B)** t-SNE plots show CNST expression of single cells from AML patients with RUNX1–RUNX1T1 (AML707B) versus other AML patients. **(C)** The detection rate of CNST expression in different AML patients by single-cell sequencing, among which AML707B is a patient with RUNX1–RUNX1T1 mutation. **(D)** Volcano plot of differentially expressed genes (DEGs) between AML patients with RUNX1-RUNX1T1 and other AML patients; **(E)** Western blot analysis of CNST in Kasumi-1 compared with KO-52 cells. **(F)** CNST mRNA expression analysis of Kasumi-1 and KO-52 cells was performed by qRT-PCR. **(G)** Changes in CNST expression at different times after adding dTAG-47. **(H)** The WashU genome browser shows the ChIP-seq data for RUNX1 and RUNX1–RUNX1T1 in different AML cell lines near the transcription start site of CNST. *$p < 0.05$, **$p < 0.01$, ***$p < 0.001$.

than normal population, which led us to believe that compared with other AML makers such as CD33 (Nguyen et al., 2006) and CD123 (Muñoz et al., 2001), the increase of expression level of CNST in AML is more common. AML is a heterogeneous disease, and the general increase of CNST in AML patients may represent the commonness between different AML patients to some extent, which also suggests the potential ability of CNST to become a biomarker of AML. The expression of CNST showed a significant variation among AML forms with different aberrations and was the highest in AML with the RUNX1–RUNX1T1 fusion protein. This is likely due to the direct transcription of CNST by RUNX1–RUNX1T1. We also found that the CNST expression level of inv (16)/CBFB–MYH11 AML was abnormally elevated in some datasets; however, unlike RUNX1–RUNX1T1, this finding did not show a uniform trend in all of the datasets. Abnormally elevated CNST in AML expressing CBFB–MYH11 fusion protein suggests that CNST expression is likely regulated by a transcriptional regulatory network shared by core-binding factor acute myeloid leukemia (CBF-AML) (Faber et al., 2016). However, the elevated expression of CNST in RUNX1–RUNX1T1 AML was not sufficient to explain the general elevation of CNST in all AML patients. Moreover, the high CNST expression represents a poor prognosis, which contradicts the usually favorable prognosis of CBF-AML (Kantarjian et al., 2021).

To explore the phenomenon that CNST expression is generally elevated in AML, we analyzed other subgroups of AML. We found that the expression of CNST was higher in AML patients with M0–M2 subtypes that were poorly differentiated. This suggests that CNST may be associated with the low degree of differentiation of hematopoietic cells, which was confirmed by the expression pattern

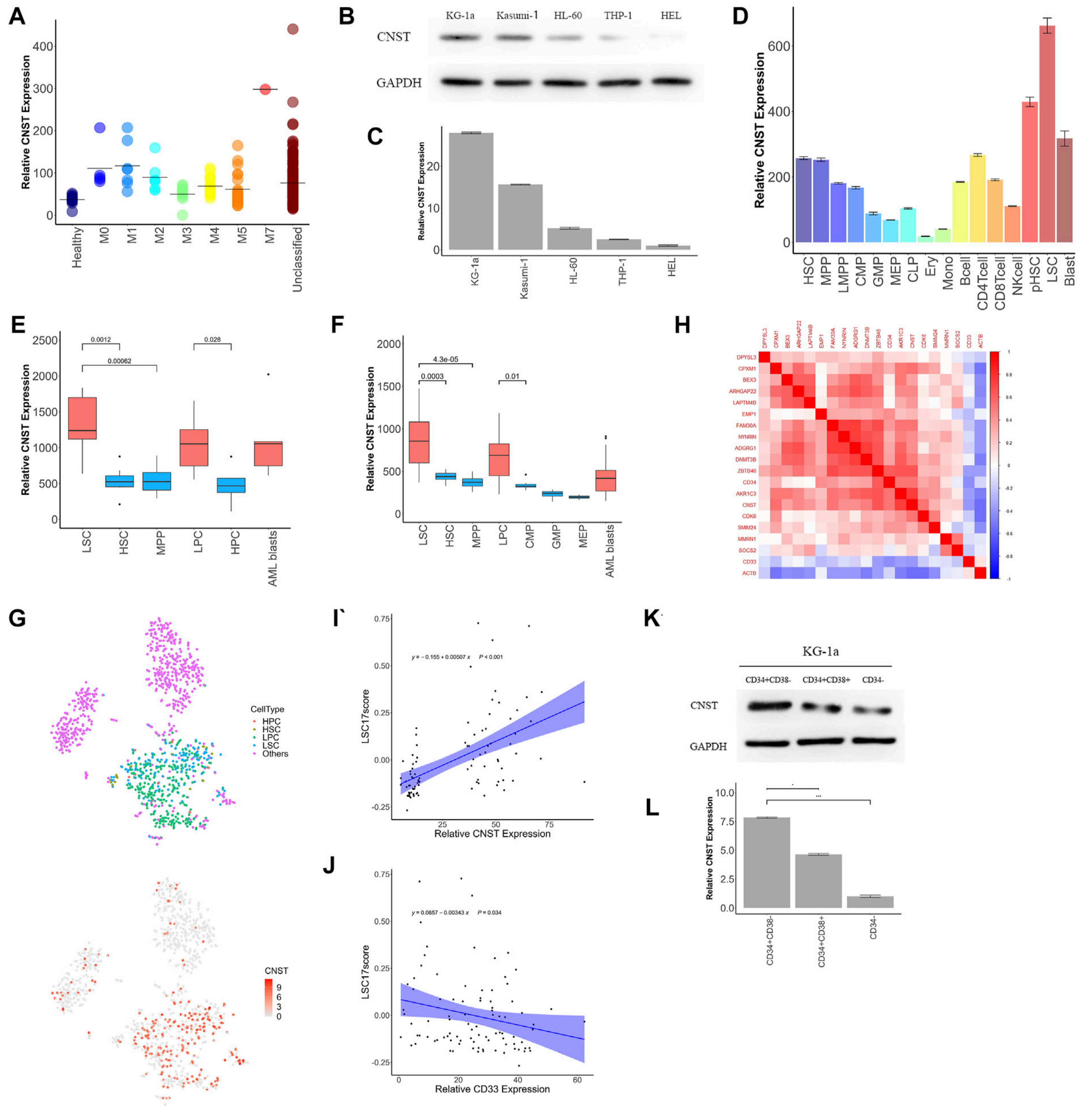

FIGURE 3 | CNST expression correlates with poor differentiation of the hematopoietic system. **(A)** The expression of CNST in different subtypes of AML patients in TCGA. **(B,C)** CNST protein and mRNA expression levels in different AML cell lines were examined by western blot and qRT-PCR. **(D)** The expression of CNST in different cells of the normal hematopoietic system and AML in GSE75384. Comparison of CNST expression levels in AML and normal bone marrow hematopoietic stem-progenitor cells in GSE63270 **(E)** and GSE24006 **(F)**. **(G)** t-SNE plots show single cells from AML556 relative expression levels of CNST in GSE116256. **(H)** Heatmap of the correlation between CNST expression and LSC17 gene expression. **(I)** Pearson's correlation between CNST and AML patients' LSC17 score; **(J)** Pearson's correlation between CD33 and AML patients' LSC17 score; **(K,L)** CNST protein and mRNA expression levels in sorted KG-1a cells were examined by western blot and qRT-PCR. *$p < 0.05$, **$p < 0.01$, ***$p < 0.001$. Abbreviations: HSC, hematopoietic stem cell; MPP, multipotent progenitor cell; LMPP, lymphoid-primed multipotent progenitor cell; CMP, common myeloid progenitor cell; GMP, granulocyte macrophage progenitor cell; MEP, megakaryocyte erythroid progenitor cell; CLP, common lymphoid progenitor cell; Ery, erythroblast cell; Mono, monocyte cell; NKcell, natural killer cell; pHSC, primary human leukemia cell; LSC, leukemia stem cell.

of CNST in the normal hematopoietic system. Thus, a question arises as to whether CNST is associated with poor differentiation levels in other tissues. However, the results indicated that CNST did not show this trend in other tissues; so, we considered CNST to be a hematopoietic system-specific marker of poor differentiation. The elevated CNST expression in LSCs also partially explains the higher CNST expression in relapsed AML patients (Long et al., 2022). Next, we considered whether CNST is differentially expressed between distinct LSC subpopulations that differ in their self-renewal and proliferative capabilities (Sachs et al., 2020); the

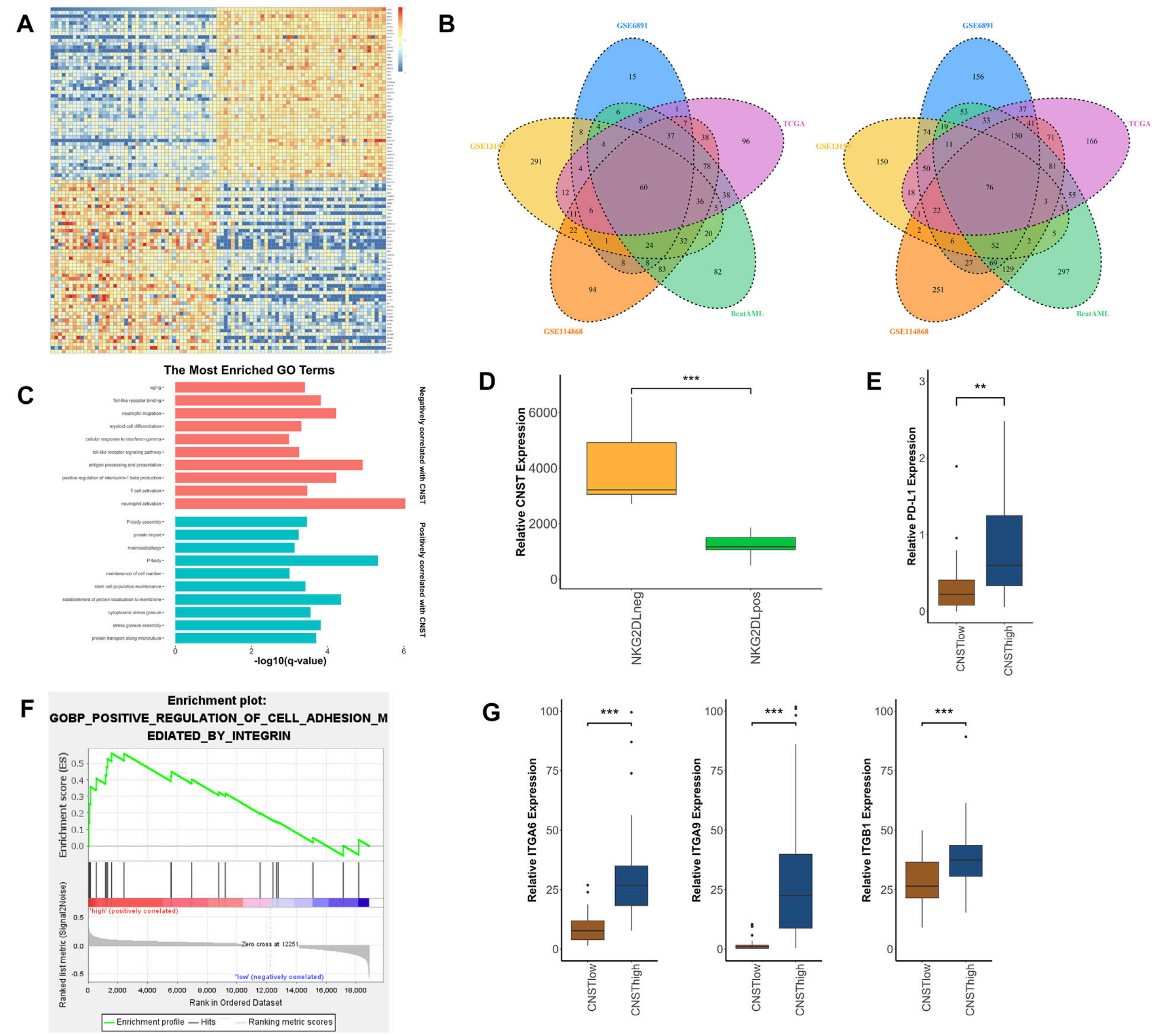

FIGURE 4 | Molecular signatures associated with CNST in AML. **(A)** Heatmap of DEGs between CNST^{high} and CNST^{low} AML patients. (cut-off point: quartile CNST expression level). **(B)** The left panel shows the enriched pathways of highly expressed genes in the CNST^{high} group in different datasets; Venn plots show pathways enriched in different datasets, where the left plot is enriched for genes positively correlated with CNST, and the right plot is the opposite. **(C)** GO analysis of gene sets positively and negatively correlated with CNST expression. **(D)** AML cells were grouped according to whether they expressed NKG2D ligands (NKG2DLs) or not, and the expression levels of CNST were compared between different groups. **(E)** Expression of PD-L1 in AML in the CNST^{high} and CNST^{low} groups. **(F)** GSEA of LSCs showed that the CNST-high expression groups were enriched in integrin-regulated cell adhesion. **(G)** Expression of ITGA6, ITGA9, and ITGB1 in LSCs in the CNST^{high} and CNST^{low} groups. $^{*}p < 0.05$, $^{**}p < 0.01$, $^{***}p < 0.001$.

results showed that there was no difference in CNST expression among the different subpopulations. In addition, we also found that CNST was highly expressed in megakaryocytes and its corresponding M7 subtype AML, which indicates that CNST may have a function in megakaryocytes.

We next considered whether the elevated expression of CNST was due to the activation of its reported function, namely sorting and cell surface targeting of transmembrane proteins through interactions with GGA adaptor proteins (del Castillo et al., 2010).

However, GGA1 and GGA2, which are reported to interact directly with CNST, and Cx32, Cx43, Cx45, and other transmembrane proteins targeted to the cytoplasmic membrane by CNST did not show a similar expression trend to CNST in the hematopoietic system and AML. Some of them even showed a negative correlation with CNST, suggesting that the high expression of CNST in HSCs and AML is likely not due to more frequent Golgi-mediated vesicular trafficking but rather due to the activation of other pathways involved in CNST. This is consistent with reports in the literature that, in addition to GGA, CNST may also recruit other proteins to play its role (del Castillo et al., 2010) [1]. Our study shows that in addition to Golgi vesicle transport, the CNST-related transcriptional network also includes multiple pathways such as microtubule-dependent transport, cytoskeleton-dependent intracellular transport, intracellular localization of protein complexes, and autophagy, suggesting that CNST is likely involved in various other intracellular transport pathways.

For the possible role of CNST in AML, according to our analysis of the signaling network involved in CNST in AML, we propose the following three possibilities: first, CNST affects the drug resistance of AML by participating in stress granule assembly. SGs are membraneless ribonucleoprotein-based cellular compartments in the cytoplasm that are formed when translation initiation is impaired (Protter and Parker, 2016). SGs are involved in posttranscriptional regulation and translational control. SGs have been found in a variety of tumors and are thought to improve the tolerance of tumor cells to stress stimuli and chemotherapeutic agents (Grabocka and Bar-Sagi, 2016; Li et al., 2021). SGs may be related to the formation of the P-body because a certain proportion of RNA-binding proteins (RBPs) and mRNAs shared by SGs and PBs have been found to shuttle between the two when the SG assembly is induced (Kedersha et al., 2005; Moon et al., 2019). A large number of genes related to PBs and SGs exist in the gene pathways related to CNST, including EIF-2A, TIA-1, DCP1, FAST, and RAP55 (Buchan and Parker, 2009). Intrinsically disordered regions (IDRs) exist in the structure of CNST. IDRs play a central role in phase separation, which underlies the assembly of SGs and PBs(Hofmann et al., 2021). IDRs can confer the ability of CNST to bind to other proteins or RNAs(Mittag and Parker, 2018). Therefore, we speculate that CNST may be involved in the intermolecular interactions in SGs or PBs as “scaffolds.” Then, CNST may promote immune evasion in AML. Our analysis of the network that CNST may be involved in AML shows that in the CNST^{high} AML patients, various immune-related pathway genes showed low expression, suggesting that CNST may be involved in immune evasion (Teague and Kline, 2013), which is believed to be involved in the relapse of AML and to affect the prognosis of AML (Taghiloo and Asgarian-Omran, 2021). Two mechanisms involving AML immune evasion have been identified, one of which is mainly mediated by CD14$^+$ monocyte-like AML through the LILRB4/SHP-2/NF-κB/uPAR/ARG1 signaling pathway (Deng et al., 2018; van Galen et al., 2019), which is inconsistent with the low expression of CNST in monocytes. At the same time, we performed a correlation analysis of these proteins with CNST in AML; the results showed that CNST was not closely related to these proteins. Therefore, we believe that CNST is more likely to be involved in immune evasion mediated by another mechanism, that is, immune evasion by LSCs, and we validated the relationship between CNST and markers of immune evasion in the data analysis (Zhang et al., 2009; Paczulla et al., 2019).

Finally, CNST participates in LSC niche retention. HSC niche is a concept first proposed by Schofield (Schofield, 1978), which defines the bone marrow microenvironment structures required to maintain a stable HSC pool. Within the niche, there are key bidirectional signals that ensure normal HSC populations and maintain a quiescent long-term HSC pool (Schepers et al., 2015). LSCs can occupy HSC niche and utilize mechanisms that maintain HSCs, thereby resulting in enhanced self-renewal and proliferation, enforced quiescence, and resistance to chemotherapeutic agents (Yamashita et al., 2020). LSC niche retention requires a variety of adhesion molecules to interact with the bone marrow microenvironment (Grenier et al., 2021), and the co-expression of CNST with these adhesion molecules in LSCs leads us to speculate that CNST mediates the membrane localization of these adhesion molecules.

Taken together, our results suggest that CNST, a marker of poor differentiation of blood cells, may play multiple biological roles in AML. CNST may influence the prognosis of AML by participating in SG assembly, immune evasion, or LSC niche retention. The specific high expression of CNST in AML also indicates that targeting CNST and its related pathways is a potential therapeutic option. However, as it is a key protein in vesicle trafficking in cells, direct targeting of CNST may lead to serious side effects. Therefore, further in-depth study of the role of CNST in cells is needed to formulate more targeted treatment options.

DATA AVAILABILITY STATEMENT

The datasets presented in this study can be found in online repositories. The names of the repository/repositories and accession number(s) can be found in the article/Supplementary Material.

ETHICS STATEMENT

Written informed consent was obtained from the individual(s) for the publication of any potentially identifiable images or data included in this article.

AUTHOR CONTRIBUTIONS

XL and WZ designed the research. HL, XZ, ZZ, and HZ performed the experiments. HL, XZ, DL, YY, FZ, YW, LZ, and ZD analyzed the data. HL, XZ, and XL wrote and revised the manuscript. All authors have read and approved the final manuscript.

ACKNOWLEDGMENTS

This work was supported by National Key R&D Program of China (2016YFE0129200), National Natural Science Foundation of China (No. 31571321, 81800161, 81601337).

REFERENCES

Bamopoulos, S. A., Batcha, A. M. N., Jurinovic, V., Rothenberg-Thurley, M., Janke, H., Ksienzyk, B., et al. (2020). Clinical Presentation and Differential Splicing of SRSF2, U2AF1 and SF3B1 Mutations in Patients with Acute Myeloid Leukemia. *Leukemia.* 34 (10), 2621–2634. doi:10.1038/s41375-020-0839-4

Buchan, J. R., and Parker, R. (2009). Eukaryotic Stress Granules: the Ins and Outs of Translation. *Mol. Cell.* 36 (6), 932–941. doi:10.1016/j.molcel.2009.11.020

Cancer Genome Atlas Research, N., Ley, T. J., Miller, C., Ding, L., Raphael, B. J., Mungall, A. J., et al. (2013). Genomic and Epigenomic Landscapes of Adult De Novo Acute Myeloid Leukemia. *N. Engl. J. Med.* 368 (22), 2059–2074. doi:10.1056/NEJMoa1301689

Carter, J. L., Hege, K., Yang, J., Kalpage, H. A., Su, Y., Edwards, H., et al. (2020). Targeting Multiple Signaling Pathways: the New Approach to Acute Myeloid Leukemia Therapy. *Signal. Transduct Target. Ther.* 5 (1), 288. doi:10.1038/s41392-020-00361-x

Corces, M. R., Buenrostro, J. D., Wu, B., Greenside, P. G., Chan, S. M., Koenig, J. L., et al. (2016). Lineage-specific and Single-Cell Chromatin Accessibility Charts Human Hematopoiesis and Leukemia Evolution. *Nat. Genet.* 48 (10), 1193–1203. doi:10.1038/ng.3646

del Castillo, F. J., Cohen-Salmon, M., Charollais, A., Caille, D., Lampe, P. D., Chavrier, P., et al. (2010). Consortin, a Trans-golgi Network Cargo Receptor for the Plasma Membrane Targeting and Recycling of Connexins. *Hum. Mol. Genet.* 19 (2), 262–275. doi:10.1093/hmg/ddp490

Deng, M., Gui, X., Kim, J., Xie, L., Chen, W., Li, Z., et al. (2018). LILRB4 Signalling in Leukaemia Cells Mediates T Cell Suppression and Tumour Infiltration. *Nature.* 562 (7728), 605–609. doi:10.1038/s41586-018-0615-z

Dombret, H., and Gardin, C. (2016). An Update of Current Treatments for Adult Acute Myeloid Leukemia. *Blood.* 127 (1), 53–61. doi:10.1182/blood-2015-08-604520

Erickson, P., Gao, J., Chang, K. S., Look, T., Whisenant, E., Raimondi, S., et al. (1992). Identification of Breakpoints in T(8;21) Acute Myelogenous Leukemia and Isolation of a Fusion Transcript, AML1/ETO, with Similarity to Drosophila Segmentation Gene, Runt. *Blood.* 80 (7), 1825–1831. doi:10.1182/blood.v80.7.1825.bloodjournal8071825

Faber, Z. J., Chen, X., Gedman, A. L., Boggs, K., Cheng, J., Ma, J., et al. (2016). The Genomic Landscape of Core-Binding Factor Acute Myeloid Leukemias. *Nat. Genet.* 48 (12), 1551–1556. doi:10.1038/ng.3709

Gentles, A. J., Plevritis, S. K., Majeti, R., and Alizadeh, A. A. (2010). Association of a Leukemic Stem Cell Gene Expression Signature With Clinical Outcomes in Acute Myeloid Leukemia. *JAMA* 304 (24), 2706–2715. doi:10.1001/jama.2010.1862

Ginestet, C. (2011). ggplot2: Elegant Graphics for Data Analysis. *J. R. Stat. Soc. Ser. a-Statistics Soc.* 174, 245–246. doi:10.1111/j.1467-985X.2010.00676_9.x

Grabocka, E., and Bar-Sagi, D. (2016). Mutant KRAS Enhances Tumor Cell Fitness by Upregulating Stress Granules. *Cell.* 167 (7), 1803–e12. doi:10.1016/j.cell.2016.11.035

Grenier, J. M. P., Testut, C., Fauriat, C., Mancini, S. J. C., and Aurrand-Lions, M. (2021). Adhesion Molecules Involved in Stem Cell Niche Retention During Normal Haematopoiesis and in Acute Myeloid Leukaemia. *Front. Immunol.* 12, 756231. doi:10.3389/fimmu.2021.756231

Hackl, H., Steinleitner, K., Lind, K., Hofer, S., Tosic, N., Pavlovic, S., et al. (2015). A Gene Expression Profile Associated with Relapse of Cytogenetically normal Acute Myeloid Leukemia Is Enriched for Leukemia Stem Cell Genes. *Leuk. Lymphoma.* 56 (4), 1126–1128. doi:10.3109/10428194.2014.944523

Haferlach, T., Kohlmann, A., Wieczorek, L., Basso, G., Kronnie, G. T., Béné, M. C., et al. (2010). Clinical Utility of Microarray-Based Gene Expression Profiling in the Diagnosis and Subclassification of Leukemia: Report from the International Microarray Innovations in Leukemia Study Group. *J. Clin. Oncol.* 28 (15), 2529–2537. doi:10.1200/jco.2009.23.4732

Hasserjian, R. P. (2021). Controversies in the Recent (2016) World Health Organization Classification of Acute Myeloid Leukemia. *Best Pract. Res. Clin. Haematol.* 34 (1), 101249. doi:10.1016/j.beha.2021.101249

Hofmann, S., Kedersha, N., Anderson, P., and Ivanov, P. (2021). Molecular Mechanisms of Stress Granule Assembly and Disassembly. *Biochim. Biophys. Acta Mol. Cell Res.* 1868 (1), 118876. doi:10.1016/j.bbamcr.2020.118876

Huang, H. H., Chen, F. Y., Chou, W. C., Hou, H. A., Ko, B. S., Lin, C. T., et al. (2019). Long Non-coding RNA HOXB-AS3 Promotes Myeloid Cell Proliferation and its Higher Expression Is an Adverse Prognostic Marker in Patients with Acute Myeloid Leukemia and Myelodysplastic Syndrome. *Bmc Cancer.* 19, 617. ARTN 617. doi:10.1186/s12885-019-5822-y

Jensen, K., Schaffer, L., Olstad, O. K., Bechensteen, A. G., Hellebostad, M., Tjønnfjord, G. E., et al. (2010). Striking Decrease in the Total Precursor B-Cell Compartment during Early Childhood as Evidenced by Flow Cytometry and Gene Expression Changes. *Pediatr. Hematol. Oncol.* 27 (1), 31–45. doi:10.3109/08880010903420687

Jung, N., Dai, B., Gentles, A. J., Majeti, R., and Feinberg, A. P. (2015). An LSC Epigenetic Signature Is Largely Mutation Independent and Implicates the HOXA Cluster in AML Pathogenesis. *Nat. Commun.* 6, 8489. ARTN 8489. doi:10.1038/ncomms9489

Kantarjian, H. M., Kadia, T. M., DiNardo, C. D., Welch, M. A., and Ravandi, F. (2021). Acute Myeloid Leukemia: Treatment and Research Outlook for 2021 and the MD Anderson Approach. *Cancer.* 127 (8), 1186–1207. doi:10.1002/cncr.33477

Kedersha, N., Stoecklin, G., Ayodele, M., Yacono, P., Lykke-Andersen, J., Fritzler, M. J., et al. (2005). Stress Granules and Processing Bodies Are Dynamically Linked Sites of mRNP Remodeling. *J. Cell Biol.* 169 (6), 871–884. doi:10.1083/jcb.200502088

Khwaja, A., Bjorkholm, M., Gale, R. E., Levine, R. L., Jordan, C. T., Ehninger, G., et al. (2016). Acute Myeloid Leukaemia. *Nat. Rev. Dis. Primers.* 2, 16010. doi:10.1038/nrdp.2016.10

Le Dieu, R., Taussig, D. C., Ramsay, A. G., Mitter, R., Miraki-Moud, F., Fatah, R., et al. (2009). Peripheral Blood T Cells in Acute Myeloid Leukemia (AML) Patients at Diagnosis Have Abnormal Phenotype and Genotype and Form Defective Immune Synapses with AML Blasts. *Blood.* 114 (18), 3909–3916. doi:10.1182/blood-2009-02-206946

Li, D., Hsu, S., Purushotham, D., Sears, R. L., and Wang, T. (2019). WashU Epigenome Browser Update 2019. *Nucleic Acids Res.* 47 (W1), W158–W165. doi:10.1093/nar/gkz348

Li, H., Lin, P. H., Gupta, P., Li, X., Zhao, S. L., Zhou, X., et al. (2021). MG53 Suppresses Tumor Progression and Stress Granule Formation by Modulating G3BP2 Activity in Non-small Cell Lung Cancer. *Mol. Cancer.* 20 (1), 118. doi:10.1186/s12943-021-01418-3

Li, S., Garrett-Bakelman, F. E., Chung, S. S., Sanders, M. A., Hricik, T., Rapaport, F., et al. (2016). Distinct Evolution and Dynamics of Epigenetic and Genetic Heterogeneity in Acute Myeloid Leukemia. *Nat. Med.* 22 (7), 792–799. doi:10.1038/nm.4125

Li, Y., Wang, H., Wang, X., Jin, W., Tan, Y., Fang, H., et al. (2016). Genome-wide Studies Identify a Novel Interplay between AML1 and AML1/ETO in T(8;21) Acute Myeloid Leukemia. *Blood.* 127 (2), 233–242. doi:10.1182/blood-2015-03-626671

Li, Z., Huang, H., Li, Y., Jiang, X., Chen, P., Arnovitz, S., et al. (2012). Up-regulation of a HOXA-PBX3 Homeobox-Gene Signature Following Down-Regulation of miR-181 Is Associated with Adverse Prognosis in Patients with Cytogenetically Abnormal AML. *Blood.* 119 (10), 2314–2324. doi:10.1182/blood-2011-10-386235

Long, N. A., Golla, U., Sharma, A., and Claxton, D. F. (2022). Acute Myeloid Leukemia Stem Cells: Origin, Characteristics, and Clinical Implications. *Stem Cell Rev Rep.* doi:10.1007/s12015-021-10308-6

Metzelder, S. K., Michel, C., von Bonin, M., Rehberger, M., Hessmann, E., Inselmann, S., et al. (2015). NFATc1 as a Therapeutic Target in FLT3-ITD-Positive AML. *Leukemia.* 29 (7), 1470–1477. doi:10.1038/leu.2015.95

Mills, K. I., Kohlmann, A., Williams, P. M., Wieczorek, L., Liu, W. M., Li, R., et al. (2009). Microarray-based Classifiers and Prognosis Models Identify Subgroups with Distinct Clinical Outcomes and High Risk of AML Transformation of Myelodysplastic Syndrome. *Blood.* 114 (5), 1063–1072. doi:10.1182/blood-2008-10-187203

Mittag, T., and Parker, R. (2018). Multiple Modes of Protein-Protein Interactions Promote RNP Granule Assembly. *J. Mol. Biol.* 430 (23), 4636–4649. doi:10.1016/j.jmb.2018.08.005

Mohan, S., Hu, Y., and Edderkaoui, B. (2013). Identification of Gender-Specific Candidate Genes that Influence Bone Microarchitecture in Chromosome 1. *Calcif Tissue Int.* 92 (4), 362–371. doi:10.1007/s00223-012-9687-1

Moon, S. L., Morisaki, T., Khong, A., Lyon, K., Parker, R., and Stasevich, T. J. (2019). Multicolour Single-Molecule Tracking of mRNA Interactions with RNP Granules. *Nat. Cell Biol.* 21 (2), 162–168. doi:10.1038/s41556-018-0263-4

Mootha, V. K., Lindgren, C. M., Eriksson, K. F., Subramanian, A., Sihag, S., Lehar, J., et al. (2003). PGC-1alpha-responsive Genes Involved in Oxidative Phosphorylation Are Coordinately Downregulated in Human Diabetes. *Nat. Genet.* 34 (3), 267–273. doi:10.1038/ng1180

Muñoz, L., Nomdedéu, J. F., López, O., Carnicer, M. J., Bellido, M., Aventín, A., et al. (2001). Interleukin-3 Receptor Alpha Chain (CD123) Is Widely Expressed in Hematologic Malignancies. *Haematologica.* 86 (12), 1261–1269.

Newell, L. F., and Cook, R. J. (2021). Advances in Acute Myeloid Leukemia. *BMJ.* 375, n2026. doi:10.1136/bmj.n2026

Ng, S. W., Mitchell, A., Kennedy, J. A., Chen, W. C., McLeod, J., Ibrahimova, N., et al. (2016). A 17-gene Stemness Score for Rapid Determination of Risk in Acute Leukaemia. *Nature.* 540 (7633), 433–437. doi:10.1038/nature20598

Nguyen, D. H., Ball, E. D., and Varki, A. (2006). Myeloid Precursors and Acute Myeloid Leukemia Cells Express Multiple CD33-Related Siglecs. *Exp. Hematol.* 34 (6), 728–735. doi:10.1016/j.exphem.2006.03.003

Paczulla, A. M., Rothfelder, K., Raffel, S., Konantz, M., Steinbacher, J., Wang, H., et al. (2019). Absence of NKG2D Ligands Defines Leukaemia Stem Cells and Mediates Their Immune Evasion. *Nature.* 572 (7768), 254–259. doi:10.1038/s41586-019-1410-1

Protter, D. S. W., and Parker, R. (2016). Principles and Properties of Stress Granules. *Trends Cell Biol.* 26 (9), 668–679. doi:10.1016/j.tcb.2016.05.004

Radpour, R., Riether, C., Simillion, C., Höpner, S., Bruggmann, R., and Ochsenbein, A. F. (2019). $CD8^+$ T Cells Expand Stem and Progenitor Cells in Favorable but Not Adverse Risk Acute Myeloid Leukemia. *Leukemia.* 33 (10), 2379–2392. doi:10.1038/s41375-019-0441-9

Rapin, N., Bagger, F. O., Jendholm, J., Mora-Jensen, H., Krogh, A., Kohlmann, A., et al. (2014). Comparing Cancer vs normal Gene Expression Profiles Identifies New Disease Entities and Common Transcriptional Programs in AML Patients. *Blood.* 123 (6), 894–904. doi:10.1182/blood-2013-02-485771

Ritchie, M. E., Phipson, B., Wu, D., Hu, Y., Law, C. W., Shi, W., et al. (2015). Limma powers Differential Expression Analyses for RNA-Sequencing and Microarray Studies. *Nucleic Acids Res.* 43 (7), e47. doi:10.1093/nar/gkv007

Rundberg Nilsson, A., Soneji, S., Adolfsson, S., Bryder, D., and Pronk, C. J. (2016). Human and Murine Hematopoietic Stem Cell Aging Is Associated with Functional Impairments and Intrinsic Megakaryocytic/Erythroid Bias. *Plos One.* 11 (7), e0158369. ARTN e0158369. doi:10.1371/journal.pone.0158369

Sachs, K., Sarver, A. L., Noble-Orcutt, K. E., LaRue, R. S., Antony, M. L., Chang, D., et al. (2020). Single-Cell Gene Expression Analyses Reveal Distinct Self-Renewing and Proliferating Subsets in the Leukemia Stem Cell Compartment in Acute Myeloid Leukemia. *Cancer Res.* 80 (3), 458–470. doi:10.1158/0008-5472.CAN-18-2932

Salvarani, N., Maguy, A., De Simone, S. A., Miragoli, M., Jousset, F., and Rohr, S. (2017). TGF-β_1 (Transforming Growth Factor-B_1) Plays a Pivotal Role in Cardiac Myofibroblast Arrhythmogenicity. *Circ. Arrhythm Electrophysiol.* 10 (5), e004567. doi:10.1161/CIRCEP.116.004567

Schepers, K., Campbell, T. B., and Passegué, E. (2015). Normal and Leukemic Stem Cell Niches: Insights and Therapeutic Opportunities. *Cell Stem Cell.* 16 (3), 254–267. doi:10.1016/j.stem.2015.02.014

Schofield, R. (1978). The Relationship between the Spleen colony-forming Cell and the Haemopoietic Stem Cell. *Blood Cells* 4 (1-2), 7–25.

Stengel, K. R., Ellis, J. D., Spielman, C. L., Bomber, M. L., and Hiebert, S. W. (2021). Definition of a Small Core Transcriptional Circuit Regulated by AML1-ETO. *Mol. Cell.* 81 (3), 530–e5. e535. doi:10.1016/j.molcel.2020.12.005

Subramanian, A., Tamayo, P., Mootha, V. K., Mukherjee, S., Ebert, B. L., Gillette, M. A., et al. (2005). Gene Set Enrichment Analysis: a Knowledge-Based Approach for Interpreting Genome-wide Expression Profiles. *Proc. Natl. Acad. Sci. U S A.* 102 (43), 15545–15550. doi:10.1073/pnas.0506580102

Taghiloo, S., and Asgarian-Omran, H. (2021). Immune Evasion Mechanisms in Acute Myeloid Leukemia: A Focus on Immune Checkpoint Pathways. *Crit. Rev. Oncol. Hematol.* 157, 103164. doi:10.1016/j.critrevonc.2020.103164

Tang, Z., Li, C., Kang, B., Gao, G., Li, C., and Zhang, Z. (2017). GEPIA: a Web Server for Cancer and normal Gene Expression Profiling and Interactive Analyses. *Nucleic Acids Res.* 45 (W1), W98–w102. doi:10.1093/nar/gkx247

Teague, R. M., and Kline, J. (2013). Immune Evasion in Acute Myeloid Leukemia: Current Concepts and Future Directions. *J. Immunother. Cancer.* 1 (13), 1–11. doi:10.1186/2051-1426-1-13

Tomasson, M. H., Xiang, Z., Walgren, R., Zhao, Y., Kasai, Y., Miner, T., et al. (2008). Somatic Mutations and Germline Sequence Variants in the Expressed Tyrosine Kinase Genes of Patients with De Novo Acute Myeloid Leukemia. *Blood.* 111 (9), 4797–4808. doi:10.1182/blood-2007-09-113027

Tregnago, C., Manara, E., Zampini, M., Bisio, V., Borga, C., Bresolin, S., et al. (2016). CREB Engages C/EBPδ to Initiate Leukemogenesis. *Leukemia.* 30 (9), 1887–1896. doi:10.1038/leu.2016.98

Tyner, J. W., Tognon, C. E., Bottomly, D., Wilmot, B., Kurtz, S. E., Savage, S. L., et al. (2018). Functional Genomic Landscape of Acute Myeloid Leukaemia. *Nature.* 562 (7728), 526–531. doi:10.1038/s41586-018-0623-z

van Galen, P., Hovestadt, V., Wadsworth Ii, M. H., Hughes, T. K., Griffin, G. K., Battaglia, S., et al. (2019). Single-Cell RNA-Seq Reveals AML Hierarchies Relevant to Disease Progression and Immunity. *Cell.* 176 (6), 1265–e24. e1224. doi:10.1016/j.cell.2019.01.031

Wouters, B. J., Löwenberg, B., Erpelinck-Verschueren, C. A., van Putten, W. L., Valk, P. J., and Delwel, R. (2009). Double CEBPA Mutations, but Not Single CEBPA Mutations, Define a Subgroup of Acute Myeloid Leukemia with a Distinctive Gene Expression Profile that Is Uniquely Associated with a Favorable Outcome. *Blood.* 113 (13), 3088–3091. doi:10.1182/blood-2008-09-179895

Yamashita, M., Dellorusso, P. V., Olson, O. C., and Passegué, E. (2020). Dysregulated Haematopoietic Stem Cell Behaviour in Myeloid Leukaemogenesis. *Nat. Rev. Cancer.* 20 (7), 365–382. doi:10.1038/s41568-020-0260-3

Yu, G., Wang, L. G., Han, Y., and He, Q. Y. (2012). ClusterProfiler: an R Package for Comparing Biological Themes Among Gene Clusters. *OMICS.* 16 (5), 284–287. doi:10.1089/omi.2011.0118

Zhang, L., Gajewski, T. F., and Kline, J. (2009). PD-1/PD-L1 Interactions Inhibit Antitumor Immune Responses in a Murine Acute Myeloid Leukemia Model. *Blood.* 114 (8), 1545–1552. doi:10.1182/blood-2009-03-206672

Conflict of Interest: The authors declare that the research was conducted in the absence of any commercial or financial relationships that could be construed as a potential conflict of interest.

Publisher's Note: All claims expressed in this article are solely those of the authors and do not necessarily represent those of their affiliated organizations, or those of the publisher, the editors and the reviewers. Any product that may be evaluated in this article, or claim that may be made by its manufacturer, is not guaranteed or endorsed by the publisher.

Copyright © 2022 Liu, Zhang, Zhao, Zhu, Li, Yang, Zhao, Zhang, Wang, Zhu, Ding and Li. This is an open-access article distributed under the terms of the Creative Commons Attribution License (CC BY). The use, distribution or reproduction in other forums is permitted, provided the original author(s) and the copyright owner(s) are credited and that the original publication in this journal is cited, in accordance with accepted academic practice. No use, distribution or reproduction is permitted which does not comply with these terms.

frontiers | Frontiers in Oncology

MINI REVIEW
published: 26 May 2022
doi: 10.3389/fonc.2022.916681

Individualized Treatment for Advanced Non-Small Cell Lung Cancer: A Case Report and Literature Review

*Qianqian Sun, Weiqing Li, Taorui Liu and Huiqin Guo**

Department of Thoracic Surgery, Beijing Shijitan Hospital, Capital Medical University, Beijing, China

The incidence of lung cancer is high and about 75% of the patients with lung cancer are found in the middle and advanced stage, which has a limited treatment strategy. Non-small cell lung cancer (NSCLC) accounts for about 85% of all lung cancers. In this article, we delineate the treatment process of a middle-aged male patient with advanced-stage lung cancer to explain the significance of individualized chemotherapy combined with immunotherapy and surgery. This patient has extensive bone metastasis with PS scores of 2. After nine cycles of preoperative neoadjuvant chemotherapy, surgery, and two cycles of postoperative adjuvant chemotherapy, the patient achieved complete response (CR) and his PS score was 0. Although there is a standard chemotherapy regimen for lung adenocarcinoma, the treatment effect varies because of individual differences. Comprehensive analysis of the characteristics of patients through a variety of means to develop a precise individualized chemotherapy plan will be a major direction of lung cancer treatment in the future. Additionally, surgical treatment for advanced lung cancer patients after chemotherapy can effectively reduce the primary lesion and prolong the survival time of patients.

Keywords: individualized treatment, NSCLC, surgery, chemotherapy, immunotherapy, targeted therapy

OPEN ACCESS

Edited by:
Dong-Hua Yang,
St. John's University, United States

Reviewed by:
Youping Deng,
Rush University Medical Center, United States
Li Su,
Harvard University, United States

***Correspondence:**
Huiqin Guo
guohuiqin@mail.ccmu.edu.cn

Specialty section:
This article was submitted to Pharmacology of Anti-Cancer Drugs, a section of the journal Frontiers in Oncology

Received: *09 April 2022*
Accepted: *21 April 2022*
Published: *26 May 2022*

Citation:
Sun Q, Li W, Liu T and Guo H (2022) Individualized Treatment for Advanced Non-Small Cell Lung Cancer: A Case Report and Literature Review. Front. Oncol. 12:916681. doi: 10.3389/fonc.2022.916681

INTRODUCTION

Lung cancer is a major health problem worldwide. About 2.1 million people are diagnosed with lung cancer and 1.8 million people die of lung cancer every year (1). Lung cancer is the leading cause of cancer death in the world. So far, there is still no effective method to screen for lung cancer, but studies have shown that annual low-dose chest CT (LDCT) can reduce lung cancer mortality by 20% and overall mortality by 6.7% compared with chest X-ray (CXR) (2). The US Preventive Services Task Force suggests that adults, aged 50 to 80, who have been smoking for 20 years, are still smoking, or have given up smoking for more than 15 years should be screened for lung cancer by LDCT (3). Lung cancer includes non-small cell lung cancer (NSCLC) and small cell lung cancer (SCLC). Adenocarcinoma is the most common pathological type in NSCLC (4), and squamous cell carcinoma ranks second (5). In recent years, the incidence of squamous-cell carcinoma has decreased significantly, which might be related to the lower smoking rate in high-income countries and changes in the composition of cigarettes (6).

Once lung cancer is suspected, diagnosis and staging must be made, because the treatment of lung cancer depends on its subtype and stage. The 5-year survival rates of NSCLC patients with stage I, stage II to stage III, and stage IV were 80%, 13-60%, and 0-10% respectively (7). Surgical resection is the standard treatment in stages I, II, and some IIIA (8). Adjuvant chemotherapy can improve the survival rate of stage II, IIA, or IB patients by 5% - 10%, but it also has side effects (9). For early NSCLC patients who are not suitable for surgery, stereotactic ablation radiotherapy (SABR) can be considered (10). Platinum-based chemotherapy (such as cisplatin and carboplatin) 2-drug regimen is standard for patients with stage IV NSCLC. Although chemotherapy is still indispensable in the treatment of lung cancer, targeted therapy for specific gene mutations has made progress in the past few years (11). The first-generation targeted drugs (gefitinib and erlotinib) and second-generation targeted drugs (afatinib and dacomitinib) for EGFR mutations can significantly improve progression-free survival time (PFS) and overall survival (OS) compared with double platinum chemotherapy (12–17). Crizotinib, a drug targeting ALK mutations, shows better survival than chemotherapy as the first-and second-line therapy in a phase III trial (18–20). In addition, targeted therapy against ROS1, BRAF, NTRK, MET, RET, KRAS, HER2, and other genes has achieved good results in clinical trials.

Compared with the second-line chemotherapy for NSCLC, patients with anti-PD-1 and anti-PD-L1 antibodies always maintain a higher survival rate, which has become an important treatment for primary NSCLC (21–24). In NSCLC, two recognized active immune checkpoints are the CTLA-4 and PD-1 axes. CTLA-4 is usually expressed on CD4 and CD8 positive T lymphocytes and inhibits T cell activation. PD-1 is expressed in T cells, B cells, and NK cells and regulates central and peripheral immune tolerance. The expression of PD-L1 in tumor cells leads to immune escape (25). In the study of non-squamous NSCLC, such as the phase 3 KEYNOTE-189 trial (26–28), PD-1 or PD-L1 antibody combined with platinum chemotherapy is better than chemotherapy alone. Now, patients whose PD-L1 expression is 50% or more can use pembrolizumab or atezolizumab monotherapy, chemotherapy plus immunotherapy, or dual-drug immunotherapy with or without chemotherapy (8). For patients with PD-L1 expression of less than 50%, chemotherapy combined with PD-1 or PD-L1 inhibitors is the standard treatment (8). However, rare toxic effects associated with immunotherapy can happen at any point. It has been reported that immune checkpoint inhibitors (ICIs) can be used for two years (22). If properly treated, immune-related side effects are usually transient, but in some cases, they can be fatal. However, there is a problem with drug resistance in both targeted therapy and immunotherapy. Dealing with the problem of drug resistance is critical for lung cancer treatment.

In recent years, the diagnosis and treatment of lung cancer have made some progress, but the effect is still not satisfactory. Individualized treatment of lung cancer has gradually become a newer trend. In this article, we present a case of a middle-aged male patient with advanced lung adenocarcinoma who underwent a descending surgery after 9 cycles of individualized chemotherapy combined with targeted immunotherapy and continued adjuvant chemotherapy until the condition reached complete response (CR). Here we will elaborate on the choice of treatment and the significance of surgery for patients with advanced lung cancer, to emphasize the importance of individualized therapy.

CASE PRESENTATION

The patient, a 69-year-old male, coughed intermittently with white mucous sputum after catching a cold for more than five months, developed left chest pain for more than two months, and felt wheezing and these symptoms aggravated after activity. Chest CT in the out-patient clinic suggested a tumor in the right lower hilum and multiple military nodules in both lungs and pleura. These findings indicated that central lung cancer should be considered. Pathological consultation revealed adenocarcinoma of the lung. Genetic examination showed EGFR exon20 insertion mutation. Carboplatin plus pemetrexed treatment was not effective, so he was transferred to our hospital. There is nothing special about past history, personal history, and family history. The patient was hoarse, suffocated, and in a wheelchair. PS scores: 2 points. On admission, tumor markers: CA125:93.8U/ml (normal value: 0-24U/ml) and CEA:1.74ng/ml (normal value: 0-5U/ml). Chest CT suggested that the space-occupying lesion in the lower lobe of the right lung was consistent with the manifestation of lung cancer (**Figure 1**). PET/CT: soft tissue mass was seen near the right hilum, FDG uptake increased unevenly, SUVmax9.2; left atlas, right 9th rib, left 10th rib, right humerus and sacrum showed multiple abnormal increased FDG uptake, SUVmax11.6. It was suggested that the

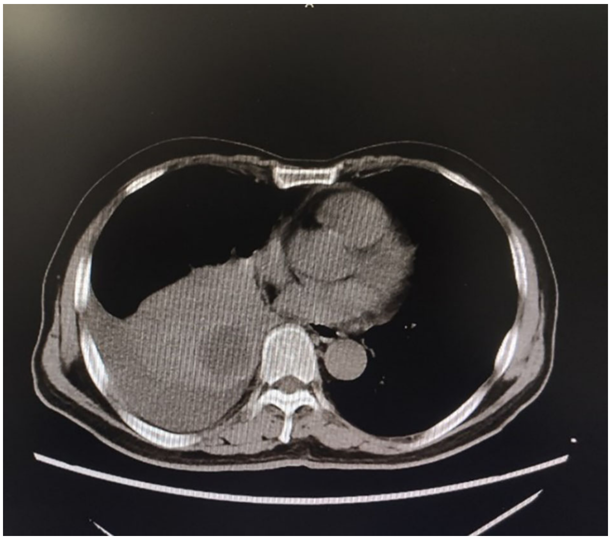

FIGURE 1 | Chest CT for the first time in our hospital showed a space-occupying mass in the lower lobe of the right lung.

hypermetabolic mass adjacent to the right hilum should be considered as the residual metabolic activity of the tumor after the treatment. Brain MRI: no abnormality. Pathological stage: T4N3M1c, stage IVB. Immunohistochemistry of drug sensitivity showed: BRCA-1 (-), ERCC-1 (+), TS (-), MSH-2 (+++), MSH-6 (+++),VEGF(-),PD-L1 (TPS=0). Combined with the examination results, we decided to carry out the first and second cycles of chemotherapy combined with targeted immunotherapy. The specific regimens were as follows: bevacizumab 500mg + pemetrexed 900mg + carboplatin 500mg + durvalumab 1000mg.However, the effect was not good, and the myelosuppression was obvious, so the adjusted regimen was bevacizumab 600mg + pemetrexed 900mg + nedaplatin 100mg + durvalumab 1000mg. After the third cycle of chemotherapy combined with targeted immunotherapy, the patients had few adverse reactions, so we continued to carry on the 4th-9th cycles. After nine cycles of chemotherapy, the re-examination of chest CT (**Figure 2**) and PET/CT showed that the metabolic activity of most of the films in the lower lobe of the right lung increased, SUVmax6.6, significantly reduced from the previous range, and the activity decreased (**Figure 3**). However, there was no change compared with the recent, and the tumor markers did not decrease, so we judged that drug resistance occurred. The relevant examination indexes were in accordance with the surgical indications, so a right lower lobe lobectomy was performed. Examination of postoperative freezing specimens showed: invasive lung adenocarcinoma in the lower lobe of the right lung, with two foci, one moderately differentiated (acinar type 70%, papillary type 20%, solid type 10%), and the other poorly differentiated (solid type 90%, acinar type 10%). The tumor surrounded the bronchial wall and there was a tumor thrombus inside blood vessels. Immunohistochemical results showed: CK7 (+), CK20 (+), TTF-1 (+), NapsinA (weak +), CK5 (-), P40 (-), ALK (D5F3) (-), Ki-67 (hot spot index 15%), P53 (wild type), MLH1 (+), MSH2 (+), MSH6 (+), PMS2 (+), PD-1 (UMAB199) (TILS:20%), NTRK (-). The cutting edge was negative, that is, R0 resection. The patients recovered well after the surgery (**Figure 4**) and received two cycles of postoperative adjuvant chemotherapy combined with targeted immunotherapy. The specific regimens were as follows: bevacizumab 600mg + pemetrexed 900mg + nedaplatin 100mg + durvalumab 1000mg. The tumor marker CA125:6.6 U/ml, CEA:2.0ng/ml, was significantly lower than that before treatment (**Figure 5**). Chest CT (**Figure 6**) suggested that the right pleural effusion decreased significantly after surgery. After two weeks of postoperative treatment, patients with mass elimination, negative lymph nodes, negative bone metastasis, normal tumor markers, PS score: 0, and no indication of progression, had reached CR, so we suspended chemotherapy, used immune maintenance therapy alone, requiring the patient to return regularly. It took one year from the beginning of the treatment to the time that the patient reached CR.

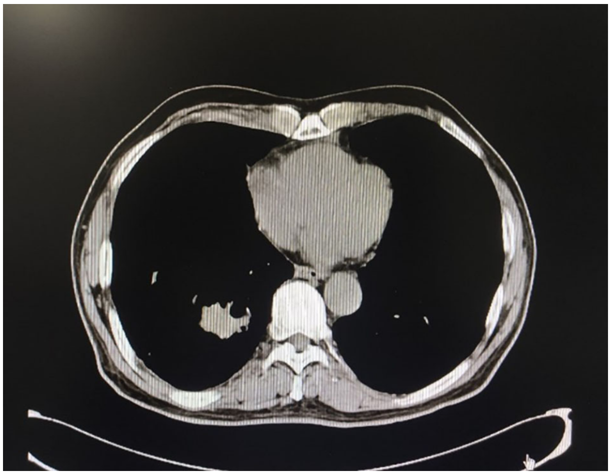

FIGURE 2 | Chest CT after nine cycles of treatment, the space-occupying mass in the lower lobe of the right lung was significantly reduced.

DISCUSSION AND LITERATURE REVIEW

Non-small cell lung cancer accounts for about 85% of lung cancer (29). With the understanding of gene mutation in NSCLC, the emergence of new drugs (30), and the use of immune checkpoint inhibitors, the treatment of NSCLC has improved. For most patients, chemotherapy is still an important part of systemic treatment, but for about 50% of advanced NSCLC patients (31), molecular targeted therapy or immunotherapy instead of chemotherapy is the standard first-line treatment.

According to the immunohistochemical results of the patients, it is suggested that carboplatin, nedaplatin, and pemetrexed can be used and immunotherapy is effective. Therefore, the external hospital regime: carboplatin combined with pemetrexed is selected first, but because of obvious myelosuppression, nedaplatin is used instead, and the effect is remarkable. Although immunohistochemistry indicates the effectiveness of the drug, it is still necessary to flexibly adjust the treatment regimen according to the patient's condition, to maximize the effect of chemotherapeutic drugs and minimize the adverse reactions, which reflects the necessity of individualized chemotherapy. The nine cycles of chemotherapy before surgery can be carried out smoothly because we provide patients with adequate support treatment and the patient's systemic condition and immunity are maintained at a good level. Because drug resistance develops after nine cycles of chemotherapy, and the tumor mass becomes small which is in line with surgical indication, surgery is considered. After the operation, the patient has no progress in metastatic focus. In our view, surgery not only removes the primary lesion, but also reduces the possibility of metastasis and recurrence. Postoperative pathology shows tumor heterogeneity and positive vascular thrombus, which provides a reference for further consolidation of chemotherapy.

Cancer patients with specific gene mutations can benefit from targeted therapy. 69% of patients with advanced NSCLC may have potential operable molecular targets (32). Targeted therapy is effective for adenocarcinoma, most of these patients are young

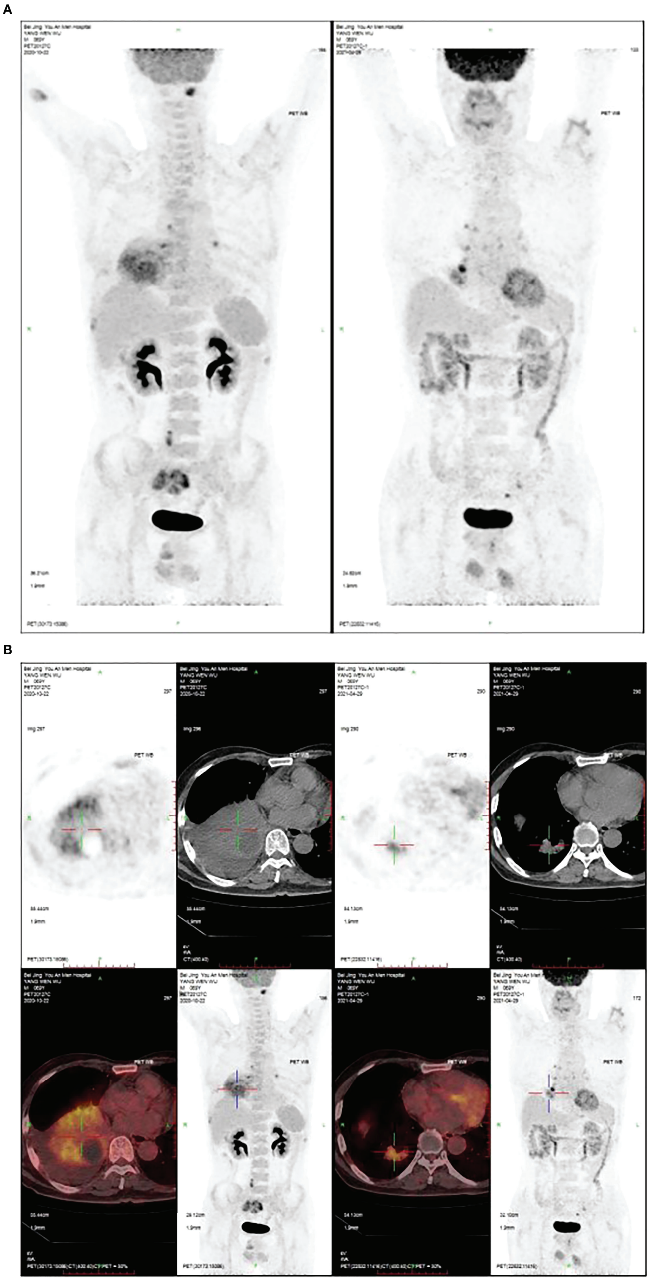

FIGURE 3 | **(A)** After nine cycles of treatment, the PET/CT of the hand and chest showed the space-occupying mass in the lower lobe of the right lung was significantly reduced. **(B)** The PET/CT of hand and chest after nine cycles of treatment. The space-occupying mass in the lower lobe of the right lung was significantly reduced.

and have never smoked (33).. Platinum dual therapy with or without bevacizumab is the most common choice for advanced NSCLC patients who cannot be treated with targeted therapy, which is also the standard first-line treatment. The understanding of tumor immune patterns, including immune escape, makes a breakthrough in the treatment and lays a foundation for the development of treatment in the future. In this case, although VEGF (-), but for non-squamous non-small cell lung cancer, the vascular targeting drug bevacizumab can be used. Attention needs to by being paid to side effects such as hypertension, hemoptysis, albuminuria, and others. As early as 2015, the BEYOND study (34) for the Chinese population confirms that bevacizumab combined chemotherapy can notably prolong PFS, and median total survival time (mOS) compared with chemotherapy alone. Meanwhile, the bevacizumab combined treatment group significantly improved the objective remission rate (ORR) and

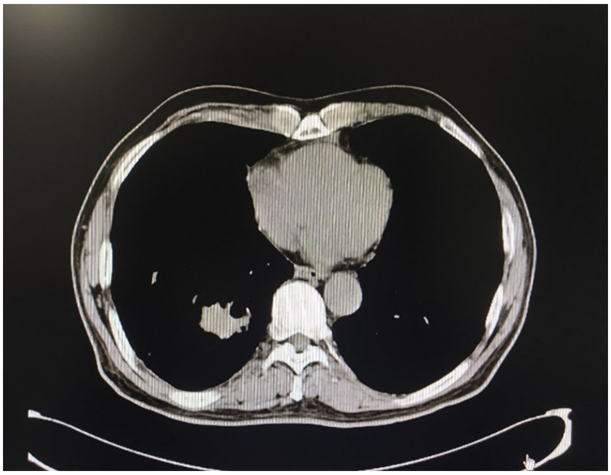

FIGURE 4 | Chest CT one month after surgery.

disease control rate (DCR). In 2018, the State Drug Administration (NMPA) approves the first-line treatment of platinum-containing dual-drug chemotherapy combined with bevacizumab for advanced NSCLC. According to the 2021 Chinese Society of Clinical Oncology (CSCO) guidelines for the diagnosis and treatment of non-small cell lung cancer (35), platinum-containing dual-drug chemotherapy or platinum-containing dual-drug chemotherapy plus bevacizumab (lung squamous cell carcinoma) should be included as first-line treatment for patients with EGFR mutant NSCLC in stage IV, and bevacizumab should be given the first choice for patients with stage IV NSCLC without driving gene and NSCLC. Although this patient has an EGFR mutation, it is specific to exon 20 insertion mutation (EGFR20ins). According to NCCN's latest guidelines on NSCLC (36): for EGFR20ins NSCLC patients, first-line treatment is chemotherapy combined with immunotherapy; when the disease progresses, targeted drugs, Amivantamab or Mobocertinib, are recommended. Because the effect of neoadjuvant therapy is better, we do not recommend patients take targeted drugs.

Immune checkpoint inhibitors (ICIs) are relatively new immunotherapy-based drugs. Different from traditional chemotherapy drugs, ICIs play a role in enhancing the natural tumor-killing response of the human body. Nivolumab and Pembrolizumab (PD-1 inhibitors), Atezolizumab and Durvalumab (PD-L1 inhibitors) have been approved by FDA in subsequent line therapy for advanced NSCLC patients without the sensitive mutation. They have been shown to improve the survival rate of advanced NSCLC. Although ICIs are not used in the guidelines for first-line treatment of advanced lung cancer patients with low expression of PD-L1, several new reports suggest that chemotherapy combined with immunotherapy as first-line treatment can effectively improve survival, regardless of PD-L1 expression level such as IMpower131、IMpower150. In one report (37), in the PD-L1 < 1% subgroup, the immune plus chemotherapy (I+C) regimen was more effective than chemotherapy in both OS and PFS. In the subgroup with PD-L1 ≥ 50%, the OS and PFS of the I+C regimen were also longer than those of chemotherapy. Therefore, for advanced NSCLC with different PD-L1 expressions, it is recommended to choose PD-1/PD-L1 inhibitors combined with chemotherapy in the first line and pay close attention to adverse events. Therefore, this patient chose chemotherapy combined with PD-L1 as the first choice. During the period of treatment, the tumor decreased significantly, and there were no immune-mediated adverse events in this patient. However, many factors must be considered in the treatment plan, such as therapeutic toxicity.

There is growing evidence that surgical resection is beneficial to survival in selective advanced patients. The

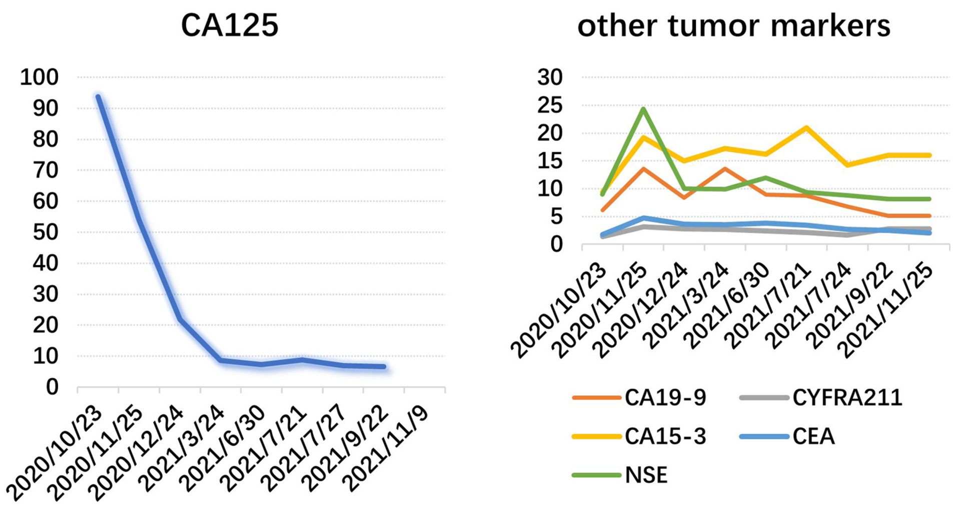

FIGURE 5 | Major abnormal tumor markers.

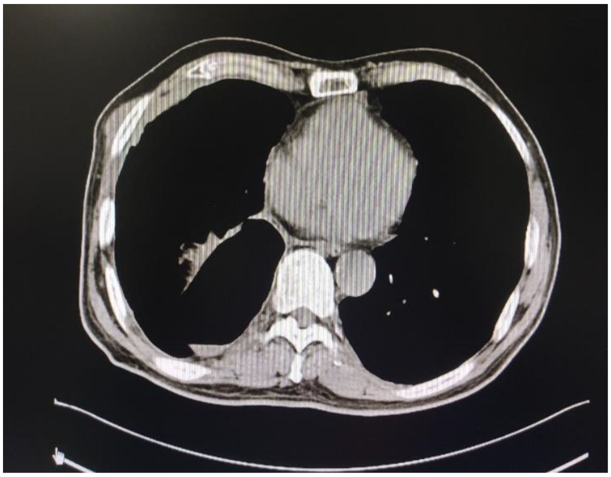

FIGURE 6 | Chest CT after lung surgery and after two cycles of postoperative treatment. The right pleural effusion decreased significantly.

surgery prolongs the survival time of some selected patients with stage IV NSCLC (38–40).. A national analysis (41) of long-term prognosis after surgery showed that the 5-year OS of patients with cT1-2, N0-1, M1 or cT3, N0, M1 was superior to non-operative treatment. These data supported surgical resection of specific advanced NSCLC patients. In a study (42) of a case with comprehensive treatment, the surgical prognoses of patients with stage IV NSCLC were analyzed, and the 1 -, 2-and 3-year OS rates were 75.9%, 59.1%, and 42.2% respectively. It is concluded that lung surgery may be a good choice for patients with IV stage NSCLC during comprehensive treatment. Surgical resection of malignant lesions can reduce the tumor load and restore the immune function of patients (43). Even in the case of pleural effusion (pleural dissemination or effusion is a contraindication for surgical treatment of NSCLC), the 5-years of OS after the surgery can reach 33.1%, and the patient recovers well after the surgery, and the primary tumor can be controlled (44). Many data suggest that radical surgery may be an option for symptom relief and further systematic treatment.

Lung cancer has strong temporal and spatial heterogeneity, which will affect its diagnosis and treatment. Understanding the heterogeneity of tumors may lead to new treatments, thus prolonging the survival time of patients with lung cancer in the future. It is the existence of tumor heterogeneity that makes individual differences in treatment methods. After a comprehensive evaluation of this patient, we worked out an accurate and individualized treatment plan; different treatment methods were given to different reactions due to individual differences in the process of treatment. The difference in pathological type and location of the patients determined the type of operation, which reflected the importance of individualized treatment. In short, the future treatment of lung cancer is inseparable from individualization.

CONCLUSION

The incidence and mortality of lung cancer are still high. Therefore, improving the therapeutic effect of lung cancer patients is an urgent task. In-depth study and understanding of tumor heterogeneity, continuing to find new treatment methods and individualized treatment for patients, will further improve the treatment outcome of lung cancer.

AUTHOR CONTRIBUTIONS

All authors contributed to the article and approved the submitted version.

REFERENCES

1. Bray F, Ferlay J, Soerjomataram I, Siegel RL, Torre LA, Jemal A. Global Cancer Statistics 2018: GLOBOCAN Estimates of Incidence and Mortality Worldwide for 36 Cancers in 185 Countries. *CA Cancer J Clin* (2018) 68:394–424. doi: 10.3322/caac.21492
2. Nasim F, Sabath BF, Eapen GA. Lung Cancer. *Med Clin North Am* (2019) 103 (3):463–73. doi: 10.1016/j.mcna.2018.12.006
3. Potter AL, Bajaj SS, Yang CJ. The 2021 USPSTF Lung Cancer Screening Guidelines: A New Frontier. *Lancet Respir Med* (2021) 9(7):689–91. doi: 10.1016/S2213-2600(21)00210-1
4. Curado M-P, Edwards B, Shin HR. *Cancer Incidence in Five Continents* Vol. Vol IX. Lyon: International Agency for Research on Cancer (2007).
5. Travis WD, Brambilla E, Burke A, Marx A, Nicholson AG. WHO Classification of Tumours of the Lung, Pleura, Thymus and Heart. *Lyon: Int Agency Res Cancer* 4:78–9 (2015).
6. Alberg AJ, Brock MV, Ford JG, Samet JM, Spivack SD. Epidemiology of Lung Cancer: Diagnosis and Management of Lung Cancer, 3rd Ed: American College of Chest Physicians Evidencebased Clinical Practice Guidelines. *Chest* (2013) 143(5 suppl):e1–29S. doi: 10.1378/chest.12-2345
7. Goldstraw P, Chansky K, Crowley J, Rami-Porta R, Asamura H, Eberhardt WE, et al. The IASLC Lung Cancer Staging Project: Proposals for Revision of the TNM Stage Groupings in the Forthcoming (Eighth) Edition of the TNM Classification for Lung Cancer. *J Thorac Oncol* (2016) 11:39–51. doi: 10.1016/j.jtho.2015.09.009
8. Thai AA, Solomon BJ, Sequist LV, Gainor JF, Heist RS. Lung Cancer. *Lancet* (2021) 398(10299):535–54. doi: 10.1016/S0140-6736(21)00312-3
9. Pignon JP, Tribodet H, Scagliotti GV, Douillard JY, Shepherd FA, Stephens RJ, et al. Lung Adjuvant Cisplatin Evaluation: A Pooled Analysis by the LACE Collaborative Group. *J Clin Oncol* (2008) 26:3552–59. doi: 10.1200/JCO.2007.13.9030
10. Tokes WA, Rusthoven CG. Surgery vs. SBRT in Retrospective Analyses: Confounding by Operability is the Elephant in the Room. *J Thorac Dis* (2018) 10(Suppl 17):S2007–10. doi: 10.21037/jtd.2018.05.40
11. Socinski MA, Evans T, Gettinger S, Hensing TA, VanDam Sequist L, Ireland B, et al. Treatment of Stage IV non-Small Cell Lung Cancer: Diagnosis and Management of Lung Cancer, 3rd Ed: American College of Chest Physicians Evidence-Based Clinical Practice Guidelines. *Chest* (2013) 143(5 Suppl): e341S–68S. doi: 10.1378/chest.12-2361
12. Mok TS, Wu Y-L, Thongprasert S, Yang CH, Chu DT, Saijo N, et al. Gefitinib or Carboplatinpaclitaxel in Pulmonary Adenocarcinoma. *N Engl J Med* (2009) 361:947–57. doi: 10.1056/NEJMoa0810699

13. Zhou C, Wu YL, Chen G, Feng J, Liu XQ, Wang C, et al. Final Overall Survival Results From a Randomised, Phase III Study of Erlotinib Versus Chemotherapy as First-Line Treatment of EGFR Mutation-Positive Advanced Non-Smallcell Lung Cancer (OPTIMAL, CTONG-0802). *Ann Oncol* (2015) 26:1877–83. doi: 10.1093/annonc/mdv276
14. Rosell R, Carcereny E, Gervais R, Vergnenegre A, Massuti B, Felip E, et al. Erlotinib Versus Standard Chemotherapy as First-Line Treatment for European Patients With Advanced EGFR Mutation-Positive Non-Small-Cell Lung Cancer (EURTAC): A Multicentre, Open-Label, Randomised Phase 3 Trial. *Lancet Oncol* (2012) 13:239–46. doi: 10.1016/S1470-2045(11)70393-X
15. Wu YL, Zhou C, Liam CK, Wu G, Liu X, Zhong Z, et al. First-Line Erlotinib Versus Gemcitabine/Cisplatin in Patients With Advanced EGFR Mutationpositive Non-Small-Cell Lung Cancer: Analyses From the Phase III, Randomized, Open-Label, ENSURE Study. *Ann Oncol* (2015) 26:1883–89. doi: 10.1093/annonc/mdv270
16. Yang JJ, Zhou Q, Yan HH, Zhang XC, Chen HJ, Tu HY, et al. A Phase III Randomised Controlled Trial of Erlotinib vs Gefitinib in Advanced Non-Small Cell Lung Cancer With EGFR Mutations. *Br J Cancer* (2017) 116:568–74. doi: 10.1038/bjc.2016.456
17. Sequist LV, Yang JC, Yamamoto N, O'Byrne K, Hirsh V, Mok T, et al. Phase III Study of Afatinib or Cisplatin Plus Pemetrexed in Patients With Metastatic Lung Adenocarcinoma With EGFR Mutations. *J Clin Oncol* (2013) 31:3327–34. doi: 10.1200/JCO.2012.44.2806
18. Kwak EL, Bang YJ, Camidge DR, Shaw AT, Solomon B, Maki RG, et al. Anaplastic Lymphoma Kinase Inhibition in Non-Small-Cell Lung Cancer. *N Engl J Med* (2010) 363:1693–703. doi: 10.1056/NEJMoa1006448
19. Camidge DR, Bang YJ, Kwak EL, Iafrate AJ, Varella-Garcia M, Fox SB, et al. Activity and Safety of Crizotinib in Patients With ALK-Positive Non-Small-Cell Lung Cancer: Updated Results From a Phase 1 Study. *Lancet Oncol* (2012) 13:1011–19. doi: 10.1016/S1470-2045(12)70344-3
20. Solomon BJ, Kim DW, Wu YL, Nakagawa K, Mekhail T, Felip E, et al. Final Overall Survival Analysis From a Study Comparing First-Line Crizotinib Versus Chemotherapy in ALK-Mutation-Positive Non-Small-Cell Lung Cancer. *J Clin Oncol* (2018) 36:2251–58. doi: 10.1200/JCO.2017.77.4794
21. Garon EB, Rizvi NA, Hui R, Leighl N, Balmanoukian AS, Eder JP, et al. Pembrolizumab for the Treatment of Non-Small-Cell Lung Cancer. *N Engl J Med* (2015) 372:2018–28. doi: 10.1056/NEJMoa1501824
22. Herbst RS, Baas P, Kim DW, Felip E, Pérez-Gracia JL, Han JY, et al. Pembrolizumab Versus Docetaxel for Previously Treated, PD-L1-Positive, Advanced Non-Small-Cell Lung Cancer (KEYNOTE-010): A Randomised Controlled Trial. *Lancet* (2016) 387(10027):1540–50. doi: 10.1016/S0140-6736(15)01281-7
23. Vokes EE, Ready N, Felip E, Horn L, Burgio MA, Antonia SJ, et al. Nivolumab Versus Docetaxel in Previously Treated Advanced Non-Small-Cell Lung Cancer (CheckMate 017 and CheckMate 057): 3-Year Update and Outcomes in Patients With Liver Metastases. *Ann Oncol* (2018) 29:959–65. doi: 10.1093/annonc/mdy041
24. Rittmeyer A, Barlesi F, Waterkamp D, Park K, Ciardiello F, von Pawel J, et al. Atezolizumab Versus Docetaxel in Patients With Previously Treated Non-Small-Cell Lung Cancer (OAK): A Phase 3, Open-Label, Multicentre Randomised Controlled Trial. *Lancet* (2017) 389:255–65. doi: 10.1016/S0140-6736(16)32517-X
25. Zarour HM. Reversing T-Cell Dysfunction and Exhaustion in Cancer. *Clin Cancer Res* (2016) 22:1856–64. doi: 10.1158/1078-0432.CCR-15-1849
26. Gadgeel SM, Garassino MC, Esteban E, Speranza G, Felip E, Hochmair MJ, et al. KEYNOTE-189: Updated OS and Progression After the Next Line of Therapy (PFS2) With Pembrolizumab (Pembro) Plus Chemo With Pemetrexed and Platinum vs Placebo Plus Chemo for Metastatic Nonsquamous NSCLC. *Proc Am Soc Clin Oncol* (2019) 37(suppl):9013. doi: 10.1200/JCO.2019.37.15_suppl.9013
27. Gadgeel S, Rodríguez-Abreu D, Speranza G, Esteban E, Felip E, Dómine M, et al. Updated Analysis From KEYNOTE-189: Pembrolizumab or Placebo Plus Pemetrexed and Platinum for Previously Untreated Metastatic Nonsquamous Non-Small-Cell Lung Cancer. *J Clin Oncol* (2020) 38:1505–17. doi: 10.1200/JCO.19.03136
28. Gandhi L, Rodríguez-Abreu D, Gadgeel S, Esteban E, Felip E, De Angelis F, et al. Pembrolizumab Plus Chemotherapy in Metastatic Non-Small-Cell Lung Cancer. *N Engl J Med* (2018) 378:2078–92. doi: 10.1056/NEJMoa1801005
29. Govindan R, Page N, Morgensztern D, Read W, Tierney R, Vlahiotis A, et al. Changing Epidemiology of Small-Cell Lung Cancer in the United States Over the Last 30 Years: Analysis of the Surveillance, Epidemiologic, and End Results Database. *J Clin Oncol* (2006) 24(28):4539–44. doi: 10.1200/JCO.2005.04.4859
30. Jordan EJ, Kim HR, Arcila ME, Barron D, Chakravarty D, Gao J, et al. Prospective Comprehensive Molecular Characterization of Lung Adenocarcinomas for Efficient Patient Matching to Approved and Emerging Therapies. *Cancer Discov* (2017) 7(6):596–609. doi: 10.1158/2159-8290.CD-16-1337
31. Arbour KC, Riely GJ. Systemic Therapy for Locally Advanced and Metastatic Non-Small Cell Lung Cancer: A Review. *JAMA* (2019) 322(8):764–74. doi: 10.1001/jama.2019.11058
32. Tsao AS, Scagliotti GV, Bunn PAJr, Carbone DP, Warren GW, Bai C, et al. Scientifi C Advances in Lung Cancer 2015. *J Thorac Oncol* (2016) 11:613–38. doi: 10.1016/j.jtho.2016.03.012
33. Hirsch FR, Scagliotti GV, Mulshine JL, Kwon R, Curran WJJr, Wu YL, et al. Lung Cancer: Current Therapies and New Targeted Treatments. *Lancet* (2017) 389(10066):299–311. doi: 10.1016/S0140-6736(16)30958-8
34. Zhou C, Wu YL, Chen G, Liu X, Zhu Y, Lu S, et al. BEYOND: A Randomized, Double-Blind, Placebo-Con- Trolled, Multicenter, Phase IIIstudy of First-Line Carboplatin/Paclitaxel Plus Bevacizumab or Placebo in Chinese Patients With Advanced or Recurrent Nonsquamous Non-Small-Cell Lung Cancer. *J Clin Oncol* (2015) 33(19):2197–204. doi: 10.1200/JCO.2014.59.4424
35. People's Medical Publishing House(PMPH). *Guidelines Working Committee of the Chinese Society of Clinical Oncology the 2021 Chinese Society of Clinical Oncology (CSCO) Guidelines for the Diagnosis and Treatment of Non-Small Cell Lung Cancer* (2021) Beijing: People's Medical Publishing House (PMPH)
36. NCCN.org. *NCCN Clinical Practice Guidelines in Oncology, Non-Small Cell Lung Cancer, Version 6* (2021) Plymouth Meeting, USA: National Comprehensive Cancer Network (NCCN)
37. Liang H, Liu Z, Cai X, Pan Z, Chen D, Li C, et al. PD-(L)1 Inhibitors vs. Chemotherapy vs. Their Combination in Front-Line Treatment for NSCLC: An Indirect Comparison. *Int J Cancer* (2019) 145(11):3011–21. doi: 10.1002/ijc.32366
38. Hanagiri T, Takenaka M, Oka S, Shigematsu Y, Nagata Y, Shimokawa H, et al. Results of a Surgical Resection for Patients With Stage IV Non-Small-Cell Lung Cancer. *Clin Lung Cancer* (2012) 13:220–4. doi: 10.1016/j.cllc.2011.05.006
39. Kawano D, Takeo S, Katsura M, Tsukamoto S, Masuyama E, Nakaji Y. Surgical Treatment of Stage IV Non-Small Cell Lung Cancer. *Interact Cardiovasc Thorac Surg* (2012) 14:167–70. doi: 10.1093/icvts/ivr036
40. Collaud S, Stahel R, Inci I, Hillinger S, Schneiter D, Kestenholz P, et al. Survival of Patients Treated Surgically for Synchronous Single-Organ Metastatic NSCLC and Advanced Pathologic TN Stage. *Lung Cancer* (2012) 78:234–8. doi: 10.1016/j.lungcan.2012.09.011
41. Yang CJ, Gu L, Shah SA, Yerokun BA, D'Amico TA, Hartwig MG, et al. Long-Term Outcomes of Surgical Resection for Stage IV Non-Small-Cell Lung Cancer: A National Analysis. *Lung Cancer* (2018) 115:75–83. doi: 10.1016/j.lungcan.2017.11.021
42. Zhang C, Wang L, Li W, Huang Z, Liu W, Bao P, et al. Surgical Outcomes of Stage IV Non-Small Cell Lung Cancer: A Single-Center Experience. *J Thorac Dis* (2019) 11(12):5463–73. doi: 10.21037/jtd.2019.11.30
43. Jin WB, Liang CY, Peng YH, Zhou NK. Pleuropneumonectomy for Diffuse Pleural Metastasis in Primary Lung Cancer. *J Cancer Res Ther* (2013) 9:S92–7. doi: 10.4103/0973-1482.119115
44. Iida T, Shiba M, Yoshino I, Miyaoka E, Asamura H, Date H, et al. Surgical Intervention for Non-Small-Cell Lung Cancer Patients With Pleural Carcinomatosis: Results From the Japanese Lung Cancer Registry in 2004. *J Thorac Oncol* (2015) 10:1076–82. doi: 10.1097/JTO.0000000000000554

Conflict of Interest: The authors declare that the research was conducted in the absence of any commercial or financial relationships that could be construed as a potential conflict of interest.

Publisher's Note: All claims expressed in this article are solely those of the authors and do not necessarily represent those of their affiliated organizations, or those of the publisher, the editors and the reviewers. Any product that may be evaluated in this article, or claim that may be made by its manufacturer, is not guaranteed or endorsed by the publisher.

Copyright © 2022 Sun, Li, Liu and Guo. This is an open-access article distributed under the terms of the Creative Commons Attribution License (CC BY). The use, distribution or reproduction in other forums is permitted, provided the original author(s) and the copyright owner(s) are credited and that the original publication in this journal is cited, in accordance with accepted academic practice. No use, distribution or reproduction is permitted which does not comply with these terms.

frontiers | Frontiers in Oncology

ORIGINAL RESEARCH
published: 13 June 2022
doi: 10.3389/fonc.2022.889049

Identification and Validation of an Apoptosis-Related Gene Prognostic Signature for Oral Squamous Cell Carcinoma

Shuqin Wang [1,2†], ***Sien Zhang*** [1†], ***Zhi Lin*** [3], ***Jingxin Ma*** [1], ***Lijun Zhu*** [2,4*] ***and Guiqing Liao*** [1*]

[1] Hospital of Stomatology, Guanghua School of Stomatology, Sun Yat-sen University, Guangdong Provincial Key Laboratory of Stomatology, Guangzhou, China, [2] Department of Oral and Maxillofacial Surgery, Guangdong Provincial People's Hospital & Guangdong Academy of Medical Sciences, Guangzhou, China, [3] Department of Stomatology, The Sixth Affiliated Hospital, Sun Yat-sen University, Guangzhou, China, [4] School of Stomatology, Southern Medical University, Guangzhou, China

OPEN ACCESS

Edited by:
Dong-Hua Yang,
St. John's University, United States

Reviewed by:
Hailong Ma,
Shanghai Jiao Tong University, China
Pranav Gupta,
Albert Einstein College of Medicine,
United States

***Correspondence:**
Guiqing Liao
liaogq@mail.sysu.edu.cn
Lijun Zhu
Zhulijun114@126.com

[†]These authors have contributed equally to this work and share first authorship

Specialty section:
This article was submitted to Pharmacology of Anti-Cancer Drugs, a section of the journal Frontiers in Oncology

Received: 03 March 2022
Accepted: 25 April 2022
Published: 13 June 2022

Citation:
Wang S, Zhang S, Lin Z, Ma J, Zhu L and Liao G (2022) Identification and Validation of an Apoptosis-Related Gene Prognostic Signature for Oral Squamous Cell Carcinoma. Front. Oncol. 12:889049. doi: 10.3389/fonc.2022.889049

To identify an apoptosis-related gene (ARG) prediction model for oral squamous cell carcinoma (OSCC), we analyzed and validated the data from TCGA and GEO, respectively. Kaplan–Meier survival analysis and ROC curves showed a good prognostic ability of the model both in the internal training set and in the external testing set. Furthermore, we built a nomogram using these ARGs to forecast the survival probability of OSCC patients. Moreover, we evaluated the rate of immune cells infiltrating in the tumor samples and found obvious, different patterns between the high and low risk groups. GO and KEGG analyses demonstrated multiple molecular biological processes and signaling pathways connecting with this prognostic model in OSCC. The expression of these risk genes in clinical specimens was higher in the non-survival patients than in the well-survival patients by immunohistochemical staining analysis. In conclusion, we established a signature made up of six risk apoptosis-related genes to predict the survival rate of OSCC. These genes could also be targets for the treatment of OSCC.

Keywords: oral squamous cell carcinoma, apoptosis-related genes, prognosis, nomogram, the cancer genome atlas

INTRODUCTION

In 2020, almost 377,713 new cases and 177,757 deaths of OSCC occurred all around the world (1). Traditionally, risk factors for OSCC include tobacco smoking, chewing betel nut, alcohol, excessive sunlight exposure, HPV infection, and poor oral hygiene (2).The primary treatment for oral squamous cell cancer (OSCC) patients is surgical resection plus chemotherapy and radiotherapy. Despite of the advancements in all these treatments nowadays, the 5-year survival rate remains poor (3). For decades, attempts to improve the prognosis have failed because of the complicated heterogeneity of tumors. Several patients are still over- or undertreated due to the unsatisfactory forecasting efficiency of conventional prognostic indicators and the uniformity of therapy guidelines (4). Currently, no molecular subtype that can guide individual targeted therapy has been recognized. Therefore, researchers are eager to identify the specific carcinogenesis and prognostic genes of OSCC.

Apoptosis or programmed cell death (PCD) is an evolutionarily conserved process to promote the development of organisms and keep the balance of tissue homeostasis (5). This progress is described as the cell suicide process. Overactivation or inactivation of apoptosis leads to diseases, such as Parkinson's disease and tumorigenesis (6, 7). Escaping from apoptosis was considered as one of the 10 hallmarks of cancer. A great number of studies have indicated the key role of apoptosis in tumorigenesis and chemotherapy resistance (8). Researchers tried to restore each defect of the apoptosis signaling pathway and wiped out the cancer cells. They are focused on targeting the anti-apoptotic Bcl-2 family member (9), p53 (10), c-FLIP, and caspase families (11) (12). For example, myeloid cell leukemia-1 (MCL1), one of the anti-apoptotic proteins, has been identified as a prospective therapeutic target. Previous studies showed the potential value of apoptosis-related genes or proteins such as Bcl-2 and Survivin in the diagnosis and treatment of OSCC (13).

Our research hopes to identify the key prognostic genes and establish the core network of OSCC by using comprehensive bioinformatics analysis based on apoptosis-related genes.

MATERIALS AND METHODS

The Collection of Apoptosis-Related Genes

We extracted the apoptosis-related gene sets from the Gene Set Enrichment Analysis (GSEA) dataset (http://www.gsea-msigdb.org/gsea/index.jsp), Reactome dataset (https://reactome.org/), and KEGG dataset (https://www.kegg.jp/kegg/). A total of 438 apoptosis-related genes (ARGs) were picked out and used for analysis.

Data Acquisition

We got the RNA sequences and clinical information of 213 OSCC patients and 16 healthy human from TCGA database. Another dataset including 97 OSCC patients with complete follow-up data (GSE41613) was extracted from the GEO database. The data from TCGA were recognized as an internal training dataset, and the data from GEO were used as an external testing dataset.

Identification of the Prognostic ARGs and Construction of the Prognostic Model

In TCGA dataset, we conducted univariate Cox analysis and Kaplan–Meier (K-M) survival analysis to seek ARGs associated with overall survival (OS) of OSCC. When ARGs met the criteria of p-value <0.05 in the two tests referred above, they were recognized as prognosis-related ARGs. These ARGs were selected for least absolute shrinkage and selection operator (LASSO). Next, we used multiple Cox analyses to select the independent ARGs. The risk score could be calculated by the following formula: Risk score=*Expression level of gene*1 × β1 + *Expression level of gene*2 × β2 + *Expression level of gene*3 × β3 + ⋯.

β represents the coefficient. Therefore, we can acquire the risk score of OSCC patients easily. Based on the median risk score, all the patients were assigned into low-risk and high-risk groups. Then, K-M analysis was conducted to value the difference in survival rate between these two groups. In the study, the receiver operating characteristic (ROC) curve was applied. The value of the corresponding area under the ROC curve (AUC) could be used to test the sensitivity of this model and compare the forecasting accuracy with traditional clinical factors (14). In addition, we conducted univariate and multivariate analyses to assess the independent ability for predicting prognosis. Moreover, the external testing dataset from GEO was used to check the prognostic capability of the model.

Construction of Nomogram

Furthermore, we created a nomogram to predict the OS of the OSCC patients on the basis of the independent prognostic ARGs. A calibration curve was applied to assess the efficiency of the nomogram. Finally, we verified the prognostic nomogram in the external testing dataset in the same way.

Tumor-Infiltrating Immune Cell Analysis

To assess the infiltration pattern of immune cells in two risk groups, we applied the CIBERSORT analysis (15). In order to know more about the relationship between the immune microenvironment and apoptosis, we conducted the correlation analysis of nine types of immune cell and risk score.

Functional Enrichment Analysis

We conducted Gene Ontology (GO) and Kyoto Encyclopedia of Genes and Genomes (KEGG) analyses for these six ARGs. These analyses discovered a series of molecular biological process and multiple signaling pathways *via* the R package clusterProfiler 4.0 (16). Moreover, an interaction network was built to display the correlation of six ARGs.

Unsupervised Clustering Analysis

Unsupervised clustering analysis was used to distinguish patient subgroups with different apoptosis modification patterns based on the expression of the six ARGs. With the "Consensus Cluster Plus" R package, patients were assigned by k-means, with k from 2 to 9. On the grounds of the dispersion of the resulting consensus clustering matrix, a cumulative distribution function (CDF) curve, and the likelihood ratio, we obtained the optimal number of clusters. Moreover, we compared the different prognoses among the apoptosis clusters with K-M analysis.

The Pan-Cancer Analysis

We acquired the expression data of the six genes in pan-cancer through GEPIA2. Then, we got the Cox proportional hazard ratio by R survival package to explore the relationship of the six genes and OS of pan-cancer.

Immunohistochemical Staining and Evaluation

Immunohistochemical (IHC) staining of MCL1, GPI, and ARHGAP10 was performed using rabbit polyclonal anti-MCL1, anti-GPI, anti-ARHGAP10 antibodies (the concentration was 1:2,000, Cat. 16225-1-AP, 15171-1-AO, 55139-1-AP, respectively, Proteintech, Wuhan, China). All sections were scanned on an Aperio AT2 scanner (Leica Biosystems, Wetzlar, Germany) with a ×20 objective lens. We used Aperio ImageScope software to obtain the digital images of sample sections. Five random fields of the same size were selected in each slide. The H-score was carried out using the Aperio ImageScope software (17). All the samples were acquired from the first oral cancer radical surgery of the patients who had not received radiotherapy or chemotherapy yet. The patients who were diagnosed with oral squamous cell carcinoma for the first time were free of other cancers.

Statistical Analysis

We conducted all statistical analyses and graphs through R software. Cox proportional hazard regression analysis was used for univariate and multivariate analyses. Overall survival times were calculated by the Kaplan–Meier analysis. The H-scores of different groups were compared with paired T test, and significant difference was considered when $p < 0.05$.

RESULT

Selection of Crucial Genes and Identification of ARGs Associated With OSCC Survival

We collected 438 ARGs from the GSEA gene set and the Reactome and KEGG databases. Based on the criteria set as $p < 0.05$, and hazard ratio >1, 18 ARGs were selected which are shown in the forest plot (**Figure 1A**). These hub genes were incorporated in LASSO analysis. Detailed information of the LASSO model optimal parameter and LASSO coefficient profiles is displayed in **Figures 1B, C**. Then, we used the multivariate Cox regression analysis to filter these candidates and constructed a prognostic signature. Finally, six ARGs (CTH, DNAJC3, IER3, MCL1, GPI, ARHGAP10) were identified to establish an apoptosis-related signature. Among these genes, MCL1, GPI, and ARHGAP10 are associated with a higher risk than others because of the higher hazard ratios (**Figure 1D**).

Prognosis Model Construction and Risk Score Analysis

We used the six prognostic genes selected above as independent factors to construct the prediction model. The expression value of six genes could define the risk score accurately: Risk score = (0.4874×expression value of CTH) + (0.5198×expression value of

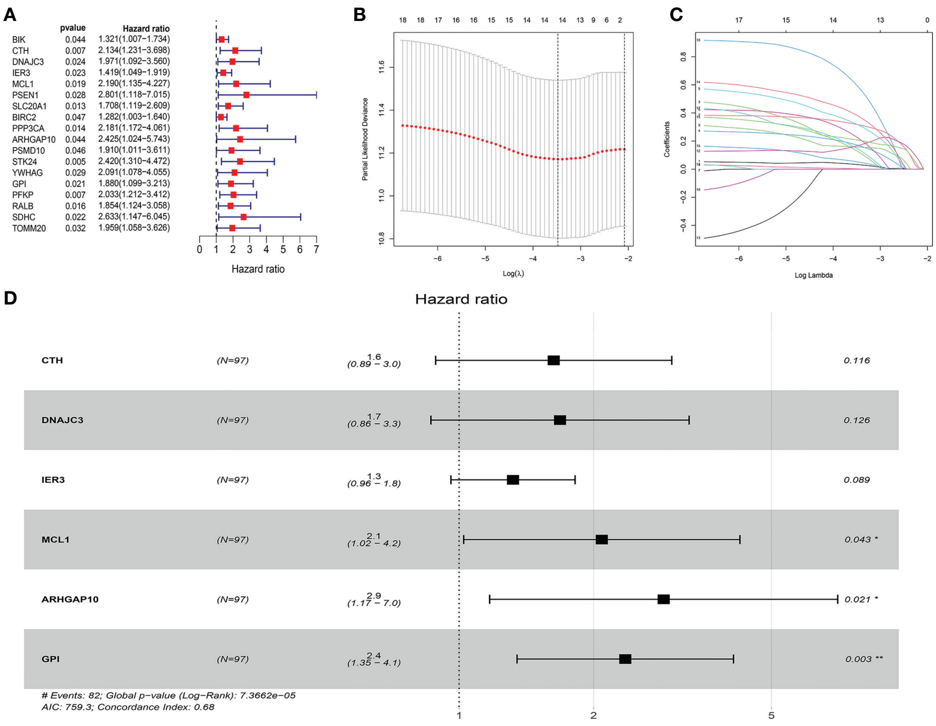

FIGURE 1 | Construction of the ARG model in the internal training dataset. **(A)** Forest plot showed that 18 risk genes were identified as prognostic ARGs through univariate Cox regression analysis (HR >1, $p < 0.05$). **(B, C)** LASSO analysis further picked up 14 ARGs. **(D)** The multiple Cox regression screened six independent predictors (CTH, DNAJC3, IER3, MCL1, GPI, ARHGAP10) of OSCC.

DNAJC3) + (0.2777× expression value of IER3) + (0.7352× expression value of MCL1) + (1.0540×expression value of ARHGAP10) + (0.8561×expression value of GPI). The median risk score allocated patients into low-risk and high-risk groups (**Figure 2A**). The results showed that the low-risk group has a longer survival time than the high-risk one (**Figure 2B**). A heat map reveals the different expression profile of six ARGs (**Figure 2C**). The patients in the low- and high-risk groups were gathered from different directions (**Figure 2D**). In addition, K-M analysis also supported that the low-risk group had a higher probability to survive (**Figure 2E**).

The ROC curves of the model showed a relatively good property, and the corresponding AUCs for 1-, 3-, and 5-year survival were 0.733, 0.720, and 0.760, which are displayed in **Figure 3A**. Univariate analysis results illustrated that the risk score ($p < 0.001$) significantly correlated with survival time as well as clinical stage ($p = 0.001$), N stage ($p = 0.001$), and T stage ($p < 0.001$) (**Figure 3C**). Then, the multivariable analysis also showed that the risk score was the best independent predictor ($p < 0.001$) as shown in **Figure 3D**. Moreover, the AUC of the risk score was the highest compared to other factors such as age, gender, clinical stage, and T and N stage, which demonstrated the superior forecasting performance of our gene model (**Figure 3B**).

External Validation of the ARG Model

As supplements of **Figure 2**, we did the external validation of the ARG signature. The patients were divided into two groups in the external testing dataset with the same method as the internal database (**Figure 4A**). **Figure 4B** shows a scattergram of risk score, survival time, and status for the external testing dataset. The six ARGs presented a similar expression profile in the heatmap (**Figure 4C**). The K-M analysis presented noticeably different survival times between the two groups (**Figure 4D**). The ROC curve and corresponding AUCs in the external testing dataset were showed in (**Figure 4E**).

Nomogram to Predict Survival Probability of OSCC

We developed a nomogram to estimate the survival time of OSCC quantificationally. As shown in **Figure 5A**, six ARGs were appointed with specific points according to its contribution to survival. The calibration curves to predict the survival rate were closer to diagonal, which showed an excellent effect in both the internal and external datasets (**Figures 5B, C**).

Immune Cell Infiltration Between Low-Risk and High-Risk Groups

We analyzed the component of 22 immune cells in tumor samples. Whether in the internal database or in the external database, great differences of immune cell infiltration were detected in the two groups divided by the median risk score (**Figures 6A, B**). The immune cells patiently played an appropriate role in some way through the six ARGs.

In TCGA internal database, the infiltration amount of NK cells resting, mast cells activated, dendritic cells activated, and eosinophils in the high-risk group were much more abundant. However, T-cells regulating (Tregs), T-cells CD8, mast cells resting, and NK cells activated in the high-risk group were much less obvious (**Figure 6C**). In the GEO external validating database, the infiltration of eosinophils and Tregs also showed

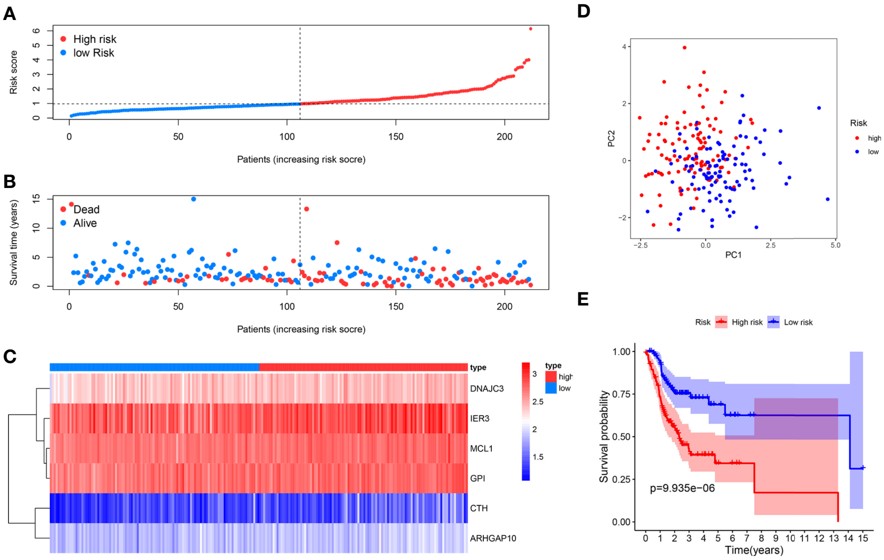

FIGURE 2 | Prognosis analysis of the internal training dataset. **(A)** The median risk score allocated OSCC patients in TCGA into two groups. From left to right, the risk scores were ascending and each dot represents an individual. **(B)** Patients with different survival times and statuses were arranged with the increasing risk score from left to right; clearly, the dead patients have higher risk score. **(C)** The heatmap showed expression profile of the six risk genes. The expression level from high to low was manifested with the colors from red to blue. **(D)** The high- and low-risk groups were gathered in two directions through the PCA analysis. **(E)** Kaplan–Meier analysis showed different prognosis between the two groups.

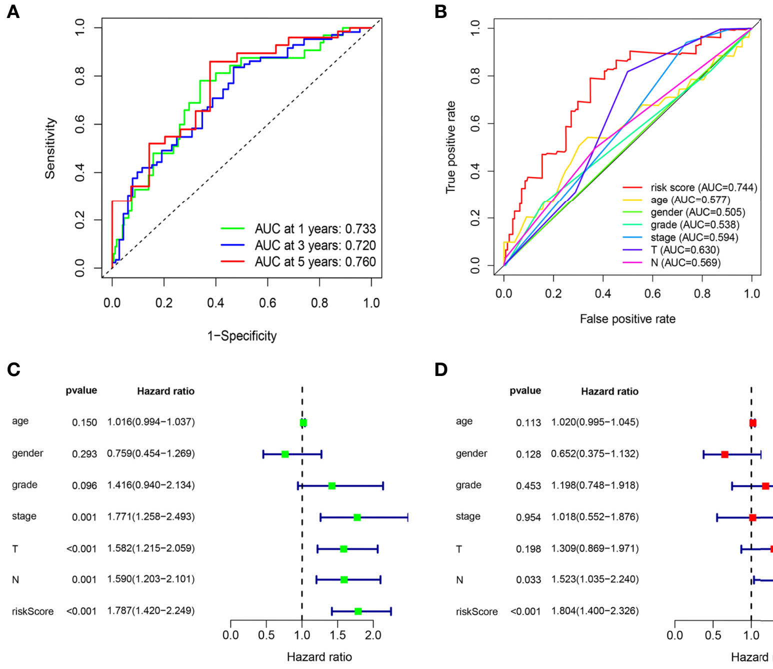

FIGURE 3 | The ARG prognostic signature shows good predictive performance in the internal training dataset. **(A)** The ROC curves of the ARG model for the 1-, 3-, and 5-year survival rates, and the corresponding AUC was 0.733, 0.720, and 0.760. **(B)** The AUC value of the risk score (0.744) showed superior predictive performance than age (0.577), gender (0.505), grade (0.538), stage (0.594), T stage (0.630), and N stage (0.569). **(C)** The risk score was a significant dangerous factor to influence the OS with HR = 1.787 (95% CI = 1.420–2.249, p <0.001). Other clinical factors such as stage with HR = 1.771 (95% CI = 1.258–2.439, p = 0.001), T stage with HR = 1.582 (95% CI = 1.215–2.059, p < 0.001), and N stage with HR = 1.590 (95% CI = 1.203–2.101, p = 0.001) were significant as well. **(D)** The risk score had excellent independent prediction ability with HR = 1.804 (95% CI = 1.400–2.326, p < 0.001) in multivariate Cox regression analysis.

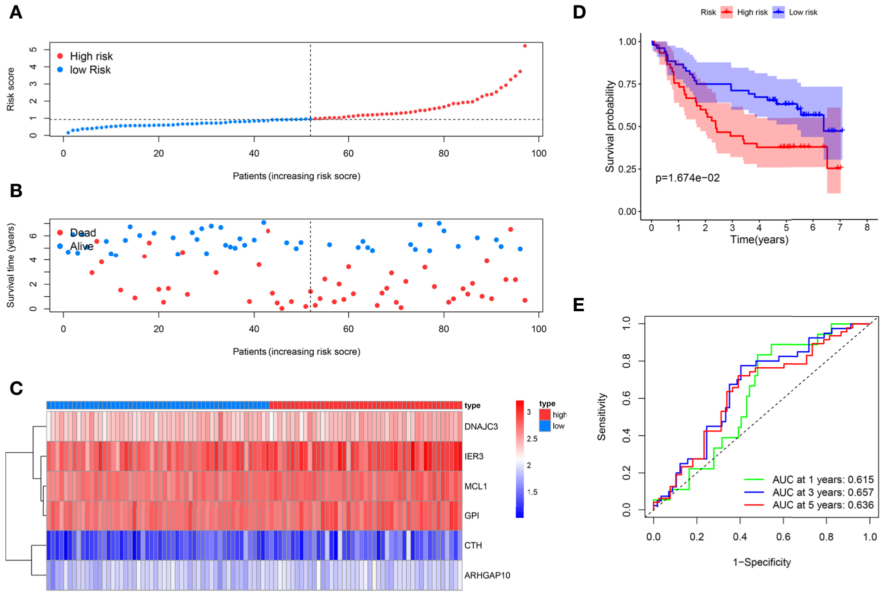

FIGURE 4 | External testing of the ARG model. **(A)** Patient with different risks were separated into two groups *via* the same median risk score in the internal database. **(B)** Patients in the external dataset with different survival times and statuses were arranged by the increasing risk score from left to right. **(C)** The heatmap of the six risk ARGs in the external database showed the same expression pattern. **(D)** Kaplan–Meier analysis showed different prognoses between the two groups as well. **(E)** The ROC curves of the models for survival rate in the external testing dataset.

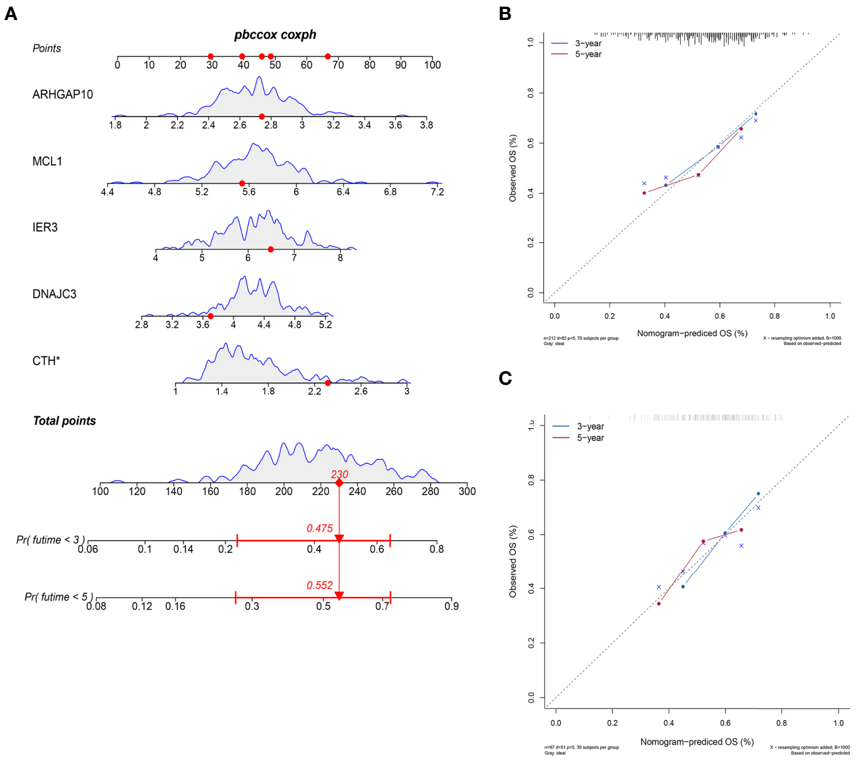

FIGURE 5 | Nomogram to predict the survival probability. **(A)** The six ARGs formed the prognostic nomogram that can be used to calculate 3- and 5-year survival rates. The expression values of each gene were assigned to a unique point. The total points of six genes from one patient correspond to the specific survival rate of 3 or 5 years. **(B)** The calibration plots showed that the predicted OS of nomogram is close to the observed OS rate in the internal dataset. **(C)** The calibration plots showed the same accuracy of nomogram in the external dataset.

the same tendency between the two groups (**Figure 6D**). Then, the correlation analysis further shed light on the relevance of risk score and nine immune cells (**Figure 7**). Plasma cells, macrophages M0, mast cells activated, eosinophils, and NK cells resting had positive correlations with the risk score. In contrast, T cells CD8, Tregs, mast cells resting, and NK cells activated correlated with the risk score in a negative way. Based on the formula of risk score, we knew that the correlation of genes and immune cells is consistent with the correlation of risk score and immune cells. Therefore, the higher the expression of risk genes, the higher the ratios of plasma cells, macrophages M0, mast cells activated, eosinophils, and NK cells infiltrated in the tumor.

Functional Enrichment Analysis and Correlation Network of the Six Prognostic ARGs

Significant enrichments were found in cellular response to unfolded proteins, endoplasmic reticulum unfolded protein response, cellular response to topologically incorrect proteins, response to unfolded proteins, and so on ($p < 0.05$, FDR < 0.05) (**Figure 8A**). Moreover, KEGG analysis demonstrated that these ARGs were prominently enriched in nucleotide and sugar metabolism, response to unfolded proteins, glycolysis/gluconeogenesis, starch and sucrose metabolism, and bacterial invasion of epithelial cells (**Figure 8B**).

An interaction network of the potential correlation between the six ARGs was established. The network contained nine edges and six nodes (CTH, DNAJC3, IER3, MCL1, ARHGAP10, GPI), as shown in **Figure 8C**. The correlation between MCL1, GPI, IER3, and ARHGAP10 was negative, while the remaining correlations were positive.

Unsupervised Clustering Analysis

Unsupervised clustering analysis was used to divide patient subgroups with different apoptosis modification patterns based on the expression of six ARGs. The clustering heatmap and changes in area under the proportion of the ambiguous cluster curve are shown in **Figures 9A, B**. One hundred sixty-two cases in TCGA-OSCC and GSE41613 OSCC cohorts were assigned to apoptosis cluster A, while 147 cases were included in cluster B. The survival analysis showed a significant survival difference between two apoptosis clusters (log-rank p value <0.001) (**Figure 9C**).

Pan-Cancer Analysis

In order to have a more comprehensive understanding of these six risk genes with various types of cancer, we conducted some work of pan-cancer analysis. The expression of genes in pan-cancer is

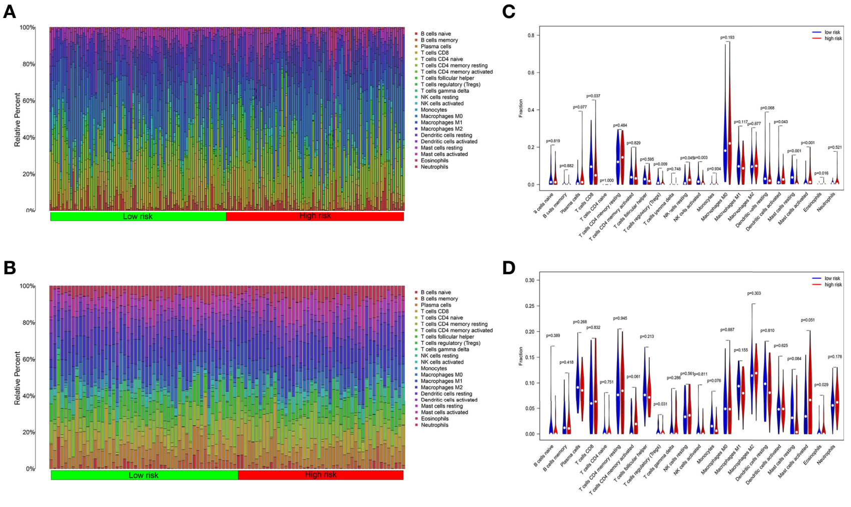

FIGURE 6 | Tumor immune cell infiltration analysis. **(A)** Ratio of 22 kinds of immune cells infiltrated in OSCC tumor samples from TCGA. **(B)** Ratio of 22 kinds of immune cells infiltrated in OSCC tumor samples from GEO. **(C)** The ratio of immune cells in the high-risk group is different from the low group in TCGA. **(D)** The ratio of immune cells in the high-risk group is different from the low group in GEO.

shown in a heatmap of (**Supplementary Figure 1**). The expression level of genes is specific to cancer species. We also get the hazard ratio of each gene in different cancers (**Supplementary Figure 2**).

Immunohistochemical Validation

We collected the pathological samples from the non-survival and survival patients. MCL1, GPI, and ARHGAP10 were strongly positive in the samples from non-survival patients and negative in the survival groups (**Figure 10A**). The semiquantitative comparison of the H-score between two groups also showed that these three genes were expressed more highly in non-survival patients (**Figure 10B**). Therefore, our experiment also validated that MCL1, GPI, and ARHGAP10 were risk genes which can predict the prognosis of OSCC.

DISCUSSION

In the present study, we acquired information and gene sets from 213 OSCC patients for analysis, and p values <0.05 were singled out for further analyses. We constructed a model made up of six biomarkers to estimate the survival time of OSCC patients. In accordance with the risk score, OSCC patients were successfully allocated into low- and high-risk groups with distinct prognosis.

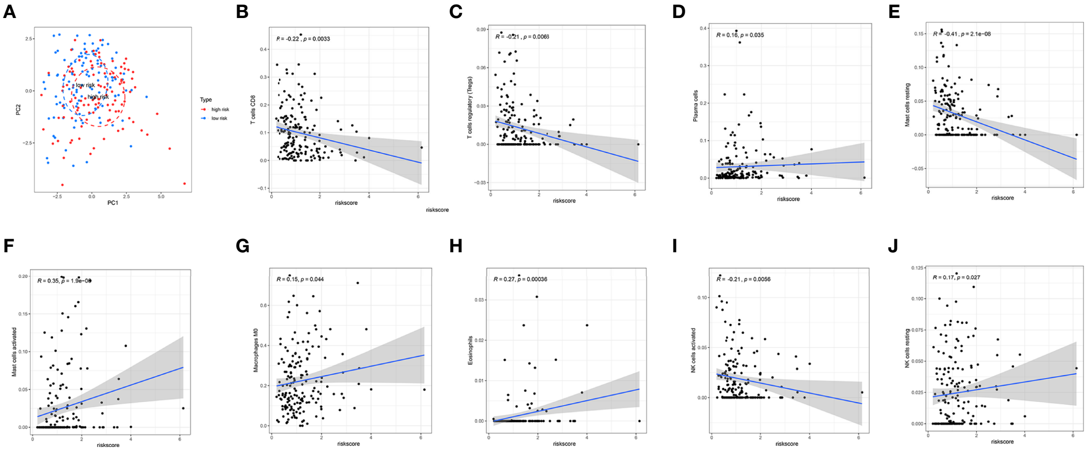

FIGURE 7 | Correlation analysis of immune cell infiltration and risk scores. **(A)** PCA analysis showed a distinct immune cell infiltration pattern in two groups. **(B–J)** Correlation analysis of risk scores and nine types of the immune cells.

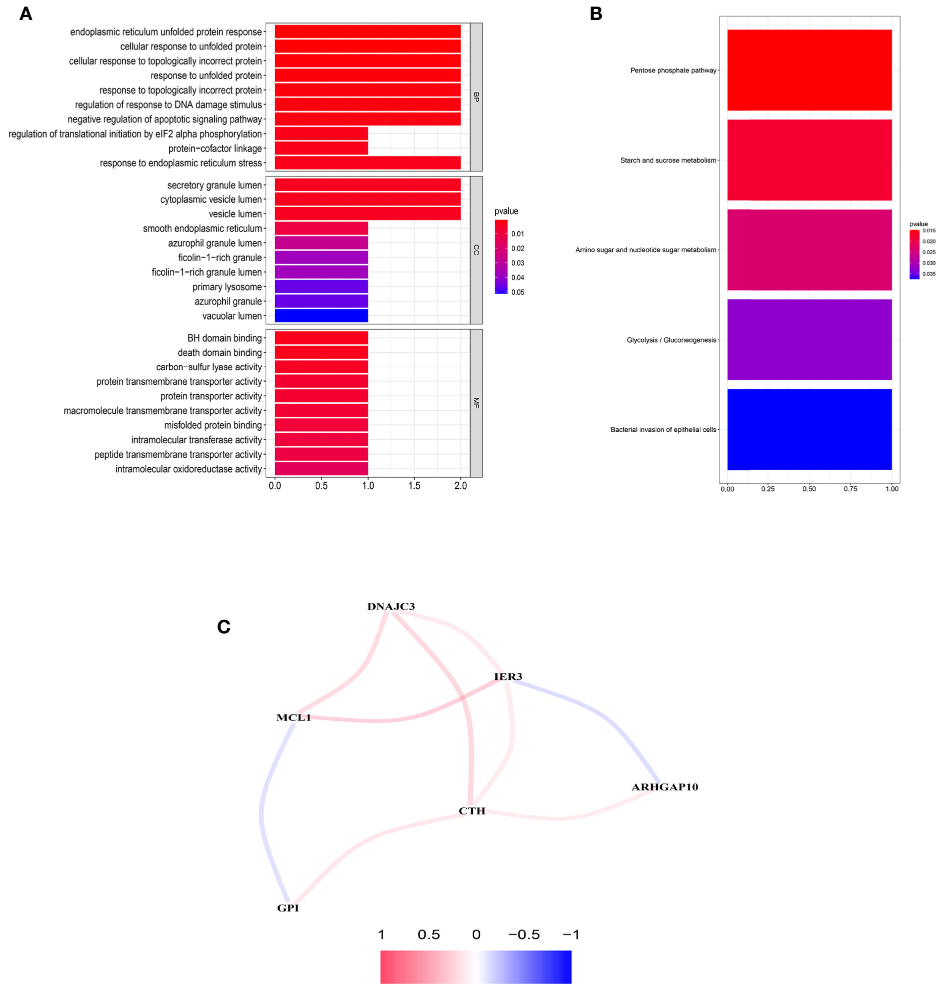

FIGURE 8 | Functional enrichment analysis and the construction of network. **(A)** GO analysis of the six prognostic ARGs. **(B)** KEGG analysis of the six prognostic ARGs. **(C)** Correlation network of the six prognostic ARGs. Red means a positive interaction, and blue indicates a negative interaction.

Moreover, the ARG model was an independent forecasting factor with better efficiency compared to previous traditional clinical factors. Moreover, we used the six genes to build a novel nomogram that can provide superior estimation of OS. However, the underlying mechanisms of these results still need to be further investigated.

In recent years, numerous studies have confirmed the relationship between apoptosis and cancer (1, 7, 11). Apoptotic signal pathways can be changed at transcriptional, translational, and posttranslational levels in cancer cells. Several proteins, such as the BCL-2 family, have been shown to function in the process of apoptosis and cancer (18, 19). Myeloid cell leukemia-1 (MCL1), which is well known for its anti-apoptotic role in the Bcl-2 family, is a distinct cell regulatory protein. MCL1 is required for cell survival, differentiation, and maintenance (20). Recent studies have also revealed that MCL1 is a therapeutic prospective target in cancers (21, 22). Knocking down MCL1 could induce the apoptosis of OSCC cells through increasing the sensitivity to drugs. Moreover, MCL1 antagonist Sabutoclax could increase cancer cell death in OSCC as well (23).

Glucose-6-phosphate isomerase (GPI) is one of the members in the glucose phosphate isomerase protein family. GPI plays a crucial part in the process of glycolysis and gluconeogenesis (24, 25). Earlier studies showed that GPI could be used as a prognostic biomarker in cancer because of its important work in the cell cycle (26, 27). In our study, GPI was a risk gene because a higher expression was associated with poor prognosis. However, the role of GPI in OSCC needs to be explored in detail.

ARHGAP10 is a member of the RhoGAP protein group, which can convert the active form to inactive form (28). Downregulating the expression of ARHGAP10 could lead to a more advanced stage and a higher Ki-67 index in breast cancer (29). Luo pointed out that ARHGAP10 may serve as a tumor inhibitor through suppressing adhesion, migration, and invasion of the ovarian cancer cells (30). Teng also found the same phenomenon in lung cancer (31). These results seem opposite

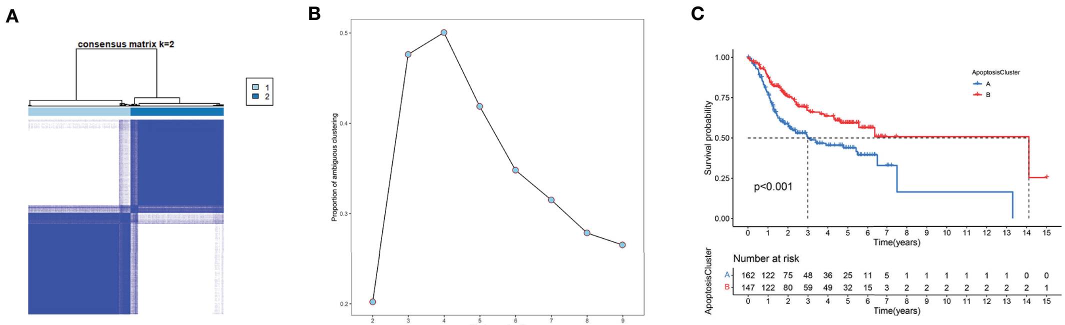

FIGURE 9 | Unsupervised clustering analysis. **(A)** The clustering heatmap relevant to the consensus matrix for k = 2 acquired by consensus clustering. **(B)** Corresponding changes in area under proportion of ambiguous cluster curve with k from 2 to 9. **(C)** K-M analysis demonstrated an obvious survival difference in two apoptosis clusters.

to our analysis and IHC validation in OSCC. However, in prostate cancer, Hua Gong claimed that a high expression of ARHGAP10 correlates with poor prognosis, which supports our result (32). The mechanisms underlying the paradox that the same molecule plays a different role in different cancers need to be further studied.

The immune microenvironment has great impact on the tumorigenesis of OSCC (33). TIL plays a key part in cancer genesis, especially in immune evasion (34, 35). In our research, the correlation analysis sheds light on the connection of risk score and immune cells. It is meaningful to explore the mutual effect of tumor cells and immune cells. Studies about CAR T cells

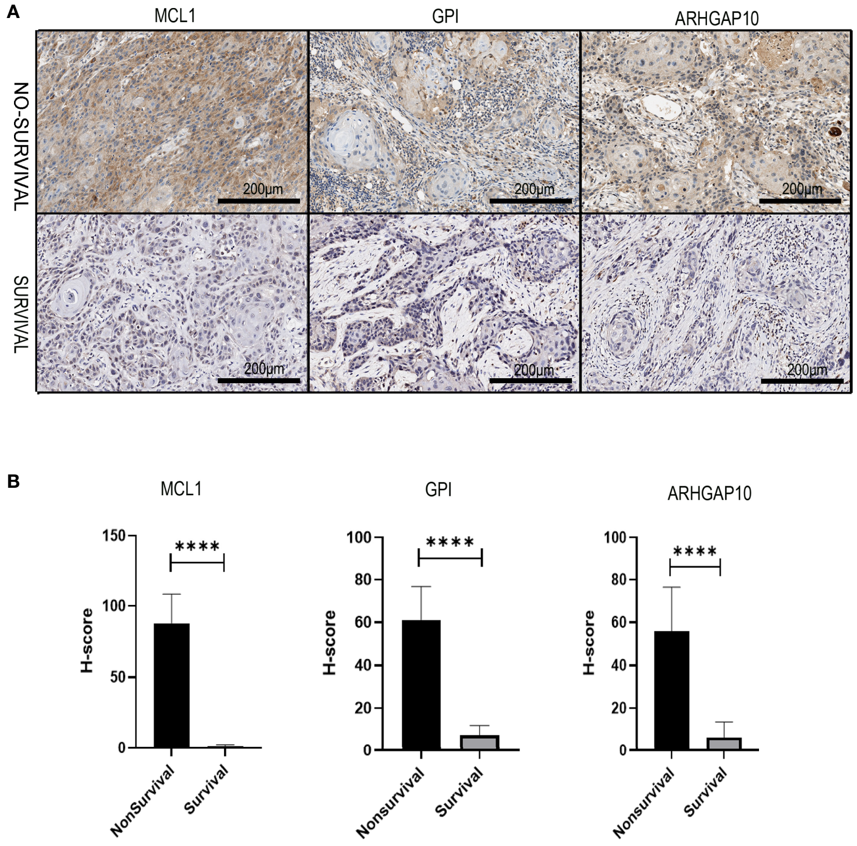

FIGURE 10 | The experiment validation of the apoptosis-related prognostic gene model. **(A)** The protein expressions of three apoptosis-related prognostic genes were dramatically different in dead and alive patients who had oral cancer 3 years ago. **(B)** Corresponding H-score of protein expression of three apoptosis-related prognostic genes. **** means $p < 0.0001$.

targeting solid tumors (36), B cell-based immunotherapy for lung cancer (37), dendritic cell-based vaccination, and so on, provided a new insight to develop more effective therapy regimens (38). Other research focused on the TILs and OSCC also revealed similar results (39), although how the TILs interact with these six prognostic ARGs specifically still requires deeper research.

Some limitations still need to be considered in our study. The construction and validation of prognostic signature were based on the previous published database. If we could use the data from a real-life clinical cohort, maybe we can acquire more reliable and meaningful discoveries. The six prognostic ARGs and nomogram should be tested in subsequent studies and clinical trials.

In conclusion, we identified six risk biomarkers, namely, MCL1, GPI, ARHGAP10, CTH, DNAJC3, and IER3, associated with prognosis of OSCC through a comprehensive bioinformatics analysis based on TCGA database and apoptosis-related gene sets. The gene signature and nomogram might provide a precise prognostic prediction of OSCC, which will help clinicians to formulate individual treatment strategies for their patients. These genes identified could also be therapeutic targets for OSCC.

DATA AVAILABILITY STATEMENT

Publicly available datasets were analyzed in this study. These data can be found here: OSCC cohort from TCGA database, https://portal.gdc.cancer.gov/; GSE41613 from GEO database, https://www.ncbi.nlm.nih.gov/geo.

ETHICS STATEMENT

The studies involving human participants were reviewed and approved by the Research Ethics Committee of Guangdong Provincial Hospital & Guangdong Academy of Medical Sciences. Written informed consent was provided by the participating patient(s).

AUTHOR CONTRIBUTIONS

SW, LZ, and GL conceived and contributed to the study concept and design. SZ contributed to the data acquisition. SW collected the specimens and developed the data analysis workflows. SW, ZL, and JM performed the data analysis and interpreted the results. ZL and JM finished the immunohistochemical stain. SW wrote the manuscript. SZ mended the manuscript. GL and LZ supervised the study. All authors contributed to the article and approved the submitted version.

FUNDING

This research was supported by grant 2019A1515012218 (SZ) funded by the Foundation and Applied Foundation Research Fund project of Guangdong Province and grant 201904010008 funded by Guangzhou Science and Technology Project.

SUPPLEMENTARY MATERIAL

The Supplementary Material for this article can be found online at: https://www.frontiersin.org/articles/10.3389/fonc.2022.889049/full#supplementary-material

Supplementary Figure 1 | The heatmap showed expression profile of the 6 risk genes in pan-cancer.

Supplementary Figure 2 | Forest plot showed the correlation of 6 risk genes with the prognosis in pan-cancer.

REFERENCES

1. Sung H, Ferlay J, Siegel RL, Laversanne M, Soerjomataram I, Jemal A, et al. Global Cancer Statistics 2020: GLOBOCAN Estimates of Incidence and Mortality Worldwide for 36 Cancers in 185 Countries. *CA Cancer J Clin* (2021) 71(3):209–49. doi: 10.3322/caac.21660
2. D'souza S, Addepalli V. Preventive Measures in Oral Cancer: An Overview. *BioMed Pharmacother* (2018) 107(May):72–80. doi: 10.1016/j.biopha.2018.07.114
3. Weber M, Wehrhan F, Baran C, Agaimy A, Büttner-Herold M, Kesting M, et al. Prognostic Significance of PD-L2 Expression in Patients With Oral Squamous Cell Carcinoma-A Comparison to the PD-L1 Expression Profile. *Cancer Med* (2019) 8(3):1124–34. doi: 10.1002/cam4.1929
4. Bettendorf O, Piffkò J, Bànkfalvi A. Prognostic and Predictive Factors in Oral Squamous Cell Cancer: Important Tools for Planning Individual Therapy? *Oral Oncol* (2004) 40(2):110–9. doi: 10.1016/j.oraloncology.2003.08.010. PMID:14693233
5. Elmore S. Apoptosis: A Review of Programmed Cell Death. *Toxicol Pathol* (2007) 35(4):495–516. doi: 10.1080/01926230701320337
6. Liu J, Liu W, Yang H. Balancing Apoptosis and Autophagy for Parkinson's Disease Therapy: Targeting BCL-2. *ACS Chem Neurosci* (2019) 10(2):792–802. doi: 10.1021/acschemneuro.8b00356
7. Mohammad RM, Muqbil I, Lowe L, Yedjou C, Hsu HY, Lin LT, et al. Broad Targeting of Resistance to Apoptosis in Cancer. *Semin Cancer Biol* (2015) 35 Suppl(0):S78–S103. doi: 10.1016/j.semcancer.2015.03.001
8. Strasser A, Vaux DL. Cell Death in the Origin and Treatment of Cancer. *Mol Cell* (2020) 78(6):1045–54. doi: 10.1016/j.molcel.2020.05.014
9. Singh R, Letai A, Sarosiek K. Regulation of Apoptosis in Health and Disease: The Balancing Act of BCL-2 Family Proteins. *Nat Rev Mol Cell Biol* (2019) 20 (3):175–93. doi: 10.1038/s41580-018-0089-8
10. Hu J, Cao J, Topatana W, Juengpanich S, Li S, Zhang B, et al. Targeting Mutant P53 for Cancer Therapy: Direct and Indirect Strategies. *J Hematol Oncol* (2021) 14(1):157. doi: 10.1186/s13045-021-01169-0
11. Goldar S, Khaniani MS, Derakhshan SM, Baradaran B. Molecular Mechanisms of Apoptosis and Roles in Cancer Development and Treatment. *Asian Pac J Cancer Prev* (2015) 16(6):2129–44. doi: 10.7314/apjcp.2015.16.6.2129
12. Boice A, Bouchier-Hayes L. Targeting Apoptotic Caspases in Cancer. *Biochim Biophys Acta Mol Cell Res* (2020) 1867(6):118688. doi: 10.1016/j.bbamcr.2020.118688
13. Sasahira T, Kirita T. Hallmarks of Cancer-Related Newly Prognostic Factors of Oral Squamous Cell Carcinoma. *Int J Mol Sci* (2018) 19(8):2413. doi: 10.3390/ijms19082413

14. Li J, Ma S. Time-Dependent ROC Analysis Under Diverse Censoring Patterns. *Stat Med* (2011) 30(11):1266–77. doi: 10.1002/sim.4178
15. Newman AM, Liu CL, Green MR, Gentles AJ, Feng W, Xu Y, et al. Robust Enumeration of Cell Subsets From Tissue Expression Profiles. *Nat Methods* (2015) 12(5):453–7. doi: 10.1038/nmeth.3337
16. Wu T, Hu E, Xu S, Chen M, Guo P, Dai Z, et al. Cluster Profiler 4.0: A Universal Enrichment Tool for Interpreting Omics Data. *Innovation (N Y).* (2021) 2(3):100141. doi: 10.1016/j.xinn.2021.100141
17. Ng KL, Ellis RJ, Samaratunga H, Morais C, Gobe GC, Wood ST. Utility of Cytokeratin 7, S100A1 and Caveolin-1 as Immunohistochemical Biomarkers to Differentiate Chromophobe Renal Cell Carcinoma From Renal Oncocytoma. *Transl Androl Urol* (2019) 8(Suppl 2):S123–37. doi: 10.21037/tau.2018.11.02
18. Pistritto G, Trisciuoglio D, Ceci C, Garufi A, D'Orazi G. Apoptosis as Anticancer Mechanism: Function and Dysfunction of its Modulators and Targeted Therapeutic Strategies. *Aging (Albany NY)* (2016) 8(4):603–19. doi: 10.18632/aging.100934
19. Knight T, Luedtke D, Edwards H, Taub JW, Ge Y. A Delicate Balance - The BCL-2 Family and Its Role in Apoptosis, Oncogenesis, and Cancer Therapeutics. *Biochem Pharmacol* (2019) 162:250–61. doi: 10.1016/j.bcp.2019.01.015
20. Sancho M, Leiva D, Lucendo E, Orzáez M. Understanding MCL1: From Cellular Function and Regulation to Pharmacological Inhibition. *FEBS J* (2021). doi: 10.1111/febs.16136. Epub ahead of print
21. Wu X, Luo Q, Liu Z. Ubiquitination and Deubiquitination of MCL1 in Cancer: Deciphering Chemoresistance Mechanisms and Providing Potential Therapeutic Options. *Cell Death Dis* (2020) 11(7):556. doi: 10.1038/s41419-020-02760-y
22. Wei AH, Roberts AW, Spencer A, Rosenberg AS, Siegel D, Walter RB, et al. Targeting MCL-1 in Hematologic Malignancies: Rationale and Progress. *Blood Rev* (2020) 44:100672. doi: 10.1016/j.blre.2020.100672
23. Maji S, Samal SK, Pattanaik L, Panda S, Quinn BA, Das SK, et al. Mcl-1 Is an Important Therapeutic Target for Oral Squamous Cell Carcinomas. *Oncotarget* (2015) 6(18):16623–37. doi: 10.18632/oncotarget.3932
24. Aguilera-Romero A, Sabido-Bozo S, Lopez S, Cortes-Gomez A, Rodriguez-Gallardo S, Perez-Linero AM, et al. Determination of the Lipid Composition of the GPI Anchor. *PloS One* (2021) 16(8):e0256184. doi: 10.1371/journal.pone.0256184
25. Lebreton S, Zurzolo C, Paladino S. Organization of GPI-Anchored Proteins at the Cell Surface and Its Physiopathological Relevance. *Crit Rev Biochem Mol Biol* (2018) 53(4):403–19. doi: 10.1080/10409238.2018.1485627
26. Han J, Deng X, Sun R, Luo M, Liang M, Gu B, et al. GPI Is a Prognostic Biomarker and Correlates With Immune Infiltrates in Lung Adenocarcinoma. *Front Oncol* (2021) 11:752642. doi: 10.3389/fonc.2021.752642
27. Gamage DG, Hendrickson TL. GPI transamidase And GPI Anchored Proteins: Oncogenes and Biomarkers for Cancer. *Crit Rev Biochem Mol Biol* (2013) 48(5):446–64. doi: 10.3109/10409238.2013.831024
28. Sekiguchi M, Sobue A, Kushima I, Wang C, Arioka Y, Kato H, et al. ARHGAP10, Which Encodes Rho GTPase-Activating Protein 10, Is a Novel Gene for Schizophrenia Risk. *Transl Psychiatry* (2020) 10(1):247. doi: 10.1038/s41398-020-00917-z
29. Li Y, Zeng B, Li Y, Zhang C, Ren G. Downregulated Expression of ARHGAP10 Correlates With Advanced Stage and High Ki-67 Index in Breast Cancer. *PeerJ* (2019) 7:e7431. doi: 10.7717/peerj.7431
30. Luo N, Guo J, Chen L, Yang W, Qu X, Cheng Z. ARHGAP10, Downregulated in Ovarian Cancer, Suppresses Tumorigenicity of Ovarian Cancer Cells. *Cell Death Dis* (2016) 7(3):e2157. doi: 10.1038/cddis.2015.401
31. Teng JP, Yang ZY, Zhu YM, Ni D, Zhu ZJ, Li XQ. The Roles of ARHGAP10 in the Proliferation, Migration and Invasion of Lung Cancer Cells. *Oncol Lett* (2017) 14(4):4613–8. doi: 10.3892/ol.2017.6729
32. Gong H, Chen X, Jin Y, Lu J, Cai Y, Wei O, et al. Expression of ARHGAP10 Correlates With Prognosis of Prostate Cancer. *Int J Clin Exp Pathol* (2019) 12 (10):3839–46.
33. Lei X, Lei Y, Li JK, Du WX, Li RG, Yang J, et al. Immune Cells Within the Tumor Microenvironment: Biological Functions and Roles in Cancer Immunotherapy. *Cancer Lett* (2020) 470:126–33. doi: 10.1016/j.canlet.2019.11.009
34. Jie HB, Srivastava RM, Argiris A, Bauman JE, Kane LP, Ferris RL. Increased PD-1+ and TIM-3+ TILs During Cetuximab Therapy Inversely Correlate With Response in Head and Neck Cancer Patients. *Cancer Immunol Res* (2017) 5(5):408–16. doi: 10.1158/2326-6066.CIR-16-0333
35. Chen L, Diao L, Yang Y, Yi X, Rodriguez BL, Li Y, et al. CD38-Mediated Immunosuppression as a Mechanism of Tumor Cell Escape From PD-1/PD-L1 Blockade. *Cancer Discovery* (2018) 8(9):1156–75. doi: 10.1158/2159-8290.CD-17-1033
36. Martinez M, Moon EK. CAR T Cells for Solid Tumors: New Strategies for Finding, Infiltrating, and Surviving in the Tumor Microenvironment. *Front Immunol* (2019) 10:128. doi: 10.3389/fimmu.2019.00128
37. Wang SS, Liu W, Ly D, Xu H, Qu L, Zhang L. Tumor-Infiltrating B Cells: Their Role and Application in Anti-Tumor Immunity in Lung Cancer. *Cell Mol Immunol* (2019) 16(1):6–18. doi: 10.1038/s41423-018-0027-x
38. Sabado RL, Balan S, Bhardwaj N. Dendritic Cell-Based Immunotherapy. *Cell Res* (2017) 27(1):74–95. doi: 10.1038/cr.2016.157
39. Succaria F, Kvistborg P, Stein JE, Engle EL, McMiller TL, Rooper LM, et al. Characterization of the Tumor Immune Microenvironment in Human Papillomavirus-Positive and -Negative Head and Neck Squamous Cell Carcinomas. *Cancer Immunol Immunother* (2021) 70(5):1227–37. doi: 10.1007/s00262-020-02747-w

Conflict of Interest: The authors declare that the research was conducted in the absence of any commercial or financial relationships that could be construed as a potential conflict of interest.

Publisher's Note: All claims expressed in this article are solely those of the authors and do not necessarily represent those of their affiliated organizations, or those of the publisher, the editors and the reviewers. Any product that may be evaluated in this article, or claim that may be made by its manufacturer, is not guaranteed or endorsed by the publisher.

Copyright © 2022 Wang, Zhang, Lin, Ma, Zhu and Liao. This is an open-access article distributed under the terms of the Creative Commons Attribution License (CC BY). The use, distribution or reproduction in other forums is permitted, provided the original author(s) and the copyright owner(s) are credited and that the original publication in this journal is cited, in accordance with accepted academic practice. No use, distribution or reproduction is permitted which does not comply with these terms.

frontiers | Frontiers in Oncology

ORIGINAL RESEARCH
published: 17 June 2022
doi: 10.3389/fonc.2022.898047

Sclerostin Suppression Facilitates Uveal Melanoma Progression Through Activating Wnt/β-Catenin Signaling *Via* Binding to Membrane Receptors LRP5/LRP6

Hanqing Wang [1,2]***, Sidi Zhao*** [2]***, Yang Liu*** [3]***, Fengyuan Sun*** [1,2]***, Xiaoming Huang*** [1,2*] ***and Tong Wu*** [1,2*]

[1] Department of Orbital Disease and Oculoplastic Surgery, Sichuan Eye Hospital, Aier Eye Hospital Group, Chengdu, China, [2] Department of Orbital Disease and Oculoplastic Surgery, Tianjin Medical University Eye Hospital, Tianjin, China, [3] Research and Development Department, Microsensor Labs, Chicago, IL, United States

OPEN ACCESS

Edited by:
Haichang Li,
The Ohio State University,
United States

Reviewed by:
Xiulin Jiang,
Kunming Institute of Zoology (CAS),
China
Leming Sun,
Northwestern Polytechnical University,
China

****Correspondence:***
Tong Wu
victortongwu@126.com
Xiaoming Huang
hxm@tmu.edu.cn

Specialty section:
This article was submitted to
Pharmacology of Anti-Cancer Drugs,
a section of the journal
Frontiers in Oncology

Received: *16 March 2022*
Accepted: *28 April 2022*
Published: *17 June 2022*

Citation:
Wang H, Zhao S, Liu Y, Sun F,
Huang X and Wu T (2022)
Sclerostin Suppression Facilitates
Uveal Melanoma Progression
Through Activating Wnt/β-Catenin
Signaling Via Binding to Membrane
Receptors LRP5/LRP6.
Front. Oncol. 12:898047.
doi: 10.3389/fonc.2022.898047

Objective: Uveal melanoma (UM) is the most frequent primary eye cancer in adults with a 50% mortality rate. Characterizing the fundamental signaling pathways that drive UM is of importance for the development of targeted therapy. This study aims to probe the impact of sclerostin (SOST) on malignant progression of UM and regulation of Wnt/β-catenin signaling.

Methods: Epithelial-type (n=20) and spindle-type (n=16) UM tissues were collected for immunohistochemical staining of SOST, Wnt-1, and β-catenin expressions. SOST was silenced in three UM cell lines (primary spindle-type OCM-1 cells, metastatic epithelial Mum-2B cells, and metastatic spindle-type Mum-2C cells) through transfecting specific siRNA. RT-qPCR and Western blot were presented for examining the levels of SOST, and markers in Wnt/β-catenin signaling. Flow cytometry, MTT, EdU, transwell, and tube formation assays were conducted, respectively. By implanting BALB/c nude murine models *in situ*, the function of SOST on tumor growth was investigated, followed by immunofluorescence double staining of SOST and LRP5/6.

Results: Low SOST expression as well as high Wnt-1 and β-catenin expressions were found in epithelial-type (high malignancy) than spindle-type (low malignancy) UM tissues. Silencing SOST activated the markers in Wnt/β-catenin signaling as well as accelerated cell cycle progression, migration, invasion, angiogenesis, and reduced apoptosis in UM cells. *In situ* tumor formation in murine eyes showed that SOST knockdown promoted tumor growth. Moreover, SOST interacted with LRP5/LRP6.

Conclusion: SOST silencing may facilitate the malignant progression of UM cells through activating Wnt/β-catenin signaling. Mechanistically, SOST may exert this function by interacting with LRP5/LRP6 membrane receptors.

Keywords: uveal melanoma, sclerostin, Wnt/β-catenin signaling, LRP5/LRP6, progression

INTRODUCTION

Uveal melanoma (UM) represents the most frequent primary intraocular tumor in adults as well as the second most frequent form of melanoma (1). It originates from the pigmented uveal tract, composed of choroid (~85%), ciliary body (5-8%), and iris (3-5%) (2, 3). In accordance with the WHO classification of histological types in 1980, UM is categorized as spindle cell type with low malignancy, epithelioid cell type with high malignancy, mixed cell type, and other types (4). Current therapeutic strategies include surgery, radiotherapy, and chemotherapy as well as targeted therapy, and the local control rate of UM has reached as high as 96.4% following active treatment (5). Nevertheless, approximately 50% of cases will develop metastasis within 15 years following the initial diagnosis (6, 7). Regrettably, there is still no effective treatment against metastasis (8). UM possesses an extremely high predilection to liver metastasis, and exceeding 90% of metastatic patients have hepatic lesions (9). At present, the prognosis of tumor invasion and metastasis cannot be accurately and objectively predicted in clinical practice, and there are not many corresponding effective treatment methods, which are the main factors affecting the curative effect and patient survival rate of UM (10). Therefore, it is necessary to conduct in-depth research on the mechanism of tumorigenesis and tumor metastasis, and to clarify the molecular biological characteristics of this disease.

Wnt/β-catenin signaling exerts a crucial role in tumor progression (11), and blockage of this signaling may suppress growth, migration, and invasion of UM cells (12–14). Sclerostin (SOST) secreted by osteocytes is a negative regulator of bone formation, and is an antagonist of the DAN/Cerberus protein family of BMP (15). Evidence suggests that SOST acts as a potential antagonist of Wnt/β-catenin pathway and inactivated SOST leads to the hyper-activation of this signaling (16). Several studies have reported that SOST-mediated Wnt/β-catenin pathway participates in retinoblastoma progression (17) and osteosarcoma (18). Evidence suggests that SOST can antagonize Wnt signaling in human cells *via* binding to the extracellular domain of LRP5/6 Wnt co-receptors as well as destroying Wnt-triggered Frizzled-LRP complexes (19). Nevertheless, the roles of SOST-triggered Wnt/β-catenin pathway in UM development as well as its clinical implication remain unclear. Hence, our study was conducted for probing the impact of SOST on malignant progression of UM and regulation of Wnt/β-catenin signaling.

MATERIALS AND METHODS

Patients and Specimens

Twenty epithelial-type UM tissue specimens and 16 spindle-type UM tissue specimens were retrieved from UM patients who underwent enucleation in Tianjin Medical University Eye Hospital from October 2015 to April 2018. All patients were confirmed by pathological examination after operation, who were classified according to the 1980 WHO classification of histological types. The age range was 24-67 years. The inclusion criteria were as follows (1): the pathological diagnosis was primary UM; (2) the submitted tissue sections were relatively complete; (3) the patient had no other types of cancer; and (4) the patient had not received radio- or chemotherapy. This study was approved by the Ethics Committee of Tianjin Medical University Eye Hospital (2017KY (L)-53). All patients provided written informed consent.

Immunohistochemistry

The patients' eye tumor specimens were fixed in neutral formalin and embedded in paraffin, followed by sectioning, deparaffinization, antigen retrieval, blocking, antibody incubation, DAB (diaminobenzidine) staining, hematoxylin staining, back blue, and dehydration coverslips. Primary antibodies were anti-rabbit (Proteintech, China), and secondary antibodies were goat anti-rabbit IgG (H+L) (Jackson Immuno Research Inc., US). As previously described, the staining scoring was calculated according to the following formula: H-score = staining intensity * number of positive cells/total number of cells (20). Three random fields were chosen, and the staining intensity was manually evaluated: 0 point for no yellow precipitate, 1 point for light yellow precipitate, 2 points for brownish-yellow precipitate, and 3 points for dark brown-yellow precipitate; positive cell counts were manually counted using Image J software.

Cell Culture

Human retinal epithelial cell line (APRE-19), human umbilical vein endothelial cells (HUVEC) as well as three human UM cell lines were acquired from the Chinese Academy of Sciences (Shanghai, China), including primary spindle-type OCM-1 cells, metastatic epithelial Mum-2B cells, and metastatic spindle-type Mum-2C cells. All cells were cultured in an incubator (Thermo Fisher Scientific, US) with 37°C, 5% CO_2. Subculture was carried out when the cells adhered and reached about 80% confluence. After discarding the medium, they were washed with Dulbecco's Phosphate-Buffered Saline (DPBS; Gibco, US), and digested with 1 mL of 0.25% trypsin-EDTA (Gibco, US). Thereafter, Dulbecco's modified eagle medium (DMEM) containing 100 U/mL penicillin, 100 μg/mL streptomycin, and 10% fetal bovine serum (FBS; Gibco, US) was used to terminate the digestion. The cells were centrifuged at 1000 rpm and resuspended in DMEM for future experiments.

Western Blot

UM cells were lysed by RIPA cell lysate, and protein concentrations were measured utilizing BCA Protein Assay Kit

---

Abbreviations: UM, uveal melanoma; SOST, sclerostin; HUVEC, human umbilical vein endothelial cells; DMEM, Dulbecco's modified eagle medium; FBS, fetal bovine serum; si-NC, negative control siRNA; si-SOST, SOST siRNA; RT-qPCR, real-time quantitative polymerase chain reaction; GAPDH, glyceraldehyde phosphate dehydrogenase; MTT, methyl thiazolyl tetrazolium; sh-SOST, SOST shRNA; sh-NC, negative control shRNA; ANOVA, one-way analysis of variance.

(Thermo Scientific, US). There were 20 μg proteins separated by 10% SDS-PAGE electrophoresis as well as transferred onto polyvinylidene fluoride membrane. The membrane was sealed with 5% nonfat dry milk and then incubated with primary antibodies against SOST (1:1000; 21933-1-AP; Proteintech, China), Wnt-1 (1:1000; 27935-1-AP), β-catenin (1:5000; 51067-2-AP), cyclin-D1 (1:2000; 26939-1-AP), MMP2 (1:500; 10373-2-AP), and MMP9 (1:500; 10375-2-AP) as well as β-Tubulin (1:1000; 10094-1-AP) at 4°C overnight. The next day, the membrane was incubated with goat anti-rabbit secondary antibody (Cell Signaling Technology, US) for 1 h at room temperature. Exposure was performed using Amersham ECL prime chemiluminescent fluid (GE Healthcare, US) in a dark room. The gray value was determined with ImageJ software.

Cell Transfection

The design and synthesis of the sequences of siRNA targeting human SOST (gene ID: 50964) and negative control siRNA (si-NC) were achieved by Shanghai Sangon Bioengineering Co., Ltd., (China). The sequence of SOST siRNA (si-SOST) was 5′-GGCGTTCAAGATGATGCCACGGAA-3′. OCM-1, Mum-2B, and Mum-2C cell lines were randomly divided into three groups: blank group (no transfection), si-NC group (transfection with si-NC plasmid), and si-SOST group (transfection with si-SOST plasmid). The full length SOST cDNA was synthesized and sub-cloned into the pcDNA3.1 vector to construct pcDNA3.1-SOST overexpression (OE-SOST) plasmid. OCM-1, Mum-2B, and Mum-2C cell lines were randomly divided into two groups: empty vector group and OE-SOST group. These cells were trypsinized at 0.25% as well as centrifuged at 1000 rpm lasting 5 min. Then, they were resuspended in medium and counted using an automated cell counter (Invitrogen, US), and 4×10^5 cells/well were seeded onto a six-well culture plate. When the cell confluency reached 50-80%, the complete medium was replaced with serum- and penicillin-free medium. Four hours later, using Lipofectamine 2000 (Invitrogen, US), plasmids encoding target sequences or siRNAs were transfected into the UM cell line. Twenty-four hours after transfections, the complete medium was exchanged for subculture. During this period, cellular morphology was investigated under a microscope (Olympus, Tokyo, Japan).

Real-Time Quantitative Polymerase Chain Reaction (RT-qPCR)

Total RNAs of UM cells were extracted utilizing Trizol kit (Invitrogen, US). The extracted RNAs were utilized for reverse transcription. Cellular cDNA synthesis was conducted according to the instructions of the reverse transcription kit (Transgen, Beijing, China). The PCR amplification reaction was carried out according to the instructions of RT-qPCR kit (Transgen, Beijing, China). **Table 1** lists the primer sequences that were synthesized by Shanghai Sangon Bioengineering Co., Ltd. (China). The reaction condition contained pre-denaturation at 94°C lasting 4 min, denaturation at 94°C lasting 30 sec, annealing at 56°C lasting 30 sec, and extending at 72°C lasting 30 sec, in total 45 cycles. The reaction system contained 10 μl Premix Ex Taq or SYBR Green Mix, 1 μl forward primer, 1 μl reverse primer, 1 μl cDNA template, and ddH_2O supplemented to 20 μl. Glyceraldehyde phosphate dehydrogenase (GAPDH) acted as an internal reference gene, and the Ct values (threshold of amplification curves) were examined with the control group set to 1. The iQ5 Real-Time PCR Amplifier was purchased from the Bio-Rad company (US). Relative expression values were calculated by the $2^{-\Delta\Delta Ct}$ method.

TABLE 1 | The primer sequence utilized for RT-qPCR.

Gene name	Primer sequence (5'-3')
SOST	Forward: TGAGACCAAAGACGTGTCCG
	Reverse: CTTGAGCTCCACTGGTTGT
WNT1	Forward: CGATGGTGGGGTATTGTGAAC
	Reverse: CCGGATTTTGGCGTATCAGAC
CTNNB1	Forward: ATGATGGTCTGCCAAGTGGG
	Reverse: GGCCATCTCTGCTTCTTGGT
CCND1	Forward: GCTGCGAAGTGGAAACCATC
	Reverse: CCTCCTTCTGCACACATTTGAA
MMP2	Forward: TACAGGATCATTGGCTACACACC
	Reverse: GGTCATCGCTCCAGACT
MMP9	Forward: TGTACCGCTATGGTTACACTCG
	Reverse: GGCAGGGACAGTTGCTTCT
GAPDH	Forward: GGAGCGAGATCCCTCCAAAAT
	Reverse: GGCTGTTGTCATACTTCTCATGG

Cell Cycle Detection by Flow Cytometry

UM cells were collected and digested with trypsin, followed by centrifugation at 1000 rpm for 5 min. After rinsing the cells with sterile PBS, 1 ml of pre-cooled 70% ethanol was utilized to resuspend the cells as well as fixed overnight at 4°C. They were then rinsed with PBS to remove the ethanol solution, followed by incubation with 500 μl of PI staining solution at room temperature lasting 15 min in the dark. The cell cycle was detected by flow cytometry.

Apoptosis Detection *via* Flow Cytometry

UM cells were trypsinized, followed by centrifugation at 1000 rpm lasting 5 min. After rinsing the cells utilizing pre-cooled sterile PBS at 4°C, the cellular concentrations were adjusted to 5×10^4/mL. Then, 10 μl of Annexin V-FITC and 10 μl of PI were added to 200 μl of the cell suspension and incubated for 10 min at room temperature in the dark, followed by the addition of 500 μl PBS. Apoptotic levels were examined by flow cytometry (BD, US) as well as analyzed with FlowJo flow cytometry software.

Methyl Thiazolyl Tetrazolium (MTT)

Following adjustment of the cellular concentration to 1×10^4/mL, the cells were seeded in 96-well plates, with six duplicate wells for each group. The edge wells were filled with 0.01 mol/L sterile PBS. After 24 h at constant temperature, the medium in the wells was aspirated and discarded, and 90 μL sterile PBS supplemented with 10 μL 0.5% MTT (Sigma-Aldrich, US) were added. After 4 h, the culture was terminated. Thereafter, 100 μl of dimethyl sulfoxide (DMSO; Sigma-Aldrich, US) was added to each well. The plate was shaken well for 10 min, and the absorbance (optical density, OD) value at 490 nm wavelength of each well was measured with a microplate reader (Promega, US).

EdU Staining

UM cells were seeded in 24-well plates (1 mL/well) containing 1 cm × 1 cm sterile glass slides. The plates were pre-incubated for 24 h at 37°C in a 5% CO_2 incubator. After transfection, 20 μM EdU working solution pre-warmed at 37°C was added to a 24-well plate. The cells continued to incubate for 2 h. After removing the culture medium, the cells were fixed with 1 ml of 4% paraformaldehyde for 15 min at room temperature. After washing, the cells were incubated with 1 ml of 0.3% TritonX-100 in PBS per well lasting 10 min at room temperature, followed by 0.5 ml Click addictive reaction lasting 30 min in the dark. DAPI (1000×) was diluted 1:1000 in PBS. After removing the washing solution, they were incubated with 200 μl of 1× DAPI solution at room temperature lasting 5 min in the dark. Finally, fluorescence detection was performed.

Transwell Assays

For invasion assay, Matrigel was diluted 8:1 with serum-free DMEM. Then 100 μL diluted Matrigel was added to the upper chamber of the transwell, and the whole process was performed on ice to prevent it from solidifying. The residual liquid was aspirated from the culture plate. UM cells were trypsinized, resuspended, and concentration adjusted. The upper chamber of a 24-well plate transwell covered with Matrigel was evenly seeded 1×10^5 cells/well as well as maintained by adding serum-free DMEM. Meanwhile, 600 μl of complete medium with 10% FBS was added to the lower chamber. Following 24 h, the chamber was removed, rinsed twice with PBS, and then gently wiped with a cotton swab to remove unpenetrated cells on the upper layer of the chamber membrane. The cells were fixed with 4% paraformaldehyde for 30 min in a 24-well plate, stained with crystal violet staining solution lasting 15 min. The cells invaded through Matrigel were observed under an inverted microscope. Three areas were randomly selected to count the number of invasive cells through Matrigel. The experimental procedure for the migration assay was the same as for the invasion assay, except that Matrigel was not added.

Tube Formation Assay

UM cells transfected with si-NC or si-SOST were co-cultured with HUVEC, and the tube formation ability was detected. Briefly, Matrigel was removed from -20°C and placed in a 4°C refrigerator overnight. The next day, 50 μl Matrigel was added to pre-cooled 96-well plates, and maintained in a 37°C incubator for 45 min. The co-cultured HUVEC was routinely digested, resuspended in cell medium containing 10% FBS. Thereafter, they were seeded into 96-well plates (1×10^4 cells/well) as well as incubated at 37°C. The tube formation was investigated under an inverted microscope.

Animal Experiment

The primer of SOST was designed by querying the CDS sequence on the NCBI website as well as the Thermo fisher website, with a primer sequence of 5'- AAAAGCAGGCGTTCAAGAATG ATGCTTGGATCCAAGCATCATTCTTGAACGCCTGC-3'. The primer was synthesized by Shanghai Sangon Bioengineering Co., Ltd. (China). With pENTRTM H1/TO as vector, shRNA SOST (sh-SOST) or negative control (sh-NC) plasmids were constructed by enzyme digestion, ligation, transformation, and other operations, and then the plasmid identification was carried out. There were 293 T cells used to package the target plasmid, and when the density of OCM-1 cells reached 40%-50%, a stable transfection cell line was constructed after screening.

Six-week-old BALB/c nude female mice (14 ± 2 g) were purchased from Vital River Company (Beijing, China). All experiments gained the approval of the Laboratory Animal Care and Use Committee of Tianjin Medical University Eye Hospital (TJYY2020122054). All animals were separated into four groups (3 mice/group), containing a control group, model group, model + sh-NC group, and model + sh-SOST group. Normal OCM-1 cells or OCM-1 cells stably transfected with sh-NC or sh-SOST were trypsinized, centrifuged as well as suspended in Hanks' balanced salt at 1×10^7/mL. The abdominal skin of the mice was disinfected with iodophor, and the mice were anesthetized by intraperitoneal injection of 0.5% pentobarbital sodium. The right eye of the mice was instilled with proparacaine for ocular surface anesthesia, and the left eye was coated with ophthalmic gel to prevent keratitis. Under the operating microscope, a 30G needle was pointed at the oblique angle to create a tunnel *via* the sclera, and to penetrate the choroid without retina. There were 34G blunt needles attached to 10 μL Hamilton syringes inserted into the subretinal space with the bevel toward the inner eye. The mice in the model group, model + sh-NC group, and model + sh-SOST group were separately injected by 5 μL (5×10^4 cells) of the cell suspension of normal OCM-1 cells or OCM-1 cells stably transfected by sh-NC or sh-SOST. For the control group, the mice did not receive any treatment. After the injection, a white bump was found in the fundus of the mouse, indicating that the injection was successful. Tobramycin ophthalmic ointment was then applied to the eye to reduce the risk of infection. After successful injection, the state of the mice was observed and weighed every other week, and the time of tumor formation in the eyes of the mice was recorded. After six weeks, all mice were euthanized, and their eyeballs were enucleated. The length (L) as well as width (W) of the murine eyeballs were measured utilizing a vernier caliper. The tumor volume (V) was measured in accordance with the following formula: $V = \pi\times L\times W^2\times1/6$.

TUNEL Staining

A TUNEL kit was purchased from the Roche Company (Switzerland). The tissue slides were soaked in xylene for 10 min to dewax. For hydration, the sections were soak in graded ethanol (100%, 95%, 85%, 70%, 50%) for 30 sec, respectively. After washing twice with 1×PBS for 5 min each, 20 μg/ml proteinase K was dropwise added. After 15 min at 37°C, the sections were washed 3 times with 1×PBS. The labeling solution was mixed with buffer evenly at a volume ratio of 1:9. Thereafter, 100 μL TUNEL reaction solution was dropwise added. The reaction area with a cover glass was covered, and reacted at 37°C in a humid, dark environment for 60 min. After washing three times with 1×PBS, 50 μL of DAPI buffer (0.1 mg/mL; Sigma, US) was added to each well, and incubated in the dark at room temperature for 5 min. After washing 3 times with 1×PBS, images were photographed under a fluorescence microscope.

Immunofluorescence

Paraffin sections of murine *in situ* UM tumors in eyeball were deparaffinized, antigen retrieved, blocked with 5% BSA, incubated with primary and secondary antibodies, and finally stained with DAPI (Sigma, US) and mounted with resin. Primary antibodies included SOST, LRP5, and LRP6 antibodies (Affinipure, Jackson, US), and fluorescent-labeled secondary antibodies included Alex Fluor 488 and Alex Fluor 610 goat anti-rabbit antibodies (Affinipure, Jackson, US). The sections were then observed under a fluorescence microscope and three fields of view were randomly selected to be photographed. The nuclei stained with DAPI were blue under the excitation of ultraviolet, and the positive expression was fluorescein-labeled green or red.

Statistical Analysis

All statistical analysis was carried out utilizing GraphPad Prism software (version 8.0.1, GraphPad Software, US). Student's t-test was implemented for comparisons between two groups, and one-way analysis of variance (ANOVA) was implemented for comparisons between multiple groups. Pearson correlation test was used for correlation analysis. $P<0.05$ was considered statistically significant.

RESULTS

Down-Regulated SOST and Up-Regulated Wnt-1 and β-Catenin in Epithelial Type Than Spindle Type UM Tissues

Our study analyzed the expressions of SOST and Wnt-1 as well as β-catenin in 20 cases of epithelial type UM tissues with a high degree of malignancy and 16 cases of spindle type UM with a low degree of malignancy *via* immunohistochemistry. The results showed that SOST expression was lower as well as Wnt1 and β-catenin expressions were higher in epithelial type in comparison to spindle type UM tissues (**Figures 1A, B**). This indicated that low SOST expression as well as activation of Wnt/β-catenin signaling were linked to malignant progression of UM. We also calculated the correlation between SOST and Wnt1 and β-catenin in UM. Our results showed that SOST was negatively correlated to Wnt1 ($p=0.0003$ and $r=-0.9869$) and β-catenin

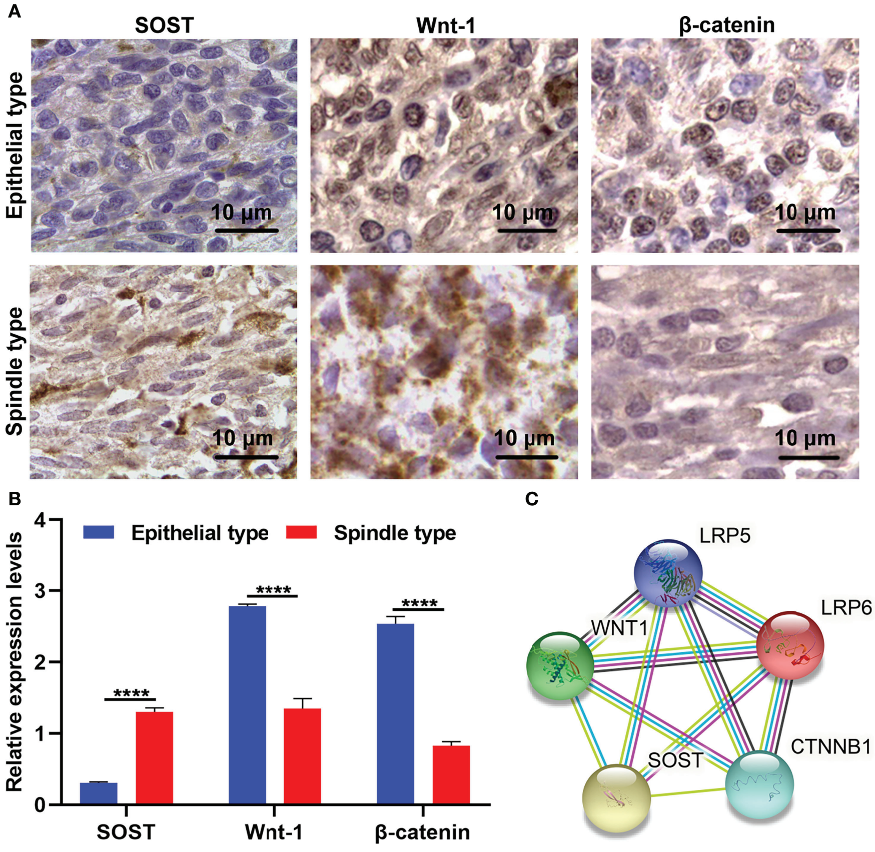

FIGURE 1 | Abnormal expressions of SOST and Wnt-1 as well as β-catenin in spindle type than epithelial type UM tissues. **(A)** Representative immunohistochemistry images for SOST and Wnt-1 as well as β-catenin in human spindle type and epithelial type UM tissues. Magnification, ×100. Scale bar, 10 μm. **(B)** Immunohistochemistry staining scoring of SOST and Wnt-1 as well as β-catenin levels in human spindle type (n=16) and epithelial type (n=20) UM specimens. **(C)** The protein-protein interactions of SOST, Wnt-1, β-catenin, LRP5, and LRP6. ****p<0.0001.

(p<0.0001 and r=-0.9953). The STRING online database also confirmed their protein-protein interactions (**Figure 1C**).

SOST Knockdown Activates Wnt/β-Catenin Signaling in UM Cells

SOST expression was further examined in human retinal epithelial cell line (APRE-19) and three human UM cell lines containing primary spindle-type OCM-1 cells, metastatic epithelial Mum-2B cells, and metastatic spindle-type Mum-2C cells. As shown in **Figures 2A, B**, SOST expression was lower in three human UM cell lines in comparison to APRE-19 cells. Compared with OCM-1 cells, lower SOST expression was found in Mum-2B and Mum-2C cells. Meanwhile, SOST expression was lower in Mum-2C cells than Mum-2B cells. This indicated the down-regulation of SOST in metastatic cells. To silence the expression of SOST, siRNA against SOST was transfected into OCM-1, Mum-2B, and Mum-2C cells. In **Figure 2C**, 48 h after transfection, the expression of SOST mRNA was successfully decreased in three human UM cell lines. Further analysis showed that the expressions of WNT1, CTNNB1, CCND1, MMP2, and MMP9 mRNAs were decreased in si-SOST-transfected OCM-1, Mum-2B, and Mum-2C cells than controls (**Figures 2D–H**). As expected, SOST protein was reduced following si-SOST transfection than control in three human UM cell lines (**Figures 2I, J**). Additionally, Wnt-1, β-catenin, Cyclin-D1, MMP2, and MMP9 proteins presented higher levels when SOST expression was knocked out (**Figures 2K–O**). Collectively, silenced SOST could activate the Wnt/β-catenin pathway in UM cells.

Low SOST Expression Accelerates Cell Cycle Progression As Well As Reduces Apoptosis in UM Cells

Flow cytometry showed that after si-SOST transfection, the proportion of G1 phase was lower as well as the proportions of S phase and G2 phase were higher in three cell lines OCM-1, Mum-2B, and Mum-2C compared with that of the si-NC group, indicating that silencing SOST expression was capable of increasing the proportion of UM cells in interphase (**Figures 3A–F**). Additionally, the apoptotic levels of si-SOST-transfected OCM-1, Mum-2B, and Mum-2C cells were decreased in comparison to that of the si-NC group (**Figures 3G–L**). Altogether, SOST knockdown

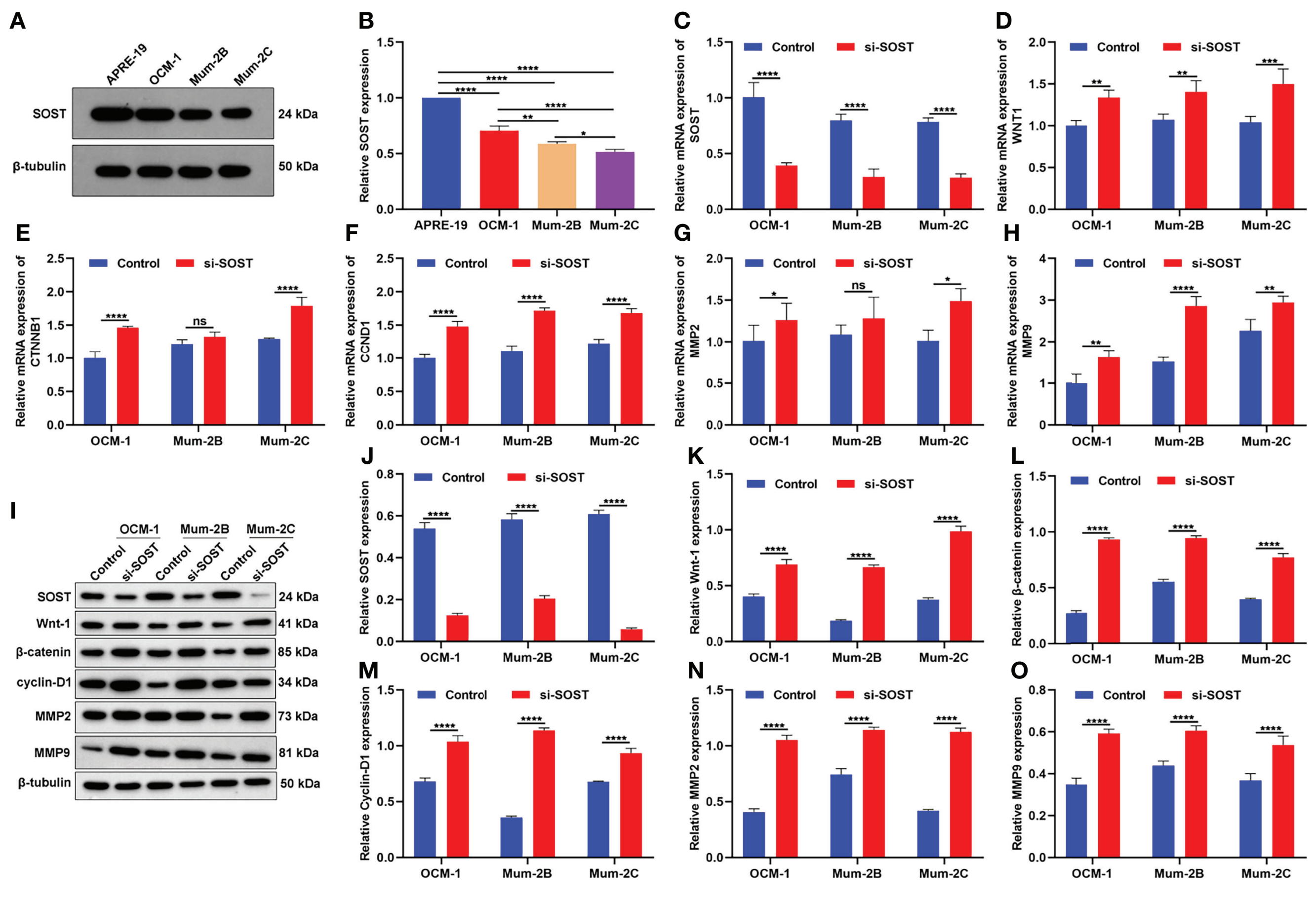

FIGURE 2 | SOST knockdown activates Wnt/β-catenin signaling in UM cells. **(A, B)** Western blot of SOST expression in APRE-19 cells as well as three human UM cell lines OCM-1, Mum-2B, and Mum-2C. **(C–H)** RT-qPCR of the expressions of WNT1, CTNNB1, CCND1, MMP2, and MMP9 mRNAs in si-SOST-transfected OCM-1, Mum-2B, and Mum-2C cells and controls. **(I-O)** Western blot of SOST, Wnt-1, β-catenin, Cyclin-D1, and MMP2 as well as MMP9 levels in si-SOST-transfected OCM-1, Mum-2B, and Mum-2C cells and controls. Ns, no significance; *p<0.05; **p<0.01; ***p<0.001; ****p<0.0001.

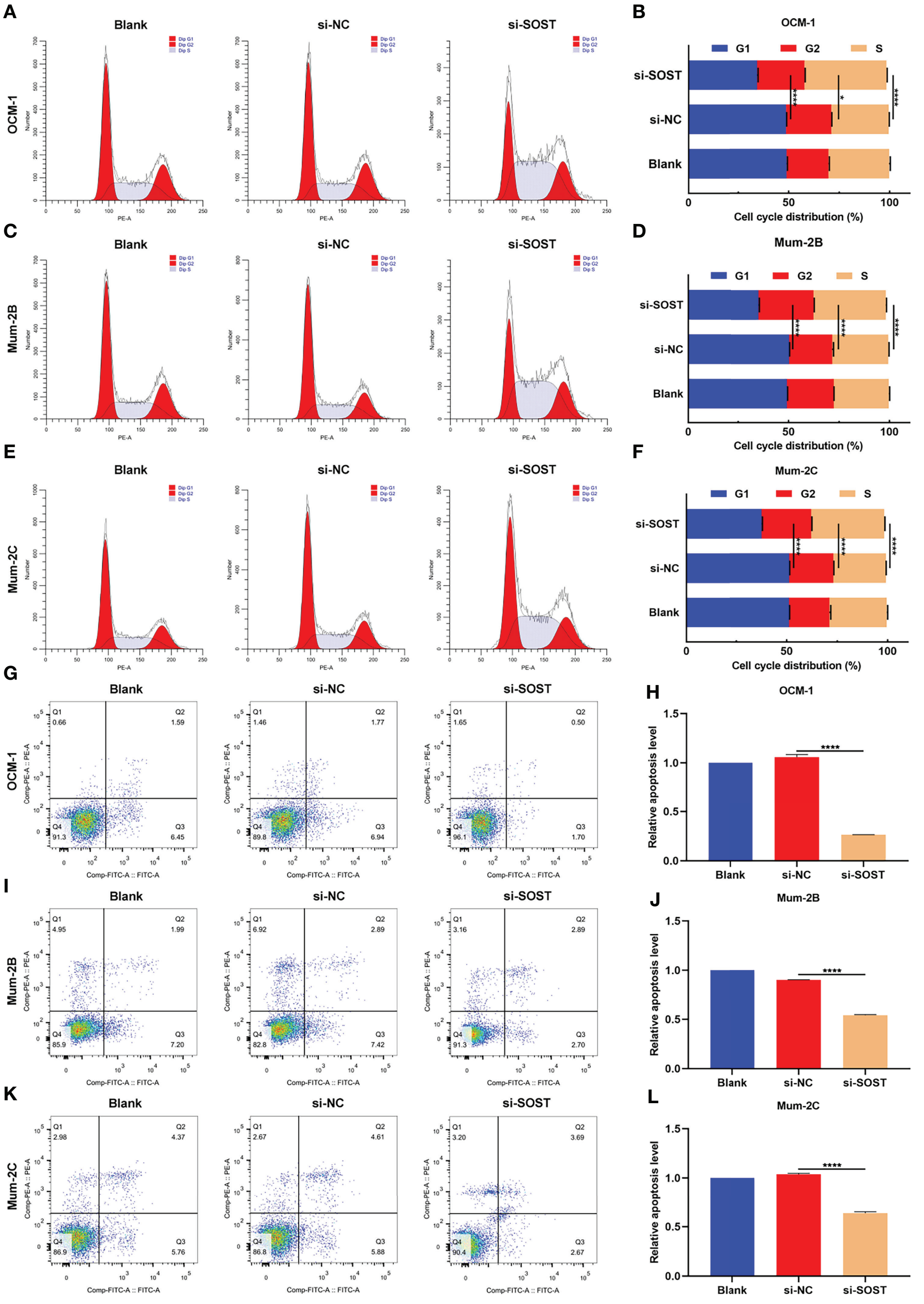

FIGURE 3 | Low SOST expression accelerates cell cycle progression and reduces apoptosis in UM cells. **(A–F)** Cell cycle distribution of normal, si-NC-, or si-SOST-transfected OCM-1 and Mum-2B as well as Mum-2C cells. **(G–L)** Apoptotic levels of normal, si-NC-, or si-SOST-transfected OCM-1, Mum-2B, and Mum-2C cells. *p<0.05; ****p<0.0001.

enabled us to accelerate cell cycle progression as well as decrease apoptosis in UM cells.

SOST Knockdown Strengthens Proliferative Capacities of UM Cells

Through CCK-8 as well as EdU staining assays, this research evaluated the effects of SOST on proliferation of UM cells. As depicted in **Figures 4A–C**, the cell viability of si-SOST-transfected OCM-1, Mum-2B, and Mum-2C cells was elevated in comparison to that of the si-NC group. To overexpress SOST, UM cells were transfected with OE-SOST plasmid. RT-qPCR confirmed that SOST expression was significantly up-regulated in UM cells (**Figure 4D**). Lower cell viability was found in SOST-overexpressed OCM-1, Mum-2B, and Mum-2C cells (**Figure 4E**). Moreover, proliferation levels of three human UM cell lines were enhanced by si-SOST transfection (**Figures 4F, G**) as well as weakened by SOST overexpression (**Figures 4H, I**). Thus, reduced expression of SOST enabled us to strengthen proliferative capacities of UM cells.

Silencing SOST Facilitates Migration, Invasion, and Angiogenesis of UM Cells

Transwell experiment results showed that compared with the si-NC group, the number of OCM-1, Mum-2B, and Mum-2C cells that penetrated the upper chamber of transwell in the si-SOST group was elevated in the si-SOST group (**Figures 5A, B**). This indicated the increase in migration capacities of UM cells. In **Figures 5C, D**, the number of three human UM cell lines invaded through Matrigel was increased in the si-SOST group in comparison to the si-NC group, indicating the enhancement in invasion capacities of UM cells. Following co-culture with si-SOST-transfected OCM-1, Mum-2B, and Mum-2C cells, the tube formation number of HUVEC was increased (**Figures 5E, F**). Altogether, SOST knockdown could enhance migration and invasion as well as angiogenesis of UM cells.

SOST Suppression Strengthens Tumor Growth in Murine Models

To further verify the impact of SOST on UM, we constructed a stable SOST knockdown expression OCM-1 cells as well as ocular orthotopic tumor models in nude mice. Following six weeks, we removed the eyeballs and measured the tumor volume. In comparison to the control group, the tumor volume of the model group was increased. Meanwhile, higher tumor volume was found in the model + sh-SOST group than the model + sh-NC group (**Figures 6A, B**), indicating that SOST suppression accelerated tumor growth. TUNEL staining also demonstrated that proliferative capacity of tumor cells in the model + sh-SOST group was heightened in comparison to that of the model + sh-NC group (**Figure 6C**).

SOST Suppression Activates Wnt/β-Catenin Signaling in Ocular Orthotopic Tumor Models

Immunohistochemistry demonstrated that SOST expression was lower in tumor cells of the model + sh-SOST group in comparison to that of the model + sh-NC group (**Figure 7**). Additionally, Wnt-1, β-catenin, cyclin-D1, MMP2, and MMP9 as well as Ki-67 levels were higher in tumor cells of the model + sh-SOST group than that of the model + sh-NC group, demonstrating that SOST suppression was capable of activating Wnt/β-catenin signaling in ocular orthotopic tumor models.

Interaction Between SOST and LRP5/6 in UM Cells

Further analysis showed that LRP5 and LRP6 membrane receptors presented lower expressions in tumor cells of the model + sh-SOST group than that of the model + sh-NC group, demonstrating that SOST suppression could decrease the expressions of LRP5 and LRP6 (**Figures 8A, B**). Also, SOST co-localized with LRP5/6 in UM cells, indicating that SOST was interacted with LRP5/6.

DISCUSSION

UM is an aggressive malignancy that originates from ocular melanocytes, which is an incurable melanoma and the mortality rate is as high as 50% (21, 22). The experimental results from this study demonstrated that SOST silencing could heighten the proliferation, migration, and invasion as well as angiogenesis of human UM cells *via* activating Wnt/β-catenin signaling *via* binding to membrane receptors LRP5/LRP6.

Low SOST expression as well as high Wnt-1 and β-catenin expressions were found in epithelial-type (high malignancy; n=20) in comparison to spindle-type (low malignancy; n=16) UM tissues. Silencing SOST activated Wnt/β-catenin signaling in three human UM cell lines. Moreover, its knockdown accelerated cell cycle reduced apoptosis as well as facilitated migration, invasion, and angiogenesis of UM cells. SOST is primarily expressed in osteocytes, as a negative regulator of bone formation (23, 24). SOST deficiency facilitates bone formation *via* Wnt/β-catenin signaling pathway as well as compensates particle-triggered osteolysis (25). Accumulated evidence has demonstrated that SOST mediates cancer progression. Hudson et al. found that SOST participates in the early onset of bone metastasis of prostate cancer, which can inhibit the invasion of prostate cancer cells as well as subsequent bone metastasis (26). SOST deficiency triggers proliferative and invasive capacities and decreases apoptotic levels of human retinoblastoma cells (17) and osteosarcoma cells (18) *via* activation of Wnt/β-catenin signaling. Hesse et al. reported that suppressing SOST is capable of alleviating breast cancer-triggered bone metastasis and muscle weakness (27). In postmenopausal Romanian women with osteoporosis, there is a close association between LRP5 and SOST polymorphisms (28). Evidence suggests that LRP5/6 co-deletion in bone markedly reduces the skeletal gain from SOST antibody treatment (29). Herein, our immunofluorescence double staining demonstrated the interactions between SOST and LRP5/6 in UM cells, proving that SOST directly bound to LRP5/6 membrane receptors, thereby inhibiting Wnt/β-catenin signaling during UM progression.

To confirm the above demonstration, this study also used the human UM cell line OCM-1 to construct a stable SOST knockdown expression cell line. Thereafter, we established an

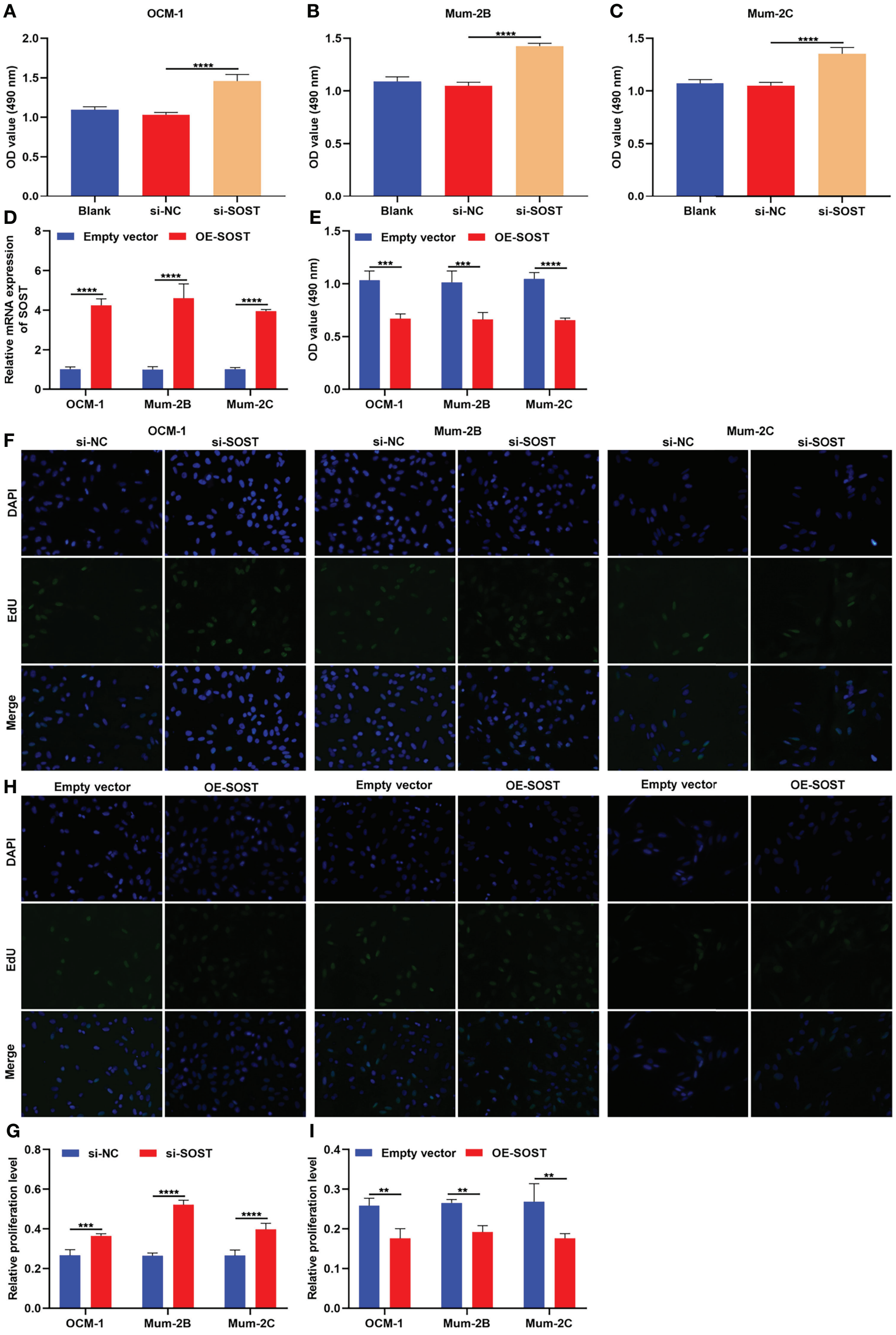

FIGURE 4 | SOST knockdown strengthens proliferative capacities of UM cells. **(A–C)** CCK-8 for the cell viability of normal, si-NC-, or si-SOST-transfected OCM-1, Mum-2B, and Mum-2C cells. **(D)** RT-qPCR for the expression of SOST in empty vector- or OE-SOST-transfected OCM-1, Mum-2B, and Mum-2C cells. **(E)** CCK-8 for the cell viability of empty vector- or OE-SOST-transfected OCM-1, Mum-2B, and Mum-2C cells. **(F, G)** EdU staining for the proliferation of normal, si-NC-, or si-SOST-transfected OCM-1, Mum-2B, and Mum-2C cells. **(H, I)** EdU staining for the proliferation of empty vector- or OE-SOST-transfected OCM-1, Mum-2B, and Mum-2C cells. Magnification, ×200. Scale bar, 10 µm. **p<0.01; ***p<0.001; ****p<0.0001.

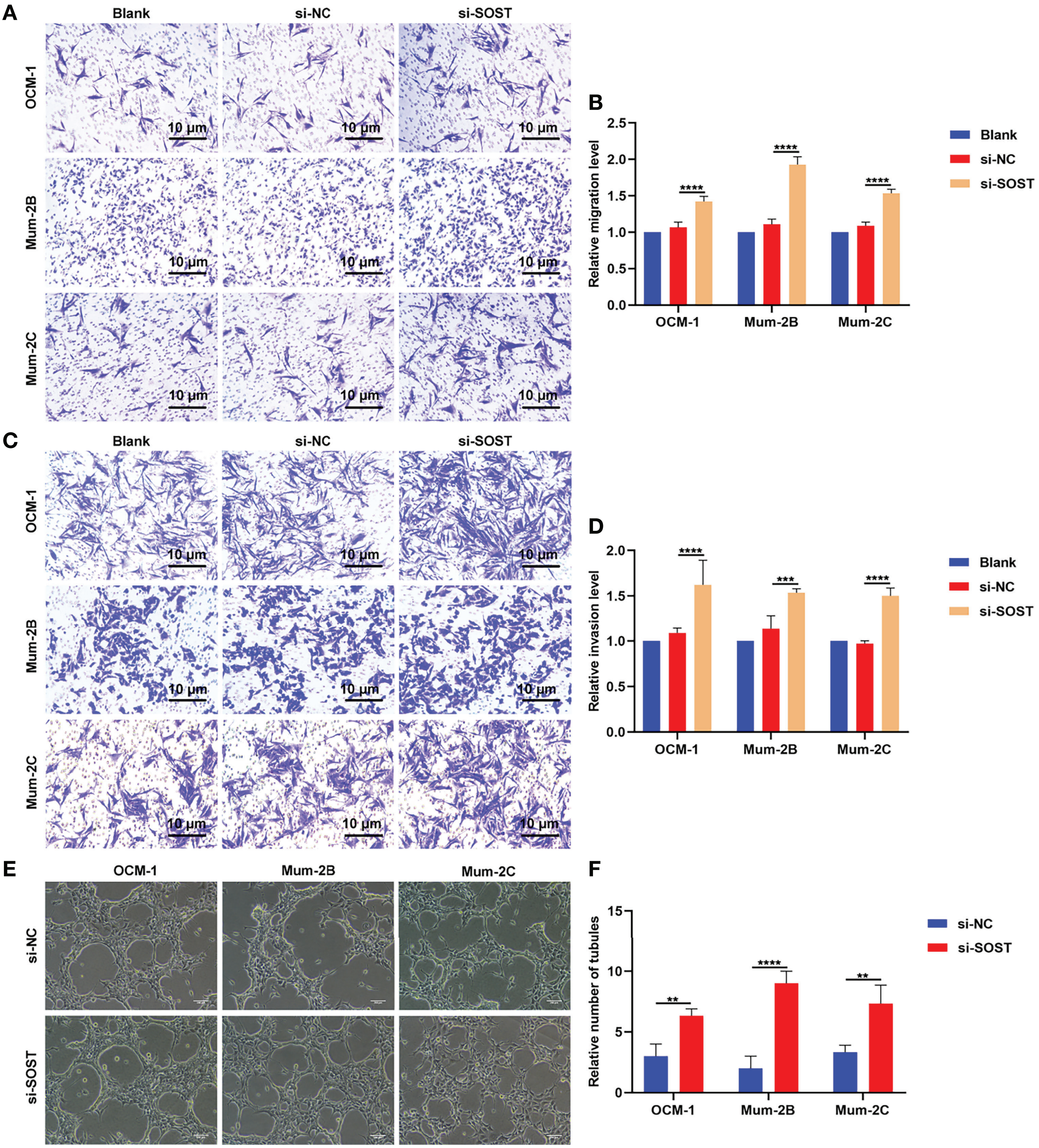

FIGURE 5 | Silencing SOST facilitates migration and invasion as well as angiogenesis of UM cells. **(A, B)** Transwell experiments for the migration of normal, si-NC-, or si-SOST-transfected OCM-1, Mum-2B, and Mum-2C cells. Magnification, ×40. Scale bar, 10 μm. **(C, D)** Transwell experiments for the invasion of normal, si-NC-, or si-SOST-transfected OCM-1, Mum-2B, and Mum-2C cells. Magnification, ×40. Scale bar, 10 μm. **(E, F)** Tube formation experiment of HUVEC co-cultured with normal, si-NC-, or si-SOST-transfected OCM-1, Mum-2B, and Mum-2C cells. Magnification, ×40. Scale bar, 200 μm. **p<0.01; ***p<0.001; ****p<0.0001.

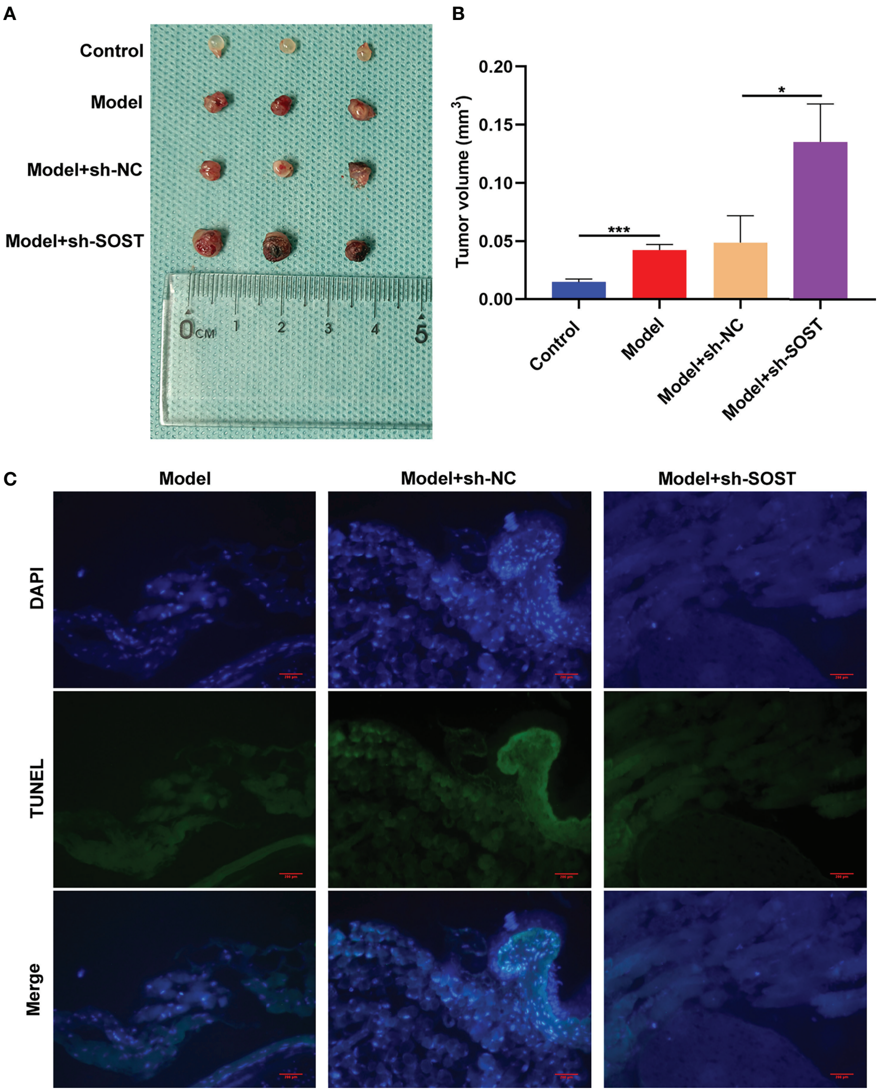

FIGURE 6 | SOST suppression strengthens tumor growth in murine models. **(A)** Representative images of tumors in eyeballs from control mice or those injected with normal, sh-NC-, or sh-SOST-transfected OCM-1 cells after six weeks. **(B)** Measurement of tumor volume of each group. $^{*}p<0.01$; $^{***}p<0.001$. **(C)** TUNEL staining of tumor sections from mice injected with normal, sh-NC-, or sh-SOST-transfected OCM-1 cells after six weeks. Magnification, ×40. Scale bar, 200 μm.

animal model of ocular orthotopic tumor implantation in BALB/c nude mice to verify the effects of SOST inhibition on UM tumor formation. The results showed that when SOST expressions were knocked down in human UM cells, the tumor volume of ocular tumors of nude mice was larger. Additionally, the expressions of Wnt-1, β-catenin, Cyclin-D1, and MMP2 as well as MMP9 were all increased when the expression of SOST was suppressed in UM cells. As demonstrated by Kim et al. SOST is capable of inactivating Wnt signaling in Xenopus embryos (30). Furthermore, Zhou et al. further proved that the expression of cyclin-D1 is linked with the progression of UM, and high Let-7b expression may weaken the expression of cyclin-D1 and heighten cell cycle arrest to increase the radiosensitivity of UM cells (31). Hou et al. demonstrated that MMP2 is a downstream effector affecting UM metastasis, and miR-34a negatively modulates LGR4, reducing the expression of MMP2 to inhibit UM cell migration and invasion (32). Chang et al. verified that epigallocatechin gallate may downregulate the activity of secreted MMP-2 *via* suppression of ERK1/2 phosphorylation, and thus reduces the migration of UM cells (33). Cheng et al. demonstrated that HMGA1 can accelerate the progression of UM *via* positively modulating the activity of PI3K/Akt/MMP9 signaling in xenograft murine models (34). The above evidence demonstrated that SOST suppression may heighten UM progression through activating Wnt/β-catenin signaling *via* binding to membrane receptors LRP5/LRP6.

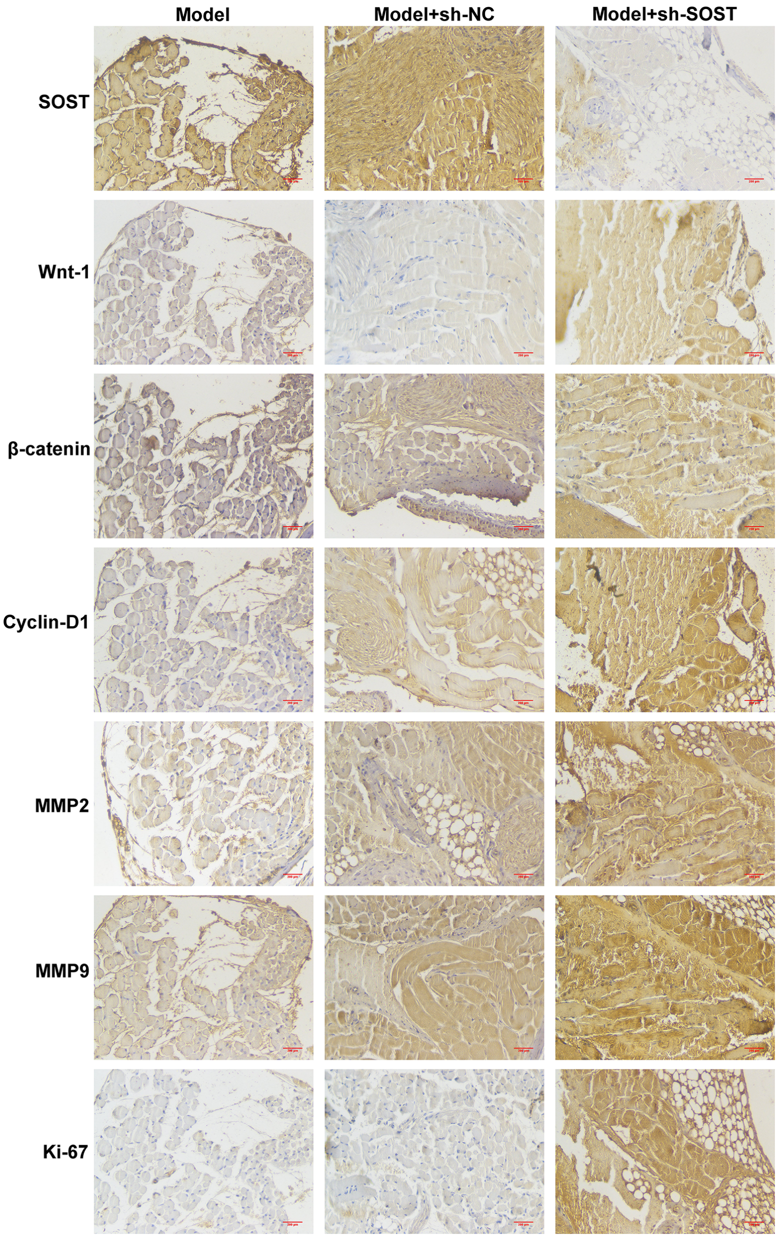

FIGURE 7 | SOST suppression activates Wnt/β-catenin pathway in ocular orthotopic tumor models. Immunohistochemistry staining for SOST, Wnt-1, β-catenin, cyclin-D1, MMP2, and MMP9 as well as Ki-67 in tumor sections from mice injected with normal, sh-NC-, or sh-SOST-transfected OCM-1 cells after six weeks. Magnification, ×40. Scale bar, 200 μm.

CONCLUSION

Taken together, this research proposed that SOST suppression may activate the Wnt/β-catenin pathway, thereby accelerating UM malignant progression. We also have reasons to believe that the SOST-triggered Wnt/β-catenin pathway might represent a promising therapeutic as well as adjunctive regimen against UM. Despite this, future clinical trials are needed for determining the safety as well as effects of this therapy. Due to the small number of subjects, it is difficult to generalize the results. To gain a deeper understanding of the biological behaviors of UM cells as well as better assess the prognosis of patients, clinical trials and clinical studies on a larger population based on the SOST-triggered Wnt/β-catenin pathway are also needed.

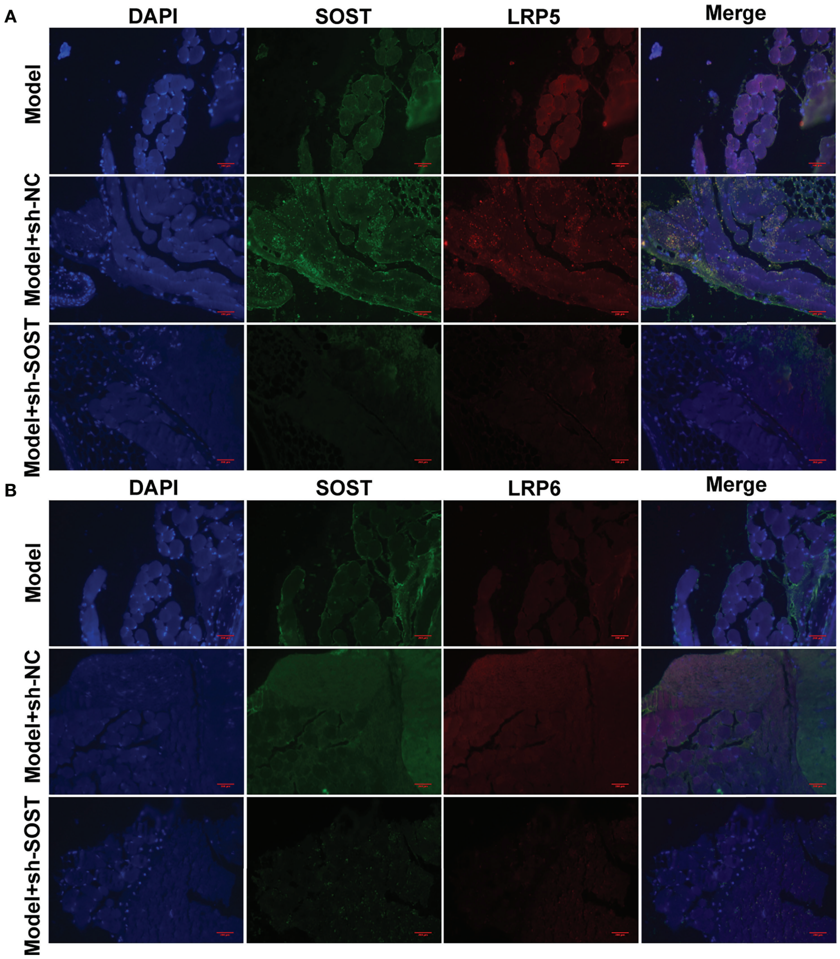

FIGURE 8 | Interaction between SOST and LRP5/6 in UM cells. **(A, B)** Immunofluorescence double staining of SOST and LRP5/6 in tumor sections from mice injected with normal, sh-NC-, or sh-SOST-transfected OCM-1 cells after six weeks. Magnification, ×40. Scale bar, 200 μm.

DATA AVAILABILITY STATEMENT

The original contributions presented in the study are included in the article/supplementary material. Further inquiries can be directed to the corresponding authors.

ETHICS STATEMENT

The studies involving human participants were reviewed and approved by Tianjin Medical University Eye Hospital (2017KY (L)-53). The patients/participants provided their written informed consent to participate in this study. The animal study was reviewed and approved by Tianjin Medical University Eye Hospital (TJYY2020122054).

AUTHOR CONTRIBUTIONS

TW and XH conceived and designed the study. HW and SZ conducted most of the experiments and data analysis and wrote the manuscript. YL and FS participated in collecting data and helped to draft the manuscript. All authors reviewed and approved the manuscript.

FUNDING

This study was supported by grants from The Science& Technology Development Fund of Tian jin Education Commission for Higher Education (NO.2020KJ176).

REFERENCES

1. Bustamante P, Piquet L, Landreville S, Burnier JV. Uveal Melanoma Pathobiology: Metastasis to the Liver. *Semin Cancer Biol* (2021) 71:65–85. doi: 10.1016/j.semcancer.2020.05.003
2. Beasley AB, Chen FK, Isaacs TW, Gray ES. Future Perspectives of Uveal Melanoma Blood Based Biomarkers. *Br J Cancer* (2022) 126(11):1511–28. doi: 10.1038/s41416-022-01723-8
3. Ambrosini G, Rai AJ, Carvajal RD, Schwartz GK. Uveal Melanoma Exosomes Induce a Prometastatic Microenvironment Through Macrophage Migration Inhibitory Factor. *Mol Cancer Res* (2022) 20(4):661–9. doi: 10.1158/1541-7786.Mcr-21-0526
4. Medina CA, Biscotti CV, Singh N, Singh AD. Diagnostic Cytologic Features of Uveal Melanoma. *Ophthalmology* (2015) 122(8):1580–4. doi: 10.1016/j.ophtha.2015.04.013
5. Seibel I, Cordini D, Rehak M, Hager A, Riechardt AI, Böker A, et al. Local Recurrence After Primary Proton Beam Therapy in Uveal Melanoma: Risk Factors, Retreatment Approaches, and Outcome. *Am J Ophthalmol* (2015) 160(4):628–36. doi: 10.1016/j.ajo.2015.06.017
6. Jang GF, Crabb JS, Hu B, Willard B, Kalirai H, Singh AD, et al. Proteomics of Primary Uveal Melanoma: Insights Into Metastasis and Protein Biomarkers. *Cancers (Basel)* (2021) 13(14):3520. doi: 10.3390/cancers13143520
7. Kim S, Kim SA, Nam GH, Hong Y, Kim GB, Choi Y, et al. *In Situ* Immunogenic Clearance Induced by a Combination of Photodynamic Therapy and Rho-Kinase Inhibition Sensitizes Immune Checkpoint Blockade Response to Elicit Systemic Antitumor Immunity Against Intraocular Melanoma and its Metastasis. *J Immunother Cancer* (2021) 9 (1):e001481. doi: 10.1136/jitc-2020-001481
8. Pandiani C, Strub T, Nottet N, Cheli Y, Gambi G, Bille K, et al. Single-Cell RNA Sequencing Reveals Intratumoral Heterogeneity in Primary Uveal Melanomas and Identifies HES6 as a Driver of the Metastatic Disease. *Cell Death Differ* (2021) 28 (6):1990–2000. doi: 10.1038/s41418-020-00730-7
9. Koch EAT, Petzold A, Wessely A, Dippel E, Gesierich A, Gutzmer R, et al. Immune Checkpoint Blockade for Metastatic Uveal Melanoma: Patterns of Response and Survival According to the Presence of Hepatic and Extrahepatic Metastasis. *Cancers (Basel)* (2021) 13(13):3359. doi: 10.3390/cancers13133359
10. Cherepakhin OS, Argenyi ZB, Moshiri AS. Genomic and Transcriptomic Underpinnings of Melanoma Genesis, Progression, and Metastasis. *Cancers (Basel)* (2021) 14(1):123. doi: 10.3390/cancers14010123
11. Ren R, Du Y, Niu X, Zang R. ZFPM2-AS1 Transcriptionally Mediated by STAT1 Regulates Thyroid Cancer Cell Growth, Migration and Invasion *via* miR-515-5p/TUSC3. *J Cancer* (2021) 12(11):3393–406. doi: 10.7150/jca.51437
12. Zhao G, Yin Y, Zhao B. miR-140-5p Is Negatively Correlated With Proliferation, Invasion, and Tumorigenesis in Malignant Melanoma by Targeting SOX4 *via* the Wnt/β-Catenin and NF-κb Cascades. *J Cell Physiol* (2020) 235(3):2161–70. doi: 10.1002/jcp.29122
13. Wu S, Han M, Zhang C. Overexpression of microRNA-130a Represses Uveal Melanoma Cell Migration and Invasion Through Inactivation of the Wnt/β-Catenin Signaling Pathway by Downregulating USP6. *Cancer Gene Ther* (2021). doi: 10.1038/s41417-021-00377-7
14. Zheng L, Pan J. The Anti-Malarial Drug Artesunate Blocks Wnt/β-Catenin Pathway and Inhibits Growth, Migration and Invasion of Uveal Melanoma Cells. *Curr Cancer Drug Targets* (2018) 18(10):988–98. doi: 10.2174/1568009618666180425142653
15. Dean DB, Watson JT, Jin W, Peters C, Enders JT, Chen A, et al. Distinct Functionalities of Bone Morphogenetic Protein Antagonists During Fracture Healing in Mice. *J Anat* (2010) 216(5):625–30. doi: 10.1111/j.1469-7580.2010.01214.x
16. Kim SP, Da H, Wang L, Taketo MM, Wan M, Riddle RC. Bone-Derived Sclerostin and Wnt/β-Catenin Signaling Regulate Pdgfrα(+) Adipoprogenitor Cell Differentiation. *FASEB J* (2021) 35(11):e21957. doi: 10.1096/fj.202100691R
17. Wu T, Wang LN, Tang DR, Sun FY. SOST Silencing Promotes Proliferation and Invasion and Reduces Apoptosis of Retinoblastoma Cells by Activating Wnt/β-Catenin Signaling Pathway. *Gene Ther* (2017) 24(7):399–407. doi: 10.1038/gt.2017.31
18. Zou J, Zhang W, Li XL. Effects of SOST Gene Silencing on Proliferation, Apoptosis, Invasion, and Migration of Human Osteosarcoma Cells Through the Wnt/β-Catenin Signaling Pathway. *Calcif Tissue Int* (2017) 100(6):551–64. doi: 10.1007/s00223-016-0231-6
19. Semënov M, Tamai K, He X. SOST is a Ligand for LRP5/LRP6 and a Wnt Signaling Inhibitor. *J Biol Chem* (2005) 280(29):26770–5. doi: 10.1074/jbc.M504308200
20. Wang X, Cheng G, Miao Y, Qiu F, Bai L, Gao Z, et al. Piezo Type Mechanosensitive Ion Channel Component 1 Facilitates Gastric Cancer Omentum Metastasis. *J Cell Mol Med* (2021) 25(4):2238–53. doi: 10.1111/jcmm.16217
21. Pelster MS, Gruschkus SK, Bassett R, Gombos DS, Shephard M, Posada L, et al. Nivolumab and Ipilimumab in Metastatic Uveal Melanoma: Results From a Single-Arm Phase II Study. *J Clin Oncol* (2021) 39(6):599–607. doi: 10.1200/jco.20.00605
22. Nathan P, Hassel JC, Rutkowski P, Baurain JF, Butler MO, Schlaak M, et al. Overall Survival Benefit With Tebentafusp in Metastatic Uveal Melanoma. *N Engl J Med* (2021) 385(13):1196–206. doi: 10.1056/NEJMoa2103485
23. Chang JC, Christiansen BA, Murugesh DK, Sebastian A, Hum NR, Collette NM, et al. SOST/Sclerostin Improves Posttraumatic Osteoarthritis and Inhibits MMP2/3 Expression After Injury. *J Bone Miner Res* (2018) 33(6):1105–13. doi: 10.1002/jbmr.3397
24. van Bezooijen RL, ten Dijke P, Papapoulos SE, Löwik CW. SOST/sclerostin, an Osteocyte-Derived Negative Regulator of Bone Formation. *Cytokine Growth Factor Rev* (2005) 16(3):319–27. doi: 10.1016/j.cytogfr.2005.02.005
25. Li J, Xue J, Jing Y, Wang M, Shu R, Xu H, et al. SOST Deficiency Aggravates Osteoarthritis in Mice by Promoting Sclerosis of Subchondral Bone. *BioMed Res Int* (2019) 2019:7623562. doi: 10.1155/2019/7623562
26. Hudson BD, Hum NR, Thomas CB, Kohlgruber A, Sebastian A, Collette NM, et al. SOST Inhibits Prostate Cancer Invasion. *PloS One* (2015) 10(11):e0142058. doi: 10.1371/journal.pone.0142058
27. Hesse E, Schröder S, Brandt D, Pamperin J, Saito H, Taipaleenmäki H. Sclerostin Inhibition Alleviates Breast Cancer-Induced Bone Metastases and Muscle Weakness. *JCI Insight* (2019) 5(9):e125543. doi: 10.1172/jci.insight.125543
28. Ciubean AD, Ungur RA, Irsay L, Ciortea VM, Borda IM, Dogaru GB, et al. Polymorphisms of FDPS, LRP5, SOST and VKORC1 Genes and Their Relation With Osteoporosis in Postmenopausal Romanian Women. *PloS One* (2019) 14 (11):e0225776. doi: 10.1371/journal.pone.0225776
29. Lim KE, Bullock WA, Horan DJ, Williams BO, Warman ML, Robling AG. Co-Deletion of Lrp5 and Lrp6 in the Skeleton Severely Diminishes Bone Gain From Sclerostin Antibody Administration. *Bone* (2021) 143:115708. doi: 10.1016/j.bone.2020.115708
30. Kim J, Han W, Park T, Kim EJ, Bang I, Lee HS, et al. Sclerostin Inhibits Wnt Signaling Through Tandem Interaction With Two LRP6 Ectodomains. *Nat Commun* (2020) 11(1):5357. doi: 10.1038/s41467-020-19155-4
31. Zhou Y, Zhang L, Fan J, Jia R, Song X, Xu X, et al. Let-7b Overexpression Leads to Increased Radiosensitivity of Uveal Melanoma Cells. *Melanoma Res* (2015) 25 (2):119–26. doi: 10.1097/cmr.0000000000000140
32. Hou Q, Han S, Yang L, Chen S, Chen J, Ma N, et al. The Interplay of MicroRNA-34a, LGR4, EMT-Associated Factors, and MMP2 in Regulating Uveal Melanoma Cells. *Invest Ophthalmol Vis Sci* (2019) 60(13):4503–10. doi: 10.1167/iovs.18-26477
33. Chang CW, Hsieh YH, Yang WE, Yang SF, Chen Y, Hu DN. Epigallocatechingallate Inhibits Migration of Human Uveal Melanoma Cells *via* Downregulation of Matrix Metalloproteinase-2 Activity and ERK1/2 Pathway. *BioMed Res Int* (2014) 2014:141582. doi: 10.1155/2014/141582
34. Cheng Y, Cheng T, Zhao Y, Qu Y. HMGA1 Exacerbates Tumor Progression by Activating miR-222 Through PI3K/Akt/MMP-9 Signaling Pathway in Uveal Melanoma. *Cell Signal* (2019) 63:109386. doi: 10.1016/j.cellsig.2019.109386

Conflict of Interest: The authors declare that the research was conducted in the absence of any commercial or financial relationships that could be construed as a potential conflict of interest.

Publisher's Note: All claims expressed in this article are solely those of the authors and do not necessarily represent those of their affiliated organizations, or those of the publisher, the editors and the reviewers. Any product that may be evaluated in this article, or claim that may be made by its manufacturer, is not guaranteed or endorsed by the publisher.

Copyright © 2022 Wang, Zhao, Liu, Sun, Huang and Wu. This is an open-access article distributed under the terms of the Creative Commons Attribution License (CC BY). The use, distribution or reproduction in other forums is permitted, provided the original author(s) and the copyright owner(s) are credited and that the original publication in this journal is cited, in accordance with accepted academic practice. No use, distribution or reproduction is permitted which does not comply with these terms.

frontiers | Frontiers in Oncology

MINI REVIEW
published: 20 June 2022
doi: 10.3389/fonc.2022.862462

Emerging Role of *Helicobacter pylori* in the Immune Evasion Mechanism of Gastric Cancer: An Insight Into Tumor Microenvironment-Pathogen Interaction

Zhifang Li[1,2], Wenqing Zhang[2], Jinyang Bai[3], Jing Li[2] and Hong Li[2]*

[1] Shanxi Medical University, Taiyuan, China, [2] The Second Hospital of Shanxi Medical University, Taiyuan, China,
[3] Shanxi Traditional Chinese Medicine Hospital, Taiyuan, China

OPEN ACCESS

Edited by:
Haichang Li,
The Ohio State University,
United States

Reviewed by:
Leming Sun,
Northwestern Polytechnical University,
China
Qing Li,
Daping Hospital, China

****Correspondence:***
Hong Li
lihong@sxmu.edu.cn

Specialty section:
This article was submitted to
Pharmacology of Anti-Cancer Drugs,
a section of the journal
Frontiers in Oncology

Received: *25 January 2022*
Accepted: *25 March 2022*
Published: *20 June 2022*

Citation:
Li Z, Zhang W, Bai J, Li J and Li H (2022) Emerging Role of Helicobacter pylori in the Immune Evasion Mechanism of Gastric Cancer: An Insight Into Tumor Microenvironment-Pathogen Interaction.
Front. Oncol. 12:862462.
doi: 10.3389/fonc.2022.862462

Helicobacter pylori (*H. pylori*) infection is the strongest causative factor of gastric cancer. Growing evidence suggests that the complex crosstalk of *H. pylori* and the tumor microenvironment (TME) exerts a profound influence on gastric cancer progression. Hence, there is emerging interest to in-depth comprehension of the mechanisms of interplay between *H. pylori* and the TME. This review discusses the regulatory mechanisms underlying the crosstalk between *H. pylori* infection and immune and stromal cells, including tumor-associated macrophages (TAMs), neutrophils, dendritic cells, myeloid-derived suppressor cells (MDSCs), natural killer (NK) cells, B and T cells, cancer associated fibroblasts (CAFs), and mesenchymal stem cells (MSCs), within the TME. Such knowledge will deepen the understanding about the roles of *H. pylori* in the immune evasion mechanism in gastric cancer and contribute to the development of more effective treatment regimens against *H. pylori*-induced gastric cancer.

Keywords: gastric cancer, *Helicobacter pylori*, tumor microenvironment, immune evasion, stromal cells

INTRODUCTION

Gastric cancer is a global health issue, with over 1 million newly diagnosed cases globally each year (1). Despite the descended morbidity and mortality of this malignancy during the last five years, it is still the third major cause of cancer-related deaths (2). The prognosis of advanced gastric cancer is undesirable with a five-year survival rate of less than 30%. Platinum-fluoropyrimidine combination

---

Abbreviations: TME, tumor microenvironment; ECM, extracellular matrix; *H. pylori*, *Helicobacter pylori*; TAMs, tumor-associated macrophages; NK, natural killer; CAFs, cancer associated fibroblasts; EMT, epithelial–mesenchymal transition.

chemotherapy represents the first-line therapeutic option against advanced patients (1). However, patients usually have a low complete response rate to chemotherapy, with substantial toxicity. Gastric cancer is diagnosed histologically following endoscopic biopsy as well as staged utilizing computed tomography, endoscopic ultrasound, positron emission tomography, and laparoscopy. Currently, histopathological classification schemes designate gastric cancer as intestinal or diffuse in accordance with the morphology, differentiation, and cohesion of glandular cells. Intestinal gastric cancer is preceded through alterations in the gastric mucosa as the Correa cascade that evolves *via* inflammatory response, metaplasia, dysplasia, or adenocarcinoma. Diffuse gastric cancer lacks cell adhesion and exhibits a diffuse aggressive growth feature. Recently, comprehensive evaluation of the Cancer Genome Atlas (TCGA) has categorized this malignancy as 4 molecular subtypes: genome stable (GS), microsatellite instability (MSI), EBV infection, as well as chromosomal instability (CIN) (3). Moreover, the Asian Cancer Research Group (ACRG) project offers a new molecular classification, including MSI subtype, microsatellite stable with epithelial to mesenchymal transition (MSS/EMT), MSS/TP53 mutant (MSS/TP53+), and MSS/TP53 wild-type (MSS/TP53-) subtypes (4). In terms of histopathological or molecular classifications, gastric cancer is not an isolated mass of cancerous epithelial cells. In contrast, these tumors present a complex morphology in which tumor cells are surrounded by the tumor microenvironment (TME) (5). The TME contains extracellular matrix (ECM), stromal cells, immune cells, and secreted factors, which present high correlations to gastric cancer progression and therapeutic responses (6). The innate immune cell populations (macrophage, neutrophil, dendritic cell, innate lymphoid cell, myeloid-derived suppressor cell, natural killer cell) as well as adaptive immune cell populations (T cell and B cell) trigger gastric cancer progression within the TME (7). Innate and adaptive immune responses exert critical functions in tumor immune surveillance as well as suppression of tumor progression. Tumor cells inhibit the immune system, and thus evade immune disruption and facilitate tumor growth, and metastases. Tumor immune surveillance is capable of recognizing and eliminating tumor cells. Tumor immune escape permits tumor cells to proliferation and metastases following escaping immune surveillance and thus results in unfavorable clinical outcomes. Numerus factors participate in the process of tumor immune escape, especially *Helicobacter pylori* (*H. pylori*) infection.

H. pylori is a gram-negative microaerobic spiral rod-shaped bacteria that colonizes the surface of human stomach mucosa (2). It is a highly invasive microorganism and is one of the reasons for the highest incidence of chronic infections in the world, though more than 80% of infected patients are still asymptomatic (2). At present, several virulence-related genes in the genome of *H. pylori* have been confirmed, mainly cytotoxin-associated gene A (cagA), vacuum toxin gene A (vacA), induced by contact epithelium (iceA), blood group antigen-binding Adhesin gene (babA), etc. (2). Over 50% of individuals are infected with *H. pylori* across the globe. Nearly all cases of gastric cancer are linked with *H. pylori* infection (8). *H. pylori* eradication is capable of preventing gastric cancer progression and quadruple therapy (bismuth quadruple and concomitant) is the recommended first-line therapeutic option (8). However, antibiotic resistance with a growing prevalence is the main reason for the therapeutic failure of *H. pylori*. Growing evidence suggests the crucial roles of *H. pylori* infection in immune evasion mechanisms during gastric cancer progression (8). The persistence of *H. pylori* infection results in an immunosuppressive microenvironment as well as allows gastric carcinoma cells to evade immune surveillance (8). In this review, we summarize a comprehensive outline of research advances of the molecular mechanisms concerning the crosstalk of *H. pylori* with components within the TME of gastric cancer, suggesting the crucial roles of *H. pylori* infection in tumor immune escape.

THE CROSSTALK OF *H. PYLORI* WITH INNATE IMMUNE CELLS WITHIN THE TUMOR MICROENVIRONMENT

Tumor-Associated Macrophages

Within the TME, macrophages, known as TAMs, are the most abundant immune cells. TAMs are categorized as two subtypes: M1 and M2 (9). M1 macrophages (also called as classical macrophages) can be primarily stimulated by IFN-γ, TNF-α, and LPS; M2 macrophages can be induced by IL-4 (9). The polarization and recruitment of macrophages produce pro-inflammatory and pro-cancerogenic cytokines and thus sustain the initiation and progression of gastric carcinoma (9). *H. pylori*-induced chronic inflammation exerts a crucial regulatory role in gastric carcinogenesis and TAMs involved in this process. The polarization and recruitment of macrophages supply pro-inflammatory and pro-tumorigenic cytokines and thus support the development and progression of gastric cancer (9). The degree of *H. pylori* infection is linked with macrophage polarization by interplay of reactive oxygen species (ROS) with hypoxia inducible factor 1 subunit α (HIF-1α) (10). HIF-1α can directly or indirectly trigger tumor development *via* modulating immune surveillance escape through inducing immunosuppressive factors and downstream targets. Inhibition of macrophage polarization can ameliorate *H. pylori*-induced gastric injury (11). Exosomes are small extracellular vesicles, which are critical mediators of cell-cell communication. *H. pylori* infection triggers the up-regulation of mesenchymal-epithelial transition factor (MET) in exosomes and activates tumor-associated macrophages through IL-1β, thereby promoting gastric cancer progression (12). *H. pylori* triggers nitric oxide (NO) release in macrophages that leads to methylation of runx3 in gastric epithelial cells (13). Runx3 methylation is linked with differentiation, nodal metastases, and unfavorable clinical outcomes of gastric cancer.

Experimental evidence shows that suppression of runx3 triggers gastric carcinoma progression as well as metastases. *H. pylori* also promotes the release of TNF-α from macrophages and thus up-regulates the expression of C-X-C motif chemokine receptor 4 (CXCR4) in gastric cancer cells (14). CXCR4 is a seven-span transmembrane G-protein coupled receptor, which is the main receptor of CXCL12. CXCL12 is released from stromal cells within the TME and thus binds to CXCR4 on the surface of tumor cells, eventually promoting tumor metastases and unfavorable survival outcomes. Notch signaling can facilitate the activation and bactericidal activities of macrophages, and one of its ligands Jagged1 enhances macrophage-mediated response to *H. pylori* (15). CXCL12/CXCR4 signaling-mediated macrophage polarization can trigger gastric cancer metastases (16). MiR-22 inhibits gastric cancer cell growth through triggering a deficiency in endogenous S-adenosylmethionine, which can sustain NLRP3 expression and attenuate *H. pylori*-induced gastric cancer initiation (17). *H. pylori* infection weakens miR-22 expression and thus up-regulates NLRP3 inflammasome activation and release of oncogenic mature IL-1β, thereby triggering uncontrolled proliferation of epithelial cells and the occurrence of gastric cancer (8).

Neutrophils

Neutrophils are the most abundant circulating leukocytes in cancer patients, which present two forms: circulating neutrophils that circulate freely and are recruited into tumors as well as peripheral neutrophils that bind to the capillary endothelium (18). Persisting and increasing neutrophil infiltrations are linked with gastric cancer progression (18). Hepatoma-derived growth factor (HDGF) displays high expression in gastric carcinoma tissues, which is linked with lymph node metastases and undesirable clinical outcomes. Additionally, the differentiation of mesenchymal stem cells into myofibroblast-like cells induced by HDGF triggers the progression of *H. pylori*-induced gastric cancer. Recent research has proposed that HDGF expression is up-regulated both in tumors and peripheral blood of *H. pylori*-infected patients, which mediates *H. pylori*-triggered neutrophil recruitment or activation of inflammatory TNF-α/COX-2 pathway, and thus promotes gastric carcinogenesis (19).

Dendritic Cells

Dendritic cells are professional antigen-presenting cell populations, which can induce antigen-specific adaptive immune response that is of importance for immune surveillance and tolerance (20). Impaired function of dendritic cells results in the ineffective innate and adaptive immune responses against *H. pylori* for gastric cancer populations (20). *H. pylori* suppresses the maturation of dendritic cells through IL-10-independent activation of the signal transducer and activator of transcription 3 (STAT3) signaling, potentially favoring chronic infection, and promoting gastric carcinogenesis (21). *H. pylori*-induced immune evasion is mediated by dendritic cell-induced Th17/Treg balance towards Treg-biased responses and inhibition of Th17 immunity (22). MiR-375 expression is frequently decreased in gastric carcinoma as well as weakens cell proliferation through targeting JAK2 oncogene. *H. pylori* infection downregulates its expression in gastric cancer cells and promotes the release of cytokines IL-6, IL-10, and VEGF *via* the JAK2-STAT3 signaling, and thus induces the maturation of dendritic cells and the reduction in the number of CD4+ and CD8+ T cells (23).

Myeloid-Derived Suppressor Cells

MDSCs are a heterogeneous subset of immature myeloid cell populations with immunosuppressive function. MDSCs have been considered as a main obstacle of immunotherapy (24). Numerous scientists are exploring the inhibitory products against MDSCs and exploiting novel therapies that may enhance the efficacy of immunotherapies. Although immunotherapies mainly focus on the manipulation of T cells, targeting MDSCs provides another insight for anti-cancer therapy. The differentiation and function of MDSCs may be mediated by *H. pylori* infection. CXCL8 is a crucial inflammatory chemokine induced by *H. pylori* infection. This chemokine is up-regulated in gastric cancer and is linked with an undesirable survival outcome and tumor metastases (24). CXCL8 can promote the recruitment of MDSCs to tumors *via* binding CXCR1/2. MDSCs restrain the antitumor immune response primarily through weakening T cell function. Kruppel-like factor 4 (KLF4) is an underlying tumor suppressor in gastric carcinoma. *H. pylori* infection results in KLF4 inactivation in gastric carcinoma with a Tet Methylcytosine Dioxygenase 1 (TET1)-independent DNA methylation mechanism (25). *H. pylori* infection up-regulates CXCL8 expression through down-regulating KLF4 expression in gastric cancer cells and thus facilitates the recruitment of MDSCs, thereby shaping an immunosuppressive microenvironment (26). Hence, effective inhibition and blockade of CXCL8 and disruption of the immunosuppressive microenvironment are of importance for improving the effects of immunotherapy in gastric cancer. *H. pylori*-induced programmed death ligand-1 (PD-L1) expression within the gastric epithelium is mediated through the Hedgehog (Hh) pathway that is a contributor of *H. pylori*-induced atrophic gastritis progressing to gastric cancer. MDSCs require the activation of the Hh pathway-mediated transcription factor GLI1 and thus promotes neoplastic transformation (27). The myeloid differentiation factor Schlafen4 (Slfn4) represents a subpopulation of MDSCs in the gastric with *H. pylori*-induced spasmolytic polypeptide-expressing metaplasia (SPEM). MiR-130b is required for the T-cell suppressor phenotype displayed by the SLFN4-positive cells, which promotes *H. pylori*-induced gastric carcinogenesis (28). Depletion of MDSCs can sensitize gastric cancer cells to anti-programmed death-1 (PD-1)/PD-L1 agents (29).

Natural Killer Cells

NK cells, large granular innate lymphoid cells, are a main contributor to immunosurveillance as well as control of tumor progression through mediating apoptosis of gastric cancer cells

(30). NK cells mainly mediate cytotoxic resistance through two mechanisms: cancer cells escape NK cell-induced response through co-suppressive signals, resulting in anergic or irresponsiveness states of the immune subpopulation, and cancer cells escape NK cell effector activities following recognition of target cells (such as ineffective perforin binding) (30). High NK-cell infiltration is an indicator of more favorable clinical outcomes of gastric carcinoma subjects, constituting the first line of defense against cancers. *H. pylori* infection alters NK cell function within the TME. NK cells in the peripheral blood of gastric cancer patients possess a serious suppression capacity in producing IFN-γ following *H. pylori* infection (30). IFN-γ is an important cytokine secreted from NK and NK T cells or activated T cells within the TME. Innate and adaptive antitumor immune responses can trigger the secretion of IFN-γ. Oppositely, IFN-γ induces feedback suppression, thereby compromising antitumor immune responses. Moreover, IFN-γ upregulates the expression of immune suppressive factors within the TME. Especially, IFN-γ can activate the PD-1 pathway *via* directly upregulating PD-L1/2 in cancer, immune as well as stromal cell populations, and thus interacts with PD-1 on T cells, thereby downregulating the cytotoxic responses. NK cells can kill susceptible target tumor cells with a perforin-dependent mechanism. Perforin is a pore-forming protein expressed only in killer cells, allowing cytotoxic proteases (31). *H. pylori* down-regulates perforin production in gastric cancer cells-co-cultured CD56+ NK cells, indicating the decrease in killing efficiency of NK cells (32).

THE CROSSTALK OF *H. PYLORI* WITH ADAPTIVE IMMUNE CELLS WITHIN THE TUMOR MICROENVIRONMENT

B and T cells are central mediators of adaptive immunity (33). *H. pylori* infection deregulates T and B cells to mediate immune escape of gastric epithelial cells (34). Immune score has been exploited for estimating the adaptive immune compositions within the TME. In accordance with immune score, tumors are categorized into four subtypes: hot, altered-excluded, altered-immunosuppressed, as well as cold (35). Hot tumors present the features of enhanced infiltrations of PD-1- or CTLA4-expressing cytotoxic T lymphocytes as well as tumor cells expressing costimulatory molecules that are capable of maintaining T-cell functions (36). Intriguingly, hot tumors present the features of the presence of local inflammatory responses as well as high responses to immunotherapy. T-cell exclusion inside the tumors, triggered by the presence of abnormal vasculature and fibrotic nets, represents a major characteristic of altered-excluded immune tumors. Altered-immunosuppressed tumors present the intermediate infiltrations of exhausted T cells and the increased density of soluble inhibitory factors and immune-suppressive cell populations. Cold tumors present the characteristics of the absence of T-cell infiltrations because the cells or mechanisms underlying T-cell priming or activation are lacking. *H. pylori*-induced adrenomedullin facilitates IFN-γ-producing T-cell responses within the gastric microenvironment (37). The production of suppressive cytokine IL-10 in *H. pylori*-infected gastric cancer patients is elevated and thus results in a decreased cytotoxic anti-tumor T-cell response in the gastric mucosa, thereby contributing to gastric carcinogenesis (38). *H. pylori* VacA targets myeloid cells in the gastric mucosa and thus creates a tolerogenic environment that promotes regulatory T-cell (Treg) differentiation and suppresses effector T-cell priming and functionality (39).

Figure 1 summarizes the crosstalk of *H. pylori* with innate immune cells within the TME, including TAMs, neutrophils, dendritic cells, MDSCs, and NK cells.

THE CROSSTALK OF *H. PYLORI* WITH CANCER ASSOCIATED FIBROBLASTS WITHIN THE TUMOR MICROENVIRONMENT

CAFs are a major stromal component that display massive infiltrations within the TME (40). CAFs are mainly distributed around blood vessels or in the fibrous interstitium around tumors, secreting cytokines, ECM components, and related enzyme molecules (41). ECM provides physical support for cells in the TME and plays an important role in cell adhesion and infiltration. ECM deposition can produce dense fibrous interstitium that envelops tumors, which makes tumor tissues more brittle and firmer than normal tissues, thereby forming a physical barrier that hinders immune cell infiltration, and inhibiting anti-tumor drugs from targeting the TME (40). Moreover, the matrix metalloproteinases secreted by CAFs can reshape ECM, release chemokines, growth factors, and pro-angiogenesis factors, and promote the malignant transformation of tumors. With the rapid growth of tumors and vascular alienation, insufficient blood supply often occurs in the tumors and long-term hypoxia (42). Meanwhile, cell metabolism will increase the accumulation of lactose and hydrogen ions to form the acidic TME. The activation of a cascade of signals caused by vascular defects and metabolic disorders promotes the formation of immunosuppressive TME (43). CAF mainly affects TME through four perspectives: tumor cell proliferation and metastases, angiogenesis, ECM remodeling, and immune inhibition. *H. pylori* can activate gastric fibroblasts into cells possessing CAFs. *H. pylori* infection increases vascular adhesion molecule 1 (VCAM1) expression in CAFs within the TME through activating the JAK/STAT1 pathway, and CAF-derived VCAM1 interacts with integrin αvβ1/5 in gastric cancer cells to trigger cancer invasion (40). *H. pylori* infection induces the cyclooxygenase-2 (COX-2)/prostaglandin E2 (PGE2) pathway and enhances PGE2 production, leading to the hypermethylation of miR-149 in CAFs as well as the increase in IL-6 secretion. Epigenetic silencing of miR-149 in CAFs mediates the interplay of CAFs with gastric cancer cells within the TME (44).

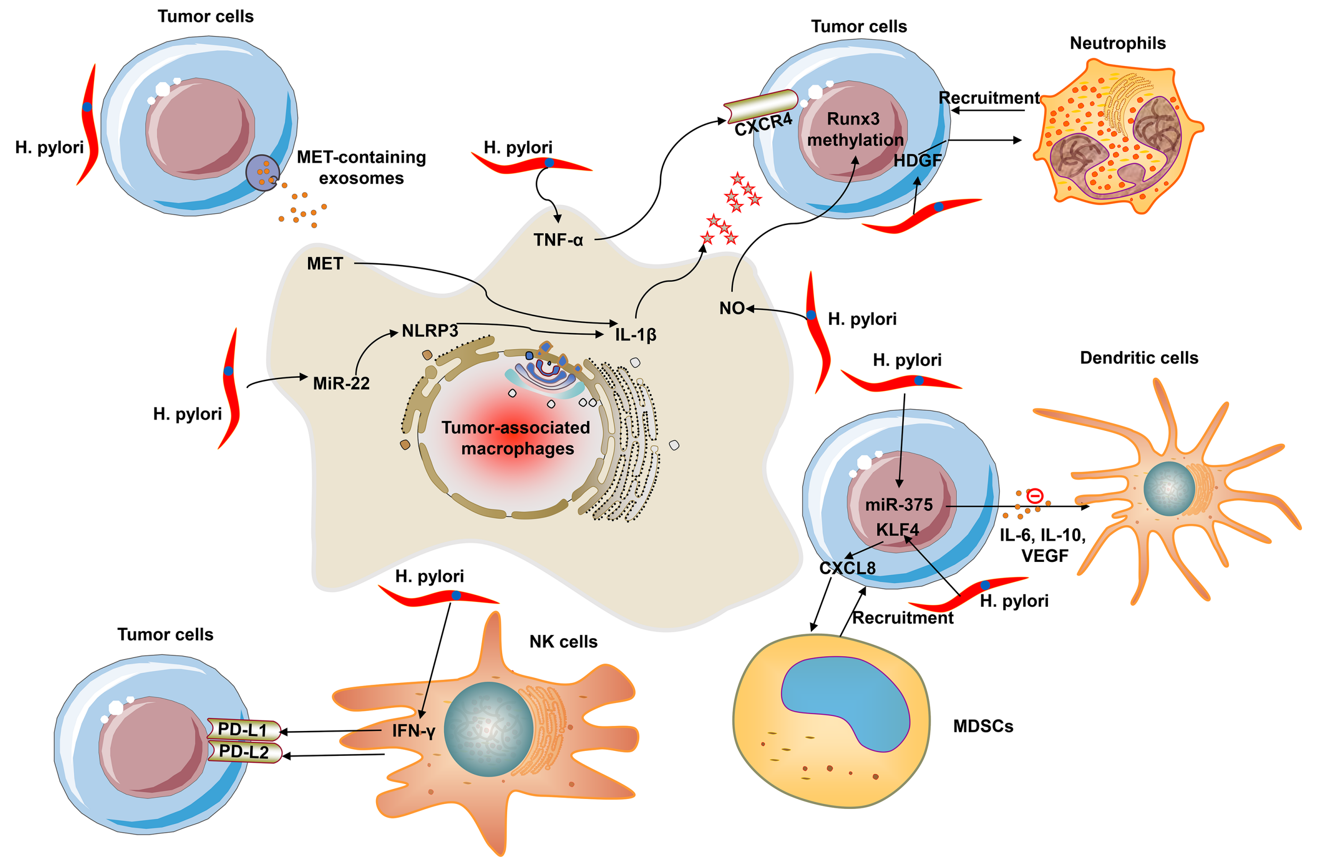
Tumor cells
H. pylori
MET-containing exosomes
H. pylori
TNF-α
MET
Tumor cells
CXCR4
Runx3 methylation
Recruitment
HDGF
Neutrophils
NLRP3
IL-1β
NO
H. pylori
H. pylori
MiR-22
Tumor-associated macrophages
H. pylori
Dendritic cells
miR-375
KLF4
IL-6, IL-10, VEGF
CXCL8
H. pylori
Recruitment
H. pylori
Tumor cells
NK cells
PD-L1
PD-L2
IFN-γ
MDSCs

FIGURE 1 | The crosstalk of H. pylori with innate immune cells within the tumor microenvironment (TME). Innate immune cells mainly contain tumor-associated macrophages (TAMs), neutrophils, dendritic cells, myeloid-derived suppressor cells (MDSCs), and natural killer (NK) cells.

THE CROSSTALK OF *H. PYLORI* WITH MESENCHYMAL STEM CELLS WITHIN THE TUMOR MICROENVIRONMENT

Epithelial–mesenchymal transition (EMT) process may confer mesenchymal phenotype and characteristics to epithelial cells (45, 46), with the abnormality of epithelial polarization and cell-to-cell junction as well as acquiring mesenchymal and motile phenotypic changes (47). *H. pylori* infection triggers the EMT of epithelial cell populations in the stomach mucosa. Moreover, this process can result in the appearance of CSC characteristics in gastric cancer. CSCs are a rare cell subset in tumors, which can initiate the progression and spread of tumors to induce distant metastasis. *H. pylori* infection can unveil CSC-like properties through inducing EMT-like alterations in gastric epithelial cells *via* CagA (47). Hippo pathway effectors yes-associated protein (YAP) along with transcriptional co-activator with PDZ binding motif (TAZ) mediates gastric carcinoma occurrence or development. TAZ activation responding to *H. pylori* can result in *H. pylori*-triggered EMT as well as CSC features. Thus, TAZ up-regulation constitutes a contributor of early conversion during *H. pylori*-induced gastric cancer initiation (48). Bone marrow-derived MSCs facilitate *H. pylori*-induced gastric cancer progression *via* secretion of thrombospondin-2 (49).

DISCUSSION

H. pylori infection has been considered as a microorganism that is highly effective in triggering inflammatory response within the stomach. Recent research has revealed a synergistic interplay of *H. pylori* infection with the components within the TME. An in-depth comprehension of how *H. pylori* and these cell populations interact can provide novel ideas and perspectives in treating gastric cancer and promising biomarkers for early detection. As mentioned, the interactions of *H. pylori* infection with TAMs, neutrophils, dendritic cells, MDSCs, NK cells, B and T cells, CAFs, and MSCs exert crucial roles in gastric carcinogenesis.

FUTURE PERSPECTIVES

Because *H. pylori* infection can induce strong immune response in the stomach, the resulting inflammation can facilitate gastric cancer progression. Most studies investigating the influence of *H. pylori* infection on the mentioned cell populations within the TME have been conducted *in vitro*. Furthermore, the exact mechanisms underlying the interplay of *H. pylori* infection with the TME should be addressed, assisting better expounding of the roles of *H. pylori* infection in gastric carcinogenesis. More biomedical or pharmaceutical regimens specifically targeting *H. pylori* infection can offer potential treatment methods for gastric cancer prevention.

AUTHOR CONTRIBUTIONS

All authors made substantial contributions to conception and design, acquisition of data, or analysis and interpretation of data; took part in drafting the article or revising it critically for important intellectual content; gave final approval of the version to be published; and agree to be accountable for all aspects of the work.

FUNDING

This work was funded by Shanxi Provincial Health Commission Project (RK-26); Shanxi Provincial Science and Technology Department Project (2018041056-6); The Second Hospital of Shanxi Medical University Fund Project (201702-2); Research on the current situation and countermeasures of the transformation of scientific and technological achievements in large general hospitals (202104031402141); Research on the implementation of medical alliance management model in public hospitals and primary medical and health service institutions (202104031402138).

REFERENCES

1. Kim W, Chu TH, Nienhüser H, Jiang Z, Del Portillo A, Remotti HE, et al. PD-1 Signaling Promotes Tumor-Infiltrating Myeloid-Derived Suppressor Cells and Gastric Tumorigenesis in Mice. *Gastroenterology* (2021) 160(3):781–96. doi: 10.1053/j.gastro.2020.10.036
2. Baj J, Korona-Głowniak I, Forma A, Maani A, Sitarz E, Rahnama-Hezavah M, et al. Mechanisms of the Epithelial-Mesenchymal Transition and Tumor Microenvironment in *Helicobacter pylori*-Induced Gastric Cancer. *Cells* (2020) 9(4):1055. doi: 10.3390/cells9041055
3. Derks S, de Klerk LK, Xu X, Fleitas T, Liu KX, Liu Y, et al. Characterizing Diversity in the Tumor-Immune Microenvironment of Distinct Subclasses of Gastroesophageal Adenocarcinomas. *Ann Oncol* (2020) 31(8):1011–20. doi: 10.1016/j.annonc.2020.04.011
4. Cristescu R, Lee J, Nebozhyn M, Kim KM, Ting JC, Wong SS, et al. Molecular Analysis of Gastric Cancer Identifies Subtypes Associated With Distinct Clinical Outcomes. *Nat Med* (2015) 21(5):449–56. doi: 10.1038/nm.3850
5. Sathe A, Grimes SM, Lau BT, Chen J, Suarez C, Huang RJ, et al. Single-Cell Genomic Characterization Reveals the Cellular Reprogramming of the Gastric Tumor Microenvironment. *Clin Cancer Res* (2020) 26(11):2640–53. doi: 10.1158/1078-0432.Ccr-19-3231
6. Cai WY, Dong ZN, Fu XT, Lin LY, Wang L, Ye GD, et al. Identification of a Tumor Microenvironment-Relevant Gene Set-Based Prognostic Signature and Related Therapy Targets in Gastric Cancer. *Theranostics* (2020) 10 (19):8633–47. doi: 10.7150/thno.47938
7. Hinshaw DC, Shevde LA. The Tumor Microenvironment Innately Modulates Cancer Progression. *Cancer Res* (2019) 79(18):4557–66. doi: 10.1158/0008-5472.Can-18-3962
8. Li S, Liang X, Ma L, Shen L, Li T, Zheng L, et al. MiR-22 Sustains NLRP3 Expression and Attenuates *H. pylori*-Induced Gastric Carcinogenesis. *Oncogene* (2018) 37(7):884–96. doi: 10.1038/onc.2017.381
9. Tang L, Tang B, Lei Y, Yang M, Wang S, Hu S, et al. *Helicobacter pylori*-Induced Heparanase Promotes *H. pylori* Colonization and Gastritis. *Front Immunol* (2021) 12:675747. doi: 10.3389/fimmu.2021.675747
10. Lu Y, Rong J, Lai Y, Tao L, Yuan X, Shu X. The Degree of *Helicobacter pylori* Infection Affects the State of Macrophage Polarization Through Crosstalk Between ROS and HIF-1α. *Oxid Med Cell Longev* (2020) 2020:5281795. doi: 10.1155/2020/5281795
11. Krakowiak MS, Noto JM, Piazuelo MB, Hardbower DM, Romero-Gallo J, Delgado A, et al. Matrix Metalloproteinase 7 Restrains *Helicobacter pylori*-Induced Gastric Inflammation and Premalignant Lesions in the Stomach by Altering Macrophage Polarization. *Oncogene* (2015) 34(14):1865–71. doi: 10.1038/onc.2014.135
12. Che Y, Geng B, Xu Y, Miao X, Chen L, Mu X, et al. *Helicobacter pylori*-Induced Exosomal MET Educates Tumour-Associated Macrophages to Promote Gastric Cancer Progression. *J Cell Mol Med* (2018) 22(11):5708–19. doi: 10.1111/jcmm.13847
13. Katayama Y, Takahashi M, Kuwayama H. *Helicobacter pylori* Causes Runx3 Gene Methylation and its Loss of Expression in Gastric Epithelial Cells, Which is Mediated by Nitric Oxide Produced by Macrophages. *Biochem Biophys Res Commun* (2009) 388(3):496–500. doi: 10.1016/j.bbrc.2009.08.003
14. Zhao C, Lu X, Bu X, Zhang N, Wang W. Involvement of Tumor Necrosis Factor-Alpha in the Upregulation of CXCR4 Expression in Gastric Cancer Induced by *Helicobacter pylori*. *BMC Cancer* (2010) 10:419. doi: 10.1186/1471-2407-10-419
15. Wen J, Chen C, Luo M, Liu X, Guo J, Wei T, et al. Notch Signaling Ligand Jagged1 Enhances Macrophage-Mediated Response to *Helicobacter pylori*. *Front Microbiol* (2021) 12:692832. doi: 10.3389/fmicb.2021.692832
16. Tang C, Lei X, Xiong L, Hu Z, Tang B. HMGA1B/2 Transcriptionally Activated-POU1F1 Facilitates Gastric Carcinoma Metastasis *via* CXCL12/CXCR4 Axis-Mediated Macrophage Polarization. *Cell Death Dis* (2021) 12 (5):422. doi: 10.1038/s41419-021-03703-x
17. Tong D, Zhang J, Wang X, Li Q, Liu L, Lu A, et al. MiR-22, Regulated by MeCP2, Suppresses Gastric Cancer Cell Proliferation by Inducing a Deficiency in Endogenous S-Adenosylmethionine. *Oncogenesis* (2020) 9 (11):99. doi: 10.1038/s41389-020-00281-z
18. Fu H, Ma Y, Yang M, Zhang C, Huang H, Xia Y, et al. Persisting and Increasing Neutrophil Infiltration Associates With Gastric Carcinogenesis and E-Cadherin Downregulation. *Sci Rep* (2016) 6:29762. doi: 10.1038/srep29762
19. Chu TH, Huang ST, Yang SF, Li CJ, Lin HW, Weng BC, et al. Hepatoma-Derived Growth Factor Participates in *Helicobacter pylori*-Induced Neutrophils Recruitment, Gastritis and Gastric Carcinogenesis. *Oncogene* (2019) 38(37):6461–77. doi: 10.1038/s41388-019-0886-3
20. Chang LL, Wang SW, Wu IC, Yu FJ, Su YC, Chen YP, et al. Impaired Dendritic Cell Maturation and IL-10 Production Following *H. pylori* Stimulation in Gastric Cancer Patients. *Appl Microbiol Biotechnol* (2012) 96 (1):211–20. doi: 10.1007/s00253-012-4034-z
21. Rizzuti D, Ang M, Sokollik C, Wu T, Abdullah M, Greenfield L, et al. *Helicobacter pylori* Inhibits Dendritic Cell Maturation *via* Interleukin-10-Mediated Activation of the Signal Transducer and Activator of Transcription 3 Pathway. *J Innate Immun* (2015) 7(2):199–211. doi: 10.1159/000368232
22. Kao JY, Zhang M, Miller MJ, Mills JC, Wang B, Liu M, et al. *Helicobacter pylori* Immune Escape is Mediated by Dendritic Cell-Induced Treg Skewing and Th17 Suppression in Mice. *Gastroenterology* (2010) 138(3):1046–54. doi: 10.1053/j.gastro.2009.11.043

23. Zhang Z, Chen S, Fan M, Ruan G, Xi T, Zheng L, et al. *Helicobacter pylori* Induces Gastric Cancer *via* Down-Regulating miR-375 to Inhibit Dendritic Cell Maturation. *Helicobacter* (2021) 26(4):e12813. doi: 10.1111/hel.12813
24. Lin C, He H, Liu H, Li R, Chen Y, Qi Y, et al. Tumour-Associated Macrophages-Derived CXCL8 Determines Immune Evasion Through Autonomous PD-L1 Expression in Gastric Cancer. *Gut* (2019) 68(10):1764–73. doi: 10.1136/gutjnl-2018-316324
25. Zhao R, Liu Z, Xu W, Song L, Ren H, Ou Y, et al. *Helicobacter pylori* Infection Leads to KLF4 Inactivation in Gastric Cancer Through a TET1-Mediated DNA Methylation Mechanism. *Cancer Med* (2020) 9(7):2551–63. doi: 10.1002/cam4.2892
26. Liu Z, Wu X, Tian Y, Zhang W, Qiao S, Xu W, et al. *H. pylori* Infection Induces CXCL8 Expression and Promotes Gastric Cancer Progress Through Downregulating KLF4. *Mol Carcinog* (2021) 60(8):524–37. doi: 10.1002/mc.23309
27. Merchant JL, Ding L. Hedgehog Signaling Links Chronic Inflammation to Gastric Cancer Precursor Lesions. *Cell Mol Gastroenterol Hepatol* (2017) 3 (2):201–10. doi: 10.1016/j.jcmgh.2017.01.004
28. Ding L, Li Q, Chakrabarti J, Munoz A, Faure-Kumar E, Ocadiz-Ruiz R, et al. MiR130b From Schlafen4(+) MDSCs Stimulates Epithelial Proliferation and Correlates With Preneoplastic Changes Prior to Gastric Cancer. *Gut* (2020) 69 (10):1750–61. doi: 10.1136/gutjnl-2019-318817
29. Koh V, Chakrabarti J, Torvund M, Steele N, Hawkins JA, Ito Y, et al. Hedgehog Transcriptional Effector GLI Mediates mTOR-Induced PD-L1 Expression in Gastric Cancer Organoids. *Cancer Lett* (2021) 518:59–71. doi: 10.1016/j.canlet.2021.06.007
30. Lindgren Å, Yun CH, Sjöling Å, Berggren C, Sun JB, Jonsson E, et al. Impaired IFN-γ Production After Stimulation With Bacterial Components by Natural Killer Cells From Gastric Cancer Patients. *Exp Cell Res* (2011) 317(6):849–58. doi: 10.1016/j.yexcr.2011.01.006
31. Voskoboinik I, Whisstock JC, Trapani JA. Perforin and Granzymes: Function, Dysfunction and Human Pathology. *Nat Rev Immunol* (2015) 15(6):388–400. doi: 10.1038/nri3839
32. Chochi K, Ichikura T, Kinoshita M, Majima T, Shinomiya N, Tsujimoto H, et al. *Helicobacter pylori* Augments Growth of Gastric Cancers *via* the Lipopolysaccharide-Toll-Like Receptor 4 Pathway Whereas its Lipopolysaccharide Attenuates Antitumor Activities of Human Mononuclear Cells. *Clin Cancer Res* (2008) 14(10):2909–17. doi: 10.1158/1078-0432.Ccr-07-4467
33. Chen L, Wang G, Qiao X, Wang X, Liu J, Niu X, et al. Downregulated miR-524-5p Participates in the Tumor Microenvironment of Ameloblastoma by Targeting the Interleukin-33 (IL-33)/Suppression of Tumorigenicity 2 (ST2) Axis. *Med Sci Monit* (2020) 26:e921863. doi: 10.12659/msm.921863
34. Reyes VE, Peniche AG. *Helicobacter pylori* Deregulates T and B Cell Signaling to Trigger Immune Evasion. *Curr Top Microbiol Immunol* (2019) 421:229–65. doi: 10.1007/978-3-030-15138-6_10
35. Ugel S, Canè S, De Sanctis F, Bronte V. Monocytes in the Tumor Microenvironment. *Annu Rev Pathol* (2021) 16:93–122. doi: 10.1146/annurev-pathmechdis-012418-013058
36. Chen L, Niu X, Qiao X, Liu S, Ma H, Shi X, et al. Characterization of Interplay Between Autophagy and Ferroptosis and Their Synergistical Roles on Manipulating Immunological Tumor Microenvironment in Squamous Cell Carcinomas. *Front Immunol* (2021) 12:739039. doi: 10.3389/fimmu.2021.739039
37. Kong H, You N, Chen H, Teng YS, Liu YG, Lv YP, et al. *Helicobacter pylori*-Induced Adrenomedullin Modulates IFN-γ-Producing T-Cell Responses and Contributes to Gastritis. *Cell Death Dis* (2020) 11(3):189. doi: 10.1038/s41419-020-2391-6
38. Lundin BS, Enarsson K, Kindlund B, Lundgren A, Johnsson E, Quiding-Järbrink M, et al. The Local and Systemic T-Cell Response to *Helicobacter pylori* in Gastric Cancer Patients is Characterised by Production of Interleukin-10. *Clin Immunol* (2007) 125(2):205–13. doi: 10.1016/j.clim.2007.07.011
39. Altobelli A, Bauer M, Velez K, Cover TL, Müller A. *Helicobacter pylori* VacA Targets Myeloid Cells in the Gastric Lamina Propria To Promote Peripherally Induced Regulatory T-Cell Differentiation and Persistent Infection. *mBio* (2019) 10(2):e00261-19. doi: 10.1128/mBio.00261-19
40. Shen J, Zhai J, You Q, Zhang G, He M, Yao X, et al. Cancer-Associated Fibroblasts-Derived VCAM1 Induced by *H. pylori* Infection Facilitates Tumor Invasion in Gastric Cancer. *Oncogene* (2020) 39(14):2961–74. doi: 10.1038/s41388-020-1197-4
41. Qiu XT, Song YC, Liu J, Wang ZM, Niu X, He J. Identification of an Immune-Related Gene-Based Signature to Predict Prognosis of Patients With Gastric Cancer. *World J Gastrointest Oncol* (2020) 12(8):857–76. doi: 10.4251/wjgo.v12.i8.857
42. Liu X, Niu X. Qiu Z. A Five-Gene Signature Based on Stromal/Immune Scores in the Tumor Microenvironment and Its Clinical Implications for Liver Cancer. *DNA Cell Biol* (2020) 39(9):1621–38. doi: 10.1089/dna.2020.5512
43. Zhao J, Zhong S, Niu X, Jiang J, Zhang R, Li Q. The MHC Class I-LILRB1 Signalling Axis as a Promising Target in Cancer Therapy. *Scand J Immunol* (2019) 90(5):e12804. doi: 10.1111/sji.12804
44. Li P, Shan JX, Chen XH, Zhang D, Su LP, Huang XY, et al. Epigenetic Silencing of microRNA-149 in Cancer-Associated Fibroblasts Mediates Prostaglandin E2/interleukin-6 Signaling in the Tumor Microenvironment. *Cell Res* (2015) 25(5):588–603. doi: 10.1038/cr.2015.51
45. Wang X, Cheng G, Miao Y, Qiu F, Bai L, Gao Z, et al. Piezo Type Mechanosensitive Ion Channel Component 1 Facilitates Gastric Cancer Omentum Metastasis. *J Cell Mol Med* (2021) 25(4):2238–53. doi: 10.1111/jcmm.16217
46. Zhu X, Chen L, Liu L, Niu X. EMT-Mediated Acquired EGFR-TKI Resistance in NSCLC: Mechanisms and Strategies. *Front Oncol* (2019) 9:1044. doi: 10.3389/fonc.2019.01044
47. Bessède E, Staedel C, Acuña Amador LA, Nguyen PH, Chambonnier L, Hatakeyama M, et al. *Helicobacter pylori* Generates Cells With Cancer Stem Cell Properties *via* Epithelial-Mesenchymal Transition-Like Changes. *Oncogene* (2014) 33(32):4123–31. doi: 10.1038/onc.2013.380
48. Tiffon C, Giraud J, Molina-Castro SE, Peru S, Seeneevassen L, Sifré E, et al. TAZ Controls *Helicobacter pylori*-Induced Epithelial-Mesenchymal Transition and Cancer Stem Cell-Like Invasive and Tumorigenic Properties. *Cells* (2020) 9(6):1462. doi: 10.3390/cells9061462
49. Shi H, Qi C, Meng L, Yao H, Jiang C, Fan M, et al. Bone Marrow-Derived Mesenchymal Stem Cells Promote *Helicobacter pylori*-Associated Gastric Cancer Progression by Secreting Thrombospondin-2. *Cell Prolif* (2021) 54 (10):e13114. doi: 10.1111/cpr.13114

Conflict of Interest: The authors declare that the research was conducted in the absence of any commercial or financial relationships that could be construed as a potential conflict of interest.

Publisher's Note: All claims expressed in this article are solely those of the authors and do not necessarily represent those of their affiliated organizations, or those of the publisher, the editors and the reviewers. Any product that may be evaluated in this article, or claim that may be made by its manufacturer, is not guaranteed or endorsed by the publisher.

Copyright © 2022 Li, Zhang, Bai, Li and Li. This is an open-access article distributed under the terms of the Creative Commons Attribution License (CC BY). The use, distribution or reproduction in other forums is permitted, provided the original author(s) and the copyright owner(s) are credited and that the original publication in this journal is cited, in accordance with accepted academic practice. No use, distribution or reproduction is permitted which does not comply with these terms.

frontiers | Frontiers in Pharmacology

ORIGINAL RESEARCH
published: 11 August 2022
doi: 10.3389/fphar.2022.923585

Oxaliplatin Eluting CalliSpheres Microspheres for the Treatment of Unresectable or Recurrent Hepatocellular Carcinoma

*Yonghua Bi†, Kewei Ren†, Jianzhuang Ren, Ji Ma and Xinwei Han**

Department of Interventional Radiology, The First Affiliated Hospital of Zhengzhou University, Zhengzhou, China

OPEN ACCESS

Edited by:
Dong-Hua Yang,
St. John's University, United States

Reviewed by:
Haibo Shao,
China Medical University, China
Ming Zhao,
Sun Yat-sen University Cancer Center (SYSUCC), China

****Correspondence:***
Xinwei Han
dreamweaver08@126.com

†These authors contributed equally to this work and share co-First authors

Specialty section:
This article was submitted to Pharmacology of Anti-Cancer Drugs, a section of the journal Frontiers in Pharmacology

Received: *19 April 2022*
Accepted: *16 June 2022*
Published: *11 August 2022*

Citation:
Bi Y, Ren K, Ren J, Ma J and Han X (2022) Oxaliplatin Eluting CalliSpheres Microspheres for the Treatment of Unresectable or Recurrent Hepatocellular Carcinoma. Front. Pharmacol. 13:923585. doi: 10.3389/fphar.2022.923585

Aim: Drug-eluting beads-transarterial chemoembolization (DEB-TACE) has been widely used in unresectable and advanced hepatocellular carcinoma (HCC). However, no study reported the clinical outcomes of drug-eluting beads TACE (DEB-TACE) with oxaliplatin-eluting CalliSpheres microspheres in the treatment of HCC. This study reports the preliminary outcomes of DEB-TACE loaded with oxaliplatin for the treatment of patients with unresectable or recurrent HCC.

Methods: From November 2019 to November 2021, 29 patients with unresectable or recurrent HCC were recruited from our department and treated by DEB-TACE loaded with oxaliplatin. The primary endpoint was progression-free survival (PFS), and the secondary endpoints were disease control rate and safety. Tumor response was investigated at 1, 3, and 6 months after DEB-TACE according to the criteria of the response evaluation in solid tumor (RECIST) criteria and the modified RECIST criteria (mRECIST). Survival curve was generated with the Kaplan–Meier method.

Results: A total of 49 DEB-TACE sessions were performed, with a technical success rate of 100%. The overall response rate and disease control rate were 52.4 and 95.2%, 64.7 and 76.5%, and 54.5 and 63.3%, respectively, at 1, 3, and 6 months after DEB-TACE (mRECIST). The PFS was 5.9 months, and the median overall survival was 18.8 months. The 6- and 12-month overall survival rate was 82.5% and 67.5%, respectively, No treatment-related mortality or severe adverse events were observed. Minor complications were observed in 21 patients (72.4%), and abdominal pain (41.4%) was the most common treatment-related complication.

Conclusion: DEB-TACE loaded with oxaliplatin-eluting CalliSpheres microspheres could be a safe, feasible, and efficacious palliative regimen in unresectable or recurrent HCC patients.

Keywords: hepatocellular carcinoma (HCC), drug-eluting beads transarterial chemoembolization (DEB-TACE), CalliSpheres beads, oxaliplatin, TACE

INTRODUCTION

Hepatocellular carcinoma (HCC) is one of the most common malignant tumors and the leading cause of cancer-related mortality worldwide (Torre et al., 2012; Mittal and El-Serag, 2013). Unfortunately, more than 70% of patients are diagnosed with late-stage HCC and cannot be treated with curative treatments such as transplantation or liver resection (Mazzaferro et al., 2014; Morise et al., 2014), so the prognosis of HCC remains poor. Transarterial chemoembolization (TACE), as an efficacious palliative treatment, has been widely used in patients with unresectable and advanced HCC (Llovet and Bruix, 2003; Bruix and Sherman, 2011). Oxaliplatin is the third generation of platinum anticancer drugs and shows an excellent inhibitory effect on various cancers (Ibrahim et al., 2004; Nobili et al., 2008). However, adverse effects, such as cardiotoxicity and neurotoxicity, are observed in some patients due to high blood concentration (Bullinger et al., 2011).

Drug-eluting beads TACE (DEB-TACE), as a relatively new drug-delivering device, showed an advantage of sustained release of chemotherapy drugs and increased local drug concentration (Wu et al., 2018; Bi et al., 2021a). DEB-TACE with oxaliplatin-eluting hepasphere microspheres has been used to reduce toxicities for patients with unresectable intrahepatic cholangiocarcinoma and liver metastasis of colorectal cancer (Poggi et al., 2008; Poggi et al., 2009). CalliSpheres microsphere is the first drug-eluting bead developed in China, which has been applied for loading and releasing oxaliplatin in an *in vitro* study (Han et al., 2019). However, no study reported the outcomes of oxaliplatin-eluting CalliSpheres microspheres in the treatment of HCC. In this study, we aim to report the preliminary outcomes of DEB-TACE loaded with oxaliplatin for the treatment of patients with unresectable or recurrent HCC.

Patients and Methods

Selection of Patients

Patients who were clinically or histologically diagnosed with primary HCC, either matter unresectable or recurrent tumor, were recruited from our department between November 2019 and November 2021. Contrast-enhanced computed tomography (CT) and/or magnetic resonance imaging (MRI) were carried out at baseline (**Figures 1A,B**; **Figure 2A**; **Figure 3A**). The inclusion criteria were 1) age 18–81 years, with a life expectancy more than 3 months; 2) Barcelona Clinic Liver Cancer (BCLC) stage B or C; and 3) Child–Pugh class A or B. Exclusion criteria were 1) allergy to study drugs; 2) liver metastatic cancer; 3) severe cardiovascular comorbidities including unstable angina, myocardial infarction, or uncontrolled hypertension; 4) coagulopathy or bleeding diathesis; 5) BCLC stage D; and 6) Child–Pugh class C. This study was approved by the Medical Ethics Committee of our hospital. Informed consent for the DEB-TACE procedure was obtained from all patients before the procedure.

DEB-TACE Procedures

The femoral artery was accessed after local anesthesia and a 5F right hepatic catheter (Terumo, Japan) was introduced. Tumor-feeding vessels were catheterized and super-selected by a 2.7-F microcatheter (Progreat, Terumo, Japan). For diffuse lesions, the right hepatic and/or left hepatic artery was catheterized for embolization, avoiding the embolization of gallbladder artery and gastroduodenal artery. Oxaliplatin (100 mg) was pre-loaded with one vial of 100–300 μm or

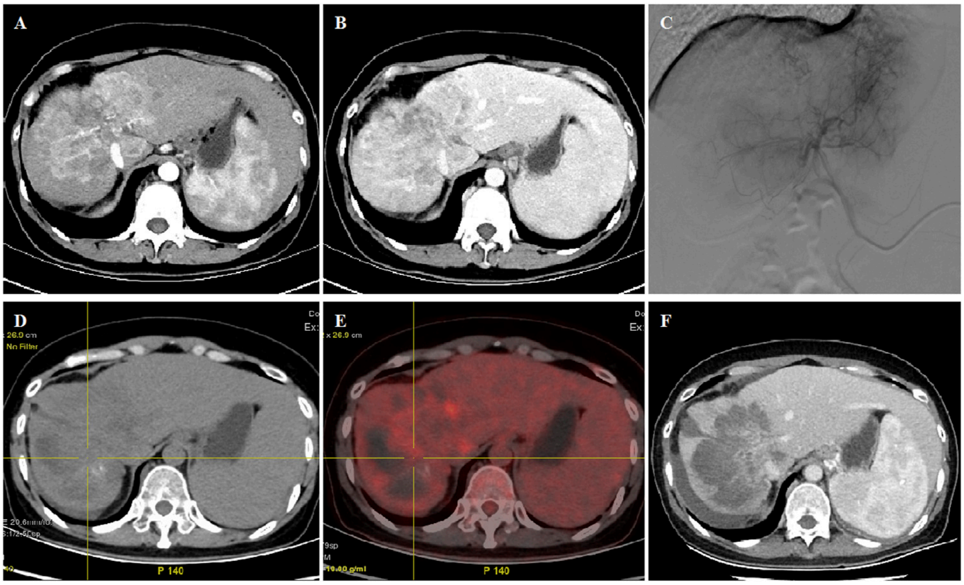

FIGURE 1 | 45 year old female patient treated with CalliSpheres beads for advanced primary HCC. **(A–B)** CT examination on admission revealed HCC in the right lobe. **(C)** Huge tumor staining was shown and was embolized by 300–500 μm oxaliplatin-loaded beads. **(D–E)** PET-CT showed significant reduction of the tumor and no residual tumor at 2.2 months' follow-up. **(F)** Complete response was shown by mRECIST criteria at 5.0 months' follow-up and still alive 15.5 months later.

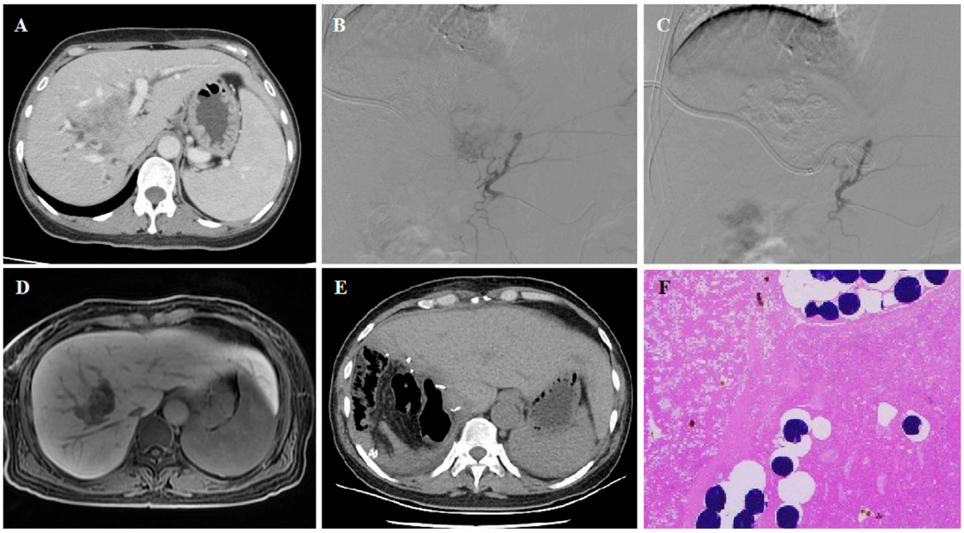

FIGURE 2 | 54 years female patient treated with CalliSpheres beads for advanced primary HCC. **(A)** CT revealed a tumor in the right lobe and the obstructed bile duct. **(B–C)** Tumor artery was super selectively incubated and embolized by 100–300 μm oxaliplatin-loaded beads. **(D)** MR revealed a shrunk tumor 4.6 months after DEB-TACE. **(E–F)** Tumor was resected 4.9 months after DEB-TACE, and no residual tumor was shown by pathological examination.

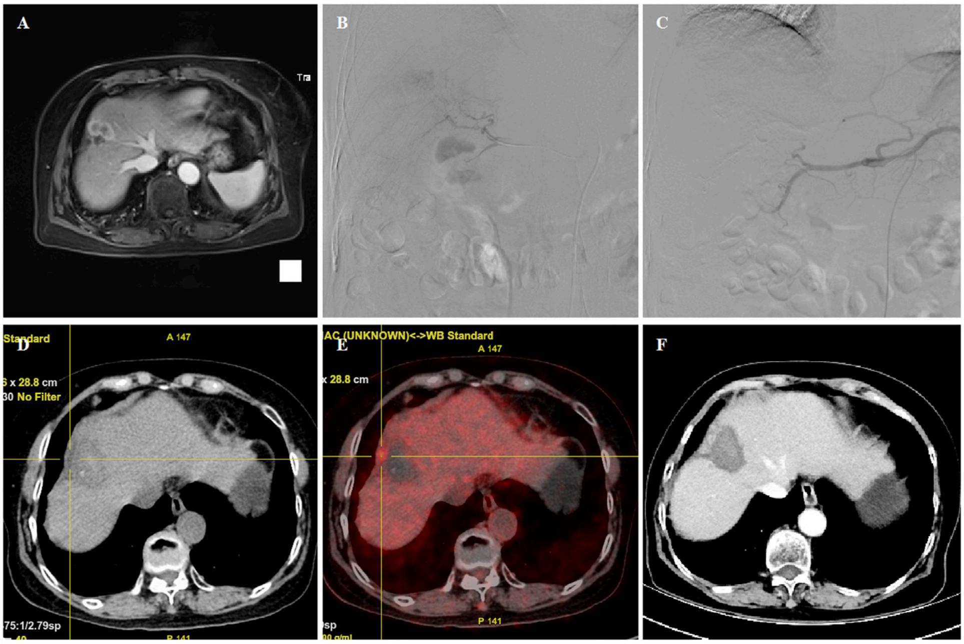

FIGURE 3 | 70 years female patient treated with CalliSpheres beads for advanced primary HCC. **(A)** MR revealed HCC in the right lobe. **(B–C)** Tumor staining was shown, and the right hepatic artery was embolized by 100–300 μm oxaliplatin-loaded beads. **(D–E)** PET-CT revealed a shrunk tumor with a small residual node 4.8 months later. **(F)** Tumor was found to shrink with no enhancement after 6.5 month follow-up. The patient passed away with tumor progression after 18.8 months.

300–500 μm CalliSpheres beads (Jiangsu Hengrui Medicine Co. Ltd., Jiangsu, China) for 30 min and then mixed with iodixanol at a ratio of 1:1. After infusion of raltitrexed (4 mg) or fluorouracil (500 mg), a bottle of CalliSpheres beads was used for embolization of the tumor-feeding vessels. Gelatin sponge particles or polyvinyl alcohol particles (Merit, American) were used if embolization was insufficient (**Figure 1C**; **Figure 2BC**; **Figure 3BC**).

Efficacy and Safety Evaluation

The progression-free survival (PFS) was the primary endpoint. CT and/or MRI images were used for assessment of tumor

TABLE 1 | Patient characteristics at admission.

Parameters	Data
Male, n (%)	20 (69.0%)
Mean age, years	58.1 ± 10.6
Lesion types	
Right lobe	14 (48.3%)
Left lobe	1 (3.4%)
Bi-lobar	14 (48.3%)
Symptom duration, months	1.0 (0.4, 10.5)
Recurrence after surgery	5 (17.2%)
Systemic treatments	21 (72.4%)
Targeted therapy	9 (31.0%)
Immunotherapy	2 (6.9%)
Targeted and immunotherapy	10 (34.5%)
Hepatitis B virus infection	14 (48.3%)
BCLC stage B/C	8 (27.6%)/21 (72.4%)
Child–Pugh class A/B	20 (69.0%)/9 (31.0%)
Multinodular/bulky tumor/diffuse	5 (17.2%)/11 (37.9%)/13 (44.8%)
Portal vein trunk or IVC invasion	5 (17.2%)
Portal vein or hepatic vein branch invasion	7 (24.1%)
Extrahepatic sites	13 (44.8%)
Lung	2 (6.9%)
Lymph node	10 (34.5%)
Bone	2 (6.9%)
Spleen	1 (3.4%)
Tumor diameter, mm	91.6 ± 41.2
a-Fetoprotein level	24 (82.8%)
Normal	7 (24.1%)
<400 ng/ml	4 (13.8%)
400–10,000 ng/ml	8 (27.6%)
>10,000 ng/ml	5 (17.2%)

IVC = Inferior vena cava.

TABLE 2 | Clinical data on DEB-TACE.

Variables	Data
Inpatient duration, months	9.0 (7.0, 12.0)
Hospitalization cost, $\times 10^4$ ¥	6.7 ± 2.0
DEB-TACE sessions	1.7 ± 0.9
Additional embolization	
Gelatin sponge particles	5 (17.2%)
Embolization microspheres	6 (20.7%)
Polyvinyl alcohol particles	4 (13.8%)
Complications, n (%)	21 (72.4%)
Fever	3 (10.3%)
Nausea	5 (17.2%)
Vomiting	3 (10.3%)
Thrombocytopenia	3 (10.3%)
hyperbilirubinemia	5 (17.2%)
Leukopenia	2 (6.9%)
Abdominal pain	12 (41.4%)
Raised ALT/AST	8 (27.6%)
Other interventional treatments, n (%)	13 (44.8%)
Conventional TACE	8 (31.0%)
PTCD	3 (10.3%)
^{125}I seed implantation	1 (3.4%)
Thermal ablation	3 (10.3%)
Drainage of liver abscess	1 (3.4%)

ALT = Alanine aminotransferase; AST = Aspartate aminotransferase; TACE = Transcatheter arterial chemoembolization; PTCD = Percutaneous transhepatic cholangial drainage.

TABLE 3 | Local tumor response assessed using RECIS criteria.

Response	1 month	3 months	6 months
Complete response	0 (0.0%)	1 (5.3%)	1 (7.7%)
Partial response	1 (4.3%)	4 (21.1%)	1 (7.7%)
Stable disease	21 (91.3%)	9 (47.4%)	5 (38.5%)
Progressive disease	1 (4.3%)	5 (26.3%)	6 (46.2%)
Overall response rate	1 (4.3%)	5 (26.3%)	2 (15.4%)
Disease control rate	22 (95.7%)	14 (73.7%)	7 (53.8%)

response according to the response evaluation criteria in solid tumors (RECIST) (Eisenhauer et al., 2009) and modified RECIST (mRECIST) (Lencioni and Llovet, 2010). Patients were followed up by CT and/or MRI examination on 1, 3, and 6 months after the procedure and every 2 months thereafter until the end of the study, complete response, or patient death (**Figures 1D–F**; **Figures 2D–F**; **Figures 3D–F**). One patient was lost to follow-up in this study. The phone call follow-up was performed for the remaining 28 patients, and the last follow-up date was 20 January 2022. Disease control rate and safety were the secondary endpoints. Safety and toxicity were assessed according to the National Cancer Institute Common Toxicity Criteria (version 3.0) (Trotti et al., 2003).

RESULTS

Patient Characteristics

Twenty-nine patients were enrolled in this study, including 20 males and nine females (mean age 58.1 ± 10.6 years). Disease characteristics and baseline demographics are shown in **Table 1**. Extrahepatic metastases were present in 13 patients (44.8%), and portal vein trunk or inferior vena cava invasion was found in five patients (17.2%). Eighteen patients (62.1%) complained of abdominal pain or distension, and median duration of symptom was 1.0 months. Twenty-one patients (72.4%) received synchronous treatments, including targeted therapy (n = 9), immunotherapy (n = 2), and targeted combined with immunotherapy (n = 10). For 10 patients who received combination treatment, targeted immunotherapy was used continuously.

DEB-TACE Treatments

As shown in **Table 2**, a total of 49 DEB-TACE sessions were performed in 29 patients, with a mean DEB-TACE cycle of 1.7 ± 0.9. Thirteen patients completed at least two cycles of DEB-TACE. All DEB-TACE procedures were successfully performed, with a technical success rate of 100%. Except for 13 sessions of DEB-TACE performed with CalliSpheres beads of 300–500 μm, the remaining 36 sessions of DEB-TACE were performed by using CalliSpheres beads of 100–300 μm in diameter. All patients received a bottle of beads; additional embolization was performed by 350–560 μm polyvinyl alcohol particles in four patients (13.8%) or 350–560 μm gelatin sponge particles in five patients (17.2%), or 300–500 μm embolization microsphere in six patients (20.7%). Thirteen patients (44.8%) received other interventional treatments, including conventional TACE (n = 8), percutaneous

TABLE 4 | Local tumor response assessed using mRECIS criteria.

Response	1 month	3 months	6 months
Complete response	4 (19.0%)	5 (29.4%)	3 (27.3%)
Partial response	7 (33.3%)	6 (35.3%)	3 (27.3%)
Stable disease	9 (42.9%)	2 (11.8%)	1 (9.1%)
Progressive disease	1 (4.8%)	4 (23.5%)	4 (36.4%)
Overall response rate	11 (52.4%)	11 (64.7%)	6 (54.5%)
Disease control rate	20 (95.2%)	13 (76.5%)	7 (63.3%)

transhepatic cholangial drainage (*n* = 3), and thermal ablation in three patients (*n* = 3).

Tumor Response

According to the RECIST criteria, only one patient achieved a complete response 3 and 6 months after DEB-TACE. Partial response was observed in one, four, and one patients at 1-, 3-, and 6-month follow-up. The overall response rates were 4.3, 26.3, and 15.4%, respectively, at 1, 3, and 6 months (**Table 3**). According to the mRECIST criteria, tumor enhancement decreased significantly after DEB-TACE, and higher rates of complete response and overall response were observed. The overall response rates were 52.4, 64.7, and 54.5% at 1, 3, and 6 months, respectively. The disease control rates were similar, whether assessed using RECIST criteria or mRECIST criteria (**Table 4**).

Survival

One patient was lost to follow-up, with a follow-up rate of 96.6%. The PFS was 5.9 months, and the median overall survival was 18.8 months (**Figure 4**). The 6- and 12-month overall survival rates were 82.5 and 67.5%, respectively. There was no significant difference in PFS between unresectable HCC and recurrent HCC (*p* = 0.41). The median overall survival was 18.8 months for unresectable HCC and 19.7 months for recurrent HCC, with no significant difference (*p* = 0.51). Twenty-one patients received DEB-TACE plus systemic therapy, and only nine patients received only DEB-TACE. The median overall survival was 18.8 months for patients who received only DEB-TACE and 16.7 months for patients who received DEB-TACE combined with targeted or immunotherapy. However, there was no significant difference in overall survival or PFS between these two groups.

Safety and Toxicity

Minor complications were observed in 21 patients (72.4%), with no severe adverse events or treatment-related mortality. Abdominal pain (41.4%) was the most common treatment-related nonhematologic complication. All reported toxicities were grades 1 and 2.

DISCUSSION

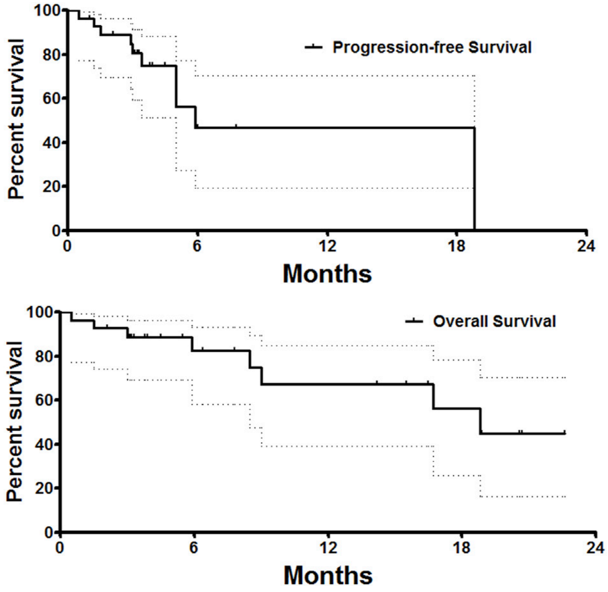

FIGURE 4 | Survival follow-up. The PFS was 5.9 months, and the median overall survival was 18.8 months.

HCC has the highest incidence in Southeast Asia and the major risk factor of HCC is hepatitis B virus transmission (McGlynn et al., 2015). More than 70% of HCC patients are diagnosed in the intermediate or advanced stage and cannot be treated with curative treatments such as liver transplantation or liver resection (Mazzaferro et al., 2014; Morise et al., 2014). For patients with BCLC tumor stage B, TACE is recommended as the first-line therapy (Bruix and Llovet, 2002). As the third generation of platinum anticancer drugs, oxaliplatin shows an excellent inhibitory effect on cancers (Ibrahim et al., 2004; Nobili et al., 2008). Oxaliplatin-based TACE, oxaliplatin combined with fluorouracil or doxorubicin, is usually used clinically for the treatment of HCC. However, adverse effects are observed due to high blood concentration, leading to cardiotoxicity and neurotoxicity (Bullinger et al., 2011) (Ransom et al., 2014).

As a relatively new drug-delivering device, DEB-TACE showed an advantage of sustained release of chemotherapeutic drugs, increased local drug concentration, and reduced toxicities (Bi et al., 2021b; Bi et al., 2021c). CalliSpheres microsphere is the first drug-eluting bead developed in China, which has been applied for loading and releasing oxaliplatin in an *in vitro* study (Han et al., 2019). Poggi et al. reported that DEB-TACE with oxaliplatin-eluting Hepasphere microspheres associated with chemotherapy is a safe and feasible treatment in advanced unresectable intrahepatic cholangiocarcinoma and liver metastasis of colorectal cancer (Poggi et al., 2008; Poggi et al., 2009). However, only nine patients with intrahepatic cholangiocarcinoma and eight patients with colorectal carcinoma liver metastases were enrolled, rather than those with primary HCC. Currently, no study reported the outcomes of oxaliplatin-eluting CalliSpheres microspheres in the treatment of HCC.

In this study, a total of 49 DEB-TACE sessions were performed in 29 patients with unresectable or recurrent HCC, with a technical success rate of 100%. The overall response rate and disease control rate were 52.4 and 95.2%, 64.7 and 76.5%, and 54.5 and 63.3%, respectively, at 1, 3, and 6 months after DEB-TACE according to mRECIST criteria. A higher overall response rate was determined by mRECIST criteria than by the RECIST criteria, which was consistent with our previous study (Zhao et al., 2016). The complete response was only one if assessed by RECIST, which was similar to the previous report (Rougier et al., 1997). The mRECIST may be more suitable for response assessment after DEB-TACE, considering that most patients showed a significant decrease in tumor enhancement after DEB-TACE procedure.

In this study, we also evaluated the safety of DEB-TACE loaded with oxaliplatin in unresectable or recurrent HCC patients. Our data suggested that abdominal pain (41.4%) was the most common treatment-related complication, which was similar to our previous study (Zhao et al., 2016). No treatment-related mortality or severe adverse events was observed in this study.

Doxorubicin is a regularly used drug in DEB-TACE. Huang et al. (Huang et al., 2021) reported the overall survival was 14.0 months for patients who received DEB-TACE with beads loaded with 60 mg doxorubicin, and the PFS was 6.3 months. These results were similar to the outcomes of our study. In addition, nausea/vomiting (18.8%), neutropenia (7.8%), and thrombocytopenia (12.5%) were observed in Huang's study, which was also similar to our study.

There are some limitations in this study. Unresectable and recurrent HCC are different in prognosis and response to the treatment. However, the sample size of recurrent HCC was too small to compare the difference. Oxaliplatin release was very quick in CalliSpheres beads, and further studies are needed to prove the advantage of oxaliplatin-loaded DEB-TACE.

In conclusion, our preliminary results showed that DEB-TACE loaded with oxaliplatin-eluting CalliSpheres microspheres is safe and tolerable in patients with unresectable HCC.

DATA AVAILABILITY STATEMENT

The raw data supporting the conclusions of this article will be made available by the authors, without undue reservation.

ETHICS STATEMENT

The studies involving human participants were reviewed and approved by the Medical Ethics Committee of First Affiliated Hospital of Zhengzhou University. The patients/participants provided their written informed consent to participate in this study.

AUTHOR CONTRIBUTIONS

All authors made substantial contributions to conception and design, acquisition of data, and analysis; took part in drafting the manuscript or revising it; agreed to submit to the current journal; gave final approval for the version to be published; and agreed to be accountable for all aspects of the work.

REFERENCES

Bi, Y., Shi, X., Ren, J., Yi, M., Han, X., and Song, M. (2021a). Clinical Outcomes of Doxorubicin-Eluting CalliSpheres(R) Beads-Transarterial Chemoembolization for Unresectable or Recurrent Esophageal Carcinoma. *BMC Gastroenterol.* 21 (1), 231. doi:10.1186/s12876-021-01816-3

Bi, Y., Shi, X., Yi, M., Han, X., and Ren, J. (2021b). Pirarubicin-loaded CalliSpheres(R) Drug-Eluting Beads for the Treatment of Patients with Stage III-IV Lung Cancer. *Acta Radiol.* 63(3), 311–318. doi:10.1177/0284185121994298

Bi, Y., Wang, Y., Zhang, J., Shi, X., Wang, Y., Xu, M., et al. (2021c). Clinical Outcomes of Uterine Arterial Chemoembolization with Drug-Eluting Beads or Advanced-Stage or Recurrent Cervical Cancer. *Abdom. Radiol. (NY)* 46 (12), 5715–5722. doi:10.1007/s00261-021-03267-6

Bruix, J., and Llovet, J. M. (2002). Prognostic Prediction and Treatment Strategy in Hepatocellular Carcinoma. *Hepatology* 35 (3), 519–524. doi:10.1053/jhep.2002.32089

Bruix, J., and Sherman, M. (2011). Management of Hepatocellular Carcinoma: an Update. *Hepatology* 53 (3), 1020–1022. doi:10.1002/hep.24199

Bullinger, K. L., Nardelli, P., Wang, Q., Rich, M. M., and Cope, T. C. (2011). Oxaliplatin Neurotoxicity of Sensory Transduction in Rat Proprioceptors. *J. Neurophysiol.* 106 (2), 704–709. doi:10.1152/jn.00083.2011

Eisenhauer, E. A., Therasse, P., Bogaerts, J., Schwartz, L. H., Sargent, D., Ford, R., et al. (2009). New Response Evaluation Criteria in Solid Tumours: Revised RECIST Guideline (Version 1.1). *Eur. J. Cancer* 45 (2), 228–247. doi:10.1016/j.ejca.2008.10.026

Han, X., Chen, Q., Sun, Y., Han, L., and Sha, X. (2019). Morphology, Loadability, and Releasing Profiles of CalliSpheres Microspheres in Delivering Oxaliplatin: An *In Vitro* Study. *Technol. Cancer Res. Treat.* 18, 1533033819877989. doi:10.1177/1533033819877989

Huang, J., Huang, W., Zhan, M., Guo, Y., Liang, L., Cai, M., et al. (2021). Drug-Eluting Bead Transarterial Chemoembolization Combined with FOLFOX-Based Hepatic Arterial Infusion Chemotherapy for Large or Huge Hepatocellular Carcinoma. *J. Hepatocell. Carcinoma* 8, 1445–1458. doi:10.2147/JHC.S339379

Ibrahim, A., Hirschfeld, S., Cohen, M. H., Griebel, D. J., Williams, G. A., and Pazdur, R. (2004). FDA Drug Approval Summaries: Oxaliplatin. *Oncologist* 9 (1), 8–12. doi:10.1634/theoncologist.9-1-8

Lencioni, R., and Llovet, J. M. (2010). Modified RECIST (mRECIST) Assessment for Hepatocellular Carcinoma. *Semin. Liver Dis.* 30 (1), 52–60. doi:10.1055/s-0030-1247132

Llovet, J. M., and Bruix, J. (2003). Systematic Review of Randomized Trials for Unresectable Hepatocellular Carcinoma: Chemoembolization Improves Survival. *Hepatology* 37 (2), 429–442. doi:10.1053/jhep.2003.50047

Mazzaferro, V., Lencioni, R., and Majno, P. (2014). Early Hepatocellular Carcinoma on the Procrustean Bed of Ablation, Resection, and Transplantation. *Semin. Liver Dis.* 34 (4), 415–426. doi:10.1055/s-0034-1394365

McGlynn, K. A., Petrick, J. L., and London, W. T. (2015). Global Epidemiology of Hepatocellular Carcinoma: an Emphasis on Demographic and Regional Variability. *Clin. Liver Dis.* 19 (2), 223–238. doi:10.1016/j.cld.2015.01.001

Mittal, S., and El-Serag, H. B. (2013). Epidemiology of Hepatocellular Carcinoma: Consider the Population. *J. Clin. Gastroenterol.* 47 (Suppl. l), S2–S6. doi:10.1097/MCG.0b013e3182872f29

Morise, Z., Kawabe, N., Tomishige, H., Nagata, H., Kawase, J., Arakawa, S., et al. (2014). Recent Advances in the Surgical Treatment of Hepatocellular Carcinoma. *World J. Gastroenterol.* 20 (39), 14381–14392. doi:10.3748/wjg.v20.i39.14381

Nobili, S., Checcacci, D., Filippelli, F., Del Buono, S., Mazzocchi, V., Mazzei, T., et al. (2008). Bimonthly Chemotherapy with Oxaliplatin, Irinotecan, Infusional

5-fluorouracil/folinic Acid in Patients with Metastatic Colorectal Cancer Pretreated with Irinotecan- or Oxaliplatin-Based Chemotherapy. *J. Chemother.* 20 (5), 622–631. doi:10.1179/joc.2008.20.5.622

Poggi, G., Amatu, A., Montagna, B., Quaretti, P., Minoia, C., Sottani, C., et al. (2009). OEM-TACE: a New Therapeutic Approach in Unresectable Intrahepatic Cholangiocarcinoma. *Cardiovasc Interv. Radiol.* 32 (6), 1187–1192. doi:10.1007/s00270-009-9694-4

Poggi, G., Quaretti, P., Minoia, C., Bernardo, G., Bonora, M. R., Gaggeri, R., et al. (2008). Transhepatic Arterial Chemoembolization with Oxaliplatin-Eluting Microspheres (OEM-TACE) for Unresectable Hepatic Tumors. *Anticancer Res.* 28 (6B), 3835–3842.

Ransom, D., Wilson, K., Fournier, M., Simes, R. J., Gebski, V., Yip, D., et al. (2014). Final Results of Australasian Gastrointestinal Trials Group ARCTIC Study: an Audit of Raltitrexed for Patients with Cardiac Toxicity Induced by Fluoropyrimidines. *Ann. Oncol.* 25 (1), 117–121. doi:10.1093/annonc/mdt479

Rougier, P., Ducreux, M., Kerr, D., Carr, B. I., Francois, E., Adenis, A., et al. (1997). A Phase II Study of Raltitrexed ('Tomudex') in Patients with Hepatocellular Carcinoma. *Ann. Oncol.* 8 (5), 500–502. doi:10.1023/a:1008249328792

Torre, L. A., Bray, F., Siegel, R. L., Ferlay, J., Lortet-Tieulent, J., and Jemal, A. (2012). Global Cancer Statistics, 2012. *CA Cancer J. Clin.* 65 (2), 87–108. doi:10.3322/caac.21262

Trotti, A., Colevas, A. D., Setser, A., Rusch, V., Jaques, D., Budach, V., et al. (2003). CTCAE v3.0: Development of a Comprehensive Grading System for the Adverse Effects of Cancer Treatment. *Semin. Radiat. Oncol.* 13 (3), 176–181. doi:10.1016/S1053-4296(03)00031-6

Wu, B., Zhou, J., Ling, G., Zhu, D., and Long, Q. (2018). CalliSpheres Drug-Eluting Beads versus Lipiodol Transarterial Chemoembolization in the Treatment of Hepatocellular Carcinoma: a Short-Term Efficacy and Safety Study. *World J. Surg. Oncol.* 16 (1), 69. doi:10.1186/s12957-018-1368-8

Zhao, C., Fan, L., Qi, F., Ou, S., Yu, L., Yi, X., et al. (2016). Raltitrexed Plus Oxaliplatin-Based Transarterial Chemoembolization in Patients with Unresectable Hepatocellular Carcinoma. *Anticancer Drugs* 27 (7), 689–694. doi:10.1097/CAD.0000000000000371

Conflict of Interest: The authors declare that the research was conducted in the absence of any commercial or financial relationships that could be construed as a potential conflict of interest.

Publisher's Note: All claims expressed in this article are solely those of the authors and do not necessarily represent those of their affiliated organizations, or those of the publisher, the editors, and the reviewers. Any product that may be evaluated in this article, or claim that may be made by its manufacturer, is not guaranteed or endorsed by the publisher.

Copyright © 2022 Bi, Ren, Ren, Ma and Han. This is an open-access article distributed under the terms of the Creative Commons Attribution License (CC BY). The use, distribution or reproduction in other forums is permitted, provided the original author(s) and the copyright owner(s) are credited and that the original publication in this journal is cited, in accordance with accepted academic practice. No use, distribution or reproduction is permitted which does not comply with these terms.

frontiers | Frontiers in Oncology

TYPE Original Research
PUBLISHED 23 September 2022
DOI 10.3389/fonc.2022.868866

Check for updates

OPEN ACCESS

EDITED BY
Olivier Feron,
Université catholique de Louvain,
Belgium

REVIEWED BY
Aleš Dvořák,
Charles University, Czechia
Haibing Zhou,
Wuhan University, China

*CORRESPONDENCE
Xiangzhi Li
xiangzhi@sdu.edu.cn

†These authors have contributed
equally to this work

SPECIALTY SECTION
This article was submitted to
Pharmacology of Anti-Cancer Drugs,
a section of the journal
Frontiers in Oncology

RECEIVED 03 February 2022
ACCEPTED 05 September 2022
PUBLISHED 23 September 2022

CITATION
Zhang X, Yang Y, Li D, Wu Z,
Liu H, Zhao Z, Zhu H, Xie F and
Li X (2022) MOF negatively regulates
estrogen receptor α signaling *via*
CUL4B-mediated protein
degradation in breast cancer.
Front. Oncol. 12:868866.
doi: 10.3389/fonc.2022.868866

COPYRIGHT
© 2022 Zhang, Yang, Li, Wu, Liu, Zhao, Zhu, Xie and Li. This is an open-access article distributed under the terms of the Creative Commons Attribution License (CC BY). The use, distribution or reproduction in other forums is permitted, provided the original author(s) and the copyright owner(s) are credited and that the original publication in this journal is cited, in accordance with accepted academic practice. No use, distribution or reproduction is permitted which does not comply with these terms.

MOF negatively regulates estrogen receptor α signaling *via* CUL4B-mediated protein degradation in breast cancer

Xu Zhang[1†], Yang Yang[2†], Danyang Li[1,3], Zhen Wu[1], Haoyu Liu[1], Ziyan Zhao[1], Hongying Zhu[1], Fei Xie[1] and Xiangzhi Li[1*]

[1]Shandong Provincial Key Laboratory of Animal Cells and Developmental Biology, School of Life Sciences, Shandong University, Qingdao, China, [2]School of Pharmacy, Binzhou Medical University, Yantai, China, [3]Rehabilitation Center, Qilu Hospital, Cheelo College of Medicine, Shandong University, Jinan, China

Estrogen receptor α (ERα) is the dominant tumorigenesis driver in breast cancer (BC), and ERα-positive BC (ERα+ BC) accounts for more than two-thirds of BC cases. MOF (males absent on the first) is a highly conserved histone acetyltransferase that acetylates lysine 16 of histone H4 (H4K16) and several non-histone proteins. Unbalanced expression of MOF has been identified, and high MOF expression predicted a favorable prognosis in BC. However, the association of MOF with ERα and the regulatory mechanisms of MOF in ERα signaling remain elusive. Our study revealed that the expression of MOF is negatively correlated with that of ERα in BC. In ERα+ BC cells, MOF overexpression downregulated the protein abundance of ERα in both cytoplasm and nucleus, thus attenuating ERα-mediated transactivation as well as cellular proliferation and *in vivo* tumorigenicity of BC cells. MOF promoted ERα protein degradation through CUL4B-mediated ubiquitin–proteasome pathway and induced HSP90 hyperacetylation that led to the loss of chaperone protection of HSP90 to ERα. We also revealed that suppression of MOF restored ERα expression and increased the sensitivity of ERα-negative BC cells to tamoxifen treatment. These results provide a new insight into the tumor-suppressive role of MOF in BC *via* negatively regulating ERα action, suggesting that MOF might be a potential therapeutic target for BC.

KEYWORDS

MOF, ERα, breast cancer, protein degradation, CUL4B, tumor suppression

Introduction

As the most common malignancy for women, breast cancer (BC) represents around 30% of female cancers and becomes the second leading cause of cancer-related mortality in women worldwide ([1], [2]). BC is a highly heterogeneous cancer with differential expression of tumorigenic marker genes like estrogen receptor α (ERα, or simply ER) or human epidermal growth factor receptor 2 (HER2) (3). Among them, ERα-expressing tumors, namely, ERα-positive BC (ERα+ BC), arise in 60%–80% of BC cases (4). As a steroid hormone nuclear receptor, ERα can be bound and activated by estrogen 17β-estradiol (E2) and serves as a transcription factor for the transactivation of oncogenes, like c-Myc and cyclin D1, thereby promoting cell proliferation and tumor progression of BC (5–7). In the absence of E2 stimulation, inactive ERα interacts with molecule chaperone heat shock protein 90 (HSP90) and can be maintained in a stable conformation for ligand binding (8). After binding with E2, ERα undergoes dissociation from HSP90 and translocates into the nucleus for the transcriptional activation/repression of target genes that encourage BC cell survival and growth (8, 9).

Therefore, as the major tumorigenesis driver in BC, modulation of ERα expression and function plays indispensable roles in the progression and treatment of BC (10). For instance, hypermethylation of ERα promoter leads to ERα deficiency, whereas treatment with DNA demethylating reagents plus inhibitors for histone deacetylases (HDACs) would restore ERα expression and tamoxifen (TAM) sensitivity in ERα-negative BC (ERα– BC) cells (11–13). ERα co-activators CBP/p300, functioning as histone acetyltransferases (HATs), enhance H3K27ac for facilitating ERα-mediated transcriptional activity, whereas pharmacological inhibition of CBP/p300 by A-485 and GNE-049 could downregulate ERα to suppress oncogenic c-Myc and cyclin D1 expression and the proliferation of ERα+ BC cells (4, 14, 15).

MOF (males absent on the first), also known as lysine acetyltransferase (KAT) 8 or histone acetyltransferase 1 (MYST1), is a highly conserved histone acetyltransferase (HAT) that specifically acetylates lysine 16 of histone H4 (H4K16) as well as non-histone proteins such as protein 53 kDa (P53),interferon regulatory factor 3 (IRF3), and lysine-specific demethylase 1 (LSD1) (16–19). MOF vigorously involves in diverse biological processes, such as transcriptional regulation, DNA damage repair, cell growth and differentiation, stem cell development, and tumorigenesis (20–22). Unbalanced expression of MOF is frequently observed in various tumors, such as colorectal carcinoma, gastric cancer, renal cell carcinoma, ovarian cancer, hepatocellular carcinoma (HCC), medulloblastoma, and primary breast carcinoma (20, 21). In particular, MOF was identified to suppress epithelial-to-mesenchymal transition (EMT) *via* the acetylation of histone demethylase LSD1 in lung cancer and BC, and higher expression of MOF is correlated with favorable prognosis in these two cancers (19, 23, 24).

Because of the inhibitory effect of MOF in BC tumor invasion and the essential role of ERα in tumor promotion, we are interested in the association of MOF with ERα as well as the modulatory effects of MOF on ERα expression and function to exert its carcinostasis potential in BC. We herein reported that MOF is negatively correlated with ERα expression in BC. In ERα+ BC, MOF negatively regulated the expression and nuclear localization of ERα to inhibit ER-mediated transactivation as well as the growth and tumorigenicity of ERα+ BC cells. MOF overexpression promotes ERα protein degradation *via* Cullin 4b (CUL4B)–mediated ubiquitin–proteasome pathway and HSP90 hyperacetylation that disrupts the chaperone binding of HSP90 with ERα. On the other hand, inhibited MOF by knockdown or inhibitor MG149 restored ERα expression and enhanced TAM sensitivity in ERα– BC cells. Our study provide new insights into the prohibitory function of MOF on ERα action in BC, suggesting that MOF might be a potential therapeutic target for BC.

Material and methods

Cell culture and cell transfection

MCF7, T47D, MDA-MB-231, and HCC1937 cells were obtained from the American Type Culture Collection. Cells were cultured in Dulbecco's modified Eagle's medium (DMEM) or Roswell Park Memorial Institute-1640 (RPMI-1640) (Macgene, Beijing, China) with 10% fetal bovine serum (FBS) (LONSA SCIENCE, Shanghai, China) and maintained in a humidified atmosphere containing 5% CO_2 at 37°C. Cells were transfected with specific plasmid by JetPRIME (Polyplus, Strasbourg, France) according to the manufacturer's protocol. The BC tissue chip was purchased from Guge Biotechnology Company (Wuhan, China).

Antibodies and reagents

Anti-MOF (sc-81765) and breast-cancer susceptibility gene 1 (BRCA1) (Santa Cruz, sc-6954) were obtained from Santa Cruz Biotechnology. Antibodies including CUL4A (14851-1), CUL4B (12916-1), glyceraldehyde-3-phosphate dehydrogenase (GAPDH) (60004-1-Ig), and Flag (66008-2) were purchased from Proteintech (Wuhan, China). Other antibodies were listed as follows: H4K16ac (Epitomics, EPR1004), ERα (Cell Signaling Technology, Inc (CST), #8644), Ki67 (Abcam, ab16667), murine double minute 2 (MDM2) (Wanleibio, WL01906), HSP90 (Sangon Biotech, D120009), HSP90 K294ac (Rockland, 600-401-981), and acetylated lysine (CST, #9441). Inhibitors including MG149, cycloheximide (CHX), and MG132 were purchased from MedChemExpress (MCE, Princeton, NJ, USA). TAM was purchased from Sigma. CHX, MG149, MG132, and TAM were dissolved in dimethyl sulfoxide (DMSO).

Immunohistochemistry staining

Immunohistochemistry (IHC) staining was performed to detect the expression of MOF and ERα in BC tissue chips. Following deparaffinization and quenching of endogenous peroxidase, the tissue section was treated by deparaffinization and quenching of endogenous peroxidase and then subjected to antigen retrieval with sodium citrate buffer. Then, the section was incubated with 5% FBS and then incubated with ERα (1:100) and MOF (1:100) antibodies overnight at 4°C. After incubation with secondary antibody at 37°C, the section was subjected to staining by the DAB Detection Kit (Polymer) (GeneTech, Shanghai, China) and counterstaining with hematoxylin (Solarbio, Beijing, China) for the observation with a light microscope (Nikon, Tokyo, Japan). All slides were scored in an open discussion by two experienced pathologists, who were blinded to the outcome. Immunostaining was scored on the basis of the intensity score and quantity of positive cell score. Intensity score: negative, 0; weak, 1; moderate, 2; and intense, 3. Quantity of positive cell score: <5%, 0; 5%–25%, 1; 26%–50%, 2; 51%–75%, 3; and >75%, 4. The product of intensity score and quantity of positive cell score was used as the total score.

Immunofluorescence staining

Cells were seeded onto coverslips in 24-well plate for growth to 70% cell confluence. Cells were fixed using 4% paraformaldehyde and blocked by 5% FBS and then subjected to incubation with the primary antibody for MOF or ERα (1:100) overnight at 4°C. After incubation with corresponding secondary antibody, cells were mounted with DAPI (4',6-diamidino-2-phenylindole) (C0060, Solarbio), and images were taken from a DP74 color fluorescence camera (Olympus, Tokyo, Japan)

RNA extraction and qRT-PCR

Total RNA was isolated using RNAiso Plus (TaKaRa, Kyoto, Japan). RNA was reverse-transcribed by the RevertAid First Strand cDNA Synthesis Kit (Thermo Fisher Scientific, Waltham, MA, USA). Quantitative reverse transcriptase PCR (qRT-PCR) was performed using the SYBR qPCR Mix (TOYOBO). GAPDH was used as an internal control. Primers for qRT-PCR were listed in Supplementary Table 1. Then, relative quantitation of gene expression was calculated using the $2^{-\Delta\Delta CT}$ method.

Western blotting

Total protein was extracted using the sodium dodecyl sulfate (SDS) lysis buffer (1% sodium dodecyl sulfate, 5% glycerol, 1 mM ethylenediamine tetraacetic acid (EDTA), 25 mM Tris, 150 mM NaCl, and 1 mM phenylmethylsulfonyl fluoride (PMSF)). Protein samples were separated by SDS-polyacrylamide gel electrophoresis (PAGE) and transferred to polyvinylidene fluoride (PVDF) membranes (Millipore, Bedford, MA, USA). After blocking with 5% non-fat milk powder and incubation with specific antibody at 4°C overnight, membranes were subjected to corresponding secondary antibody and then visualized by an ECL detection kit (Wanleibio, Dalian, China).

Immunoprecipitation

Proteins were extracted from cells using BC-200 lysis buffer (20 mM 2-[4-(2-hydroxyethyl)piperazin-1-yl]ethanesulfonic acid (HEPES), 200 mM KCl, 10 mM β-mercaptoethanol, 1 mM EDTA, 10% glycerol, and 0.1% NP-40) containing protease inhibitor cocktail (APExBIO, Houston, TX, USA). Extracted proteins were immunoprecipitated by incubation with 1 μg of antibody and followed by binding with Protein A/G magnetic beads (Bimake, Shanghai, China). After washing with lysis buffer, proteins were extracted by SDS sample buffer and detected by Western blotting.

Chromatin immunoprecipitation assay

Chromatin immunoprecipitation (ChIP) assay was conducted using the SimpleChIP Plus Sonication Chromatin IP Kit (Cell Signaling Technology). Cells were cross-linked by 1% formaldehyde followed by sonication. The immunoprecipitated DNA was analyzed by qPCR with specific primers listed in Supplementary Table 2.

Cell proliferation and colony formation

For cell proliferation assay, cells were seeded into 96-well plate and then treated with 10 μl of CCK8 (Biosharp) per 100 μl of culture medium at specific time points. After incubation at 37°C for 4 h, the absorbance value was determined at 450 nm by a SPECTROstar Nano instrument for calculating cell proliferation curves. In the colony formation assay, cells were seeded in 6-cm culture dish (200 cells per dish) and culture in 37°C incubator for 10–14 days. After termination of culture, cells were fixed with methanol and stained by crystal violet. The colonies with more than 50 cells per colony were counted.

Xenograft tumor growth

Female NSG mice aged 6–8 weeks were prepared. MCF7 cells (5×10^7 cells) with stable MOF transfection or control vector were subcutaneously injected into one flank of each mouse, respectively. The tumor growth was observed every 2 days. After 3 weeks, mice were sacrificed, and tumors were taken out for size measurement. Tumors were fixed with 4% paraformaldehyde and followed by IHC staining. Animal experiments were performed with the approval from the Animal Research Ethical Inspection Form of Shandong University School of Life Sciences (SYDWLL-2018-19).

Statistical analysis

Data were statistically analyzed using GraphPad Prism software (San Diego, CA, USA) and were shown as means ±

S.D. in three independent experiments. A Chi-square test was applied for analyzing pathological data. One-way ANOVA analysis was performed for time-course studies, and Student's *t*-test was applied for comparisons of two groups. $P < 0.05$ was considered to be statistically significant.

Results

The expression of MOF is negatively correlated with that of ERα in BC tissues and cells

MOF is reported as a critical suppressor in BC by inhibiting EMT and tumor invasion, suggesting a favorable prognosis (19); whereas ERα functions as the crucial oncogenic driver for the progression of BC (4). However, the relationship between the expression of MOF and ERα still remains elusive. To evaluate the correlation between MOF and ERα, we examined the protein expression level of MOF and ER in BC tissues from 78 patients. The immunohistochemical staining (IHC) results demonstrated the staining of MOF/ERα defined as either low/negative (weak or none) or high/positive (strong or moderate) based on the relative intensity of staining (Figure 1A). Statistical analysis of IHC results showed that around 64.5% of BC tumors with low MOF expression exhibited ERα-positive staining, whereas the majority (68.8%) of tumors with high MOF expression displayed ERα-negative staining, indicating that there is a negative correlation between MOF and ERα expression in BC tissues (Table 1, Figure 1B). Moreover, we examined the MOF and ERα expression in multiple BC cell lines. Western blot analyses revealed that the protein abundance of MOF with histone H4K16 acetylation exhibited a remarkably attenuated expression in ERα+ BC cells (MCF7 and T47D) compared with that in ERα− BC cells (MDA-MB-231 and HCC1937), and histone H4K16 acetylation also showed a similar pattern with MOF expression (Figure 1C). Taken together, these results suggested that MOF functions as a tumor suppressor in BC tumors and that the expression of MOF was negatively associated with that of ERα in BC tissues and cells.

MOF negatively regulates ERα protein level in ERα+ BC cells

To investigate whether and how MOF plays roles in the expression of ERα, plasmids of Flag-HA-MOF (for MOF overexpression) and pGPU6-shMOF (for MOF knockdown) were transfected into ERα+ BC cell lines (MCF7 and T47D), respectively. qRT-PCR analysis showed that the mRNA level of MOF was significantly upregulated or reduced in these cell lines, whereas the mRNA level of ERα had indistinguishable change (Figures 2A, C), suggesting that the expression of MOF did not regulate ERα expression at the transcriptional level. However, the protein abundance of ERα was obviously influenced by MOF overexpression or knockdown in a negatively regulatory manner (Figures 2B, D). Namely, both MCF7 and T47D cells transfected with Flag-HA-MOF plasmid (MOF overexpression) showed an increased amount of MOF and a decreased level of ERα protein (Figure 2B). Conversely, in the pGPU6-shMOF–transfected cells (MOF knockdown), the protein abundance of ERα was elevated (Figure 2D). In addition, when increased doses of Flag-HA-MOF plasmid were transfected into MCF7 cells, the ERα protein levels showed the corresponding downward trend with the gradually advanced expressions of MOF and H4K16ac (Figure 2E).

As a steroid hormone nuclear receptor, ER could be activated by estrogen 17β-estradiol (E2) (25). After binding with E2, homodimerized ER would translocate into the nucleus and functions as a transcription factor to regulate target gene transcription (25). Hence, we explored whether MOF-mediated regulation of ERα expression would be affected by E2 stimulation. After transfection with Flag-HA-MOF plasmid or empty vector as control for 48 h, cells were treated with E2 for 3 h. As depicted in Figure 2F, MOF overexpression could induce a significant reduction of ERα protein in the presence or absence of E2, suggesting that MOF downregulates the ERα protein level in an estrogen-independent manner. In addition, nuclear and cytoplasmic separation assay demonstrated that protein abundance of ERα in both cytoplasm and nucleus obviously decreased after MOF overexpression regardless of the presence of E2 (Figure 2G). Similar results were also observed by immunofluorescence staining that the distribution of ER in cytoplasm/nucleus was reduced in MOF-overexpressed MCF7 cells with or without E2 treatment (Figure 2H). These results suggest that MOF overexpression inhibited ERα protein levels in both cytoplasm and nucleus with or without E2 treatment.

MOF prohibits the transactivation activity of ERα and cellular proliferation induced by estrogen and *in vivo* tumorigenicity

We next determined the effect of MOF on ERα-mediated transactivation upon E2 stimulation. MOF-overexpressed MCF7 cells were treated with E2 for specified incubation time, and the results showed that the mRNA expression of the three endogenous target genes (TFF1, CCND1, and GREB1) of ERα were significantly upregulated by E2 after 3 h of incubation in the control group cells. Whereas MOF overexpression abrogated this expression raise of ERα target genes by E2 (Figure 3A), suggesting that the transactivation abilities of ERα on target genes upon E2 treatment was prohibited by MOF overexpression. ChIP analysis further demonstrated that under the stimulation of E2, the recruitment of ERα at the promoters of TFF1, CCND1, and GREB1 was inhibited by ectopic expression of MOF (Figure 3B).

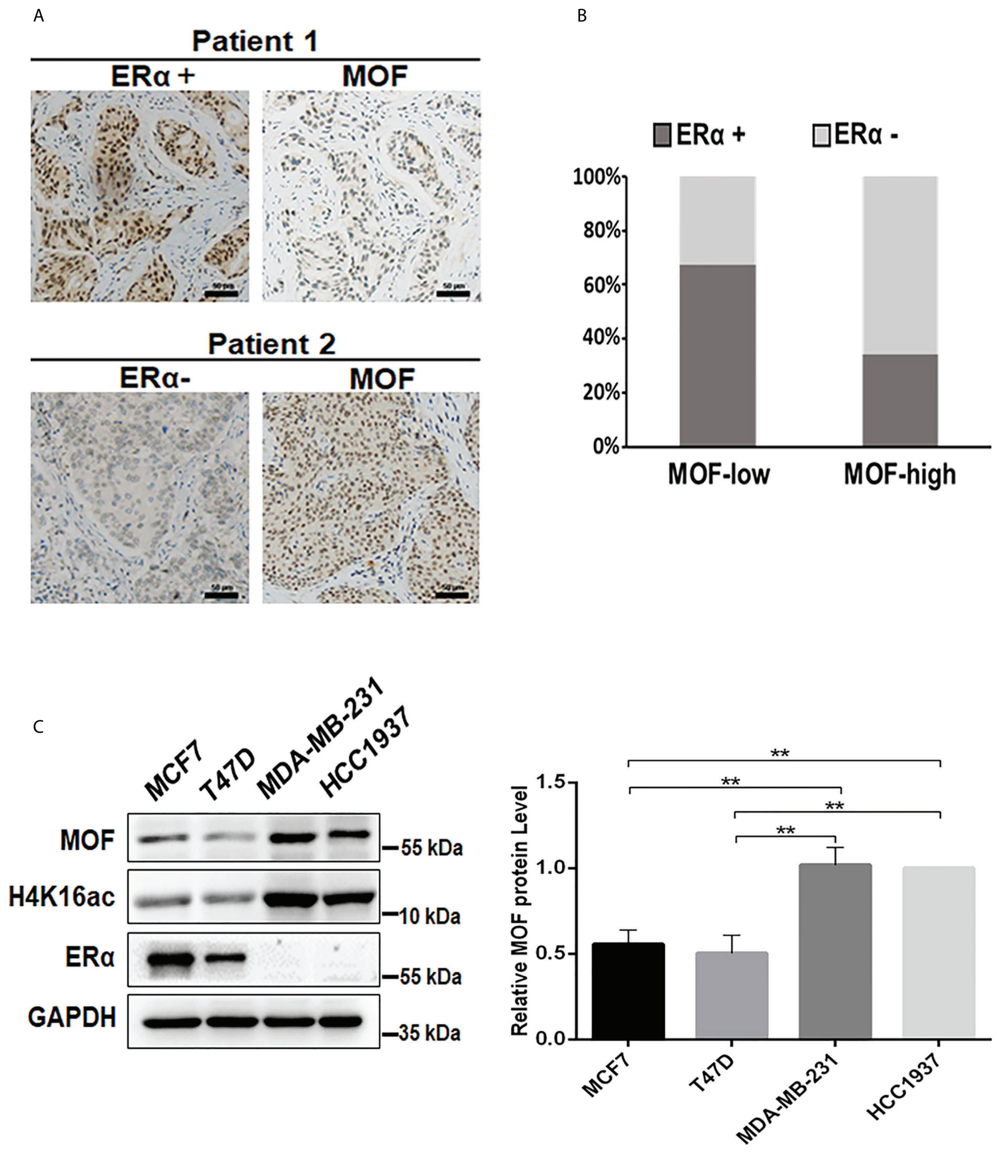

FIGURE 1
Analysis of the expression correlation of MOF and ERα in BC tissues and cells. **(A)** The protein abundance of MOF and ERα in BC tissue chip was determined by IHC staining, and the representative images were shown as high/positive and low/negative levels of MOF and ERα. Bar = 50 μm. **(B)** The staining results were quantified to demonstrate the correlation between MOF and ERα expression in BC tissues (n = 78). The staining was defined as high/positive (strong or moderate) and low/negative (weak or none) levels of expression. **(C)** The protein levels of MOF and ERα was analyzed by Western blot in BC cells, including ERα+ BC cells (MCF7 and T47D) and ERα– BC cells (MDA-MB-231). $^{**}P < 0.01$ vs. control group.

TABLE 1 IHC analysis of MOF and ERα in BC tissues.

	ERα-positive	ERα-negative	Total
MOF-low	40 (64.5%)	22 (35.5%)	62
MOF-high	5 (31.2%)	11 (68.8%)	16
Total	45	33	78

Two-sided Pearson's Chi-square test was conducted. P = 0.0163.
P < 0.05 was considered as statistical significance.

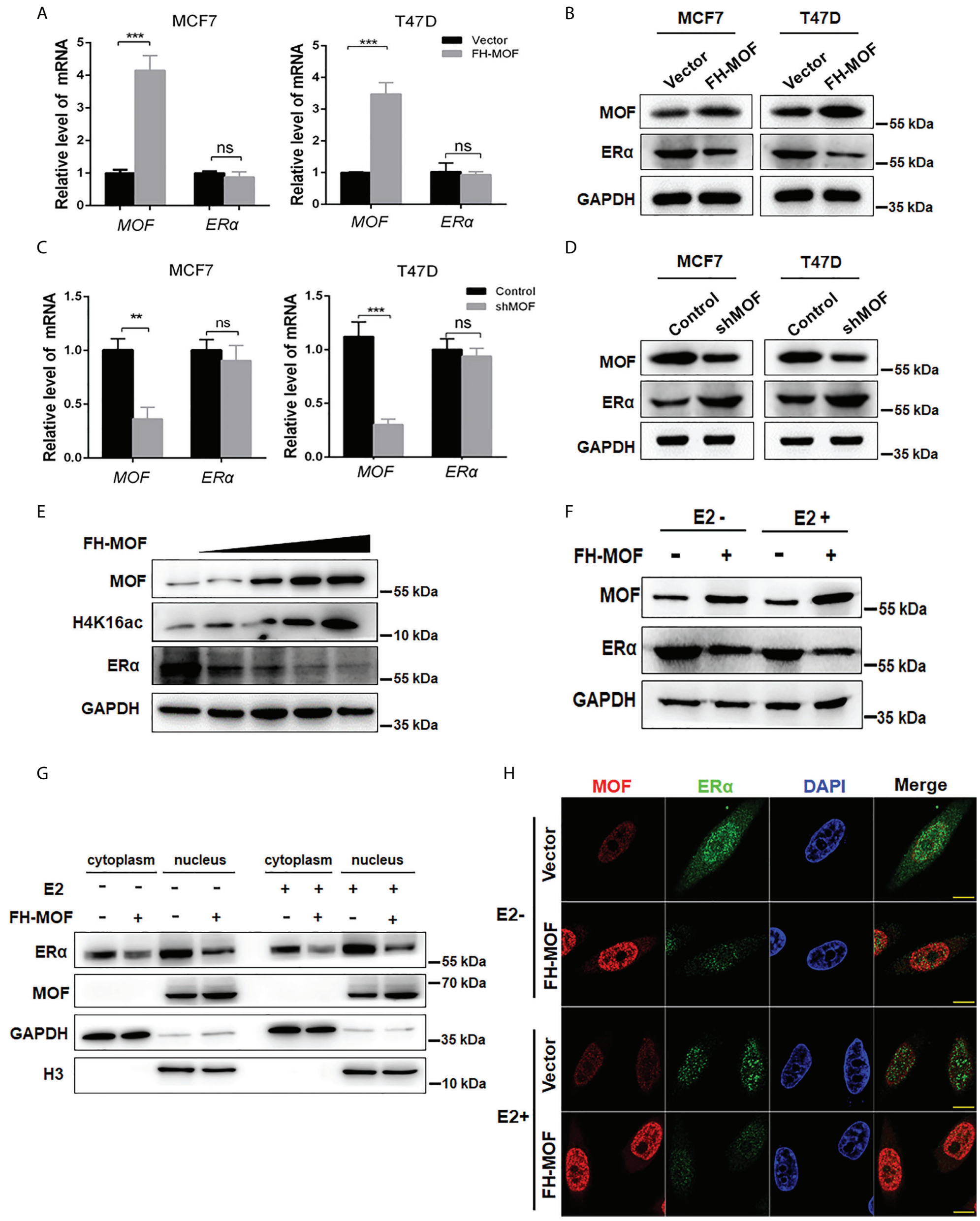

FIGURE 2
Effects of MOF overexpression on the expression of ERα in BC cells. **(A, B)** Effects of MOF overexpression on the steady-state mRNA levels and protein abundance of ERα in MCF7 and T47D cells were examined by qRT-PCR and Western blot assays. **(C, D)** MOF knockdown was performed by shMOF plasmid transfection to determine the expression of ERα at the mRNA and protein levels. **(E)** Increased doses of Flag-HA-MOF plasmid were transfected into MCF7 cells to examine the alteration trend of ERα protein levels. **(F)** Examination of the ERα protein level by MOF overexpression in the absence or presence of E2 treatment. After transfection with Flag-HA-MOF plasmid or empty vector as control for 48 h, MCF7 cells were treated with 10 nM E2 for 3h. **(G)** The protein expression of ERα by MOF in both cytoplasm and nucleus was determined by nuclear and cytoplasmic separation assay regardless of the presence of E2 in MCF7 cells. **(H)** Immunofluorescence staining assay was conducted to detect the expression of ERα in MOF-overexpressed MCF7 cells. Bar = 10 μm. ***P < 0.001 and **P < 0.01 vs. control group. ns, not significant vs. control.

We further investigate the biological function of MOF in ERα+ BC cells. Moreover, stable cell lines with MOF overexpression were established by lentivirus infection of MCF7 cells, and CCK8 assay was performed to determine the functional role of MOF in BC cell proliferation. As shown Figure 3C, E2 stimulation significantly promoted cell proliferation of ERα+ BC MCF7 cells in the control group, whereas in MOF-overexpressed cells, this E2-stimulated raise

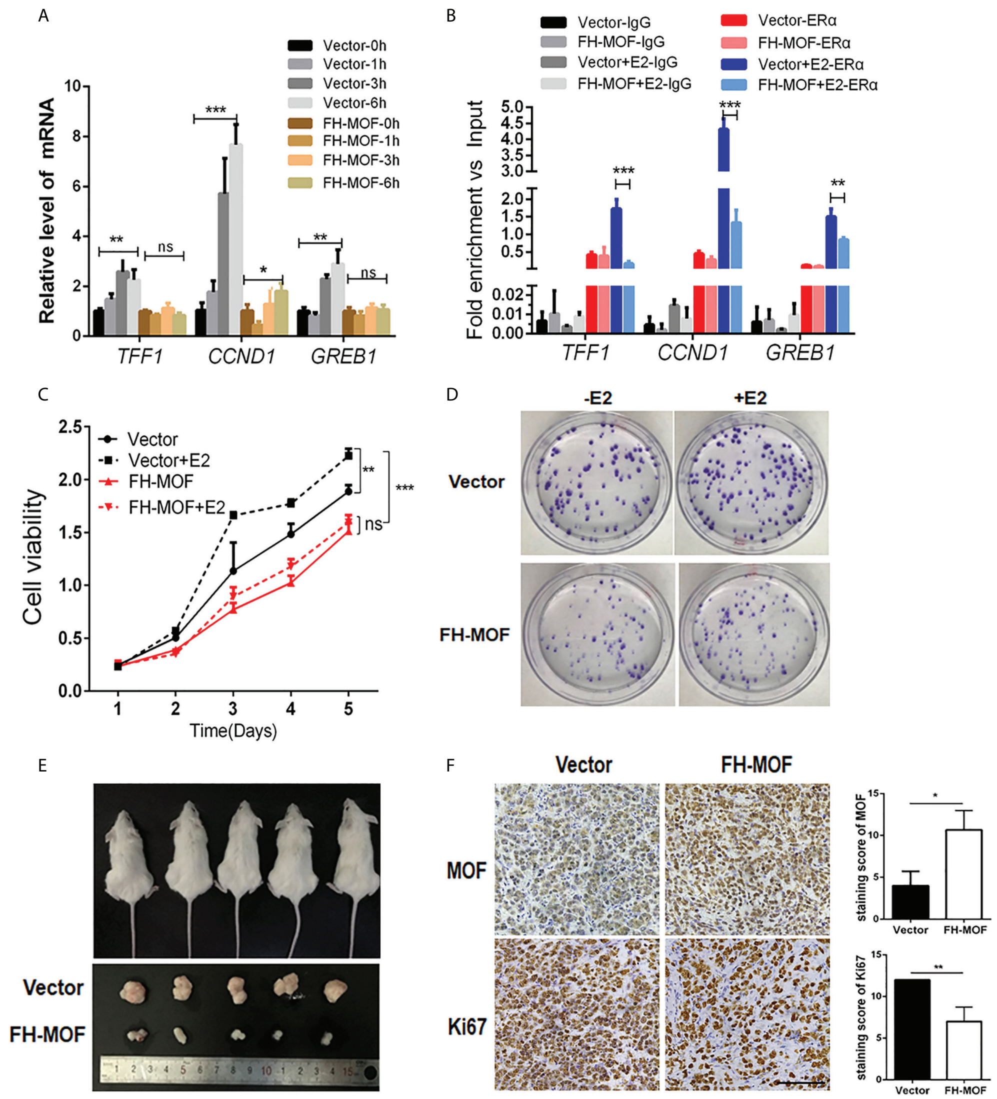

FIGURE 3
The inhibitory roles of MOF in ERα signaling, cellular proliferation, and tumorigenicity of BC cells. **(A)** The effects of MOF overexpression on ERα-mediated transcription activity of target genes (TFF1, CCND1, and GREB1) by qRT-PCR assay in E2-treated MCF7 cells. **(B)** The recruitment of ERα on the promoters of TFF1, CCND1, and GREB1 was analyzed by ChIP assay in MOF-overexpressed MCF7 cells under E2 stimulation. **(C)** Cell proliferation of MCF7 was prohibited by ectopic expression of MOF in CCK8 assay. **(D)** MOF restrained the colony formation ability of MCF7 cells whatever E2 is present. **(E)** Xenograft tumor-forming assay was conducted to determine the effect of MOF on in vivo tumorigenicity of MCF7 cells. MCF7 cells with stable MOF transfection or control were subcutaneously injected into one flank of each mice. Tumors were dissected from mice after 3 weeks of injection. **(F)** IHC staining (left) and staining score (right) showed the reduced expression of proliferation marker Ki67 in xenograft tumor tissue with MOF overexpression. Bar = 100 μm. $^{***}P < 0.001$, $^{**}P < 0.01$, and $^{*}P < 0.05$ vs. control group. ns, not significant vs. control. MOF restrained the colony formation ability of MCF7 cells, whatever E2 is present.

was abolished, suggesting that MOF overexpression inhibited E2-induced proliferation of BC cells. In addition, the inhibitory effect of MOF on MCF7 cell prol9iferation occurred regardless of the presence or absence of E2 (Figure 3C), indicating that MOF prohibits cell proliferation of ERα+ BC cells in an E2-independent manner. In addition, MCF7 cells with shMOF transfection showed that MOF knockdown led to increased cell proliferation (Figure S1A). Colony formation assay further showed that MOF overexpression restrained the colony formation ability of MCF7 cells whenever E2 is present (Figure 3D). *In vivo* tumor formation experiments revealed that the size of tumor formed by MOF-overexpressed MCF7 cells was obviously smaller than that of control group cells (Figure 3E), indicating that MOF overexpression significantly impeded the growth of subcutaneous tumors formed by ERα+ BC cells in mice. In addition, IHC staining showed that, compared with the control tumor, reduced expression of proliferation marker Ki67 was observed in the tumor tissue with MOF overexpression (Figure 3F). Taken together, these results demonstrated that MOF overexpression prevented cell proliferation and tumorigenicity of ERα+ BC cells through the inhibition on ERα function.

MOF promotes ERα protein turnover through ubiquitin–proteasome pathway

MOF downregulates ERα protein abundance in MCF7 cells. We speculated that the protein stability of ERα might be affected by MOF for the negative effect on ERα expression. By using CHX, an inhibitor of protein translation, to block *de novo* protein synthesis, we found that ERα protein stability was attenuated by MOF overexpression (Figure 4A). Under CHX treatment, the degradation of ERα protein was overtly accelerated by MOF overexpression compared with the control group. The half-life of ERα was reduced down to around 4 h in the MOF-overexpressed MCF7 cells compared with that to around 9 h in the control group (Figure 4A). Conversely, we found that the application of MG132 (an inhibitor of proteasome function) could strikingly prevent ERα protein degradation induced by MOF. With the time extension of MG132 treatment, ERα protein expression increased gradually in MOF-overexpressed MCF7 cells and reached a similar level as the control group at 6 h (Figure 4B), suggesting that MOF-induced ERα protein degradation occurred by the proteasome pathway. Furthermore, polyubiquitination of ERα protein by MOF was observed in co-immunoprecipitation (Co-IP) assay. MOF overexpression strengthened the polyubiquitination of ERα, as shown by more intense ladder band of polyubiquitin-conjugated ERα protein in Flag-MOF–transfected cells (Figure 4C). In addition, MOF knockdown resulted in the abrogation of ERα polyubiquitination to promote ERα protein

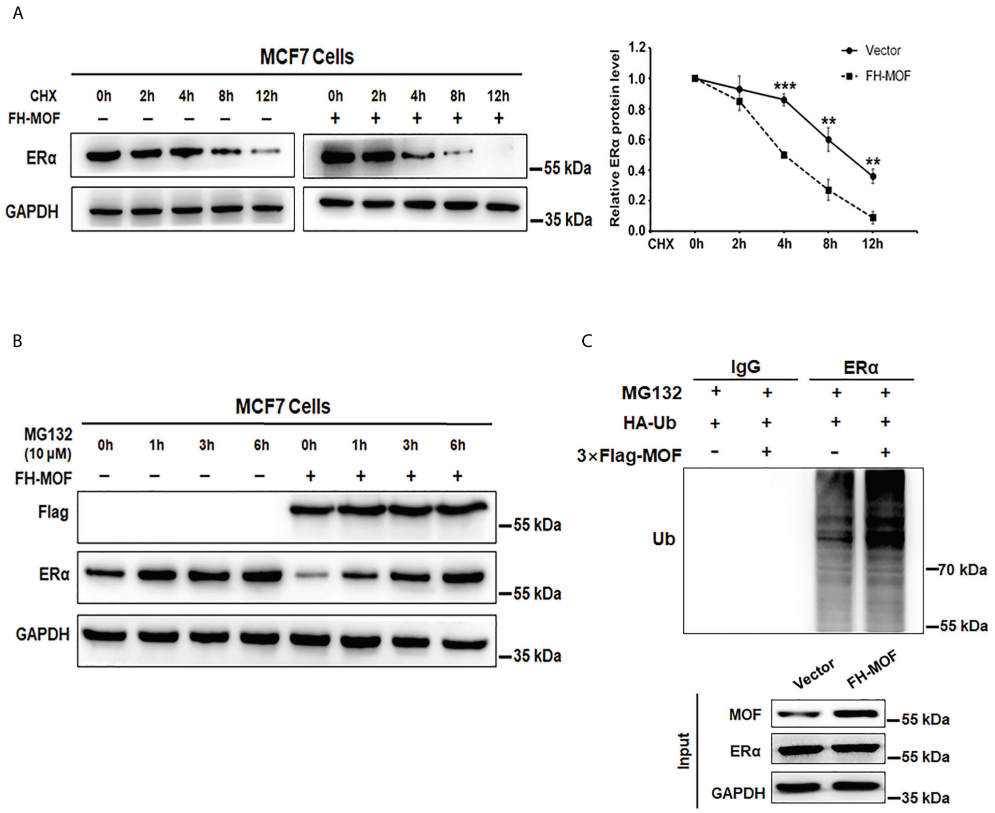

FIGURE 4
MOF promotes ERα protein degradation via ubiquitin–proteasome pathway. **(A)** CHX (10 µg/ml) assay was performed to examine the protein degradation of ERα under MOF overexpression. CHX (10 µg/ml) was applied for MCF7 cells with FH-MOF or control transfection, and cells were terminated at specified time points to calculate the half-life of ERα protein. **(B)** Proteasome inhibitor MG-132 could prevent ERα protein degradation induced by MOF overexpression. **(C)** Co-IP assay was performed in the presence of MG-132 to detect the polyubiquitin-conjugated ERα protein level in Flag-MOF–transfected cells. ***P < 0.001 and **P < 0.01 vs. control group.

stability (Figure S1C). These results indicated that MOF promoted ERα protein degradation through ubiquitin–proteasome pathway.

CUL4B is the functional E3 ligase involved in MOF-mediated ERα protein destabilization

We further explored the E3 ubiquitin ligase responsible for the MOF-induced ERα ubiquitination and degradation. Several E3 ligases like MDM2, CHIP, RNF31, and BRCA1 have been reported to trigger polyubiquitination of ERα for ubiquitin/proteasome-mediated proteolysis (26–29). Our RNA-seq raw data suggested a possible upregulation of CUL4A, which belongs to the Culling-Ring E3 ligase subfamily, in MOF-overexpressed MCF7 cells. After investigating the expression of several E3 ligase candidates in MCF7 cells harboring overexpression or knockdown of MOF, it was found that CUL4A and CUL4B can be positively modulated by MOF in a qRT-PCR assay (Figure 5A). In addition, the protein abundance of CUL4A and CUL4B could be upregulated by MOF overexpression (Figure 5B). To further confirm the involvement of CUL4A or CUL4B in MOF-mediated ERα degradation, cells were co-transfected with FH-MOF plasmids and CUL4A or CUL4B small interfering RNA (siRNA). It was demonstrated that blockage of CUL4B but not CUL4A could abrogate MOF-induced ERα protein degradation (Figure 5C). Moreover, Co-IP assay revealed that CUL4B and ERα proteins could physically interact with each other (Figure 5D). In addition, CUL4B knockdown abolished MOF-encouraged ubiquitination of ERα as revealed by the reduced amount of polyubiquitin-conjugated ER in CUL4B siRNA-transfected cells (Figure 5E). These results indicated that MOF promoted the ubiquitination and protein degradation of ERα *via* upregulated CUL4B functioning as an E3 ligase.

MOF promotes HSP90 hyperacetylation to inhibit its chaperon association with ERα

Molecular chaperone HSP90 binds with ERα to maintain the conformational stability of ER for ligand binding and to protect ERα from protein degradation, whereas hyperacetylation of HSP90 inhibits its chaperone function for ERα (9). By Co-IP assay, it was shown that the acetylation level of HSP90 was overtly raised in MOF-overexpressed MCF7 cells, whereas the acetylation level of ERα was not obviously affected (Figure 6A). In addition, MOF knockdown also did not overtly affect the acetylation level of ERα but markedly decreased that of HSP90 (Figure S1B) It was further confirmed that MOF-induced hyperacetylation of HSP90 occurred through the K294 acetylation site (Figure 6B), which was reported to be determinant for the chaperone binding of HSP90 with its client proteins (30). Co-IP assay further revealed that when MOF was overexpressed in MCF7 cell, the interaction between HSP90 and ER was undermined, whereas more association of ER with CUL4B was observed instead (Figure 6C). Taken together, it is suggested that MOF enhanced the acetylation level of HSP90 at K294 site to attenuate the chaperone association of HSP90 with ERα, thereby liberating ERα to more interact with CUL4B for ubiquitin-mediated proteasomal degradation of ERα.

Inhibition of MOF restores ERα protein abundance and increases TAM sensitivity in ERα− BC cells

In addition to the negative regulation of MOF overexpression on ERα protein stability in ERα+ BC cells, we also examined the effect of MOF inhibition on ERα− BC cells. As shown in Figure 7A, knockdown of MOF in ERα-negative HCC1937 cells resulted in a recovery of ERα protein expression. As an HAT inhibitor, MG149 could inhibit MOF within a certain concentration range (47 ± 14 μM) because higher concentration would work on other histone acetylases (like 74 ± 20 μM for Tip60) (31, 32). First, the inhibitory effect of MG149 was verified in ERα+ MCF7 cells, where increased doses of MG149 could result in the raised abundance of ERα protein and reduced H4K16ac (Figure 7B). Then, treatment of 35 μM MG149 in ER− HCC1937 cells could obviously restore ERα protein expression similar as the effect of MOF knockdown (Figure 7C). Because reactivation of ERα expression could restore endocrine therapy sensitivity in patients with ERα− BC (12, 13), we further investigated the effect of MG149 on the sensitivity of ER− BC cells to TAM. Compared with the inhibition concentration $IC50_{50}$ of TAM at 41.06 μM in HCC1937 treated with TAM alone for 24 h, IC_{50} was reduced to 21.26 μM with a combinatory treatment of TAM and MG149 for 24 h (Figure 7D), suggesting that MOF inhibitor MG149 could effectively improve the response of ERα− BC cells to TAM treatment by the restoration of ERα protein abundance.

Discussion

ERα, encoded by the gene of estrogen receptor 1 (ESR1), is one of the major tumorigenic drivers in BC and uterine cancer (10, 33). ERα-expressing BC, also called luminal BC, accounts for more than two-thirds of patients with BC (10). Because of the full weight of ER functioning in fueling tumor behavior, post-translational modifications of ERα protein and/or epigenetic regulation of ESR1 gene have drawn much attention for their roles in the expression and activity of ERα for controlling the growth and tumorigenicity of cancer cells (34–36). MOF, functioning as a lysine acetyltransferase for the acetylation of H4K16ac as well as multiple non-histone proteins, is currently identified for its aberrant expression and playing regulatory roles in diverse cancers (37–39). For instance, MOF overexpression

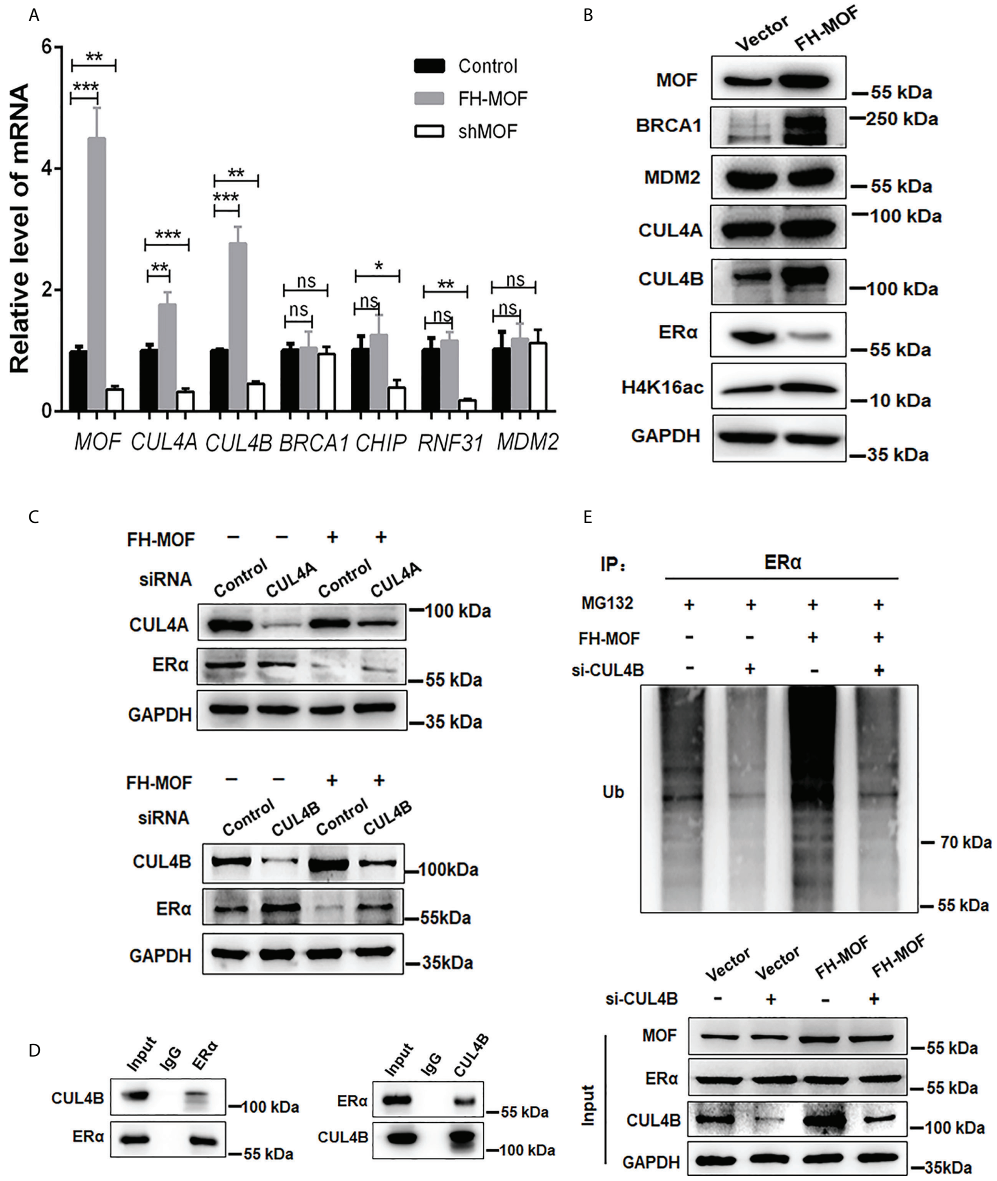

FIGURE 5
CUL4B is required for MOF-induced ERα protein degradation. **(A, B)** The mRNA and protein levels of candidate E3 ligases were determined by qRT-PCR and Western blotting in MCF7 cells with MOF overexpression. **(C)** Knockdown of CUL4B but not CUL4A could abrogate MOF-induced ERα protein degradation by WB assay. **(D)** Co-IP was performed to detect the physical interaction between MOF and ERα by using specific antibodies against the two proteins. **(E)** The levels of polyubiquitin-conjugated ERα was determined by Co-IP to examine the involvement of CUL4B in the ubiquitination and protein degradation of ERα. ***P < 0.001, **P < 0.01, and *P < 0.05 vs. control group. ns, not significant vs. control. .

promoted the cell proliferation, migration, and drug resistance of lung non–small cell lung cancer cells (39), whereas the lack of MOF resulted in the hypoxia tolerance and multidrug resistance of HCC cells through upregulated hypoxia-inducible factor-1α (HIF-1α) (40). It was reported that in large cohort of patients with BC or lung cancer, high MOF expression showed a favorable prognosis (19, 23, 24), which is consistent with the demonstration in the present study that the expression of MOF is negatively correlated with that of ERα in BC tissues and cells. We unraveled that MOF overexpression downregulated ERα expression to inhibit the transactivation potential of ERα as well as the proliferation and tumorigenicity of ERα+ BC cells.

The reduced ERα expression by MOF overexpression occurred at the post-translational level *via* promoting ER

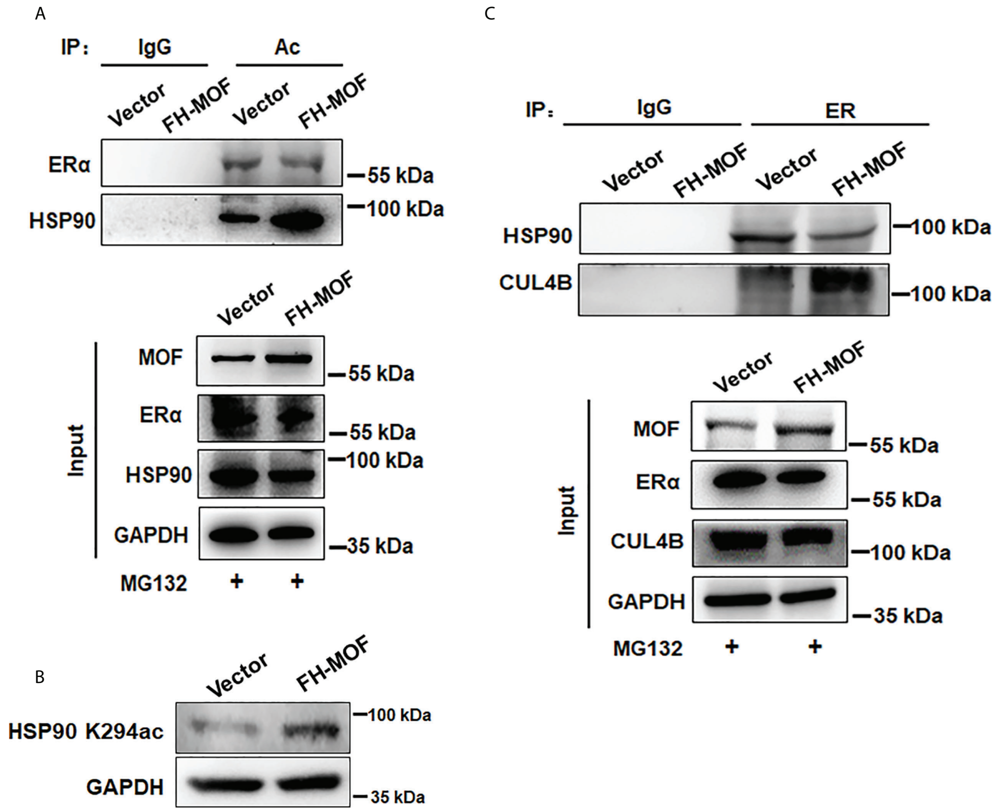

FIGURE 6

MOF promotes HSP90 hyperacetylation to inhibit its chaperon association with ERα. **(A)** The acetylation level of ERα and HSP90 was investigated by Co-IP using acetylated lysine antibody for IP and antibodies against ERα and HSP90 for Western blotting in FH-MOF–transfected MCF7 cells. **(B)** HSP90 K294 acetylation site was identified to be functioning in MOF-induced hyperacetylation of HSP90 by Western blotting assay using specific HSP90 K294ac antibody. **(C)** MOF overexpression enhanced the protein interaction between ERα and CUL4B but undermined the chaperon association of HSP90 with ERα in Co-IP assay.

protein degradation but not at the mRNA level. MOF-mediated ERα degradation requires the activation of CUL4B to speed up ERα protein turnover by the proteasome machinery. CUL4B belongs to the Cullin-Ring E3 ubiquitin ligase subfamily whose members were reported to participate in the proteolysis *via* catalyzing polyubiquitination of various substrates for proteasomal degradation and are implicated in the regulation of some pathological processes (41). For instance, CUL5 is responsible for IFN-gamma–induced proteasomal degradation of HER2 in BC, resulting in diminished cell growth and tumor senescence (42). In addition, CUL4B is responsible for long noncoding RNA Nron-mediated ERα protein stability in osteoporosis (43). Similar with these findings, our data showed that CUL4B destabilized ERα when MOF was overexpressed in BC cells because MOF promoted more expression and interaction of CUL4B with ERα for its polyubiquitination and degradation. As for the two Cullin 4 genes (CUL4A and CUL4B), they shared high identity of protein sequence (44) and possessed overlapping functions in certain scenario (45, 46), like in DNA damage response and polyubiquitination of p53 for degradation (47, 48). However, distinct roles for these two Cul4 proteins have also been revealed recently (49, 50). Accordingly, in our study, both CUL4A and CUL4B were positively regulated by MOF; nevertheless, only the knockdown of CUL4B could abrogate MOF-induced ERα protein degradation.

Apart from the role of CUL4B in MOF-induced ERα protein destabilization, our data also showed that the acetylation of HSP90 might be associated with the effect of MOF on ERα expression. As a molecular chaperone HSP90 interacts with ERα to maintain a stable conformation of ERα for ligand binding and being protected from degradation (8, 9). Previous studies have revealed that hyperacetylation of HSP90 induced by HDAC6 depletion or HDAC inhibitors would restrain the chaperone function of HSP90, thereby promoting the polyubiquitylation and proteasomal degradation of client proteins, like c-Raf, Akt, cyclin D1, and ERα, to evoke growth arrest and apoptosis of cancer cells (9, 51). Similarly, our data showed that MOF overexpression heightened the acetylation of HSP90 and thereby hampered the interaction between HSP90 and ERα, implying the contribution of MOF-induced hyperacetylation of

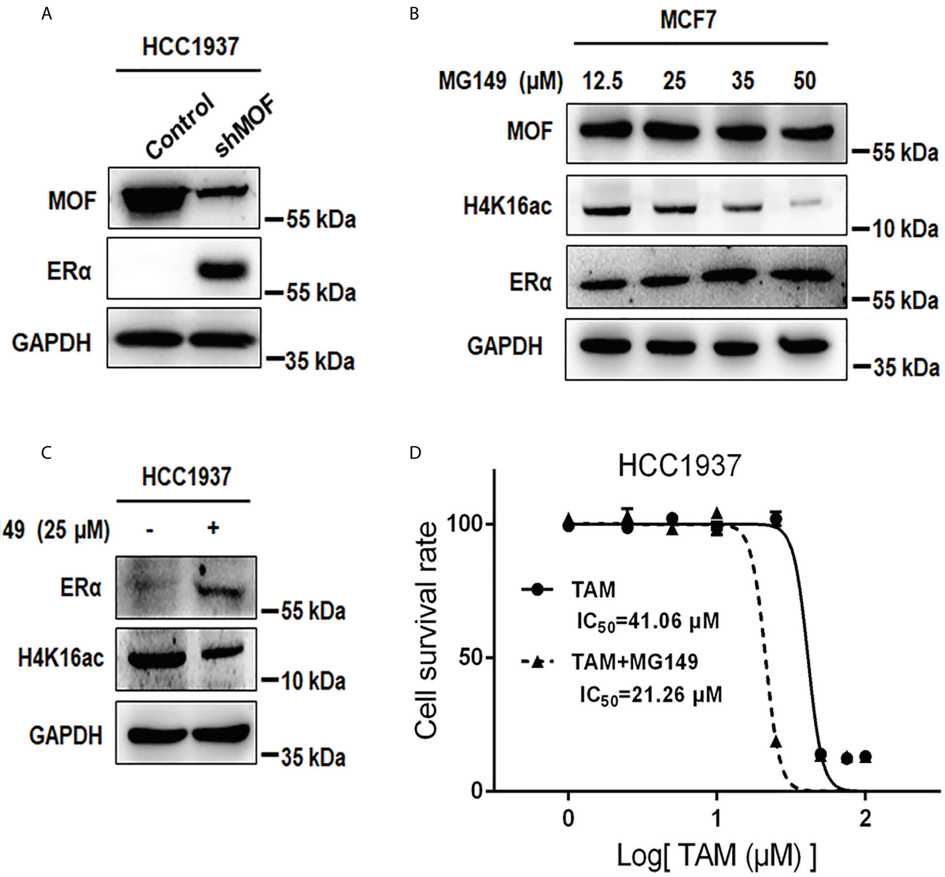

FIGURE 7
Effects of MOF inhibition on ERα protein expression and cell viability in ERα– HCC1937 cells. **(A)** MOF knockdown restored ERα protein abundance in ERα– HCC1937 cells transfected with pGPU6-shMOF plasmid as determined by Western blotting. **(B)** Different concentration of MOF inhibitor MG-149 was applied to examine its enhanced effect on ERα protein expression in MCF7 cells. **(C)** ERα protein expression was reactivated by 35 μM MG149 in ERα– HCC1937 cells. **(D)** Cell viability assay was performed to investigate the effect of MG149 on the sensitivity of ERα– HCC1937 cells to tamoxifen (TAM) treatment. IC_{50} was calculated to compare the combinatory effect of TAM and MG149 with TAM alone treatment for 24 h.

HSP90 in the promotion of ERα degradation. Moreover, the acetylation of HSP90 K294 site was known to be essential for weakening the chaperone association of HSP90 with diverse client proteins such as ErbB2, mutant p53, HIF-1, and androgen receptor (30). In our study, HSP90 K294 site can be specifically acetylated by MOF overexpression, implicating that HSP90 K294ac might play a functional role in MOF-elicited dissociation of ER from HSP90 that results in ER protein instability. Taken together, MOF promoted the hyperacetylation of HSP90 to liberate ERα from the chaperone binding, and subsequently, more CUL4B was recruited to ERα for inducing ER polyubiquitination and proteasomal degradation. A similar scenario was demonstrated where inhibited HSP90 function would destroy the chaperone binding of HSP90 with mutant p53, thereby triggering the protein degradation of released mutant p53 *via* E3 ligases MDM2 and CHIP-mediated ubiquitin–proteasome pathway (52).

On the basis of its role in histone H4K16 acetylation, MOF serves as co-activator of nuclear factor–κB and androgen receptor for upregulating their transactivation capacity in prostate cancer (53, 54). Dimethylation of ERα by G9a could be recognized by MOF complex to induce transcriptional activation of ERα target genes (55). In addition, MOF-mediated acetylation of non-histone proteins plays essential roles in distinct cancer cells. For instance, MOF acetylates the histone demethylase LSD1 to impede its binding with epithelia genes for their transactivation, thus suppressing EMT and tumor progression in lung cancer and BC (19). MOF-mediated acetylation of HIF-1α causes the ubiquitination and degradation of HIF-1α to affect hypoxia susceptibility and drug resistance in HCC (40). On the contrary, MOF acetylates ERα to maintain ERα stability *via* reduced polyubiquitination, thus promoting ER signaling and inhibiting HCC progression (56). This discrepancy in ERα protein stability elicited by the same acetylase activity of MOF on non-histone proteins could be due to different functional characteristics of ERα caused by distinct cellular environment in diverse cancer types and various acetylation targets that MOF acts on.

At present, hormonal therapies have been extensively applied for the treatment of ERα+ BC, like aromatase inhibitors for suppressing estrogen synthesis and antiestrogens competing with estrogens for the interaction with ERα to hinder ERα signaling pathway, which are the most common cure strategies (57, 58). However, for congenital ERα-negative tumors and relapsed tumors losing ER expression after endocrine treatment, they would exhibited intrinsical or acquired resistance to hormonal therapies due to lack of ERα expression (3, 59). Hence, restored expression of lost ERα will be an effective strategy for the sensitivity recovery to endocrine treatment. On account of the negative correlation between MOF and ERα in BC, we further identified that inhibition of MOF by knockdown or inhibitor MG149 could enhance ER expression in BC cells. In particular, in ER-negative HCC1937 cells, recovered abundance of ER protein by MG149 would partially restore the sensitivity of BC cells to TAM treatment. Hypermethylation of ERα gene was reported to be an important cause of suppressed ERα expression (9, 11), and the combination of DNA demethylating agents with HDAC inhibitors would restore ERα expression and TAM sensitivity in ERα– BC cells (12, 13). However, on the other hand, other studies reported that pan-HDAC inhibitors induce HSP90 hyperacetylation to inhibit its binding to ERα and promote ERα degradation (9, 60, 61). Consequently, we provided that the functional role of MOF in ER expression is prone to be similar with the action of HDAC inhibitors through HSP90 acetylation. A high level of MOF in ERα– BC cells resulted in the instability of ER protein due to HSP90 hyperacetylation and loss of chaperone function, whereas MOF inhibition would abrogate the foregoing effects to restore ERα abundance and partial sensitivity to endocrine therapy.

In summary, we unraveled the inverse correlation between MOF and ERα in BC tissues and cells, and MOF overexpression promoted ERα protein degradation *via* CUL4B-mediated ubiquitin–proteasome pathway and HSP90 hyperacetylation that lead to the loss of chaperone binding of HSP90 with ERα, thus inhibiting transcriptional activation and cellular proliferation induced by estrogen and *in vivo* tumorigenicity of ERα+ BC cells. In addition, suppression of MOF restored ERα expression and increased the sensitivity of ERα– BC cells to TAM treatment. These findings highlight an essential role of MOF in modulating ER signaling in BC and rationalize MOF as a potential therapeutic target, like developing specific MOF activator for anti-ER treatment in ERα+ BC or combination therapy of MG149 with TAM for resistance amelioration in ERα– BC.

Data availability statement

The original contributions presented in the study are included in the article/Supplementary Material. Further inquiries can be directed to the corresponding author.

Ethics statement

The animal study was reviewed and approved by Animal Research Ethical Inspection Form of Shandong University School of Life Sciences.

Author contributions

XL designed this work. XZ, YY, DL, ZW, HL, ZZ, HZ, and FX performed the experiments. XZ and YY analyzed the data. XZ, YY, and XL wrote this manuscript. All authors have reviewed and approved the manuscript.

Funding

This work was supported by the National Key R&D Program of China (2016YFE0129200) and the National Natural Science Foundation of China (Nos. 31571321, 31171428, 71974113 and 81601337).

Conflict of interest

The authors declare that the research was conducted in the absence of any commercial or financial relationships that could be construed as a potential conflict of interest.

Publisher’s note

All claims expressed in this article are solely those of the authors and do not necessarily represent those of their affiliated organizations, or those of the publisher, the editors and the reviewers. Any product that may be evaluated in this article, or claim that may be made by its manufacturer, is not guaranteed or endorsed by the publisher.

Supplementary material

The Supplementary Material for this article can be found online at: https://www.frontiersin.org/articles/10.3389/fonc.2022.868866/full#supplementary-material

SUPPLEMENTARY FIGURE 1

MOF knockdown increased cellular proliferation of MCF7 cells and abrogated polyubiqutination but not acetylation of ERα. (A) CCK8 assay showed that cell proliferation was increased in MOF knockdown MCF7 cells. (B) Co-IP assay was performed in the presence of MG-132 to detect polyubiquitin-conjugated ERα protein level in pGPU6-shMOF–transfected cells. (C) The acetylation level of ERα and HSP90 was investigated by Co-IP using acetylated lysine antibody in pGPU6-shMOF–transfected MCF7 cells. ** P < 0.01 vs. control group.

References

1. Burguin A, Diorio C, Durocher F. Breast cancer treatments: Updates and new challenges. *J Pers Med* (2021) 11(8):80–61. doi: 10.3390/jpm11080808

2. Siegel RL, Miller KD, Jemal A. Cancer statistics, 2020. *CA Cancer J Clin* (2020) 70(1):7–30. doi: 10.3322/caac.21590

3. Onitilo AA, Engel JM, Greenlee RT, Mukesh BN. Breast cancer subtypes based on ER/PR and Her2 expression: comparison of clinicopathologic features and survival. *Clin Med Res* (2009) 7(1-2):4–13. doi: 10.3121/cmr.2008.825

4. Waddell A, Mahmud I, Ding H, Huo Z, Liao D. Pharmacological inhibition of CBP/p300 blocks estrogen receptor alpha (ERalpha) function through suppressing enhancer H3K27 acetylation in luminal breast cancer. *Cancers (Basel)* (2021) 13(11)::2799–823. doi: 10.3390/cancers13112799

5. Yasar P, Ayaz G, User SD, Gupur G, Muyan M. Molecular mechanism of estrogen-estrogen receptor signaling. *Reprod Med Biol* (2017) 16(1):4–20. doi: 10.1002/rmb2.12006

6. Wang C, Mayer JA, Mazumdar A, Fertuck K, Kim H, Brown M, et al. Estrogen induces c-myc gene expression via an upstream enhancer activated by the estrogen receptor and the AP-1 transcription factor. *Mol Endocrinol* (2011) 25 (9):1527–38. doi: 10.1210/me.2011-1037

7. Prall OW, Rogan EM, Musgrove EA, Watts CK, Sutherland RL. C-myc or cyclin D1 mimics estrogen effects on cyclin e-Cdk2 activation and cell cycle reentry. *Mol Cell Biol* (1998) 18(8):4499–508. doi: 10.1128/MCB.18.8.4499

8. Fliss AE, Benzeno S, Rao J, Caplan AJ. Control of estrogen receptor ligand binding by Hsp90. *J Steroid Biochem Mol Biol* (2000) 72(5):223–30. doi: 10.1016/S0960-0760(00)00037-6

9. Fiskus W, Ren Y, Mohapatra A, Bali P, Mandawat A, Rao R, et al. Hydroxamic acid analogue histone deacetylase inhibitors attenuate estrogen receptor-alpha levels and transcriptional activity: a result of hyperacetylation and inhibition of chaperone function of heat shock protein 90. *Clin Cancer Res* (2007) 13(16):4882–90. doi: 10.1158/1078-0432.CCR-06-3093

10. Porras L, Ismail H, Mader S. Positive regulation of estrogen receptor alpha in breast tumorigenesis. *Cells* (2021) 10(11):2966–90. doi: 10.3390/cells10112966

11. Ottaviano YL, Issa JP, Parl FF, Smith HS, Baylin SB, Davidson NE. Methylation of the estrogen receptor gene CpG island marks loss of estrogen receptor expression in human breast cancer cells. *Cancer Res* (1994) 54(10):2552–5.

12. Yang X, Phillips DL, Ferguson AT, Nelson WG, Herman JG, Davidson NE., et al. Synergistic activation of functional estrogen receptor (ER)-alpha by DNA methyltransferase and histone deacetylase inhibition in human ER-alpha-negative breast cancer cells. *Cancer Res* (2001) 61(19):7025–9.

13. Sharma D, Saxena NK, Davidson NE, Vertino PM. Restoration of tamoxifen sensitivity in estrogen receptor-negative breast cancer cells: tamoxifen-bound reactivated ER recruits distinctive corepressor complexes. *Cancer Res* (2006) 66 (12):6370–8. doi: 10.1158/0008-5472.CAN-06-0402

14. Hanstein B, Eckner R, Direnzo J, Halachmi S, Liu H, Searcy B, et al. p300 is a component of an estrogen receptor coactivator complex. *Proc Natl Acad Sci United States America* (1996) 93(21):11540–5. doi: 10.1073/pnas.93.21.11540

15. Waddell AR, Huang H, Liao D. CBP/p300: Critical Co-activators for nuclear steroid hormone receptors and emerging therapeutic targets in prostate and breast cancers. *Cancers (Basel)* (2021) 13(12):2872–905. doi: 10.3390/cancers13122872

16. Taipale M, Rea S, Richter K, Vilar A, Lichter P, Imhof A, et al. HMOF histone acetyltransferase is required for histone H4 lysine 16 acetylation in mammalian cells. *Mol Cell Biol* (2005) 25(15):6798–810. doi: 10.1128/MCB.25.15.6798-6810.2005

17. Sykes SM, Mellert HS, Holbert MA, Li K, Marmorstein R, Lane WS, et al. Acetylation of the p53 DNA-binding domain regulates apoptosis induction. *Mol Cell* (2006) 24(6):841–51. doi: 10.1016/j.molcel.2006.11.026

18. Huai W, Liu X, Wang C, Zhang Y, Chen X, Chen X, et al. KAT8 selectively inhibits antiviral immunity by acetylating IRF3. *J Exp Med* (2019) 216(4):772–85. doi: 10.1084/jem.20181773

19. Luo H, Shenoy AK, Li X, Jin Y, Jin L, Cai Q, et al. MOF acetylates the histone demethylase LSD1 to suppress epithelial-to-Mesenchymal transition. *Cell Rep* (2016) 15(12):2665–78. doi: 10.1016/j.celrep.2016.05.050

20. Singh M, Bacolla A, Chaudhary S, Hunt CR, Pandita S, Chauhan R, et al. Histone acetyltransferase MOF orchestrates outcomes at the crossroad of oncogenesis, DNA damage response, proliferation, and stem cell development. *Mol Cell Biol* (2020) 40(18):e00232–43. doi: 10.1128/MCB.00232-20

21. Su J, Wang F, Cai Y, Jin J. The functional analysis of histone acetyltransferase MOF in tumorigenesis. *Int J Mol Sci* (2016) 17(1):99–116. doi: 10.3390/ijms17010099

22. Li XZ, Pandey R, Byun JS, Gardner K, Qin ZH, et al. The histone acetyltransferase MOF is a key regulator of the embryonic stem cell core transcriptional network. *Cell Stem Cell* (2012) 11(2):163–78. doi: 10.1016/j.stem.2012.04.023

23. Gyorffy B, Surowiak P, Budczies J, Lanczky A. Online survival analysis software to assess the prognostic value of biomarkers using transcriptomic data in non-Small-Cell lung cancer. *PloS One* (2013) 8(12). doi: 10.1371/journal.pone.0082241

24. Gyorffy B, Lanczky A, Eklund AC, Denkert C, Budczies J, Li Q, et al. An online survival analysis tool to rapidly assess the effect of 22,277 genes on breast cancer prognosis using microarray data of 1,809 patients. *Breast Cancer Res Treat* (2010) 123(3):725–31. doi: 10.1007/s10549-009-0674-9

25. Pfister S, Rea S, Taipale M, Mendrzyk F, Straub B, Ittrich C, et al. The histone acetyltransferase hMOF is frequently downregulated in primary breast carcinoma and medulloblastoma and constitutes a biomarker for clinical outcome in medulloblastoma. *Int J Cancer* (2008) 122(6):1207–13. doi: 10.1002/ijc.23283

26. Fan M, Park A, Nephew KP. CHIP (carboxyl terminus of Hsc70-interacting protein) promotes basal and geldanamycin-induced degradation of estrogen receptor-alpha. *Mol Endocrinol* (2005) 19(12):2901–14. doi: 10.1210/me.2005-0111

27. Saji S, Okumura N, Eguchi H, Nakashima S, Suzuki A, Toi M, et al. MDM2 enhances the function of estrogen receptor alpha in human breast cancer cells. *Biochem Biophys Res Commun* (2001) 281(1):259–65. doi: 10.1006/bbrc.2001.4339

28. Witus SR, Stewart MD, Klevit RE. The BRCA1/BARD1 ubiquitin ligase and its substrates. *Biochem J* (2021) 478(18):3467–83. doi: 10.1042/BCJ20200864

29. Zhu J, Zhuang T, Yang H, Li X, Liu H, Wang H. Atypical ubiquitin ligase RNF31: the nuclear factor modulator in breast cancer progression. *BMC Cancer* (2016) 16:538. doi: 10.1186/s12885-016-2575-8

30. Scroggins BT, Robzyk K, Wang D, Marcu MG, Tsutsumi S, Beebe K, et al. An acetylation site in the middle domain of Hsp90 regulates chaperone function. *Mol Cell* (2007) 25(1):151–9. doi: 10.1016/j.molcel.2006.12.008

31. Ghizzoni M, Wu J, Gao TL, Haisma HJ, Dekker FJ, Zheng YG. 6-alkylsalicylates are selective Tip60 inhibitors and target the acetyl-CoA binding site. *Eur J Med Chem* (2012) 47:337–44. doi: 10.1016/j.ejmech.2011.11.001

32. Valerio DG, Xu HM, Chen CW, Hoshii T, Eisold ME, Delaney C, et al. Histone acetyltransferase activity of MOF is required for MLL-AF9 leukemogenesis. *Cancer Res* (2017) 77(7):1753–62. doi: 10.1158/0008-5472.CAN-16-2374

33. Ascenzi P, Bocedi A, Marino M. Structure-function relationship of estrogen receptor alpha and beta: impact on human health. *Mol Aspects Med* (2006) 27 (4):299–402. doi: 10.1016/j.mam.2006.07.001

34. Jeffreys SA, Powter B, Balakrishnar B, Mok K, Soon P, Franken A, et al. Endocrine resistance in breast cancer: The role of estrogen receptor stability. *Cells* (2020) 9(9):2077–99. doi: 10.3390/cells9092077

35. Le Romancer M, Poulard C, Cohen P, Sentis S, Renoir JM, Corbo L, et al. Cracking the estrogen receptor's posttranslational code in breast tumors. *Endocr Rev* (2011) 32(5):597–622. doi: 10.1210/er.2010-0016

36. Sukocheva OA, Lukina E, Friedemann M, Menschikowski M, Hagelgans A, Aliev G, et al. The crucial role of epigenetic regulation in breast cancer anti-estrogen resistance: Current findings and future perspectives. *Semin Cancer Biol* (2020) 82:35–59. doi: 10.1016/j.semcancer.2020.12.004

37. Li X, Corsa CA, Pan PW, Wu L, Ferguson D, Yu X, et al. MOF and H4 K16 acetylation play important roles in DNA damage repair by modulating recruitment of DNA damage repair protein Mdc1. *Mol Cell Biol* (2010) 30(22):5335–47. doi: 10.1128/MCB.00350-10

38. Li X, Wu L, Corsa CA, Kunkel S, Dou Y. Two mammalian MOF complexes regulate transcription activation by distinct mechanisms. *Mol Cell* (2009) 36 (2):290–301. doi: 10.1016/j.molcel.2009.07.031

39. Chen Z, Ye X, Tang N, Shen S, Li Z, Niu X, et al. The histone acetylranseferase hMOF acetylates Nrf2 and regulates anti-drug responses in human non-small cell lung cancer. *Br J Pharmacol* (2014) 171(13):3196–211. doi: 10.1111/bph.12661

40. Wang M, Liu H, Zhang X, Zhao W, Lin X, Zhang F, et al. Lack of MOF decreases susceptibility to hypoxia and promotes multidrug resistance in hepatocellular carcinoma via HIF-1alpha. *Front Cell Dev Biol* (2021) 9:718707. doi: 10.3389/fcell.2021.718707

41. Gong L, Cui D, Xiong X, Zhao Y. Targeting cullin-RING ubiquitin ligases and the applications in PROTACs. *Adv Exp Med Biol* (1217) p:317–47. doi: 10.1007/978-981-15-1025- 0_19

42. Jia Y, Kodumudi KN, Ramamoorthi G, Basu A, Snyder C, Wiener D, et al. Th1 cytokine interferon gamma improves response in HER2 breast cancer by modulating the ubiquitin proteasomal pathway. *Mol Ther* (2021) 29(4):1541–56. doi: 10.1016/j.ymthe.2020.12.037

43. Jin F, Li J, Zhang YB, Liu X, Cai M, Liu M, et al. A functional motif of long noncoding RNA nron against osteoporosis. *Nat Commun* (2021) 12(1):3319. doi: 10.1038/s41467-021-23642-7

44. Zou Y, Mi J, Cui J, Lu D, Zhang X, Guo C, et al. Characterization of nuclear localization signal in the n terminus of CUL4B and its essential role in cyclin e degradation and cell cycle progression. *J Biol Chem* (2009) 284(48):33320–32. doi: 10.1074/jbc.M109.050427

45. Kerzendorfer C, Whibley A, Carpenter G, Outwin E, Chiang SC, Turner G, et al. Mutations in cullin 4B result in a human syndrome associated with increased camptothecin-induced topoisomerase I-dependent DNA breaks. *Hum Mol Genet* (2010) 19(7):1324–34. doi: 10.1093/hmg/ddq008

46. Hu J, Mccall CM, Ohta T, Xiong Y. Targeted ubiquitination of CDT1 by the DDB1-CUL4A-ROC1 ligase in response to DNA damage. *Nat Cell Biol* (2004) 6 (10):1003–9. doi: 10.1038/ncb1172

47. Thirunavukarasou A, Singh P, Govindarajalu G, Bandi V, Baluchamy S. E3 ubiquitin ligase Cullin4B mediated polyubiquitination of p53 for its degradation. *Mol Cell Biochem* (2014) 390(1-2):93–100. doi: 10.1007/s11010-014-1960-3

48. Nag A, Bagchi S, Raychaudhuri P. Cul4A physically associates with MDM2 and participates in the proteolysis of p53. *Cancer Res* (2004) 64(22):8152–5. doi: 10.1158/0008-5472.CAN-04-2598

49. Liu L, Lee S, Zhang J, Peters SB, Hannah J, Zhang Y, et al. CUL4A abrogation augments DNA damage response and protection against skin carcinogenesis. *Mol Cell* (2009) 34(4):451–60. doi: 10.1016/j.molcel.2009.04.020

50. Kopanja D, Roy N, Stoyanova T, Hess RA, Bagchi S, Raychaudhuri P. Cul4A is essential for spermatogenesis and male fertility. *Dev Biol* (2011) 352(2):278–87. doi: 10.1016/j.ydbio.2011.01.028

51. George P, Bali P, Annavarapu S, Scuto A, Fiskus W, Guo F, et al. Combination of the histone deacetylase inhibitor LBH589 and the hsp90 inhibitor 17-AAG is highly active against human CML-BC cells and AML cells with activating mutation of FLT-3. *Blood* (2005) 105(4):1768–76. doi: 10.1182/blood-2004-09-3413

52. Li D, Marchenko ND, Schulz R, Fischer V, Velasco-Hernandez T, Talos F, et al. Functional inactivation of endogenous MDM2 and CHIP by HSP90 causes aberrant stabilization of mutant p53 in human cancer cells. *Mol Cancer Res* (2011) 9(5):577–88. doi: 10.1158/1541-7786.MCR-10-0534

53. Kim JY, Yu JD, Abdulkadir SA, Chakravarti D. KAT8 regulates androgen signaling in prostate cancer cells. *Mol Endocrinol* (2016) 30(8):925–36. doi: 10.1210/me.2016-1024

54. Jaganathan A, Chaurasia P, Xiao GQ, Philizaire M, Lv X, Yao S, et al. Coactivator MYST1 regulates nuclear factor-kappaB and androgen receptor functions during proliferation of prostate cancer cells. *Mol Endocrinol* (2014) 28 (6):872–85. doi: 10.1210/me.2014-1055

55. Zhang X, Peng DN, Xi YX, Yuan C, Sagum CA, Klein BJ, et al. G9a-mediated methylation of ER alpha links the PHF20/MOF histone acetyltransferase complex to hormonal gene expression. *Nat Commun* (2016) 7:10810–21. doi: 10.1038/ncomms10810

56. Wei S, Liu W, Sun N, Wu Y, Song H, Wang C, et al. MOF upregulates the estrogen receptor alpha signaling pathway by its acetylase activity in hepatocellular carcinoma. *Cancer Sci* (2021) 112(5):1865–77. doi: 10.1111/cas.14836

57. Traboulsi T, El Ezzy M, Gleason JL, Mader S. Antiestrogens: structure-activity relationships and use in breast cancer treatment. *J Mol Endocrinol* (2017) 58(1):R15–31. doi: 10.1530/JME-16-0024

58. Caciolla J, Bisi A, Belluti F, Rampa A, Gobbi S.. Reconsidering aromatase for breast cancer treatment: New roles for an old target. *Molecules* (2020) 25 (22):5351–79. doi: 10.3390/molecules25225351

59. Gutierrez MC, Detre S, Johnston S, Mohsin SK, Shou JN, Allred DC, et al. Molecular changes in tamoxifen-resistant breast cancer: Relationship between estrogen receptor, HER-2, and p38 mitogen-activated protein kinase. *J Clin Oncol* (2005) 23(11):2469–76. doi: 10.1200/JCO.2005.01.172

60. Bali P, Pranpat M, Bradner J, Balasis M, Fiskus W, Guo F, et al. Inhibition of histone deacetylase 6 acetylates and disrupts the chaperone function of heat shock protein 90: a novel basis for antileukemia activity of histone deacetylase inhibitors. *J Biol Chem* (2005) 280(29):26729–34. doi: 10.1074/jbc.C500186200

61. Kovacs JJ, Murphy PJ, Gaillard S, Zhao X, Wu JT, Nicchitta CV, et al. HDAC6 regulates Hsp90 acetylation and chaperone-dependent activation of glucocorticoid receptor. *Mol Cell* (2005) 18(5):601–7. doi: 10.1016/j.molcel.2005.04.021

Frontiers in
Pharmacology

Explores the interactions between chemicals and living beings

The most cited journal in its field, which advances access to pharmacological discoveries to prevent and treat human disease.

Discover the latest
Research Topics

See more →

frontiers
Frontiers in
Pharmacology

Frontiers

Avenue du Tribunal-Fédéral 34
1005 Lausanne, Switzerland

Contact us

+41 (0)21 510 17 00
frontiersin.org/about/contact